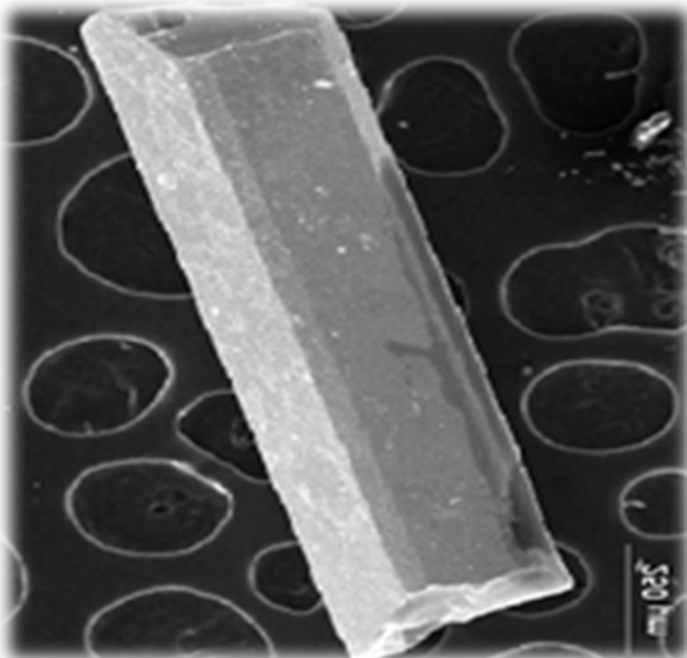
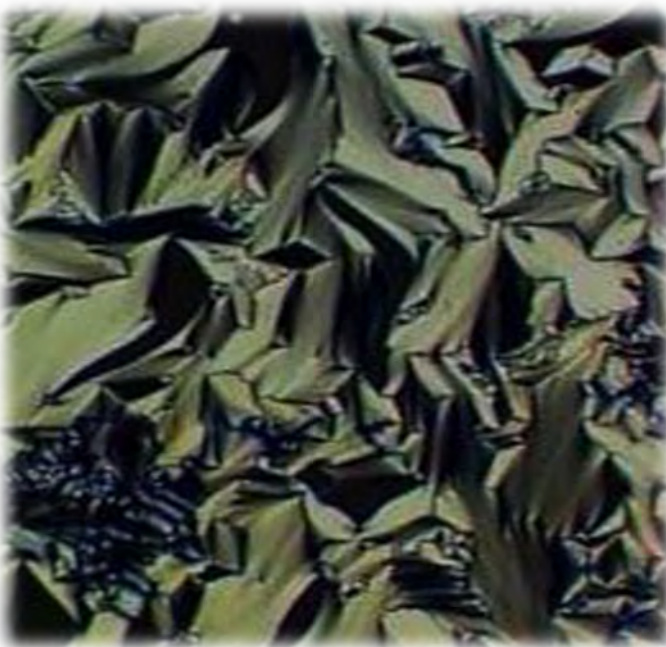
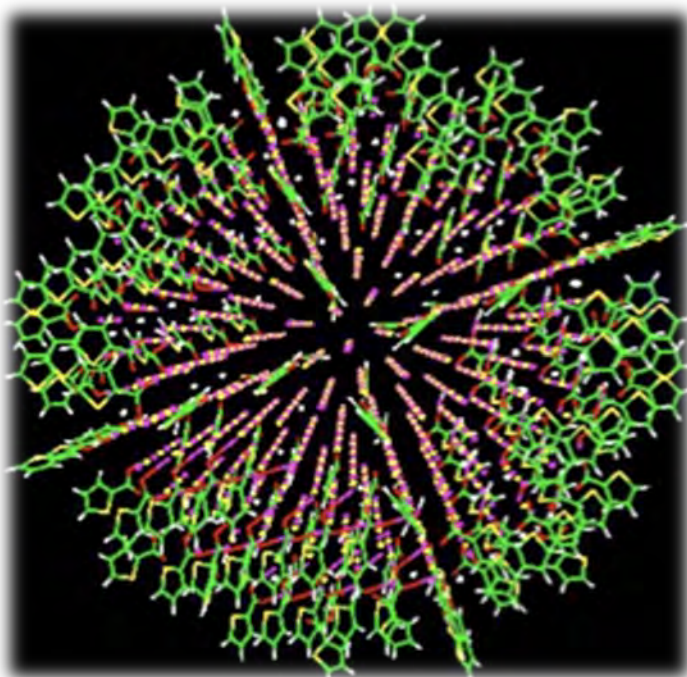
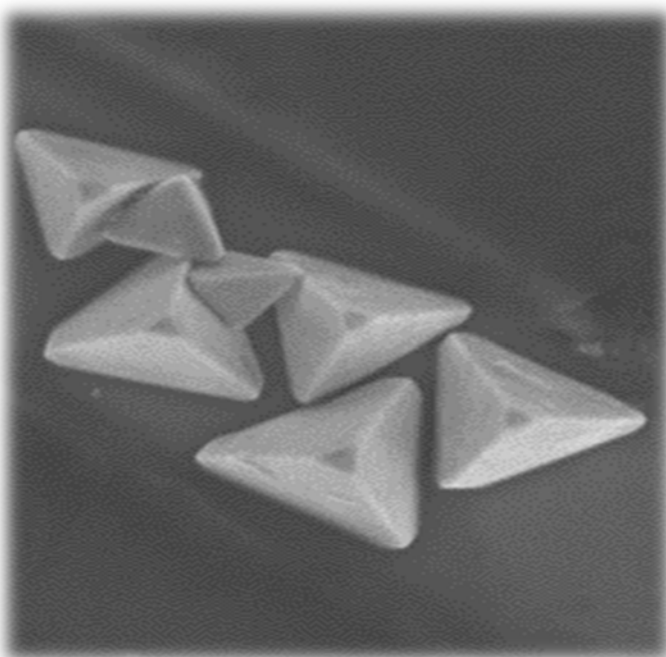


Materials Chemistry Principal Investigators' Meeting—2012

July 15-18, 2012

DoubleTree Hotel, Annapolis, MD



U.S. DEPARTMENT OF
ENERGY

Office of Basic Energy Sciences
Materials Sciences and Engineering Division

On the Cover

- Top Left: Template-assisted assembly of the anisotropic core-shell microparticles driven by electrostatic interactions.
Courtesy: Dr. Vladimir Tsukruk, Georgia Institute of Technology
- Top Right: Simulation of passivation of a PbS nanoparticle with 2,5-thiophenedicarboxylic acid.
Courtesy: Dr. Lin-Wang Wang, Lawrence Berkeley National Laboratory
- Bottom Left: Crossed polarized optical texture micrograph of a bent-core chiral mesogen.
Courtesy: Dr. Satyendra Kumar, Kent State University
- Bottom Right: Scanning electron micrograph (SEM) image of a flux-grown $\text{Yb}_3\text{AuGe}_2\text{In}_3$ single crystal.
Courtesy: Dr. Mercouri Kanatzidis, Northwestern University / Argonne National Laboratory

This document was produced under contract number DE-AC05-06OR23100 between the U.S. Department of Energy and Oak Ridge Associated Universities.

The research grants and contracts described in this document are supported by the U.S. DOE Office of Science, Office of Basic Energy Sciences, Materials Sciences and Engineering Division.

Foreword

This document is a collection of abstracts of the presentations made at the Principal Investigators' Meeting of the Materials Chemistry program, sponsored by the Materials Sciences and Engineering Division (MSED) in the Office of Basic Energy Sciences (BES) of the U. S. Department of Energy (DOE). The meeting was held on July 15–18, 2012 at the DoubleTree Hotel, Annapolis, Maryland, and is one of a series of principal investigators' meetings organized by BES. The purpose of the meeting is to bring together all the principal investigators with currently active projects in the Materials Chemistry program for the multiple purposes of raising awareness among PIs of the overall program content and of each other's research, encouraging exchange of ideas, promoting collaboration and stimulating innovation. The meeting also provides an opportunity for the program manager and MSED/BES management to get a comprehensive overview of the program on a periodic basis, which provides opportunities to identify program needs and potential new research directions. The opening session of the meeting, titled *Frontiers of Materials Chemistry*, includes a selection of presentations chosen to illustrate a cross section of the diverse research being conducted in the Materials Chemistry program. The balance of the meeting agenda is organized in eight sessions around major topical areas in contemporary materials research that broadly encompass many of the projects in the current Materials Chemistry portfolio. These include Electronic and Magnetic Materials, Solar Energy Conversion Materials, Tools and Techniques for Materials Characterization, Materials Relevant to Fuel Cells, Nanostructured Materials, Materials Behavior at Surfaces and Interfaces, and Energy Storage Materials. Recent BES workshops and other reports have identified the concept of “materials by design” as a Grand Challenge goal, defined as the ability to design and synthesize new materials with specific properties tailored and optimized for use in next-generation technologies. In support of the materials-by-design objective, the Materials Chemistry program supports basic research in the discovery, design, and synthesis of materials with an emphasis on elucidating the complex relationships between a material's functional properties and its composition, atomic and molecular structure, and higher-order morphology. Major focus areas of the program include the discovery, synthesis, and characterization of new materials and the manipulation of materials' structure across a range of length scales using *chemistry*.

I thank all of the meeting attendees, including the invited speakers, for their active participation and for sharing their ideas and new research results. The assistance of the meeting chairs, Geri Richmond and Mercouri Kanatzidis, in organizing this meeting is greatly appreciated. Sincere thanks also go to Teresa Crockett in MSED and Lee-Ann Talley and her colleagues at the Oak Ridge Institute for Science and Education (ORISE) for their excellent work providing all the logistical support for the meeting.

Michael Sennett
Program Manager, Materials Chemistry
Materials Sciences and Engineering Division
Office of Basic Energy Sciences
U.S. Department of Energy

Agenda

Meeting Chairs
Geraldine Richmond and **Mercouri Kanatzidis**
University of Oregon
Northwestern University/Argonne National Laboratory

Agenda

Sunday, July 15, 2012

- 3:00 – 6:00 pm Arrival and Registration
- 5:00 – 6:00 pm Reception (No Host)
- 6:00 – 7:00 pm *****Working Dinner*****
Welcome and Presentation of Meeting Agenda
Michael Sennett, Program Manager, Materials Chemistry
- 7:00 – 7:30 pm *Introductory Remarks*
Linda Horton
Director, Materials Sciences and Engineering Division, Basic Energy Sciences
- 7:30 – 7:50 pm Meeting Chairs: **Geraldine Richmond** and **Mercouri Kanatzidis**
University of Oregon/Northwestern University-Argonne National Laboratory

Session I Frontiers of Materials Chemistry

Chair: **Mercouri Kanatzidis**, Northwestern University/Argonne National Laboratory

- 7:50 – 8:20 pm **Paul Alivisatos**, University of California, Berkeley/LBNL
Physical Chemistry of Inorganic Nanostructures 3
- 8:20 – 8:50 pm **Geraldine Richmond**, University of Oregon
*Molecular Processes Underlying the Structure and Assembly of Thin Films
and Nanoparticles at Complex Interfaces* 285
- 8:50 – 9:20 pm **Jennifer Lewis**, University of Illinois, Urbana-Champaign
Deterministic Assembly of Fluid and Solid Inks 246
- 9:20 – 11:00 pm Small Group Discussions

Monday, July 16, 2012

- 7:00 – 8:00 am ***** Breakfast*****

Session II Electronic and Magnetic Materials

Chair: **Joel Miller**, University of Utah

- 8:00 – 8:30 am **Robert Cava**, Princeton University
New Superconducting Materials 123

8:30 – 9:00 am	Kim Dunbar , Texas A&M University <i>Molecular Magnets Based on a Modular Approach: Investigation of Coupling, Anisotropy and Electronic Factors on Bistability</i>	142
9:00 – 9:30 am	Howard Katz , Johns Hopkins University <i>Charging and Polarization of Organic Semiconductors in Energy-Efficient Circuits and Energy Capture Modules: Synthesis, Electronics, and Spectroscopy</i>	238
9:30 – 10:00 am	Elsa Reichmanis (Invited) , Georgia Institute of Technology <i>Conjugated Polymer Semiconductors: Insights into Ordering at the Nano-through Macro-scales</i>	340
10:00 – 10:30 am	***** Break *****	

Session III Solar Energy Conversion Materials
Chair: **Fred Wudl**, University of California Santa Barbara

10:30 – 11:00 am	Tobin Marks , Northwestern University <i>Materials Science of Electrodes and Interfaces for High-Performance Organic Photovoltaics</i>	254
11:00 – 11:30 am	Song Jin , University of Wisconsin-Madison <i>Fundamental Studies of Charge Transfer in Quantum-Confined Nanostructure Heterojunctions and Applications to Solar Energy Conversion</i>	222
11:30 – 12:00 pm	Cherie Kagan , University of Pennsylvania <i>Bi-Continuous Multi-Component Nanocrystal Superlattices for Solar Energy Conversion</i>	226
12:00 – 12:30 pm	Xiaoyang Zhu , University of Texas, Austin <i>Extracting Hot Carriers from Photo-Excited Semiconductor Nanocrystals</i>	327
12:30 – 2:00 pm	***** Working Lunch***** <i>Introduction of Poster Session 1 Presenters with Highlights</i> Michael Sennett , Program Manager, Materials Chemistry	
2:00 – 2:30 pm	Ramamoorthy Ramesh (Invited) , DOE <i>The DOE SunShot Initiative: Science and Technology to Enable Solar Electricity at Grid Parity</i>	339
2:30 – 2:45 pm	<i>Project Reporting Requirements and Delineation of Support</i> Michael Sennett , Program Manager, Materials Chemistry Program BES	

Session IV Tools and Techniques for Materials Characterization
Chair: **Geraldine Richmond**, University of Oregon

2:45 – 3:15 pm	Alex Pines , University of California, Berkeley/LBNL <i>Nuclear Magnetic Resonance</i>	53
3:15 – 3:45 pm	Harald Ade , North Carolina State University <i>Fundamental Science of High Open Circuit Voltage Excitonic Solar Cells</i>	107

3:45 – 4:15 pm	Kelly Gaffney (Invited) , Stanford National Accelerator Laboratory (SLAC) <i>Ultrafast X-ray Laser Studies of Electronic Excited State Dynamics in Model Photocatalytic Coordination Complexes</i> 337
4:15 – 5:30 pm	Small Group Discussions
5:30 – 7:00 pm	***** Working Dinner ***** <i>Scientific Highlights of the Day – Discussion and Input from Attendees</i> Michael Sennett , Program Manager, Materials Chemistry
7:00 – 10:00 pm	***** Poster Session 1 *****

Tuesday, July 17, 2012

7:00 – 8:00 am ***** Breakfast*****

Session V

Materials Relevant to Fuel Cells

Chair: **Vojislav Stamenkovic**, Argonne National Laboratory

8:00 – 8:30 am	Nenad Markovic , Argonne National Laboratory <i>Energy and Fuels from Multi-functional Electrochemical Interfaces</i> 36
8:30 – 9:00 am	Bryan Pivovar , National Renewable Energy Laboratory <i>Hydroxide Conductors for Energy Conversion Devices</i> 57
9:00 – 9:30 am	Ralph Nuzzo , University of Illinois, Urbana-Champaign <i>Cathode Catalysis in Hydrogen/Oxygen Fuel Cells: New Catalysts, Mechanism, and Characterization</i> 158
9:30 – 10:00 am	Allan Jacobson , University of Houston <i>Enhanced Mixed Electronic-Ionic Conductors through Cation Ordering</i> 214
10:00 – 10:30 am	*****Break*****

Session VI

Nanostructured Materials

Chair: **James Heath**, California Institute of Technology

10:30 – 11:00 am	Vladimir Tsukruk and Mostafa El-Sayed , Georgia Institute of Technology <i>Guided Assembly of Anisotropic Micro- and Nano-structures into Mesoscale Hierarchies of New Properties</i> 319
11:00 – 11:30 am	Adam Matzger , University of Michigan <i>Symmetry Breaking for the Synthesis of Nanostructured Porous Materials</i> 258
11:30 – 12:00 pm	Ting Xu , University of California, Berkeley <i>Self-Assembly of Organic/Inorganic Nanocomposites</i> 89
12:00 – 12:30 pm	Jennifer Hollingsworth , Los Alamos National Laboratory <i>"Giant" Nanocrystal Quantum Dots: Controlling Charge Recombination Processes for High-Efficiency Solid-State Lighting</i> 28

12:30 – 2:00 pm	***** Working Lunch***** <i>Introduction of Poster Session 2 Presenters with Highlights</i> Michael Sennett , Program Manager, Materials Chemistry	
2:00 – 2:30 pm	John Hemminger (Invited) , University of California, Irvine/BESAC <i>Quantum to the Continuum: Opportunities for Mesoscale Science</i>	338
Session VII Inorganic Materials		
	<u>Chair:</u> James Ibers , Northwestern University	
2:30 – 3:00 pm	Mercouri Kanatzidis , Northwestern University/Argonne National Laboratory <i>Rational Synthesis of Superconductors</i>	234
3:00 – 3:30 pm	John Corbett , Ames National Laboratory <i>Gold's Ability to Bridge Classes of Metal-Rich "Electron Compounds": From Polar Intermetallics to Hume-Rothery Phases and Quasicrystals</i>	49
3:30 – 4:00 pm	Danny Fredrickson , University of Wisconsin <i>Chemical Frustration: A Design Principle for the Discovery of New Complex Intermetallic and Alloy Phases</i>	154
4:00 – 5:30 pm	Small Group Discussions	
5:30 – 7:00 pm	***** Working Dinner ***** <i>Scientific Highlights of the Day – Discussion and Input from Attendees</i> Michael Sennett , Program Manager, Materials Chemistry	
7:00 – 10:00 pm	***** Poster Session 2 *****	

Wednesday, July 18, 2012

7:00 – 8:00 am	***** Breakfast *****	
Session VIII Materials Behavior at Surfaces and Interfaces		
	<u>Chair:</u> Gabor Somorjai , University of California Berkeley	
8:00 – 8:30 am	Miquel Salmeron , Lawrence Berkeley National Laboratory <i>Chemical and Mechanical Properties of Surfaces, Interfaces and Nanostructures: Subtask #1: Mechanical and Physical Properties</i>	61
8:30 – 9:00 am	Jacob Israelachvili , University of California, Santa Barbara <i>Relationships between the Adhesion, Friction and Nano/Micro-Structure of Materials, Surfaces and Films</i>	210
9:00 – 9:30 am	Charles Rosenblatt , Case Western Reserve University <i>Nanosopic Manipulation and Imaging of Liquid Crystals</i>	289
9:30 – 10:00 am	Mike Savina , Argonne National Laboratory <i>Directed Energy Interactions with Surfaces</i>	73
10:00 – 10:30 am	***** Break *****	

Session IX**Energy Storage Materials**

Chair: **Sheng Dai**, Oak Ridge National Laboratory

- 10:30 – 11:00 am **Arumgam Manthiram**, University of Texas, Austin
Materials and Interfacial Chemistry for Next Generation Electrical Energy Storage 166
- 11:00 – 11:30 am **Wesley Henderson**, North Carolina State University
Linking Ion Solvation and Lithium Battery Electrolyte Properties 202
- 11:30 – 12:00 pm **Amy Marschilok**, SUNY Stony Brook
Bimetallic Electrochemical Displacement Materials Yielding High Energy, High Power and Improved Reversibility 311
- 12:00 – 12:30pm *Remarks – Discussion of Meeting Highlights*
Geraldine Richmond and **Mercouri Kanatzidis**, Meeting Chairs
Michael Sennett, Program Manager, Materials Chemistry
- 12:30 – 1:30pm *****Working Lunch*****
Meeting Feedback – Questionnaire: Suggestions for Future Meetings
Michael Sennett, Program Manager, Materials Chemistry
(optional box lunches available)

Poster Session 1: Monday, July 16, 2012 7:00 – 10:00 pm

- 1a. Electronic and Magnetic Materials
- 1b. Solar Energy Conversion Materials
- 1c. Tools and Techniques for Materials Characterization
- 1d. Materials Relevant to Fuel Cells

Poster Session 2: Tuesday, July 17, 2012 7:00 – 10:00 pm

- 2a. Nanostructured Materials
- 2b. Inorganic Materials
- 2c. Materials Behavior at Surfaces and Interfaces
- 2d. Energy Storage Materials

Table of Contents

Table of Contents

Foreword	i
Agenda	v
Table of Contents	xiii
 Laboratory Projects	
<i>Physical Chemistry of Inorganic Nanostructures: Subtask 1: Physical Chemistry of Semiconductor Nanocrystals</i>	
A. Paul Alivisatos, Peidong Yang, and Stephen R. Leone	3
<i>Physical Chemistry of Inorganic Nanostructures: Subtask 2: Fundamentals of Semiconductor Nanowires</i>	
A. Paul Alivisatos, Peidong Yang, and Stephen R. Leone	7
<i>Physical Chemistry of Inorganic Nanostructures: Subtask 3: Microscopy Investigations of Nanostructured Materials</i>	
A. Paul Alivisatos, Peidong Yang, and Stephen R. Leone	11
<i>Physical Chemistry of Inorganic Nanostructures: Subtask 4: Model Photocatalytic Nanostructures</i>	
A. Paul Alivisatos, Peidong Yang, and Stephen R. Leone	15
<i>Nanostructured Carbon Materials</i>	
L. A. Curtiss, S. Vajda, P. Zapol, M. J. Pellin, and N. Markovic	19
<i>Materials and Interfacial Chemistry for Next Generation Electrical Energy Storage</i>	
S. Dai, M. P. Paranthaman, C. A. Bridges, R. R. Unocic, X. G. Sun, D.-E. Jiang, G. M. Veith, J. B. Goodenough, and A. Manthiram	24
<i>“Giant” Nanocrystal Quantum Dots: Controlling Charge Recombination Processes for High-Efficiency Solid-State Lighting</i>	
Jennifer A. Hollingsworth and Han Htoon	28
<i>¹²⁵Te NMR and Transport Properties of Complex Thermoelectric Tellurides</i>	
E. M. Levin and K. Schmidt-Rohr	32
<i>Energy and Fuels from Multi-functional Electrochemical Interfaces</i>	
Nenad M. Markovic and Vojislav R. Stamenkovic	36
<i>Energy and Fuels from Multi-functional Electrochemical Interfaces: Subtask: Electrocatalysis at Mesoscale</i>	
Nenad M. Markovic and Vojislav R. Stamenkovic	40

<i>Diamondoid Science and Applications</i> Nick Melosh, Thomas Devereaux, Hari Manoharan, Peter Scheiner, and Z. X. Shen	44
<i>Gold’s Ability to Bridge Classes of Metal-Rich “Electron Compounds”: From Polar Intermetallics to Hume-Rothery Phases and Quasicrystals</i> Gordon J. Miller, John D. Corbett, Qisheng Lin, and Srinivasa Thimmaiah	49
<i>Nuclear Magnetic Resonance</i> Alexander Pines	53
<i>Hydroxide Conductors for Energy Conversion Devices</i> Bryan Pivovar, Clay Macomber, Chai Engtrakul, Hai Long, Jim Boncella, and Joe Edson	57
<i>Chemical and Mechanical Properties of Surfaces, Interfaces, and Nanostructures: Subtask 1: Mechanical and Physical Properties</i> Miquel Salmeron, Gabor Somorjai, Peidong Yang	61
<i>Chemical and Mechanical Properties of Surfaces, Interfaces, and Nanostructures: Subtask 2: Surface Chemical Properties</i> Gabor A. Somorjai	65
<i>Chemical and Mechanical Properties of Surfaces, Interfaces and Nanostructures: Subtask 3: Synthesis and Assembly of Metal and Oxide Nanoparticles</i> Miquel Salmeron, Gabor Somorjai, and Peidong Yang	69
<i>Directed Energy Interactions with Surfaces</i> Michael Savina and Igor Veryovkin	73
<i>Solid-State NMR of Complex Materials</i> K. Schmidt-Rohr, M. Hong, and E. M. Levin	77
<i>Polymer-Based Multicomponent Materials</i> A. P. Sokolov, B. G. Sumpter, V. S. Urban, J. W. Mays, M. D. Dadmun, F. Bates, and K. Schweizer	81
<i>Polymer-Based Multicomponent Materials: Research on Multiblock Copolymer Systems</i> A. P. Sokolov, B. G. Sumpter, V. S. Urban, J. W. Mays, M. D. Dadmun, F. Bates, and K. Schweizer	85
<i>Self-Assembly of Organic/Inorganic Nanocomposites</i> Ting Xu, A. Paul Alivisatos, Tanja Cuk, Jean Fréchet, Yi Liu, Miquel Salmeron, and Lin-Wang Wang	89

<i>Self-Assembly of Organic/Inorganic Nanocomposite Materials: Subtask 1: Transport and Doping in Nanocrystal Solids with Electronically Active Organic Ligands</i> Ting Xu, A. Paul Alivisatos, Tanja Cuk, Yi Liu, J. Fréchet, Miquel Salmeron, and Lin-Wang Wang	93
<i>Self-Assembly of Organic/Inorganic Nanocomposite Materials: Subtask 2: Directed Hierarchical Assemblies of Nanocomposites</i> Ting Xu, A. Paul Alivisatos, Tanja Cuk, Yi Liu, J. Fréchet, Miquel Salmeron, and Lin-Wang Wang	97
<i>Self-Assembly of Organic/Inorganic Nanocomposite Materials: Subtask 3: Characterization</i> Ting Xu, A. Paul Alivisatos, Tanja Cuk, Yi Liu, J. Fréchet, Miquel Salmeron, and Lin-Wang Wang	101
 University Grant Projects	
<i>Fundamental Science of High Open Circuit Voltage Excitonic Solar Cells</i> H. Ade	107
<i>The Influence of Electrolyte Structure and Electrode Morphology on the Performance of Ionic-Liquid Based Supercapacitors: A Combined Experimental and Simulation Study</i> Dmitry Bedrov, Yury Gogotsi, Wesley Henderson, and Oleg Borodin	111
<i>Synthesis and Structured Characterization of Novel Intermetallic Clathrates—Prospective Materials for Thermoelectric Applications</i> Svilen Bobev	115
<i>Mitigating Breakdown in High Energy Density Perovskite Polymer Nanocomposite Capacitors</i> Richard L. Brutchey	119
<i>New Superconducting Materials</i> R. J. Cava	123
<i>The Synthesis, Structures and Chemical Properties of Macrocyclic Ligands Covalently Bonded into Layered Arrays</i> Abraham Clearfield and Donald T. Reed	127
<i>Tuning Sorption Properties of Metal-Organic Frameworks via Postsynthetic Covalent Modification</i> Seth M. Cohen	130
<i>Electronic and Ionic Conductors from Ordered Microporous Materials</i> Mircea Dincă	134

<i>Synthesis, Characterization and Properties of Nanoparticles of Intermetallic Compounds</i> Frank DiSalvo	137
<i>Rational Design and Nanoscale Integration of Multi-heterostructures as Highly Efficient Photocatalysts</i> Xiangfeng Duan	141
<i>Molecular Magnets Based on a Modular Approach: Investigation of Coupling, Anisotropy, and Electronic Factors on Bistability</i> Kim R. Dunbar	142
<i>Design and Synthesis of Chemically and Electronically Tunable Nanoporous Organic Polymers for Use in Hydrogen Storage Applications</i> Hani M. El-Kaderi	146
<i>Pore Space Engineering and Functionalization in Porous Metal-Organic Framework Materials</i> Pingyun Feng	150
<i>Chemical Frustration: A Design Principle for the Discovery of New Complex Intermetallic and Alloy Phases</i> Daniel C. Fredrickson	154
<i>Cathode Catalysis in Hydrogen/Oxygen Fuel Cells: New Catalysts, Mechanism, and Characterization</i> Andrew A. Gewirth, Paul J. A. Kenis, Ralph G. Nuzzo, and Thomas B. Rauchfuss	158
<i>Low Temperature Synthesis of Carbide-Derived–Carbons from Binary and Ternary Carbides in the Si-Ti-C System</i> Yury Gogotsi	162
<i>Materials and Interfacial Chemistry for Next Generation Electrical Energy Storage</i> J. B. Goodenough, A. Manthiram, S. Dai, M. Paranthaman, C. A. Bridges, R. R. Unocic, X. Sun, D. Jiang, and G. M. Veith	166
<i>Dynamic Supracolloidal Assemblies</i> Steve Granick	170
<i>Spectroscopic Studies of Materials for Electrochemical Energy Storage</i> Steven G. Greenbaum	174
<i>Solid State Electronic Structure and Properties of Neutral Carbon-Based Radicals</i> Robert C. Haddon	178

<i>Controlling Magnetic and Ferroelectric Order through Geometry-Synthesis, Ab Initio Theory, and Characterization of New Multi-ferroic Fluoride Materials</i> P. Shiv Halasyamani and Craig Fennie	182
<i>Crystallization-Driven Assembly of Conjugated-Polymer-Based Nanostructures</i> Ryan C. Hayward	187
<i>Surface Science at the Nanoscale</i> James R. Heath	190
<i>Charge Recombination, Transport Dynamics, and Interfacial Effects in Organic Solar Cells</i> Alan J. Heeger, Guillermo C. Bazan, Thuc-Quyen Nguyen, and Fred Wudl	194
<i>Optical Spectroscopy and Scanning Tunneling Microscopy Studies of Molecular Adsorbates and Anisotropic Ultrathin Films</i> John C. Hemminger	198
<i>Linking Ion Solvation and Lithium Battery Electrolyte Properties</i> Wesley Henderson	202
<i>Actinide Transition-Metal Chalcogenides and Pnictides</i> James A. Ibers and Lynda Soderholm	206
<i>Relationships between the Adhesion, Friction and Nano/Micro-Structure of Materials, Surfaces and Films</i> Jacob Israelachvili	210
<i>Enhanced Mixed Electronic-Ionic Conductors through Cation Ordering</i> Allan J. Jacobson, Dane Morgan, and Clare Grey	214
<i>Molecular and Nanoscale Engineering of High Efficiency Excitonic Solar Cells</i> Samson A. Jenekhe, Guozhong Cao, and David S. Ginger	218
<i>Fundamental Studies of Charge Transfer in Quantum-Confined Nanostructure Heterojunctions and Applications to Solar Energy Conversion</i> Song Jin, John C. Wright, and Robert J. Hamers	222
<i>Bi-Continuous Multi-Component Nanocrystal Superlattices for Solar Energy Conversion</i> Cherie R. Kagan, Christopher B. Murray, James M. Kikkawa, and Nader Engheta	226
<i>Chemistry and Properties of Complex Intermetallics from Metallic Fluxes</i> Mercouri G. Kanatzidis	230
<i>Rational Synthesis of Superconductors</i> Mercouri G. Kanatzidis	234

<i>Charging and Polarization of Organic Semiconductors in Energy-Efficient Circuits and Energy Capture Modules: Synthesis, Electronics, and Spectroscopy</i> Howard E. Katz, Andreas G. Andreou, and William L. Wilson	238
<i>Biaxiality in Thermotropic Bent-Core and Tetrapodic Nematic Liquid Crystals</i> Satyendra Kumar, Quan Li, Sam Sprunt, Alejandro Rey, and Mohan Srinivasarao	242
<i>Deterministic Assembly of Fluid and Solid Inks</i> Jennifer A. Lewis	246
<i>Functional Architectures for Light Capture and Utilization</i> Xiuling Li	250
<i>Materials Science of Electrodes and Interfaces for High-Performance Organic Photovoltaics</i> Tobin J. Marks, R. P. H. Chang, A. J. Freeman, T. O. Mason, and K. R. Poeppelmeier	254
<i>Symmetry Breaking for the Synthesis of Nanostructured Porous Materials</i> Adam J. Matzger and Antek G. Wong-Foy	258
<i>Synthesis of Molecule/Polymer-Based Magnetic Materials</i> Joel S. Miller	262
<i>Mechanistic Studies of Charge Injection from Metallic Electrodes into Organic Semiconductors Mediated by Ionic Functionalities</i> Thuc-Quyen Nguyen, Guillermo C. Bazan, and Alexander Mikhailovsky	266
<i>RAFT Polymerization of Emulsified Microemulsions</i> Jennifer O'Donnell	270
<i>Measuring the Importance of Valence to the Chemistry of Nanocrystal Surfaces</i> Jonathan S. Owen	274
<i>Basic Surface Chemistry and Physics of Carbon-Based Electronic Materials Modified by Silane Molecular Layers</i> Vitaly Podzorov	277
<i>Activation of Hydrogen under Ambient Conditions and Unusual Element Hydride Reactivity by Main Group Molecules</i> Philip P. Power	281
<i>Molecular Processes Underlying the Structure and Assembly of Thin Films and Nanoparticles at Complex Interfaces</i> Geraldine L. Richmond	285

<i>Nanoscopic Manipulation and Imaging of Liquid Crystals</i> Charles Rosenblatt	289
<i>Improved Electrical Energy Storage with Electrochemical Double Layer Capacitance Based on Novel Carbon Electrodes, New Electrolytes, and Thorough Development of a Strong Science Base</i> Rod Ruoff	293
<i>Interfacial Behavior of Polymers: Using Interfaces to Manipulate Polymers</i> T. P. Russell	297
<i>Dielectric Ceramics in Nanosheet Form</i> Tina T. Salguero	301
<i>Luminescence in Conjugated Molecular Materials under Sub-bandgap Excitation</i> Franky So	303
<i>Nanoscale Materials and Architectures for Energy Conversion</i> Mahendra K. Sunkara and Madhu Menon	307
<i>Bimetallic Electrochemical Displacement Materials Yielding High Energy, High Power and Improved Reversibility</i> Esther S. Takeuchi, Kenneth J. Takeuchi, and Amy C. Marschilok	311
<i>Solvation and Phase Behavior of Lithium Trifluoromethanesulfonate in Ethylene Carbonate, γ-Butyrolactone, or Propylene Carbonate</i> Paul C. Trulove, Christopher J. Worosz, Kurt Sweely, Matthew P. Foley, Wesley A. Henderson, Paul D. Boyle, and Daniel M. Seo	315
<i>Guided Assembly of Anisotropic Micro- and Nano-structures into Mesoscale Hierarchies of New Properties</i> Vladimir Tsukruk and Mostafa El-Sayed	319
<i>Optical and Magnetic Probes of Charge Dynamics in Organic Donor-Acceptor Bulk Heterojunction for Photovoltaic Applications</i> Z. Valy Vardeny	323
<i>Extracting Hot Carriers from Photo-Excited Semiconductor Nanocrystals</i> Xiaoyang Zhu	327
<i>Spectroscopy of Charge Carriers and Traps in Field-Doped Single Crystal Organic Semiconductors</i> Xiaoyang Zhu and C. Daniel Frisbie	331

Invited Talks

Ultrafast X-ray Laser Studies of Electronic Excited State Dynamics in Model Photocatalytic Coordination Complexes
Kelly J. Gaffney.....337

Quantum to the Continuum: Opportunities for Mesoscale Science
John C. Hemminger.....338

The DOE SunShot Initiative: Science and Technology to Enable Solar Electricity at Grid Parity
Ramamoorthy Ramesh.....339

Conjugated Polymer Semiconductors: Insights into Ordering at the Nano- through Macro-scales
Elsa Reichmanis.....340

Poster Sessions List.....342

Author Index.....350

Participant List.....352

***LABORATORY
PROJECTS***

Physical Chemistry of Inorganic Nanostructures

A. Paul Alivisatos, Peidong Yang, Stephen R. Leone

University of California, Lawrence Berkeley National Laboratory

Program Scope – Subtask 1: Physical Chemistry of Semiconductor Nanocrystals

Control of materials on the nanometer scale offers great opportunities to tailor the properties of energy conversion systems, yet the realization of these goals depends critically on improvements in our abilities to make complex nanostructures with precision. This program emphasizes the fundamental science of the synthesis of inorganic nanomaterials as well as the characterization of physical properties of these materials. The program consists of four subtasks: Physical Chemistry of Colloidal Nanocrystals, Fundamentals of Inorganic Nanowires, Microscopy Investigations of Nanostructured Materials, and Model Nanoscale Photo-catalytic Systems. The goal of the first subtask is to develop the science of colloidal inorganic nanocrystals with special emphasis on understanding and controlling their synthesis. Recent work has included highly specific synthesis of nanoheterostructures by cation exchange, post-synthesis improvement of luminescence efficiency, and synthesis of semiconductor nanostructures featuring tunable plasmon resonances. Another aspect of this first subtask is the investigation of fundamental optical, electrical, structural, and thermodynamic properties of nanocrystals. The Alivisatos lab has recently exploited novel in situ imaging techniques to achieve unprecedented structural information about nanocrystals and their growth in solution.

Recent Progress

1. High resolution nanocrystal imaging in solution using a graphene liquid cell. A major challenge in the study of nanocrystals is imaging their behavior and especially their growth in the solution phase. Previous work from our lab has succeeded in using transmission electron microscopy (TEM) to image nanocrystals in solution.[1] However, the resolution achieved using a microfabricated liquid cell was limited by the width of both the silicon nitride “window” layer and the liquid layer. The imaging conditions are further limited by leaking of liquid from the cell into the TEM vacuum chamber. We have recently achieved liquid phase images of unprecedented resolution by making use of a liquid cell based on two layers of graphene. Initial studies were conducted in the solid state, by drop casting nanocrystal solutions onto a layer of graphene and allowing the solvent to evaporate. A second layer of graphene was layered over the first, resulting in encapsulation of the nanocrystals.

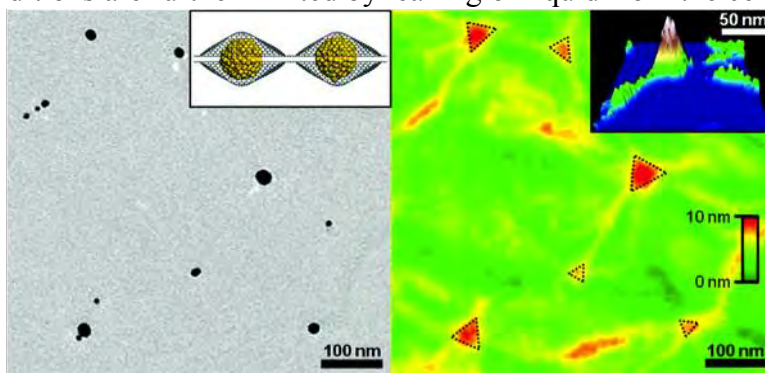


Figure 1. TEM (left) and AFM (right) images of nanocrystals trapped between two layers of graphene.

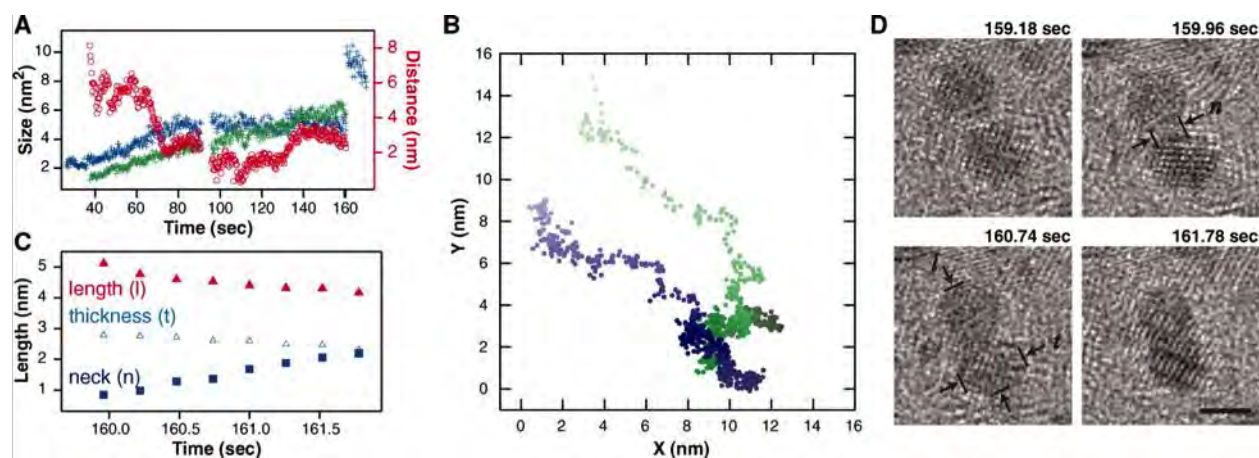


Figure 2. (a) Time course of the size evolution and distance between two Pt nanocrystals. (b) Position of the two nanocrystals over the time observed. (c) Plot of the total length, thickness, and neck diameter of the two nanocrystals during coalescence. (d) TEM images of the two nanocrystals.

In these proof-of-principle experiments we were able to image the nanocrystals using both TEM and atomic force microscopy (AFM) (Fig. 1).[2].

By adding the second graphene layer prior to drying of the solvent we were able to encapsulate ultra-thin layers of nanocrystal solution. These solution pockets were stable upon exposure of the cell to vacuum, and allow for ultra high resolution TEM imaging.[3] We were able to resolve lattice fringes and observe crystalline twinning in solution. More impressive, we were able to monitor nanocrystal growth and coalescence events in real time and to observe the specific facets involved in coalescence and the evolution of particle crystallinity after coalescence (Fig. 2). Figure 2C is a plot of the change in length (l , along the center-to-center direction), thickness (t , perpendicular to the length), and neck diameter (n) of the coalesced nanocrystals. Neck growth is accompanied by a decrease in l and t , which indicates that the atoms migrate to the neck region, presumably by surface diffusion. After coalescence, the nanocrystal gradually reorganizes, evolving truncated surfaces. Observations at this high level of detail promise to yield unprecedented information about the behavior of nanocrystals in solution.

2. Nanocrystal heterostructures by cation exchange. Rapid cation exchange reactions on nanocrystals have proven to be a highly versatile method for synthesis of otherwise inaccessible nanocrystal phases and morphologies.[4,5] The process has been shown to leave the anion lattice unaffected, thus opening up numerous routes to interesting heterostructures.[6] An exciting aspect of nanocrystal heterostructures is the potential for creating semiconductor heterojunctions within a single nanocrystal. This potential has been realized in studies of aligned CdS nanorods.[7] Rod alignment over large areas on a variety of substrates was demonstrated previously.[8] Given the uniform nature of the resulting film, it was deemed likely that cation exchange would proceed selectively from the top of the film, yielding an array of aligned nanorods each containing the same heterojunction. The anticipated affect was indeed observed: partial cation exchange from CdS to Cu₂S yielded a film with aligned rods made up of CdS near the bottom surface and Cu₂S facing solution (Fig. 3, right). The depth profile of the film was determined using Rutherford backscattering (RBS). Cation exchange could be driven to completion by addition of excess Cu^I. Subsequently, exchange of Cu₂S to PbS was demonstrated using an analogous procedure, with partial or complete exchange achieved by addition of an appropriate amount of Pb^{II}. These aligned films present a unique opportunity for electronic

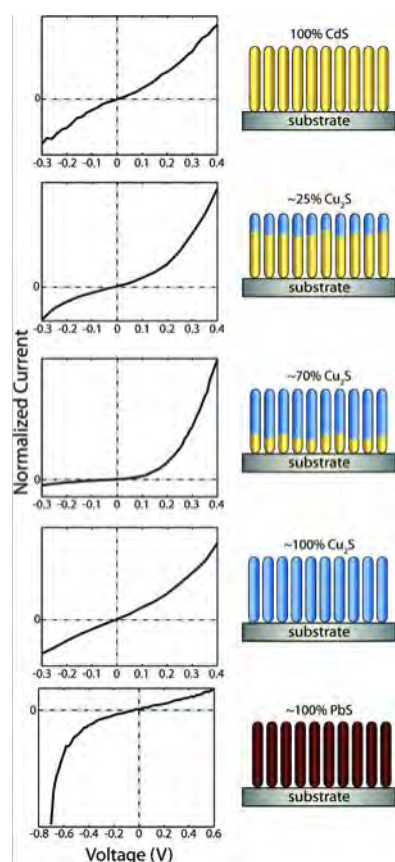


Figure 3. Voltage-current plots for aligned nanocrystal heterojunction devices.

characterization. One would expect a conventional thin film of these materials to display electronic rectification. Indeed, electrical measurements indicate that the films are rectified in exactly the expected way (Fig. 3, left). While these films are too thin to act as efficient absorber layers in solar cells, these experiments demonstrate the great promise of cation exchange in controlling both the structure and the properties of nanocrystals.

3. Tunable plasmon resonances in semiconductor nanocrystals. Localized surface plasmon resonances (LSPRs) typically arise in nanostructures of noble metals resulting in enhanced and geometrically tunable absorption and scattering resonances. LSPRs, however, are not limited to nanostructures of metals and can also be achieved in semiconductor nanocrystals with appreciable free carrier concentrations. We have demonstrated well-defined LSPRs arising from p-type carriers in vacancy-doped semiconductor nanocrystals.[9] Vacancies were introduced into Cu_2S nanocrystals by exposure to O_2 gas (ambient air), which induces formation of p-type Cu_{2-x}S . Concomitant with this reaction we observe the rise of an optical absorption peak in the near-infrared region. We confirm that this peak is due to an LSPR resonance by examining its position dependence on the refractive index of the nanocrystal solvent; a characteristic of plasmon resonance. By controlling the extent of reaction with O_2 we were able to tune the optical absorption wavelength of the LSPR. The capability to tune the

plasmon through doping is unique to semiconductor nanocrystals. This added degree of flexibility may introduce possibilities for application of these nanocrystals to sensing. These LSPRs are not only observed in the Cu_2S system. We recently showed that a known optical absorption in oxygen-deficient line phases of tungsten oxide, $\text{WO}_{3-\delta}$, is due to an LSPR.[10] As with Cu_2S , the position of the plasmon can be tuned by altering the degree of oxygen deficiency.

Future Plans

1. Cation exchange from II-V to III-V nanocrystals. III-V semiconductor nanocrystals such as InP, InAs, GaP, and GaAs have been vigorously sought due to their great potential for use in optoelectronic devices (LEDs, solar cells, etc.). However, high quality III-V colloidal nanocrystals remain synthetically challenging. Cation exchange is a promising method for generating monodisperse III-V nanocrystals. Standard colloidal synthetic strategies have recently been developed for II-V semiconductor systems such as Cd_3P_2 and Cd_3As_2 offering a monodisperse template for cation exchange. We are encouraged by preliminary results indicating efficient Cd^{II} to In^{III} exchange which preserves sample monodispersity. This strategy will provide facile access to a wide array of III-V materials of interest for optoelectronic applications.

2. Microfluidic liquid cell fabrication for imaging nanocrystal reactions in-situ. While the graphene liquid cell described above is a pivotal development in the effort to image nanocrystals in solution, it is also of great interest to images nanocrystals in dynamic solution conditions; a

goal for which a microfluidic liquid TEM cell would be an important tool. Using anisotropic etching methods it is possible to fabricate microfluidic silica or silicon nitride channels with extremely thin walls (~20-100 nm) with a channel diameter on the order of hundreds of nanometers. We have begun fabrication of this device and plan to use it to inspect nanocrystals as they undergo reaction such as cation exchange, metal tipping, growth and etching.

References

1. Zheng, H. *et al.* Observation of single colloidal platinum nanocrystal growth trajectories. *Science* **2009**, *324*, 1309-1312.
2. Yuk, J. *et al.* Graphene Veils and Sandwiches. *Nano Lett.* **2011**, *11*, 3290-3294.
3. Yuk, J. M. *et al.* High-Resolution EM of Colloidal Nanocrystal Growth Using Graphene Liquid Cells. *Science* **2012**, *336*, 61-64.
4. Son, D. H.; Wittenberg, J. S.; Alivisatos, A. P. Cation exchange reactions in ionic nanocrystals. *Science* **2004**, *306*, 1009-1012.
5. Luther, J. M.; Zheng, H. M.; Sadtler, B.; Alivisatos, A. P. Synthesis of PbS Nanorods and Other Ionic Nanocrystals of Complex Morphology by Sequential Cation Exchange Reactions. *J. Am. Chem. Soc.* **2009**, *131*, 16851-16857.
6. Jain, P. K.; Amirav, L.; Aloni, S.; Alivisatos, A. P. Nanoheterostructure Cation Exchange: Anionic Framework Conservation. *J. Am. Chem. Soc.* **2010**, *132*, 9997-9999.
7. Baker, J. L. *et al.* Device-Scale Perpendicular Alignment of Colloidal Nanorods. *Nano Lett.* **2010**, *10*, 195-201.
8. Rivest, J. B. *et al.* Assembled Monolayer Nanorod Heterojunctions. *ACS Nano* **2011**, *5*, 3811-3816.
9. Luther, J. M.; Jain, P. K.; Ewers, T.; Alivisatos, A. P. Localized surface plasmon resonances arising from free carriers in doped quantum dots. *Nature Materials* **2011**, *10*, 361-366.
10. Manthiram, K.; Alivisatos, A. P. Tunable Localized Surface Plasmon Resonances in Tungsten Oxide Nanocrystals *J. Am. Chem. Soc.* **2012**, *134*, 3995-3998.

Publications

1. Yuk, J. *et al.* Graphene Veils and Sandwiches. *Nano Lett.* **2011**, *11*, 3290-3294.
2. Yuk, J. M. *et al.* High-Resolution EM of Colloidal Nanocrystal Growth Using Graphene Liquid Cells. *Science* **2012**, *336*, 61-64.
3. Jain, P. K.; Amirav, L.; Aloni, S.; Alivisatos, A. P. Nanoheterostructure Cation Exchange: Anionic Framework Conservation. *J. Am. Chem. Soc.* **2010**, *132*, 9997-9999.
4. Rivest, J. B. *et al.* Assembled Monolayer Nanorod Heterojunctions. *ACS Nano* **2011**, *5*, 3811-3816.
5. Luther, J. M.; Jain, P. K.; Ewers, T.; Alivisatos, A. P. Localized surface plasmon resonances arising from free carriers in doped quantum dots. *Nature Materials* **2011**, *10*, 361-366.
6. Manthiram, K.; Alivisatos, A. P. Tunable Localized Surface Plasmon Resonances in Tungsten Oxide Nanocrystals *J. Am. Chem. Soc.* **2012**, *134*, 3995-3998.

Physical Chemistry of Inorganic Nanostructures

A. Paul Alivisatos, Peidong Yang, Stephen R. Leone
University of California, Lawrence Berkeley National Laboratory

Program Scope – Subtask 2: Fundamentals of Semiconductor Nanowires

Semiconductor nanowires have witnessed an explosion of interest in the last decade due to advances in synthesis and the unique thermal, optoelectronic, chemical, and mechanical properties of these materials. The potential applications of single-crystalline nanowires are truly impressive, including computational technology, communications, spectroscopic sensing, alternative energy, and the biological sciences. This subtask on “Fundamentals of Semiconductor Nanowires” can be considered as the fundamental research program with the aim of establishing and developing the core science and technology for semiconductor nanowires, and with an emphasis on growth, assembly and fundamental optical and electronic properties characterization.

Recent Progress

1. Cation exchange chemistry for nanowire heterostructure. The cation exchange reaction in nanostructures can be very different when compared to bulk solids. Work on colloidal nanocrystals in subtask 1 of this FWP illustrates how the reaction speed is much faster in nanostructures due to a larger surface to volume ratio, and therefore novel nanostructures could be produced¹⁻⁴. Subtask 2 is leveraging this experience to explore cation exchange in nanowires. We have shown that a Cu₂S-CdS core-shell nanowire can be produced by a short (~10s) cation exchange reaction in CuCl aqueous solution. The resulting Cu₂S shell is around 10 nm thick and coherently attached to CdS. By using a longer reaction time (>30s), the Cu⁺ continues to replace Cd²⁺ in CdS lattice. However, due to a high lattice mismatch between the core and shell, increasing the shell thickness is prohibited by high lattice strain. As shown in Figure 1b and 1c, instead of forming a thicker Cu₂S shell, periodic Cu₂S inclusion layers are observed inside the CdS nanowire. To further confirm the superlattice (SL) formation, the CdS was selectively etched with diluted HCl, and a hollow Cu₂S tube with inclusion layers was observed (Figure 1d).

It is well known that CdS-Cu₂S form a good type II junction which is useful for solar cell application. Photoluminescence (PL) spectra clearly demonstrated the fluorescence quenching due to effective charge separation in this heterostructured nanowire (Figure 2a). The CdS PL at ~510nm was completely suppressed and a broad weak emission centered ~590nm was observed, which may due to the charge recombination at the CdS - Cu₂S interface. The efficient charge separation is further supported by fluorescence lifetime measurements (Figure 2b), which clearly show that the decay becomes faster from Cu₂S inclusions. The cation exchange reaction provides a facile method for producing high

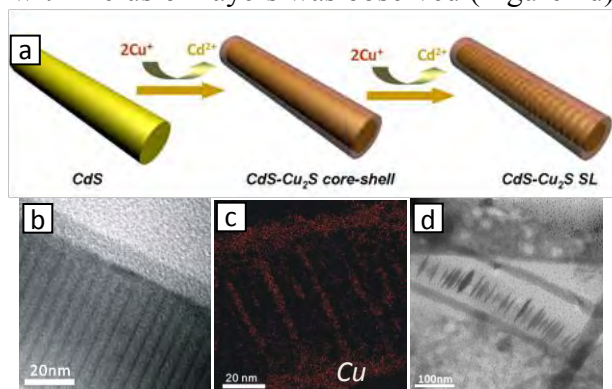


Figure 1. CdS to Cu₂S cation exchange reaction. a. schematic of nanowire cation exchange reaction. b. TEM image of as formed CdS-Cu₂S SL nanowire. c. EELS elemental mapping for Cu. d. TEM image of CdS-Cu₂S SL nanowire after selective CdS removal by diluted HCl.

quality heterojunctions and novel nanostructures. More experiments will be done to further understand the mechanism of superlattice formation, as well as the charge transport properties across the CdS-Cu₂S heterojunction. Also, cation exchange chemistry will be extended into other nanowire material systems to realize functions such as solar cells and light emitting diodes.

2. Conversion chemistry of oxide

nanowires: one atomic layer at a time. Alloys of zinc oxide (ZnO) with indium oxide and other trivalent metal oxides (IMZO, In_{2-x}M_xO₃(ZnO)_n, M=In, Ga, Fe) have been examined for potential applications in thermoelectric devices, low-indium transparent conducting oxides, and photoelectrochemical cells. Previously, we developed a new conversion scheme, by depositing metal onto ZnO nanowire arrays and annealing at high temperature, which allows for rational control of nanowire dimensions, density, orientation, and alloy concentration. At 300 K, InGaO₃(ZnO)_n nanowires (IGZO) exhibit a thermal conductivity of 3.3 W m⁻¹ K⁻¹, which is lower than what has been observed for IZO in the bulk (3.5 W m⁻¹ K⁻¹, n = 3,4) and ZnO nanowires (~20 W m⁻¹ K⁻¹) despite very low In and Ga loading. Improved visible light absorption and chemical stability were also observed for IZO and IFZO nanowires. High resolution TEM and STEM on the IZO and IFZO structures have provided great insight into the crystal structure of this family of compounds. The nanowire platform allowed us to easily image thin segments of IZO where the structure was only partially formed, showing that the basal InO₂⁻ layer begins at the nanowire surface and is bounded by a partial dislocation, as seen in Figure 3. These dislocations propagate into the nanowire by vacancy diffusion, and indium precipitates at the defects. In addition, modulating contrast forms between the basal layers, with an angle that depends on the composition of M. Our structural model has been confirmed by DFT calculations.

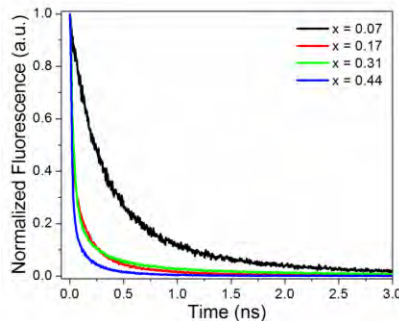


Figure 4. Fluorescence decay curves of different In_xGa_{1-x}N nanowire arrays.

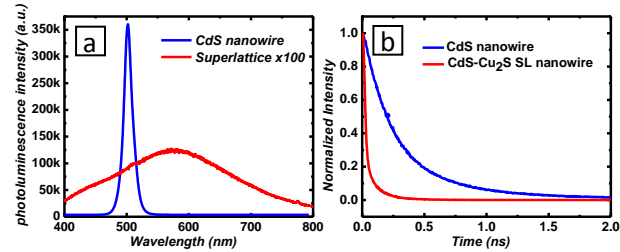


Figure 2. Photoluminescence spectra (a) and lifetime spectra (b) of a CdS-Cu₂S SL nanowire compared to a CdS nanowire.

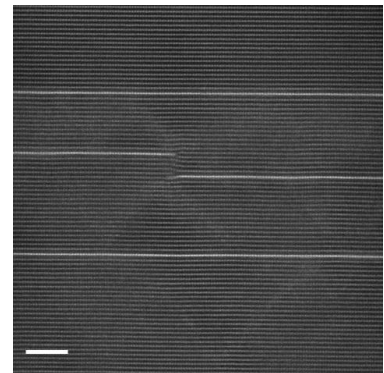


Figure 3. HRSTEM of an IFZO nanowire, showing two partial inclusions between two fully formed basal layers. Scale bar is 25 nm.

3. Growth and chemical modification of In_xGa_{1-x}N nanowires. Recently, there has been much interest in the InGaN ternary alloy due to its UV to IR bandgap tunability. However, the large thermodynamic miscibility gap (0.1 < x < 0.9) presents a significant challenge towards the synthesis of the majority of alloy compositions. Previously, we developed a method to produce single phase InGaN within the miscibility gap by using the nanowire geometry⁵. Although initial LED and photoanode testing proved to be successful, devices were limited by the poor internal quantum efficiency (QE) of InGaN nanowires. Therefore, time resolved fluorescence studies were used to examine the excited state decay of InGaN nanowires. Fluorescence lifetimes clearly decrease (Figure 4) with

increasing indium incorporation, most likely due to carrier localization from statistical fluctuations in composition. Due to the short fluorescence lifetimes and low QE, we conclude that InGaN nanowires have a large nonradiative decay rate.

Factors that could contribute to the fast nonradiative decay rate include increased surface recombination from the nanowire geometry, partial dislocations/point defects, and efficient Auger recombination pathways in InGaN. Therefore, we examined the effect of thermal treatments in NH_3 gas on these factors. Although no change in partial dislocations was observed by TEM, all compositions displayed increased photoluminescence intensities after annealing. Integrated PL intensities show (Figure 5A) the largest increase in QE for the highest indium compositions. Fluorescence lifetime measurements on annealed InGaN nanowires (Figure 5B) showed an order of magnitude decrease in lifetime when compared to as made samples. Therefore, we conclude that perturbations from thermal treatment increase the QE of InGaN nanowires by increasing the radiative rate rather than reducing the nonradiative rate. A similar treatment could be used for LEDs to maximize device performance. However, for applications which require carrier extraction, it will be necessary to reduce the nonradiative recombination rate. Surface passivation and growth modification will be done in conjunction with fluorescence lifetime measurements to observe the effect of these treatments on the nonradiative decay rate.

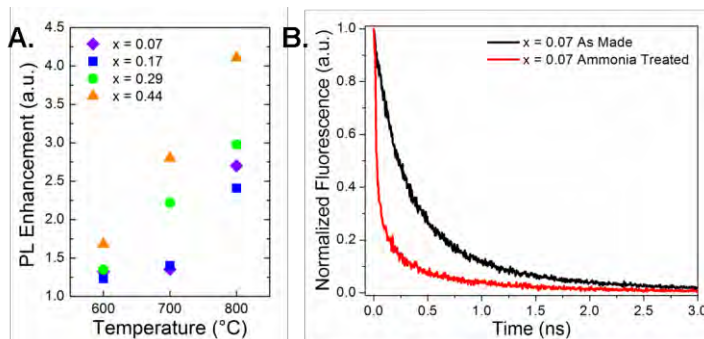


Figure 5. Integrated PL (a) peaks indicated annealing is increasing the quantum efficiency. A sharp decrease in fluorescence lifetime (b) was seen for annealed nanowires.

Future Plans

In close collaboration with the Alivisatos and Leone groups, we will continue to develop novel synthetic chemistry for semiconductor nanowires and their heterostructures. We will continue to systematically explore the optical and electrical properties of these novel semiconductor nanowires. In addition, a collection of optical and electrical characterization tools will be used to probe these nanostructures as function of synthetic conditions with high spatial resolution. This would include, for example, spatial resolved cathodoluminescence, scanning confocal optical imaging; single nanowire imaging and spectroscopy, temperature-dependent PL, quantum efficiency measurements with integrating sphere, ultrafast spectroscopy, X-ray absorption/emission spectroscopy, impedance spectroscopy and field-effect transistor measurement of carrier concentration and mobility.

As part of our continuing efforts on oxide nanowire research, we will pursue reproducible p-doping in ZnO nanowires. During ZnO nanowire growth, Li impurities can be introduced through an *in situ* CVT scheme. As-grown, these Li-doped wires exhibited decreased electrical properties as measured by single nanowire transconductance. However, on-device annealing at 500°C in O_2 converts the FET response of the same nanowire to p-type. Single nanowire Seebeck voltage measurements were performed to corroborate the majority carrier type switching. With confirmation of p-type conduction in ZnO nanowires, we hope to integrate these nanowires into ZnO homojunction light emitting diodes and solar cells. However, various storage conditions and

operating temperatures may change the electrical properties of the nanowires due to the relative instability of the Li acceptor state. By gathering fundamental information about the mechanism of majority type-conversion and subsequent reversion, chemical methods of surface and dopant passivation will be designed for long-term stability.

In addition, we will also expand our efforts into transition metal doped TiO₂ nanowires. TiO₂ is a unique material for photocatalysis since it is nontoxic, abundant, stable and photoactive. However, the wide bandgap of TiO₂ limits its photocatalytic performance in the visible part of the solar spectrum. Doping TiO₂ with transition metals can create localized electronic states within the TiO₂ bandgap, which can enhance the material's optical absorption. Our group has already developed a very simple molten salt flux method to synthesize transition metal doped TiO₂ nanowires in large scales. A variety of transition metals such as Cr, Co, Ni, Fe, Mn, Mo, Nb, Ta, W, V, Ru, Rh can be incorporated into the TiO₂ lattice to tune the nanowire optical, electrical and surface catalytic properties. Further work will be done using x-ray absorption spectroscopy (Subtask 3) to examine the local coordination environment of the incorporated transition metal elements, and correlate with their electrochemical or photoelectrochemical properties.

References

1. Luther, J. M.; Zheng, H.; Sadtler, B.; Alivisatos, A. P. *J. Am. Chem. Soc.* **2009**, *131*, 16851.
2. Park, J.; Zheng, H.; Jun, Y.-w.; Alivisatos, A. P. *J. Am. Chem. Soc.* **2009**, *131*, 13943.
3. Robinson, R. D. *et al. Science* **2007**, *317*, 355.
4. Sadtler, B.; Demchenko, D. O.; Zheng, H.; Hughes, S. M.; Merkle, M. G.; Dahmen, U.; Wang, L.-W.; Alivisatos, A. P. *J. Am. Chem. Soc.* **2009**, *131*, 5285.
5. Kuykendall, T.; Ulrich, P.; Aloni, S.; Yang, P. *Nat. Mat.* **2007**, *6*, 951.

Publications

1. "Solution processed core-shell nanowires for efficient photovoltaic cells", J. Tang, Z. Huo, S. Britzman, P. Yang, *Nature Nanotech.*, *6*, 568, 2011.
2. "Atomic-Level Control of the Thermoelectric Properties in Polytypoid Nanowires", S. C. Andrews, M. A. Fardy, M. C. Moore, S. Aloni, M. Zhang, V. Radmilovic, P. Yang, *Chem. Sci.*, *2*, 706, 2011.
3. "Epitaxial growth of InGaN nanowire arrays for light emitting diodes", C. Hahn, Z. Zhang, A. Fu, C. H. Wu, Y. J. Hwang, D. J. Gargas, P. Yang, *ACS Nano*, *5*, 3970, 2011.
4. "Si/InGaN Core/Shell Hierarchical Nanowire Arrays and their Photoelectrochemical Properties", Y. J. Hwang, C. H. Wu, C. Hahn, H. E. Jeong, P. Yang, *Nano Lett.*, *12*, 1678, 2012.
5. "Nanowire-based Single Cell Endoscopy", R. Yan, J. Park, Y. Choi, C. Heo, S. Yang, L. P. Lee, P. Yang, *Nature Nanotech.*, *7*, 191, 2012.
6. "High Quantum Efficiency of Band-Edge Emission from ZnO Nanowires", D. Gargas, H. Gao, P. Yang, *Nano Lett.* *11*, 3792, 2011.
7. "Semiconductor Nanowires: What's Next?", P. Yang, M. Fardy, R. Yan, *Nano Lett.* *10*, 1529, 2010.
8. "Semiconductor nanowires for energy application", A. Hochbaum, P. Yang, *Chem. Rev. (Invited Review)*, *110*, 527, 2010.

Physical Chemistry of Inorganic Nanostructures

A. Paul Alivisatos, Peidong Yang, Stephen R. Leone

University of California, Lawrence Berkeley National Laboratory

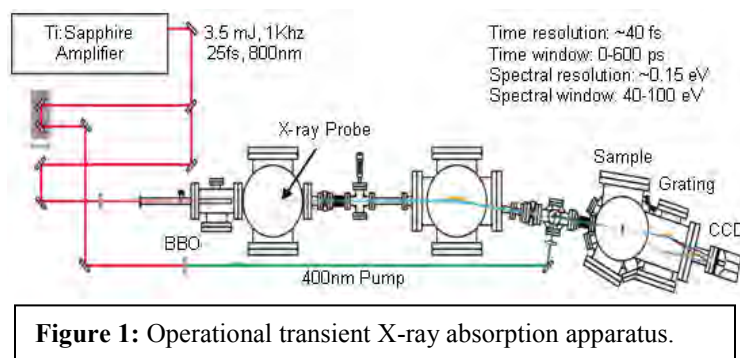
Program Scope - Subtask 3: Microscopy Investigations of Nanostructured Materials

The goal of the third subtask in this program is to develop and use novel spectroscopic techniques to obtain a detailed understanding of charge carrier dynamics in nanostructured materials. This work is organized along two lines of inquiry: ultrafast x-ray transient absorption of excited-state dynamics in semiconductors and single-particle studies of quantum dot blinking and surface plasmon resonances. A tabletop x-ray transient absorption system combines the elemental and oxidation state specificity of x-ray absorption with the femtosecond time resolution of Ti:Sapphire laser amplifiers. This allows the determination of the rates of energy and charge transfer in multicomponent nanostructures. Single molecule fluorescence microscopy and time-resolved spectroscopy are applied to study the fluorescence intermittency, or blinking, of single semiconducting nanostructures. The research seeks to uncover the physical processes that lead to this blinking, focusing on the role of charge carriers. In addition, blinking is a sensitive probe of the interactions between single nanostructures and their environment, such as quantum dots embedded in polymer and inorganic matrices relevant to solar energy conversion. Finally, far-field scattering measurements are combined with near-field imaging to investigate the impact of nanostructure shape and environment on localized surface plasmon resonances (LSPRs).

Recent Progress

1. Transient X-ray Absorption of Semiconductors

Transient absorption spectroscopy in the visible and infrared regions is commonly used to probe the excited-state dynamics of nanomaterials. However, as nanostructures become more complex, the broad and often overlapping spectral features make it difficult to differentiate between competing relaxation mechanisms. X-ray absorption, on the other hand, can map the conduction band density of states with element- and oxidation-state specificity. This level of detail is essential for determining the photophysics of multicomponent nanostructures such as the nanowire superlattices in Subtask 2 and the seeded/cation-exchanged rods in Subtasks 1 and 4. A new instrument has been developed that creates tens-of-fs pulses of extreme ultraviolet/soft x-ray light from high-harmonic generation by an intense 800 nm laser pulse (Figure 1). The spectral range of the system, from 40 to 100 eV, is ideal for studying the shallow-core to valence absorption



of transition metals and II-VI or III-V semiconductors. For example, the $\text{Se}_{3d \rightarrow 3p}$ and $\text{Te}_{4d \rightarrow 4p}$ resonances at 55 and 41 eV, respectively, are well separated and will provide a direct probe of hole localization in core/shell CdSe/CdTe Type-II quantum dots. The instrument was used to determine the excited-state electronic structure of $\alpha\text{-Fe}_2\text{O}_3$ (hematite), an earth-abundant

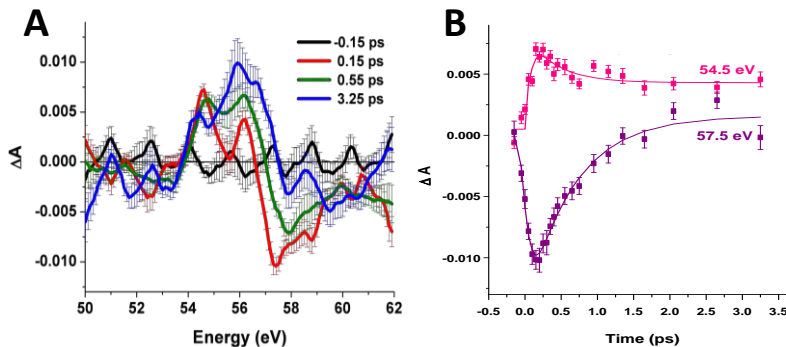


Figure 2: (a) Excited-state x-ray absorption of $\alpha\text{-Fe}_2\text{O}_3$ after excitation at 400 nm. (b) Kinetic traces at 54.5 and 57.5 eV

photocatalyst for water splitting prepared by Subtask 2. Photoexcitation of the sample at 400 nm causes the growth of an x-ray absorption feature consistent with a ligand-to-metal charge transfer (LMCT) state ($\text{O}^{2-}\text{Fe}^{3+} \rightarrow \text{O}^1\text{Fe}^{2+}$). Some theory suggests a d-d transition at this excitation energy⁵, which is not observed here. The transient signal rises in <200 fs and changes shape on a sub-picosecond timescale as the LMCT state relaxes to a d-d excitation, highlighting the ability of this technique to probe ultrafast changes in electronic structure.

2. Single-Particle Studies

Previous work in this subtask suggested that rate fluctuations of the charge trapping process play an important role in QD blinking.¹ Current work focuses on the role of these fluctuations and how they relate to distributed kinetics and memory effects in blinking events. A strong correlation is observed between on-state memory and distributed blinking kinetics, suggesting that both originate from the same fluctuation-based blinking mechanism. Monte-Carlo simulations show that introducing an ionization-induced charge trapping process causes a decrease in the on-state memory and less distributed blinking kinetics. These simulations reproduce the experimental data, suggesting that the combined effect of two charge trapping processes (one fluctuation-based and one ionization-based) are responsible for fluorescence blinking of a single QD.

Blinking is also used as a probe of the nanoparticle-environment interaction. Previous work in this subtask revealed surprising differences in the trap state distribution for QDs in two polymer hosts: the semiconducting N,N'-diphenyl-N,N'-bis(3-methylphenyl)-(1,1'-biphenyl)-4,4'-diamine (TPD) and the insulating poly(methylmethacrylate) (PMMA).² Current work extends these studies by investigating excitation-intensity dependent behavior. As with QDs on other conducting surfaces, the fluorescence decay time and quantum yield is reduced in TPD. However, in contrast to QDs in insulating and other conducting environments, QDs in TPD exhibit an increase in the probability of long on durations with an increase in power density (Figure 3a). This trend could be indicative of facile transfer of holes to the QDs from the TPD valence band.³

In coordination with Subtask 1, fluorescence blinking statistics are used as a probe of the interaction between CdSe/CdS QDs and a new class of chalcogenidometalate (ChaM) ligands, specifically $\text{Sn}_2\text{S}_6^{4-}$ or $\text{In}_2\text{Se}_4^{2-}$. These ChaM-QD systems are of interest because of the enhanced carrier mobilities reported for films of ChaM-capped QDs, which were attributed to favorable energy alignment between the QD and ChaM band structures, as well as the small inter-QD

spacing within the films. The single nanoparticle studies currently under way focus on the interaction between the individual QD and ChaM complexes. Preliminary results suggest photoexcitation leads to hole trapping on the ChaM ligand complex. The ChaM-capped QDs are largely non-fluorescent, spending only 11% of the measurement time in the on-state, compared to 82% time in the on-state of organically capped QDs (Figure 3b). Additionally an increase in the charge trapping rate occurs with decreasing CdS shell thickness.

Previous work in this subtask on the localized surface plasmon resonance of rod-in-ring gold nanostructures showed that conductive coupling between the rod and ring leads to sharp quadrupolar and octupolar resonances.⁴ Current work focuses on the effect of the underlying substrate on the LSPR. A 2 nm titanium layer between the nanostructure and the glass substrate increases the plasmon dephasing rate, drastically reduces the plasmon amplitude, and red-shifts the resonance peak. This effect can be reasonably well simulated by finite-difference time domain calculations, which use the bulk dielectric constants of Au and Ti to model the nanostructure. However, the observed redshift is greater than expected due to interface reactions and intermetallic diffusion. Titanium is often used as an adhesion layer in electron-beam lithography, and this damping effect reduces the usefulness of LSPRs for sensing applications. Vapor-deposited (3-mercaptopropyl) trimethoxysilane performs well as an adhesion layer without damping the sharp plasmon resonances.

Future Plans

1. Transient X-ray Absorption of Semiconductors. Ultrafast x-ray absorption will be used to probe the excited-state dynamics of semiconductor thin films and multi-component nanostructures. The absorption spectrum of the photocatalyst Co_3O_4 is composed of several distinct features attributed to metal-to-metal charge transfer between Co^{2+} and Co^{3+} ions, as well as LMCT transitions from O^{2-} to $\text{Co}^{2+/3+}$. Specific transitions will be excited using a tunable pump pulse and both the initial excited state electronic structure and the rate of relaxation through the ladder of excited states will be observed. The elemental specificity of x-ray absorption will be employed to measure charge separation in Type-II heterostructures such as PbSe quantum dots embedded in a Sb_2S_3 thin film. This material, synthesized by Subtask 1, is a promising candidate for all-inorganic photovoltaic devices. By measuring the rate of charge transfer between the PbSe and Sb_2S_3 as a function of QD size and excitation wavelength, processes such as hot electron injection and multiple-exciton generation will be investigated. Transient x-ray absorption of transition metal doped TiO_2 nanowires (Subtask 2) will reveal the rate of electron and/or hole localization on the dopant after photoexcitation and enable the engineering of nanowires with long-lived charge separated states necessary for photocatalysis.

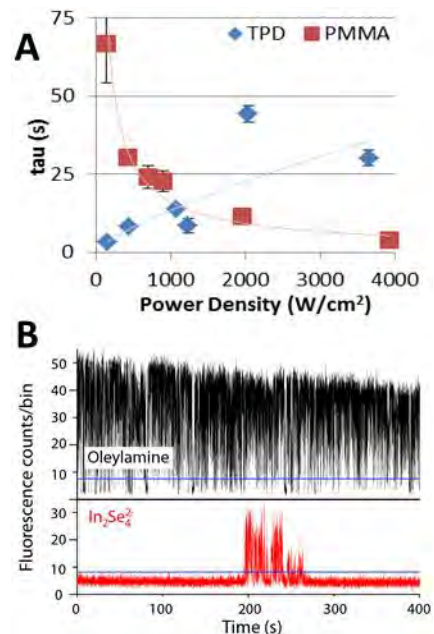


Figure 3: (a) Crossover time τ vs. excitation power density for QDs in PMMA and TPD. (b) Fluorescence blinking traces for single oleylamine and $\text{In}_2\text{Se}_4^{2-}$ -capped CdSe/CdS QDs

2. Single-Particle Studies. Future work in this subtask aims to uncover the mechanism for charge trapping rate fluctuations occurring during the off state.¹ The source of these fluctuations may correlate with the nature of the surface ligand coverage. It has been shown theoretically that some ligand molecules are highly mobile, able to randomly walk across the surface of a quantum dot altering the trap state energy levels.⁶ Future work will monitor the trapping rate fluctuations and blinking statistics of QDs with various capping ligand mobilities. In addition to ligand mobility, ligand-QD binding types are also considered.⁷ QDs with both covalent and dative ligand binding will be measured. The ligand exchange procedures necessary for this work will be done in collaboration with Subtask 1. Electric-field poling of QDs in TPD will also be investigated to elucidate the details of current-density enhancement in composite photovoltaic devices.⁸ A modification of surface trap states via nanoscale charge migration would modify the blinking statistics of an individual QD, whereas macroscale rearrangement of permanent dipoles in the semiconductor host would alter the polarization of its emission.

Based on the observation of the dramatic effect of a thin Ti underlayer on the LSPR of gold nanostructures, this line of inquiry will be extended to other substrates of interest. Specifically, far-field scattering and near-field microscopy will be used to study the coupling of π electrons in few-layer graphene to the LSPRs of gold disks. The band structure of graphene is sensitive to both the number of layers and an applied gate voltage,⁹ and the interplay of the optical response and electronic structure of the graphene with the LSPRs will serve as a sensitive probe of the coupling between the two components.

References

- (1) Cordones, A. A.; Bixby, T. J.; Leone, S. R. *Nano Lett.* **2011**, *11*, 3366.
- (2) Bixby, T. J.; Cordones, A. A.; Leone, S. R. *Chem. Phys. Lett.* **2012**, *521*, 7.
- (3) Jin, S.; Song, N.; Lian, T. *ACS Nano* **2010**, *4*, 1545.
- (4) Habteyes, T. G.; Dhuey, S.; Cabrini, S.; Schuck, P. J.; Leone, S. R. *Nano Lett.* **2011**, *11*, 1819
- (5) Liao, P. L.; Carter, E. A. *J. Phys. Chem. C* **2011**, *115*, 20795.
- (6) Voznyy, O. *J. Phys. Chem. C* **2011**, *115*, 15927.
- (7) Chon, B. et al.; *Phys. Chem. Chem. Phys.* **2010**, *12*, 9312.
- (8) Kumari, K.; Chand, S.; Vankar, V. D.; Kumar, V. *Appl. Phys. Lett.* **2009**, *94*, 213503.
- (9) Mak, K. F.; Sfeir, M. Y.; Misewich, J. A.; Heinz, T. F. *PNAS.* **2010**, *107*, 14999.

Publications

1. A. A. Cordones, T. J. Bixby, and S. R. Leone, *Evidence for multiple trapping mechanisms in single CdSe/ZnS quantum dots from fluorescence intermittency measurements over a wide range of excitation intensities*, *J. Phys. Chem. C* **115**, 6341 (2011).
2. A. A. Cordones, T. J. Bixby, and S.R. Leone, *Direct measurement of off-state trapping rate fluctuations in single quantum dot fluorescence*, *Nano Lett.* **11**, 3366 (2011).
3. T. G. Habteyes; S. Dhuey; S. Cabrini; P. J. Schuck; S. R. Leone, *Theta-Shaped Plasmonic Nanostructures: Bringing "Dark" Multipole Plasmon Resonances into Action via Conductive and Capacitive Coupling*, *Nano Lett.* **11**, 1819–1825 (2011).
4. T. J. Bixby, A. A. Cordones, and S. R. Leone, *CdSe/ZnS quantum dot intermittency in the semiconducting polymer N,N'-diphenyl-N,N'-bis(3-methylphenyl)-(1,1'-biphenyl)-4,4'-diamine (TPD)*, *Chem. Phys. Lett.* **521**, 7 (2012).

Physical Chemistry of Inorganic Nanostructures

A. Paul Alivisatos, Peidong Yang, Stephen R. Leone
University of California, Lawrence Berkeley National Laboratory

Program Scope – Subtask 4: Model Photocatalytic Nanostructures

In this newly established sub-task, we will use the latest advances in nanomaterials fabrication from subtask 1 to construct model nanoscale systems that can be used to separately investigate individual key underlying issues in artificial photosynthesis. In a complete first generation artificial photosynthetic system, the disparate functions of light absorption, charge separation, photo-voltage generation, and electrochemical water-splitting catalysis must be combined within a single nanostructured construct.^{1,2} We propose to deploy the most recent advances in the synthesis of colloidal nanostructures to enable the well defined assembly of semiconductor, oxide, metallic, and molecular components, specifically designed to test and develop our knowledge of each of these fundamental processes that underpin efficient artificial photosynthesis.³ The overarching goal of this work will be to create model systems designed to probe and answer long-standing basic questions in artificial photosynthesis. One goal for instance will be to specifically create a system to overcome photo-oxidation of a compound semiconductor light absorber, by creating a rapid alternative productive pathway for hole consumption, through systematic adjustment of the physical, quantum, and chemical parameters of the system. Work in this subtask will be tightly integrated with subtask 1 as well as subtask 3.

Recent Progress

Observations of photocatalysis from single seeded quantum rod systems. We have exploited nanoscale semiconductor systems as light absorbers with extremely high luminescence quantum yields before any catalysts are attached to them to perform what we believe are the first single particle studies of nanoscale semiconductor photocatalysts. We use a hydrogen evolving nanorod heterostructure photocatalyst⁴ composed of a platinum-tipped cadmium sulfide rod with an embedded cadmium selenide seed (illustrated in Figure 1). This interesting model system offers a systematic way of both manipulating and probing charge carriers within the photocatalyst, providing a useful system to better understand the underlying photophysical and photochemical phenomena. In such structures holes are three-dimensionally confined to the cadmium selenide (fast hole localization in the seed), whereas the delocalized electrons are generally transferred to the metal tip (with an estimated lifetime of 1 ps). Consequently, the electrons are now separated from the holes over three different components, and by a tunable physical length. Electron transfer to the Pt results in strong photoluminescence quenching. The quenching of the photoluminescence by the metal tip is not complete however, and occasionally the electron hole pair will recombine radiatively. Due to the exceptionally strong original quantum yield of the non-tipped seeded rods, this residual photoluminescence is sufficient for monitoring, and may be utilized as an internal inverse probe of catalytic activity. Using far-field optical microscopy we explore the fluence-dependent photoluminescence from photo-catalysts on the single particle level. We find that individual catalysts exhibit strong optical nonlinearities that allow direct determination of the number of charges participating in a catalytic reaction and the rate of photo-

induced charge transfer. These studies enable new approaches to examining rate limiting kinetics, through studies in which the luminescence is probed as a function of the incident photon flux.

Future Plans

(1) *Structure*: We will design novel multicomponent nano-heterostructures that draw upon the synthetic advances from subtask 1. Emphasis will be placed on diversity in (1) the atomic composition of each component, (2) nanocrystal shape and faceting, and (3) the arrangement and interconnectivity of each component. Compositional control will be achieved using cation/anion exchange strategies pioneered in our research group. Recent work of this nature is described in sub-task 1. Shape control will be achieved by making use of standard anisotropic growth techniques wherein preferential ligation of surfactant molecules to particular crystal facets during the synthesis to affords directional growth.^{5,6} Control over the interconnectivity of each

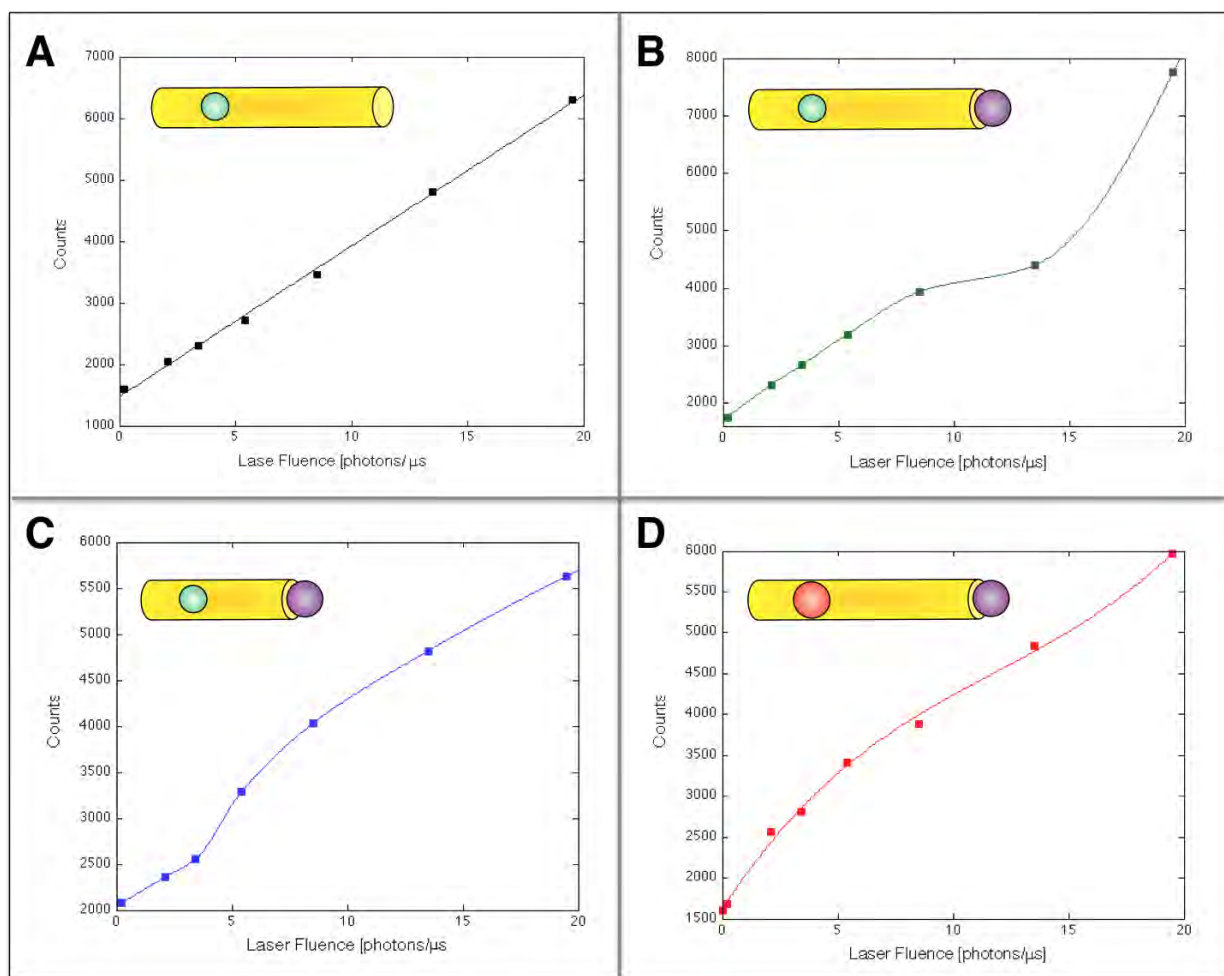


Figure 1. Characteristic fluence-dependent photoluminescence obtained in gaseous argon from a few dozen of individual photocatalysts consisting of (A) colloidal CdSe quantum dot embedded asymmetrically within a CdS quantum rod; (B) with reduction Pt catalyst placed on the opposite end of the rod. (C) The quantum dot size is held fixed, and the rod length decreases from 60 nm to 40 nm. (D) The rod length is held constant, and the dot diameter is increased from 2.3 nm to 3.9 nm.

component will be achieved using seeded growth methods, which furnish heterostructures wherein the components lie in intimate contact and can be induced to grow preferentially on specific facets of an anisotropic seed structure, as in the structures discussed in Figure 1. Finally, ligand exchange reactions on the heterostructures and individual components will be used to impart water solubility and to display molecular functionality, including charge transfer relays and molecular catalysts, at the nanocrystal-solution interface.

(2) *Energetics*: Exciton dissociation and charge carrier migration in colloidal nano-heterostructures occur along electrochemical potential gradients. As such, a fundamental objective of the proposed work is to measure the energetic landscape across the composite nanostructures we synthesize. In addition to measuring the band edge potentials of the semiconducting components we will determine the potential of zero charge and charging energies of the metallic catalytic components as well as the redox potentials of molecular surface moieties. Additionally, the proposed work will distinguish itself from contemporary reports by striving to operate photocatalytic reactions under conditions of well-defined overall driving force using *reversible* electron and hole scavengers. In this fashion, we will be able to draw rigorous correlations between the energy storage efficiency and quantum efficiency of each water splitting half reaction.

(3) *Kinetics*: The kinetic competition between productive fuel-forming and unproductive recombination pathways defines the quantum efficiency of solar energy storage via artificial photosynthesis. In order to determine the quantum-yield-limiting competition steps, we will isolate the rate constants of each charge transfer step (semiconductor to catalyst, catalyst to solution) at the ensemble level using both steady state (quantum yield) and time resolved (transient absorption, transient fluorescence) techniques. As nanocrystal systems are invariably characterized by particle-to-particle inhomogeneity, the kinetics of fuel formation at nano-heterostructures will be characterized at the single particle, single turnover level using model turn-on fluorescent molecular probes. For these studies, aspects of both static and dynamic disorder will be determined for each system.

References

-
- (1) Cook, T. R. *et al.* “Solar Energy Supply and Storage for the Legacy and Non-legacy Worlds” *Chem. Rev.* **2010**, *110*, 6474–6502.
 - (2) Walter, M. G. *et al.* “Solar Water Splitting Cells” *Chem. Rev.* **2010**, *110*, 6446–6473.
 - (3) Mokari, T. “Synthesis and characterization of hybrid nanostructures” *Nano Reviews* **2011**, *2*, 5983.
 - (4) Amirav, L. and Alivisatos, A. P. “Photocatalytic Hydrogen Production with Tunable Nanorod Heterostructures” *J. Phys. Chem. Lett.* **2010**, *1*, 1051.
 - (5) Manna, L.; Scher, E. C.; Alivisatos, A. P. “Synthesis of soluble and processable rod-, arrow-, teardrop-, and tetrapod-shaped CdSe nanocrystals” *J. Am. Chem. Soc.* **2000**, *122*, 12700-12706.
 - (6) Manna, L.; Scher, E. C.; Alivisatos, A. P. “Shape control of colloidal semiconductor nanocrystals” *J. Clust. Sci.* **2002**, *13*, 521-532.

Publications

-
1. Amirav, L.; Alivisatos, A. P. "Photocatalytic Hydrogen Production with Tunable Nanorod Heterostructures" *J. Phys. Chem. Lett.* **2010**, *1*, 1051.

Nanostructured Carbon Materials

L. A. Curtiss (PI), S. Vajda, P. Zapol, M. J. Pellin, N. Markovic

Program Scope

The Nanostructured Carbon Materials Program focuses on new frontiers in nanocarbon-based materials with capability to make and break specific bonds under electrochemical conditions for the next generation of energy storage and production systems. The new form of diamond referred to as ultrananocrystalline diamond (UNCD) discovered in this program has many unique properties due to combining sp^3 diamond grains with sp^2 -like carbon grain boundaries in one material. Among the unique properties of UNCD is its large electrochemical window, electrochemically inert surface, and increased n-type conductivity via doping that makes it very attractive as an electrode material. These properties make it ideal to develop as a support for small metal and metal oxide clusters that we have recently shown to be highly active and selective for catalytic reactions. We have unique capabilities to synthesize ultrasmall clusters of specific size and composition. This program uses *in situ* characterization and computational capabilities to both understand the electrocatalytic properties of the new nanocarbon composites as well as to perform screening to help choose optimal candidate clusters for catalysis to be integrated with the nanocarbon supports. Fundamental understanding of the properties of the UNCD/cluster hybrids has important implications for energy applications such as in the production of fuels by reduction of CO_2 and new energy storage materials. We are exploring the effects of supports other than carbon to assess their effect and we are using principles from other types of catalysis such as heterogeneous catalysis to understand the reactions mechanisms.

Recent progress

During the past year we have focused on understanding the stability of clusters on UNCD and assessing the electrocatalytic properties of these new materials for water oxidation. We have also initiated investigations of other supports for comparison with the UNCD results. Finally, computations are being carried out in support of the above experiments, as well exploratory studies on lithium oxide clusters and CO_2 electroreduction. Some of the highlights of this work are given below.

Stability of Co clusters on UNCD. The composition and stability of oxidized cobalt subnanometer clusters composed of four metal atoms supported on ultrananocrystalline diamond (UNCD) and alumina surfaces were studied using a combination of grazing-incidence X-ray absorption near-edge spectroscopy (GIXANES), grazing incidence small angle X-ray scattering (GISAXS) and density functional calculations. GIXANES data revealed partially oxidized subnanometer cobalt clusters upon exposure to air, with similarity in the total degree of oxidation on both supports. The clusters were exposed to elevated temperatures of up to 300 °C and were found by GISAXS to be agglomeration resistant as shown in [Figure 1](#). DFT calculations of cluster binding to model surfaces for UNCD indicate that the stability of the cobalt oxide clusters

on UNCD is the result of electrostatic and dispersive interactions for the pristine hydrogen-terminated surfaces and covalent bonding between the cluster and defect sites on the surfaces. On alumina the origin of the stability is interactions between the cobalt and surface oxygens or the cluster oxygen with the surface aluminum atoms. These properties indicate that oxidized subnanometer cobalt clusters supported on UNCD and alumina are suitable candidates hybrid nanostructures for use as supported catalysts.

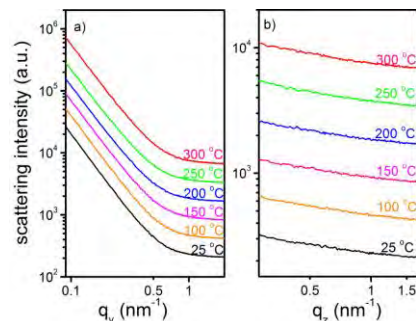


Figure 1. Horizontal (a) and vertical (b) cuts of the GISAXS images of UNCD-supported $\text{Co}_{4+/-1}$ clusters as function of temperature.

Electrocatalysis results for water oxidation. Tests of various size clusters supported on a carbon-base support, ultrananocrystalline diamond (UNCD) were performed under harsh conditions of water splitting, with pH reaching 14 and potentials up to 1.8 V. Figure 2 shows the results of these tests. The current densities shown refer to the current from the clusters only, after subtracting the contribution of the bare (i.e. cluster-free) support. The current density measured on the blank support reached around 0.16 mA/cm^2 at 1.8 V. The calculated per second and active site (cluster) turnover of elementary charges is on the order of 10^{+2} , which is much higher than turn-over rates reported for heterogeneous electrocatalyst to date. Results from repeated cycles hint towards a promising stable cluster-diamond hybrid material for use under electrocatalytic conditions. While clusters of sizes #1 and #2 exhibit very high activity, the current density of sample #3 drops below the current measured on the blank support under identical conditions. We hypothesize that the negative current is caused by Size #3 clusters blocking the active sites in the support. If this assumption correct, it opens an avenue to 1) selectively block unwanted reactive sites/defects in the support which would otherwise cause a deterioration of the support material and 2) use these strongly bond clusters as anchors for other active particles deposited in subsequent step(s). An analysis of the *ex situ* X-ray data obtained during the last month beam time is under progress, to provide information on what (if any) permanent changes may have taken place in the composition or morphology of the clusters or support. Based on several test cycles, which did not indicate a degradation of performance of this cluster/support combination, we assume that this system did not undergo considerable change under the applied harsh conditions.

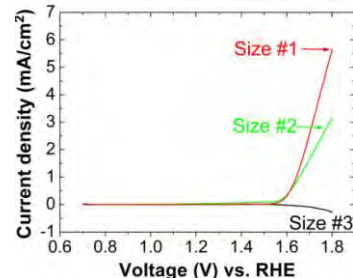


Figure 2. Water splitting (oxygen evolution reaction, OER) at pH 14, on metal clusters of three sizes. (Background corrected data, after the subtraction of the current measured on identical blank support without clusters)

Support studies. In order to better understand and improve the electrocatalysis of precious metal and oxide clusters made of more abundant metals, we have begun to examine the role of the support, by examining other support materials. In this regard, for example, Fe_2O_3 is an intriguing counterpoint to UNCD as a support layer. Hematite has some catalytic activity for water oxidation and has also attracted considerable attention as a photocatalyst for this reaction. Like

UNCD, hematite shows unique stability under the harsh electrode conditions necessary for electrocatalysis and is a very promising material for electrochemical water oxidation. Like n-type UNCD, hematite is also conductive over short distances (<10 nm). It also takes advantage of more recent atomic layer deposition (ALD) synthetic work that produces high growth rates and a highly conformal, pinhole free electrode support layer only a few nanometers thick. A recent paper, using a 20 nm thick Si-modified hematite, reported considerably increased current densities in OER. [1] Preliminary tests in our lab, with the addition of well defined size-selected clusters on a ~3ML hematite film show a dramatic increase in turnover rates, of up to two orders of magnitude on a deposited metal atom basis over the reported Si-modified hematite. While the results are preliminary, it is already clear that this combination of support and catalyst is quite interesting and is likely to be among the most active for this reaction.

Computational materials design First-principles calculations have been carried out to evaluate four metal atom clusters that will be of potential interest in CO₂ reduction. It is widely believed that the rate limiting step in CO₂ reduction is transfer of the first electron to the CO₂ molecule. Results were obtained for adsorption of CO₂ molecule on a series of metal clusters. We have investigated both linear and bent configurations of CO₂ on the clusters. As shown in Figure 3, Co₄ and Ni₄ clusters have bent adsorbed CO₂ molecules with significant binding to the cluster and electron transfer, which suggests that they are good candidates for CO₂ activation. The Cu₄ and Pt₄ clusters also produce a bent configuration as the most stable adsorbed CO₂ structure. On the other hand, Ir₄, Pd₄ and Au₄ exhibit preference for linear configuration, without charge transfer, and a small binding energy. Based on this study, we have focused on Co₄ clusters. In the presence of O₂ molecules, Co₄ gets oxidized easily with a

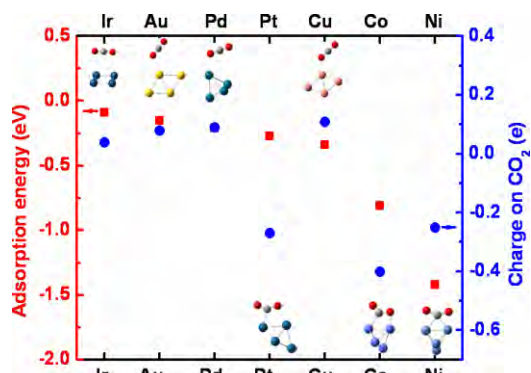


Figure 3. Calculated adsorption energies and charges for CO₂ on M₄ clusters.

spontaneous O₂ dissociation. We have evaluated reactions of Co clusters containing up to 6 O atoms with CO₂. The bare Co₄ cluster has the strongest binding to CO₂. The most stable configuration of CO₂ on CO₄ results from dissociation to CO and O with an energy gain of 1.87 eV, as compared to the sum of energies of individual systems. A Co₄O₂ cluster can still dissociate CO₂, but with a lower binding strength 1.56 eV as compared to the bare Co₄ cluster. The non-dissociative adsorption has a much smaller binding energy, although there are barriers to dissociation in each case. Dissociation of CO₂ on a Co₄O₄ cluster is unfavorable and instead forms a carbonate-like configuration. To make connection of DFT calculations to electrocatalysis involving CO₂ reduction as well as water oxidation we will use a formalism that has been successfully applied to electrocatalytic reactions on metal surfaces with aqueous electrolytes in previous studies, e.g. [2]. This will result in electrode potentials required for different steps along the pathway.

Future Plans

Experimental investigation of size and support effects will be carried out on clusters of various metals and oxides with the goal to understand these effects on electrocatalytic reactions and relationship to other types of catalysis. The knowledge will be used to screen for new composite materials in a close feedback-loop with predictions from theory. This will allow us to exploit the electrocatalytic properties of multi-component clusters and optimized support compositions.

Computational studies will be continued on the CO₂ electroreduction and expanded to include water oxidation on pertinent clusters and supports. In both cases once we have developed mechanistic understanding, we will perform calculations with different cluster sizes and compositions to establish trends in electrocatalytic activity, correlate with experimental results, and screen for optimal clusters.

References

- [1.] Jun, K.; Lee, Y. S.; Buonassisi, T.; Jacobson, J. M. *Angewandte Chemie-International Edition* **2012**, *51*, 423
- [2.] J. K. Nørskov, J. Rossmeisl, A. Logadottir, L. Lindqvist, J. R. Kitchin, T. Bligaard and H. Jo'ansson, *J. Phys. Chem. B* **2004**, *108*, 17886-17892

Publications (last two years)

"Assessment of Gaussian-4 theory for energy barriers", L. A. Curtiss, P. C. Redfern, and K. Raghavachari, *Chemical Physics Letters* **499**, 168 (2010).

"Bulk and surface thermal stability of ultra nanocrystalline diamond films with 10-30 nm grain size prepared by chemical vapor deposition", S. Michaelson, A. Stacey, J. Orwa, A. Cimmino, S. Praver, B. C. C. Cowie, O. A. Williams, D. M. Gruen, and A. Hoffman, *Journal of Applied Physics* **107** (9), 7 (2010).

"Gn Theory", L. A. Curtiss, P. C. Redfern, and K. Raghavachari, *WIRES* **1** 810 (2011).

"Carbon nanotunnels formed from single-walled carbon nanotubes interacting with a diamond (100)-(2 X 1) surface," D. A. Horner, M. Sternberg, P. Zapol, L. A. Curtiss, *Diam. and Rel. Mater.* **20**, 1103 (2011).

"Effect of Al and B Substitution on the Electronic Structure and Thermoelectric Properties of Silicon Carbide Nanoparticles", P. C. Redfern, D. M. Gruen, Curtiss L. A., Bruno. P., Routbort J., and Singh D., *Nanoscience and Nanotechnology Letters* **3**, 1 (2011).

"Simultaneous Measurement of X-ray Small Angle Scattering, Absorption, and Reactivity: A Continuous Flow Catalysis Reactor", S. Lee, B. Lee, S. Seifert, S. Vajda and R. E. Winans *Nucl. Instr. and Meth. A*, **649**. 200-203 (2011).

"Suppression of Sintering of Size-Selected Pd Clusters under Realistic Reaction Conditions for Catalysis", F. Yin, S. Lee, A. Abdela, S. Vajda, and R. E. Palmer, *J. Chem. Phys* **134**, 141101-1-4 (2011).

“Cleavage of the C-O-C bond on Size-Selected Subnanometer Cobalt Catalysts and on ALD-Cobalt Coated Nanoporous Membranes”, W. Deng, S. Lee, J. A. Libera, J. W. Elam, S. Vajda, and C. L. Marshall, *Appl. Catal. A: General* **393**, 29-35 (2011).

“Increased Stability Toward Oxygen Reduction Products for Lithium-Air Batteries with Oligoether-Functionalized Silane Electrolytes”, Z. Zhang, J. Lu, R.S. Assary, P. Du, H.-H. Wang, Y.-K. Sun, Y. Qin, K.C. Lau, J. Greeley, P.C. Redfern, H. Iddir, L.A. Curtiss, K. Amine, *J. Phys. Chem. C*, **115**, 25535-25542, 2011.

“Size-Dependent Selectivity and Activity of Silver Nanoclusters in the Partial Oxidation of Propylene to Propylene Oxide and Acrolein: A Joint Experimental and Theoretical Study”, L. M. Molina, S. Lee, K. Sell, G. Barcaro, A. Fortunelli, B. Lee, S. Seifert, R. E. Winans, J. W. Elam, M. J. Pellin, I. Barke, A. Kleibert, V. von Oeynhausen, Y. Lei, R. J. Meyer, J. A. Alonso, A. Fraile-Rodríguez, S. Giorgio, C. R. Henry, K.-H. Meiwes-Broer and S. Vajda, *Catal. Today* **160**, 116-130 (2011). *Invited Article*

J. Russell, P. Zapol, P. Král, L. A. Curtiss, Methane bond activation by Pt and Pd subnanometer clusters supported on graphene and carbon nanotubes, *Chem. Phys. Lett.* **536** (2012) 9–13

“Exploring Computational Design of Size-Specific Subnanometer Clusters Catalysts” G. A. Ferguson, F. Mehmood, R. Rankin, J. P. Greeley, S. Vajda, and L. A. Curtiss, *Top. Catal.* **55**, p. 353-365 (2012), *invited article*

“Physical Fabrication of Nanostructured Heterogeneous Catalysts”, C. Yin, E. Tyo and S. Vajda Chapter 3 in “*Heterogeneous Catalysis at the Nanoscale for Energy Applications*”, Eds. F. Tao, W. Schneider, and P. Kamat, Wiley-VCH, *invited chapter, in Press* (2012)

“A First-Principle Theoretical Approach to Heterogeneous Nanocatalysis”, F. R. Negreiros, E. Aprà, G. Barcaro, L. Sementa, S. Vajda, and A. Fortunelli, *Nanoscale* **4**, 1208-1219 (2012).

“Oxidative Dehydrogenation of Cyclohexene on Size Selected Subnanometer Cobalt Clusters: Improved Catalytic Performance via Evolution of Cluster-Assembled Nanostructures”, S. Lee, M. Di Vece, B. Lee, S. Seifert, R. E. Winans and S. Vajda, *Phys. Chem. Chem. Phys.*, *invited paper, Advance Article on-line, DOI: 10.1039/c2cp40162b* (2012)

“Theoretical Studies of UNCD Properties” S. Adiga, P. Zapol, and L. A. Curtiss, Invited Chapter for Book on Ultrananocrystalline Diamond, Edited by O. Shenderova and D. Gruen, in press.

“Support-Dependent Performance of Size-Selected Subnanometer Cobalt Cluster-Based Catalysts in the Dehydrogenation of Cyclohexene”, S. Lee, M. Di Vece, B. Lee, S. Seifert, R. E. Winans and S. Vajda, *Chem. Cat. Chem.*, *invited paper, submitted*

“Stable Subnanometer Cobalt Oxide Clusters on Ultrananocrystalline Diamond and Alumina Supports: Oxidation State and the Origin of Sintering-Resistance”, G. A. Ferguson, C. Yin, G. Kwon, S. Lee, J. P. Greeley, P. Zapol, B. Lee, S. Seifert, R. E. Winans, and S. Vajda*, and L. A. Curtiss*, *J. Phys. Chem. C*, *submitted*

“CO oxidation by subnanometer Ag_xAu_{3-x} supported clusters via DFT simulations”, F. R. Negreiros, L. Sementa, G. Barcaro, S. Vajda, E. Aprà, and A. Fortunelli, *submitted*

Materials and Interfacial Chemistry for Next Generation Electrical Energy Storage

S. Dai, M. P. Paranthaman, C. A. Bridges, R. R. Unocic, X. G. Sun, D.-E. Jiang,
G. M. Veith - Oak Ridge National Laboratory, Oak Ridge, TN 37831
J. B. Goodenough, A. Manthiram – The University of Texas at Austin, Austin, TX 78712

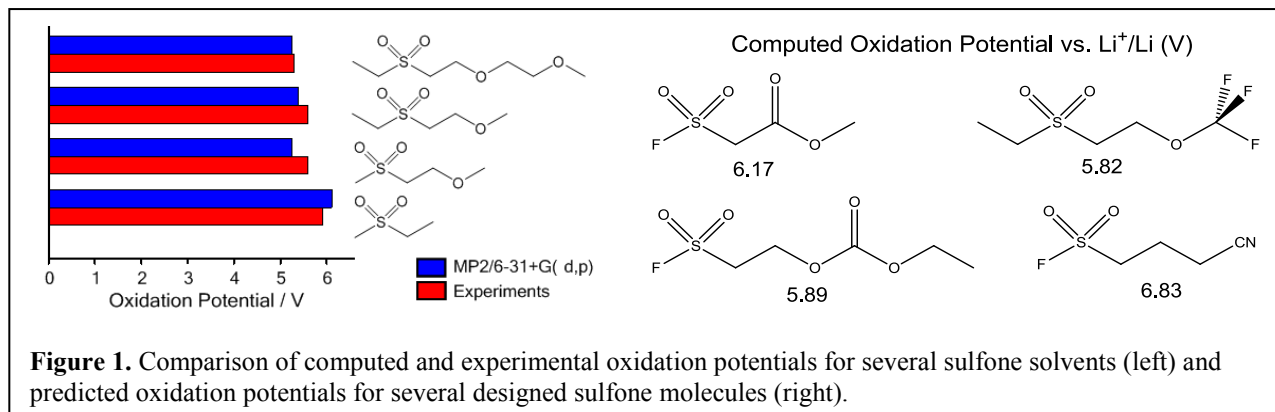
Program Scope

The overarching goal is to *investigate fundamental principles governing energy storage through integrated synthesis and advanced characterization*. Our current research is focused on fundamental investigation of electrolytes based on ionic liquids and rational synthesis of novel electrode architectures through Fermi level engineering of anode and cathode redox levels by employing porous structures and surface modifications as well as advanced operando characterization techniques including neutron diffraction and scattering. The key scientific question concerns the relationship between chemical structures and their energy-storage efficacies.

Recent Progress

Rational Synthesis of Ionic-Liquid Electrolytes

Sulfone-based electrolytes are promising for the development of high-voltage based lithium-ion batteries as electrolytes with electrochemical windows greater than 5 V. We computed the electrochemical windows for experimentally tested sulfone electrolytes by different levels of theory in combination with various solvation models (as shown in Fig. 1). The MP2 method



combined with the polarizable continuum model is shown to be the most accurate method to predict oxidation potentials of sulfone-based electrolytes with mean deviation less than 0.29 V.

Ionic liquids have many advantages such as non-volatility, high thermal stability, non-flammability, wide electrochemical window (>5.0V), and also very flexible in structure design. Our primary goal is first understand the basic relationship between structure and properties of ionic liquids, in order to design new ionic liquids with improved compatibility with graphite anode for application in lithium ion batteries. Thus, five room temperature ionic liquids (**1–5**) based on C-2 substituted imidazolium cations and

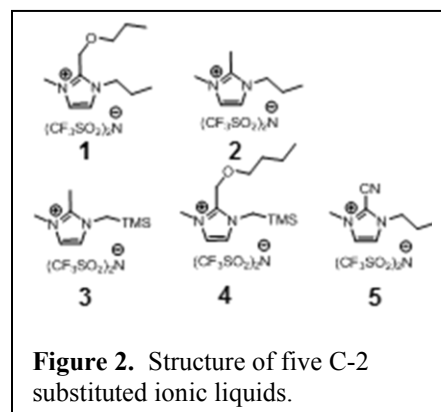


Figure 2. Structure of five C-2 substituted ionic liquids.

bis(trifluoromethanesulfonyl)imide (TFSI) anion were synthesized and their physiochemical properties were systematically investigated and the results will be presented in detail (Fig.2).

Mesoporous Electrode Architectures

Research on anode materials is to design new architectures and seek new anode materials with capacity well beyond graphite's 372 mAh/g. ORNL mesoporous carbon-MWNT composite exhibits a capacity of 120 mAh/g at 20C whereas the capacity of graphite drops to nearly zero (as shown in Fig. 3). The enhanced rate capability coupled with the advantages of soft-templating approach to prepare MC-MWNTs nanocomposites make these materials ideal candidate electrodes in Lithium ion batteries. We have also designed and synthesized TiO₂ with novel architecture, which combines the features of the TiO₂-B polymorph with mesoporous structure and microsphere morphology. Mesoporous TiO₂-B spheres show superior rate performance with 165 mAh/g at 10 cycles, 130 mAh/g at 30 cycles and 115 mAh/g at 60 cycles (as shown in Fig. 4).

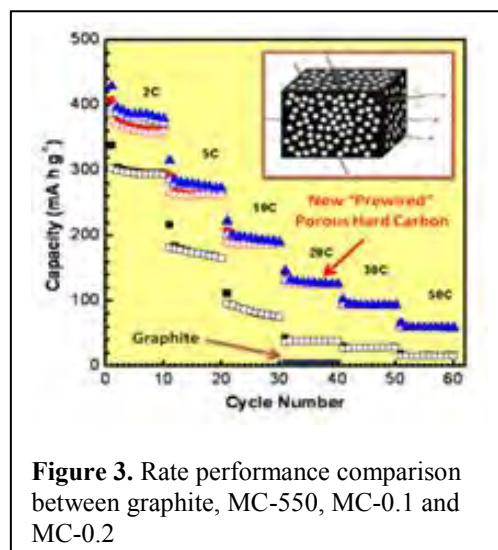


Figure 3. Rate performance comparison between graphite, MC-550, MC-0.1 and MC-0.2

Fluorinated Mesoporous Carbons

High surface area mesoporous graphitic carbons were fluorinated using pure F₂ at temperatures below 235 °C forming carbon fluorides (CF_x; x = 0.18-0.75). X-ray photoelectron spectroscopy results showed an increase in specific capacity with the increase in sp³ type carbon in the sample due to the formation of more reactive sites for Li storage. In addition, the median potential of the samples, versus lithium increased from 2.2V to 3.2V by increasing the concentration of C-C bonds. The increase in C-C bonds resulted in increased electron conduction through the sample thus reducing the materials overpotential.

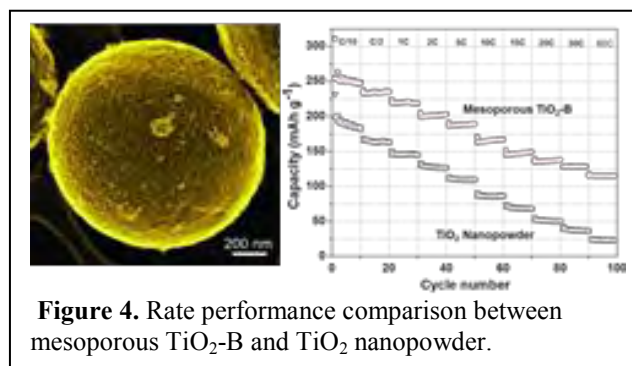


Figure 4. Rate performance comparison between mesoporous TiO₂-B and TiO₂ nanopowder.

SEI Observation via In Situ SANS

A novel approach based on small angle neutron scattering (SANS) enables the observation of electrochemical processes during the cycling of high capacity lithium ion batteries. Better understanding of processes such as solid-electrolyte interphase (SEI) formation have been of great interest to overcome performance limitations of batteries for vehicle and grid applications. Changes in neutron scattering intensity associated with mesopore ordering show the processes of SEI formation and lithium intercalation (see Fig. 5). Using a lithium-ion half-cell and different solvent deuteration levels, these results demonstrate that SANS can be employed to better understand complicated electrochemical processes occurring in rechargeable batteries.

Cation Ordering and Surface-Segregation in High-voltage Spinel Cathodes via Neutron Diffraction

Neutron diffraction has been used as part of a collaborative effort between UT-Austin and ORNL to better understand the atomic structure of the high-voltage doped spinel oxides $\text{LiMn}_{1.5}\text{Ni}_{0.5-x}\text{M}_x\text{O}_4$ ($\text{M} = \text{Cr, Fe, and Ga}$; $0 \leq x \leq 0.08$). Spinel synthesized at $900\text{ }^\circ\text{C}$ have been investigated systematically before and after post-annealing at $700\text{ }^\circ\text{C}$. Neutron diffraction studies reveal that the cation-ordered domain size tends to increase on annealing at $700\text{ }^\circ\text{C}$. Time-of-flight secondary-ion mass spectroscopy (TOF-SIMS) data reveal that the dopant cations $\text{M} = \text{Cr, Fe, and Ga}$ segregate preferentially to the surface. The doping with Cr and Fe stabilizes the structure with a significant disordering of the cations in the $16d$ sites even after post-annealing at $700\text{ }^\circ\text{C}$, resulting in high rate-capability due to low charge-transfer resistance and polarization loss.

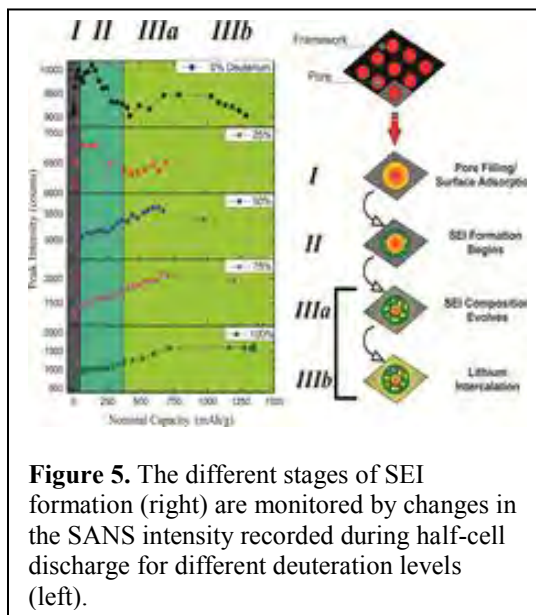


Figure 5. The different stages of SEI formation (right) are monitored by changes in the SANS intensity recorded during half-cell discharge for different deuteration levels (left).

Future Plans

- Explore the transport of lithium ions in novel ionic-liquid electrolytes through classical molecular dynamics simulations.
- Further understand the structure-property relationship of ionic liquids and design new ionic liquids with good SEI formation ability to be compatibility with graphite.
- Understanding the limiting factors in rate performance of anode and cathode materials and design novel electrode materials with enhanced rate capability.
- Further explore the understanding gained from small angle neutron scattering (SANS) on the electrochemical processes occurring at the surface and in the bulk of both anode and cathode electrode materials
- Continue to work with UT-Austin to develop a more comprehensive picture of next-generation electrode and electrolyte materials being investigated as a part of this project
- Experiment on model systems to better understand the effects of surface modification on surface chemistry and cycle stability in high voltage electrode materials
- Explore the synthesis of Na-intercalation batteries and understand how the surface reactivity of these materials changes in comparison with their Li analogs.

Publications

1. Shao, N.; Sun, X.-G.; Dai, S.; Jiang, D. E. Oxidation Potentials of Functionalized Sulfone Solvents for High-Voltage Li-Ion Batteries: A Computational Study. *J. Phys. Chem. B* **2012**, *116*, 3235-3238
2. Shao, N.; Sun, X.-G.; Dai, S.; Jiang, D. E. Electrochemical Windows of Sulfone-Based Electrolytes for High-Voltage Li-Ion Batteries. *J. Phys. Chem. B* **2011**, *115*, 12120-12125
3. C. Liao, N. Shao, K. S. Han, X. G. Sun, D. E. Jiang, E. W. Hagaman, S. Dai, Physicochemical Properties of Imidazolium-derived Ionic Liquids with Different C-2 Substitutions, *Physical Chemistry Chemical Physics* **2011**, *13*, 21503.

4. C. Liao, X. Zhu, X. G. Sun, S. Dai, Investigation of carbon-2 substituted imidazoles and their corresponding ionic liquids, *Tetrahedron Letters*, **2011**, 52, 5308-5310.
5. Griffin, P., Agapov, A. L., Kisliuk, A., Sun, X. G., Dai, S., Novikov, V. N., and Sokolov, A. P. Decoupling charge transport from the structural dynamics in room temperature ionic liquids. *J. Chem. Phys.* **2011**, 135.
6. B. K. Guo, X.Q. Wang, P.F. Fulvio, M.F. Chi, S.M. Mahurin, X.G. Sun, S. Dai, S, "Soft-Templated Mesoporous Carbon-Carbon Nanotube Composites for High Performance Lithium-ion Batteries," *Adv. Mater.*, **2011**, 23, 4661.
7. P. F. Fulvio, S. S. Brown, J. Adcock, R.T. Mayes, B.K. Guo, X.G. Sun, S.M. Mahurin, G.M. Veith, S. Dai, "Low-Temperature Fluorination of Soft-Templated Mesoporous Carbons for a High-Power Lithium/Carbon Fluoride Battery," *Chem. Mater.*, **2011**, 23, 4420-4427.
8. Guo, B.; M. Chi; X.G. Sun; S. Dai, Mesoporous carbon-Cr₂O₃ composite as an anode material for lithium ion batteries, *J. Power Sources*, **2012**, 205, 495-499.
9. Liu, H.; Z. Bi; X-G. Sun; R. R. Unocic; M. P. Paranthaman; S. Dai, and G.M. Brown, "Mesoporous TiO₂-B Microspheres with Superior Rate Performance for Lithium Ion Batteries", *Adv. Mater.*, **2011**, 23, 3450.
10. Bridges, C. A.; Sun, X.-G.; Zhao, J.; Paranthaman, M. P.; Dai, S.; "In Situ Observation of Solid Electrolyte Interphase Formation in Ordered Mesoporous Hard Carbon by Small-Angle Neutron Scattering", *J. Phys. Chem. C* **2012**, 116, 7701.
11. Yoon, S.; Liao, C.; Sun, X. G.; Bridges, C. A.; Unocic, R. R.; Nanda, J.; Dai, S.; Paranthaman, M. P.; "Conductive surface modification of LiFePO₄ with nitrogen-doped carbon layers for lithium-ion batteries", *J. Mater. Chem.* **2012**, 22, 4611.
12. Gupta, A.; Murugan, R.; Paranthaman, M. P.; Bi, Z.; Bridges, C. A.; Nakanishi, M.; Sokolov, A. P.; Han, K. S.; Hagaman, E. W.; Xie, H.; Mullins, C. B.; Goodenough, J. B.; "Optimum lithium-ion conductivity in cubic Li_{7-x}La₃Hf_{2-x}Ta_xO₁₂", *J. Power Sources* **2012**, 209, 184.
13. Qiao, Z.; S. S. Brown; J. Adcock; G. M. Veith; and S. Dai, "A new topotactic synthetic methodology for highly fluorine-doped mesoporous metal oxides" *Angew. Chem. Intl. Ed.* **2012**, 51, 2888-2893.
14. Carroll, K. J.; M. Yang; G. M. Veith; N. J. Dudney; Y. S. Meng, "Intrinsic surface stability in LiMn_{2-x}Ni_xO_{4-δ} (x = 0.45, 0.5) high voltage spinel materials for lithium ion batteries" *Electrochemical and Solid State Letters* **2012**, 15, A72-A75.
15. Martha, S. K.; J. Nanda; G. M. Veith; N. J. Dudney "Electrochemical and Interfacial Studies of High-Voltage Lithium-Rich Composition: Li_{1.2}Mn_{0.525}Ni_{0.175}Co_{0.1}O₂" *J. Power Sources* **2012**, 199, 220-226.
16. Xie, H.; Y. Li; J. Han; Y. Dong; M. P. Paranthaman; L. Wang; M. Xu; A. Gupta; Z. Bi; C. A. Bridges; M. Nakanishi; A. P. Sokolov; J. B. Goodenough, "Li₆La₃SnMO₁₂ (M=Sb,Nb,Ta) a new family of lithium garnets with high Li-ion conductivity, *J. Power Sources*, in press.

“Giant” Nanocrystal Quantum Dots: Controlling Charge Recombination Processes for High-Efficiency Solid-State Lighting

**Dr. Jennifer A. Hollingsworth and Dr. Han Htoon, Materials Physics & Applications
Division: Center for Integrated Nanotechnologies, Los Alamos National Laboratory, Los Alamos, NM**

Program Scope

Solid-state lighting (SSL) has the potential to replace less efficient and robust lighting technologies, such as incandescent and fluorescent lamps. Significant inroads into the commercial and residential general-lighting markets have been made in recent years as light-emitting diodes (LEDs) find consumer acceptance. That said, science challenges remain as underpinning drivers of fundamental research required for *disruptive advances* in SSL. Existing technologies (nitride and organic-LEDs) suffer from some combination of flaws: non-optimal efficiencies and/or manufacturing/materials costs, insufficient access to a full-spectrum ‘color palette,’ inadequate longevity, etc. A fundamental understanding of the processes that impact the conversion of electricity into light is still needed. As recently observed (DOE/EERE 2011 Joint Roundtable), nanostructures can serve as *platforms for understanding* such fundamental processes, but also as *solutions* to realizing control over exciton→photon conversion pathways. In our work, we study and develop a new class of optical nanomaterial – the “giant” nanocrystal quantum dot (g-NQD). g-NQDs are thick-shell core/shell NQDs that exhibit unique photo-physical/chemical behavior (non-blinking, non-photobleaching, suppressed non-radiative Auger recombination, large Stokes shift, surface-independent emission) resulting from effects of a thick shell, a relatively large per-particle volume, at least partial spatial separation of the excited-state electron-hole pair, and/or possibly compositional alloying at the core/shell interface. By judicious nanoscale-heterostructuring, we are able to influence these parameters and, thereby, to alter the interplay between radiative/nonradiative carrier-recombination processes. Through three Research Goals, we aim to establish g-NQDs as functional “building blocks” for SSL with combined attributes of high-efficiency, robustness, low-cost, and color tunability: (1) Establish quantitative g-NQD “structure-function” relationships for fully predictable/consistent performance and new g-NQD development, (2) Understand/control exciton (*and multi-exciton*)→photon conversion pathways via strategic manipulation of intrinsic and extrinsic g-NQD properties, and (3) Demonstrate performance-benchmarking in light-emitting devices.

Recent Progress

Research Goal 1. We recently explored key reaction variables in the Successive Ionic Layer Adsorption and Reaction (SILAR) synthesis of thick-shell or “giant” NQDs (Fig. 1). In the

case of conventional thin-shell NQDs (~1-3 monolayers of shell material), the exact choice and implementation of these parameters does not significantly impact the resulting core/shell product. In contrast, we have now shown that these variables can dramatically affect structure and function in g-NQDs, dictating both ensemble quantum yield (QY) and single-NQD blinking properties, as well as particle shape and crystal structure.¹ In addition, we addressed the issues of within-batch and across-batch particle size/shape variability. Initially, we attributed such irreproducibility to the tendency of CdSe/CdS g-NQDs to flocculate during the shelling process at some “threshold” shell thickness (“titrated” away by S addition, only to reappear with each addition of Cd). We considered that the resulting decrease in reaction homogeneity influenced the processes by which Cd and S ad-atoms interact with the NQD surface (e.g., atom adsorption-desorption and surface migration). Such processes are critical for obtaining high-quality, crystalline and uniform NQDs. They are well supported in homogeneous reaction solutions that afford efficient reactant transfer between the NQD surface and the solvent phase. In contrast, we surmised, such processes in the case of “partially precipitated” NQDs would be less well supported and more variable, potentially resulting in particle-size/shape inhomogeneity.

To achieve greater control over the shell addition process at the atomic level, we varied choice of non-coordinating solvent, dilution, identity and concentrations of coordinating ligands (especially 1° vs. 2° amines), and precursor:NQD ratios.¹ We were able to tune reaction parameters to eliminate the aggregation process; however, in all such cases emission properties suffered dramatically, and particle shape and/or crystalline phase were completely altered, suggesting that methods that afforded reduced (not eliminated) and late-onset aggregation produced the highest-quality g-NQDs (structurally and optically). We have now improved QYs (consistently ~50% for ultra-thick shell g-NQDs), and demonstrated for the first time: *complete suppression of blinking* in g-NQDs, a clear structure:function correlation, and, interestingly, that *blinking and PL lifetimes trend explicitly with g-NQD volume* (Fig. 2).¹

Research Goal 2. To understand the effect of electronic structure – as an ‘intrinsic’ property of core/shell NQDs – on g-NQD properties, we synthesized a range of InP/II-VI core/shell systems. Surmounting synthetic challenges to handling InP NQDs, the realized compositions (InP/ZnS, InP/ZnSe, InP/CdS, InP/CdSe) allowed us to achieve extreme color tunability from the green to the IR (~500-1100 nm) as a function of core size, shell thickness,

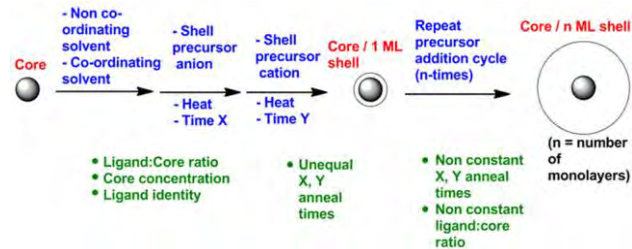


Figure 1. SILAR shell-addition process. Blue text denotes general reaction parameters and flow, while green text shows options for modifying specific reaction conditions.

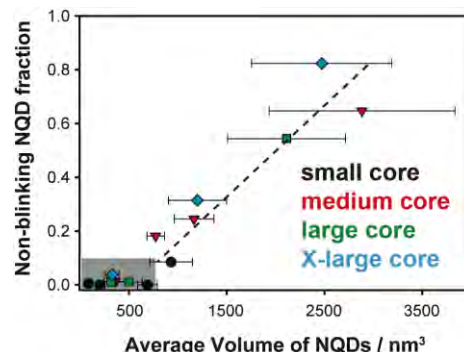


Figure 2. Non-blinking NQD fraction vs. particle volume for different starting core sizes; shaded region: NQD volumes that fall below “threshold volume” of ~750 nm³.

and shell composition, as a result of tuning electronic structure from type I (co-localized electron and hole) to quasi-type II (partially spatially separated carriers) to type II (fully spatially separated carriers). Furthermore, in the case of InP/CdS, we studied ensemble and single-dot level optical properties from thin shells to giant shells to understand carrier recombination processes as a function of shell thickness. Here, we demonstrated for the first time suppressed blinking in the near-IR (Fig. 3), as well as extremely enhanced biexciton lifetimes, which increased by ~ 125 -fold from nominally 1-shell to 10-shell monolayers (to ~ 7 ns). The long biexciton lifetimes (comparable to the prototype CdSe/CdS g-NQDs) are thought to result from suppressed non-radiative Auger recombination² and imply that InP/CdS g-NQDs should support realization of optical gain and stimulated emission toward NQD-based lasers. *Thus, this new system has achieved two of the key signatures of “g-NQD functionality:” suppressed blinking and suppressed Auger and represents an important extension of the approach beyond CdSe/CdS g-NQDs.*

In addition to advances in the area of g-NQD synthesis, we have developed novel spectroscopic capabilities and provided new insights into the underlying processes governing carrier recombination processes. In the case of the new InP/CdS system, for example, we have recently discovered that, in contrast to conventional NQDs, PL intensity fluctuations at the single-dot level are *not* correlated with fluctuations in lifetime, with both highly emissive and low-emissive states exhibiting the characteristic long lifetimes of this type II structure. The underlying mechanism for this behavior was previously described by us in the context of so-called “B-type blinking,”³ which relates decreased emission intensities with hot-electron capture to NQD-surface traps, rather than NQD charging (or “A type” standard blinking behavior). The new blinking model (i.e., two types of blinking: “A” and “B”) was made possible by our development of a novel single-NQD spectroelectrochemistry technique.³

As Auger recombination (AR) detrimentally impacts NQD emission efficiencies in both spontaneous and stimulated-emission modes, we have aimed to understand and control this process. Our preliminary studies revealed that AR in CdSe/CdS g-NQDs is strongly suppressed compared to conventional core/shell NQDs.² Beyond this ensemble level study, we have also conducted a series of single-NQD-spectroscopy studies. We have studied PL intensity and lifetime fluctuations in individual CdSe/CdS NQDs as a function of shell thickness.⁴ We quantitatively determined the emission efficiency of multiexciton states in these g-NQDs and studied how this value varied among the nominally identical individual g-NQDs, observing that some ultra-thick-shell g-NQDs exhibit $\sim 100\%$ biexciton QYs.⁵ More recently, we have explored

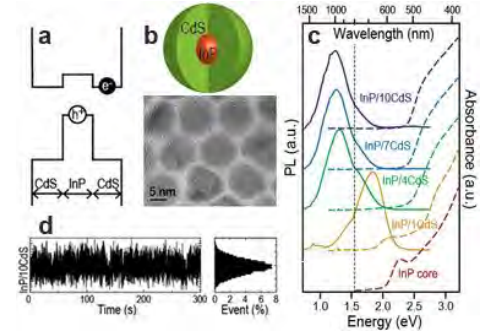


Figure 3. (a) Relative bulk bandgap alignments of InP and CdS. (b) InP/CdS g-NQD schematic and TEM image of InP/CdS g-NQDs after 10 successive shell depositions. (c) Absorption (dashed) and PL (solid) spectra of InP and InP/CdS NQDs. (d) Single-particle PL: representative emission trace (InP/10CdS) (left) and corresponding histogram demonstrating the relative frequency of ‘on’ and ‘off’ states (right; \sim all ‘on’).

g-NQD photon emission statistics in the presence of a rough silver film⁶ made of nanoflakes. We demonstrated for the first time that the interaction with localized plasmons can transform the photon emission statistics of g-NQDs from photon antibunching to strong photon-bunching. The ability to manipulate this statistical property of a quantum emitter could bring transformational breakthroughs in its utilization as single and/or entangled photon pair sources.⁷

Research Goal 3. We have recently demonstrated the unique attributes of g-NQDs as ‘building blocks’ for either direct-charge-injection LEDs or down-conversion devices.^{8,9} For the former, despite the simplicity of our device,⁸ we obtained external electroluminescence quantum efficiencies nearly 2 orders-of-magnitude higher than comparable conventional-NQD devices (~0.17%) and luminance of 2000 Cd/m². We directly assessed the effect of shell thickness from 4-16 CdS monolayers,⁸ revealing significantly enhanced solid-state performance in the case of the thickest shells without adverse effects on charge injection. We also incorporated g-NQDs into down-conversion devices and observed greater stability and a dramatic reduction in self-reabsorption compared to standard NQDs. Finally, we described the advantages of shell→core energy relaxation vs. core→core energy transfer as mechanisms for energy down-conversion.⁹

Future Plans

To further optimize our ensemble-level g-NQD optical properties and to support our understanding of structure-function correlations, we will develop new methods for electro-phoretic fractioning of g-NQD sub-populations, as well as continue to work with collaborators at Northwestern Un. (Prof. Lauhon) to characterize the g-NQD core/shell interface. We also aim to answer fundamental questions pertaining to the nature of Auger recombination as g-NQD physical/electronic structure is tuned, e.g., carriers are alternatively confined such that the electron resides in the core and the hole extends into the shell. To this end, we remain committed to developing new g-NQD compositions that encompass a range of electronic/interface structures. We will also emphasize the influence of plasmonic effects on radiative and non-radiative processes that determine both exciton and multiexciton carrier recombination pathways, where plasmon-multiexciton interactions constitute an exciting new direction in the field.

References

1. Ghosh, Y. *et al. J. Am. Chem. Soc.* Accepted. 2. Garcia-Santamaría, F., *et al. Nano Lett.* **9**, 3482, (2009). 3. Galland, C. *Nature* **479**, 203-U275, (2011). 4. Malko, A. V. *et al. Nano Lett.* **11**, 5213-5218, (2011). 5. Park, Y. S. *Phys. Rev. Lett.* **106**, 187401, (2011). 6. Mack, N. H. *Langmuir* **27**, 4979-4985, (2011). 7. Bennett, C. H. *et al. Nature* **404**, 247-255, (2000). 8. Pal, B. N. *et al. Nano Lett.* **12**, 331 (2012). 9. Kundu, J. *et al. Nano Lett.* DOI: 10.1021/nl3008659.

Publications

References **1, 4, 5, 8, 9 above** and • Garcia-Santamaría, F. *et al. Nano Lett.* **11**, 687-693 (2011).
• Brovelli *et al. Nature Comm.* **2**, 280 (2011).

Project: ^{125}Te NMR and transport properties of complex thermoelectric tellurides

PI's: E.M. Levin^{1,2}, K. Schmidt-Rohr^{1,3}

¹ – Division of Materials Sciences and Engineering, Ames Laboratory US DOE, ² – Department of Physics and Astronomy, ³ – Department of Chemistry, Iowa State University, Ames, IA 50011

Project Scope

The direct conversion of heat to electricity using the Seebeck effect, or of electricity to heat removal using the Peltier effect, are fundamentally interesting physical phenomena, and simultaneously attractive and elegant processes for energy conversion. Potential use of thermoelectric devices in automobiles, power plants, wireless and solar cells systems [1a] requires intensive study and improvement of fundamental properties of various types of thermoelectric materials [2a-5a].

Enhancement of the efficiency of thermoelectric devices requires materials with a high figure of merit $ZT = S^2/(\rho\kappa)$ where S is the Seebeck coefficient (thermopower), ρ is the electrical resistivity, and κ is the thermal conductivity; the latter has two contributions, $\kappa = \kappa_{\text{lat}} + \kappa_{\text{car}}$, where κ_{lat} and κ_{car} are thermal conductivities due to the lattice and free charge carriers, respectively. However, because κ_{car} and ρ are coupled via the Wiedemann-Franz law [3a], there is a fundamental limitation that needs to be overcome by decoupling these parameters using mechanisms such as resonance scattering [5a], potential barriers [6a], or nanostructuring [2a]. Generally, the enhancement can be achieved via two approaches: (i) discover a material with quite unique properties, and/or (ii) better understand and modify well-known thermoelectric materials, e.g. complex tellurides [3a,4a]. We believe that a detailed understanding of correlations between *materials chemistry* (composition, local structure, bonding, lattice distortion) and *materials physics* (electronic and thermal transport) is required for significant improvement of thermoelectric properties.

There are two well-known groups of thermoelectric tellurides that exhibit high efficiency, still attract great attention, and can be used as matrixes for further improvement: PbTe- and GeTe-based materials. For characterization of thermoelectric materials, we use NMR (DSX-400), two measuring systems for electrical resistivity and Seebeck coefficient (LSR-3) and thermal conductivity (XFA-500), and XRD (Scintag SDS-2000). Our long-term goal is to correlate structural insights from NMR with thermoelectric properties of complex tellurides and other materials, and develop materials with enhanced thermoelectric efficiency.

In our study we also use capabilities and expertise available at Ames Laboratory US DOE [Dr. S. L. Bud'ko and Dr. P.L. Canfield (low-temperature magnetic measurements), and Dr. M. J. Kramer (elemental analysis and electron microscopy)] and at external institutions [Dr. M.G. Kanatzidis, Argonne National Lab US DOE and Northwestern University (PbTe-based materials), and Dr. J.P. Heremans, Ohio State University and Revolutionary Materials for Solid State Energy Conversion Center, Michigan State University (PbTe-based materials)].

Recent Progress

Two types of complex tellurides were synthesized and studied within the project: (i) PbTe- and (ii) GeTe-based materials. The first group includes $\text{Pb}_{1-x}(\text{Ag}_y\text{Sb}_z)\text{Te}$ [1b,2b], $\text{Pb}_{1-x}\text{Sb}_x\text{Te}$ and $\text{PbSb}_x\text{Te}_{1-x}$ [3b], $\text{Pb}_{1-x}\text{Cr}_x\text{Te}$ [4b], $\text{Pb}_{1-x}\text{S}_x\text{Te}$, $\text{Pb}_{1-x}\text{Sn}_x\text{Te}$, and $\text{Pb}_{1-x}\text{Ge}_x\text{Te}$ alloys where Pb or Te are replaced with Ag, Sb, S, or Ge. ^{207}Pb and/or ^{125}Te NMR spectra show several signals, which can be attributed to different chemical environments and concentrations of charge carriers (electrons or holes) and allow us to better understand complex thermoelectric tellurides.

The second group includes $\text{Ag}_{x/2}\text{Sb}_{x/2}\text{Ge}_{50-x}\text{Te}_{50}$ (TAGS) alloys where Ge is replaced by Ag and Sb. Like GeTe, the alloys have p -type conductivity, which is due to holes generated by Ge vacancies and can be varied via the Te/Ge ratio. The Hall effect data suggest that the hole concentration in TAGS materials is very high, $p \approx 40 \times 10^{20} \text{ cm}^{-3}$ [7a], which is inconsistent with thermopower data. Using ^{125}Te NMR, we have discovered that the hole concentration in TAGS is in fact $\sim 6 \times 10^{20} \text{ cm}^{-3}$, similar as in GeTe [7b]. Fig.1(a) shows ^{125}Te NMR spin-lattice relaxation time, T_1 , vs. saturation recovery time for GeTe-based materials. T_1 varies only between 3.1 and 4.7 ms, indicating that the hole concentration in these alloys is high and similar (compare T_1 for GeTe-based and PbTe: {Ag,Sb} materials). Fig. 1(b) shows the dependence of the carrier concentration in p -type GeTe-based materials obtained from ^{125}Te NMR (our data [7b]) and from Hall effect (literature data [7a]) vs. {Ag+Sb} content on the Ge sublattice. The discrepancy can be attributed to a reduction in the Hall effect signal arising from an n -type component, which results in an artificially high hole concentration.

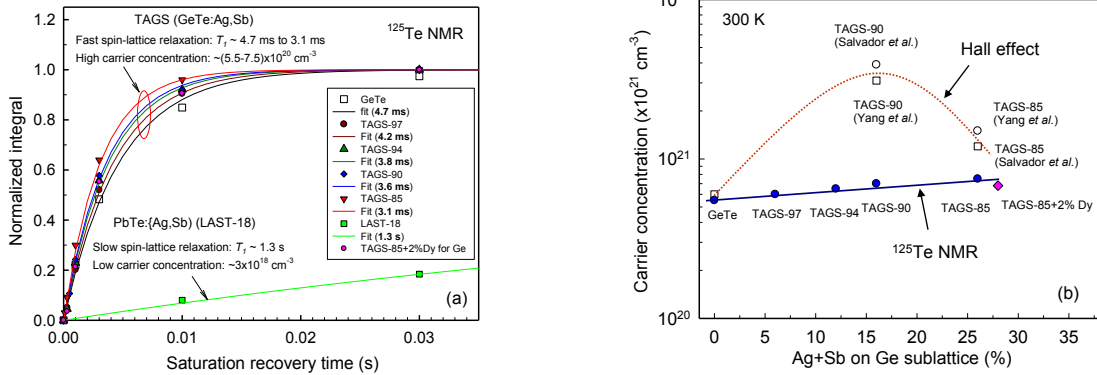


FIG. 1. (a) ^{125}Te NMR spin-lattice relaxation time, T_1 , vs. saturation recovery time for GeTe-based materials; data for PbTe: {Ag,Sb} sample (LAST-18) with low carrier concentration and long T_1 shown for comparison; (b) carrier concentration in GeTe-based materials obtained from ^{125}Te NMR (filled circles and diamond [7b]) and Hall effect (open circles and squares [7a]) vs. {Ag+Sb} content on Ge sublattice.

We have also synthesized $\text{Ag}_{6.5}\text{Sb}_{6.5}\text{Ge}_{37}\text{Te}_{50}$ (TAGS-85) with additions of rare-earth elements of different sizes and effective magnetic moments (Ce, Gd, Dy, and Yb) on Te or Ge sites, and studied thermoelectric properties and ^{125}Te NMR parameters. ^{125}Te NMR and XRD data [5b,6b] show that rare earth atoms are incorporated into the TAGS lattice [see Fig. 2(a) for TAGS-85 doped with Dy]. ^{125}Te NMR in GeTe-based materials shows a strong local lattice distortion [see Fig. 2(b)], which can play an important role for electronic and thermal transport properties of the alloys.

Magnetic data also confirmed that rare earth atoms are incorporated into the lattice [5b,6b], but details of the chemical bonding of Ce, Gd, Dy, and Yb with Ge or Te need to be better understood.

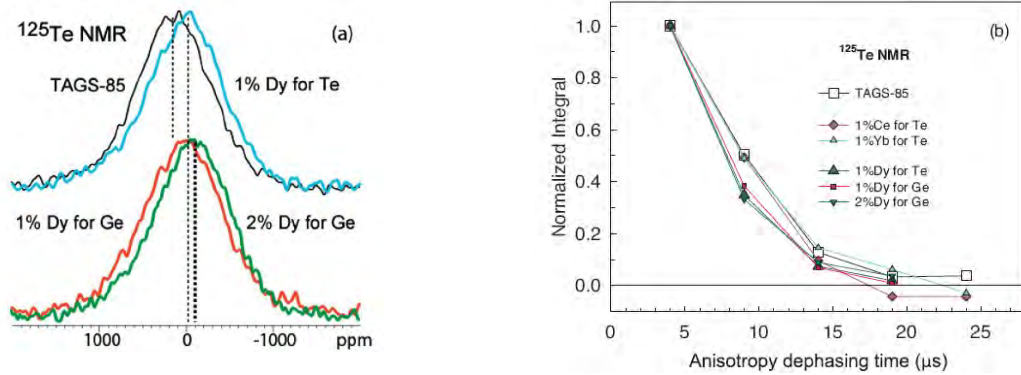


FIG 2. (a) ^{125}Te NMR spectra of TAGS-85, TAGS-85 + 1% Dy for Te, TAGS-85 + 1% Dy for Ge, and TAGS-85 + 2% Dy for Ge [5b]; (b) intensity of the ^{125}Te NMR signal as a function of anisotropy dephasing time in an experiment probing orientation-dependent interactions of the ^{125}Te nuclei for TAGS-85 doped with Dy [6b]; data for TAGS-85 doped with Ce or Yb for Te [5b] are shown for comparison.

Fig. 3(a) shows the temperature dependence of the absolute Seebeck coefficient of the initial and doped TAGS-85 samples, indicating its enhancement due to doping. However, reports of a large enhancement of thermoelectric efficiency due to doping, which have periodically appeared in literature, sometimes cannot be confirmed. Fig. 3(b) shows the variation of the absolute Seebeck coefficient of initial TAGS-85 and doped with Dy vs. the distance from the ingot top at 305 and 700 K, clearly demonstrating enhanced Seebeck coefficient of TAGS-85+Dy alloys along the ingot. The enhancement may be due to potential barriers [6a] formed by rare earth atoms [6b].

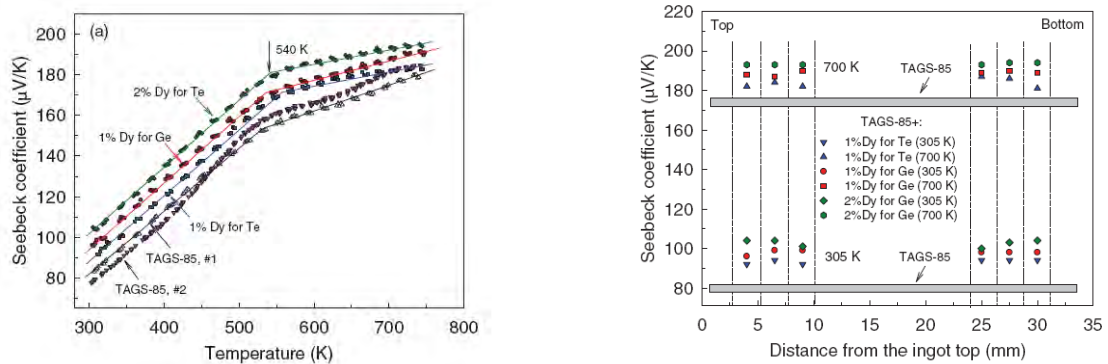


FIG. 3. (a) Temperature dependence of the absolute Seebeck coefficient and (b) its variation vs. the distance from the ingot top at 305 and 700 K [6b].

At 730 K, the initial TAGS-85 shows a power factor, PF , and figure of merit, ZT , of $PF \approx 29 \mu\text{W cm}^{-1} \text{K}^{-2}$ and $ZT \leq 1.3$. For TAGS-85 doped with rare-earth elements $PF \geq 35 \mu\text{W cm}^{-1} \text{K}^{-2}$ and $ZT \geq 1.5$ [6b]; these parameters are among the best reported for p -type thermoelectric materials.

Future Plans

- Synthesize complex GeTe- and PbTe-based and other thermoelectric materials without and with small additions of magnetic (*4f*- and *3d*-elements carrying localized magnetic moments) and non-magnetic dopants.
- Measure ^{125}Te NMR of thermoelectric tellurides to characterize the distribution of dopants, local symmetry, local bonding, charge-carrier concentrations, inhomogeneities, and the Seebeck coefficient, electrical resistivity, Hall effect, thermal conductivity, and other relevant properties on the same samples.
- Perform analysis of effects of doping complex tellurides with non-magnetic and magnetic atoms on spin-lattice relaxation, vacancies, charge-carrier concentration and mobility, carriers and phonon scattering, and thermoelectric properties; consider a model of potential barriers formed at the atomic level as a reason for enhancement of thermoelectric efficiency in complex tellurides.
- Establish a better understanding of materials chemistry - materials physics relations in GeTe- and PbTe-based materials; using this knowledge, design thermoelectric materials with enhanced efficiency.

References

- [1a] L.E. Bell, *Science* **321**, 321, 1457 (2008); J. Karni, *Nat. Mater.* **10**, 481 (2011).
- [2a] M. S. Dresselhaus *et al.* *Adv. Mater.* **19**, 1043 (2007).
- [3a] G. J. Snyder and E. S. Toberer. *Nat. Mater.* **7**, 105 (2008).
- [4a] M.G. Kanatzidis, *Chem. Mater.* **22**, 648 (2010).
- [5a] J.P. Heremans *et al.* *Science* **321**, 554 (2008); Y. Pei *et al.* *Nature* **2011**, 473, 66.
- [6a] S.V. Faleev and F. Leonard, *Phys. Rev. B* **77**, 214304 (2008).
- [7a] E.A. Skrabek and D.S. Trimmer, in *CRC Handbook of Thermoelectrics* (Ed. by D.M. Rowe) CRC Press LLC, **1995**, chapter 22; S.H. Yang *et al.* *Nanotechnology* **19**, 245707 (2008); J.R. Salvador *et al.* *J. Solid State Chem.* **182**, 2088 (2009); Y. Gelbstein *et al.* *J. Electr. Mater.* **39**, 2049 (2010).

Recent Publications

- [1b] Yan-Yan Hu, E.M. Levin, and K. Schmidt-Rohr, *J. Am. Chem. Soc.* **131**, 8390 (2009).
- [2b] E. M. Levin, B. A. Cook, K. Ahn, M. G. Kanatzidis, and K. Schmidt-Rohr, *Phys. Rev. B* **80**, 115211 (2009).
- [3b] C.M. Jaworski, J. Tobola, E.M. Levin, K. Schmidt-Rohr, J.P. Heremans, *Phys. Rev. B* **80**, 125208 (2009).
- [4b] M.D. Nielsen, E.M. Levin, C.M. Jaworski, K. Schmidt-Rohr, J.P. Heremans, *Phys. Rev. B* **85**, 045210 (2012).
- [5b] E.M. Levin, B.A. Cook, J.L. Haringa, S.L. Budko, R. Venkatasubramanian, and K. Schmidt-Rohr, *Adv. Funct. Mater.* **21**, 441 (2011).
- [6b] E.M. Levin, S.L. Bud'ko, and K. Schmidt-Rohr, *Adv. Funct. Mater.* Published online April 10, 2012.
- [7b] E.M. Levin, J.D. Acton, and K. Schmidt-Rohr, 2012 APS March Meeting, Boston, MA.

Energy and Fuels from Multi-Functional Electrochemical Interfaces

PIs: Nenad M. Markovic and Vojislav R. Stamenkovic
Materials Science Division Argonne National Laboratory

Program Scope

We propose an interdisciplinary, atomic/molecular level approach, integrating both experimental- and- computational-based methodologies to design, synthesize, and characterize electrochemical interfaces for efficient transformation of chemical energy into electricity and/or to utilize the energy of electrons for the synthesis of chemicals that can be stored and re-used. The proposal describes a science based approach to developing new materials, and interfaces with specific focus on the electrocatalytic reactions involving the **water cycle** ($\text{H}_2 + \text{O}_2 \leftrightarrow \text{H}_2\text{O}$) and the **carbon cycle** ($\text{C}_x\text{H}_y\text{O}_z + \text{O}_2 \leftrightarrow x\text{CO}_2 + 1/2y \text{H}_2\text{O}$). These two cycles are expected to constitute the core building blocks for an efficient, green and viable energy landscape required for the design and synthesis of multi-functional electrochemical interfaces with specifically tailored properties. A two-fold strategy is proposed. The first centers on the design of novel energy-efficient *multi-functional materials* with tailored properties, such as metals and metal alloys, complex oxides, metal-metal oxides and chemically modified electrodes. The second strategy centers on the understanding and design of *multi-functional double layers*, a “solution-phase” of electrochemical interfaces established in the vicinity of catalytic materials. To develop a multi-scale capability for tailoring electrochemical interfaces, we will rely on the research facilities at Argonne National Laboratory and a set of unique, state-of-the-art, *ex-situ* and *in-situ* surface-sensitive probes. The synergy obtained from the combination of experimental and computational methods, together with the application of knowledge, concepts, and tools developed in this program, will lead to a new generation of *multi-functional interfaces* for efficient energy conversion and fuel production.

Recent Progress

The development of new multi-functional electrochemical interfaces that can solve challenging problems of clean energy production, storage, and conversion, as well as carbon sequestration is of paramount importance in the quest to find alternatives to fossil fuel use and to ultimately tackle environmental concerns. Electrocatalysis – the study of electrode processes where the rate (charge transfer) of reaction has a strong dependence on the nature of electrochemical interfaces – lies at the heart of the spectrum of electrochemical transformations relevant for resolving these challenges. The creation of new electrochemical interfaces has always proceeded hand-in hand with advances in our ability first to define the nature, arrangement, and transformations of catalyst surface atoms and hydrated ions in the double layer and the correlation of these interfacial properties with the kinetics of electron transfer as well as our theories to explain and predict such phenomena. The success of this approach will be demonstrated further below.

Tailoring Metal-Oxide Materials for Hydrogen Production: Improving the sluggish kinetics for the electrochemical reduction of water to molecular hydrogen in alkaline environments is the key to reducing energy losses in water-alkali and chlor-alkali electrolyzers. Working with well

controlled single crystal surfaces, our group has demonstrated that targeted functionality can be achieved by bottom up design [1]. A controlled and well characterized arrangement of nanometer-scale Ni(OH)₂ clusters on platinum single crystal electrode surfaces manifests a 10-fold activity increase in catalyzing the hydrogen evolution reaction (HER) over that obtained on state-of-the-art metal and metal-oxide catalysts. In a bi-functional effect, the edges of the Ni(OH)₂ clusters promote the dissociation of water leading to the production of hydrogen intermediates that then adsorb (H_{ad}) on the nearby Pt surfaces and recombine into molecular hydrogen. This process is completely transformational to real Pt-Ni(OH)₂ nanocatalysts supported on carbon. Again, this work illustrates how fundamental understanding leads quickly to innovative new technologies.

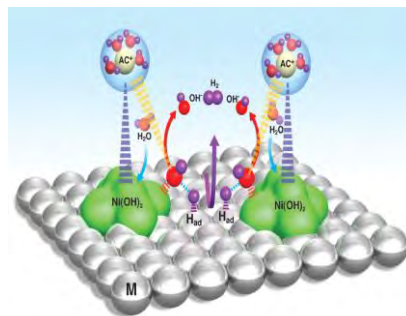


Figure 1. Schematic of water dissociation, formation of H_{ad} intermediates and subsequent recombination to H₂[1].

This work has been recently highlighted on the Office of Science’s webpage of the DOE as a significant contribution to the research field.

Trends in Activity for the Water Electrolyzer Reactions: we have used well characterized M^{2+δ}O^δ(OH)_{2-δ} /Pt(111) catalyst surfaces (M=Ni,Co,Fe,Mn) to establish clear trends in activity

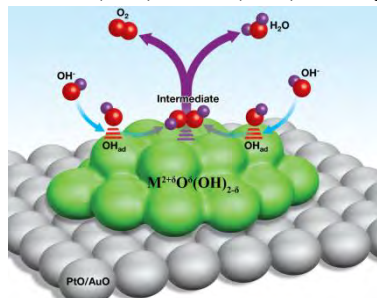


Figure 2. Schematic showing the formation of O₂ and H₂O from OH⁻ via formation of OH_{ad} intermediates [2].

for the HER and the OER of a complex oxide system where the conventional methods of comparing high surface area materials present a lot of uncertainties. We determined, using the OH_{ad}---M^{2+δ} interaction as the primary descriptor, that the activity for the HER and the OER for these 3d-M hydr(oxy)oxide systems follows the order Ni>Co>Fe>Mn. The importance of this interaction (OH_{ad}---M^{2+δ}) was identified by probing oxophilicity trends in adsorption of OH⁻ in the butterfly region and CO oxidation reaction in the H_{upd} region [2]. Although the same descriptor can be effectively used to study both the HER and the OER on these 3d-M hydr(oxy)oxide systems, the reaction mechanisms were found to be different. While the HER is controlled by a pure bi-functional mechanism (metal sites to recombine H_{ad} and “oxides” to dissociate water), the activities for the OER are controlled exclusively by the oxophilicities of the corresponding 3d-M hydr(oxy)oxides (mono-functional). The increasing OER activities for the 3d-M systems (always greater than Pt), as a function of the decreasing strength of the OH_{ad}---Mⁿ⁺ interaction, provides us with the necessary toolkit to tune transition metal oxide catalysts for the OER. We anticipate that by further, descriptor-guided tuning of these oxides, even greater improvements in alkaline electrocatalyst performance will be possible by focused design of the elusive ‘active centers’ in catalysis.

Tailoring Stability by Tuning Selectivity: While the methods to improve catalytic activity are diverse, the methods to improve stability of cathode materials are limited. To overcome this limitation we designed chemically modified Pt electrodes with a self-assembled monolayer of calx[4]arene. These molecules effectively block the undesired oxygen reduction reaction while fully preserving high activity for the hydrogen oxidation reaction. This selectivity is highly transformational, applicable not only to long range ordered single crystal surfaces [3] but also to

nanocatalysts [4]. This methodology has many potential applications in analytical, synthetic, and materials chemistry as well as in chemical energy conversion and storage.

Future Work

An interdisciplinary, atomic/molecular level approach, integrating both experimental- and computational-based methodologies, will be applied to define the landscape for design of *multi-functional interfaces* that will resolve many challenging problems related to clean energy generation and fuel production. To fully design and develop these interfaces, with main focus on catalytic materials and the double-layer properties, we will employ a rigorous, *science-based* approach, that will involve four major steps: (i) *design* novel states of catalytic interfaces by manipulating their electronic and structure properties; (ii) *characterize* atomic and electronic properties of such interfaces by developing and using ex-situ and in-situ surface characterization techniques and state-of-the-art theoretical methods to explore structure/property relationships; (iii) *understand* at atomic/molecular level, fundamental principles that govern efficient bond-making and bond-breaking processes at electrochemical interfaces; and (iv) *optimize* the active sites by an iterative process, guided by the fundamental understanding of the structure-property relationships at complex electrochemical interfaces. Our strategy will allow further design of multi-functional interfaces that can transform chemical energy into electricity or utilizing the energy of electrons for the syntheses of chemicals that can be stored and re-used in energy conversion systems.

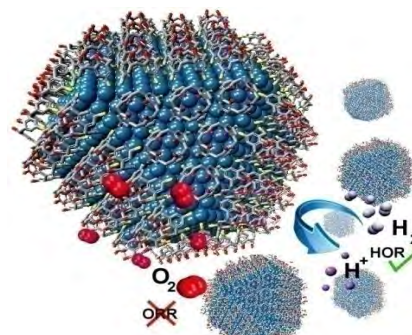


Figure 3. Schematic demonstrating selectivity for the HOR and ORR [4]

References:

1. R. Subbaraman, D. Tripkovic, D. Strmcnik, K-C. Chang, M. Uchimura, A. P. Paulikas, V. Stamenkovic and N. M. Markovic; “Enhancing Hydrogen Evolution Activity in Water Splitting by Tailoring L^+ -Ni(OH)₂-Pt Interfaces”; *Science*, **334** (2011) 1256-1260.
2. R. Subbaraman, D. Tripkovic, K-C. Chang, D. Strmcnik, A. P. Paulikas, H.P. Hurinsit, M. Chan, J. Greeley, V. Stamenkovic and N. M. Markovic; “Trends in Activity for the Water Electrolyzer Reactions on 3d-M(Ni,Co,Fe,Mn)-Hydr(oxy)oxide Catalysts”; *Nature Materials*, DOI 10 1038/NMAT3313 (2012).
3. B. Genorio, D. Strmcnik, R. Subbaraman, D. Tripkovic, G. Karapetrov, V. R. Stamenkovic, S. Pejovnik, N. M. Markovic; “Selective Catalysts for the Hydrogen Oxidation and Oxygen Reduction Reactions by Patterning of Platinum with Calix[4]arene Molecules”; *Nature Materials*, **9** (2010) 998–1003.
4. B. Genorio, R. Subbaraman, D. Strmcnik, D. Tripkovic, V.R. Stamenkovic, N.M. Markovic; “Tailoring the Selectivity and Stability of Chemically Modified Platinum Nanocatalysts To Design Highly Durable Anodes for PEM Fuel Cells”; *Anew. Chem. Int. Ed.*, **123** (2011) 5582–5586.

Publications:

1. R. Subbaraman, D. Tripkovic, K-C. Chang, D. Strmcnik, A. P. Paulikas, H.P. Hurinsit, M. Chan, J. Greeley, V. Stamenkovic and N. M. Markovic; “Trends in Activity for the Water Electrolyzer Reactions on 3d-M(Ni,Co,Fe,Mn)-Hydr(oxy)oxide Catalysts”; *Nature Materials*, DOI 10 1038/NMAT3313 (2012).

2. R. Subbaraman, D. Tripkovic, D. Strmcnik, K-C. Chang, M. Uchimura, A. P. Paulikas, V. Stamenkovic and N. M. Markovic; "Enhancing Hydrogen Evolution Activity in Water Splitting by Tailoring L^+ -Ni(OH)₂-Pt Interfaces"; *Science*, **334** (2011) 1256-1260.
3. D. Strmcnik, D. van der Vliet, K-C. Chang, V. Komanicky, K. Kodama, H. You, V. R. Stamenkovic, N.M. Markovic; "Effects of Li^+ , K^+ , and Ba^{2+} , Cations on the ORR at Model and High Surface Area Pt and Au Surfaces in Alkaline Solutions"; *J. Phys. Chem. Lett.*, **2** (2011) 2733-2736.
4. C. A. Lucas, P. Thompson, Y. Gründer, N. M. Markovic; "The structure of the electrochemical double layer: Ag(111) in alkaline electrolyte"; *Electrochemistry Communications*, **13** (2011) 1205-1208.
5. M. Escudero-Escribano, Z. Michoff, E.P. Leiva, N.M. Marković, N. M., C. Gutiérrez, A. Cuesta; "Quantitative Study of Non-Covalent Interactions at the Electrode–Electrolyte Interface Using Cyanide-Modified Pt(111) Electrodes"; *ChemPhysChem*, **12** (2011) 2230–2234.
6. B. Genorio, R. Subbaraman, D. Strmcnik, D. Tripkovic, V.R. Stamenkovic, N.M. Markovic; "Tailoring the Selectivity and Stability of Chemically Modified Platinum Nanocatalysts To Design Highly Durable Anodes for PEM Fuel Cells"; *Anew. Chem. Int. Ed.*, **123** (2011) 5582–5586.
7. B. Genorio, D. Strmcnik, R. Subbaraman, D. Tripkovic, G. Karapetrov, V. R. Stamenkovic, S. Pejovnik, N. M. Markovic; "Selective Catalysts for the Hydrogen Oxidation and Oxygen Reduction Reactions by Patterning of Platinum with Calix[4]arene Molecules"; *Nature Materials*, **9** (2010) 998–1003.
8. C. Stoffelsma, P. Rodriguez, G. Garcia, N. Garcia-Araez, D. Strmcnik, N. M. Markovic, M. T. Koper; "Promotion of the Oxidation of Carbon Monoxide at Stepped Platinum Single-Crystal Electrodes in Alkaline Media by Lithium and Beryllium Cations"; *J. Am. Chem. Soc.*, **132** (2010) 16127-16133.
9. D. Strmcnik, M. Escudero, K. Kodama, V.R. Stamenkovic, A. Cuesta, N.M. Markovic, "Enhanced Electrocatalysis of the Oxygen Reduction Reaction Based on Patterning of Platinum Surfaces with Cyanide"; *Nature Chemistry*, **2** (2010) 880-885.
10. R. Subbaraman, D. Strmcnik, V. Stamenkovic, N.M. Markovic, "O₂ Reduction at Three Phase Interfaces: A Case Study for Pt(hkl), Pt₃Ni(111) and High Surface Area Catalysts-Nafion Interfaces"; *PhysChemPhys.*, **11** (2010) 2825-2833.
11. R. Subbaraman, D. Strmcnik, V. Stamenkovic, N.M. Markovic, "Three Phase Interfaces at Electrified Metal-Solution Interfaces- Study of the Pt(hkl) - Nafion Interface"; *J. Phys. Chem. C*, **114** (2010) 8414-8422.
12. D. Strmcnik, N. Hodnik, S. B. Hocevar, D. van der Vliet, M. Zorko, V.R. Stamenkovic, B. Pihlar, N.M. Markovic, "Novel Method for Fast Characterization of High Surface Area Electrocatalytic Materials Using Carbon Fiber Microelectrode"; *J. Phys. Chem. C*, **114** (2010) 2640-2644.
13. D. Strmcnik, K. Kodama, D. van der Vliet, J. Greeley, V. Stamenkovic, N.M. Markovic, "The Role of Noncovalent Interactions in Electrocatalytic Fuel Cell Reactions on Platinum"; *Nature Chemistry*, **1** (2009) 466-472.
14. C. Lucas, P. Thomson, M. Cormack, A. Brownrigg, B. Fowler, D. Strmcnik, V. Stamenkovic, J. Greeley, A. Menzel, H. You, and N.M. Markovic; " Temperature-induced Ordering of Metal-adsorbates Structures at Electrochemical Interfaces", *J. Am. Chem. Soc.*, **131** (2009) 7654-7661.
15. H. Gasteiger and N.M. Markovic; " Just a Dream-or Future Reality ", *Science*, **324** (2009) 48-49.

Energy and Fuels from Multi-Functional Electrochemical Interfaces

Subtask: **Electrocatalysis at Mesoscale**

PIs: Nenad M. Markovic and Vojislav R. Stamenkovic

Materials Science Division Argonne National Laboratory

Program Scope

The main focus of this effort is placed on an interdisciplinary, atomic/molecular level approach, which integrates experimental-based methodologies to design, synthesize, and characterize electrochemical interfaces for efficient transformation of chemical energy into electricity and/or to utilize the energy of electrons for the synthesis of chemicals that can be stored and re-used. The proposal describes a science based approach to developing new materials, and interfaces with specific focus on the electrocatalytic reactions involving the *water cycle* ($H_2 + O_2 \leftrightarrow H_2O$) and the *carbon cycle* ($C_xH_yO_z + O_2 \leftrightarrow xCO_2 + 1/2y H_2O$). These two cycles are expected to constitute the core building blocks for an efficient, green and viable energy landscape required for the design and synthesis of multi-functional electrochemical interfaces with specifically tailored properties. A two-fold strategy is proposed. The first centers on the design of novel energy-efficient *multi-functional materials* with tailored properties, such as metals and metal alloys, complex oxides, metal-metal oxides and chemically modified electrodes. The second strategy centers on the understanding and design of *multi-functional double layers*, a “solution-phase” of electrochemical interfaces established in the vicinity of catalytic materials. The knowledge obtained from the combination of experimental methods, together with the application of novel concepts developed in this program, will lead to *multi-functional interfaces* for efficient energy conversion and fuel production.

Recent Progress

The fundamental understanding of the structure-function relationships can ultimately lead the design and development of multi-functional electrochemical interfaces that can be utilized for clean energy production, storage, and conversion. In electrocatalysis – the surface properties such as structure, composition and associated electronic structure have strong influence on the electrochemical reaction rates. At the same time, the dependence on nature of interactions at electrified solid-liquid interfaces and the presence of non-reactive species from electrolyte have also direct influence on catalytic performance. Ability to control these critical parameters can provide extraordinary potential in fine tuning of the functional properties of electrochemical interfaces. These parameters can be described by mesoscale phenomena that control and connect the world of molecules at the interfaces and tailored extended-, micro-, and/or nano- scale surfaces. The ability to orchestrate mesoscale properties in order to provide maximal utilization of electrochemical interfaces will be presented in several examples that point out the most recent progress from our research.

Mesostructured Thin-Films as Electrocatalysts with Tunable Composition and Morphology:

Great expectations are held for technologies such as fuel cells and lithium-air batteries that rely on electrochemical processes. In both cases, satisfactory energy density can be attained; however, a major challenge lays in the insufficient activity and durability of materials that are currently employed as cathode catalysts for electrochemical reduction of oxygen. These limitations inevitably lead to a lower operating efficiency of the devices, which highlights the need for development of more active and durable oxygen reduction reaction (ORR) catalysts.

In past¹ we have shown how surface morphology can greatly affect catalytic properties by utilizing unique structure-function properties of nanosegregated extended-surfaces. Here, we present that superior catalytic behavior can be achieved in ultra-thin films by tuning of the thin film surface structure and inducing mesostructured morphology.

Molecular Patterning and non-Covalent Interactions of Mesoscale Surfaces: The successful deployment of advanced energy conversion systems depends critically on understanding of the fundamental bonding interactions at electrified metal-liquid interfaces.

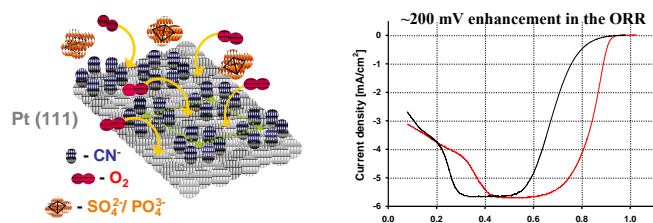


Figure 2. Molecular patterning of mesoscale Pt(111) surfaces by irreversible adsorbed cyanide molecules has induced enhancement of more than 200 mV for the ORR.

been considered: (i) direct bond formation between adsorbates and electrodes, involving chemisorption, electron transfer, and release of the ion hydration shell; and (ii) relatively weak electrostatic metal-ion forces that may affect the concentration of ions in the vicinity of the electrode but do not involve direct metal-adsorbate bonding. The range of physical phenomena associated with these two classes of bonds is unusually broad, ranging from ionic hydration and electron-charge transfer processes to adsorption and catalysis. The energy of adsorption of reactants/intermediates, as well as of species from supporting electrolytes, varies strongly from metal to metal, thereby leading to significant variation in the electrocatalytic reaction rates.

Highly Durable Mesoscale Surfaces: Thermodynamically established segregation trends for alloys can be reversed by adsorbates. For instance, in case of Pt-Au alloys strong Pt-O interaction drives Pt atoms to remain on the surface and induces a unique mechanism of stabilization of Pt surface atoms, which is opposed to tendency of Au to be on the topmost surface layer. Inspired by this example, other combinations that rely on a negative segregation trend of altered near-surface segregated profiles between transition metals from IB group (Au, Ag, Cu) and catalytically active elements (Pt, Pd, Ru, Ir alloyed with Ni, Co, Fe, Cr, Mn etc.) including metallic oxides have been examined. Based on the

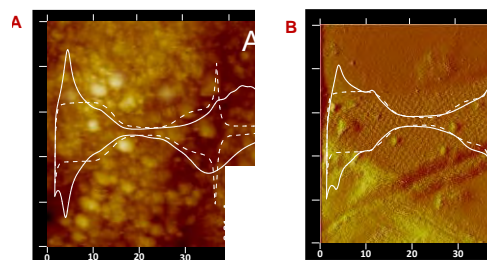


Figure 1. STM images: (A) as-deposited nanostructured thin film and (B) thermally treated mesostructured thin film with large [111] oriented facets. Cyclic voltammograms of Pt(111), as-deposited and mesostructured thin films of Pt (solid curves).

In general, the interface between a metal and an electrolyte solution is characterized by the presence of an electric double layer, formed by an electrical charge on the metal surface and an opposing charge in the adjacent solution. In aqueous electrolytes, depending on the nature of the reacting species^{2,3}, the supporting electrolyte, and the metal electrodes, two types of interactions have traditionally

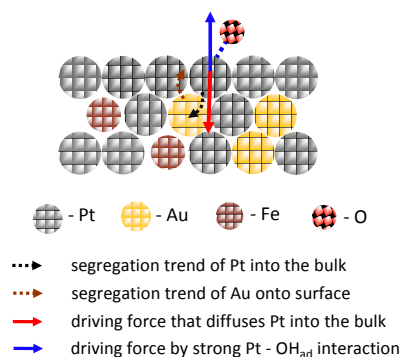


Figure 3. Illustration of counterbalance between the two opposing forces: strong interaction between Pt and surface oxides and tendency of Au to segregate over Pt

fine balance between the segregation forces that originate from the fundamental-thermodynamic and adsorbate induced segregation, the durability of the multimetallic system can be tuned for the OER and ORR. Materials that are promising for metal-air batteries are also studied for the first time at this fundamental level in the form of bimetallic and multimetallic systems. As a part of the same effort, well-defined systems are optimized by thin film studies in order to get maximal output in performance with the minimal content of precious metals.

Future Work

An interdisciplinary, atomic/molecular level experimental-approach will be applied to define the advanced design of mesoscale multi-functional interfaces that may address challenging problems related to clean energy generation, storage and fuel production. To fully design and develop these interfaces, with main focus on catalytic materials, we apply science-based approach that involve four major steps: (i) design novel states of catalytic interfaces by manipulating their electronic and structure properties; (ii) characterize atomic and electronic properties to establish structure/property relationships; (iii) understand at atomic/molecular level, fundamental principles that govern efficient bond-making and bond-breaking processes at mesoscale electrochemical interfaces; and (iv) optimize the active sites by an iterative process, guided by the fundamental understanding of the structure-property relationships at complex electrochemical interfaces.

References:

1. V.R. Stamenkovic, B. Fowler, B.S. Mun, G. Wang, P.N. Ross, C.A. Lucas, N.M. Markovic “*Improved Oxygen Reduction Activity on Pt₃Ni(111) via Increased Surface Site Availability*”, *Science*, **315**(2007)493-497.
2. D.Strmcnik, K. Kodama, D.vander Vliet, J. Greeley, **V.R. Stamenkovic**, N.M.Markovic, “*The Role of Non-Covalent Interactions in Electrocatalytic Fuel-Cell Reactions on Platinum*” *Nature Chemistry*, **1**(2009)446.
3. D.Strmcnik, M.Escudero, K.Kodama, **V.Stamenkovic**, A.Cuesta, N.M.Markovic, “*Electrocatalysis based on Molecular Patterning: the Oxygen Reduction Reaction on CN-modified Pt*”, *Nature Chemistry*, **2**(2010)880-885.

Publications:

1. R. Subbaraman, D. Tripkovic, K-C. Chang, D. Strmcnik, A. P. Paulikas, H.P. Hurinsit, M. Chan, J. Greeley, V. Stamenkovic and N. M. Markovic; “Trends in Activity for the Water Electrolyzer Reactions on 3d-M(Ni,Co,Fe,Mn)-Hydr(oxy)oxide Catalysts”; *Nature Materials*, DOI 10.1038/NMAT3313 (2012).
2. D.vanderVliet, C.Wang, D.Tripkovic, D.Strmcnik, A.P.Paulikas, N.M.Markovic, and V.R.Stamenkovic, “Unique Electrochemical Adsorption Properties of Pt-Skin Surfaces”, *Angewandte Chemie International Edition*, 51(2012)3139-3142.
3. R. Subbaraman, D. Tripkovic, D. Strmcnik, K-C. Chang, M. Uchimura, A. P. Paulikas, V. Stamenkovic and N. M. Markovic; “Enhancing Hydrogen Evolution Activity in Water Splitting by Tailoring L⁺-Ni(OH)₂-Pt Interfaces”; *Science*, **334** (2011) 1256-1260.

4. D. Strmcnik, D. van der Vliet, K-C. Chang, V. Komanicky, K. Kodama, H. You, V. R. Stamenkovic, N.M. Markovic; "Effects of Li^+ , K^+ , and Ba^{2+} Cations on the ORR at Model and High Surface Area Pt and Au Surfaces in Alkaline Solutions"; *J. Phys. Chem. Lett.*, **2** (2011) 2733-2736.
5. C. A. Lucas, P. Thompson, Y. Gründer, N. M. Markovic; "The structure of the electrochemical double layer: Ag(111) in alkaline electrolyte"; *Electrochemistry Communications*, **13** (2011) 1205-1208.
6. M. Escudero-Escribano, Z. Michoff, E.P. Leiva, N.M. Marković, N. M., C. Gutiérrez, A. Cuesta; "Quantitative Study of Non-Covalent Interactions at the Electrode–Electrolyte Interface Using Cyanide-Modified Pt(111) Electrodes"; *ChemPhysChem*, **12** (2011) 2230–2234.
7. B. Genorio, R. Subbaraman, D. Strmcnik, D. Tripkovic, V.R. Stamenkovic, N.M. Markovic; "Tailoring the Selectivity and Stability of Chemically Modified Platinum Nanocatalysts To Design Highly Durable Anodes for PEM Fuel Cells"; *Angew. Chem. Int. Ed.*, **123** (2011) 5582–5586.
8. B. Genorio, D. Strmcnik, R. Subbaraman, D. Tripkovic, G. Karapetrov, V. R. Stamenkovic, S. Pejovnik, N. M. Markovic; "Selective Catalysts for the Hydrogen Oxidation and Oxygen Reduction Reactions by Patterning of Platinum with Calix[4]arene Molecules"; *Nature Materials*, **9** (2010) 998–1003.
9. C. Stoffelsma, P. Rodriguez, G. Garcia, N. Garcia-Araez, D. Strmcnik, N. M. Markovic, M. T. Koper; "Promotion of the Oxidation of Carbon Monoxide at Stepped Platinum Single-Crystal Electrodes in Alkaline Media by Lithium and Beryllium Cations"; *J. Am. Chem. Soc.*, **132** (2010) 16127-16133.
10. D. Strmcnik, M. Escudero, K. Kodama, V.R. Stamenkovic, A. Cuesta, N.M. Markovic, "Enhanced Electrocatalysis of the Oxygen Reduction Reaction Based on Patterning of Platinum Surfaces with Cyanide"; *Nature Chemistry*, **2** (2010) 880-885.
11. R. Subbaraman, D. Strmcnik, V. Stamenkovic, N.M. Markovic, "O₂ Reduction at Three Phase Interfaces: A Case Study for Pt(hkl), Pt₃Ni(111) and High Surface Area Catalysts-Nafion Interfaces"; *PhysChemPhys.*, **11** (2010) 2825-2833.
12. R. Subbaraman, D. Strmcnik, V. Stamenkovic, N.M. Markovic, "Three Phase Interfaces at Electrified Metal-Solution Interfaces- Study of the Pt(hkl) - Nafion Interface"; *J. Phys. Chem. C*, **114** (2010) 8414-8422.
13. D. Strmcnik, N. Hodnik, S. B. Hocevar, D. van der Vliet, M. Zorko, V.R. Stamenkovic, B. Pihlar, N.M. Markovic, "Novel Method for Fast Characterization of High Surface Area Electrocatalytic Materials Using Carbon Fiber Microelectrode"; *J. Phys. Chem. C*, **114** (2010) 2640-2644.
14. D. Strmcnik, K. Kodama, D. van der Vliet, J. Greeley, V. Stamenkovic, N.M. Markovic, "The Role of Noncovalent Interactions in Electrocatalytic Fuel Cell Reactions on Platinum"; *Nature Chemistry*, **1** (2009) 466-472.
15. C. Lucas, P. Thomson, M. Cormack, A. Brownrigg, B. Fowler, D. Strmcnik, V. Stamenkovic, J. Greeley, A. Menzel, H. You, and N.M. Markovic; " Temperature-induced Ordering of Metal-adsorbates Structures at Electrochemical Interfaces", *J. Am. Chem. Soc.*, **131** (2009) 7654-7661.
16. H. Gasteiger and N.M. Markovic; " Just a Dream-or Future Reality ", *Science*, **324** (2009) 48-49.

Diamondoid Science and Applications

PIs: Nick Melosh, SIMES, SLAC

Thomas Devereaux, SIMES, SLAC

Hari Manoharan, Dept of Physics, Stanford University

Peter Scheiner, Dept of Chemistry, University of Giessen

ZX Shen, SIMES, SLAC

Program Scope

Diamondoids are unique new carbon-based nanomaterials consisting of 1-2 nanometer, fully hydrogen-terminated diamond particles (Fig 1). Unlike their conjugated counterparts, graphene or carbon nanotubes, the carbon atoms in diamondoids are sp^3 hybridized, leading to unique electronic and mechanical properties. Diamondoids behave much like small molecules, with atomic-level uniformity, flexible chemical functionalization, and systematic series of sizes, shapes and chiralities. At the same time diamondoids offer more mechanical and chemical stability than other small molecules, and vastly superior size and shape control compared to inorganic nanoparticles.

This program explores and develops diamondoids as a new class of functional nanomaterials based upon their unique electronic, mechanical, and structural properties. This includes diamondoid isolation from petroleum, chemical functionalization, and molecular assembly, as well as electronic, optical and theoretical characterization. We have currently focused on three areas of research: synthesis, electronic properties, and thin film growth. In particular the ability of these materials to control the flow of electrons and emitted electron energy at the molecular level is an exciting direction for mastering energy flow at the nanoscale.

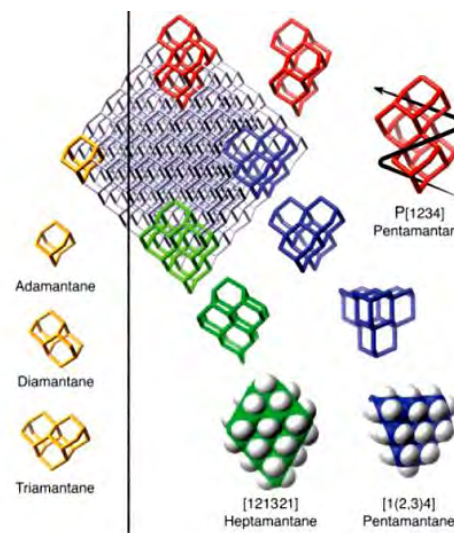


Fig 1. Molecular structures of diamondoids

Recent Progress

Based on the unique high van der Waals, low-entropy nature of the diamondoid molecules, our team was able to demonstrate extraordinarily sp^3 C-C bonds stable at high temperatures.¹ The strong van der Waals interactions between diamondoids supplanted some of

the normal C-C bond energy, enabling the bond to extend significantly from the normal 1.54 Å to 1.72 Å (Fig 2), and extraordinarily large increase that was stable up to 300°C. Supplanting some of the normal covalent bond energy for vdW forces may allow design of stable materials with more highly reactive bonds for catalysts and engineered molecules taking advantage of the ‘weak’ interactions in a way that was not possible without diamondoids.

We also discovered a remarkable application for diamondoids in X-ray PEEM imaging. Normally X-PEEM is limited by the chromatic dispersion (energy spread) of the electrons emitted by the sample. Only a few facilities have developed the multi-million dollar correction equipment necessary to achieve ~25 nm resolution with X-ray excitation. However, a single monolayer of diamondoids applied by simply dunking the sample in to a diamondoid thiol solution improved the X-PEEM resolution to <10 nm, without the use of any additional correction equipment (Fig. 3). This opens up the ability to do high resolution X-PEEM imaging on standard PEEM microscopes with very simple sample preparation. Our calculations show this result stems from the remarkable ability of diamondoids to strongly scatter and relax incident electrons to the diamondoid conduction band.

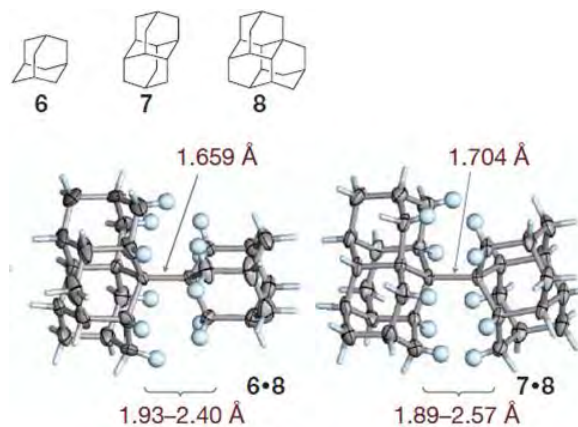


Fig 2. X-ray structures of three diamondoid conjugates with long central sp^3 bonds. Normal C-C alkane bonds are 1.54Å.

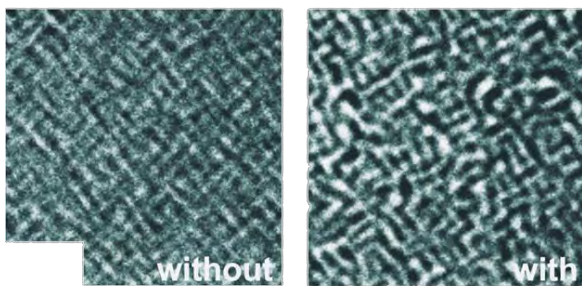


Fig 3. X-PEEM images of magnetic domains in a Co/Pd multilayer obtained at an acceleration voltage of 10kV with and without a diamondoid monolayer.

Previous research had shown that diamondoids can have exceptionally stable electron emission.² Building upon these results, we sought to create robust diamondoid enhanced field-emission guns required for commercial applications and understand its mechanism. Toward this goal, we demonstrated covalent attachment of diamondoids onto silicon and metal oxide surfaces and found that the unique monochromatic electron emission characteristic of diamondoids is retained for these surfaces. FTIR and XPS confirmed the presence of a diamondoid monolayer that is stable to ~400°C, sufficient for many gun applications. Electron field emission from diamondoid functionalized Au wires showed dramatic work function lowering (Fig 4). A new theoretical model had to be constructed to understand this phenomenon, which we attribute to localized diamondoid ionization. However, a simple charged parallel plate model did not fit the experimental data well. We then treated the full electric field emanating from a heterogeneously charged surface, and calculated the transmission coefficient

through this electrostatic landscape using the WKB approximation. This model agreed quite well with the experimental data and provides a model to understand emission from non-uniform surfaces.

The novel electronic properties of diamondoids also were observed in electronic transport through the molecules. Significantly reduced tunneling barriers were found for the larger diamondoids, but not adamantane or diamantane. This facile electron transport stimulated exploration of a new energy conversion architecture using photo-excited hot electrons to cross the insulating barrier in a metal-insulator-metal (MIM) structure. This phenomenon opens up new possibilities for photon to electron conversion for energy scavenging and photodetection.³

Our other substantial project was using diamondoids as seed particles for bulk diamond growth. Unlike detonation diamond seeds, diamondoids are nitrogen-impurity free and can be more uniformly distributed at higher density. With a simple diamondoid seed layer, we were able to synthesize small (~5-20 nm) diamond nanoparticles at high density at low temperatures (~400°C). Growths seeded with other carbon sources, such as C60 or alkanes, did not show any growth under these conditions, confirming diamondoids are critical for low temperature diamond growth.

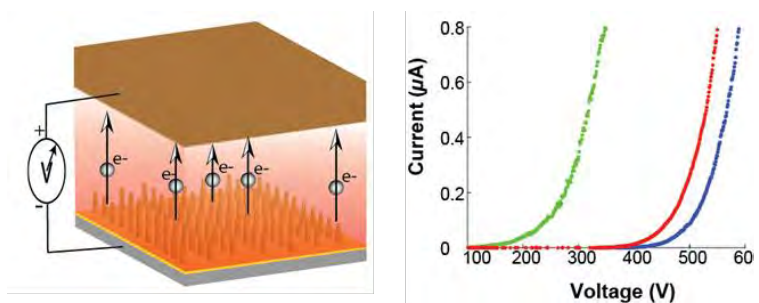


Fig 4. Field emission geometry and current-voltage emission results with bare gold (red, blue curves), and diamondoid monolayers (green curve).

Future Plans

We are focusing on four main thrust directions based on our previous results: robust monochromatic electron emission, high-density diamond growth, very small diamond nanoparticles for nitrogen-vacancy (NV) centers, and new diamondoid synthetic constructs, such as metal-oxide frameworks (MOFs). The rigid structure of the diamondoids may allow for rational design of new classes of MOFs based on their steric packing and the large vdW forces observed. These structures could have unique properties such as confined optical absorption quantum effects, superconductivity, or energy storage capacity. The size of the diamondoids would restrict the manner in which they can pack, allowing specific structures to be designed by picking particular diamondoids. Bulk diamond synthesis based on a diamondoid seed layer is a highly promising way to achieve very high diamond seeding density, thin diamond films, and NV-centers in diamond nanoparticles. We have shown growth of small diamond particles from seed diamondoid monolayers, and will extend these efforts to create even smaller nanoparticles (<5 nm) that are highly coveted for NV magnetic detectors. We plan to implant N into the

diamond nanoparticles and anneal to create optically active NV centers, and explore their opto-magnetic properties.

Our results on electron field emission show enormous promise for robust electron sources, thus we plan on pursuing this avenue and understand the failure mechanisms. This is critical both for commercial applications for partners such as KLA-Tencor, and for advanced electron guns such as at the national labs, such as LCLS. From our most recent results, we believe the diamondoids become positively charged during emission, lowering the surface workfunction. To improve emission further, a larger fraction of the molecules should become charged. We will study the field emission properties under direct photo-ionization, which should provide very high emission current and brightness.

References

1. Peter R. Schreiner, Lesya V. Chernish, Pavel A. Gunchenko, Evgeniya Yu. Tikhonchuk, Heike Hausmann, Michael Serafin, Sabine Schlecht, Jeremy E. P. Dahl, Robert M. K. Carlson, Andrey A. Fokin, "Overcoming lability of extremely long alkane carbon-carbon bonds through dispersion forces", *Nature*, 308-311, 2011
2. W. L. Yang, **J. D. Fabbri**, T. M. Willey, J. R. I. Lee, J. E. Dahl, R. M. K. Carlson, P. R. Schreiner, A. A. Fokin, B.A.Tkachenko, N. A. Fokina, W. Meevasana, N. Mannella, K. Tanaka, X. J. Zhou, T. v. Buuren, M. A. Kelly, Z. Hussain, N. A. Melosh, Z.-X. Shen. "Monochromatic Electron Emission from Negative Electron Affinity Diamondoid Monolayers," *Science* Vol. 315, pp. 1460-1462, 2007.
3. Wang, F. and N.A. Melosh, "Plasmonic energy collection through hot carrier extraction" *Nano Letters*, 11, p. 5426-30, 2011

Publications

- Peter R. Schreiner, Lesya V. Chernish, Pavel A. Gunchenko, Evgeniya Yu. Tikhonchuk, Heike Hausmann, Michael Serafin, Sabine Schlecht, Jeremy E. P. Dahl, Robert M. K. Carlson, Andrey A. Fokin, "Overcoming lability of extremely long alkane carbon-carbon bonds through dispersion forces", *Nature*, 308-311, 2011
- Clay, W.A., T. Sasagawa, A. Iwasa, Z. Liu, J.E. Dahl, R.M.K. Carlson, M. Kelly, N.A. Melosh, and Z. Shen, "Photoluminescence of Diamond Crystals" *Journal of Applied Physics*, 2011
- Wang, F. and N.A. Melosh, "Plasmonic energy collection through hot carrier extraction" *Nano Letters*, 11, p. 5426-30, 2011

Fuming, W. and N.A. Melosh, "Theoretical analysis of hot electron collection in metal-insulator-metal devices" Proceedings of the SPIE - The International Society for Optical Engineering, 8111, 2011

Gold's Ability to Bridge Classes of Metal-Rich "Electron Compounds": From Polar Intermetallics to Hume-Rothery Phases and Quasicrystals

Gordon J. Miller, John D. Corbett, Qisheng Lin, and Srinivasa Thimmaiah
Ames Laboratory and Iowa State University, Ames, Iowa 50011

Program Scope. To address the grand challenge of designing and perfecting the atom-efficient syntheses of revolutionary forms of matter with tailored properties, e.g., thermoelectric, magnetocaloric, or catalytic, we focus on the discovery and characterization of complex metal-rich solids to identify the significant chemical bonding features that stabilize their structures and influence their properties. Compound classes of interest span Zintl-type, cluster-based, Hume-Rothery-type, polar intermetallics, quasicrystalline and their approximants, and complex metallic alloys, among other (often unanticipated) possibilities, and many of these show pseudogaps in their electronic densities of states (DOS). The valence electron counts at which such pseudogaps occur are a frequent diagnostic for "stable" structures because this region of the DOS often separates occupied metal-metal bonding states from corresponding unoccupied antibonding states. Moreover, identifying pseudogaps in DOS curves often allows chemical tuning by combining appropriate mixtures of elements, thereby uncovering potentially interesting physical properties that depend on large changes of the DOS with respect to energy.

Recent exploratory syntheses of Au-rich polar intermetallics have established the substantial roles for gold in stabilizing new phases that display many fascinating structural motifs and unprecedented compositions.^{1,2} Unlike Au-poor phases, in which Au atoms are often segregated within polyanionic clusters or networks, Au-rich polar intermetallics contain Au aggregates, such as condensed Au₄ tetrahedra, 1-D rods of hexagonal stars, 2-D undulating layers, and 3-D diamond-like frameworks, all of which have resulted from our broader research portfolio. These Au fragments are reminiscent of small isolated, charged or neutral gold clusters found in the gas phase or solutions, e.g., Au_n⁻ (*n* = 1-4), Au₇, Au₁₁, Au₁₅₋₁₉, Au₂₀, etc. and of colloidal or nanocrystalline gold with beautiful shapes. Thus, the availability of various Au fragments in intermetallics may open new insights to bridging the science from atoms to clusters and to bulk materials. Also, such Au-rich polar intermetallics may exhibit interesting catalytic properties. From the viewpoint of metal-metal bonding, the study of Au-rich phases may foster new ideas for materials that are electronically positioned between electron-poor, polar intermetallics and the noble-metal Hume-Rothery phases.

Recent Progress. Ongoing productive explorations of diverse, ternary alkali-metal-gold systems containing the post-transition elements, Zn, Cd, Ga, In, Tl, Si, Ge, or Sn, benefit from strong bonding between Au and these post-transition elements. Large contributions of Au to bond populations via relativistic effects seem particularly important for stabilizing many novel, often unprecedented, compositions and structures. The new phases are typically valence electron-poor with valence electron per atom (*e/a*) ratios of ~1.4 to ~2.2. Marked differences are found among (Na, K, Rb, Cs)-Au-*Di* phases for *Di* = Cd or Zn; Cd yields a variety of new structures whereas Zn gives only two with very unusual ordering of Na ions in 1-D tunnel structures. Contrasting Au-transition metal phases include the open-shell, antiferromagnetically ordered Y₃MnAu₅ and Nd₄Mn₃Au₁₀. Other (alkali-metal)_{0.55}Au₂Ga₂ and related Zn or In phases exhibit extensive but different degrees of disorder of the cations within parallel 1D tunnels in the Au-Ga, etc. frameworks, reminiscent of zeolites. Early impressions of the substitutions of Pt, the immediate predecessor of Au, in such ternary intermetallics are that the Pt chemistry is quite different from that of Au.

Our recent systematic investigations of alkali metal–Au–Ga systems, and the Na–Au–Ga case in particular, led to the discoveries of two new polar intermetallic phases, $\text{Na}_{0.56}\text{Au}_2\text{Ga}_2$ and $\text{Na}_{13}\text{Au}_{41.2}\text{Ga}_{30.3}$, with tunnel-like structural motifs. In general, alkali metal content of stable phases is limited to lower than 35 at. % (Fig. 1). Further explorations near 33 at % Na have uncovered an icosahedral quasicrystalline phase (Fig. 2) and two, distinct Bergman type approximants. These two are: (a) conventional Bergman-type (CB) structures $\text{Na}_{26}\text{Au}_x\text{Ga}_{54-x}$ ($x \approx 18.1\text{--}19.5$), which feature empty innermost icosahedra, and (b) new stuffed Bergman-type (SB) type structures $\text{Na}_{26}\text{Au}_y\text{Ga}_{55-y}$ ($y \approx 35.2\text{--}36.0$), which contain Ga-centered innermost icosahedra. Although each approximant shows a considerable phase width, they do not merge into a continuous solid

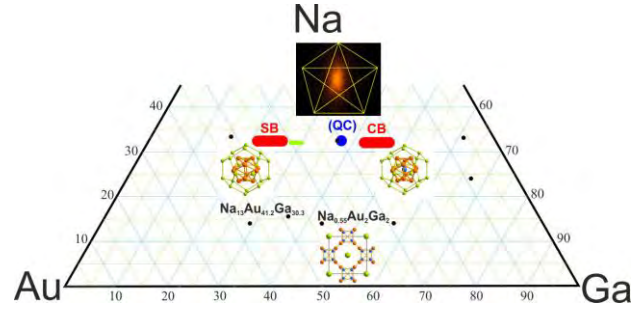


Fig. 1. Selected phases identified in the Na–Au–Ga system, including mixtures studied to elucidate the existence of icosahedral quasicrystalline phases. Compositions showing conventional (CB) and stuffed (SB) Bergman type phases are noted in red, and a new quasicrystalline phase (QC) in blue.

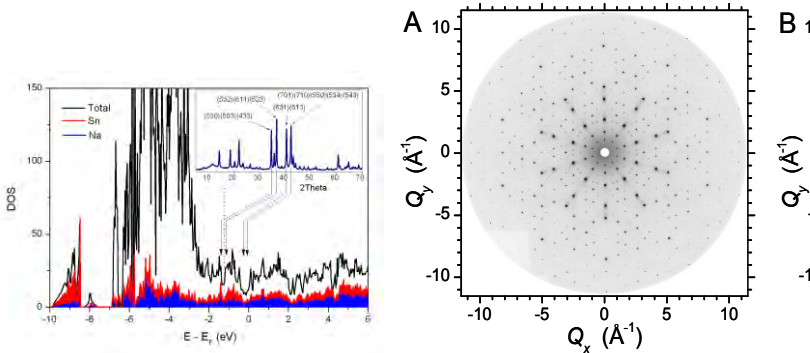


Fig. 2. (Left) Electronic DOS curve of Bergman Na–Au–Ga phases emphasizing pseudogaps and their correlation with largest structure factors. (Right) Zero-level, high-energy precession images of the fivefold reciprocal planes of the single-grain Na–Au–Ga quasicrystal.

curves that arise from the interactions between Fermi surfaces and Brillouin zones boundaries corresponding to strong diffraction intensity.

Another class of Hume-Rothery electron phases is the γ -brasses, which contain condensed metal icosahedra and occur in the e/a range of 1.59 to 1.75.³ To achieve these e/a values, we find that these structurally robust compounds use both mixed metal and non-stoichiometric site occupancies. Depending upon composition and e/a values, therefore, γ -brasses may exhibit specific atomic ordering patterns, e.g., cubic $2 \times 2 \times 2$ superstructures involving ordered vacancies, commensurately modulated superstructures, and cubic-rhombohedral distortions. In particular, ordered vacancies and mixed metal site occupancies significantly influence the occurrence of γ -brass superstructures in Pd–Zn–Al and Pd–Au–Zn systems.

The cluster centering and Au/Ga coloring correlate with the sizes of neighboring icosahedra, the size ratios between electropositive and electronegative components, and the valence electron count per atom (e/a values). According to theoretical calculations, the Bergman-type phases and, presumably, the quasicrystal all belong to Hume-Rothery electron phases, with evident pseudogaps in the DOS

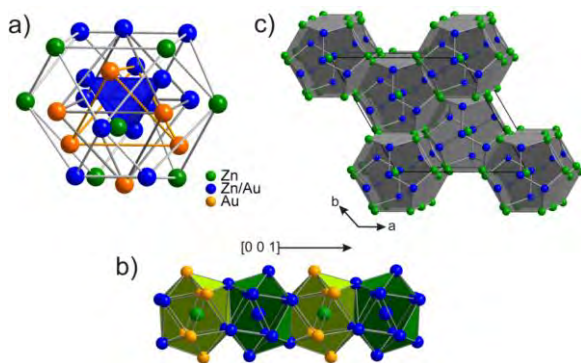


Fig. 3. Different representations of γ - Au_5Zn_8 . (a) 26-atom cluster; (b) Chain of face-shared icosahedra centered by Zn and Zn/Au atoms; and (c) 3-D network of Zn1-centered pentagonal dodecahedra, inner icosahedra omitted.

electronegativity, as revealed by recent Au substitutions into γ - Cu_9Al_4 , and previous work on γ - Cu_5Zn_8 .⁴ Although replacing Cu with Au does not change e/a values, there are significant differences in electronegativity and size between Au and Cu. Cu_9Al_4 has two distinct 26-atom clusters, $[\text{Cu}_{14}\text{Al}_{12}]$ and $[\text{Cu}_{22}\text{Al}_4]$. $\text{Cu}_{9-x}\text{Au}_x\text{Al}_4$ ($x < 5$) shows specific site occupancies for Au, linearly increasing lattice constants on increasing Au content, and, again, broad pseudogaps in the electronic DOS curves near their Fermi levels.

Future Plans. On-going explorations and characterization of novel, even unanticipated metal-rich phases will continue to employ synthesis, diffraction, and electronic structure calculations synergistically. Wider-ranging goals include:

- (a) To materially expand the fraction of the periodic table for which ternary intermetallic compound formation has been examined, and from this, to expand our knowledge of unprecedented intermetallic compositions, structures, and properties. About 61 elements are stable (semi)metals, and even half of the independent ternary combinations still amount to over 10^4 ternary systems! The simplest of searches would seem to still require good control of stoichiometry and some pains-taking care. The beginnings of broader searches are planned among alkaline-earth or rare-earth metal–gold–late metal systems. Also, we will explore Li-rich systems, a relatively poorly studied territory, to provide fundamental knowledge in understanding and material design for the next generation Li-ion battery anode materials.
- (b) To establish chemical guidelines for pseudogaps or full gaps in electronic DOS curves of metal-rich systems. Electronic pseudogaps, precursors of actual band gaps, are signatures of special, and often somewhat obscure, electronic effects and special stabilities in the solid state. Furthermore, they may also presage important physical phenomena, such as greatly diminished electrical conductivities, possible superconductivity, and potential thermoelectric behavior, depending on the location of the Fermi level with respect to this pseudogap. Density functional calculations on certain ‘pregnant’ structural examples may predict pseudogap locations well enough that subsequent compositional tuning to these points turn up such phases with different but electronically related structures. Electron-poor phases around not only quasicrystal, approximant systems but untested phases may be good bets. Such rigid band predictions more or less across a phase transition seem to be meaningful, at least among related multiply-endohedral structural examples.

Efforts to understand the γ -phase region of the Au-Zn system, i.e., 30 to 42 at.% Zn, reveal that γ - Au_5Zn_8 exhibits a rhombohedral distortion from the cubic type seen for isoelectronic γ - Cu_5Zn_8 with vacancies occurring on two specific sites and e/a ratios between 1.64 and 1.66. The electronic DOS curve shows a clear pseudogap at the Fermi level for “ Au_5Zn_8 ” as the representative composition, an outcome which is consistent with the Hume-Rothery interpretation of γ -brass.

The structural chemistry of γ -brasses also depends on atomic size and

References

1. J.D. Corbett, "Exploratory Synthesis: The Fascinating and Diverse Chemistry of Polar Intermetallic Phases," *Inorganic Chemistry*, **49**, 13 (2010).
2. G.J. Miller, "Metal-Rich Chemistry of the *d*-Metals," *Comprehensive Inorganic Chemistry*, 2012, in press.
3. U. Mizutani, *Hume-Rothery Rules for Structurally Complex Alloy Phases*, Taylor & Francis, New York: 2010.
4. O. Gourdon, et al., "Atomic Distributions in the γ -Brass Structure of the Cu-Zn System," *Inorg. Chem.* **2007**, *46*, 251.

Selected Publications (2010-2012)

- J.D. Corbett, "Exploratory Synthesis: The Fascinating and Diverse Chemistry of Polar Intermetallic Phases," *Inorg. Chem.*, **49**, 13 (2010). (Cover Article) (Award article)
- S.J. Kim, G.J. Miller, J.D. Corbett, "Zigzag Chains of Alternating Atoms in A_2AuBi ($A = Na, K$) and K_2AuSb . Synthesis, Structure, and Bonding," *Z. Anorg. Allg. Chem.*, **636**, 67 (2010).
- H. Ko, O. Gourdon, D. Gout, E.D. Mun, S. Thimmaiah, G.J. Miller, "Rhombhedrally Distorted γ -Brasses $Cr_{1-x}Fe_xGa$," *Inorg. Chem.*, **49**, 11505 (2010).
- B. Li, S.J. Kim, G.J. Miller, J.D. Corbett, " $K_{23}Au_{12}Sn_9$ -An Intermetallic Compound Containing a Large Gold-Tin Cluster: Synthesis, Structure, and Bonding," *Inorg. Chem.*, **49**, 1503 (2010).
- Q.S. Lin and J.D. Corbett, "Multiple Nonstoichiometric Phases with Discrete Composition Ranges in the $CaAu_5$ - $CaAu_4Bi$ - $BiAu_2$ System. A Case Study of the Chemistry of Spinodal Decomposition," *J. Am. Chem. Soc.*, **132**, 5662 (2010).
- S. Thimmaiah and G.J. Miller, "On the Structural Chemistry of γ -Brasses: Two Different Interpenetrating Networks in Ternary *F*-Cell Pd-Zn-Al Phases," *Chem. Eur. J.*, **16**, 5461 (2010).
- J.C. Dai, S. Gupta, J.D. Corbett, "Synthesis, Structure, and Bonding of $BaTl_4$. Size Effects on Encapsulation of Cations in Electron-Poor Metal Networks," *Inorg. Chem.*, **50**, 238 (2011).
- S. Thimmaiah, M.-K. Han, G.J. Miller, " $Zn_{13}(Cr_xAl_{1-x})_{27}$ ($x = 0.34-0.37$): A New Intermetallic Phase Containing Icosahedra as Building Units," *Z. Kristallogr.*, **226**, 557 (2011) (Cover Article).
- S. Samal and J. D. Corbett, "Relativistic Effects and Gold Site Distributions: Synthesis, Structure and Bonding in a New Polar Intermetallic $Na_6Cd_{16}Au_7$," *Inorg. Chem.* **50**, 7033 (2011).
- J. D. Corbett, "Intermetallic Studies and Bonding Concepts" (Viewpoint), *Eur. J. Inorg. Chem.* 3821 (2011).
- S. Thimmaiah, N.A. Crumpton, G.J. Miller, "Crystal Structures and Stabilities of γ - and γ' -Brass Phases in $Pd_{2-x}Au_xZn_{11}$ ($x = 0.2-0.8$): Vacancies vs. Valence Electron Concentration," *Z. Anorg. Allg. Chem.*, **637**, 1992, (2011).
- V. Smetana, J. D. Corbett, G. J. Miller, "Four Polyanionic Compounds in the K–Au–Ga System: A Case Study in Exploratory Synthesis and of the Art of Structural Analysis", *Inorg. Chem.* **51**, 1695 (2012).
- S. Gupta and J. D. Corbett, " $BaAu_xZn_{13-x}$: An Electron-Poor Cubic $NaZn_{13}$ -type Intermetallic and its Ordered Tetragonal Variant," *Inorg. Chem.* **51**, 2247 (2012).

Nuclear Magnetic Resonance

**Dr. Alexander Pines, Senior Scientist,
Materials Sciences Division, Lawrence Berkeley National Laboratory, Berkeley, CA**

1.0 Program Scope: The Nuclear Magnetic Resonance (NMR) program seeks to enhance the capabilities of NMR and MRI in the study of the molecular structure, chemistry, and dynamics of materials on length scales ranging from the nanoscopic to the macroscopic. The program is comprised of several complementary and interdependent components. The first is the development of **new theoretical methods** that treat the interaction of spins with each other and with other degrees of freedom, yielding new experiments. The second is their development and demonstration, almost always involving the **construction of unique instrumentation**, and, in some cases, micro- and nanofabrication of novel materials and substrates. Finally, we seek to apply these methods to **exemplary problems in physics, chemistry, materials science, and nanoscience**, drawn from the portfolio of possibilities presented by other MSD investigators, collaborators, and industrial laboratories. It is the unique environment of interdisciplinary research and large-scale instrumentation capabilities at the Lawrence Berkeley National Laboratory that cultivates these innovations, their diverse applications, and the rapid transfer of this technology to industry.

2.0 Recent Progress

2.1 Marriage of Optical Spectroscopy and Magnetic Resonance: While optical spectroscopy is sensitive enough to detect single molecules, it lacks the chemical sensitivity of NMR; conversely, NMR is extraordinarily sensitive to chemistry, but typically detects macroscopic ensembles of nuclei. A major thrust of our research program has been the development of experiments that marry the two techniques, preserving the sensitivity of optical spectroscopy and the chemical discrimination of NMR. We accomplish this through engineering systems in which the optical and magnetic degrees of freedom are coupled. Our recent progress has involved: (a) the **application of new instrumentation based on alkali vapor magnetometers** (see 2.2) and (b) the **engineering of novel diamond-based substrates that harbor defects in which optical and magnetic degrees of freedom are coupled, and their use as NMR detectors.**

2.2 Chemical Analysis of Materials by NMR in Low and Zero Magnetic Fields: We have explored magnetic resonance methodologies using alkali-metal atomic magnetometers, which, unlike established techniques, do not require high-field magnets or cryogens. We have also demonstrated **magnet-free NMR chemical analysis by J-spectroscopy** using a magnetometer based on a microfabricated chip-scale atomic vapor cell, distinguishing complex organic molecules. Finally, we have demonstrated **optically-detected analogues of Earth's magnetic field relaxometry experiments which form the bulk of industrial MRI applications.**

2.3 Xenon-based Molecular Sensors: We have invested the physical properties of xenon-based molecular NMR sensors to enhance their potential **for sensitive detection and recognition of**

molecules and materials. By covalently attaching individual sensor molecules to self-assembling scaffolds, we have dramatically increased the environmental compatibility, robustness, and sensitivity of these sensors, demonstrating the ability to **detect molecules in the environment at ~700 femtomolar concentration.** We have also demonstrated the ability to produce such sensors in a **combinatorial library** process.

2.5 Microfabrication & Remote Detection of NMR and MRI: A long-standing goal of our field has been the development of **portable analogues of ubiquitous, laboratory-scale NMR and MRI** instrumentation. In particular, our remote detection technique is an enabling ingredient in microfabricated, portable NMR. Using remote detection, a method by which a **single generic NMR/MRI detector can give parallel MRI images of any microfluidic geometry without modification,** we have demonstrated that high resolution MRI and NMR is possible on microfluidic devices. We have applied this technique to the measurement of **confined microfluidic flow in microscopic detail, to packed bed microreactors, and to chromatographic separations.**

2.6 Technology Transfer & Dissemination: Our recent efforts have resulted in one provisional patent application, five intellectual property disclosures, and the licensing of one invention to a start-up company. Spin-off research based on DOE-funded technology in this program has attracted industrial funding. We were awarded an **R&D 100 Award in 2011 for “Magnetic Resonance Microarray Imaging.”**

3.0 Future Plans

3.1 Marriage of Optical Spectroscopy and Magnetic Resonance: While continuing to apply the technology of alkali vapor magnetometers, we will improve the sensitivity and resolution of **solid-state, diamond-based magnetic field sensors for microfluidic applications.** We will accomplish this by optimizing the materials properties of the defect-harboring diamonds, produced by CVD and ion implantation, and by developing new quantum control and sensing methodologies. We are also constructing a diamond-based MRI microscope, capable of **chemical imaging materials on small (~100 nm) length scales.** This requires our collaboration with LBNL’s Molecular Foundry to engineer and pattern diamond substrates and probes for AFM-style microscopes. Finally, using the same coupled magneto-optical substrates, we are working on methods that **will transfer the polarization of optical photons to NMR (spin) degrees of freedom,** enhancing the sensitivity of NMR experiments.

3.2 Chemical Analysis by NMR in Low and Zero Magnetic Fields: Modern NMR is particularly successful because of correlation experiments in which chemical features are resolved in many spectral dimensions. We intend to develop **multidimensional techniques for J-based chemical analysis** in the absence of a magnetic field, using alkali vapor magnetometers. This will involve the development of **new theory and pulse sequences, and also new instrumentation** capable of executing multiple pulse NMR experiments.

3.3 Xenon-based Molecular Sensors: We are designing sensors to explore a broad range of chemical, analytical, and materials properties. These include sensors with chemical targeting groups produced through combinatorial assays, and **entirely new sensor platforms with improved fidelity and resolution, or which operate on magnetic resonance dimensions other than the chemical shift.** We are also pursuing applications of **sensors arrays in portable devices** for the non-perturbing analysis of fluids.

3.4 Microfabrication & Remote Detection of NMR and MRI: We are combining remote detection, optical magnetometry, and NMR molecular sensing, in microfabricated, micromagnetic devices that serve as **platforms for portable chemical analysis.** Novel instrumentation includes the technology for building NMR-based, functionalized microfluidic devices using soft lithography, and the development of a **microfabricated, chip-scale xenon polarizer that produces hyperpolarized xenon gas.** Methodological innovations include our development of robust techniques for the collection of multidimensional MRI images in reduced time, using a combination of compressive sampling, static (micromagnetic) position encoding (similar to an NMR “bar code), and spatial multiplexing (single scan MRI). Finally, we continue to apply intermediate elements of this portable MRI sensing platform to analytical and materials problems of interest to the DOE.

References & Publications

1. Thomas Theis, Micah P. Ledbetter, Gwendal Kervern, John W. Blanchard, Paul J. Ganssle, Mark C. Butler, Hyun D. Shin, Dmitry Budker, and Alexander Pines, [Zero Field NMR Enhanced by Parahydrogen in Reversible Exchange](#), *J. Am. Chem. Soc.*, **134 (9)**, 3987-3990 (2012)
2. M.P Ledbetter, T. Theis, J.W. Blanchard, H. Ring, P. Ganssle, S. Appelt, B. Blumich, A. Pines, and D. Budker, [Near-Zero-Field Nuclear Magnetic Resonance](#), *Phys. Rev. Lett.* **107 (10)**, 107601 (2011).
3. Thomas Z. Teisseyre, Jiri Urban, Nicholas W. Halpern-Manners, Stuart D. Chambers, Vikram S. Bajaj, Frantisek Svec, Alexander Pines, [Remotely Detected NMR for the Characterization of Flow and Fast Chromatographic Separations Using Organic Polymer Monoliths](#), *Anal. Chem.* **83 (15)**, 6004-6010 (2011).
4. David J. Michalak, Shoujun Xu, Thomas J. Lowery, C.W. Crawford, Micah Ledbetter, Louis-S. Bouchard, David E. Wemmer, Dmitry Budker, Alexander Pines, [Relaxivity of Gadolinium Complexes Detected by Atomic Magnetometry](#), *Mag. Res. Med.* **66** 605-608, (2011).
5. T. Theis, P. Ganssle, G. Kervern, S. Knappe, J. Kitching, M.P. Ledbetter, D. Budker, A. Pines, [Parahydrogen-enhanced zero-field nuclear magnetic resonance](#), *Nature Physics* **7**, 571-575 (2011).
6. N. Halpern-Manners, J. Paulsen, V. Bajaj, A. Pines, [Remotely Detected MRI Velocimetry in Microporous Bead Packs](#), *J. Phys. Chem. A* **115 (16)** 4023-4030, (2011).
7. David Trease, Vikram S. Bajaj, Jeffrey Paulsen, Alexander Pines, [Ultrafast Optical Encoding of Magnetic Resonance](#), *Chemical Physics Letters* **503**, 187-190 (2011). COVER ARTICLE

8. S. J. Seltzer, D. J. Michalak, M. H. Donaldson, M. V. Balabas, S. K. Barber, S. L. Bernasek, M.-A. Bouchiat, A. Hexemer, A. M. Hibberd, D. F. Jackson Kimball, C. Jaye, T. Karaulanov, F. A. Narducci, S. A. Rangwala, H. G. Robinson, A. K. Shmakov, D. L. Voronov, V. V. Yashchuk, A. Pines, and D. Budker, [Investigation of antirelaxation coatings for alkali-metal vapor cells using surface science techniques](#), *Journal of Chemical Physics* **33**, 144703 (2010).
9. V. Bajaj, J. Paulsen, E. Harel, A. Pines, [Zooming in on Microscopic Flow by Remotely Detected MRI](#), *Science* **330(6007)**, 1078-1081 (2010).
10. Franz Schilling, Leif Schroeder, Krishnan Palaniappan, Sina Zapf, David Wemmer, Alexander Pines, [MRI Thermometry Based on Encapsulated Hyperpolarized Xenon](#), *ChemPhysChem* **11(16)**, 3529-3533 (2010). COVER ARTICLE
11. T. Meldrum, L. Schröder, P. Denger, D. Wemmer, A. Pines, [Xenon-based molecular sensors in lipid suspensions](#), *J. of Magn. Reson.*, **205(2)**, 242-246 (2010). COVER ARTICLE
12. J. Paulsen, V.S. Bajaj, A. Pines, [Compressed Sensing of Remotely Detected MRI Velocimetry in Microfluidics](#), *J. Mag. Reson.* **205(2)**, 196-201 (2010).
13. T. Meldrum, K.L. Seim, V.S. Bajaj, K.K. Palaniappan, W. Wu, M.B. Francis, D.E. Wemmer, and A. Pines, [A Xenon-Based Molecular Sensor Assembled on an MS2 Viral Capsid Scaffold](#), *J. Am. Chem. Soc.* **132 (17)**, 5936-5937 (2010).
14. N.W. Halpern-Manners, V.S. Bajaj, T.Z. Teisseyre, and A. Pines, [Magnetic Resonance Imaging of Oscillating Electrical Currents](#), *PNAS* **107 (19)**, 8519-8524 (2010).
15. John M. Franck, Vasiliki Demas, Rachel W. Martin, Louis-S. Bouchard, Alexander Pines, [Shimmed Matching Pulses: Simultaneous Control of RF and Static Gradients for Inhomogeneity Correction](#), *Journal of Chemical Physics* **131 (23)**, 234506 (2009).
16. Xin Zhou, Dominic Graziani, and Alexander Pines, [Hyperpolarized Xenon NMR and MRI Signal Amplification by Gas Extraction](#), *Proc. of the Nat. Acad. Sci.* **106 (40)**, 16903-16906 (2009).
17. Nathan Kelso, Seung-Kyun Lee, Louis-S. Bouchard, Vasiliki Demas, Michael Mueck, Alexander Pines, John Clarke, [Distortion-Free Magnetic Resonance Imaging in the Zero-Field Limit](#), *Journal of Magnetic Resonance* **200 (2)**, 285-290 (2009).
18. M.P. Ledbetter, C.W. Crawford, A. Pines, D.E. Wemmer, S. Knappe, J. Kitching, D. Budker, [Optical Detection of NMR J-Spectra at Zero Magnetic Field](#), *Journal of Magnetic Resonance* **199 (1)**, 25-29 (2009).
19. V. Demas, J.M. Franck, L.S. Bouchard, D. Sakellariou, C.A. Meriles, R. Martin, P.J. Prado, A. Bussandri, J.A. Reimer, A. Pines., ['Ex Situ' Magnetic Resonance Volume Imaging](#), *Chemical Physics Letters* **467 (4-6)**, 398-401 (2009).
20. Louis-S. Bouchard, M. Sabieh Anwar, Gang L. Liu, Byron Hann, Z. Harry Xie, Joe W. Gray, Xueding Wang, Alexander Pines, Fanqing Frank Chen, [Picomolar sensitivity MRI and photoacoustic imaging of cobalt nanoparticles](#), *Proc. of the Nat. Acad. Sci.*, **106 (11)**, 4085-4089 (2009).

Title: Hydroxide Conductors for Energy Conversion Devices

Investigators: Bryan Pivovar (PI), Clay Macomber, Chai Engtrakul, Hai Long, National Renewable Energy Lab; Jim Boncella, Joe Edson, Los Alamos National Lab

Program Scope

There is significant current interest in hydroxide conductors for energy conversion devices, driven largely by their ability to perform efficiently and durably with non-Pt group metal (PGM) catalysts, a major concern for current proton exchange membrane (PEM) fuel cells. This project focuses on the fundamental study of hydroxide conductors for use in anion exchange membranes (AEMs). Our purpose is to evaluate the potential of anion exchange membranes as enabling components of next-generation energy conversion devices with a focus on alkaline membrane fuel cells (AMFCs) and electrolyzers. To date, our work has had a heavy focus on the chemical stability of covalently tetherable cations (the functional component of AEMs), a critical concern for requisite durability of target devices.

Beyond non-PGM catalysis, other advantages of AMFCs include increased material stability at high pH, increased electrocatalytic activity, increased fuel choices, and decreased fuel crossover rates/potentially improved water management (arising from electro-osmotic drag and the flux of hydroxide ions in the opposite direction of protons in traditional PEM fuel cells). Conversely, alkaline systems have been perceived to be limited in terrestrial applications owing to carbonate formation from CO₂ in air. Liquid KOH is susceptible to carbonate precipitation, which prevents ion transport. However, a membrane-based alkaline system would prevent precipitates from forming, although issues with carbonate displacing hydroxide must be considered. An additional difficulty with aqueous KOH systems is using a corrosive, liquid electrolyte as a cell separator and ion conductor. Water management for these systems also can be more difficult because water is consumed in the cathode reaction.

Our project has focused heavily on fundamental investigation and quantification of reaction products, mechanisms, and rates for covalently tetherable cations with hydroxide through accelerated testing methods. Our early efforts in this area determined that traditional (substituted ammonium) cations had much higher stability than was perceived in the scientific community.¹⁻⁹ In exploring the better-than-anticipated durability of traditional cations, we established the importance of hydration level and an ylide mechanism on cation degradation.²⁻⁴ Our approach has been centered on highly coupled experimental and modeling efforts to produce mechanistic understanding of degradation reactions and rates as a function of chemical composition; the goal is to use this knowledge to select and design cations of enhanced stability. The project has also included chemical synthesis, as necessary, because several of the cations studied are not commercially available.

Recent Progress

Our studies have had a heavy focus on substituted trimethylammonium (TMA⁺) cations as candidates for use in AEMs. If ammonium cations were acceptable from the standpoint of durability, they would be ideal cations because they are easily tetherable to a polymer matrix, have well established (simple, cheap) synthesis routes, and are reasonably strong bases. Trimethyl substitution is predicated on methyl being the simplest ammonium substituent, due to its lack of susceptibility to Hofmann elimination (no β -H's), and concerns about cation size and hydrophobicity that would make attempts to use other larger groups (i.e., neopentyl, benzyl) potentially more problematic when applied to multiple sites. Additionally, small cation substituents have advantages in computational studies, allowing for more simulations and higher

fidelity to be probed and thus providing a better opportunity to screen different computational approaches for relevance and obtain better agreement between model and experiment.

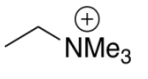
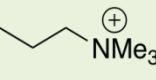
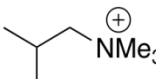
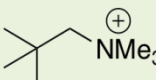
Our approach has been to explore specific cation families with systematic substitution to elucidate key factors that impact reaction mechanisms and rates. Table 1 summarizes the different cation families explored, the approaches employed, and the rationale for the studies.

Table 1: Summary of cation families investigated

Cation Family	Approaches Employed	Rationale
Substituted TMA ⁺ (varying number of β -H's) ¹⁰	Thorough experimental (wet and dry), including isotopic and computational studies.	Systematically probe Hofmann elimination by altering number of sites available and steric hindrance. Strong implications for tethering strategies.
Functionalized benzyITMA ⁺	Thorough experimental (wet and dry), including isotopic and computational studies.	Systematically probe impact of electron withdrawing/donating groups on stability. Modification of the most commonly employed cation.
Substituted TMA ⁺ (alkyl chain length) ¹¹	Reasonable computational and experimental studies.	Investigation of steric and electronic effects related to alkyl chain length. Strong implications for tethering strategies.
“Advanced” cations	Preliminary computational and experimental studies.	Guidance on systems to investigate, stability expectations.

The number of β -hydrogen atoms susceptible to Hofmann elimination were systematically varied for a series of substituted TMA⁺ cations (ethyl, n-propyl, isobutyl, and neopentyl abbreviated ETMA⁺, PTMA⁺, ITMA⁺, and NTMA⁺, respectively).¹⁰⁻¹¹ Table 2 summarizes our experimental and computational findings.

Table 2: Experimental and computational results for varying number of β -hydrogen atoms

Cation		# of β -H's	Ylide Scrambling	Hofmann Elimination	S _N 2 Attack	Peak Decay (°C)	ΔG^\ddagger Hofmann (kcal/mol)	ΔG^\ddagger S _N 2 (kcal/mol)
	ETMA ⁺	3	Yes	Yes	No	60	17.5	24.7
	PTMA ⁺	2	Yes	Yes	No	79	22.9	25.9
	ITMA ⁺	1	Yes	Yes	Yes	74	21.7	25.7
	NTMA ⁺	0	Yes	NA	Yes	74	NA	25.0

We found that Hofmann elimination is always preferred when possible but is much less preferred when β -H's are replaced with methyl groups. While these trends were expected, we were initially surprised to find that decomposition of PTMA⁺ (2 β -H's) occurred at a higher temperature peak decay temperature than ITMA⁺ (1 β -H). Our calculated energy barrier for

Hofmann elimination mirrored this trend, giving us insight into the energetics of the degradation reactions. While increased methyl substitution plays a role in inhibiting hydroxide attack and preventing Hofmann elimination, our model results showed that the increase in energy of the ground state for the sterically encumbered ITMA⁺ was larger than the increase in TS due to steric inhibition of hydroxide attack. Thus, increased steric effects actually resulted in a lower energy barrier for degradation. The ylide barrier for deuterium scrambling in all these samples has been calculated to be between 18.2 and 18.4 kcal/mol. Isotopic (ylide) scrambling of deuterium is observed in all cases shown in Table 5. Trimethylamine degradation products from ETMA⁺, however (unlike all other samples), initially did not show isotopic scrambling but did in samples degraded over longer times, confirming that our relative energy barriers for Hofmann elimination versus ylide scrambling were qualitatively reasonable. Additionally, comparisons between energy barriers calculated for S_N2 attack and Hofmann elimination also seem qualitatively reasonable when compared to the experimentally observed degradation products.

We have enhanced our understanding significantly of ammonium cations and developed and applied unique tools to their degradation mechanisms and rates. However, a primary finding from our studies on substituted TMA⁺ is that strategies employed to date have had only minimal impact on the reaction barriers observed, with only modest improvements in stability.

Future Plans

We have thoroughly explored the chemical stability of ammonium cations and now have an increased understanding of their stability, reaction mechanisms and energy barriers. Unfortunately, we still find ammonium cations to be lacking desired base stability. We have also identified fundamental gaps in the understanding of the relationship between cations in solution with those bound in polymers and the electrochemical impact of cations with bicarbonate/carbonate/hydroxide. Our future work focuses on three areas: (1) advanced cations, (2) the relationship between the properties of free cations in solution to those in bound polymer systems, and (3) the electrochemical impacts of ions.

Advanced cations in our proposed work refer to any covalently tetherable cations other than ammonium. For discussion purposes we classify these cations into non-ammonium N⁺ centered, P⁺ centered, S⁺ centered, C⁺ centered, and metal tethered (e.g, cobaltocenium, ruthenium). Non-ammonium N⁺ centered cations include cations in the imidazolium, triazolium, pyridinium, and pyrazinium families and are often employed as ionic liquids. Polymers with guanidiniums (C⁺ centered) and phosphoniums (P⁺ centered) cations are also of interest and have been reported in the literature. A new, potentially promising approach for significantly enhanced durability of AEMs is the use of metal cations immobilized onto polymers through tethers. Cobaltocenium tethered to a polymer matrix through functionalization of the cyclopentadienyl group¹² and ruthenium¹³ in a bis(terpyridine)ruthenium(II) complex and dicyclopentadiene have both been demonstrated in polymers appropriate for AEMs. The stability of these cations under appropriate conditions will be probed along lines our team has commonly employed.

Our work to date has focused on free cations in solution. The impact of the polymer environment on cation stability has not yet been explored directly by our team or anyone else. For cations tethered to polymers, conditions can be envisioned in which degradation is accelerated relative to cations in solution. For example, ylide-based decomposition routes involving intra- or inter-polymer reactions could result in reaction pathways not available in solution. Conversely, conditions could also be imagined in which steric hindrance or favorable interactions of cations with polymer chains or other cations may be beneficial in preventing

attack. We have performed initial investigations of commercially available ion-exchange polymers (ion-exchange resins) through headspace analysis. We plan to study defined systems of polymers for parallel thermal degradation studies to elucidate the relationship between the properties of free cations in solution to those in bound polymer systems.

Finally, the impacts of ions on catalysis are critical as they may fundamentally limit the use these materials in any application that has CO₂ or may impact the cations that may be employed in AEMs. For this reason it is critical to better understand the mechanisms of how these ions interact with catalysts and how these interactions impact overpotentials. Our planned work takes advantage of our unique access to multiple cations and polymers, and our significant electrochemical testing capabilities.

References

1. Einsla, B., Chempath, S., Pratt, L.R., Boncella, J., Rau, J.A., Macomber, C., and Pivovar, B.S. *ECS Transactions*, 2007. **11**(1): p. 1173-1180.
2. Macomber, C.S., Boncella, J.M., Pivovar, B.S., and Rau, J.A. *Journal of Thermal Analysis and Calorimetry*, 2008. **93**(1): p. 225-229.
3. Chempath, S., Boncella, J.M., Pratt, L.R., Henson, N., and Pivovar, B.S., *Journal of Physical Chemistry C*, 2010. **114**(27): p. 11977-11983.
4. Chempath, S., Einsla, B.R., Pratt, L.R., Macomber, C.S., Boncella, J.M., Rau, J.A., and Pivovar, B.S., *Journal of Physical Chemistry C*, 2008. **112**(9): p. 3179-3182.
5. Varcoe, J.R. and Slade, R.C.T., *Fuel Cells*, 2005. **5**(2): p. 187-200.
6. Bauer, B., Strathmann, H., and Effenberger, F., *Desalination*, 1990. **79**(2-3): p. 125-144.
7. Kneifel, K. and Hattenbach, K., *Desalination*, 1980. **34**(1-2): p. 77-95.
8. Neagu, V., Bunia, I., and Plesca, I., *Polymer Degradation and Stability*, 2000. **70**(3): p. 463-468.
9. Pivovar, B., *Alkaline Membrane Fuel Cell Workshop Final Report*. 2011: Washington, DC, http://www1.eere.energy.gov/hydrogenandfuelcells/pdfs/amfc_may2011_workshop_report.pdf
10. Edson, J.B., Macomber, C.S., Pivovar, B.S., and Boncella, J.M., *Journal of Membrane Science*. 2012 **399-400**(1): p. 49-59.
11. Long, H., Kim, K., and Pivovar, B.S., *Journal of Physical Chemistry C*, 2012, **116** (17), p. 9419-9426.
12. Ren, L.X., Zhang, J.Y., Bai, X.L., Hardy, C.G., Shimizu, K.D., and Tang, C.B., *Chemical Science*, 2012. **3**(2): p. 580-583.
13. Zha, Y., Disabb-Miller, M.L., Johnson, Z.,D., Hickner, M.A., and Tew, G.N., *J. Am. Chem. Soc.* 2012, **134**, p. 4493-4496.

Publications

1. Long, Hai, Kim, Kwiseon, Pivovar, Bryan, "Hydroxide Degradation Pathways for Substituted Trimethylammonium Cations: A DFT Study," *J. Phys Chem C*, 116 (17), 9419-9426, 2012.
2. Pivovar, B., *Alkaline Membrane Fuel Cell Workshop Final Report*. 2011: http://www1.eere.energy.gov/hydrogenandfuelcells/pdfs/amfc_may2011_workshop_report.pdf.
3. J. Edson, C. Macomber, B. Pivovar, J. Boncella, Hydroxide Based Decomposition Pathways of Alkyltrimethylammonium Cations, *J. Memb. Sci.*, 399-400, 49-59, 2012.
4. Shaji Chempath, Jim Boncella, Lawrence Pratt, Neil Henson and Bryan Pivovar, "Density Functional Theory Study of Degradation of Tetraalkylammonium Hydroxides," *J. Phys. Chem. C*, 114, 11977-11983, 2010.

Chemical and Mechanical Properties of Surfaces, Interfaces and Nanostructures.

Miquel Salmeron, Gabor Somorjai, Peidong Yang. Materials Science Division, Lawrence Berkeley National Laboratory.

Subtask 1: Mechanical and Physical Properties. PI. Miquel Salmeron

Program Scope

The overall program in this FWP is aimed at molecular level studies of surfaces, focusing on structure, adsorption, reactions, film growth, and energy transfer across interfaces, to obtain a fundamental understanding of the mechanisms that govern their physical, chemical, catalytic and tribological properties. The three subtasks comprised in the program: Mechanical and Physical Properties (Salmeron), Chemical Properties (Somorjai), and Synthesis and properties of Nanoparticles (Yang) synergistically complement each other and collaborate by sharing students and postdocs.

The goal of the first subtask is to study fundamental processes that govern the physical, chemical and tribological properties of surfaces. Specifically we study: a) structure and dynamics of adsorbed layers; b) mechanisms of energy transfer by excitation of vibrational and electronic states of adsorbed atoms and molecules; c) wetting at the molecular scale; d) friction of clean surfaces and of surfaces covered with lubricant layers. Tools used include: Scanning Tunneling and Atomic Force Microscopies (STM, AFM), and electron and photon spectroscopies. A very important activity is the development of instruments to obtain microscopy and spectroscopy information of surfaces in vacuum and in the presence of gases at ambient pressures (Fig. 1). These include Variable Temperature and Low Temperature Scanning Tunneling Microscopy (VT-STM, LT-STM), High Pressure STM (HP-STM) [1], contact and non-contact atomic force microscopy (AFM, NC-AFM), Ambient Pressure Photoelectron Spectroscopy (AP-XPS), and X-ray absorption and emission, spectroscopies (XAS, XES) [2]. The x-ray techniques, initially developed for use at the Advanced Light Source (ALS), have resulted in the creation of three dedicated beamlines that attract also many users from all over the world. Two companies now produce and sell the AP-XPS, and 10 synchrotron facilities around the world have implemented the AP-XPS technology developed in this program.

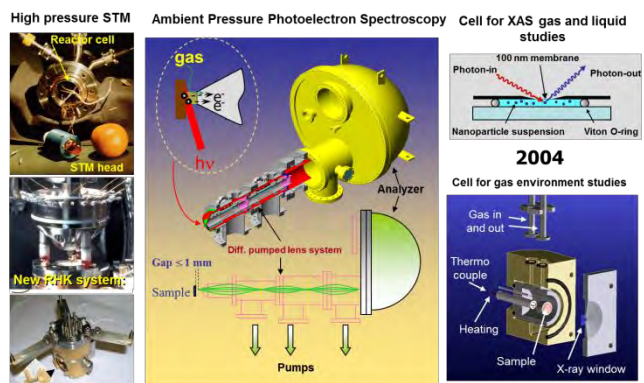


Fig. 1. This program develops instrumentation for atomic scale microscopy and electron spectroscopy studies of surfaces under ambient gases and liquids.

These include Variable Temperature and Low Temperature Scanning Tunneling Microscopy (VT-STM, LT-STM), High Pressure STM (HP-STM) [1], contact and non-contact atomic force microscopy (AFM, NC-AFM), Ambient Pressure Photoelectron Spectroscopy (AP-XPS), and X-ray absorption and emission, spectroscopies (XAS, XES) [2]. The x-ray techniques, initially developed for use at the Advanced Light Source (ALS), have resulted in the creation of three dedicated beamlines that attract also many users from all over the world. Two companies now produce and sell the AP-XPS, and 10 synchrotron facilities around the world have implemented the AP-XPS technology developed in this program.

Recent Progress

Mechanical properties of graphene: Graphene monolayers deposited on Silicon wafers were found to exhibit surprising friction anisotropy in 3 different domains, with a periodicity of 180

degrees on each domain (Fig.2). The anisotropy was shown to arise from ripple distortions of the graphene sheets along preferential directions (zig-zag, arm-chair). The ripples disappear after applying high pressure with the tip or by thermal treatment (Science, 2011).

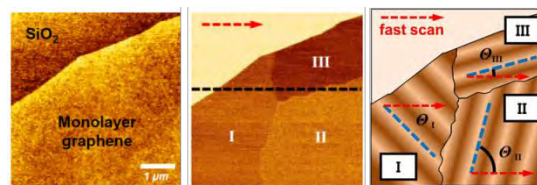


Fig.2. Left: AFM image of a graphene flake on a Si wafer. Center: friction force image showing three friction domains. Right: schematic showing the ripples formed in graphene with axis rotated 120° .

Molecular scale wetting: We have shown that the initial stages of wetting of Ru(0001) and Pd(111) is determined by the competition between O-metal bonding and H-bonding between water molecules leading to unexpected monolayer structures consisting of hexagonal water domains rotated by 30° relative to one another. Pentagon and heptagon clusters bridge the two types of hexagons. One domain is in registry with the substrate with the molecules lying flat and forming strong O-metal bonds with the substrate (Fig.3). In the other domain the molecules are raised a fraction of an angstrom, have dangling H-bonds, and are weakly bound to the substrate. This bonding motif is of similar nature to the periodic wetting structure recently reported on Pt(111), and very different from the conventional "ice-like" bilayer. First-principles Density Functional Theory simulations support these conclusions. (PRB 2012).

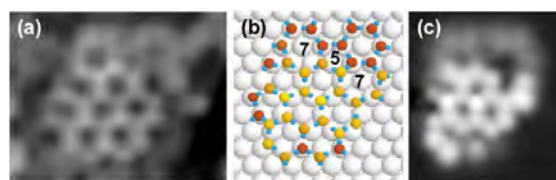


Fig.3. Experimental and calculated STM images of water on Ru(0001). (a) STM image showing water hexamers rotated by 0° and 30° relative to the surface lattice, connected by pentagons and heptagons. (b) DFT optimized model. (c) Calculated STM image.

Chemical reactivity of graphene: In another project we explored the chemical activity of graphene. Using STM we found that water reacts efficiently with the grain boundary defects in graphene on Ru(0001), where dangling or stressed C bonds are located. The chemical attack by water splits graphene into flakes at temperatures as low as 90 K, and intercalates between the graphene and Ru through the gaps opened in the overlayer (Fig.4). (JACS, 2012)

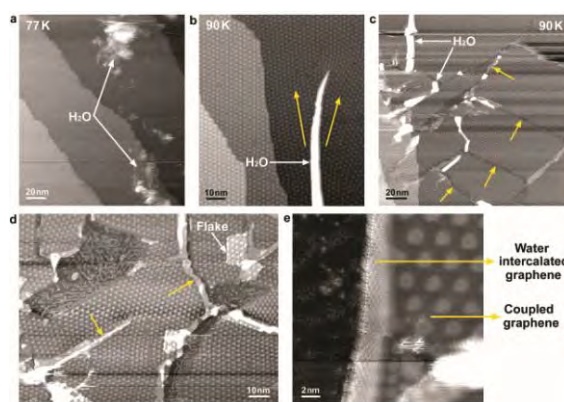


Fig.4. a) STM image of a graphene on Ru(0001); b) Water adsorbs weakly and diffuses to the grain boundaries; c,d) At 90 K water breaks C-C bonds at the domain boundaries and intercalates between Gr and Ru; e) the periodic Moire structure disappears in the regions where water intercalates.

Future Plans

We will focus on understanding the molecular scale mechanism of chemical reactions on surfaces by investigating the role of specific quantum excitations of molecules adsorbed on metals using our LT-STM. Excitations include vibrational modes (bond stretching, bending) that are coordinates for chemical reactions and diffusion. In water for

example O-H stretching leads to a variety of reactions, including diffusion by coupling to frustrated translation modes, and to dissociation when multiple quantum modes are excited. We plan to study molecules important in energy processes including CO_2 (photosynthesis), NH_3 (H

fuels), CH_x dissociation, and others. In preliminary experiments we have shown that electric fields can strongly influence the reactivity of adsorbed molecules. For example NH_3 dissociation is strongly affected by E-fields that can be generated by the tip of the STM due to its close proximity to the surface. Such fields simulate the conditions prevalent in the double layer in electrochemical systems, which have applications in the field of energy storage in batteries and fuel cells.

We plan to use our newly finished liquid helium cooled AFM to study the structure of molecules on insulating surfaces, including Al_2O_3 , Fe_2O_3 , TiO_2 and oxygen-covered metal surfaces. These include H_2O , CO_2 , and small hydrocarbons. Using non-contact, high resolution capabilities of the microscope we will study the energy landscape between the molecules and the tip atoms. In previous work with STM we have shown that molecules can be incorporated in the tip and used for imaging and force spectroscopy (Fig. 5).

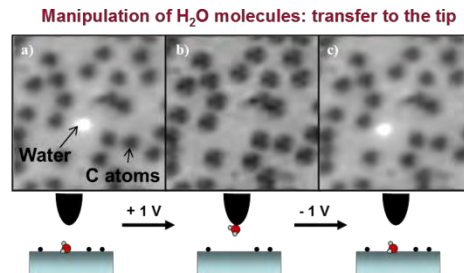


Fig. 5. STM images showing the back and forth transfer of a water molecule from the Ru(0001) surface to the tip and back. Dark spots correspond to C atoms.

In the area of friction fundamentals we will study the effect of confined layers (such as the water between graphene flakes and Ru from the previous example) in the friction properties. Confined layers provide an ideal laboratory to study lubricants forming molecularly thin layers between moving surfaces. The high resolution capabilities of AFM will allow us to correlate the atomic structure of the confining surfaces, and that of the intercalated lubricant film, and the forces measured while scanning in different crystallographic directions.

In collaboration with the Somorjai and Yang groups (subtasks 2 and 3 of this program) we will study the influence of high densities of adsorbates on the structure of the surface, both in model single crystals and nanocrystals. High adsorbate density is the result of thermodynamic equilibrium in the presence of high pressures (>1 Torr) of reactants. Thanks to the new tools (HP-STM, AP-XPS) developed in this subtask we demonstrated the reconstruction of Pt crystals [3] and of Pt-Rh alloy nanocrystals [4] in the presence of CO , H_2 , and NO (reducing and oxidizing) at coverages near unity. We plan to expand these first demonstration studies to new materials and gases that are important in catalysis, energy conversion and storage and CO_2 sequestration.

References

- [1] B.J. McIntyre, M.B. Salmeron and G.A. Somorjai. *Catal. Lett.* 14, 263 (1992)
- [2] M. Salmeron and R. Schlögl. *Surf. Sci. Rep.* 63, 169 (2008)
- [3] Feng Tao, Zhi, Sefa Dag, Lin-Wang Wang, Zhi Liu, Derek R. Butcher, Miquel Salmeron, Gabor A. Somorjai. *Science.* 327, 850 (2010)
- [4] Feng Tao, Michael E. Grass, Yawen Zhang, Derek R. Butcher, James R. Renzas, Zhi Liu, Jen Y. Chung, Bongjin S. Mun, Miquel Salmeron, and Gabor A. Somorjai *Science.* 322, 932 (2008)

Publications

1. J.T. Newberg, D.E. Starr, S. Yamamoto, S. Kaya, T. Kendelewicz, E.R. Mysak, S. Porsgaard, M.B. Salmeron, G.E. Brown Jr., A. Nilsson, H. Bluhm. Formation of hydroxyl and water layers for MgO(100) films studied with ambient pressure XPS. *Surf. Sci.* 605, 89-94 (2011).
2. Feng Tao and Miquel Salmeron. In Situ Studies of Chemistry and Structure of Materials in Reactive Environments. *Science.* 331, 171-174 (2011).
3. Lindsay R. Merte, Jan Knudsen, Falk M. Eichhorn, Soeren Porsgaard, Helene Zeuthen, Lars C. Grabow, Erik Lægsgaard, Hendrik Bluhm, Miquel Salmeron, Manos Mavrikakis and Flemming Besenbacher. CO-induced embedding of Pt adatoms in a partially-reduced FeOx film on Pt(111). *J. Am. Chem. Soc.* 133 (28) 10692-10695 (2011)
4. J. T. Newberg, D. E. Starr, S. Yamamoto, S. Kaya, T. Kendelewicz, E. R. Mysak, S. Porsgaard, M. B. Salmeron, G. E. Brown, Jr., A. Nilsson, H. Bluhm. Auto-catalytic surface hydroxylation of MgO(100) terrace sites observed under ambient conditions. *J. Phys. Chem. C.* 115, 12864 (2011)
5. J.J. Benítez, M A. San-Miguel, S. Domínguez-Meister, J. A. Heredia-Guerrero, and M. Salmeron. Structure and Chemical State of Octadecylamine Self-Assembled Monolayers on Mica. *J. Phys. Chem. C* 115, 19716–19723 (2011).
6. L. J. Giovanetti, J. M. Ramallo-López, M. Foxe, L. C. Jones, M. M. Koebel, G.A. Somorjai, A. F. Craievich, M. B. Salmeron, and F. G. Requejo. Shape changes of Pt nanoparticles induced by deposition on mesoporous silica monitored by SAXS and EXAFS. *Small.* 8 , 468 (2012).
7. S. Maier, I. Stass, T. Mitsui, M. Tatarkhanov, Peter J. Feibelman, K. Thürmer, N. C. Bartelt and M. Salmeron. Adsorbed water-molecule hexagons with unexpected rotations in islands on Ru(0001) and Pd(111). *Phys. Rev. B.* 85, 155434 (2012).
8. Z. Zhu, F. Tao, F. Zheng, R. Chang, Y. Li, L. Heinke, Z. Liu, M. Salmeron, and G. A. Somorjai. Reversible Formation of Nanometer-sized Surface Platinum Oxide Clusters on a Stepped Pt(557) Single Crystal Surface Induced by Oxygen: A High-pressure STM and Ambient Pressure XPS Study. *Nano Letters.* 12, 1491 (2012).
9. Xiaofeng Feng, Sabine Maier, Miquel Salmeron. Water splits epitaxial graphene and intercalates. *J. Am. Chem. Soc.* 134, 5662 (2012)

Chemical and Mechanical Properties of Surfaces, Interfaces and Nanostructures

Gabor A. Somorjai, Materials Sciences Division, Lawrence Berkeley National Laboratory

Subtask 2: Surface Chemical Properties. PI Gabor A. Somorjai

Program Scope

This subtask focuses on the exploration of the atomic and molecular factors of structure, bonding, and dynamics that make surfaces chemically reactive. We synthesize and characterize metal and bimetallic nanoparticles (NPs) in the form of 2D films, or supported in 3D mesoporous oxides, using a combination of techniques. We use mostly colloid synthesis to produce nanoparticles. We explore the structure of the surfaces of materials and nanoparticles in the presence of the reactive gas environments characteristic of industrial catalytic processes. To that effect we use unique tools developed in this Program, such as sum frequency generation (SFG) vibrational spectroscopy, HP-STM, AP-XPS and other synchrotron-based techniques (X-ray absorption) that make possible to investigate surfaces under reaction conditions on atomic and molecular scales. We investigate solid-liquid and solid-solid interfaces (buried interfaces) as they adsorb and react with diatomic and organic molecules in dynamic steady state at various pressures and temperatures. The research has a significant impact in catalytic energy production, by providing the basic science necessary for the development of better catalysts.

Recent Progress

We have synthesized monodispersed metals (Pt, Rh, Ru, IR) and bimetallic (Pt-Rh, Pt-Ir) nanoparticles with 2-12 nm size and controlled shape capped with a polymer (PVP) to prevent their aggregation.¹ The porous cap allows the reactants and products to enter and exit the metal NP surface without inhibiting the NP reactivity and disordering the polymer cap by hydrogen permits detection of the reaction intermediates by SFG without interference by the polymer. Mesoporous oxides were synthesized (γ -Al₂O₃, TiO₂, SiO₂) and utilized to fabricate three-dimensional (3D) nanoparticle deposits, and the Langmuir-Blodgett technique was used to form 2D NP films. Characterization of NP structure, composition and oxidation states was performed under reaction conditions by SFG and synchrotron-based techniques of AP-XPS, EXAFS, NEXAFS and by application of TEM, ethylene hydrogenation, chemisorption and STEM/EDAX before and after reactivity studies. In-situ reaction cells were constructed for studies using synchrotron techniques at solid-liquid and solid-high pressure gas interfaces.

In collaboration with the Yang group, we have fabricated a thermally stable Pt/mesoporous silica core-shell system for high-temperature reactions.² The high-temperature-stable system consists of a Pt metal core coated with a mesoporous silica shell (Pt@mSiO₂) (Fig. 1). The high thermal stability of Pt@mSiO₂ nanoparticles enabled high-temperature CO

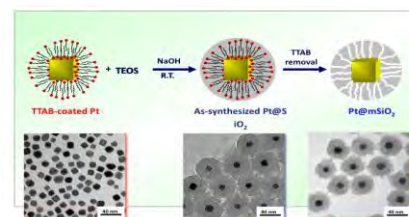


Figure 1. The synthesis approach for mesoporous-silica-coated Pt nanoparticles

oxidation studies, including ignition behaviour, which was not possible for bare Pt nanoparticles because of their deformation or aggregation.

We find that the size of the metal nanoparticles controls the selectivity of most multipath catalytic reactions.³ In the case of methylcyclopentane isomerization, the shape of platinum NPs had large effects on the formation of branched isomers.⁴ For small ≤ 2 nm metal nanoparticles the higher oxidation states dominated as compared to the metallic state for larger NPs.

In collaboration with Salmeron's group we found that stepped platinum (Pt) surfaces can undergo extensive and reversible restructuring when exposed to carbon monoxide (CO) and oxygen at pressures above 0.1 torr (Fig. 2). Scanning tunneling microscopy and photoelectron spectroscopy studies under gaseous environments near ambient pressure at room temperature revealed that as the CO or oxygen surface coverage approaches 100%, the originally flat terraces of (557) and (332) oriented Pt crystals break up into nanometer-sized clusters and revert to the initial morphology after pumping out the CO gas.⁵ Density functional theory calculations provided a rationale of the observations whereby the creation of increased concentrations of low-coordination Pt edge sites in the formed nanoclusters relieves the strong CO-CO repulsion in the highly compressed adsorbate film.

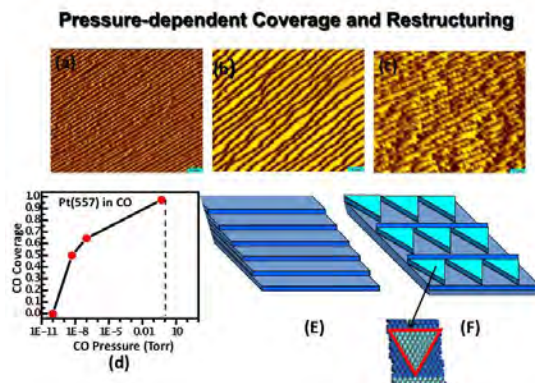


Figure 2. Reconstruction of a Pt step surface induced by high pressure exposure to CO at room temperature.

Future Plans

Exposure of metal single crystal surfaces to high pressures ≥ 1 atm causes restructuring of the surface atoms to optimize the coverage and the concentration of metal-adsorbate and metal-metal bonds. High pressure restructuring appears to be reversible but is likely to change the surface reactivity. The concentration of adsorbates dramatically increases at the solid-liquid interface as compared to the solid-gas interface, which is likely to cause restructuring. We shall be studying the pressure-induced restructuring using high pressure STM in collaboration with the Salmeron Group. We shall also use high-pressure-induced restructuring to produce nanosize clusters on metal surfaces to study the restructuring phenomena on metal NPs created by the high-pressure restructuring.

Studies of metal NP formation in the 5-30 atom range using Raman spectroscopy will allow fabrication of monodispersed NPs in this very small NP range that has not been investigated as yet. This promises to provide NPs with novel atomic and electronic structures and oxidation states with interesting chemical bonding and reactivities.

In collaboration with the Yang group we shall fabricate oxide and semiconductor nanorods with metal nanodots at their ends to produce tandem nanocatalysts that exhibit different chemical

reactivities as we change the oxide (semiconductor) nanorods and the metal nanodots at their ends.⁶

Construction of a femtosecond broad band laser enabling us to simultaneously monitor the CH and CO vibrational SFG spectra, thus allowing more accurate characterization of reaction intermediates.

We will also undertake synthesis and characterization of a variety of metal core-oxide shell NP structures as they promise high thermal stability and novel chemical reactivity.

References

1. The Colloidal Chemistry of Nanocatalysts: The Molecular View. Kwangjin An, Selim Alayoglu, Trevor Ewer, Gabor A. Somorjai. *J. Colloid and Interface Science* **373** 1-13 (2012).
2. Thermally Stable Pt/Mesoporous Silica Core-Shell Nanocatalysts for High-Temperature Reactions. Sang Hoon Joo, Jeong Young Park, Chia-Kuang Tsung, Yusuke Yamada, Peidong Yang and Gabor A. Somorjai. *Nature Materials* **8** (February), **126** (2009).
3. Nanocrystal Bilayer for Tandem Catalysis. Yusuke Yamada, Chia-Kuang Tsung, Wenyu Huang, Ziyang Huo, Susan E. Habas, Tetsuro Soejima, Cesar E Aliaga, Gabor A. Somorjai, Peidong Yang. *Nature Chemistry*, **3**, 372-376 (2011)
4. Size and Shape Dependence of Pt Nanoparticles over Methylcyclopentane/Hydrogen Ring Opening / Ring Enlargement Reaction. S. Alayoglu, C. Aliaga, C. Sprung, G. A. Somorjai. *Cat. Lett.* **141**, 914-924 (2011).
5. Break-up of Stepped Platinum Catalyst Surfaces by High CO Coverage. Feng Tao, Sefa Dag, Lin-Wang Wang, Zhi Liu, Derek R. Butcher, Hendrik Bluhm, Miquel Salmeron and Gabor A. Somorjai. *Science* **327**, 850 (2010).
6. Lee, H. J.; Habas, S. E.; Somorjai, G. A.; Yang, P. D., Localized Pd overgrowth on cubic Pt nanocrystals for enhanced electrocatalytic oxidation of formic acid. *J. Am. Chem. Soc.*, **130** (16), 5406 (2008).

Publications

1. Seedless Polyol Synthesis and CO Oxidation Activity of Monodisperse (111) and (100)-Oriented Rhodium Nanocrystals in Sub-10 nm Sizes. Yawen Zhang, Michael E. Grass, Wenyu Huang and Gabor A. Somorjai. *Langmuir*, **26**(21) 16463-16468 (2010).
2. Furan Hydrogenation over Pt(111) and Pt(100) Single-Crystal Surfaces and Pt Nanoparticles from 1 to 7 nm: A Kinetic and Sum Frequency Generation Vibrational Spectroscopy Study. Christopher J. Kliewer, Cesar Aliaga, Marco Bieri, Wenyu Huang, Chia-Kuang Tsung, Jennifer B. Wood, Kyriakos Komvopoulos, Gabor A. Somorjai. *J. Am. Chem. Soc.* **132** 13088-13095 (2010).
3. Nanocrystal Bilayer for Tandem Catalysis. Yusuke Yamada, Chia-Kuang Tsung, Wenyu Huang, Ziyang Huo, Susan E. Habas, Tetsuro Soejima, Cesar E Aliaga, Gabor A. Somorjai, Peidong Yang. *Nature Chemistry*, **3**, 372-376 (2011)
4. An SFG Study of Interfacial Amino Acids at the Hydrophilic SiO₂ and Hydrophobic Deuterated Polystyrene Surfaces. George J. Holinga, Roger L. York, Robert M. Onorato, Christopher M. Thompson, Nic E. Webb, Alfred P. Yoon and Gabor A. Somorjai. *J. Am. Chem. Soc.* **133**, 6243-6253 (2011).

5. Sum Frequency Generation Vibrational Spectroscopy and Kinetic Study of 2-Methylfuran and 2,5-Dimethylfuran Hydrogenation over 7 nm Platinum Cubic Nanoparticles. Cesar Aliaga, Chia-Kuang Tsung, Selim Alayoglu, Kyriakos Komvopoulos, Peidong Yang and Gabor A. Somorjai. *J. Phys. Chem. C* **115**, 8104-8109 (2011).
6. In-situ X-ray Adsorption Study of Evolution of Oxidation States and Structure of Cobalt in Co and CoPt Bimetallic Nanoparticles (4 nm) under Reducing (H₂) and Oxidizing (O₂) Environments. Fan Zheng, Selim Alayoglu, Jinghua Guo, Vladimir Pushkarev, Yimin Li, Per-Anders Glans, Jeng-lung Chen, Gabor A. Somorjai. *Nano Letters* **11**, 847-853 (2011)
7. Surface Composition and Catalytic Evolution of Au_xPd_{1-x} (x=0.25, 0.50 and 0.75) Nanoparticles under CO/O₂ Reaction in Torr Pressure Regime and at 200 °C. Selim Alayoglu, Franklin Tao, Virginia Altoe, Colin Specht, Zhongwei Zhu, Funda Aksoy, Derek R. Butcher, Russ J. Renzas, Zhi Liu and Gabor A. Somorjai. *Cat. Lett.* **141**, 633-640 (2011).
8. Spectroscopic Study of Platinum and Rhodium Dendrimer (PAMAM G4OH) Compounds, Structure and Stability. Yuri Borodko, Christopher M. Thompson, Wenyu Huang, Huseyin B. Yildiz, Heinz Frei and Gabor A. Somorjai. *J. Phys. Chem. C* **115**, 4757-4767 (2011).
9. CO₂ Hydrogenation Studies on Co and CoPt Bimetallic Nanoparticles under Reaction Conditions using TEM, XPS and NEXAFS. Selim Alayoglu, Fan Zheng, Vladimir V. Pushkarev, Zhi Liu, Jinghua Guo, Simon Beaumont, Viacheslav Iablokov, Haimei Zheng, Norbert Kruse and Gabor A. Somorjai. *Topics in Catalysis* **54**(13), 778-785 (2011).
10. Size and Shape Dependence of Pt Nanoparticles over Methylcyclopentane/Hydrogen Ring Opening / Ring Enlargement Reaction. S. Alayoglu, C. Aliaga, C. Sprung, G. A. Somorjai. *Cat. Lett.* **141**, 914-924 (2011).
11. Determination of Molecular Surface Structure, Composition and Dynamics under Reaction Conditions at High Pressures and at the Solid-Liquid Interface. Gabor A. Somorjai, Simon K. Beaumont and Selim Alayoglu. *Angew. Chem. Int. Ed.* **50**, 10116-10129 (2011).
12. *In-situ* Oxidation Study of Pt(110) and Its Interaction with CO. Derek R. Butcher, Michael E. Grass, Zhenhua Zeng, Funda Aksoy, Hendrik Bluhm, Wei-Sue Li, Bongjin S. Mun, Gabor A. Somorjai and Zhi Liu. *J. Am. Chem. Soc.*, **133**, 20319-20325 (2011).
13. From Single Pt Atoms to Pt Nanocrystals: Photoreduction of Pt²⁺ inside of a PAMAM Dendrimer. Yuri Borodko, Peter Ercius, Vladimir Pushkarev, Christopher Thompson, Gabor A. Somorjai. *J. Phys. Chem. Lett.* **3**, 236-241 (2012)
14. In-situ Study of Oxidation States and Structure of 4 nm CoPt Bimetallic Nanoparticles during CO Oxidation using X-ray Spectroscopies in Comparison with Reaction Turnover Frequency. Fan Zheng, Selim Alayoglu, Vladimir Pushkarev, Simon Beaumont, Colin Specht, Funda Aksoy, Zhi Liu, Jinghua Guo, Gabor A. Somorjai. *Catalysis Today* **182** 54-59 (2012).
15. Formation of Nanometer-sized Surface Platinum Oxide Clusters on a Stepped Pt(557) Single Crystal Surface Induced by Oxygen: A High-Pressure STM and Ambient-pressure XPS Study. Zhongwei Zhu, Franklin (Feng) Tao, Fan Zheng, Rui Chang, Yimin Li, Lars Leinke, Zhi Liu, Miquel Salmeron, Gabor A. Somorjai. *Nano Letters* **12**, 1491-1497 (2012).

Chemical and Mechanical Properties of Surfaces, Interfaces and Nanostructures.

Miquel Salmeron, Gabor Somorjai, Peidong Yang. Materials Science Division, Lawrence Berkeley National Laboratory.

Subtask 3: Synthesis and Assembly of Metal and Oxide Nanoparticles. PI. Peidong Yang

Program Scope

The application of shape- and size-controlled metal and oxide nanocrystals as catalyst supports has even greater potential for innovative catalyst design. It is well known that catalysis can be modulated by using different metal oxide supports, or metal oxide supports with different crystal surfaces. This subtask will focus on the design and synthesis of size and shape controlled metal and oxide nanocrystals, and their large scale assembly towards high surface-area catalysts with well-defined metal-oxide interfaces. On the metal nanocrystal side, we will focus on the development of synthetic strategies towards size and shape control of the bimetallic systems such as PtPd, PtRh, PtNi and PtCo. We propose to demonstrate the viability in building the relationship between catalyst surfaces and their catalytic properties using bimetallic nanoparticles of well controlled surface composition. The validity of our approach will be confirmed by a catalytic reaction, CO oxidation, as well as a synchrotron based nanoparticle characterization technique, extended X-ray absorption fine structure (EXAFS). On the oxide nanocrystal side, we will develop a general method to produce ultrathin, single crystalline oxide nanostructures as high surface area catalytic supports for both gas-phase and solution-phase catalysis applications.¹⁻²

Recent Progress

Platinum (Pt) nanocrystals exhibit strongly shape- and size-dependent catalytic properties.³⁻⁵ Optimizing nanocatalyst morphology has become a prolific area of investigation. Recently, we developed a solution-based method for the synthesis of colloidal Pt nanoparticles. The Pt nanocubes and nanopolyhedra with controllable size and shapes have been synthesized accordingly by controlling the reducing rate of metal precursor ions in a one-pot polyol synthesis.

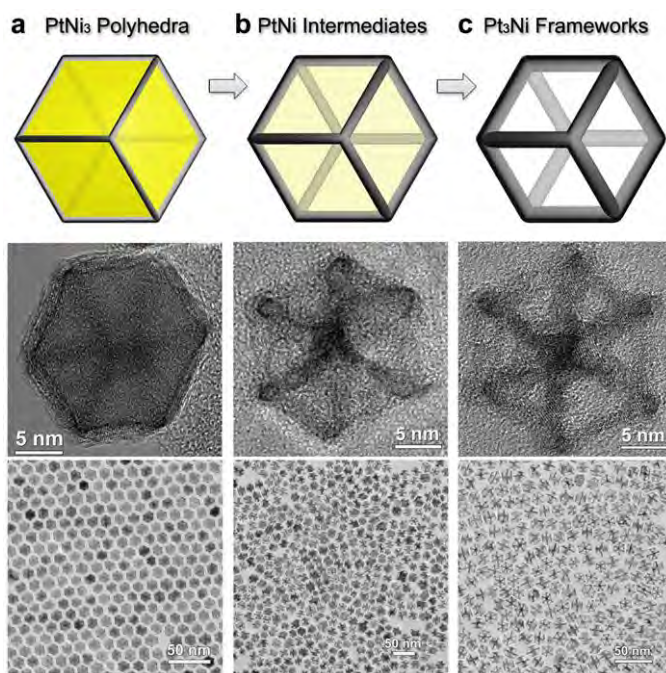


Fig. 1. Schematic illustrations and corresponding TEM images of the samples obtained at three representative stages during the evolution process. a, initial solid PtNi₃ polyhedra. b, PtNi intermediates. c, final hollow Pt₃Ni frameworks.

Structural Evolution of Bimetallic Nanocrystals: Following our early studies on pure Pt nanocrystals, we have discovered a very interesting structural evolution process for Pt-Ni bimetallic nanostructures. During this process, solid PtNi₃ polyhedra, spontaneously transform into hollow Pt₃Ni frameworks under ambient conditions (Figure 1). The initial PtNi₃ polyhedra exhibit single crystallinity and the morphology of rhombic dodecahedron, both of which are maintained in the final Pt₃Ni frameworks which consists of 24 remaining edges and an eroded interior. This structural evolution process was traced and analyzed, and a mechanism is proposed to interpret this spontaneous conversion in both composition and morphology. This discovery represents a new synthetic strategy for hollow nanostructures, and these Pt-Ni bimetallic nanostructures can potentially serve as catalysts in fuel cells and petroleum refinement.

Metal and metal oxides interface has been demonstrated to influence both the activity and selectivity in catalytic reaction. Here we developed a new concept which the as-designed metal and metal oxides interface is utilized as a new class of nanocrystal tandem catalysts for sequential reactions. Here we fabricate a nanocrystal bilayer structure formed by assembling platinum and cerium oxide nanocube monolayers of less than 10 nm on a silica substrate as shown in figure 2. The cubic shape of nanocrystals is ideal for assembling metal–metal oxide interfaces with

a large contact area. Figure 2 shows our tactic to achieve the ‘tandem’ bilayer structure with nanocubes of metal and metal oxide. First, a two-dimensional metal (Pt) nanocube array was assembled onto a flat metal oxide substrate (SiO₂) by using the Langmuir–Blodgett (LB) method to make the first metal–metal oxide interface. The second metal oxide (CeO₂) nanocube LB array was then assembled on top of the metal nanocube monolayer, which provided the second metal–metal oxide interface. The capping agents of the nanocrystals were removed by ultraviolet/ozone treatment to form clean metal–metal oxide interfaces. After removal of the capping agent, the vertical clefts between the nanocrystals ensured access to both catalytic interfaces and provided a high surface area in the close-packed array. The two distinct metal–metal oxide interfaces, CeO₂–Pt and Pt–SiO₂, can be used to catalyze two distinct sequential reactions. The CeO₂–Pt interface catalyzed methanol decomposition to produce CO and H₂, which were subsequently used for ethylene hydroformylation catalyzed by the nearby Pt–SiO₂ interface. Consequently, propanal was produced selectively from methanol and ethylene on the nanocrystal bilayer tandem catalyst. This new concept of nanocrystal tandem catalysis represents a powerful approach towards designing high-performance, multifunctional nanostructured catalysts.

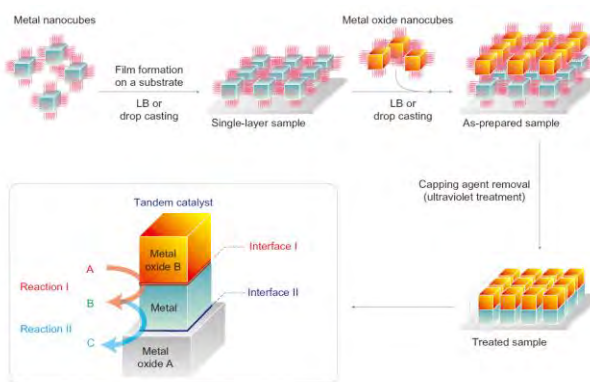


Figure 2. Assembly process for the preparation of a nanocrystal bilayer tandem catalyst.

Future Plans

We plan to expand our current synthetic methods to new metal and oxide nanoparticles to enrich the choices when we design the catalyst. We will synthesize transition metal nanoparticles and their alloy particles with controllable size and morphology. For example, cobalt (Co) particle with nanometer size, especially in 6~7nm, have been demonstrate to be efficient catalyst in Fischer–Tropsch synthesis.⁶ When the Co nanoparticles were deposited on certain oxide surface (like CeO₂), it show obvious product selectivity. More long chain alkanes could be obtained by using this metal and metal oxides interface.⁶⁻⁷ So, updating our current synthetic method to prepare non-noble metal nanocrystals and their alloys with controllable size and shape will be an important part of our future research plan.

In order to gain more insights about the interaction between metal and metal oxides and its impact on catalysis, we plan to design the new generation of tandem catalysts and apply the new catalyst in sequential reactions. Compared with the current generation tandem catalyst, the next generation tandem catalyst will have two or more metal components (like Pt and Co nanoparticles or PtCo bimetal nanoparticles).

And for the oxide support, only one metal oxide will be applied to couple with the two metals. In this design, the first metal Pt will be assembled or grew directly on the surface of CeO₂ for MeOH decomposition reaction. This reaction will supply hydrogen and carbon monoxide for the next Fischer–Tropsch synthesis reaction. The Fischer–Tropsch reaction will happen at the active interface between Co and CeO₂ to produce hydrocarbons.⁸ The over reaction will be from MeOH to hydrocarbons. The advantage of this new generation tandem catalyst is: a), the reactants are simplified. MeOH is the only reactant during the reaction; b), the catalyst will show both activity and selectivity. This new generation of tandem catalyst gives us the possibility to test the tandem catalysis selectivity using the Fischer–Tropsch process as an example. The hydrocarbon product selectivity could be investigated by GC-MS.

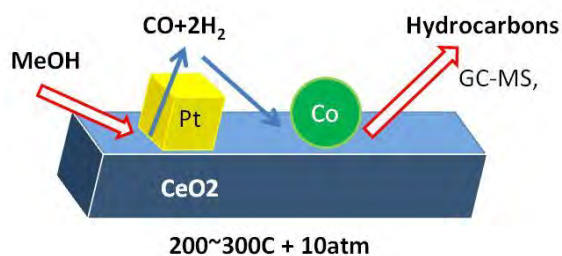


Figure 3. Schematic Illustration of next generation tandem catalyst.

We will continue to collaborate with the Somorjai and Salmeron groups to apply Ambient Pressure Photoelectron Spectroscopy and X-ray absorption and emission, spectroscopies to investigate the interface between metal and metal oxides. High and low pressure reactors will be installed into existing GC instrument in the lab (Somorjai Lab).

References

1. Aliaga, C.; Park, J. Y.; Yamada, Y.; Lee, H. S.; Tsung, C. K.; Yang, P. D.; Somorjai, G. A., Sum Frequency Generation and Catalytic Reaction Studies of the Removal of Organic

-
- Capping Agents from Pt Nanoparticles by UV-Ozone Treatment. *J. Phys. Chem. C* 2009, 113 (15), 6150-6155.
 2. Aliaga, C.; Tsung, C. K.; Alayoglu, S.; Komvopoulos, K.; Yang, P. D.; Somorjai, G. A., Sum Frequency Generation Vibrational Spectroscopy and Kinetic Study of 2-Methylfuran and 2,5-Dimethylfuran Hydrogenation over 7 nm Platinum Cubic Nanoparticles. *J. Phys. Chem. C* 2011, 115 (16), 8104-8109.
 3. Lee, H. J.; Habas, S. E.; Somorjai, G. A.; Yang, P. D., Localized Pd overgrowth on cubic Pt nanocrystals for enhanced electrocatalytic oxidation of formic acid. *J. Am. Chem. Soc.* 2008, 130 (16), 5406-+.
 4. Tao, A. R.; Habas, S.; Yang, P. D., Shape control of colloidal metal nanocrystals. *Small* 2008, 4 (3), 310-325.
 5. Lee, H.; Habas, S. E.; Kweskin, S.; Butcher, D.; Somorjai, G. A.; Yang, P. D., Morphological control of catalytically active platinum nanocrystals. *Angew. Chem.-Int. Edit.* 2006, 45 (46), 7824-7828.
 6. Iglesia, E., Design, synthesis, and use of cobalt-based Fischer-Tropsch synthesis catalysts. *Appl. Catal. A-Gen.* 1997, 161 (1-2), 59-78.
 7. Dry, M. E., The Fischer-Tropsch process: 1950-2000. *Catal. Today* 2002, 71 (3-4), 227-241.
 8. Khodakov, A. Y.; Chu, W.; Fongarland, P., Advances in the development of novel cobalt Fischer-Tropsch catalysts for synthesis of long-chain hydrocarbons and clean fuels. *Chem. Rev.* 2007, 107 (5), 1692-1744

Publications

1. L. Hung, C. Tsung, W. Huang, P. Yang, Room-temperature Formation of Hollow Cu₂O Nanoparticles, *Adv. Mater.* 22, 1910, 2010.
2. J. Henzie, M. Grnwald, A. Widmer-Cooper, P. L. Geissler, P. Yang, Self-assembly of uniform polyhedral silver nanocrystals into densely packed supercrystals, *Nature Mater.*, 11, 31, 2012.
3. Yamada, Y.; Tsung, C. K.; Huang, W.; Huo, Z. Y.; Habas, S. E.; Soejima, T.; Aliaga, C. E.; Somorjai, G. A.; Yang, P. D., Nanocrystal bilayer for tandem catalysis. *Nature Chemistry* 2011, 3 (5), 372-376.
4. Chen, C., Huo, Z. Y., Zhu, Z. W., Liu T., Somorjai, G. A.; Yang, P. D., Structural Evolution of Bimetallic Nanocrystals: From PtNi₃Polyhedra to Pt₃Ni Frameworks. *Nature* 2012 (submitted).
5. Aliaga, C.; Tsung C. K.; Alayoglu S.; et al. Sum Frequency Generation Vibrational Spectroscopy and Kinetic Study of 2-Methylfuran and 2,5-Dimethylfuran Hydrogenation over 7 nm Platinum Cubic Nanoparticles, *J. Phys. Chem. C*, 115, 8104, 2011.

Directed Energy Interactions with Surfaces

Michael Savina, Igor Veryovkin

Materials Science Division, Argonne National Laboratory

Program Scope

The Directed Energy Interactions with Surfaces program focuses on fundamental studies of the interaction of directed energy sources such as energetic ions, electrons, and photons with materials. It has at its core two integrated activities: 1) A fundamental understanding of energetic ion- and laser-solid interactions, and 2) The development of world-class trace analysis instrumentation. The interaction of directed energy sources such as energetic ions, electrons, and photons with surfaces provides the basis for modifying, patterning and analyzing materials. This program investigates the fundamentals of these complex interactions over a range of conditions using several unique, world-class methods developed in our laboratory.

Our current research explores of ion-surface interactions and the flux of material ejected during the sputtering process: 1) Characterizing the sputtered flux from a solid surface in terms of secondary atoms and molecules, both as neutrals and ions, under varying sputtering conditions. 2) Optimizing the depth resolution of ion sputtering via a dual-beam sputtering approach, resulting in a depth resolution of ~ 2 atomic layers, which is approximately the physical limit.

Recent Progress

Ion sputtering can be described by a sequence of elastic collisions between point particles in which the bombarding ion transfers its energy to the target atoms [1], thereby initiating a series of collision cascades in the near-surface region (up to a few tens of nm for a 25 keV ion). Cluster ion beams such as Au_3^+ , Bi_3^+ and C_{60}^+ provide large increases in sputtering yield compared to monatomic ion sources [2, 3] because they deposit the majority of their energy within the first few nanometers of the surface [4]. For molecular solids, the total kinetic energy and energy partitioning across fragmentation pathways are also affected by primary ion nuclearity.

Photoionization techniques provide insight into the mechanism of energy transfer from the primary ion to the surface and sub-surface atoms. We used Resonance Ionization Mass Spectrometry (RIMS) to study ion sputtering of uranium oxide [5]. Briefly, a solid is sputtered using a pulsed (300 ns), energetic (15-25 keV) ion beam and sputtered neutrals are ionized by

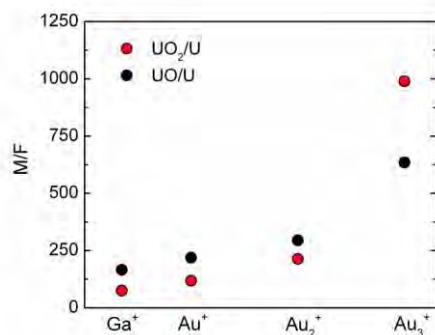


Figure 1: Molecule-to-fragment ratio of sputtered flux from U_3O_8 for various projectiles.

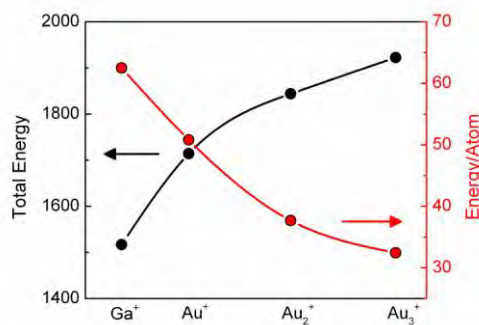


Figure 2: Total and average energy of the sputtered flux for various projectiles.

lasers tuned to resonantly excite and ionize uranium [6]. The lasers also ionize UO and UO₂ at low efficiency. The molecule-to-fragment (M/F) ratios in the sputtered flux (i.e. UO_x/U) for various primary ions are shown in Figure 1, which shows the extent of fragmentation of UO_x to U decreases with increased mass and nuclearity of the primary ion. The Stopping and Range of Ions in Matter (SRIM) 2011 software was used to gain insights into ion-atom collisions [7]. SRIM shows that the number of knock-ons increases as a function of primary ion mass and nuclearity, allowing for more direct transfer of energy to the target atoms. Additionally, the average knock-on depth becomes shallower as ion mass and nuclearity increase. Although the total energy imparted to the sputtered flux increases, the energy per sputtered species actually decreases with increasing primary ion mass and nuclearity (Fig. 2). Although the sputtering yield increases, the energy is partitioned over a much larger flux, resulting in less fragmentation.

In addition to fundamental studies, we are developing novel approaches and instrumentation for materials characterization with the goal of maximizing the information obtained by combining high lateral and depth resolution imaging mass spectrometry (detecting secondary ions, SIMS, and post-ionized secondary neutrals, LPI SNMS) with *in situ* scanning electron microscopy (SEM) and optical profilometry. This multidimensional (multi-D) sample characterization provides chemical and physical materials characterization in real time.

Figure 3 shows high resolution depth profiles of a nanolayered (~5 nm) MgO/ZnO sample obtained in SIMS mode on the SARISA instrument at Argonne. A unique dual-beam arrangement was used in which ion milling was done with Ar⁺ at either 250 or 500 eV impact energy, and SIMS analysis was performed between milling cycles with a 5 keV Ar⁺ beam. This is possible because of the unique dual-beam arrangement of the SARISA instrument, which allows the ion mill to operate at normal incidence so that the impact energy of primary ions can be precisely controlled and optimized by the target potential. We have recently equipped our ion mill column with a Wien (velocity) filter in order to avoid surface contamination with undesirable primary ions coming from ion source. The 250 eV beam is near the sputtering threshold for these materials, and gives a depth resolution of about two atomic layers (0.4 nm) which is the physical limit for sputtering-based methods. Because ion milling at ultra-low energy

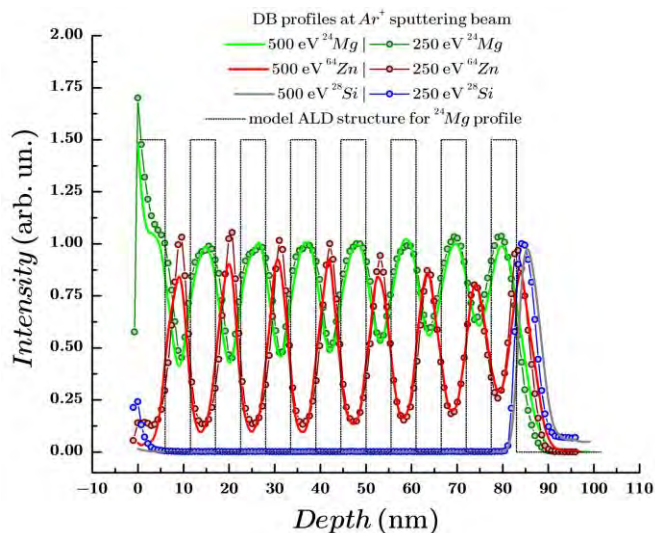


Figure 3: Dual-beam depth profiles of MgO/ZnO layers on a Si substrate obtained by 250 eV or 500 eV Ar⁺ ion milling combined with 5 keV Ar⁺ SIMS analysis between milling cycles.

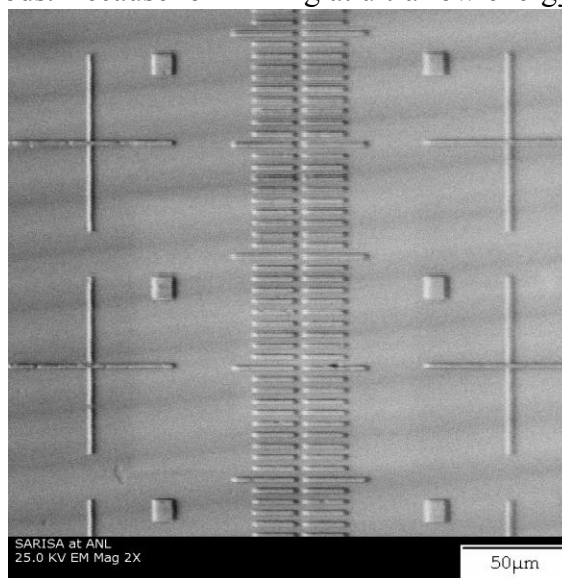


Figure 4: SEM image of a Si calibration wafer acquired in the SARISA instrument (FEI 2LE e-gun and RevolutionSEM software).

does not roughen the irradiated surface, we can use this approach to determine the roughness of buried interfaces in nanolayered structures using the mixing-roughness-information model of depth profiling (MRI) [8]. The results of using MRI in conjunction with dual beam sputter depth profiling were in good agreement with the industry standard method, the X-ray reflectivity technique, applied to the same samples. This is crucial for studies of ion mixing phenomena in ion-irradiated nanolayered structures, because it allows us to unambiguously distinguish native roughness from beam-induced interlayer mixing and diffusion.

In addition to high resolution depth profiling, we have recently enabled *in-situ* secondary electron microscopy in the SARISA instrument (Fig. 4) which allows SEM imaging before, during, and after irradiation with primary ions. At present the lateral resolution is <100 nm, and we can perform SEM imaging of surface roughness changes due to ion beam bombardment. We are now incorporating SEM imaging in the dual-beam sputter depth profiling protocol.

Future Plans

Previous work has shown that M/F ratios decrease with increasing primary ion dose [9]. We speculate that this is a convolution of projectile-dependent molecular fragmentation and ion-induced preferential sputtering of oxygen from the uranium oxide matrix at high ion doses [10]. In our experiment, the analysis and the reducing beams are the same, but operated under different sputter conditions (dynamic vs. pulsed). We plan to test our hypothesis with experiments where the analysis and the reducing beams are different (e.g. H⁺ vs. Ga⁺).

To understand effects such as ion milling on sputtered flux, which in many cases causes the observed elemental, molecular, and even isotopic ratios to appear to change as a function of ion dose, we are developing techniques to quantify the sputtered material. This requires understanding ionization effects such as isotope shifts, hyperfine splitting, Doppler broadening, Doppler shifts, laser power broadening, and mass-dependent (flight-time) effects. Techniques such as traditional scanning laser spectroscopy coupled with saturation spectroscopy and empirical and *a priori* modeling yield descriptions of laser-atom and laser-molecule interactions that enable a quantitative analysis of the sputtered flux. Sputtered ion/neutral ratios, atom/molecule ratios, photo-fragmentation rates, sputtered atom electronic state population distributions can be quantified to enable a detailed understanding of ion- and laser-surface interactions. This is important in understanding phenomena such as preferential sputtering of elements from a solid.

Future instrumental upgrades include integrating an ion nanoprobe into the dual-beam depth profiling protocol. This new tool will allow us to perform imaging mass spectrometry with lateral resolution of up to 10 nm, which is the physical limit (collision cascade size) for medium energy (keV) ion probes. Overall, this work will lead to multi-D characterization of solid samples with the best lateral and depth resolution possible with this class of tools.

We have also begun developing *in-situ* optical profilometry in order to measure ion milling rates in real time during multi-D characterization experiments. Presently, such measurements are always performed *post-mortem*, which limits the accuracy by forcing the assumption of equal sputtering yields for all layers. Our approach is Heterodyne Displacement Interferometry, which has a typical depth resolution of 0.35 nm. This system will monitor changes in irradiated surfaces in real time and will be incorporated into the dual-beam depth profiling protocol. The components are currently installed on an optical bench and are undergoing assembly and software development.

References

- [1] Andersen, H.H. and P. Sigmund, (1965), *Physics Letters*. **15**(3), 237.
- [2] Davies, N., et al., (2003), *Applied Surface Science*. **203**, 223-227.
- [3] Touboul, D., et al., (2005), *Journal of the American Society for Mass Spectrometry*. **16**(10), 1608-1618.
- [4] Ryan, K.E., et al., (2007), *Journal of Physical Chemistry C*. **111**(34), 12822-12826.
- [5] Savina, M.R., et al., (2003), *Geochimica Et Cosmochimica Acta*. **67**(17), 3215-3225.
- [6] Isselhardt, B.H., et al., (2011), *Analytical Chemistry*. **83**(7), 2469-2475.
- [7] Ziegler, J.F., et al., (2010), *Nuclear Instruments & Methods in Physics Research Section B- Beam Interactions with Materials and Atoms*. **268**(11-12), 1818-1823.
- [8] Hofmann, S. and J.Y. Wang, (2006), *Journal of Surface Analysis*. **13**(2), 142-147.
- [9] Willingham, D., et al., (2012), *Journal of Radioanalytical and Nuclear Chemistry*, in press.
- [10] Idriss, H., et al., (2007), *Journal of Physical Chemistry C*. **111**(22), 7963-7970.

Publications in the last two years

1. Mass Spectrometry of Organic Molecules and Laser Induced Acoustic Desorption: Applications, Mechanisms and Perspectives, A. Zinovev and I. Veryovkin, *Current Trends in Mass Spectrometry*, July 2011, pp. 24-29 (Supplement to Spectroscopy and LCGC, www.spectroscopyonline.com), (invited)
2. Laser Postionization Secondary Neutral Mass Spectrometry for Analysis on the Nanometer- Scale – the Followup, I.V. Veryovkin, S.V. Baryshev, A.V. Zinovev, C.E. Tripa, Q. Peng, J.W. Elam, M.J. Pellin, in: *Nanotech Conference Technical Proceedings, Nanotech 2011 Vol. 1, Nanotechnology 2011: Advanced Materials, CNTs, Particles, Films and Composites, Chapter 1: Nanoscale Materials Characterization*, (2011) pp. 24-27, ISBN: 978-1-4398-7142-3
3. Molecular Desorption by Laser-Driven Acoustic Waves: Analytical Applications and Physical Mechanisms, A. Zinovev, I. Veryovkin and M. Pellin (invited), in: *ACOUSTIC WAVES - FROM MICRODEVICES TO HELIOSEISMOLOGY*, Editor: Marco G. Beghi, Ch.16, pp.343-368, (2011), InTech - Open Access Publisher, <http://www.intechopen.com/books>
4. Baryshev, S. V., Zinovev, A. V., Tripa, C. E., Erck, R. A., and Veryovkin, I. V., 2012. White light interferometry for quantitative surface characterization in ion sputtering experiments. *Applied Surface Science* **258**, 6963-6968.
5. Willingham, D., Savina, M. R., Knight, K. B., Pellin, M. J., and Hutcheon, I. D., 2012. RIMS Analysis of Ion Induced Fragmentation of Molecules Sputtered from an Enriched U₃O₈ Matrix. *Journal of Radioanalytical and Nuclear Chemistry*, in press.
6. S.V. Baryshev, A.V. Zinovev, C.E. Tripa, M.J. Pellin, Q. Peng, J.W. Elam, and I.V. Veryovkin, High resolution SIMS depth profiling of nanolayers. *Rapid Comm. Mass Spectrom.* (2012, submitted)
7. S.V. Baryshev, J.A. Klug, A.V. Zinovev, C.E. Tripa, J.W. Elam, and I.V. Veryovkin, Measuring roughness of buried interfaces by sputter depth profiling. *Phys. Rev. B* (2012, submitted)

FWP: Solid-State NMR of Complex Materials

K. Schmidt-Rohr, M. Hong, E. M. Levin

Ames Laboratory, Division of Materials Science and Engineering, Ames, IA 50011

Program Scope

Many energy-relevant materials have a complex bulk structure with significant disorder on the 1-nm scale that prevents full characterization by diffraction or microscopy techniques. Using nuclear spins as local probes, advanced solid-state nuclear magnetic resonance (NMR) can make unique contributions to the elucidation of the structure and of structure-property relations in such complex materials. Our program focuses on NMR characterization of energy-relevant materials, such as fuel-cell membranes,¹ carbon-based electrode materials, as well as thermoelectric tellurides. In addition, we analyze biological and biomimetic materials, such as plant cell walls² and biological nanocomposites³. In all these materials, solid-state NMR can determine the composition,³⁻⁷ local proximities,² nanoparticle thickness,^{8,9} and amount of disordered phases¹⁰. It can yield information on local lattice distortions in crystals, and on segmental and polymer-chain dynamics in organic materials.^{11,12} We develop new radio-frequency pulse sequences^{7-9,13-19} and improved spectral simulation methods to increase the structural information provided by advanced solid-state NMR. Through careful analysis of all available data, we develop new, more accurate structural models of the molecular^{3,20} and nanometer-scale^{1,8} structure of the systems studied. In this abstract, we focus on organic and carbon-based materials, while thermoelectric tellurides are discussed in a different abstract.

Proton exchange membranes are at the center of H₂-O₂ fuel cells, providing high H⁺ conductivity combined with good gas-barrier properties.¹ Hydrated Nafion, a perfluorinated polymer with a Teflon backbone and ionic sidechains, has been the benchmark material for low-temperature proton exchange membranes for decades. We have elucidated its nanometer scale structure in this program, identifying water channels¹ stabilized by relatively stiff polymer backbones¹² (Figure 1). Quite recently, a superior proton-exchange membrane material, Aquivion, was introduced commercially;²¹ like Nafion, it is a perfluorinated sulfonated polymer with a (-CF₂)_n backbone, but with shorter sidechains (Figure 1b,c). For reasons not well understood, Aquivion shows better performance than Nafion at “high” temperatures (up to 130°C),²¹ which is attractive for improved catalyst performance.

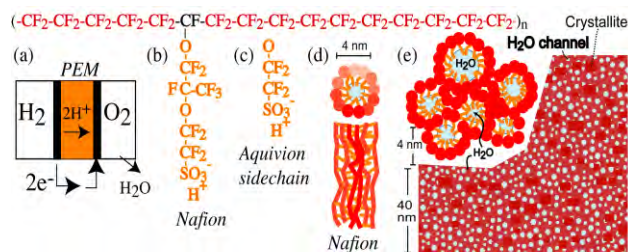


Figure 1. (a) Schematic of a H₂-O₂ fuel cell with proton-exchange membrane (PEM). (b, c) Chemical structures of (b) Nafion and (c) Aquivion. (d) Inverted polymer micelles of hydrated Nafion stabilized by the stiff backbone¹² and forming water channels that are locally parallel. (e) Resulting parallel water-channel model of Nafion developed in this program¹.

Organic-inorganic nanocomposites in the skeletons of vertebrates and invertebrates provide useful combinations of properties, such as considerable stiffness and toughness.²² They are produced at ambient pressure and temperature, and structured on the nanometer scale, in processes that we are only beginning to understand and harness for energy-efficient materials production. Our research has so far focused on the stiff and tough load-bearing material in bone, which is a nanocomposite of calcium phosphate (apatite) nanocrystals imbedded in a matrix of the fibrous protein collagen, at a 45:45 volume ratio; water accounts for the remaining 10%. We have shown that solid-state NMR can characterize many important aspects of this

nanocomposite, in particular regarding the organic-inorganic interface.

Graphitizable and nongraphitizable carbon-based materials are used in various energy-relevant applications, for instance as electrodes of batteries^{23,24} and supercapacitors²⁵. Nongraphitizable ('hard') carbon is produced from organic precursors that char as they pyrolyze,²⁶ producing irregular spaces between graphene sheets. Since these carbon materials are usually too disordered for a comprehensive analysis by diffraction techniques,^{26,27} the current picture of their local structure is rather vague, particularly for materials produced at lower temperatures (500-700°C). Defects such as cluster edges, flexible linkers, or five- and seven-membered rings are important for many properties such as adsorption and transport of ions or gases. We are developing various ¹³C, ¹H, ¹³C-¹H, ¹³C-¹³C, ²H, ^{6/7}Li, and ¹³C-⁷Li NMR techniques for characterizing structural defects in low-temperature hard-carbon materials.

Recent Progress

²H NMR to probe the water channels in Nafion. We have continued our investigations of the nanometer-scale structure of hydrated Nafion, the benchmark material for proton exchange membranes in H₂/O₂ fuel cells. In the framework of the parallel-water-channel model that we developed in this program,¹ we have estimated the straightness (persistence length) of the water channels in Nafion, through a quantitative analysis of line narrowing and T₂ relaxation in ²H NMR of D₂O in Nafion.²⁸ In drawn Nafion where scattering shows that the channels are mostly oriented along the draw direction, a ~1-kHz quadrupolar ²H splitting is observed, which means that the quadrupolar interaction tensor, essentially fixed to the D₂O molecule, does not undergo fully isotropic tumbling. The hydration dependence of the spectral splittings and relaxation times indicates exchange between bound water affected by the anisotropic environment of the channel surface and free water in the channel core. In unoriented Nafion, the splitting is ~30-fold smaller than in the drawn material. The observed ~10-fold motional averaging in the undeformed relative to the drawn film is explained by diffusion of water along coiled channels, which results in additional motional averaging. Thus, the persistence length of the channels must be much shorter than the diffusion length $\langle x^2 \rangle^{1/2} \approx 2 \mu\text{m}$ of water on the 3-ms NMR time scale. The quantitative analysis of NMR frequency exchange via diffusion along a model channel and between bundles of channels, using an exchange algorithm suitable for long channels, shows that the persistence length of the channels in Nafion is between 30 and 80 nm, which is near the lower limit of the value estimated from small-angle scattering but ~10 times greater than the persistence length of an individual polymer backbone of Nafion. Further, we have analyzed the hydration dependence of the polymer-water interfacial area in terms of various structural models, confirming the validity of the parallel-water-channel model at the typical hydration levels in fuel cells.²⁹

Strongly bound citrate stabilizes the apatite nanocrystals in bone. Nanocrystals of apatitic calcium phosphate impart the organic-inorganic nanocomposite in bone with favorable mechanical properties, but the factors preventing crystal growth beyond the favorable thickness of ~3 nm had not been identified. We have shown³ by multinuclear NMR, including ¹³C{³¹P} REDOR, ¹³C{¹H} spectral editing,⁵ and chemical-shift anisotropy dephasing,¹⁶ that the nanocrystal surfaces in bone are studded with strongly bound citrate molecules, which have no large-amplitude mobility on the 10-s scale or below, and have characterized the density (0.25 nm⁻²) and geometry of the bound citrate with the three carboxylate groups at distances of 0.3 to 0.45 nm from the apatite surface. This structural analysis was facilitated by multispin simulations developed in this program.⁸ We were able to exchange the native citrate with ¹³C-labeled molecules, confirming the peak assignment and enhancing sensitivity 30-fold for detailed

distance measurements.³ Bound citrate is highly conserved, being found in fish, avian, and mammalian bone, which indicates its critical role in interfering with crystal thickening and stabilizing the apatite nanocrystals in bone.

Characterization of hard-carbon materials. We are further developing NMR techniques and expertise for NMR analysis of low-temperature hard-carbon materials. This includes quantification of aromaticity,⁶ of the ratio of nonprotonated to protonated carbons,⁶ of the typical size of aromatic clusters by complementary spectroscopic and dipolar-dephasing methods, and of alkyl residues without overlap from sp^2 carbons.¹⁶ In addition to commercial and standard carbon materials, we study ^{13}C -enriched model materials, for instance made from ^{13}C -enriched glucose. This enhances sensitivity and spectroscopic possibilities by orders of magnitude.

Future Plans

^2H NMR to probe water channel segments in Nafion. As a critical test of the parallel-water channel model, we are trying to trap D_2O within straight channel segments in Nafion and Aquivion and measure the ^2H spectrum.²⁸ If the parallel-channel model is correct, the D_2O molecules will sample a uniaxial environment and report this in terms of a small quadrupolar biaxiality parameter. The asymmetry parameter can be read off directly from the characteristic features of the spectral pattern. If models of polymer in a hydrated matrix, such as the polymer ribbon, bundle, or channel-network models are right, (i) the environment of the D_2O molecules is not uniaxial and (ii) the diffusion of water molecules cannot be restricted to a well-defined region within which it moves freely. The proposed experiments require that the free diffusion length is smaller than the persistence length (≈ 40 nm). We are trying to achieve this by blocking channels with silica nanoparticles grown in situ.

Aquivion vs. Nafion fuel cell membranes: Chain order, dynamics, and crystallites. The mechanical properties of Aquivion in the relevant temperature range of 80–130°C are significantly better than those in Nafion.²¹ How the reduced length of the side chains produces this change is not clear. A potential explanation would be kinking of the *backbone* for favorable interactions between side groups. Using ^{19}F and ^{13}C NMR, we will compare the local order parameter of chain segments and large-amplitude rotations of backbone segments around their helical axis, as well as the sidechain dynamics, in Aquivion with those detected in Nafion,^{12,20} as a function of temperature.

The nanostructure of bone. Various models of bone assume that apatite nanocrystals are concentrated in the “gap” regions of the collagen fibrils.³⁰⁻³² This would require the presence of thick collagen layers in the apatite-poor regions. We will test these models by probing the thickness of the collagen layers in bone by long-range $^{13}\text{C}\{^{31}\text{P}\}$ NMR; thick layers would produce a nearly constant intensity at long dephasing times. We will also determine the nanoparticle size distribution in bone, based on heteronuclear NMR combined with quantitative scattering analysis. Further, we will try to determine to what extent the surface layer of biological apatite nanocrystals resembles octacalcium phosphate (OCP), by identifying the NMR and diffraction characteristics of OCP in nanocrystals. In the end, we should be able to present a well-founded comprehensive and detailed model of the local structure of the nanocomposite in bone.

^{13}C -enriched carbon materials: Probing curvature of aromatic sheets. We plan to use ^{13}C CODEX NMR¹¹ with ^{13}C spin diffusion³³ to probe to what extent graphene sheets in ^{13}C -labeled hard carbon are flat²⁶ or curved³⁴. In the interior of graphene sheets, carbons have a local three-fold symmetry, which results in a chemical-shift asymmetry or biaxiality parameter of $\eta = 0$

(quasi-uniaxial), as confirmed in naphthalene and coronene (at low temperatures to quench rotation of the rings). As a result, the chemical-shift tensors of all interior carbons (selected by C-H dephasing of signals of carbons near the periphery)⁹ in a flat graphene sheet are parallel, and spin diffusion among them will not lead to significant exchange in CODEX NMR. Thus, exchange in CODEX will be the signature of sheet curvature. Graphitizable soft carbon can serve as a reference material with flat graphene. Our ability to simulate scattering data³⁵ will help us incorporate the NMR results into a detailed picture of the local structure of hard carbon.

References

- (1) Schmidt-Rohr, K.; Chen, Q. *Nat. Mater.* **2008**, *7*, 75-83.
- (2) Dick-Pérez, M.; Zhang, Y.; Hayes, J.; Salazar, A.; Zabolina, O. A.; Hong, M. *Biochemistry*
- (3) Hu, Y. Y.; Rawal, A.; Schmidt-Rohr, K. *PNAS* **2010**, 22425-22429. **2011**, *50*, 989-1000
- (4) Schmidt-Rohr, K.; Mao, J.-D. *Chem. Phys. Lett.* **2002**, *359*, 403-411.
- (5) Schmidt-Rohr, K.; Mao, J.-D. *J. Am. Chem. Soc.* **2002**, *124*, 13938-13948.
- (6) Mao, J.-D.; Schmidt-Rohr, K. *Environ. Sci. Technol.* **2004**, *38*, 2680-2684.
- (7) Mao, J.-D.; Schmidt-Rohr, K. *J. Magn. Reson.* **2005**, *176*, 1-6.
- (8) Schmidt-Rohr, K.; Rawal, A.; Fang, X. W. *J. Chem. Phys.* **2007**, *126*, 054701-(1-16).
- (9) Mao, J.-D.; Schmidt-Rohr, K. *J. Magn. Reson.* **2003**, *162*, 217-227.
- (10) Enlow, D.; Rawal, A.; Kanapathipillai, M.; Schmidt-Rohr, K.; Mallapragada, S.; Lo, C. T.; Thiyagarajan, P.; Akinc, M. *J. Mater. Chem.* **2007**, *17*, 1570-1578.
- (11) deAzevedo, E. R.; Hu, W.-G.; Bonagamba, T. J.; Schmidt-Rohr, K. *JACS* **1999**, *121*, 8411.
- (12) Chen, Q.; Schmidt-Rohr, K. *Macromol. Chem. Physic* **2007**, *208*, 2189-2203.
- (13) Liu, S.-F.; Mao, J.-D.; Schmidt-Rohr, K. *J. Magn. Reson.* **2002**, *155*, 15-28.
- (14) Schmidt-Rohr, K.; Hong, M. *J. Am. Chem. Soc.* **2003**, *125*, 5648-5649.
- (15) Chen, Q.; Schmidt-Rohr, K. *Solid State NMR* **2004**, *26*, 11-15.
- (16) Mao, J.-D.; Schmidt-Rohr, K. *Solid State NMR* **2004**, *26*, 36-45.
- (17) Schmidt-Rohr, K.; Mao, J.-D.; Olk, D. C. *Proc. Nat. Acad. Sci.* **2004**, *101*, 6351-6354.
- (18) Hu, Y.-Y.; Schmidt-Rohr, K. *J. Magn. Reson.* **2009**, *197*, 193-207.
- (19) Hu, Y.-Y.; Schmidt-Rohr, K. *J. Am. Chem. Soc.* **2009**, *131*, 8390-8391.
- (20) Chen, Q.; Schmidt-Rohr, K. *Macromolecules* **2004**, *37*, 5995-6003.
- (21) Kreuer, K. D.; et al. *J. Power Sources* **2008**, *178*, 499-509.
- (22) Currey, J. D. *Bones*; Princeton University Press, 2002.
- (23) Dahn, J. R.; Zheng, T.; Liu, Y.; Xue, J. S. *Science* **1995**, *270*.
- (24) Leifer, N. D., et al. *J. Electrochem. Soc.* **2010**, *157*, A148-A154.
- (25) Azais, P. et al. *J. Power Sources* **2007**, *171*, 1046-1053.
- (26) Franklin, R. E. *Proc. Roy. Soc.* **1951**, *A209*. (27) Oberlin, A. *Carbon* **1984**, *22*, 521-541.
- (28) Li, J.; Wilmsmeyer, K. G.; Madsen, L. A. *Macromolecules* **2009**, *42*, 255-262.
- (29) Kong, X.; Schmidt-Rohr, K. *Polymer* **2011**, *52*, 2011.
- (30) Burger, C., et al. *J. Appl. Cryst.* **2008**, *41*, 252. (31) Fratzl, P. *Nat. Mater.* **2008**, *7*, 610.
- (32) Glimcher, M. J. *Rev. Mineral. Geochem.* **2006**, *64*, 223-282.
- (33) Reichert, D.; Bonagamba, T. J.; Schmidt-Rohr, K. *J. Magn. Reson.* **2001**, *151*, 129-135.
- (34) Harris, P. J. F. *Crit. Rev. Mat. Sci* **2005**, *30*, 235-253.
- (35) Schmidt-Rohr, K. *J. Appl. Crystallogr.* **2007**, *40*, 16-25.

Recent Publications (excluding thermoelectrics)

- References (2), (3), (29) in the list above. - Y.Y. Hu, X.P. Liu, X. Ma, A. Rawal, T. Prozorov, M. Akinc, S.K. Mallapragada, K. Schmidt-Rohr, *Chemistry of Materials*, **23**, 2481 (2011).

Polymer-based Multicomponent Materials (ERKCC02)

A.P. Sokolov

Chemical Sciences Division, Oak Ridge National Laboratory, Oak Ridge, TN 37831

B.G. Sumpter

Center for Nanophase Materials Sciences, ORNL, Oak Ridge, TN 37831

V.S. Urban

Spallation Neutron Source, ORNL, Oak Ridge, TN 37831

J.W. Mays, M.D. Dadmun

Department of Chemistry, University of Tennessee, Knoxville, TN 37996

F. Bates

Department of Chemical Engineering and Materials Science, University of Minnesota, Minneapolis, MN 55455

K. Schweizer

Department of Materials Science, University of Illinois at Urbana-Champaign, Urbana, IL

Program Scope

Multicomponent polymeric materials are widely used in various modern technologies and will have even broader applications in future technologies, from lightweight materials, to solar cells and electrical energy storage, to biomedical technologies. Yet, our fundamental understanding of the processes and interactions that control macroscopic properties in these materials remains limited. The overarching goal of our program is to develop a fundamental understanding of how interfacial properties and interactions affect structure, morphology, dynamics, and macroscopic properties of multicomponent polymeric systems, in both the liquid and solid states. The proposed research focuses on two research themes. The first seeks to correlate structure-property relationships in polymer-nanoparticle mixtures to the nanoparticle structure and interfacial interactions, while the second involves the correlation of molecular architecture, electrostatic interactions and external fields to the morphology of multiblock copolymer materials, including both neat block copolymers and those containing discrete nanoparticles. To fully understand the underlying processes and mechanisms, we pursue a comprehensive interdisciplinary approach lead by advanced theory and simulations, precise

synthesis with nano-scale control and state-of-the-art characterization (with special emphasis on neutron scattering). The fundamental knowledge developed in this program will contribute to the scientific foundation for the rational design of multicomponent polymer based materials with superior properties and function that can address many DOE challenges such as organic photovoltaics, batteries and fuel cell membranes, and stronger light-weight materials that result in energy savings. This presentation focuses on our research of polymer based nano-composite materials, and research of multi-block systems will be presented in separate contribution.

Recent Progress

Tuning nanoparticle dispersion by modifying the fundamental interactions between the polymer and nanoparticle interface was explored in detail using a combination of experiment, simulation and theory. Theory provided solid foundation for understanding dispersion of spherical nano-particles in homo-polymers and block co-polymers. Guided by theory and computational studies, optimum dispersion of single wall carbon nanotubes (SWNTs) and fullerenes in various polymer matrices with varying composition of electron donating 2-(dimethylamino)ethyl methacrylate (DMAEMA) or electron accepting acrylonitrile (AN) and cyanostyrene (CNSt) were prepared and characterized [1,11]. In qualitative agreement with theory [13], the experimental and computational results establish that chain connectivity is critical in controlling the accessibility of the functional groups to form intermolecular interactions.

A microscopic, quantitative, first principles statistical dynamical theory at the level of intermolecular forces for the violation of the Stokes-Einstein (SE) diffusion law of a spherical nanoparticle in entangled and unentangled polymer melts has been developed based on a combination of mode-coupling, Brownian motion and polymer physics ideas [12].

Among many other topics, we also started studies of composites with soft polymeric nano-particles that according to [R1,R2] exhibit unexpected miscibility and unusual viscoelastic properties. We developed synthesis strategy that provides grams quantity of polymeric nano-particles with controllable size, softness and surface roughness, with radius down to ~5nm. Initial analysis indeed revealed unexpected viscoelastic behavior of composites with these nano-particles.

Future Plans

The major objectives of our future research in this topic are: (i) Understand the influence of nanoparticle structure and softness and solvent annealing on the overall morphology and particle dispersion of the composite material; (ii) Unravel the influence of nanoparticles size, shape and softness on the dynamics, viscoelasticity and ionic conductivity of the composites.

Combining experiment, theory and simulations we will establish the role of nano-particles softness and surface roughness in their dispersion and viscoelastic properties of

composites. Understanding anomalous diffusion of nano-particles in entangled polymer melt is another focus of our experimental, simulations and theoretical studies. We will reveal critical dimensions of nano-particles relative to the distance between entanglements ('tube' diameter) and to the polymer radius of gyration. Influence of nano-particles size and their interaction with polymer on segmental and chain dynamics of polymer will be also studied. In addition, we will analyze role of solvent, its interaction with nano-particles and polymer on the dispersion of nano-particles and macroscopic properties of composite material.

References

R1. Mackay, M. E.; Tuteja, A.; Duxbury, P. M.; Hawker, C. J.; VanHorn, B.; Guan, Z. H. **Science** **311**, 1740 (2006).

R2. Mackay, M. E.; Dao, T. T.; Tuteja, A.; Ho, D. L.; VanHorn, B.; Kim, H. C.; Hawker, C. J., **Nat. Mat.** **2**, 762 (2003).

Publications (excluding topic of multi-block systems)

1. D. Linton, P. Driva, B. Sumpter, I. Ivanov, D. Geohegan, C. Feigerle, and M. D. Dadmun, "*The Importance of Chain Connectivity in the Formation of Non-Covalent Interactions between Polymers and Single-Walled Carbon Nanotubes and its Impact on Dispersion*", **Soft Matter** **6**, 2801-2814 (2010).
2. E. Cruz-Silva, A. R. Botello-Mendez, Z. M. Barnett, X. Jia, M. S. Dresselhaus, H. Terrones, M. Terrones, B. G. Sumpter, and V. Meunier, "*Controlling Edge Morphology in Graphene Layers Using Electron Irradiation: From Sharp Atomic Edges to Coalesced Layers Forming Loops*", **Phys. Rev. Lett.** **105**, 045501 (2010).
3. G. Feng, R. Qiao, J. S. Huang, B. G. Sumpter and V. Meunier, "*Atomistic Insight on the Charging Energetics in Sub-Nanometer Pore Supercapacitors*", **J. Phys. Chem. C.** **114**, 18012-18016 (2010).
4. L.M.Hall, A.Jayaraman and K.S.Schweizer, *Molecular Theories of Polymer Nanocomposites*, **Current Opinion in Solid State and Materials Science** **14**,38 (2010) (invited).
5. K.Chen and K.S.Schweizer, *Theory of Aging, Rejuvenation and the Nonequilibrium Steady State in Deformed Polymer Glasses*, **Physical Review E** **82**, 041804 (2010).
6. M. Goswami, and B. G. Sumpter, "*Anomalous Chain Diffusion in Polymer Nanocomposites for Varying Polymer-Filler Interaction Strengths*," **Phys. Rev. E** **81**(4) 041801 (2010).
7. L.M.Hall and K.S.Schweizer, *Structure, Scattering Patterns and Phase Behavior of Polymer Nanocomposites with Nonspherical Fillers*, **Soft Matter** **6**, 1015 (2010).
8. A. Agapov, A.P. Sokolov, "*Size of the Dynamic Bead in Polymers*", **Macromolecules** **43**, 9126-9130 (2010).

9. L. Hong, B. Begen, A. Kisliuk, V.N. Novikov and A. P. Sokolov, “*Influence of pressure on fast picosecond relaxation in glass-forming materials*”, **Phys. Rev. B** **81**, 104207 (2010).
10. E. Cruz-Silva, F. Lopez-Urias, E. Munoz-Sandoval, B. G. Sumpter, H. Terrones, J. C. Charlier, V. Meunier, and M. Terrones, “*Phosphorus and Phosphorus-Nitrogen Doped Carbon Nanotubes for Ultrasensitive and Selective Molecular Detection*,” **Nanoscale** **3**, 1008 (2011).
11. S.-L. Teh, D. Linton, B. G. Sumpter, M. D. Dadmun, “*Controlling Non-Covalent Interactions to Modulate the Dispersion of Fullerenes in Polymer Nanocomposites*,” **Macromolecules** **44**, 7737–7745 (2011).
12. U. Yamamoto and K.S. Schweizer, *Theory of Nanoparticle Diffusion in Unentangled and Entangled Polymer Melts*, **J. Chemical Physics** **135**, 224902 (2011).
13. L.M. Hall and K.S. Schweizer, *Effective of Monomer Sequence, Composition and Chemical Heterogeneity on Copolymer-Mediated Effective Interactions between Nanoparticles in Melts*, **Macromolecules**, **44**, 3149 (2011).
14. Ranko Richert, Alexander Agapov, Alexei P. Sokolov, *Appearance of a Debye Process at the conductivity relaxation frequency of a viscous liquid*, **J. Chem. Phys.** **134**, 104508/1-7 (2011).
15. L. Hong, V.N. Novikov, and A.P. Sokolov, “*Dynamic heterogeneities, boson peak, and activation volume in glass-forming liquids*”, **Phys. Rev. E** **83**, 061508/1-10 (2011).
16. J. J. Yoo, K. Balkrishnan, J. S. Huang, V. Meunier, B. G. Sumpter, A. Srivastava, M. Conway, A. L. M. Reddy, J. Yu, R. Vajtai, and P. M. Ajayan, “*Ultrathin Planar Graphene Supercapacitors*”, **Nano Letters** **11**, 1423 (2011).
17. E. Cruz-Silva, Z. M. Barnett, B. G. Sumpter, and V. Meunier, “*Structural, Magnetic, and Transport Properties of Substitutionally Doped Graphene Nanoribbons from First Principles*”, **Phys. Rev. B** **83**, 155445 (2011).
18. K. Chen and K.S. Schweizer, *Theory of Yielding, Strain Softening and Steady Plastic Flow in Polymer Glasses Under Constant Rate Deformation*, **Macromolecules** **44**, 3988 (2011).
19. L. Hong, V.N. Novikov, A.P. Sokolov, “*Is there a connection between fragility of glass forming systems and dynamic heterogeneity/cooperativity?*”, **J. Non-Cryst. Solids** **357**, 351-356 (2011)
20. S. Tekobo, A.G. Richter, S. A. Dergunov, S. V. Pingali, V. Urban, B. Yan, and E. Pinkhassik, “*Synthesis, characterization, and controlled aggregation of biotemplated polystyrene nanodisks*”, **Journal of Nanoparticle Research** **13**, 6427-6437 (2011).
21. Phillip Griffin, Alexander Agapov, Alexander Kisliuk, Xiao-Guang Sun, Sheng Dai, Vladimir Novikov, and Alexei P. Sokolov, “*Decoupling Charge Transport from the Structural Dynamics in Room Temperature Ionic Liquids*”, **J. Chem. Phys.** **135**, 114509/1-8 (2011).

Polymer-based Multicomponent Materials (ERKCC02): Research on Multiblock Copolymer Systems

A.P. Sokolov

Chemical Sciences Division, Oak Ridge National Laboratory, Oak Ridge, TN 37831

B.G. Sumpter

Center for Nanophase Materials Sciences, ORNL, Oak Ridge, TN 37831

V.S. Urban

Spallation Neutron Source, ORNL, Oak Ridge, TN 37831

J.W. Mays, M.D. Dadmun

Department of Chemistry, University of Tennessee, Knoxville, TN 37996

F. Bates

Department of Chemical Engineering and Materials Science, University of Minnesota, Minneapolis, MN 55455

K. Schweizer

Department of Materials Science, University of Illinois at Urbana-Champaign, Urbana, IL

Program Scope

Multicomponent polymeric materials are widely used in various modern technologies and will have even broader applications in future technologies, from lightweight materials, to solar cells and electrical energy storage to biomedical technologies. Yet, our fundamental understanding of the processes and interactions that control macroscopic properties in these materials remains limited. The overarching goal of our program is to develop a fundamental understanding of how interfacial properties and interactions affect structure, morphology, dynamics, and macroscopic properties of multicomponent polymeric systems, in both the liquid and solid states. The proposed research focuses on two research themes. The first seeks to correlate structure-property relationships in polymer-nanoparticle mixtures to the nanoparticle structure and interfacial interactions, while the second involves the correlation of molecular architecture, electrostatic interactions and external fields to the morphology of multiblock copolymer materials, including both neat block copolymers and those containing discrete nanoparticles. To fully understand the underlying processes and mechanisms, we pursue a

comprehensive interdisciplinary approach led by advanced theory and simulations, precise synthesis with nano-scale control and state-of-the-art characterization (with special emphasis on neutron scattering). The fundamental knowledge developed in this program will contribute to the scientific foundation for the rational design of multicomponent polymer based materials with superior properties and function that can address many DOE challenges such as organic photovoltaics, batteries and fuel cell membranes, and stronger light-weight materials that result in energy savings. This presentation focuses on our research on multi-block copolymer systems. Research on polymer based nano-composite materials will be presented in separate contribution.

Recent Progress

The bulk morphologies formed by a new class of charged block copolymers, 75 vol % fluorinated polyisoprene (FPI) – 25 vol% sulfonated polystyrene (PSS) with 50% sulfonation, were characterized, and the fundamental underlying forces that promote the self-assembly processes were elucidated. Our work [1] has demonstrated that the addition of charged groups to one block of a copolymer can effectively modify the morphology phase diagram and create novel morphologies (hexagonally packed cylinders of the majority FPI phase dispersed in a continuous phase of PSS). A physical understanding based on the underlying strong electrostatic interactions between the charged block and counterions was obtained using detailed Monte Carlo and Molecular Dynamics simulations [1,2]. In solution, diblock copolymers of FPI and PSS form novel tapered rods and ribbon-like micelles [16].

Recently, we reported the discovery of a new and unusually large piezoelectric response of block copolymers to electric field [15]. Piezoelectric materials contract or expand when an electric potential is applied, and this effect is widely used for high precision movement and positioning, for example in atomic force microscopes or fuel injection in diesel engines. Until now, non-polar polymers were thought to be unable to exhibit any piezoelectric effect. Our research shows that, to the contrary, nonpolar polymers can produce piezoelectric responses that are 10 times larger than the strongest piezoelectric materials known thus far, lead zirconate titanate ceramics.

Future Plans

The major objectives of our future research in this topic are: (i) Reveal the role of electrostatic interactions, conformational asymmetry, and external electric field in the formation of specific structures and morphologies of multi-block polymers and (ii) Develop a strategy for the design of block copolymer materials with coordinated bulk and surface properties.

We will expand our experimental and theoretical (SCFT) work on PCHD-containing diblock copolymers to the study of ABC triblock terpolymers containing PCHD blocks. To our knowledge morphologies of triblock terpolymers incorporating high levels of conformational asymmetry have not been previously reported. Addition of a third block type (e.g. ABC triblock) greatly expands the portfolio of ordered phases [R1]. To better control nanophase morphology,

we will study the influence of electric field on the structure of block copolymers. We have recently observed by SANS and SAXS several novel, interesting and initially surprising effects of electric fields on block copolymers.

References

R1. Bates, F. S.; Fredrickson, G. H. **Physics Today** **52**, 32 (1999).

Publications on multi-block copolymer systems

1. M. Goswami, B. G. Sumpter, T.Z. Huang, J.M. Messman, S.P. Gido, A. Isaacs-Sodeye, J. Mays, “*Tunable Morphologies from Charged Block Copolymers*”, **Soft Matter** **6**, 6146-6154 (2010).
2. M. Goswami, B. G. Sumpter, and J. Mays, “*Controllable Stacked Disc Morphologies of Charged Diblock Copolymers*”, **Chem. Phys. Lett.** **487**, 272 - 278 (2010).
3. M. J. Bluemle, J. Zhang, T. P. Lodge, F. S. Bates, “*Inverted Phases Induced by Chain Architecture in ABAC Tetrablock Terpolymers*”, **Macromolecules** **43**, 4449 (2010).
4. D. Priftis, G. Sakellariou, J. W. Mays, and N. Hadjichristidis, “*Novel Diblock Copolymer-Grafted Multi-walled Carbon Nanotubes Via a Combination of Controlled/Living Surface Polymerizations*”, **J. Polym. Sci. Part A: Polym. Chem.** **48**, 1104 - 1112 (2010)
5. D. Baskaran, J. Mays, and P. Driva, “*A New Approach to the Living Anionic Polymerization of 4-Cyanostyrene*”, **Macromolecules** **43**, 6915 - 6918 (2010)
6. C.-U. Lee, D. Roy, B. S. Sumerlin, M.D. Dadmun, “*Facile Synthesis of Thiol-terminated Poly(styrene-*ran*-vinyl phenol) (PSVPh) Copolymers via Reversible Addition-Fragmentation Chain Transfer (RAFT) Polymerization and Their Use in the Synthesis of Gold Nanoparticles with Controllable Hydrophilicity*”, **Polymer** **51**, 1244-1251 (2010).
7. S. Lee, M.J. Bluemle, F.S. Bates, “*Discovery of a Frank-Kasper sigma-Phase in Sphere Forming Block Copolymer Melts*”, **Science** **330**, 349-353 (2010).
8. R. Aggarwal and D. Baskaran, “*Effects of Hydration and Hydrophilicity on Na-Clay-Supported Aqueous Phase Catalysis for Atom Transfer Radical Polymerization*”, **J. Polym. Sci. Part A: Polym. Chem.** **49**, 5049-5056 (2011)
9. R. Aggarwal and D. Baskaran, “*Hydration Mediation in Supported Aqueous-Phase Catalysis for Atom Transfer Radical Polymerization*”, **Macromolecules** **44**, 8805-8818 (2011)
10. M. Goswami, B. G. Sumpter, and J. W. Mays, “*Dynamical Studies of Charged Di-Block Copolymer in Different Dielectric Media*”, **J. Phys. Chem. B** **115**, 3330 - 3338 (2011).

11. D. Uhrig, R. Schlegel, R. Weidisch, and J. Mays, “*Multigraft Copolymer Superelastomers: Synthesis Morphology, and Properties*”, **Eur. Polym. J.** **47**, 560-568 (2011)
12. M. Goswami, R. Kumar, B. G. Sumpter, and J. Mays, “*Breakdown of Inverse Morphologies in Charged Diblock Copolymers*”, **J. Phys. Chem. B** **115**, 3330 (2011)
13. F. Zuo, C. G. Alfonso, and F. S. Bates, “*Structure and Dynamics of Elastomeric Multiblock Terpolymers Containing Glassy, Rubbery and Semicrystalline Blocks*”, **Macromolecules** **44**, 8143–8153 (2011).
14. J. Zhang, S. Sides, F.S. Bates, “*Ordering of Sphere Forming SISO Tetrablock Terpolymers on a Simple Hexagonal Lattice*”, **Macromolecules**, ASAP (2011).
15. C. W. Pester, M. Ruppel, H. G. Schoberth, K. Schmidt, C. Liedel, P. van Rijn, K. A. Schindler, S. Hiltl, T. Czubak, J. Mays, V. S. Urban, A. Böker, “*Temperature Dependent Piezoelectric Properties of Non-polar Block Copolymers*”, **Advanced Materials** **23**, 4047 - 4052 (2011).
16. X. Wang, K. Hong, D. Baskaran, M. Goswami, B. Sumpter, and J. Mays, “*Asymmetrical Self-assembly From Fluorinated and Sulfonated Block Copolymers in Aqueous Media*,” **Soft Matter** **7**, 7960–7964 (2011).
17. R. Schlegel, Y. X. Duan, R. Weidisch, K. Schneider, M. Stamm, D. Uhrig, J.W. Mays, G. Heinrich, and N. Hadjichristidis, “*Strain Induced Deformation Mechanisms in Blockgraft and Multigraft Copolymers at High Strains*”, **Macromolecules** **44**, 9374 - 9383 (2011).
18. A.G. Richter, S. A. Dergunov, B. Ganus, Z. Thomas, S. V. Pingali, V. Urban, Y. Liu, L. Porcar, and E. Pinkhassik, “*Scattering Studies of Hydrophobic Monomers in Liposomal Bilayers: An Expanding Shell Model of Monomer Distribution*”, **Langmuir** **27**, 3792-3797 (2011).
19. J. Wang, H. Lu, R. Kamat, S. V. Pingali, V. S. Urban, J. J. Cheng, and Y. Lin, “*Supramolecular Polymerization from Polypeptide-Grafted Comb Polymers*”, **J. Am. Chem. Soc.** **133**, 12906-12909 (2011).
20. X. Wang, M. Goswami, R. Kumar, B. Sumpter, and J. Mays, “*Morphologies of Block Copolymers Composed of Charged and Neutral Blocks*”, **Soft Matter** **8**, 3036 - 3052 (2012).

Self-Assembly of Organic/Inorganic Nanocomposites

Investigators: Ting Xu, A. Paul Alivisatos, Tanja Cuk, Jean Fréchet, Yi Liu, Miquel Salmeron, Lin-Wang Wang

Materials Science Division, Lawrence Berkeley National Laboratory

Program Scope

Organic/inorganic nanocomposites with structural control over nanoparticle geometry and inter-particle electronic/optical communication can lead to development of functional hybrid materials with tailored electrical and optical properties. These materials can potentially impact in a range of applications for energy harvesting, energy storage, light management and microelectronic devices. Our goal is to design and synthesize organic and inorganic building blocks, and guide their assemblies into functional nanocomposite materials by developing a thorough understanding of the interfacial electronic properties with an ultimate goal to improve device performance of composite solar cells. This broad-based program takes advantage of local expertise in the production of inorganic nanocrystals with control over shape and composition and electroactive organic semiconductor and polymers, in directed hierarchical assemblies of multi-component systems, and in advanced characterization techniques and theoretical studies to investigate the electronic properties of nanomaterials and at the organic/inorganic interfaces.

Recent Progress

As a multi-faceted program addressing a complicated challenge, our program focuses on material design and synthesis, structural manipulation of nanocomposites and controlled optoelectronic communication at the organic/inorganic interfaces. Progresses have been made in each area through close collaboration among multiple investigators. Details of each subtask are described in three separate abstracts. The following summary abstract serves the purpose of global view of the program development and future plan.

Subtask 1. Transport and doping in nanocrystal solids with electronically active organic ligands (Alivisatos, Fréchet, Liu, Wang): In order to achieve high carrier mobilities in films, semiconducting nanocrystals rely on short molecular linkers to decrease the tunneling width for charge carrier transport. Difunctionalized conjugated ligands, including tetrathiafulvalenetetrathiolate, terthiophenedicarboxylic acid and terthiophenedithiol, were synthesized and ligand exchanged for monodisperse PbSe nanoparticle, 3-9 nm in size. The mobilities of the resulting films were measured as a function of nanoparticle size, energy level alignment between the nanocrystals and ligands, and the anchoring functionalities. The best devices have reproducibly shown field-effect mobilities achieving $1 \text{ cm}^2/\text{V}\cdot\text{s}$. To the best of our knowledge, this study is the first example where nanoparticle supercrystals have been assembled with highly conducting ligands. The results from this work will allow for the rational design of

highly conductive arrays of self-assembled nanocrystals functionalized with conjugated organic ligands.

To perform theoretical studies of interparticle transport in such supercrystals, we developed models describing the nanoparticle-ligand binding and geometry and applied them to the study of PbS (001) and (111) surfaces passivated by ligands with carboxylic acid (R-COOH) anchoring groups. We also investigated the carrier transport in a CdSe quantum dot (QD) supercrystal connected by Sn₂S₄ molecules. The carrier hopping between QDs can be described by Marcus theory and the hopping rate depends on the QD size and the molecule-QD attachment at the atomic level. The calculated carrier mobility agrees well with the experimental measurements. We plan to adapt this model to PbSe QDs with functionalized with conjugated ligands.

In addition to interparticle charge transport, we investigated the effect of organic molecules on nanoparticle doping. By exposing PbS nanocrystal thin films to solutions of known redox potential, which can be modulated by varying proportions of the oxidized and reduced forms of decamethylferrocene, the carrier concentration can be systematically, incrementally, and reversibly increased by two orders of magnitude from their native values (**Figure 2**).

Subtask 2. Directed Hierarchical Assemblies of Nanocomposites (Alivisatos, Fréchet and Xu): We developed a supramolecular approach to achieve hierarchical assemblies of nanospheres and nanorods with high precision. For nanorod-containing nanocomposites, the energetic contributions from nanorod ligand-polymer interactions, polymer chain deformation and rod-rod interactions are comparable and can be tailored to disperse nanorods with control over inter-rod ordering and the alignment of nanorods within BCP microdomains.

Additionally, we studied the phase behavior of supramolecular nanocomposites in thin films. Different from that observed previously in thin films of coil-coil block copolymers (BCPs), the entropic contributions from polymer chain conformation upon nanoparticle incorporation favor the incorporation of nanoparticles in the interior. We have obtained 3-D nanoparticle assemblies in thin films, i.e. layered nanoparticle sheets with in-plane hexagonal order and 3-D ordered arrays of single nanoparticle chains. They serve as a model system to investigate the effect of electronic percolation pathway on the charge mobility of nanoparticle ensembles.

Subtask 3. Electronic properties at the organic/inorganic interfaces (Salmeron, Cuk, Wang): We also developed unique ultra-flat electrodes in a transistor geometry (source-drain-gate) that make the study of transport in monomolecular films possible. The electronic transport properties of oligomers containing 5 thiophene rings have been studied using conductive AFM. We showed that the conduction is dominated by hole hopping, occurring preferentially in certain directions of the unit cell. Calculations confirm the experimental findings.

Future Plans

Our studies have showed that nanoparticle clusters connected with conductive ligands can be readily prepared to perform charge transport studies. Our future plans aim at a more detailed characterization of the designed materials to gain thorough understanding on electronic communication at the particle/ligand interface and between nanoparticles. We will carry out photoelectron spectroscopy at the Advanced Light Source to determine the energy level positions of ligands and nanoparticles., Structural characterization of the spatial organization of nanoparticles will be performed using conductive AFM, which allows for the study of carrier pathways in thin films and for the visualization charging/discharging events. Transient electrical experiments will be performed to study carrier trapping and its dependence on the organic linkers. We will also study charge transfer between two linked quantum dots using optical transient absorption spectroscopy. These studies will identify how charge separation occurs in a coupled quantum dot system.

In parallel, we will investigate the phase behavior of supramolecular nanocomposites containing organic semiconductors rather than alkyl molecules used in current studies. These organic semiconductors will be chemically identical or similar to those used to electronically connect nanoparticles as shown in **subtask I** and those characterized in **subtask III**. Understanding the phase behavior of these supramolecular nanocomposites will provide platform to interface with existing progress in subtask I and lead to electroactive nanocomposites.

These further studies will be coupled with theory as we plan to calculate the carrier hopping rates between PbSe quantum dots that are connected by organic linker molecules. We will investigate the dependence of the hopping rate on the organic molecule lengths and on the organic ligand and QD energy level alignments. We will carry out GW calculations on the ligand molecule to correct the band alignment problem in DFT calculations. Based on our calculations, we will suggest new molecular designs for the inter-QD connections in order to increase the conductivity of a QD supercrystal. Our realistic surface passivation model will also allow us to study the source of surface states of quantum dots that give rise to native doping and traps.

Publications

1. J. Kao, P. Bai, V. Chuang, D. J. Zhang, P. Ercius, T. Xu, Nanoparticle Assemblies in Thin Films of Supramolecular Nanocomposites, *Nano Letters*, ASAP, 2012.
2. K. Thorkelsson, A. Mastroianni, P. Ercius, T. Xu, Direct Nanorod Assembly Using Block Copolymer-based Supramolecules, *Nano Letters*, 12, 498, 2012. (The authors wish to thank J. Baker and P. Alivisatos for helpful assistance with nanorod synthesis.)
3. Virginia Altoe, Florent Martin, Allard Katan, Miquel Salmeron, and Shaul Aloni, Electron Microscopy Reveals Structure and Morphology of One Molecule Thin Organic Films *Nano Letters*. 12, 1295, 2012. (Science Editors' Choice, 9 March 2012)
4. J.B. Rivest, S.L. Swisher, L.K. Fong, H. Zheng and A. P. Alivisatos, "Assembled Monolayer Nanorod Heterojunctions," *ACS Nano* 5, 3811, 2011.

5. S. Dag, S.Z. Wang, L.W. Wang, "Large surface dipole moments in ZnO nanorods", *Nano Lett.* 11, 2348, 2011.
6. I-H. Chu, M. Radulaski, N. Vukmirovic, H.-P. Cheng, L.W. Wang, "Charge transport in a quantum dot supercrystal", *J. Phys. Chem. C* 115, 21409, 2011.
7. B. L.M. Hendriksen, F. Martin, Y. Qi, C. Mauldin, N. Vukmirovic, A. J. Katan, V. Altoe, S. Aloni, J.M.J. Frechet, L.W. Wang, M. Salmeron, "Electrical transport properties of oligothiophene based molecular films studied by current sensing atomic force microscopy", *Nano Lett.* 11, 4107, 2011.
8. Florent Martin, Bas Hendriksen, Allard Katan, Imma Ratera, Yabing Qi, Bruce Harteneck, Alex Liddle, Miquel Salmeron., Fabrication of ultra-flat coplanar electrodes for contacting molecular monolayers *Rev. Sci. Instrum.* 82, 123901, 2011.
9. J. L. Baker, A. Widmer-Cooper, M. F. Toney, P. L. Geissler, and A. P. Alivisatos, "Device-Scale Perpendicular Alignment of Colloidal Nanorods" *Nano Lett.* 10, 195, 2010.
10. R. Tangirala, J.L. Baker, A.P. Alivisatos, and D.J. Milliron, "Modular Inorganic Nanocomposites by Conversion of Nanocrystal Superlattices," *Angewandte Chemie. Int. Ed.*, 49, 2878, 2010
11. B. Rancatore, C. Mauldin, S. H. Tung, C. Wang, A. Hexemer, J. Strzalka, J. Fréchet, T. Xu, Nano-Structured Organic Semiconductor via Supramolecular Assemblies, *ACS Nano*, 4, 2721, 2010.
12. K. Thorkelsson, B. J. Rancatore, C. E. Mauldin, J. M. Luther, D. Poulsen, J. M. J. Fréchet, A. Paul Alivisatos, T. Xu, Modular Small-Molecule Directed Nanoparticle Assembly, *IEEE Proceeding*, 51, 2010.
13. Jeong Y. Park, Sabine Maier, Bas Hendriksen, and Miquel Salmeron, Sensing Current and Forces with SPM, *Materials Today*. 13, 37, 2010.
14. S. Dag, L.W. Wang, "Atomic and electronic structures of nano and amorphous CdS/Pt interfaces", *Phys. Rev. B* 82, 241303(R), 2010.
15. Y. Luo and L. W. Wang, "Electronic Structures of the CdSe/CdS Core-Shell Nanorods," *Acs Nano*, 4, 1, 91, 2010.
16. I. R. Franchini, G. Bertoni, A. Falqui, C. Giannini, L. W. Wang and L. Manna, "Colloidal Pbte-Au Nanocrystal Heterostructures," *J. of Materials Chemistry*, 20, 7, 1357, 2010.
17. C. Wadia, Y. Wu, S. Gul, S. K. Volkman, J. Guo, and A. P. Alivisatos, "Surfactant-Assisted Hydrothermal Synthesis of Single Phase Pyrite FeS₂ Nanocrystals," *J. Am. Chem. Soc.*, 21, 2568, 2009.
18. M.T. Sheldon, P.E. Trudeau, T. Mokari, L.W. Wang, A.P. Alivisatos, "Enhanced Semiconductor Nanocrystal Conductance via Solution Grown Contacts." *Nano Lett*, 9, 3676, 2009.
19. C. Wadia, Y. Wu, S. Gul, S. K. Volkman, J. Guo, and A. P. Alivisatos, "Surfactant-Assisted Hydrothermal Synthesis of Single Phase Pyrite FeS₂ Nanocrystals," *J. Am. Chem. Soc.*, 21, 2568, 2009.

Self-Assembly of Organic/Inorganic Nanocomposite Materials

Investigators: Ting Xu, A. Paul Alivisatos, Tanja Cuk, Yi Liu, J. Fréchet, Miquel Salmeron, Lin-Wang Wang

Materials Science Division, Lawrence Berkeley National Laboratory

Subtask #1: Transport and Doping in Nanocrystal Solids with Electronically Active Organic Ligands

Investigators: A. Paul Alivisatos, Jean M. J. Frechet, Yi Liu, Lin-Wang Wang

Program Scope

A nanocrystal solid is fundamentally a composite material, in which the interactions between semiconducting organic ligands and inorganic nanoparticles control both the charge transport and Fermi level of the film.¹ The objective of this program is to provide insight into the role this organic/inorganic interface plays in determining the charge mobility and free carrier concentration of the composite film. In our current studies, we aim to control the carrier concentration in porous nanocrystal thin films via redox buffers and to investigate the impact of conjugated organic linkers on interparticle charge transport.

In order to achieve high carrier mobilities in films, semiconducting nanocrystals rely on short molecular linkers to decrease the tunneling width for charge carrier transport. However, the self-assembly of nanocrystals into superlattices often requires long (> 1nm), bulky and insulating ligands to establish long-range order and controlled quasi-crystallization of nanoparticles.² In order to maximize film mobility while preserving the long-range order, we aim to functionalize lead selenide (PbSe) nanoparticles with long (1 – 1.5 nm) conjugated organic ligands with tailored lengths, HOMO-LUMO levels and binding groups. The charge transport properties of the resulting thin films can then be determined by incorporating them into field-effect transistors and measuring charge mobility. Coupled with the experimental data, theoretical calculations will be performed to investigate the role of ligand conjugation and functionalization on interparticle charge transfer. The results from this work will allow for the rational design of highly conductive arrays of self-assembled nanocrystals functionalized with conjugated organic ligands.

While our studies on conjugated ligands seek to probe the importance of energetic resonance for transport, the effects of organic ligands and inclusions on nanoparticle doping are less well understood. We are currently investigating these dynamics of organic-inorganic charge transfer doping through the use of inexpensive ferrocene-derived organometallic redox

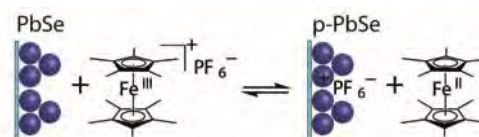


Figure 1: Mechanism and strategy for redox buffer doping. Equilibrium oxidation of a PbSe nanocrystal solid by Fe³⁺ accompanied by PF₆⁻ counterion infiltration into the film.

buffers (Figure 1). This application of redox buffers for controlled doping provides new opportunities to study the fundamentals of transport and defects in nanocrystal solids and establishes a new paradigm for the precise control of majority carrier concentration in porous semiconductor thin films.

Recent Progress

Towards investigating the interparticle charge transport in films, difunctionalized conjugated ligands, including

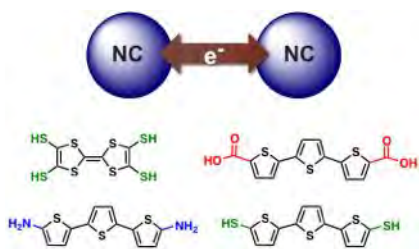


Figure 2. Structures of the conjugated ligands for studying charge transport within the inorganic component.

ligands, including tetrathiafulvalenetetrathiolate, terthiophenedicarboxylic acid and terthiophenedithiol, were synthesized (Figure 2). A library of monodisperse PbSe nanoparticle samples of sizes between 3 and 9 nm has also been synthesized, functionalized and systematically tested with the target ligands.³ The mobilities of the resulting films were measured as a function of (1) nanoparticle size, (2)

energy level alignment between the nanocrystals and ligands, and (3) the anchoring functionalities. The best devices have reproducibly shown field-effect mobilities achieving $1 \text{ cm}^2/\text{V}\cdot\text{s}$, which is unprecedented for organic ligands of this length scale. We have developed a procedure to arrive at extended, three-dimensional ordered arrays of the nanoparticle-ligand combination with the largest mobility as characterized by electron microscopy (Figure 3). To the best of our knowledge, this study is the first example where nanoparticle supercrystals have been assembled with highly conducting ligands, opening up exciting possibilities for photovoltaics, thermoelectrics and other applications.^{4,5}

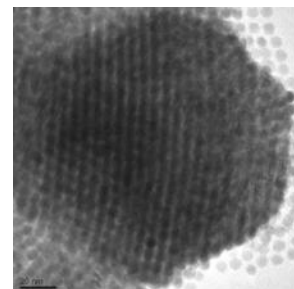


Figure 3: TEM micrograph of self-assembled PbSe nanocrystals cross-linked with a conjugated organic linker. The scale bar is 20nm.

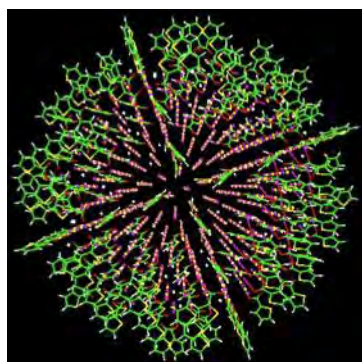


Figure 4: Simulation of passivation of a PbS nanoparticle with 2,5-thiophenedicarboxylic acid.

Supporting our mobility measurements, quantum mechanical calculations can provide insight into charge transport mechanism between nanoparticles. To perform the theoretical studies of interparticle transport in such supercrystals, we must first develop an accurate model of the nanoparticle-ligand binding and geometry. We have studied the passivation pattern of PbS (001) and (111) surfaces by 2,5-thiophenedicarboxylic acid, acetic acid and oleic acid, all of which have a carboxylic acid (R-COOH) anchoring group. For the (001) surface, every two surface PbS pairs have one molecule, and one O is attached to one S, while the OH is attached to one Pb atom. For the (111) surface with Pb termination, the R-COOH group will deprotonate. While the two oxygen atoms in $-\text{COO}^-$ locate at two centers of surface Pb-Pb lines, the hydrogen atom is at the

center of a Pb-Pb-Pb triangle. We have built a realistic QD model using these surface passivation parameters (Figure 4).

To provide a realistic model for interparticle charge transport, we investigated the carrier transport in a CdSe quantum dot (QD) supercrystal connected by a Sn₂S₄ molecule. We found that the carrier hopping from one QD to a neighboring QD can be described by Marcus theory. As a result, hopping rate depends on the QD size and the molecule-QD attachment at the atomic level. The calculated carrier mobility agrees well with the experimental measurements. We intend to adapt this model to PbSe QDs with functionalized with conjugated ligands.

In addition to studying the influence of conjugated ligands on interparticle charge transport, we are investigating the effect of organic molecules on nanoparticle doping. Chemical methods for doping nanocrystal solids have thus far provided poor control over the doping density because they rely on kinetic or stoichiometric limitations on the reaction.⁶ We have found that, by exposing PbS nanocrystal thin films to solutions of known redox potential, which can be modulated by varying proportions of the oxidized and reduced forms of decamethylferrocene, the carrier concentration can be systematically, incrementally, and reversibly increased by two orders of magnitude from their native values (Figure 5). Carrier concentrations are measured using thin-film transistor measurements, and low-temperature cyclic voltammetry provides band edge positions to allow for easy selection of an appropriate redox couple. The strength of this redox buffer technique sets the Fermi level of the film directly and exerts thermodynamic control, reaching a unique equilibrium value for each potential.

Future Plans

For the charge transport studies, our future plans aim at a more detailed characterization of the designed materials to allow for a deeper understanding of the mobility dependence in the films described above. The characterization methods will include: (1) photoelectron spectroscopy at the Advanced Light Source beam line to determine the energy level positions of all ligands and nanoparticles with greater accuracy, (2) grazing-incidence small angle X-ray scattering experiments to monitor the degree of ordering in self-assembled thin films, (3) conductive AFM measurements to reveal carrier pathways in thin films and visualize charging/discharging events, and (4) transient electrical experiments to study carrier trapping and its dependence on the organic linkers.

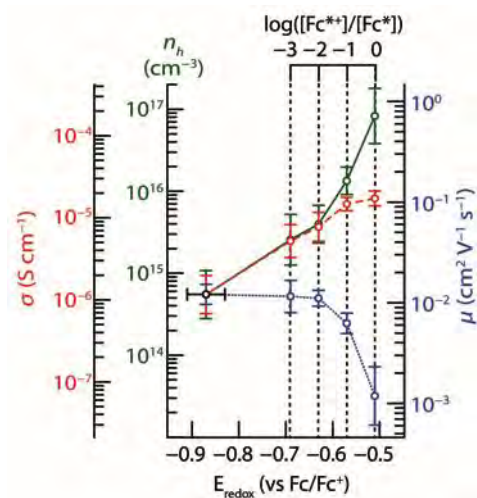


Figure 5: Dependence of doping on solution redox potential. Small field conductivity, σ (—), linear field-effect mobility, μ (■), and hole majority carrier density, n_h (—), of PbSe nanocrystal solid films as a function of the potential of the Fc^*/Fc^{*+} doping solution.

These further studies will be coupled with theory as we plan to calculate the carrier hopping rates between PbSe quantum dots that are connected by organic linker molecules. We will investigate the dependence of the hopping rate on the organic molecule lengths and on the organic ligand and QD energy level alignments. We will carry out GW calculations on the molecule to correct the band alignment problem in DFT calculations. Based on our calculations, we will suggest new molecules for the inter-QD connections in order to increase the conductivity of a QD supercrystal. Our realistic surface passivation model will also allow us to study the source of surface states of quantum dots that give rise to native doping and traps.

Finally, controlled chemical doping opens new avenues for exploring the fundamentals of transport and defects in nanocrystal solids. Measuring the effect of varying counterion size, polarizability, and concentration on transport may shed light on the nature of the Columbic interactions between free carriers and the dielectric environment of the effective medium. Additionally, the stability and efficiency of controlled doping experiments can prove to be a sensitive probe of the extent to which different surface passivation strategies reduce the concentration of surface defects.

References

1. Talapin, D. V.; Lee, J.-S.; Kovalenko, M. V.; Shevchenko, E. V. *Chemical Reviews* **2010**, *110*, 389–458.
2. Liu, Y.; Gibbs, M.; Puthussery, J.; Gaik, S.; Ihly, R.; Hillhouse, H. W.; Law, M. *Nano Letters* **2010**, *10*, 1960–1969.
3. Ma, W.; Swisher, S. L.; Ewers, T.; Engel, J.; Ferry, V. E.; Atwater, H. A.; Alivisatos, A. P. *ACS Nano* **2011**, *5*, 8140–8147.
4. Lin, Y.-M.; Dresselhaus, M. S. *Phys. Rev. B* **2003**, *68*, 075304-14.
5. Kramer, I. J.; Sargent, E. H. *ACS Nano* **2011**, *5*, 8506–8514.
6. Norris, D.J.; Efros, A.L.; Erwin, S.C. *Science* **2008**, *319*, 1776-9.

Publications

1. Engel, J. H., Surendranath, Y., Alivisatos, A. P., “Controlled Chemical Doping of Semiconductor Nanoparticles Using Redox Buffers”, *Nature Materials* (**in review**).
2. Hendriksen, B. L. M.; Martin, F.; Qi, Y.; Mauldin, C.; Vukmirovic, N.; Ren, J.; Wormeester, H.; Katan, A. J.; Altoe, V.; Aloni, S.; Fréchet, J. M. J.; Wang, L.-W.; Salmeron, M. “Electrical Transport Properties of Oligothiophene-Based Molecular Films Studied by Current Sensing Atomic Force Microscopy.” *Nano Lett.* **2011**, *11*, 4107-4112.
3. I-H. Chu, M. Radulaski, N. Vukmirovic, H.-P. Cheng, L.W. Wang, "Charge transport in a quantum dot supercrystal", *J. Phys. Chem. C* **2011**, *115*, 21409.
4. Y. Luo and L. W. Wang, "Electronic Structures of the CdSe/CdS Core-Shell Nanorods," *ACS Nano* **2010**, *4*, 91-98.

Self-Assembly of Organic/Inorganic Nanocomposite Materials

Investigators: Ting Xu, A. Paul Alivisatos, Tanja Cuk, Yi Liu, J. Fréchet, Miquel Salmeron, Lin-Wang Wang

Materials Science Division, Lawrence Berkeley National Laboratory

Subtask #2: Directed Hierarchical Assemblies of Nanocomposites

Investigators: Alivisatos, Fréchet and Xu

Program Scope

Organic/inorganic nanocomposites with structural control over nanoparticle displacement and inter-particle electronic/optical communication can lead to development of functional hybrid materials with tailored electrical and optical properties; and can potentially impact a range of applications for energy harvesting, energy storage, light management and microelectronic devices. The goal of this program is to design and synthesize organic and inorganic building blocks, guide their assemblies into functional nanocomposite materials through developing a thorough understanding of the interfacial electronic properties with an ultimate goal to improve device performance of composite solar cells. This broad-based program takes advantage of local expertise in the production of inorganic nanocrystals with control over shape and composition and electroactive organic semiconductor and polymers, the directed hierarchical assemblies in multi-component systems, the advanced characterization techniques and the theoretical studies to investigate the electronic properties of nanomaterials and at the organic/inorganic interfaces.

As the subtask II of the “Self-Assembly of Organic/Inorganic Nanocomposites” program, we aim to develop versatile approaches to control hierarchical assemblies of nanoparticles with single particle precision toward electroactive nanocomposites. Specifically, we focus on fundamentally understanding the phase behavior of blends of nanoparticles and block copolymer-based supramolecules in bulk and in thin films to generate 1-, 2- and 3-D ordered arrays of nanoparticles that are electronically connected. These hierarchically structured nanocomposites will provide model platform to develop basic understanding in the effects of electronic percolation pathway on the charge mobility of nanoparticle ensembles and overall device performance.

Recent Progress

Blends of nanoparticles and block copolymer (BCP) can result in structured nanocomposites in bulk and in thin films.¹ However, solubilizing nanoparticles in a polymeric matrix requires chemical modification of nanoparticle ligands to interact favorably with at least one BCP block. There is limited control over inter-particle ordering and the nanoparticles tend to disperse within BCP microdomains, making it difficult to electronically connect nanoparticles toward electroactive nanocomposites. We developed a supramolecular approach to direct

nanoparticle assemblies where small molecules are hydrogen bonded to the polymer side chains. The presence of small molecules effectively mediates the particle-polymer interactions and decouples the nanoparticle surface chemistry from that of BCP. Small molecules can also be used to tailor inter-particle ordering within BCP microdomains. Using a supramolecule, polystyrene-block-poly-4-vinylpyridine (3-pentadecylphenol) (PS-*b*-P4VP(PDP)), a wide variety of nanoparticles with native alkyl ligands, such as Au, PbS, PbSe and CdSe, can be assembled.² Our recent work focused on two areas to develop foundation toward electroactive nanocomposites.

Inorganic nanorods exhibit unique electronic properties desirable for composite solar cell. Blending nanorods with BCP-based supramolecules also provides a simple route to enhance macroscopic mechanical and electrical properties of

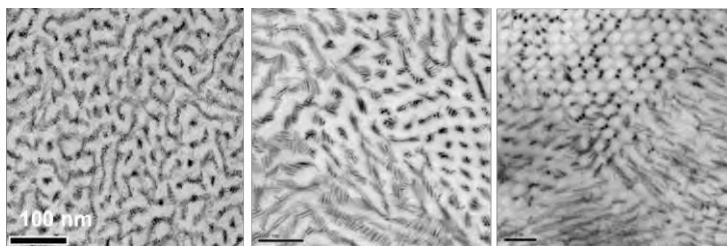


Figure 1: (left to right) TEM images showing continuous nanorod networks, nanorod clusters and highly aligned arrays of nanorods

nanocomposites. Our studies have shown that in supramolecule/nanorod blends, the energetic contributions from rod-polymer interaction, polymer chain deformation and rod-rod interactions are comparable and can be tailored to disperse nanorods with control over inter-rod ordering and relative alignment of nanorods with respect to the BCP microdomains. As shown in **Figure 1**, a wide library of nanorod assemblies including highly aligned arrays of nanorods, continuous nanorod networks, and nanorod clusters, can be readily accessed. Since the macroscopic alignment of BCP microdomains can be obtained in bulk and in thin films by the application of external fields, present studies open up a new route to manipulate macroscopic alignments of nanorods.

Many nanoparticle-based devices require 3-D ordered arrays of nanoparticles to be fabricated in thin film configurations. Hypothetically, if one can directly translate the assemblies of preformed nanoparticles in bulk into thin films with high fidelity, the present bottleneck in nanoparticle-based nanodevices would be overcome. However, various studies have shown that the thermodynamics and the assembly kinetics governing the phase behavior of BCP-based nanocomposites in thin films can be quite different from that in bulk. The second aspect

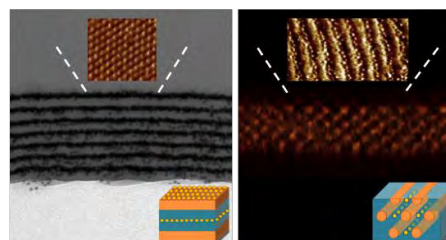


Figure 2: 3-D nanoparticle assemblies in thin films: (left) layered nanoparticle sheets with in-plane hexagonal order and (right) 3-D ordered arrays of single nanoparticle chains

of our efforts focused on the phase behavior of supramolecular nanocomposites in thin films. Different from that observed previously in thin films of coil-coil BCPs, the entropic contributions from polymer chain conformation upon nanoparticle incorporation favor the incorporation of nanoparticles in the interior of thin films. Layered nanoparticle sheets with in-plane hexagonal order and 3-D ordered arrays of single nanoparticle chains can be obtained in

thin films as shown in **Figure 2**. Fundamentally, we showed that the mechanisms to obtain 3-D nanoparticle assemblies in thin films of lamellar and cylindrical nanocomposites are different. For lamellar nanocomposites, the parallel lamellar nanocomposite thin films may be in a kinetically trapped state. For cylindrical nanocomposites, however, the nanoparticles act as filler, localizing in the interstitial regions between cylindrical microdomains to effectively release the comb block deformation. Energetically, the entropy gain overcomes the differences in the surface tension between nanoparticle and supramolecule and stabilizes 3-D nanoparticle assemblies within the film.

Future Plans

Based on these developments, our future work will focus on developing approaches to electronically connect nanoparticles in structured nanocomposites. First, we will apply ligand exchange process to remove the native alkyl ligands on the nanoparticle surface in-situ after self-assembly within the supramolecule thin film framework. This is similar to what has been routinely performed in the fabricate schottky junction solar cell. Three types of ligands will be explored. One is short alkyl dithiol, such as ethane dithiol (EDT). The second route is to perform ligand exchange using recently developed inorganic ligands by exposing the nanoparticle assembly to a $(\text{NH}_4)_2\text{S}$ solution.³ Preliminary results suggest that the structural integrity of the nanoparticle assembly was maintained after the ligand removal process. However, the potential difficulty is that both ligands are shorter than the native alkyl ligands. Ligand exchange may lead to lateral shrinkage of local particle ensemble and consequently, discontinuities in the electronic percolation pathway. The third route is to exchange using organic semiconductors developed in **subtask I**, where the length of the ligand molecule can be readily tailored to match that of native alkyl ligands. Preliminary results in **subtask I** clearly showed that charge mobilities can be maintained without lateral shrinkage upon ligand exchange using designed organic linker.

Our current approach is based on an alkyl small molecule acting as insulator between nanoparticles. Systematic studies of blends of nanoparticle and alkyl-containing supramolecules provide basic foundation to understand parameters governing the phase behavior of nanocomposites in bulk and in thin films. An important goal of our program is to generate electroactive nanocomposites for solar cell fabrication. To this end, we substituted the alkyl molecule with organic semiconductors. We have investigated the supramolecules containing organic semiconductors to provide guidance toward electroactive nanocomposites. We showed that the supramolecule containing a quaterthiophene organic semiconductor forms supramolecular assemblies that act as p-type semiconductors in field-effect transistors. In thin films, the quaterthiophenes can be readily assembled into microdomains, tens of nanometers in size, oriented normal to the surface. The supramolecules exhibited the same field-effect mobilities as that of the quaterthiophene alone ($10^{-4} \text{ cm}^2/\text{Vs}$).

We plan to investigate nanocomposites based on these organic semiconductor-containing supramolecules in bulk and in thin films. Specifically, we aim to develop systematic

understanding on the crystallization and molecular packing of organic semiconductors on the nanoparticle assemblies. We will also characterize electronic properties of this new family of nanocomposites. Since the organic semiconductors can be readily substituted, this modular supramolecular approach should be applicable to conductive ligands studied in **subtask I**. For each approach, our future efforts will be focused on structural characterization of nanocomposites upon ligand exchange and studies the electron percolation properties of the NP arrays as detailed in **subtask III**.

References

1. Balazs, A.C., Emrick, T. & Russell, T.P. Nanoparticle polymer composites: Where two small worlds meet. *Science* 314, 1107-1110 (2006).
2. Zhao, Y. et al. Small-molecule-directed nanoparticle assembly towards stimuli-responsive nanocomposites. *Nature Materials* 8, 979-985 (2009).
3. Zhang, H.T. et al. Surfactant Ligand Removal and Rational Fabrication of Inorganically Connected Quantum Dots. *Nano Letters* 11, 5356-5361.

Publications

1. J. Kao, P. Bai, V. Chuang, D. J. Zhang, P. Ericius, T. Xu, Nanoparticle Assemblies in Thin Films of Supramolecular Nanocomposites, *Nano Letters*, 2012, *ASAP*.
2. K. Thorkelsson, A. Mastroianni, P. Ericus, T. Xu, Direct Nanorod Assembly Using Block Copolymer-based Supramolecules, *Nano Letters*, 2012, 12, 498. (The authors wish to thank J. Baker and P. Alivisatos for helpful assistance with nanorod synthesis.)
3. B. Rancatore, C. Mauldin, S. H. Tung, C. Wang, A. Hexemer, J. Strzalka, J. Fréchet, T. Xu, Nano-Structured Organic Semiconductor via Supramolecular Assemblies, *ACS Nano*, 2010, 4, 2721.
4. K. Thorkelsson, B. J. Rancatore, C. E. Mauldin, J. M. Luther, D. Poulsen, J. M. J. Fréchet, A. Paul Alivisatos, T. Xu, Modular Small-Molecule Directed Nanoparticle Assembly, *IEEE Proceeding*, 2010, 51.
5. J. Kao, P. Bai, M. Lucas, A. P. Alivisatos, T. Xu, Directed Assemblies of Nanoparticle Mixtures in Thin Films, 2012, *submitted*.
6. B. Rancatore, C. Mauldin, J. Fréchet, T. Xu, Molecular Ordering of Organic Semiconductor Dictates Supramolecular Assemblies, 2012, *submitted*.

Self-Assembly of Organic/Inorganic Nanocomposite Materials

Investigators: Ting Xu, A. Paul Alivisatos, Tanja Cuk, Yi Liu, J. Fréchet, Miquel Salmeron, Lin-Wang Wang

Materials Science Division, Lawrence Berkeley National Laboratory

Subtask #3: Characterization

Investigators: Miquel Salmeron, Tanja Cuk, Liu

Program Scope

Organic/inorganic nanocomposites with structural control over nanoparticle displacement and inter-particle electronic/optical communication can lead to development of functional hybrid materials with tailored electrical and optical properties; and can potentially impact a range of applications for energy harvesting, energy storage, light management and microelectronic devices. The goal of this program is to design and synthesize organic and inorganic building blocks, guide their assemblies into functional nanocomposite materials through developing a thorough understanding of the interfacial electronic properties with an ultimate goal to improve device performance of composite solar cells. This broad-based program takes advantage of local expertise in the production of inorganic nanocrystals with control over shape and composition and electroactive organic semiconductor and polymers, the directed hierarchical assemblies in multi-component systems, the advanced characterization techniques and the theoretical studies to investigate the electronic properties of nanomaterials and at the organic/inorganic interfaces. As subtask III of the organic/inorganic nanocomposite, we focus our efforts on the characterization of organic films, nanowires and nanoparticles and their function.

Recent Progress

Transport properties of organic conductors (Salmeron). The electronic transport properties of D5TBA and 5TBA, oligopolymers containing thiophene rings have been studied using conductive AFM. These oligomers are models for a class of thiophene-based polymeric conductors used in BHJ solar cells and other molecular electronic applications. Because they crystallize in the Langmuir trough and can be easily transferred to a substrate they are ideal models to investigating the effect of their molecular scale structure on the electrical transport. WE characterized them with AFM (lattice periodicity), with TEM (unit cell structure and orientation in different domains), and X-ray Absorption Spectroscopy to determine electronic levels and angular orientation. I-V spectra with the conductive AFM tip allowed us to determine the onset of hole and electron conductivity, due to alignment of

Model organic conductors: oligothiophenes

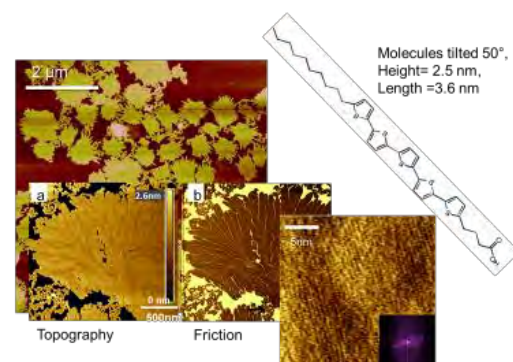


Figure 1: AFM images of crystalline islands of D5TBA molecules (schematic on top right). dot are shown. The islands are composed of monocrystalline domains separated by grain boundaries. A lattice resolved image (bottom right) and its 2D Fourier transform reveals the lattice periodicity.

the HOMO and LUMO levels with the Fermi level at the appropriate bias voltage. We confirmed that the dominant conduction mechanism is hole hopping. More interestingly we determined that conduction occurs preferentially in certain directions of the unit cell. The unit cell was revealed by TEM to contain two molecules with their thiophene planes oriented at an angle and forming a herringbone structure. In one direction the thiophene planes are parallel to each other and this is the easy electronic transport direction. Calculations by Lin-Wang Wang helped interpret the experimental findings.

Charge Transfer between Asymmetrical, Linked Quantum Dots (Cuk). Electronic tunneling between two quantum dots mimics ionic-like or covalent-like bonds depending on the degree of inter-dot coupling. As a result of inter-dot coupling and electronic tunneling, a re-distribution of charge can lead to either isolated charges on each quantum dot (ionic bonds) or delocalization across both quantum dots (covalent bonds). Coupled quantum dot systems have largely been studied in integrated, gated silicon devices with possible application for quantum computing. Previous measurements consist mainly of current-voltage curves of Coulomb blockade and

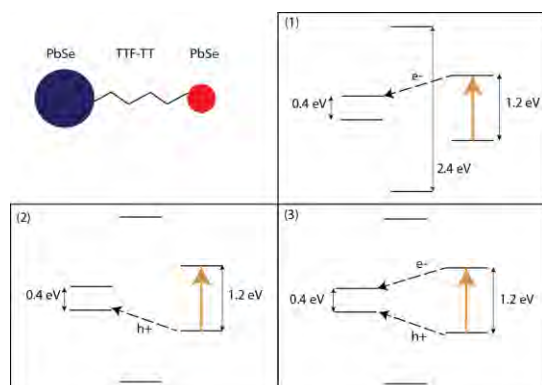


Figure 2: Two asymmetrically sized PbSe are linked by an organic ligand. Three scenarios of charge transfer excited by a light pulse resonant with the band gap of the smaller quantum dot are shown.

photon (microwave) assisted tunneling [2]. However, photo-activated devices involving coupled quantum dots, anywhere from two to an array, require knowledge of the kinetics of electron-hole pair separation and recombination pathways that cannot be obtained from current measurements. We plan to investigate two asymmetric quantum dots coupled through an organic linker using ultrafast transient absorption spectroscopy. The two asymmetric quantum dots could be, for example, two differently sized PbSe quantum dots with markedly different band gaps [3] (e.g., 1.2 eV vs. 0.4 eV) or quantum dots of two different materials, involving combinations of PbS, PbSe, CdS, and CdSe; they will be synthesized by the Alivisatos group. The relative band alignment will be designed to suppress resonance energy transfer, ensure that two distinct

spectra can be probed in the near infrared, and create a driving force for tunneling between one quantum dot and another. Previous experiments reporting optical spectra of linked dimers and trimers do show the presence of energy transfer in quantum dots of similar size; we hope to suppress this energy transfer in favor of charge transfer with quantum dots of markedly different band gaps [4]. The two quantum dots will be linked through an organic ligand with a band gap whose energy levels straddle that of either quantum dot as shown in Figure 1 or one in which the HOMO of the ligand aligns with that of the quantum dots, as in the TTF-TT systems grown by Xu. This organic linker serves as an insulating barrier through which the only avenue for charge transfer is electronic tunneling for excitation energies below the band gap of the organic ligand. This configuration replicates the structure of molecules and is the basic building block of more extensive array systems assembled in Xu's group.

In the past year, we have set up a time resolved optical and infrared system with capabilities of pumping and probing between 300nm and 20um at the ultrafast, 100fs time scale. The setup consists of a Ti:Sapphire ultrafast laser system, with 3.5mJ, 100fs, 1kHz pulses pumping an optical parametric amplifier with output between 300nm and 20um, purchased from Coherent.

Another 1.5 mJ is used to create light in the VIS and near IR range (500nm-1.4um) in a Non-collinear Optical Parametric Amplifier (NOPA) that we designed. Depending on the size of the quantum dots, we will use either the NOPA or OPA to probe their spectrum. Currently, the pump-probe optics are set up in a non-collinear, crossed geometry for thin film investigations. However, a collinear setup is in progress to investigate nanoparticles in solution. Discussions with the Alivisatos group are currently being undertaken to determine the best experimental geometry. If needed, the lab is equipped with spectrometers covering the full wavelength range; we are currently in the process of purchasing the appropriate detectors for the mid infrared regime, which will be relevant for probing the band gaps of the larger quantum dots. Future Plans (Cuk)

Future plans include designing an optical setup that will be dedicated to the investigations of linked quantum dots. Our first experiments will involve pumping the linked quantum dots with a photon of high enough energy to send the electron over the LUMO of the organic ligand. This will transiently create a charge separated state with an electron on one quantum dot and a hole on the other. These experiments do not require electron tunneling. The incoming pump pulse has enough energy to split apart the exciton, stabilizing the charge separated state over a certain time scale.

The next experiments will involve pumping precisely the band gap one quantum dot and probing the other, necessitating tunneling pathways. Figure 1 shows examples of different excitation pathways that could be investigated in the case of two differently sized quantum dots: (1) Pumping the smaller quantum dot and probing electron transfer to the larger quantum dot (2) Pumping the smaller quantum dot and probing hole transfer to the larger quantum dot (3) Pumping the smaller quantum dot and probing the transfer of the exciton to the larger quantum dot prior to recombination. The charge transfer just described—resulting from pumping either the high above the LUMO of the organic linker or a single quantum dot—will be accompanied by nuclear motion leading to “phonon assisted” charge transfer. This nuclear motion includes phonons in the lattice of the quantum dot as well as motion of the quantum dots relative to each other and the organic linker. How electron transfer relates to nuclear motion has been well-described by Marcus theory in molecules [5]; these investigations would apply that theory to coupled quantum dots.

Future Plans (Salmeron)

We plan to use our conductive AFM (in contact mode) to continue our studies of electric transport in polymer assemblies, but this time containing nanoparticles of CdS and CdSe. The films will be deposited on source-gate-drain transistor structures. Also, using non-contact AFM we plan to map the contact potential distribution during transport of charge from source to drain and as a function of gate voltage with the idea of determining the charge transfer points. For example, the preliminary result in Fig. 3 shows the potential distribution in our transistor with the gate biased at 5V. The potential map shows a good uniformity across the gap filled with the nanoparticle film. As current flows the potential changes following the path of the current.

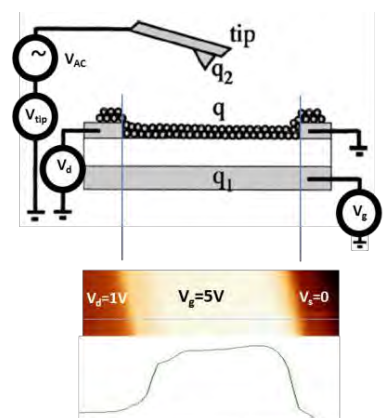


Fig. 3: Transistor geometry (source-gate-drain) to study electrical transport in organic-inorganic films. The example shows the potential distribution measured with Kelvin probe when the gate is biased at 5 V.

We plan to improve the development of ultra-flat coplanar electrodes for transport studies of molecularly thin films of organic conductive molecules (Pub. 4). These will be applied to studies of oligothiophenes and molecules of n-type character (Dodecyl Triethylamine Perylene Diimide as described in **subtask I**, in collaboration with Yi Liu).

Finally we also plan to use newly developed plasmonic tips at the Molecular Foundry [1], to perform TERS (tip enhanced Raman) as well as to excite locally (within 10-20 nm) electronic HOMO-LUMO transitions in conducting polymer films with and without nanoparticles, to study charge separation and transport in the flat electrode geometry developed in the last cycle of the program.

References

[1]. *Hyperspectral Nanoscale Imaging on Dielectric Substrates with Coaxial Optical Antenna Scan Probes*. Alexander Weber-Bargioni, Adam Schwartzberg, Matteo Cornaglia, Ariel Ismach, Jeff Urban, YuanJie Pang, Reuven Gordon, Jeff Bokor, Miquel Salmeron, D. Frank Ogletree, Stefano Cabrini, P. James Schuck. **Nano Letters**. 11, (3) 1201-1207 (2011)

[2] Wiel, W.G., *et. al.* "Electron transport through double quantum dots", *Rev. Mod. Phys.*, vol. 75, pp. 1 (2003)

[3] Moreels, I. *et. al.*, "Composition and Size-Dependent Extinction Coefficient of Colloidal PbSe Quantum Dots," *Chem. Mater.*, vol. 19, pp. 6101 (2007)

[4] Xu, X. *et. al.*, "Assembly and Separation of Semiconductor Quantum Dot Dimers and Trimers," *J. Am. Chem. Soc.*, vol. 133, pp. 18062 (2011).

[5] Marcus, R. "Electron transfer reactions in chemistry. Theory and experiment," *Rev. Mod. Phys.*, vol. 65 (1993).

Publications

1. *Electron Microscopy Reveals Structure and Morphology of One Molecule Thin Organic Films* Virginia Altoe, Florent Martin, Allard Katan, Miquel Salmeron, and Shaul Aloni

Nano Letters. 12, 1295–1299 (2012). Science Editors' Choice (Sciencewww.sciencemag.org Volume 335, Number 6073, Issue of 9 March 2012 ©2012)

2. *Fabrication of ultra-flat coplanar electrodes for contacting molecular monolayers*

Florent Martin, Bas Hendriksen, Allard Katan, Imma Ratera, Yabing Qi, Bruce Harteneck, Alex Liddle, Miquel Salmeron. **Rev. Sci. Instrum.** 82, 123901 (2011)

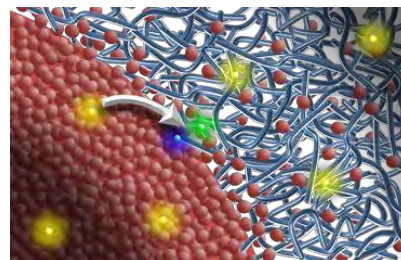
3. *Electrical transport properties of penta-thiophene based molecular films studied by current sensing AFM*. Bas L. M. Hendriksen, Florent Martin, Yabing Qi, Clayton Mauldin, Nenad Vukmirovic, JunFeng Ren, Herbert Wormeester, Allard J. Katan, Virginia Altoe, Shaul Aloni, Jean M. J. Frechet, Lin-Wang Wang, and Miquel Salmeron. **Nano Letters**. 11 (10), 4107–4112 (2011).

4. *Sensing Current and Forces with SPM*. Jeong Y. Park, Sabine Maier, Bas Hendriksen, and Miquel Salmeron. **Materials Today**. 13 (10), 37-44 (2010)

***UNIVERSITY GRANT
PROJECTS***

Fundamental Science of High Open Circuit Voltage Excitonic Solar Cells

H. Ade, Dept. of Physics, NCSU, Raleigh, NC27695



Program Scope

We develop [1-3] and use novel soft x-ray methods to characterize bulk-heterojunction (BHJ) organic photovoltaic (OPVs) devices and relate quantitative measurements about domain size, purity, interface properties, crystallization and texture, and non-crystalline ordering to device performance and molecular design. This provides a much more detailed understanding of device performance than otherwise possible, thus providing rational design paradigms in a field that has often progressed by Edisonian approaches and use of heuristic principles.

Recent Progress

We focus on the following three main areas (two of which will be described in detail below): i) We are in the process of establishing that molecular ordering near a BHJ interface is an important parameter in OPV performance. This will add a previously ignored critical parameter to the present, canonical BHJ paradigm as depicted in Fig. 1. This advance has been made possible by the development of a novel characterization method based on scattering of polarized soft x-rays that is sensitive to crystalline and non-crystalline ordering. The work has been recently published in *Nature Materials* [1]. ii) We have established that there is a high degree of miscibility between the donor polymer and the fullerene acceptor in many common OPV materials systems [4-7]. The degree of miscibility is likely directly related to device function and needs to be controlled in order to optimize devices. iii) We quantify the domain size and purity in a number of high performance OPVs systems and relate these morphological characteristics to device performance [8-12]. We find that in some cases excellent performance can be achieved with domain sizes much larger than commonly assumed necessary and shown as ~ 10 nm in size in Fig. 1 [11, 13]. Why some systems show such excellent performance in violation of the canonical assumptions remains to be determined and is likely related to specific intermolecular interactions.

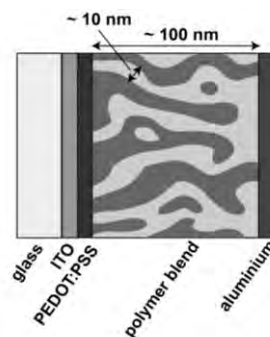


Figure 1. Schematic diagrams of a bulk-heterojunction organic solar cell, representing the present canonical paradigm.

Resonant scattering with polarized soft x-rays (P-SoXS): Molecular orientation critically influences many mechanical, chemical, optical and electronic properties of organic materials. So far, molecular-scale orientational ordering in soft matter could be characterized

with electron microscopy or x-ray techniques only if the sample exhibited sufficient crystallinity. We have shown that the resonant scattering of polarized soft X-rays by molecular orbitals is not limited by crystallinity and that it can be used to probe molecular orientation in domains as small as 10 nm. P-SoXS furthermore revealed scattering anisotropy arising from the amorphous domains of an all-polymer organic solar cell where interfacial interactions pattern orientational alignment in the matrix phase (See Fig. 2). The energy and q-dependence of the scattering anisotropy allows the identification of the composition and the degree of orientational order in the domains without the need to have complementary information from a real-space method.

Scattering anisotropy has been consistently observed in a large fraction of OPV systems investigated by us and others, including many fullerene-based devices. With very few exceptions, we observe very strong correlation of high device performance and a high degree of scattering anisotropy. This is the case even in systems that have very low crystallinity. In a particularly instructive study, fluorine substitution on the backbone resulted in high device performance and is correlated with a face-on to edge-on transition of the polymer at the BHJ interface with the fullerene. Charge separation, charge transport, and charge recombination are all affected by the molecular structure and relative orientation at the interface. Consequently, molecular orientation near a bulk heterojunction interface has to be added as an important parameter to the canonical OPV operations diagram shown in Fig. 1. P-SoXS is the only tool that can probe local, relative, crystalline and non-crystalline molecular ordering at the nanoscale and the field can now investigate this important aspect of devices. Improved insight of the structure of the interface will allow improved control of the charge dynamics. This work is thus directly related to DOE grand challenge #1.

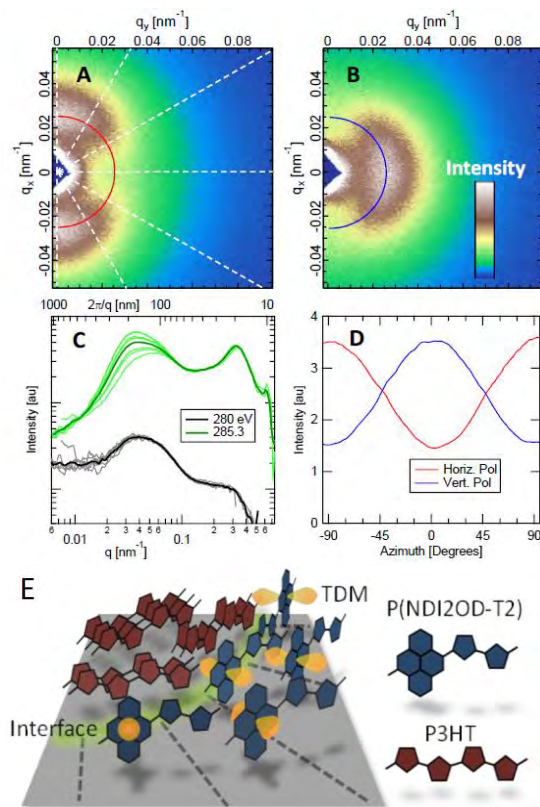


Figure 2. P-SoXS of P3HT:P(NDI2OD-T2) blend films. (a,b) Anisotropic scattering patterns obtained using linear horizontally (a) and vertically (b) polarized 285.3 eV photons. (c) Radial scattering profiles at non-resonant (black) and resonant (green) energies. Darker lines are averages over the entire azimuth whereas lighter lines are from 30° sectors along the azimuth as indicated by white dashes in part (a). (d) $I(\psi)$ for $q = 0.04 \text{ nm}^{-1}$ (color-coded circles in a) and b). (e) Molecular-scale perspective at the blend interface formed in the phase-separated materials. The green line represents the interface between material phases. P(NDI2OD-T2) transition dipole moments (shown in yellow) determine how the molecules scatter resonant X-ray photons and in this sample are aligned radially along the curved interface. This corresponds to an “edge-on” geometry relative to the BHJ interface.

Miscibility. We have measured with high precision the miscibility of phenyl- C_{61} -butyric acid methyl ester (PCBM) in the amorphous regions of poly(3-hexylthiophene) (P3HT) as a function of temperature, polymer grade [6] and supplier [4] (see Fig. 3). We have also shown that there is significant dependence on fullerene type [5] and that de-mixing and mixing pathways lead to the same measured values [7]. The original work [6, 14] lead to the invitation to write a perspective for JCPL [4]. This work has lead to active collaborations with the McGehee group from Stanford and the groups of Prof. J. Durrant and N. Stingelin from Imperial College, who are seeking complementary information that only soft x-rays can provide to their own studies. We are in the process of measuring the miscibility in systems for which these groups have already investigated considerable effort to understand the device structure and performance. Comparative studies will allow establishing the importance of miscibility as a controlling parameter.

A working hypothesis has been established that in most systems with high performance, the donor and acceptor materials are comparatively immiscible. Interestingly, from a device stability perspective and hence lifetime consideration, high miscibility is advantageous as the device is not as far from equilibrium. Hence, conflicting engineering considerations are at work: Performance seems to require low miscibility, good life-time is easier to achieve with high miscibility. Inherently, spin-cast OPV devices are systems often far from equilibrium and their reliable fabrication and stabilization far from equilibrium directly relates to DoE grand challenge #5.

Future Plans

We have build up a set of tools and methods that provide unique information on OPV systems and are now poised to exploit their capabilities to provide deep insight into OPV processing methods, impact of molecular design of constituent materials, and device function. We have established collaborations to synthetic groups (e.g. Wei You at UNC, two groups from South China University of Technology) and complementary characterization and processing groups (McGehee, Stingelin, Durrant, McNeil, and Neher). We will systematically characterize high performance systems (all-polymer and polymer-fullerene based) to learn why they work so well and how they can be further improved. The deep insight provided will accelerate the transition from discoveries in the lab to real-world applications.

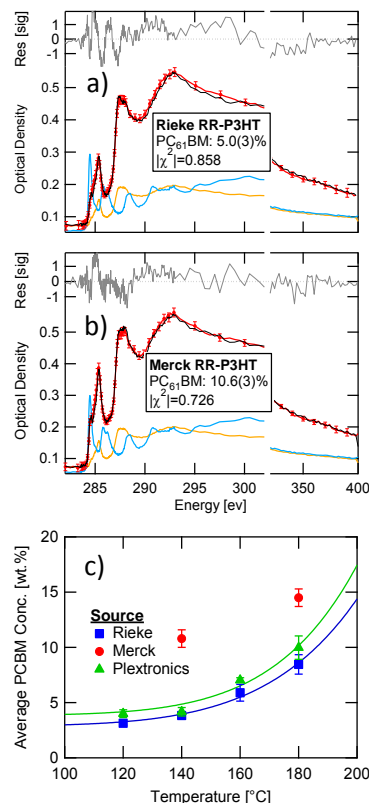


Figure 3: Manufacturer-Dependent Miscibility Study. a) & b) Least-squares fits to Rieke and Merck-sourced blend films, respectively, annealed at 140 °C until at equilibrium. c) Miscibility diagram for three P3HT batches. Lines are guides for the eye.

References

- [1] B. A. Collins *et al.*, Nat Mater **advance online publication**, DOI: 10.1038/NMAT3310 (2012).
- [2] E. Gann *et al.*, Rev Sci Instrum **83**, 045110 (2012).
- [3] B. A. Collins, and H. Ade, Journal of Electron Spectroscopy and Related Phenomena, In Press (2012).
- [4] B. A. Collins, J. Tumbleston, and H. Ade, J. Phys. Chem. Lett. **2**, 3135 (2011).
- [5] B. A. Collins *et al.*, Macromolecules **44**, 9747 (2011).
- [6] B. A. Collins *et al.*, J Phys Chem Lett **1**, 3160 (2010).
- [7] X. He *et al.*, Small, 10.1002/sml.201102382 (2012).
- [8] L. Yang *et al.*, Energy & Environmental Science, (submitted) (2012).
- [9] H. Yan *et al.*, Acs Nano **6**, 677 (2012).
- [10] A. Stuart *et al.*, (in preparation) (2012).
- [11] W. Ma *et al.*, Advanced Energy Materials, (in preparation) (2012).
- [12] B. A. Collins *et al.*, Advanced Energy Materials, (submitted) (2012).
- [13] J. R. Tumbleston *et al.*, (in preparation) (2012).
- [14] B. Watts *et al.*, Macromolecules **42**, 8392 (2009).

Publications

- [1] L. Yang *et al.*, Energy & Environmental Science, (submitted) (2012).
- [2] W. Ma *et al.*, Advanced Energy Materials, (in preparation) (2012).
- [3] X. He *et al.*, Small, 10.1002/sml.201102382 (2012).
- [4] E. Gann *et al.*, Rev Sci Instrum **83**, 045110 (2012).
- [5] B. A. Collins *et al.*, Advanced Energy Materials, (submitted) (2012).
- [6] B. A. Collins *et al.*, Nat Mater **advance online publication**, DOI: 10.1038/NMAT3310 (2012).
- [7] B. A. Collins, and H. Ade, Journal of Electron Spectroscopy and Related Phenomena, In Press (2012).
- [8] W. Zhang *et al.*, Polymers for Advanced Technologies **22**, 65 (2011).
- [9] H. Yan *et al.*, J. Appl. Phys. **110**, 102220 (2011).
- [10] B. Watts *et al.*, J. Chem. Phys. **134**, 024702 (2011).
- [11] C. Wang *et al.*, Nano Letters **11**, 3906 (2011).
- [12] B. A. Collins, J. Tumbleston, and H. Ade, J. Phys. Chem. Lett. **2**, 3135 (2011).
- [13] B. A. Collins *et al.*, Macromolecules **44**, 9747 (2011).
- [14] H. Yan *et al.*, Advanced Functional Materials **20**, 4329 (2010).
- [15] Y. T. Wang *et al.*, Macromolecules **43**, 8153 (2010).
- [16] C. Wang *et al.*, IOP Conference Series: Materials Science and Engineering **14**, 012016 (2010).
- [17] S. Swaraj *et al.*, Nano Lett. **10**, 2863 (2010).
- [18] S. Jeong *et al.*, Appl. Phys. Lett. **96**, 183305 (2010).
- [19] B. A. Collins *et al.*, J Phys Chem Lett **1**, 3160 (2010).

SISGR: The Influence of Electrolyte Structure and Electrode Morphology on the Performance of Ionic-Liquid Based Supercapacitors: A Combined Experimental and Simulation Study

Dmitry Bedrov,¹ Yury Gogotsi,² Wesley Henderson,³ Oleg Borodin⁴

¹*Department of Materials Science & Engineering, University of Utah, Salt Lake City, UT.*

²*A.J. Drexel Nanotechnology Institute and Department of Materials Science & Engineering, Drexel University, Philadelphia, PA.*

³*Department of Chemical Engineering, North Carolina State University, Raleigh, NC.*

⁴*Electrochemistry Branch, Army Research Laboratory, Adelphi, MD.*

Program Scope

The main objective of this project is to obtain fundamental understanding of correlations between electrolyte structure, electrode morphology and the performance of ionic liquid-based supercapacitors. The interdisciplinary team of materials scientists and engineers has utilized a combined simulation and experimental approach and focused the research in three main areas:

- a) Obtaining molecular level understanding of factors influencing properties of room temperature ionic liquid (RTIL) electrolytes at electro active interfaces and in nanostructured electrodes using theory and molecular dynamics (MD) simulations.
- b) Design and characterization of novel RTIL mixtures for application as electrolytes in supercapacitors. Two methodologies have been explored including the addition of solvent to an RTIL and salt mixtures. Both approaches permit the fine tuning of select properties such as ionic conductivity, viscosity, wettability, etc. Further, the mixtures enable the effects of ion solvation and ion size on the performance (capacitance and charge/discharge rate, lifetime/durability, etc.) of capacitors with porous electrodes to be explored in depth.
- c) Development of novel nanostructured carbon-based electrode materials and testing new electrolyte/electrode combinations for supercapacitors applications.

Recent Progress

Molecular simulations. Using state-of-the-art simulation methodology allowing simulating at constant potential difference between electrodes and fully atomistic model, extensive MD simulations of realistic RTILs at electroactive interfaces have been conducted as a function of RTIL structure, temperature, and applied potential. Predictions from our simulations were found to be in excellent agreement with experimental observations as well as confirmed several predictions of simplified theoretical models for RTIL-based capacitors at flat electrodes. However, our simulations also showed that atomistic level details of realistic RTILs can significantly impact the electric double layer structure and result in nontrivial dependencies of differential capacitance (DC) that are not captured by simplified theoretical models. Moreover,

we showed that the shape of DC versus the electrode potential can change *qualitatively* with the structure of the electrode surface. For example, whereas the atomically flat basal plane of graphite in contact with a RTIL generates camel-shaped DC, the atomically corrugated prismatic face of graphite with the same electrolyte complex multi-peak behavior and much larger DCs at low potentials. We showed that DC capacitance dramatically depends on the geometry of surface nanopatterning and which can be used to significantly increase the energy storage of the capacitor as illustrated in Figure 1. Molecular simulations of RTILs and carbon-based electrodes with different size nanopores showed that at high potential differences between electrodes (above 1V) no significant increase in capacitance is observed with reduction of pore sizes. However, at lower voltages (less than 1V) a substantial increase in capacitance is observed when pore dimensions are about 7.5 Å. (the volcano effect). We also found that contributions of positive and negative electrodes of the same structure to the total capacitance are noticeably different, indicating that the structure of each electrode can be optimized independently depending on the structure of the intercalating counter.

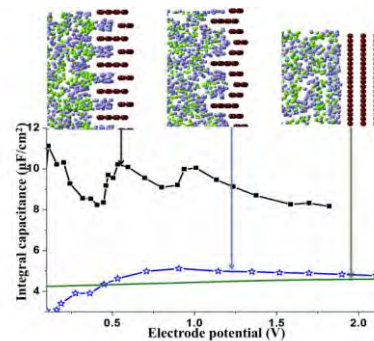


Figure 1. Integral capacitance of RTIL at graphite electrodes with different nanopatterned topography as a function of electrode potential.

Development and characterization of novel electrolytes. An experimental study has been completed for mixtures of 13 different solvents (Fig. 2) with the ionic liquid *N*-methyl-*N*-pentylpyrrolidinium bis(trifluoromethanesulfonyl)imide (PY₁₅TFSI). The conductivity of RTILs, especially at lower temperatures, can be low enough to preclude their use in commercial electrolyte applications. The addition of solvent to the RTIL resulted in a significant decrease in the viscosity and melting temperature (T_m) and a significant increase in the conductivity, even with limited amount of solvent. The link between the structure of the solvent and variable properties has been examined using MD simulations. The simulations have been validated using the experimental property measurements. This work provides insight into how the solvents interact with the ions at the molecular-level in the various concentration regions — salt-with-solvent (concentrated salt), intermediate concentration and solvent-with-salt (dilute salt) — to explain the noted properties.

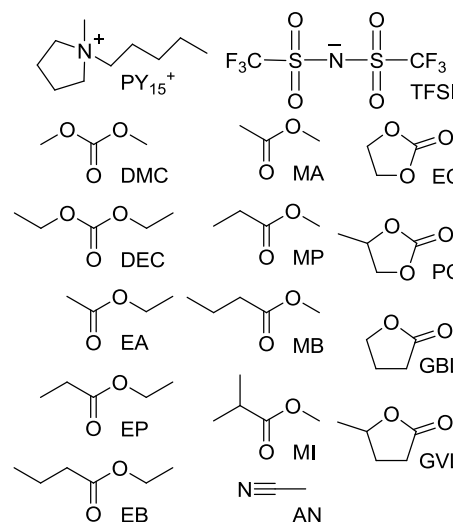


Figure 2. Chemical structures of RTILs and solvents used in this study.

Salt mixtures have been systematically explored including: (1) salts with the same anion (TFSI) and same cations, but the latter have different alkyl chain lengths, (2) salts with the same anion (TFSI) and different cations, (3) salts with the same cations, but different anions (TFSI, FSI (i.e., $N(SO_2F)_2^-$) and BF_4^-) and (4) mixtures of different RTILs with LiTFSI. The motivation for the first set of mixtures is that the conductivity of neat RTILs increases with decreasing alkyl chain length, but so does the T_m of the salts. Mixtures may allow the inclusion of significant amounts of salt with short alkyl chain length to improve the transport properties. Further, smaller organic cations may be able to interact more favorably with high surface area porous carbon electrodes with small pores. The second set of mixtures examines how the thermal phase behavior is impacted by different cations such as dialkylpyrrolidinium, piperidinium and morpholinium. Anions also have a tremendous impact of both the properties and charging behavior of electrodes. Salts with the BF_4^- anion tend to have exceptional behavior for capacitor electrolytes (as solvent-salt mixtures), but the salts also generally have a very high T_m thus precluding their use as neat RTILs. Mixtures of anions may enable the liquidus range of salt mixtures to be extended to low temperature, while simultaneously improving capacitor performance (capacitance, reduced volatility/flammability, etc.). Finally, the inclusion of limited amounts of smaller cations (i.e., Li^+ cations) may be beneficial or detrimental to the charging behavior of porous electrodes, but little is known about the performance of such electrolytes. The mixtures composition are being correlated both with properties and electrode cycling behavior to deconvolute the factors which govern device performance.

RTIL-based supercapacitors with nanostructured electrodes. We have systematically studied the effect of pore/ion size on EDLC performance, particularly on power and temperature range of operation. We have shown that while small pores (close to ion size) can lead to higher capacitance, high power or low temperature operation is negatively affected, due to kinetic limitations to ion transport.

Additionally, we have demonstrated that the temperature range of operation can be expanded through the use of carbons with easily accessible surfaces (i.e. exohedral carbons such as vertically-aligned CNT forests), and through the use of eutectic RTIL mixtures with suppressed phase transitions.

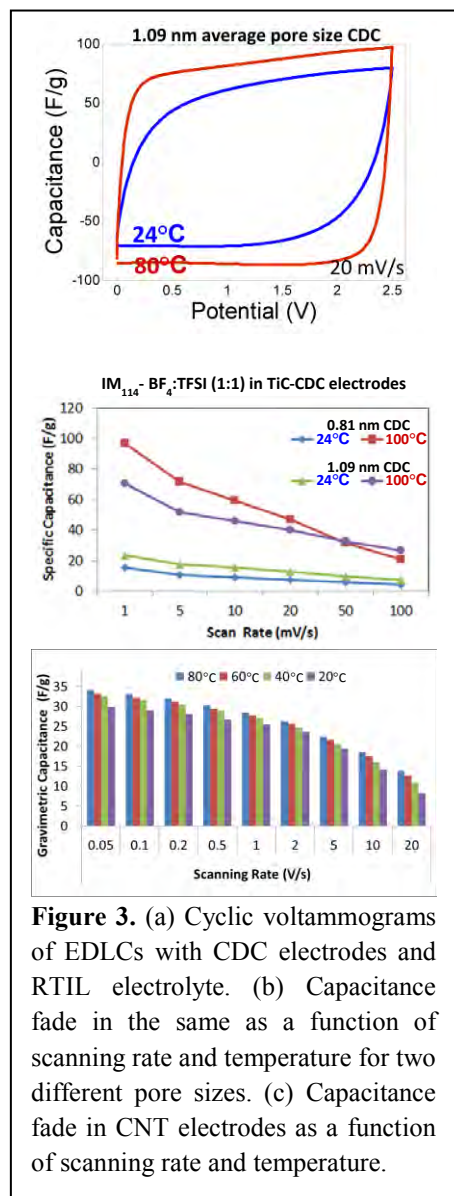


Figure 3. (a) Cyclic voltammograms of EDLCs with CDC electrodes and RTIL electrolyte. (b) Capacitance fade in the same as a function of scanning rate and temperature for two different pore sizes. (c) Capacitance fade in CNT electrodes as a function of scanning rate and temperature.

Future Plans

The mechanism by which surface-specific capacitance varies among porous carbons will be studied through simulation and experiment, with emphasis on the dynamics of the double layer formation. Simulations and experiments on optimizing each electrode simultaneously will be explored. Additionally, testing of RTILs on low temperature synthesis, nanoparticle-based CDC has produced positive results, and we will proceed to study the performance of such materials, but with higher synthesis temperatures.

Publications

Vatamanu, J., Borodin, O., Smith, G.D., “Molecular insights into the microscopic origin of the camel-shaped behavior of the differential capacitance on electrified interfaces”, *J. Am. Chem. Soc.*, **2010**, 132, 14825.

Vatamanu, J., Cao, L., Borodin, O., Bedrov, D., Smith, G.D., “On the influence of electrode surface roughness and its crystallographic orientation on the electric double layer structure and differential capacitance”, *J. Phys. Chem. Lett.* **2011**, 2, 2267-2272.

Vatamanu, J., Borodin, O., Smith, G.D., “Molecular dynamics simulations of electric double layer structure and differential capacitance for complex room temperature ionic liquids”, *J. Phys. Chem. B.*, **2011**, 115, 3073.

Vatamanu, J., Borodin, O., Bedrov, D.; Smith, G.D., “Molecular dynamics simulation study of the interfacial structure and differential capacitance of alkyimidazolium bis(trifluoromethanesulfonyl)imide [C_nmim][TFSI] ionic liquids at graphite electrodes” *J. Phys. Chem. C*, **2012**, 116, 7940-7951.

Vatamanu, J., Xing, L.; Smith, G.D., Bedrov, D.; “Nanopatterning of electrode surface as potential route to improve energy density of electric double layer capacitor: Insight from molecular simulations”, *J. Phys. Chem. Lett.* **2012** 3, 1124-1129.

Kondrat, S.; C. R. Perez, V. Presser, Y. Gogotsi, A. A. Kornyshev, *Energy Environ. Sci.* **2012**, 5, 6474.

Perez, C.R.; S-H. Yeon, J. Ségalini, V. Presser, P-L. Taberna, P. Simon, Y. Gogotsi, “Structure and Electrochemical Performance of Carbide-Derived Carbon Nanopowders”, *Advanced Functional Materials*, **2012**. (in review)

Perez, C.R.; E. Fox, W. Henderson, Y. Gogotsi, “Effect on ELDC of pore size and chain length of tri-alkyl-imidazoliums-based ionic liquids” (in preparation)

Fox, E. T.; Weaver, J. E. F.; Henderson, W. A. *J. Phys. Chem. C* **2012**, 116, 5270. Tuning Binary Ionic Liquid Mixtures: Linking Alkyl Chain Length to Phase Behavior and Ionic Conductivity

Fox, E. T.; Dickmann, J. S.; Henderson, W. A. *J. Phys. Chem. C* **2012**, in-preparation. Tuning Binary Ionic Liquid Mixtures: Linking Cation Structure to Physicochemical Properties and Performance in Electrochemical Capacitors

Fox, E. T.; Dickmann, J. S.; Weaver, J. E. F.; Allen, J. L.; Henderson, W. A. *J. Phys. Chem. C* **2012**, in-preparation. Tuning Binary Ionic Liquid Mixtures: Linking Anion Structure to Physicochemical Properties and Performance in Electrochemical Capacitors

Weaver, J. E. F.; Parrish, E. G.; Fox, E. T.; Zhou, Q.; Henderson, W. A.; Mantz, R. A. *J. Phys. Chem. C* **2012**, in-preparation. Ionic Liquid-Lithium Salt Mixtures: Linking Ion Structure with Electrolyte Transport Properties

Synthesis and Structural Characterization of Novel Intermetallic Clathrates—Prospective Materials for Thermoelectric Applications

P.I. Prof. Svilen Bobev, Department of Chemistry and Biochemistry, University of Delaware, Newark DE 19716

Program scope

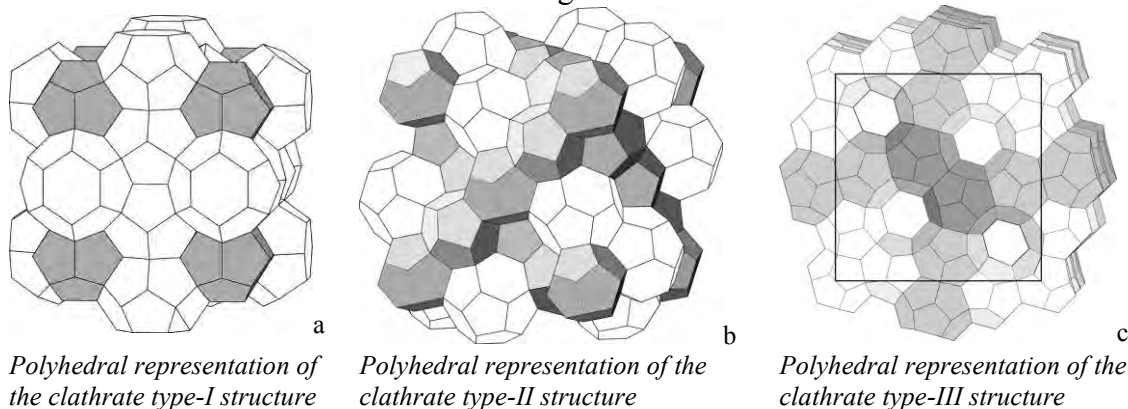
The overall objective of the project is to contribute to the development of the fundamental chemistry and physics of new intermetallic clathrates (open framework materials) that can find applications in solid-state energy conversion. Such materials are termed thermoelectric materials and they possess the unique property that a temperature gradient induces a separation of charge in them. Thermoelectric materials are of great practical importance because of their potential for widespread applications in power generation or in cooling devices.

Not too long ago, new complex inorganic materials with open framework structures, such as skutterudites and clathrates (Figure 1) have been suggested to be a breakthrough in the thermoelectric energy conversion. The basic hypothesis for the thermoelectric properties of such “host-guest” structures is that the conducting host-framework provides a high Seebeck coefficient (S) and electrical conductivity (σ), while low-lying optical modes, associated with the vibration of the guest-atoms, hybridize with the acoustic modes.

The proposed interdisciplinary efforts are the initial part of a broader, collaborative program to investigate the structure-bonding-properties relationships in related intermetallic compounds. More specifically, our work is aimed at:

1. Comprehensive and systematic investigations of the crystal chemistry and stoichiometry breadth of new semiconducting clathrates with the type-I, type-II or type-III structures.
2. Precise determination of the composition with minimum occupancy of the cages, needed for the thermodynamic stability of the clathrate framework, coupled with investigations to verify the possibility of “rattling” atoms inside the open-framework structure.
3. Extensive physical property measurements (S , σ , κ , R_H , C_p , χ_m). Ultimately, this new phenomenology will be used as a foundation for the rational tuning of potentially interesting properties of the newly synthesized materials.

Figure 1



Recent progress

Clathrates have open-framework structures, where large polyhedral cages (host) exist; they are typically filled by suitably-sized metal atoms (guest). The guest atoms inside the host

lattice are weakly bound to their neighbors, thereby could efficiently scatter phonons, while the rigid covalent framework can freely conducts electrons. Such structural characteristics provide unique combination of charge/heat transfer properties, which fit ideally the “phonon glass, electron crystal” (PGEC) concept [1].

So far, most of the studied intermetallic clathrates are based on group 14 elements, i.e., Si, Ge, and Sn, which is understandable since the cage-forming atoms are four-bonded. Clathrates that are free of group 14 metals are rarely seen. The two known exceptions include $\text{Ba}_8\text{Cu}_{16}\text{P}_{30}$, an orthorhombic superstructure of type-I clathrate that constitutes Cu and P atoms on the framework [2], and the recently published type-I antimonide clathrates $\text{Cs}_8\text{Zn}_{18}\text{Sb}_{28}$ and $\text{Cs}_8\text{Cd}_{18}\text{Sb}_{28}$ [3]. They have demonstrated the feasibility of forming clathrate compounds with elements other than group 14, which have greatly stimulated our interest in searching for new pnictide clathrate compounds. As part of our efforts in this area, we have made the first arsenide clathrates, $A_8\text{Zn}_{18}\text{As}_{28}$ ($A = \text{K}, \text{Rb}, \text{Cs}$) and $\text{Cs}_8\text{Cd}_{18}\text{As}_{28}$, which also adopt type-I structure but with their own subtleties. These examples together have expanded the scope of the chemical range for exploring clathrates, which may lead to new and improved thermoelectric materials.

Synthesis of the novel arsenide clathrate in high yield proved not an easy task. Although the antimonide clathrates could be synthesized in high yield by direct fusion of the corresponding elements [3], similar synthetic route resulted in only traces of $A_8\text{Zn}_{18}\text{As}_{28}$ ($A = \text{K}, \text{Rb}, \text{Cs}$) and $\text{Cs}_8\text{Cd}_{18}\text{As}_{28}$ in the multi-phased reaction products. This adverseness might be due to the insufficient diffusion of the starting materials since their physical properties are distinctly different. However, increasing the reaction temperature was also unfavorable since such reactions yielded KZn_4As_3 , RbZn_4As_3 , CsZn_4As_3 , and CsCd_4As_3 [4]. In order to avoid the thermodynamic trap of the latter compounds, a two-step synthetic route, which involved pre-mixing As and Zn or Cd, had been employed. The almost phase pure arsenide clathrates could be obtained by annealing the mixtures of the binary precursors and the alkali metals at a relatively low temperature for a shorter time (Figure 2).

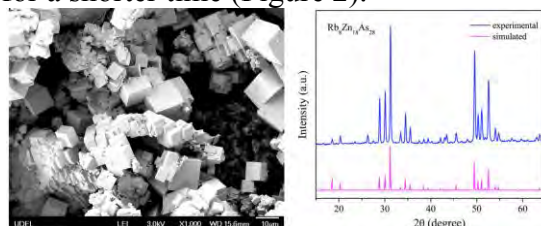


Figure 2. SEM image and powder X-ray diffraction pattern for $\text{Rb}_8\text{Zn}_{18}\text{As}_{28}$

The structures of the title compounds have been established by single-crystal X-ray diffraction. All of the four compounds crystallize with the type I clathrate structure in a primitive cubic lattice ($Pm\bar{3}n$, No. 223). There are 3 unique crystallographic sites on the open framework— $6d$, $16i$, and $24k$, occupied by either Zn (or Cd)/As and constituting two types of polyhedra: the 20-atom pentagonal dodecahedra and the 24-atom tetrakaidecahedra. By sharing the hexagonal faces, the tetrakaidecahedra form non-intersecting chains that are mutually perpendicular in the three-dimensional space. The smaller pentagonal dodecahedra are enclosed by these chains and thereby isolated from each other. Locating at the centers of the pentagonal dodecahedra and the tetrakaidecahedra are the $2a$ and $6c$ sites, respectively, occupied by the alkali metals. Unlike $\text{Cs}_8\text{Zn}_{18}\text{Sb}_{28}$ and $\text{Cs}_8\text{Cd}_{18}\text{Sb}_{28}$ in which both $2a$ and $6c$ sites are fully occupied [3], the $2a$ sites in the title arsenide clathrates all show partial occupancy (Fig. 3).

The Zn/Cd and As atoms are statistically disordered on the three framework sites ($6d$, $16i$, $24k$) with refined Cd/As ratios as follows: 0.48(1)/0.52, 0.20(1)/0.80, and 0.51(1)/0.49, respectively. Similar Zn distribution at the Sb-based framework is noted in $\text{Cs}_8\text{Zn}_{18}\text{Sb}_{28}$, too [3].

Comparing the distributions of the substituents in the pnictogen-based clathrates and those in the tetrrel-based clathrates reveals some interesting facts, which are worth of a discussion. In type I clathrate with general formula $A_8M_xTt_{46-x}$ (A = alkali metal or alkaline earth metal; M = element from group 12, 13; Tt = Si, Ge, Sn), the substituents M usually have strong preference for the $6d$ site [5]. A Mulliken population analysis on K_8Si_{46} reveals that the $6d$ site has the lowest Mulliken population and thereby should be most preferred by the more electropositive

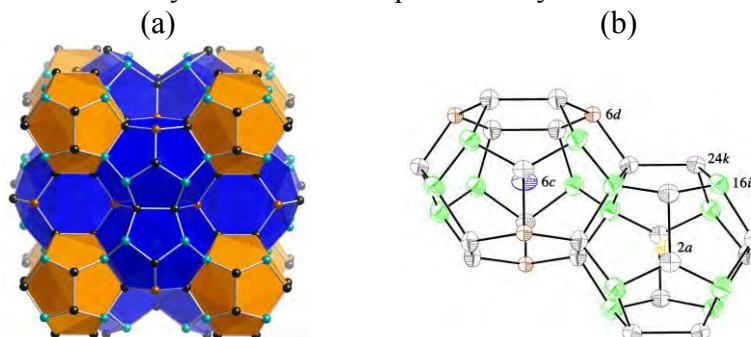


Figure 3 (a) Crystal structure of type-I clathrate; (b) Thermal ellipsoid presentation of two types of cages in $Cs_8Cd_{18}As_{28}$, drawn with 95% probability level.

substituent atoms [5]. The theoretical study on Ga distribution in $A_8Ga_{16}Tt_{30}$ (A = Sr, Ba, Tt = Si, Ge) also indicated its tendency for occupying the $6d$ site. However, in the case for $Cs_8Zn_{18}Sb_{28}$ [3] and $Cs_8Cd_{18}As_{28}$, such a preference is not as profound. As a matter of fact, Zn and Cd prefer even the $24k$ site to the $6d$ site from the refinements. In addition, pnictogens show an apparent preference for the $16i$ site, with about 80% occupancy at this site in both $Cs_8Zn_{18}Sb_{28}$ and $Cs_8Cd_{18}As_{28}$. Regardless of the size differences between the two atom pairs Zn/Sb and Cd/As, Zn and Cd still show similar distributions, which most likely indicates that in the pnictogen-based clathrates, electronegativity is a more decisive factor in determining the distribution of the substituents. Analogous to the homoatomic Ga–Ga interactions that are known to be energetically unfavorable in $A_8Ga_{16}Tt_{30}$ [5], density functional calculations on the antimonide clathrates also suggest that Cd–Cd and Zn–Zn bonds are disadvantageous to the stability of the clathrate structure [3]. This should be true for the arsenide clathrates, too, considering that the bond energies of the Cd–As/Zn–As bonds are much stronger.

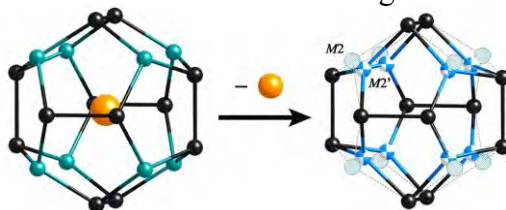


Figure 4. Schematic presentation of the split of the $16i$ site on the framework. When the cage is vacant, the atoms at the $16i$ site move toward the center of the cage (from $M2$ to $M2'$ site) in order to compensate for empty space.

As mentioned above, the partial occupancy of the $2a$ site complicates the structure even further (Figure 4). In order to compensate for the vacancy in the empty pentagonal dodecahedra, the $16i$ site has to be split (noted as $M2$ and $M2'$ sites, $M=Cd/Zn/As$). While the $M2$ site is the normal position with reasonable distances to the alkali metal, the $M2'$ site exists only when the $2a$ site is vacant, thus the very short distance between this position and the alkali metal is not real. This is the first time the splitting of $16i$ site being noted due to vacancy of the guest atom, although similar scenarios do have been reported for the type I cationic clathrate $Sn_{24}P_{19.3}I_8$ (the P partial occupancy leads to the splitting of the neighboring Sn atoms at the $24k$ site); disorder at the $16i$ site was also noted in $K_7B_7Si_{39}$ (attributed to the size difference between B and Si).

Future plans

The first arsenide clathrate compounds $A_8Zn_{18}As_{28}$ ($A = K, Rb, Cs$) and $Cs_8Cd_{18}As_{28}$ have been synthesized and characterized. A delicate charge balance is maintained by the subtle changes in the Cd/As and Zn/As ratios in corresponding to the alkali metal vacancy. More exploratory work on pnictide clathrates is worthy of pursuing since property measurements have confirmed these materials to be semiconductor/semimetals. Their bonding characteristics offer many possibilities for property-tuning, which could prove very useful for the generation of new ideas and concepts in modern thermoelectrics development.

References

- [1] Blake, N. P.; Mollnitz, L.; Kresse, G.; Metiu, H. *J. Chem. Phys.* **1999**, *111*, 3133
- [2] Alleno, E.; Maillet, G.; Rouleau, O.; Leroy, E.; Godart, C.; Carrillo-Cabrera, W.; Simon, P.; Grin, Y. *Chem. Mater.* **2009**, *21*, 1485
- [3] Liu, Y.; Wu, L.-M.; Du, S.; Corbett, J. D.; Chen, L. *Angew. Chem. Int. Ed.* **2009**, *48*, 5305
- [4] He, H.; Tyson, C.; Bobev, S. *Inorg. Chem.* **2011**, *50*, 8375
- [5] Bentien, A.; Nishibori, E.; Paschen, S.; Iversen, B. B. *Phys Rev. B* **2005**, *71*, 144107

Publications (the names of the contributing undergraduate researchers are underlined)

Synthesis, Crystal and Electronic Structures, and Properties, of the New Pnictide

Semiconductors A_2CdPn_2 ($A = Ca, Sr, Ba, Eu$; $Pn = P, As$)

Wang, J.; Yang, M.; Pan, M.-Y.; Xia, S.-Q.; Tao, X.-T.; He, H.; Darone, G. M.; **Bobev, S.** *Inorg. Chem.* **2011**, *50*, 8020

8-coordinated Arsenic in the Zintl Phases $RbCd_4As_3$ and $RbZn_4As_3$. Synthesis and Structural Characterization

He, H.; Tyson, C.; **Bobev, S.** *Inorg. Chem.* **2011**, *50*, 8375

New Compounds with $[As_7]^{3-}$ Clusters. Synthesis and Crystal Structures of the Zintl Phases Cs_2NaAs_7 , Cs_4ZnAs_{14} and Cs_4CdAs_{14}

He, H.; Tyson, C.; **Bobev, S.** *Crystals* **2011**, *1*, 87

Indium Doping in $BaSn_{3-x}In_x$ ($0 \leq x \leq 0.2$) with Ni_3Sn Structure

Schäfer, M. C.; Yamasaki, Y.; Fritsch, V.; **Bobev, S.** *Crystals* **2011**, *1*, 104

Ternary Compounds in the Sn-rich Section of the Ba–Ga–Sn System: $Ba_8Ga_{16-x}Sn_{30+x}$ ($1.1 \leq x \leq 2.8$) Clathrates of Type-I and Type-VIII, and $BaGa_{2-x}Sn_{4+x}$ ($x \approx 0.2$) with a Clathrate-like Structure

Schäfer, M. C.; Yamasaki, Y.; Fritsch, V.; **Bobev, S.** *Crystals* **2011**, *1*, 145

Synthesis and Structural Characterization of the Ternary Zintl phases $AE_3Al_2Pn_4$ and $AE_3Ga_2Pn_4$ ($AE = Ca, Sr, Ba, Eu$; $Pn = P, As$)

He, H.; Tyson, C.; Saito, M.; **Bobev, S.** *J. Solid State Chem.* **2012**, *188*, 59

Synthesis and Crystal Structures of the Quaternary Zintl Phases $RbNa_8Ga_3Pn_6$ ($Pn = P, As$) and $Na_{10}NbGaAs_6$

He, H.; Tyson, C.; **Bobev, S.** *Crystals* **2012**, *2*, 213

Synthesis and Structural Characterization of ACu_9Tt_4 ($A = Ca, Sr, Ba, Eu$; $Tt = Si, Ge, Sn$)—Tetragonally Distorted Ternary Variants of the Cubic $NaZn_{13}$ Structure Type

Schäfer, M. C.; Yamasaki, Y.; Fritsch, V.; **Bobev, S.** *Z. Anorg. Allg. Chem.* **2012**, in print

Synthesis, Structural Characteristics, and Physical Properties of Type-I Clathrates $A_8Zn_{18}As_{28}$ ($A = K, Rb, Cs$) and $Cs_8Cd_{18}As_{28}$

He, H.; Zevalkink, A.; Snyder, G. J.; **Bobev, S.** *Chem. Mater.* **2012**, submitted

Mitigating Breakdown in High Energy Density Perovskite Polymer Nanocomposite Capacitors

Richard L. Brutchey

Department of Chemistry, University of Southern California, Los Angeles, CA 90089 USA

Program Scope

Current electrical energy storage technologies do not meet the demands of transportation applications in terms of energy density. For example, the conversion from gasoline-powered vehicles to all-electric vehicles requires higher energy density pulsed power sources. Such applications require a new generation of robust dielectric capacitors that have (1) high electrical energy density (D , where $D = 0.5\epsilon'\epsilon_0 E_{bd}^2$), (2) low dielectric loss, (3) high field endurance, and (4) increased temperature stability. The most promising solution to this challenge is to utilize polymer nanocomposites, whereby high permittivity inorganic nanocrystals are integrated into a polymer matrix. In such an approach, the polymer provides the processibility, light weight, and high breakdown voltage, while the inorganic filler delivers the desired dielectric characteristics. The fundamental challenge for these composites lies in aggregation of the inorganic filler at the percolation threshold, which leads to a precipitous drop in breakdown voltage (the dominant term in electrical energy density) as the continuous particle network becomes a pathway for charge carriers. To solve this challenge, and maximize the energy density of the resulting nanocomposites, our objectives are two-fold:

- (1) Develop a low temperature solution-phase synthesis of small perovskite oxide nanocrystals with tunable properties, such as relative permittivity. An exquisite level of control over such nanocrystal properties will be accomplished by a thorough understanding of the nanocrystal structure and ability to tune nanocrystal composition.
- (2) Control perovskite oxide surface chemistry such that nanocrystal percolation may be sterically mitigated in order to maximize the breakdown voltage of a nanocomposite.

The following section will summarize our recent progress (September 1, 2011 – May 1, 2012) towards addressing the first objective.

Recent Progress

1. Aliovalent doping of perovskite oxide nanocrystals. Owing to their high thermal and chemical stability and low environmental toxicity, lanthanide-doped perovskite oxides and their corresponding solid solutions $(A,A')(B,B')O_3$ ($A, A' = Ca, Sr, Ba$; $B, B' = Ti, Zr, Hf$) are attractive candidates for nanostructured dielectrics¹ and phosphors.² Lanthanide-doped perovskite oxide micro and nanocrystals have been previously prepared *via* solid state reaction, conventional sol-gel, flame-spray pyrolysis, and hydrothermal synthesis.³⁻⁶ These methods invariably rely on the use of physical (heat and pressure) and/or chemical (salts, chelating ligands, or mineralizers) agents to induce crystallization of the perovskite and incorporation of the lanthanide ions. Physical agents such as heat induce grain growth, while chemical agents can introduce impurities into the oxide's bulk and/or surface. From this perspective, the development of a synthetic approach yielding lanthanide-doped perovskite oxide nanocrystals under ultrabenign conditions (*i.e.*, room temperature, atmospheric pressure, surfactant- and mineralizer-free, and near-neutral pH) is critical in order to realize the full potential of this family of materials in dielectric and light emission applications.

We recently demonstrated that Eu^{3+} -doped BaZrO_3 can be synthesized under ultrabenign conditions to yield a red phosphor. In this work, $x\text{Eu}:\text{BaZrO}_3$ ($x = 0\text{--}5$ mol%) nanocrystals were synthesized using a vapor diffusion sol–gel approach developed in our laboratory that relies on the kinetically controlled delivery of water vapor to an alcohol solution of $\text{Eu}(\text{acac})_3$ (acac = acetylacetonate) and a bimetallic alkoxide $\text{BaZr}(\text{OR})_6$ ($\text{R} = \text{CH}_2\text{CHCH}_3(\text{OCH}_3)$) mixed in the appropriate stoichiometric ratio.⁷ Hydrolysis and condensation of the bimetallic alkoxide occur at room temperature and yield small 10–20 nm nanocrystals of pure $x\text{Eu}:\text{BaZrO}_3$. Moreover, near unity doping efficiencies of Eu^{3+} were achieved using the vapor diffusion sol–gel route. The excitation and emission spectra of thermally treated $x\text{Eu}:\text{BaZrO}_3$ powders are both dominated by peaks arising from $f\text{--}f$ transitions of the Eu^{3+} ion, with the major emission peaks resulting from ${}^5D_0 \rightarrow {}^7F_2$ (611–625 nm) and ${}^5D_0 \rightarrow {}^7F_1$ (586–596 nm) transitions. The intensity of the excitation and emission bands increases upon increasing the Eu^{3+} concentration and reaches a maximum for 4 mol%, indicating that concentration quenching occurs at higher doping levels. The red-to-orange ratio (*i.e.*, the ratio of the integrated intensity of the ${}^5D_0 \rightarrow {}^7F_2$ to the ${}^5D_0 \rightarrow {}^7F_1$ transition) reaches a maximum value of 3.4 for 4% $\text{Eu}:\text{BaZrO}_3$, making this composition the most attractive candidate for red phosphors. The calculated CIE coordinates for this composition are (0.647, 0.353), which corresponds to a reddish pink color (Fig. 1).

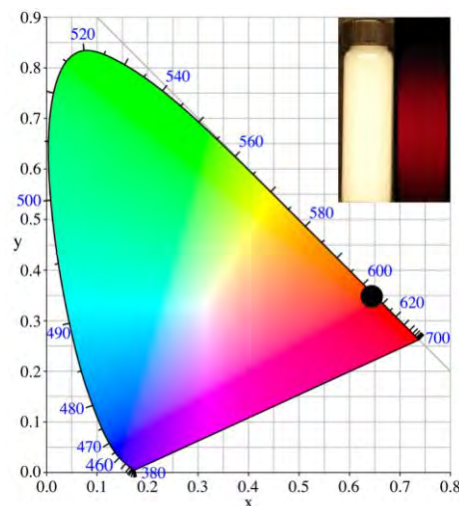


Fig 1. CIE coordinates of the emission of 4% $\text{Eu}^{3+}:\text{BaZrO}_3$ upon irradiation with near-ultraviolet light. The inset shows pictures of the nanocrystals suspended in methanol under natural (left) and ultraviolet (right) illumination.

Comparison of these findings with previous syntheses of Eu^{3+} -doped BaZrO_3 reveals that quenching of the lanthanide emission is typically observed for doping levels of less than 1 mol% when solid state reactions are used to crystallize the perovskite phase and incorporate the lanthanide ions into the host lattice.⁸ Because concentration quenching depends on the spatial distribution of the activator ions in the host lattice, this finding demonstrates that an intrinsic advantage of the vapor diffusion sol–gel approach is to yield an apparently more homogeneous spatial distribution of the lanthanide ions. In addition, a common drawback of previously synthesized Eu^{3+} -doped BaZrO_3 micro- and nanocrystals was their low red-to-orange emission ratio.^{3,8} In contrast, $x\text{Eu}:\text{BaZrO}_3$ nanocrystals synthesized *via* vapor diffusion sol–gel exhibit a marked predominance of the red over the orange emission for all the Eu^{3+} doping levels explored. It is well-known that the chromaticity of the light emitted by the Eu^{3+} ion is governed by the local symmetry of the crystallographic site in which it sits.⁹ In the case of $x\text{Eu}:\text{BaZrO}_3$ nanocrystals studied in this work, the strong predominance of the red over the orange emission suggests that Eu^{3+} ions occupy sites in a noncentrosymmetric lattice position.

2. *Structural evolution of BaTiO_3 nanocrystals synthesized via vapor diffusion sol–gel.* BaTiO_3 is one the most technologically relevant electroceramics. It exhibits a perovskite structure consisting of BaO_{12} dodecahedra and TiO_6 octahedra. The structure undergoes three temperature-dependent phase transitions: rhombohedral ($R3m$) to orthorhombic ($Amm2$) at -90 °C, orthorhombic to tetragonal ($P4mm$) at 5 °C, and tetragonal to cubic ($Pm\bar{3}\bar{m}$) at 120 °C;¹⁰

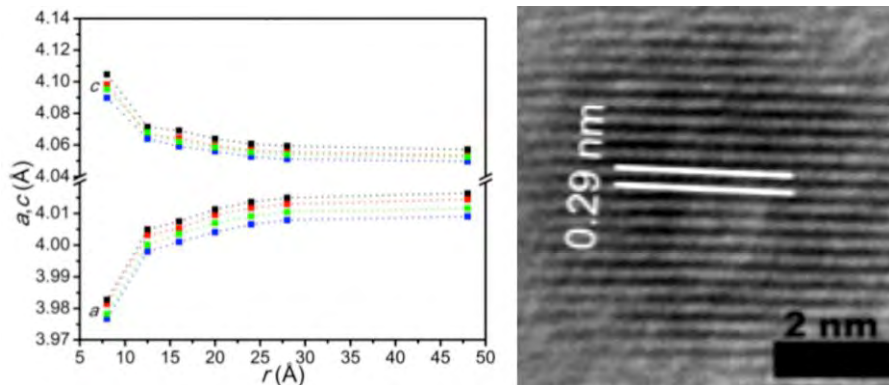


Fig 2. Lattice constants a and c of the BaTiO₃ nanocrystals (shown in TEM image) as a function of intraparticle distance.

the three low temperature phases exhibit ferroelectric character, whereas the high temperature phase is paraelectric. Understanding how the local symmetry and structural coherence, which ultimately sustain cooperative properties such as ferroelectricity and relative permittivity, change upon reducing the grain size is critical from both fundamental and applied standpoints. We followed the structural evolution of sub-10 nm BaTiO₃ nanocrystals as they nucleate and grow from an amorphous metallorganic gel at room temperature (*via* vapor diffusion sol-gel) using a series of techniques that probe the atomic structure on different length and time scales.¹¹ This allows for a comprehensive picture of the evolution of the nanocrystals to be achieved, particularly regarding their local symmetry and structural coherence, and has extremely important implications in the ferroelectric and dielectric properties of the nanocrystals.

The structural evolution of sub-10 nm BaTiO₃ nanocrystals as they assemble from an amorphous metallorganic gel under ultrabeneign conditions was investigated using a series of techniques that probe the atomic structure on different length and time scales. Upon the slow diffusion of water vapor into an alcohol solution of a bimetallic alkoxide at room temperature, hydrolysis and polycondensation occurred and the solution gelled after ~8 h. The continued flow of water vapor over this gel resulted in the formation of BaTiO₃ nuclei within an amorphous metallorganic matrix at times as early as 12 h, as evidenced by TEM analysis. Gas-liquid rather than liquid-liquid hydrolysis and the use of a bimetallic alkoxide precursor are the keys to the formation of crystalline nuclei.¹² The resulting 3–6 nm diameter nuclei continued to grow within the amorphous metallorganic matrix up until a reaction time of 27 h. During this growth stage, conventional and synchrotron XRD and Raman spectroscopy revealed a gradual increase in structural coherence and the simultaneous decrease in atomic positional disorder. After 30 h, discrete 9-nm diameter BaTiO₃ nanocrystals were obtained and the amorphous-to-crystalline phase transition quickly approached completion, as evidenced by TEM analysis.

The room-temperature crystal structure of the final 9-nm nanocrystals appeared cubic to Rietveld analysis of synchrotron XRD data; however, the presence of noncentrosymmetric regions arising from the off centering of the titanium atoms was confirmed *via* Raman spectroscopy and pair distribution function (PDF) analysis. Both techniques showed an increase in the coherence of these local off-center displacements upon approaching the completion of the amorphous-to-crystalline phase transition. Significantly, the local structure of the acentric regions present in the fully grown nanocrystals after 72 h are best described by a tetragonal $P4mm$ symmetry. An orthorhombic $Amm2$ symmetry also provided an adequate structural description, demonstrating that the coexistence of both types of local symmetries is plausible. The coherence length of the local off-center displacements of the titanium atoms was found to be on the order of 16 Å, or about 4 unit cells (Fig. 2). The presence of local dipoles whose average

magnitude ($c/a = 1.013 \text{ \AA}$) is comparable to that observed in bulk suggests that a large amount of macroscopic polarization can be obtained in these nanocrystals if the long-range coherence of their ferroelectric coupling is achieved.

Future Plans

(1) Extend our vapor diffusion sol-gel method to make compositionally more complex four cation $\text{Ba}_x\text{Sr}_{1-x}\text{Ti}_y\text{Zr}_{1-y}\text{O}_3$ nanocrystals and map the synthetic phase space over all composition ranges. PDF analysis will be used to structurally address why certain compositions exhibit maximized relative permittivity.

(2) Extend our vapor diffusion sol-gel method to the aliovalent doping of other lanthanide ions (e.g., Yb^{3+}) into perovskite oxide nanocrystal hosts for fluorescence and dielectric applications. High-resolution X-ray diffraction and XANES/EXAFS will be utilized to attempt to address where the lanthanide ion sits in the perovskite lattice.

(3) Study the effect of steric protection on the mitigation of dielectric breakdown in BaTiO_3 /polystyrene nanocomposites.

References

1. Viviani, M.; Bassoli, M.; Buscaglia, V.; Buscaglia, M. T.; Nanni, P. *J. Phys. D – Appl. Phys.* **2009**, *42*, 175407.
2. Vecht, A.; Smith, D.; Chadha, S. S.; Gibbons, C. S.; Koh, J.; Morton, D. *J. Vac. Sci. Technol.* **1994**, *12*, 781.
3. Alarcon, J.; van der Voort, D.; Blasse, G. *Mater. Res. Bull.* **1992**, *27*, 467.
4. Diallo, P. T.; Boutinaud, P.; Mahiou, R.; Cousseins, J. C. *Phys. Stat. Sol. A* **1997**, *160*, 255.
5. Chang, H.; Lenggoro, I. W.; Okuyama, K.; Jang, H. D. *Jpn. J. Appl. Phys.* **2006**, *45*, 967.
6. Zhang, X.; Zhang, J.; Jin, Y.; Zhao, H.; Wang, X.-J. *Cryst. Growth Des.* **2008**, *8*, 779.
7. Rabuffetti, F. A.; Lee, J. S.; Brutchey, R. L. *Adv. Mater.* **2012**, *24*, 1434.
8. Liu, X.; Wang, X. *Opt. Mater.* **2007**, *30*, 626.
9. C. R. Ronda, Ed. *Luminescence: From Theory to Applications*, Wiley-VCH, Weinheim **2008**.
10. Kwei, G. H.; Lawson, A. C.; Billinge, S. J. L.; Cheong, S.-W. *J. Phys. Chem.* **1993**, *97*, 2368.
11. Rabuffetti, F. A.; Brutchey, R. L. **2012**, manuscript submitted.
12. Brutchey, R. L.; Morse, D. E. *Angew. Chem., Int. Ed.* **2006**, *45*, 6564.

Publications

1. Rabuffetti, F. A.; Lee, J. S.; Brutchey, R. L. Vapor Diffusion Sol-Gel Synthesis of Fluorescent Perovskite Oxide Nanocrystals. *Advanced Materials* **2012**, *24*, 1434-1438.

New Superconducting Materials

R.J. Cava, Department of Chemistry Princeton University, Princeton NJ 08544

i) Program Scope The scope of the DOE-BES-sponsored Solid State Chemistry program at Princeton University is to find new superconducting materials and to address the structure-property correlations in known superconductors and related compounds. Much of our current work is in the area of superconductivity in intermetallic phosphides and germanides. We are also working intensively on a new thrust area in our search for new superconductors— ternary early transition metal subsulfides, which the PI believes may lead to new superconducting materials. These materials are expected to be conventional superconductors, and, by analogy to early transition metal intermetallics, may, if they can be found, have useful current-carrying properties. Finally, we have also worked on vanadium sulfides, which we believe may show superconductivity due to suppression of antiferromagnetic fluctuations through chemical doping. We have established fruitful collaborations with scientists at Argonne National Laboratory (beam line 11BM, APS) and have worked with them on many structural characterizations.

ii) Recent Progress In the past several years we have worked primarily on the determination of a new kind of bonding-structure-property relationship in superconductor-related phases, specifically between the magnetic and electronic properties of compounds with the ThCr_2Si_2

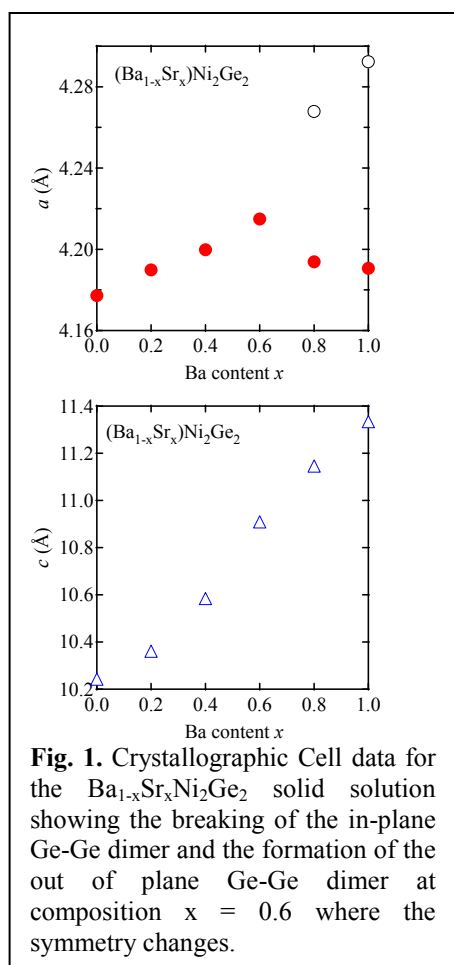
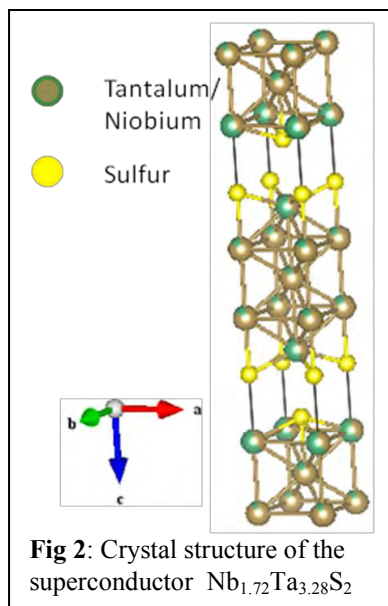


Fig. 1. Crystallographic Cell data for the $\text{Ba}_{1-x}\text{Sr}_x\text{Ni}_2\text{Ge}_2$ solid solution showing the breaking of the in-plane Ge-Ge dimer and the formation of the out of plane Ge-Ge dimer at composition $x = 0.6$ where the symmetry changes.

structure and the presence of a molecule-like bond within the crystal structure. This layered ThCr_2Si_2 “122” structure type is the most commonly observed ternary intermetallic structure type, and is the basis for the high temperature iron arsenide superconductors that are of so much recent interest. Work of theoretical chemist Roald Hoffman on the 122 structure type in the 1980s argued for the critical importance of the shape of the TX_4 tetrahedra and $X-X$ molecular dimer-like bonding across the A layers in determining the electronic states at the Fermi level. In the major thrust of our work in recent years we described the correlations between structure and properties for some important 122 structure type solid solutions to show the impact of the $X-X$ bonding on the electronic and magnetic properties. This work recently resulted in a major publication, which traces the surprising appearance of ferromagnetism in a Co-based 122 system as a result of the breaking of the $X-X$ bond.

There are many aspects of the impact of $X-X$ dimer formation on electronic properties and superconductivity in the 122 phases to follow up on. We are currently focusing on determining whether these considerations are relevant to the properties of materials based on the $4d$ and $5d$ transition metals in addition to the $3d$ transition metals. We have indications that the impact of the dimer formation is dramatic in these compounds as well, even though $4d$ orbitals are more extended than $3d$ orbitals. In the $4d$

systems, many of the compounds involved are superconducting; two specific systems that we are working on are $\text{Ba}_{1-x}\text{Sr}_x\text{Rh}_2\text{Ge}_2$ and $\text{Sr}(\text{Rh}_{1-x}\text{Pd}_x)_2\text{Ge}_2$. Our structural data shows that both systems display anomalous behavior, which we attribute to the formation or breaking of Ge-Ge bonds in the crystal structures. This work is not yet complete. Figure 1 shows a related system that we have been working on this year as well. This is the $\text{Ba}_{1-x}\text{Sr}_x\text{Ni}_2\text{Ge}_2$ system. For these 122 phases, which are based on Ge, which has one electron less than As or P, the tendency for Ge-Ge bond formation is very strong because the Ge-Ge dimer antibonding band is far above the Fermi Energy and is therefore usually empty. The result is that for BaNi_2Ge_2 even though the Ge's are too far apart to form bonds across the Ba atom layer, as we now expect based on our previous work on 122 phases, they distort the crystal structure dramatically to form in-plane Ge-Ge bonds instead. The partial Sr substitution for Ba then brings the Ge's closer together across the (Ba,Sr) layer until they become close enough to form an across-the-layer bond, evidenced by the transition back to the usual 122 tetragonal symmetry structure type. The characterization of these materials by synchrotron X-ray diffraction at the APS is almost complete, as is characterization of their magnetic properties. The synthesis of all these phases is extremely challenging.

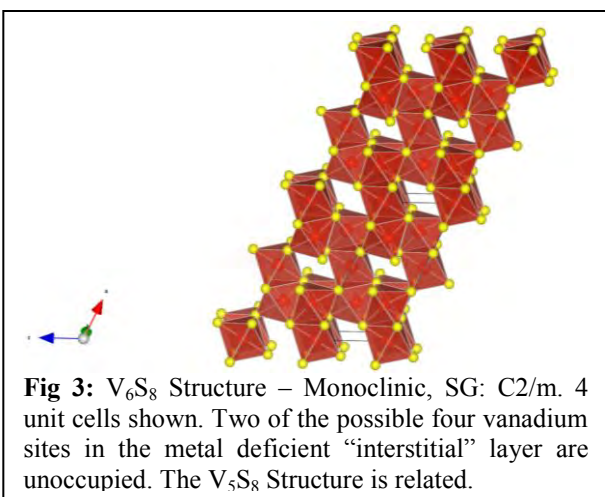


A major new research thrust in our program in recent years is based on a group of “subsulfide” compounds discovered by Hugo Franzen at ISU many years ago. These are designated as subsulfides because the sulfur content is substantially lower than is found in normal, more ionic sulfides. They can be expected to display behavior somewhere between intermetallic phases and ionic phases, and thus are believed by the PI to be excellent candidates for superconductivity. Franzen worked on binaries and pseudo-binaries of early transition metal sulfides and synthesized them at high temperatures; some of the compounds, such as $\text{Nb}_{6.74}\text{Ta}_{5.26}\text{S}_4$, were synthesized by annealing samples at $1400\text{ }^\circ\text{C}$, while others such as $\text{Nb}_{1.72}\text{Ta}_{3.28}\text{S}_2$ and $\text{Ta}_{6.08}\text{Nb}_{4.92}\text{S}_4$ were formed by arc melting pre-reacted reagents and then annealing around $1350\text{ }^\circ\text{C}$. A few of the materials his group discovered are Ta_6S , Ta_2S , Nb_{21}S_8 , Nb_{14}S_5 , Zr_{21}S_8 , Zr_9S_2 , $\text{Nb}_{6.74}\text{Ta}_{5.26}\text{S}_4$ and $\text{Nb}_{1.72}\text{Ta}_{3.28}\text{S}_2$. Some of these compounds are superconducting; Nb_{21}S_8 , for example, is superconducting at 3.7 K . In the niobium sulfides the niobium metal coordinations are capped pentagonal prisms and capped distorted cubes, while in the tantalum sulfides the coordination is typically Ta pentagonal antiprisms. When tantalum and niobium sulfides are combined in a pseudoternary niobium-tantalum-sulfide they can have a third, different type of structure. For example the compound $\text{Nb}_{1.72}\text{Ta}_{3.28}\text{S}_2$, shown in Fig. 2, is a bcc type structure with a mix of Nb and Ta statistically distributed on three different metal sites, where 2 adjacent layers of atoms out of every 7 are sulfur atoms. This compound is superconducting at about 4 K .

Based on this lead, we have been looking for new superconductors and new compounds in the high temperature phases of ternary metal rich subsulfides. We have systematically tried reactions with combinations of three elements and tested them for superconductivity. One of the elements is always sulfur, the second an early transition metal (Zr, Nb, Mo, Hf, Ta or W), and the third either a first row or second row late transition metal. These reactions have so far been performed at 1:2:1 ratio of varied transition metal to early transition metal to sulfur.

Combinations that show potential new structures or superconductivity have been explored in more detail with further reactions. Reactions have been performed at around 1400°C in sealed tantalum tubes. The samples are being analyzed by X-ray diffraction and tested for superconductivity. Our work so far has resulted in the discovery of no confirmed new compounds but many samples have shown the presence of superconductivity with T_c s between 2 and 10 K. We are presently in the process of determining whether this superconductivity arises from previously known phases or is from previously undiscovered compounds.

Finally, I describe our ongoing work on vanadium sulfides. In recent years, much attention has been given to itinerant electron magnetic superconductors. Compounds such as UGe_2 , RMo_6S_8 , RMo_6Se_8 (R = rare earth), Y_9Co_7 , $LaRh_2Si_2$ and YRh_2Si_2 exhibit itinerant electron magnetism as well as superconductivity. UGe_2 and Y_9Co_7 are ferromagnetic metals while RMo_6S_8 , RMo_6Se_8 , $LaRh_2Si_2$ and YRh_2Si_2 are antiferromagnetic (AFM) metals. Many theorists believe that the superconductivity in these systems can be explained through magnetic spin fluctuations (SF) mediating the pairing of electrons, especially for layered compounds. The study of “failed magnets” is a potentially fruitful avenue for finding new superconductors.



Another family of compounds with layered structures that have weak itinerant electron antiferromagnetic phases is the V-S series. The vanadium sulfide family has a complex phase diagram. Of particular interest are the phases VS, V_3S_4 , V_5S_8 and VS_2 . (e.g. Fig. 3) VS and VS_2 are metallic paramagnets while V_3S_4 and V_5S_8 are metallic antiferromagnets with T_N 's of 8 K and 32 K, respectively. VS_2 also has a charge density wave onset at 305 K. Neither a local moment model nor a spin fluctuation treatment has been able to fully explain the anomalously weak magnetism or the onset of the CDW in

VS_2 ; the data does, however, point to strong electron-electron correlation as being the cause for these behaviors. We hypothesize that carefully controlling the stoichiometry of crystals grown in this family may lead to a superconducting state.

In our analysis, we divide the magnetic behavior of V_6S_8 and V_5S_8 into two parts: the itinerant electron part, from the metal full layers, and the localized electron part from the metal deficient (interstitial) layers. We have worked to correlate changes in the T_N for V_6S_8 and V_5S_8 with the interstitial vanadium content (IVC) through careful synthesis. Through changing the IVC, we have been searching for superconductivity near the stoichiometries at which the compounds undergo a change in electronic state: between V_4S_8 and V_5S_8 there is a crossover from a CDW state to a weak AFM state, between V_5S_8 and V_6S_8 there is a change in T_n from from 32 K to 8 K, and between V_6S_8 and V_8S_8 the AFM ordering is destroyed.

Crystals in the range of composition $V_{4.88}S_8$ to $V_{5.44}S_8$ were obtained by vapor transport in either the V_5S_8 structure or the V_6S_8 structure. Quantitative X-ray refinements showed that neither V_5S_8 nor V_6S_8 grow stoichiometrically; that is, the IVC is variable. It is possible to continuously vary the V/S ratio within the two phases, which actually overlap in composition at certain stoichiometric ranges. The magnetic susceptibility has been measured on the crystals. T_N is clearly visible in V_5S_8 in the magnetic susceptibility, though it is not easily detected in V_6S_8 .

T_N in the V_5S_8 structure type samples shifts slightly with vanadium content. In order to investigate the dependence of the magnetic susceptibility of the compounds on the interstitial vanadium content (IVC), χ (T) was fitted to the Curie-Weiss law. The determined effective magnetic moment per mol interstitial vanadium was calculated: there is a clear relationship between the IVC and the magnetic moment: as the IVC increases, the compounds become less magnetic. Previous studies in the $V_{4.0}S_8$ - $V_{4.7}S_8$ range only measured down to 100K, so these compounds were reported as being paramagnetic. We see that this is not the case however: magnetic measurements of the $V_{4+x}S_8$ samples where $x = 0.1, 0.2, \dots, 0.9$ show a systematic decrease in T_N with decreasing vanadium content, but T_N was never destroyed. No superconductivity has been observed yet. The studies so far conducted have offered insight into the relationship between the vanadium content and the magnetic properties of the compounds, however, an investigation into the V-S compounds more than half of the interstitial vanadium sites occupied is still needed, as a superconducting state may arise on the side of the V_5S_8 solid solution where T_N is low and the overall magnetism of the compound is weaker than in V_5S_8 .

iii.) Future plans 1. Complete the work on correlations between superconductivity and dimer formation in 122 structure germanides and pnictides. 2. Complete the work on vanadium sulfides. 3. Determine whether ternary early transition-metal - late-transition metal subsulfides will lead to new conventional superconducting materials. 4. In a new thrust, determine whether TiNiSi-type AlB_2 and Fe_2P -type phases will lead to new superconducting phases at the borderline between magnetism and superconductivity.

v.) Publications supported by this grant, last two years

1. “Dimer breaking and high-temperature ferromagnetism in $LaCo_2(Ge_{1-x}P_x)_2$ ”, S.A. Jia and R.J. Cava, *Phys. Rev. B* **82** 180410 (2010).
2. “Muon spin rotation/relaxation measurements of the noncentrosymmetric superconductor $Mg_{10}Ir_{19}B_{16}$ ”, A.A. Aczel, T.J. Williams, T. Goko, J.P. Carlo, W. Yu, Y.J. Uemura, T. Klimczuk, J.D. Thompson, R.J. Cava, and G.M. Luke, *Phys. Rev.* **B82** 024520 (2010).
3. “Superconductivity at 2.3 K in the misfit compound $(PbSe)_{1.16}(TiSe_2)_2$ ”, N. Giang, Q. Xu, Y.S. Hor, A.J. Williams, S.E. Dutton, H.W. Zandbergen, and R.J. Cava, *Phys. Rev.* **B82** 024503 (2010).
4. “Magnetic and structural properties of $Ca(Fe_{1-x}Co_x)_2P_2$ and $Ca(Ni_{1-x}Co_x)_2P_2$ ”, S.A. Jia, S.X. Chi, J.W. Lynn, and R.J. Cava, *Phys. Rev.* **B81** 214446 (2010).
5. “Density of phonon states in superconducting FeSe as a function of temperature and pressure”, V. Ksenofontov, G. Wortmann, A.I. Chumakov, T. Gasi, S. Medvedev, T.M. McQueen, R.J. Cava, and C. Felser, *Phys. Rev.* **B81** 184510 (2010).
6. “Multiple electronic transitions and superconductivity in Pd_xTiSe_2 ”, E. Morosan, K.E. Wagner, L.L. Zhao, Y.S. Hor, A.J. Williams, J. Tao, Y. Zhu, and R.J. Cava, *Phys. Rev.* **B81** 094524 (2010).
7. “Pressure-restored superconductivity in Cu-substituted FeSe”, L.M. Schoop, S.A. Medvedev, V. Ksenofontov, A. Williams, T. Palasyuk, I.A. Troyan, J. Schmitt, F. Casper, C.H. Wang, M. Eremets, R.J. Cava and C. Felser, *Phys. Rev. B* **84** 174505 (2011).
8. “Ferromagnetic quantum critical point induced by dimer-breaking in $SrCo_2(Ge_{1-x}P_x)_2$ ”, Shuang Jia, Pawina Jiramongkolchai, M. R. Suchomel, B. H. Toby, J. G. Checkelsky, N. P. Ong and R. J. Cava, *Nature Physics* **7** 207 (2011).

The Synthesis, Structures and Chemical Properties of Macrocyclic Ligands Covalently Bonded into Layered Arrays, DE-FG02-03ER15420

Abraham Clearfield, Texas A&M University

College Station, TX 77843-3255

Phone: (979) 845-2936; Fax: (979) 845-2370

e-mail: clearfield@chem.tamu.edu

Jonathan D. Burns, Graduate Student, Texas A&M University

Eliazar Candanoza, Undergraduate, Texas A&M University

Sean Springer, Undergraduate, Texas A&M University

Collaborator: Donald T. Reed, Team Leader, Actinide Chemistry and Repository Science, Los Alamos National Laboratory, Carlsbad, NM 88220, dreed@lanl.gov

Overall Research Goals:

To utilize unconventional metal-organic frameworks (UMOFs) for the separation of lanthanides as a group from actinides and further separate individual actinides from one another.

Recent Progress:

1. We have discovered that the selectivities for 3+ and 4+ ions, recorded as K_d values, are greatly enhanced by synthesizing materials using Na_3PO_4 in place of H_3PO_4 in the synthesis of the mixed ligand phosphonates of Sn(IV) and Zr(IV).
2. The actinides follow the same selectivity sequence as the lanthanides in that the selectivity sequence is $\text{An}^{4+} > \text{AnO}_2^{2+} \geq \text{An}^{3+}/\text{Ln}^{3+} \gg \text{AnO}_2^+$.
3. We have developed an new method for synthesizing and stabilizing AmO_2^+ with lifetimes of days to weeks using $\text{Na}_2\text{S}_2\text{O}_8$ and $\text{Ca}(\text{OCl})_2$ as oxidant and stabilizing agents, respectively.

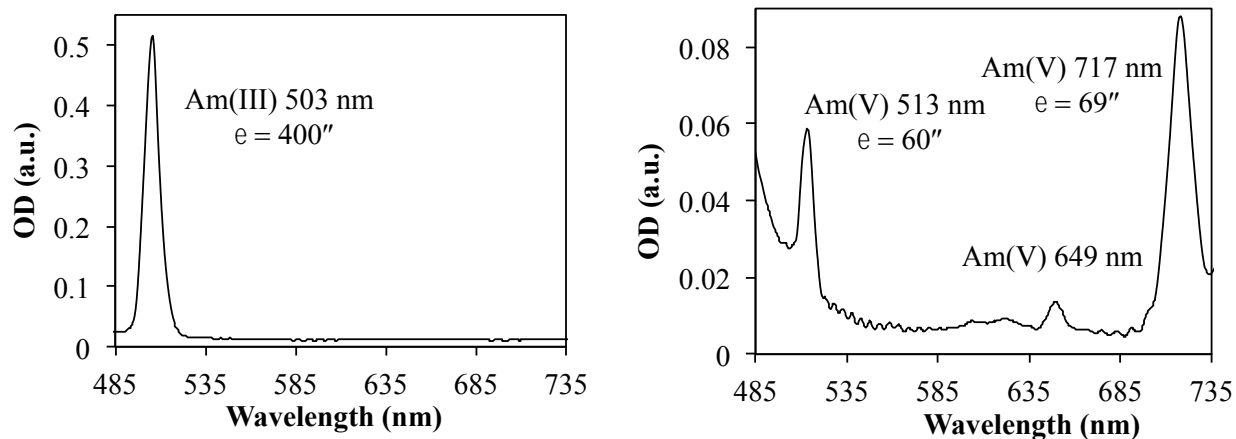
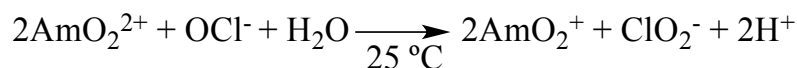
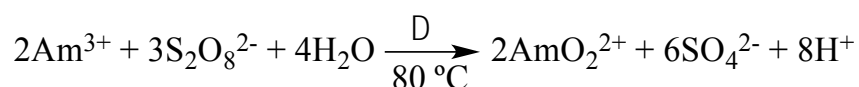


Figure 1: Absorbance spectrum of Am(III) before oxidation (left) and AmO_2^+ after oxidation (right).

4. Our ability to work with Np, Pu, Am, and Cm is due to the collaborations with Donald T. Reed and David T. Hobbs who have graciously allowed Jon Burns to spend time at Los Alamos National Laboratory-Carlsbad Operations (LANL-CO) and Savannah River National Laboratory (SRNL), respectively.
5. Direct separations have been observed for a mixture of AmO_2^+ , Nd^{3+} , and Eu^{3+} resulting in separation factors as high as 58 at pH 2 (LANL-CO).
6. Direct separations have been observed for a mixture of AmO_2^+ and Cm^{3+} resulting in separation factors as high as 20 at pH 2 (SRNL).
7. Direct separation have been observed for mixtures of Nd^{3+} and Ni^{2+} , Nd^{3+} and Sr^{2+} , and Nd^{3+} and Cs^+ with separation factors as high as 1,000, 2,400, and 800 at pH 2, respectively.

Future Plans:

1. Determine the ideal pH range for separation of Am from Cm.
2. Develop program for new materials based in aluminum.
3. Develop a chromatographic scheme implementing mixed metal phosphate phosphonates as the stationary phase.
4. Perform a separation of Am from a mixture of lanthanides in concentration close to the expected waste stream.
5. Investigate the structure of these UMOFs by means of EXAFS, EXANES, atomic pair distribution, and positron annihilation studies.
6. Add soft ligands with nitrogen or sulfur functions to the UMOFs for interaction with soft metal ions and extend the range of separations.

References:

1. Mincher, B. J.; Martin, L. R.; Schmitt, N. C., Tributylphosphate extraction behavior of bismuthate-oxidized americium. *Inorg. Chem.* **2008**, *47* (15), 6984-6989. Doi 10.1021/Ic800667h
2. Magirus, S.; Carnall, W. T.; Kim, J. I., Radiolytic Oxidation of Am(III) to Am(V) in NaCl Solutions. *Radiochim. Acta* **1985**, *38* (1), 29-32.
3. Runde, W. H.; Mincher, B. J., Higher Oxidation States of Americium: Preparation, Characterization and Use for Separations. *Chem. Rev.* **2011**, *111* (9), 5723-5741. Doi 10.1021/Cr100181f
4. Clark, D. L.; Hecker, S. S.; Jarvinen, G. D.; Neu, M. P., Plutonium. In *The Chemistry of the Actinide and Transactinide Elements*, 4th ed.; Morss, L. R.; Edelstein, N. M.; Fuger, J., Eds. Springer: Netherlands, 2011; Vol. 2, pp 813-1264.
5. Nash, K. L.; Madic, C.; Mathur, J. N.; Lacquement, J., Actinide Separation Science and Technology. In *The Chemistry of the Actinide and Transactinide Elements*, 4th ed.;

Morss, L. R.; Edelstein, N. M.; Fuger, J., Eds. Springer: Netherlands, 2011; Vol. 4, pp 2622-2798.

6. *2011 Fuel Cycle Technologies Annual Review Meeting Transaction Report*; Argon National Laboratory: November 8-10, 2011.
7. Brunet, E.; Cerro, C.; Juanes, O.; Rodriguez-Ubis, J. C.; Clearfield, A., Hydrogen storage in highly microporous solids derived from aluminium biphenyldiphosphonate. *J. Mater. Sci.* **2008**, *43* (3), 1155-1158. Doi 10.1007/S10853-007-2377-0

Publications:

1. Burns, J. D.; Clearfield, A.; Shehee, T. C.; and Hobbs, D. T., Separation of americium from curium by oxidation and ion exchange. *J. Am. Chem. Soc.*, **submitted**.
2. Burns, J. D.; Borkowski, M.; Clearfield, A.; and Reed, D. T., Separation of oxidized americium from lanthanides by use of pillared metal(IV) phosphate-phosphonate hybrid materials. *Radiochim. Acta*, (**2012**) in press.
3. Clearfield, A.; Medvedev, D. G.; Kerlegon, S.; Bosser, T.; Burns, J. D.; Jackson, M.; Rate of exchange of Cs⁺ and Sr²⁺ for poorly crystalline sodium titanium silicate (CST) in nuclear waste systems. *Solvent Extr Ion Exc.* (**2012**) in press.
4. Burns, J. D.; Clearfield, A.; Borkowski, M.; and Reed, D. T., Pillared metal(IV) phosphate-phosphonate extraction of actinides. *Radiochim. Acta*, (**2012**) DOI: 10.1524/ract.2012.1929.
5. Kevin, J. Gagnon, Houston P. Perry, Abraham Clearfield, Conventional and Unconventional Metal–Organic Frameworks Based on Phosphonate Ligands: MOFs and UMOFs. *Chem. Rev.* (**2012**), *112*(2), 1034-1054, DOI: 10.1021/cr2002257.
6. Christopher S. Fewox, Abraham Clearfield and Aaron J. Celestian, In situ X-ray Diffraction Study of Cesium Exchange in Synthetic Umbite, *Inorg. Chem.*, (**2011**), *50*(8), 3596-3604, DOI: 10.1021/ic102546w.
7. T. Moller, N. Bestaoui, M. Wierzbicki, T. Admas and A. Clearfield, Separation of lanthanum, hafnium barium and radiotracers yttrium-88, barium-133 for Ra-223 radioisotope generator, *Appl. Radiat. Isot.*, (**2011**), *69*(7), 947-954, DOI: 10.1016/j.apradiso.2011.02.033.

Tuning Sorption Properties of Metal-Organic Frameworks via Postsynthetic Covalent Modification

Seth M. Cohen, Department of Chemistry and Biochemistry, University of California, San Diego, La Jolla, California, 92093-0358

Program Scope

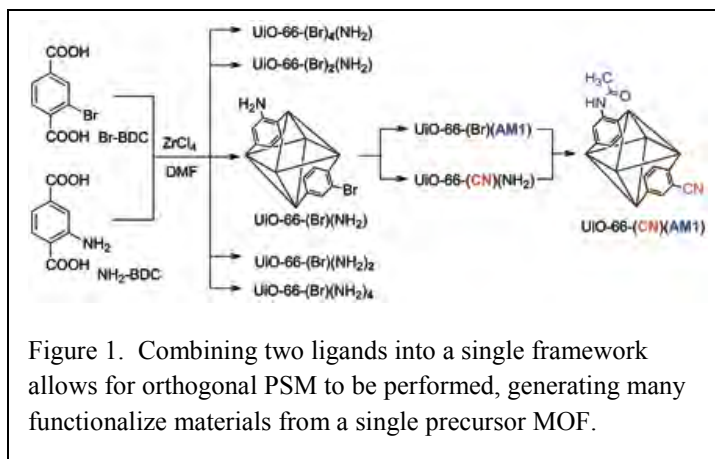
This continuing proposal in the area of Materials Chemistry describes a systematic approach to the postsynthetic modification (PSM) of metal-organic framework (MOF) materials. To further advance the utility of MOFs in the area of gas storage and other applications (particularly in energy applications), the ability to chemically modify these structures in a predictable and reliable fashion is essential. Realization of this goal will allow for the preparation of functionalized MOFs, which will have unparalleled properties, such as controlled framework flexibility and highly unsaturated metal sites. This continuing research program fulfills at least two, of the four, stated research goals of the Office of Basic Energy Sciences: a) the fabrication and characterization of new materials, and b) the understanding and control of chemical reactivity.

This research program will develop new methods to chemically modify MOFs. We will expand the scope of reactions that can be performed within MOFs by introducing new chemical ‘handles’ within the framework. Our studies focus on the commonly used 1,4-benzenedicarboxylate (BDC) ligand, and extended analogues, possessing amino-, nitro-, or bromo-substituents. Other substituents can also be used by application of a new method, termed postsynthetic deprotection (PSD). Ligands with these chemical handles have been assembled into a variety of known MOFs, including IRMOF, UMCM, MIL-53, and UiO-66 architectures. We have also developed bifunctional systems that contain two or more, orthogonal chemical handles on a single ligand (e.g., a bromo- and amine- group). These allow for control over the relative orientation of newly introduced functional groups, a feat not previously achieved in PSM chemistry. Slightly more applied studies will focus specifically on using PSM (or PSD) to control the selectivity, energetics, and capacity of gas sorption in MOFs. Our findings show that PSM can be used to control MOF flexibility (‘breathing’), improve heats of binding (for H₂), and facilitate introduction of unsaturated metal centers. Better understanding and control over these features will be pursued in our ongoing investigations. The overall scope of our program serves to advance the energy-related applications of MOFs via PSM. Our improved capacity to modify MOFs in this manner will be important for the synthesis of new materials, altering the physical properties of these materials, and ultimately the use of these materials in advanced energy applications.

Recent Progress

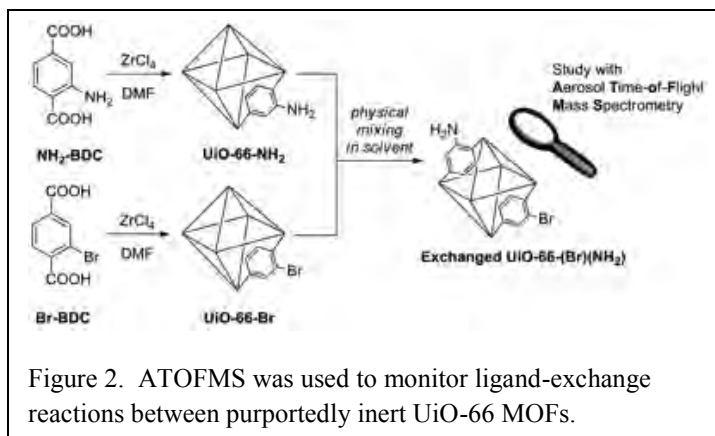
Our recent progress on this project has expanded in several different directions, all of which provide interesting opportunities for new research directions. Each of these different directions is concisely summarized below.

- As proposed, we have prepared a series of mixed, bifunctional metal–organic frameworks that could be modified in a postsynthetic manner at two, orthogonal sites (Figure 1). The use of differentially ‘tagged’ ligands combined with PSM provides a facile route to a large number of functionally diverse materials. In related work, we prepared bifunctional BDC



ligands with two, orthogonal functional groups on the same ligand. These ligands were found to produce MOFs with modulated breathing. PSM studies on these systems are ongoing.

- A new discovery in our laboratory has been in the area of the dynamics and stability of MOFs. We recently reported the exchange of ligands from an intact MOF can be exploited as a means to introduce functionalized ligands into MOFs under mild conditions. Such exchange reactions in MOFs have been reported, with

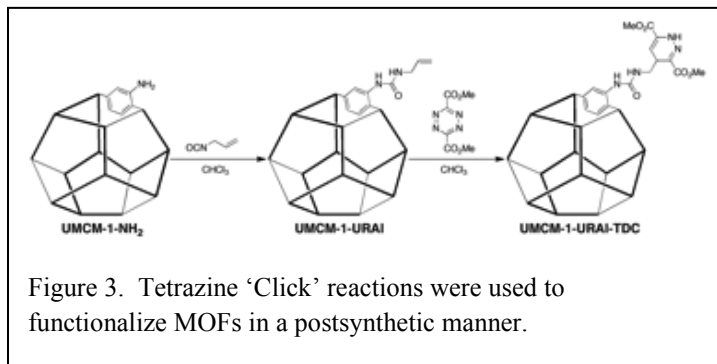


both metals and ligands (with a flurry of recent reports appearing in in the last year).

However, what was surprising about our findings was that ligand exchange occurred with the ‘inert’ Zr(IV)-based UiO-66 MOFs (Figure 2). In line with our other work, we termed this process ‘postsynthetic exchange’ (PSE) and showed that it provides access to MOFs that are not readily prepared by solvothermal methods. In addition to the exploration of this PSE methodology, we introduced, in collaboration with Prof. Kimberly Prather (U.C. San Diego), the use of aerosol time-of-flight mass spectrometry (ATOFMS) to monitor these reactions on MOF particles (micron-sized). ATOFMS was used to analyze the chemical composition of

microcrystalline MOFs on the single particle level, providing information not available through bulk analysis. ATOFMS is a powerful method, widely used in environmental chemistry, but essentially absent in the field of nanomaterials chemistry. PSE is an important postsynthetic approach to the modification of MOFs, and the ligand exchange revealed by ATOFMS requires a re-evaluation of the assumed ‘stability’ of even the most robust MOFs.

- In our efforts to develop fundamentally new PSM reactions, we have demonstrated that tetrazine-based “Click” reactions are amenable for MOF modification (Figure 3). It was



found that the efficacy of this modification procedure was dependent on the topology of the MOF and, in the case of an isorecticular MOF (IRMOF) system, required the formation of a mixed-ligand IRMOF with a suitable ratio of BDC and an olefin-tagged BDC derivative. On the basis of the versatile use of tetrazine “Click” chemistry in bioconjugate chemistry, we expect that this scheme will prove to be a useful reaction for modifying MOFs.

Future Plans

Our future plans seek to continue our investigations along the several lines of research described above. Some of these projects are of sufficient scope and interest, they may be spun-off into independent projects, but that decision will be made as progress on each research subject continues. Fundamental studies on the PSM induced flexibility of MOFs and the ability to control selective gas sorption will be continued. In addition, we are collaborating with Prof. F. Paesani (U.C. San Diego), a new theoretical chemist in our department, on computational/theoretical studies to help us understand these complex phenomena. Studies on the gas uptake selectivity and moisture stability of differentially-functionalized UiO-66 MOFs will continue as well. These studies are being performed in close collaboration with Prof. K. Walton (Georgia Tech U.). Indeed, a postdoctoral research from the Cohen group (Dr. Min Kim) made a visit to the Walton group in Spring 2012 to help move this collaborative study forward.

Most certainly our group will continue to develop of new postsynthetic methods, such as the tetrazine-derived click chemistry described above. Our group is intent on remaining at the forefront of developing new synthetic methods for functionalizing MOFs, and this includes the discovery of new reactions as well as new methodologies such as PSM, PSD, and PSE. All of these techniques can serve to augment MOF research and produce materials with unprecedented

properties. The wide adoption of postsynthetic methods by MOF researchers around the world is evidence of the continued importance of further augmenting these methods.

Finally, our investigations on MOFs containing unsaturated metal centers (introduced by postsynthetic methods) will be a primary area of future study. Although a common theme in MOF chemistry, the postsynthetic approaches we have discovered often lead to the introduction of rather distinct unsaturated metal centers, involving metal-ligand combinations beyond those commonly reported in other MOF materials. The ability of such materials to enhance gas sorption, including CO₂ and H₂, is a well-established, but still growing area of research. We have exciting, new results on the cyclometallation of MOFs, providing a distinct platform for enhancing gas sorption.

References

See list below for references to the work described.

Publications (due to page restrictions this is only a partial list of recent DOE-funded work)

1. Min Kim, Jake A. Boissonault, Corrine A. Allen, Phuong V. Dau, and Seth M. Cohen, "Functional Tolerance in an Isoreticular Series of Highly Porous Metal-organic Frameworks" *Dalton Trans.* **2012**, 41, 6277-6282.
2. Sang Ho Lim, Yongxuan Su, and Seth M. Cohen, "Supramolecular Tetrahedra of Phosphines and Coinage Metals" *Angew. Chem. Int. Ed.* **2012**, Early View.
3. Min Kim and Seth M. Cohen, "Discovery, Development, and Functionalization of Zr(IV)-Based Metal-Organic Frameworks" *CrystEngComm* **2012**, Advanced Article.
4. Seth M. Cohen, "Postsynthetic Methods for the Functionalization of Metal-Organic Frameworks" *Chem. Rev.* **2012**, 112, 970-1000.
5. Min Kim, John F. Cahill, Yongxuan Su, Kimberly A. Prather, and Seth M. Cohen, "Postsynthetic Ligand Exchange as a Route to Functionalization of 'Inert' Metal-Organic Frameworks" *Chem. Sci.* **2012**, 3, 126-130.
6. Chao Chen, Corinne A. Allen, and Seth M. Cohen, "Tandem Postsynthetic Modification of Metal-Organic Frameworks Using an Inverse-Electron-Demand Diels-Alder Reaction" *Inorg. Chem.* **2011**, 50, 10534-10536.
7. Min Kim, John F. Cahill, Kimberly A. Prather, and Seth M. Cohen, "Postsynthetic Modification at Orthogonal Reactive Sites on Mixed, Bifunctional Metal-Organic Frameworks" *Chem. Commun.* **2011**, 47, 7629-7631.
8. Min Kim, Sergio J. Garibay, and Seth M. Cohen, "Microwave-Assisted Cyanation of an Aryl Bromide Directly on a Metal-Organic Framework" *Inorg. Chem.* **2011**, 50, 729-731.

Project Title: Electronic and Ionic Conductors from Ordered Microporous Materials

PI: Mircea Dincă (mdinca@mit.edu)

Institution: Department of Chemistry, Massachusetts Institute of Technology

Program Scope

This project aims to establish microporous metal-organic (MOFs) and covalent-organic frameworks (COFs) as new classes of high-surface area, crystalline electronic and ionic conductors. This effort is part of the PI's interest in exploring the physical and chemical properties of these materials and their non-traditional uses such as gas separation and storage. With this project, we hope to provide new types of electrode materials, ionic membranes, or electrocatalysts and to provide fundamentally new platforms for studying processes such as ion diffusion in monodisperse sub-nanometer pores and electron delocalization and transport in molecular materials. Our approach to imparting electronic conductivity in MOFs, which are prototypical insulators, is to employ a series of electroactive organic building blocks containing chalcogenide atoms and is inspired by similar approaches in conducting organic polymers. Our approach to obtain ionic conductors from MOFs involves post-synthetic cation metathesis, which we are establishing as a new synthetic route towards MOFs with predefined structures, but novel electronic properties.

Recent Progress

Towards ion conductors from MOFs – we found that post-synthetic cation metathesis can be employed to access highly sought-after MOF phases that could not be previously produced by direct synthesis. In particular, we showed $3d$ transition-metal analogues of $\text{Zn}_4\text{O}(\text{BDC})_3$ (MOF-5; BDC = 1,4-benzenedicarboxylate), one of the most iconic materials in this class can be directly substituted with Co^{2+} and Ni^{2+} by post-synthetic ion exchange. Having established $\text{Ni}_x\text{Zn}_{4-x}\text{O}(\text{BDC})_3$ as a thermodynamic product relative to MOF-5 itself, we also developed direct synthetic routes for substituted MOF-5 analogues. In doing so, we observed that the maximal Ni^{2+} incorporation rate was 25% (one Ni ion per Zn_4O cluster) regardless of the synthetic conditions (post-synthetic metathesis or direct synthesis from the respective metal nitrates) or reactant ratio (Figure 1). We

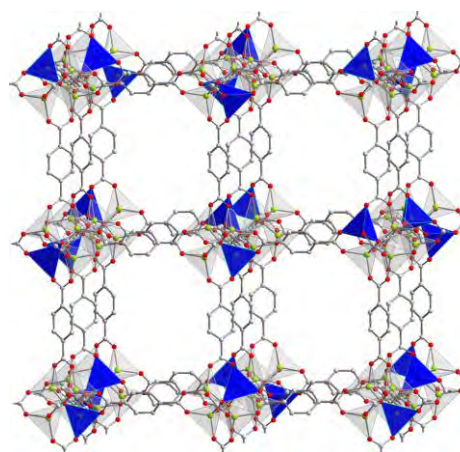


Figure 1 Part of the crystal structure of $\text{Ni}_x\text{Zn}_{4-x}\text{O}(\text{BDC})_3$ ($x = 1$). Green, red, and grey spheres represent Zn, O, and C atoms, respectively. Hydrogen atoms are omitted for clarity. We were thus able to establish the partially-substituted MOF-5 structures as *kinetically-trapped intermediates* in the molecular energy surface of basic zinc acetate clusters. Furthermore, we showed that the substituted MOF-5 materials retain identical structures, surface area, and stability to the parent all-Zn MOF-5 material, and that a very unusual tetrahedral Ni^{2+} ion in an

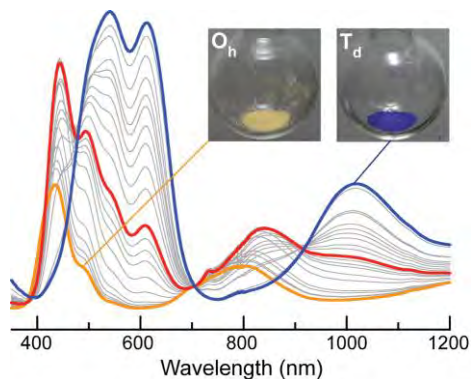


Fig. 2 In-situ diffuse-reflectance spectra depicting the octahedral-to-tetrahedral transformations of the Ni^{2+} centers within Ni-substituted MOF-5. The inset shows optical images of the yellow (O_h) and blue (T_d) crystals.

all-oxygen (strong) ligand field environment results by heating the Ni-substituted MOF-5 analogues under high vacuum. These findings establish post-synthetic ion metathesis as a new method to access previously unknown MOF phases (Figure 2).

Important in the context of accessing ion conductors from MOFs, our findings show that MOFs that were previously believed rigid, such as MOF-5, are in fact under dynamic equilibrium with other divalent metal ions in solution. Moreover, we showed that insertion of Ni^{2+} involves an octahedral Ni^{2+} intermediate which occupies a tetrahedral Zn^{2+} site without otherwise disrupting the MOF structure. This suggests that even "rigid" MOFs can accommodate

relatively large distortions without compromising structural integrity, an important aspect of our future studies where we will attempt to incorporate divalent metal ions in coordination environments previously occupied by trivalent metals with different ionic radii and coordination numbers.

Towards electronically-conducting MOFs. Efforts here were focused on the synthesis of chalcogenide analogues of carboxylic acids and new organic bridging ligands containing chalcogenide atoms in the backbone. Dithioic acids and thioamides were explored initially and found to be sensitive to the reaction conditions typically required for MOF synthesis, which led to oxidation of the reduced sulfur ligands. More recently, employing carboxylate ligands containing sulfur atoms in the organic backbone we were able to obtain permanently porous MOFs with BET surface areas of approximately $600 \text{ m}^2/\text{g}$. Transient microwave spectroscopy in three of these new materials has revealed high charge mobility values in line with those of good organic conducting polymers. Further studies of these materials are currently underway.

Future Plans

- ionic conductors: we will extend our post-synthetic ion metathesis studies to systems where ion exchange will not only result in intra-framework ion substitution, but will also leave mobile, uncoordinated monovalent ions such as Li^+ within the pores of the targeted materials. With these new materials in hand, we will undertake systematic ion exchange and ion conductivity studies. By varying the nature of the mobile ion, pore size, pore polarity, and pore topology, we seek to understand trends in ion conduction in nanometer and sub-nanometer-sized pores.
- electronic conductors: two distinct pathways will be undertaken here: 1) we will continue the exploration of electroactive, π -stacking ligands as useful synthons for the construction of high-charge-mobility MOFs. First, we will increase linker size in an

isorecticular fashion, aiming to increase the pore size and pore volume of our current materials to allow infiltration of electron acceptor molecules for charge-transfer interactions. 2) we will continue the characterization of newly synthesized materials using UV Photoelectron Spectroscopy and terahertz spectroscopy (in a new collaboration at MIT) and will test their efficacy towards devices such as photovoltaic cells, owing to their broadband absorption in the visible.

Publications in the Period Aug 2011 – May 2012

Brozek, C. K.; Dincă, M. "Lattice-Imposed Geometry in Metal-Organic Frameworks: Lacunary Zn_4O Clusters in MOF-5 Serve as Tripodal Chelating Ligands for Ni^{2+} " *Chemical Science* **2012**, 3, 2110-2113.

Synthesis, Characterization and Properties of Nanoparticles of Intermetallic Compounds

Frank DiSalvo, Department of Chemistry, Cornell University, Ithaca, NY 14850

Program Scope

Our research program is focused on developing a “universal” method to prepare alloys or ordered intermetallic compound (binary, ternary and beyond) nanoparticles in order to understand their structural and electrochemical behavior, as well as their durability in use. An eventual application to electrochemical catalysis, such as in fuel cells, is hoped for, but our main focus is on developing methods to synthesize compositionally complex nanoparticle systems and to understand the kinetics of formation and phase diagrams of compound nanoparticles as a function of annealing temperature and composition.

We have developed a solution method that allows reduction of mixed metal cations from group III to XIV and are exploring methods of controlled particle growth and specific structures by thermal processing. We use THF as the solvent, since it is non-reactive with all the metals in these groups. We have shown that almost all metal cations of interest are moderately to highly soluble in THF either as binary chlorides (e.g. TiCl_4 , FeCl_3 , ZnCl_2 , SnCl_2 , SnCl_4) or as ternary Li salts (e.g. Li_3CrCl_6 , Li_2NiCl_4 or Li_6NiCl_8 , Li_2PtCl_6 , Li_2CuCl_4). (See **Figure I**) We avoid the use of organic anions or ligands in the reactants, since we find that they often react with, or are included in, or strongly bound to the surfaces of the nanoparticles. Similarly, almost all surfactants are avoided, since they often cannot be removed from the nanoparticles without leaving residues that poison the catalyst.

										MCl_x			
										Li_yMCl_x			
										5 B Boron 10.811	6 C Carbon 12.0107	7 N Nitrogen 14.00674	
										13 Al Aluminum 26.981538	14 Si Silicon 28.0855	15 P Phosphorus 30.973761	
21 Sc Scandium 44.955910	22 Ti Titanium 47.867	23 V Vanadium 50.9415	24 Cr Chromium 51.9961	25 Mn Manganese 54.938049	26 Fe Iron 55.845	27 Co Cobalt 58.933200	28 Ni Nickel 58.6934	29 Cu Copper 63.546	30 Zn Zinc 65.39	31 Ga Gallium 69.723	32 Ge Germanium 72.61	33 As Arsenic 74.92160	
39 Y Yttrium 88.90585	40 Zr Zirconium 91.224	41 Nb Niobium 92.90638	42 Mo Molybdenum 95.94	43 Tc Technetium (98)	44 Ru Ruthenium 101.07	45 Rh Rhodium 102.90550	46 Pd Palladium 106.42	47 Ag Silver 107.8682	48 Cd Cadmium 112.411	49 In Indium 114.818	50 Sn Tin 118.710	51 Sb Antimony 121.760	
57 La Lanthanum 138.9055	72 Hf Hafnium 178.49	73 Ta Tantalum 180.9479	74 W Tungsten 183.84	75 Re Rhenium 186.207	76 Os Osmium 190.23	77 Ir Iridium 192.217	78 Pt Platinum 195.078	79 Au Gold 196.96655	80 Hg Mercury 200.59	81 Tl Thallium 204.3833	82 Pb Lead 207.2	83 Bi Bismuth 208.98038	

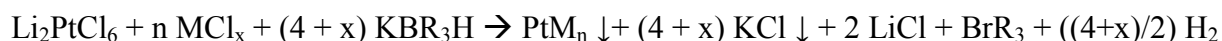
Figure 1. Table of THF soluble metal chloride salts. Virtually every metal in the periodic table can be put in THF solution at useful concentrations (Exceptions: Na – Cs, Mg-Ba, Hg - Pb). When both MCl_x and Li_yMCl_x salts are available and soluble, the latter usually have higher solubility.

The next challenges were: 1) to keep the nanoparticles from agglomerating in all stages of processing, 2) to carefully grow the nanoparticle size by heating (annealing), and 3) to transfer and bind the nanoparticles to an appropriate support.

Recent Progress

The reducing agents used are alkali alkylborohydride salts [1] [2] (ABR_3H , with $A = Li, Na$ or K and R typically ethyl). Here we focus on $A = K$, and on reactions that produce Pt containing intermetallics. We emphasize, however, that the method is widely applicable and can be utilized to prepare nanoparticles of a large variety of intermetallic phases of metals from groups III to XIV.

A prototypical reaction scheme carried out in THF under air free conditions is:



Upon adding the borohydride, a very fast reaction (few seconds) occurs and the two solid products precipitate together as very small intermetallic nanoparticles (2 nm) trapped in a KCl matrix (denoted as Np-KCl). Note that LiCl and BR_3 are quite soluble in THF and are easily removed by decanting and washing in neat THF. The amount of precipitating KCl can be considerably increased by adding LiCl to the initial reaction mixture and adding a THF soluble K^+ source to the reducing agent. If M is from group III, IV, V or is Cr, the product may contain some hydrogen (as a hydride) but in the cases we have studied this is removed upon annealing.

Controlled particle growth occurs when the Np-KCl is annealed under vacuum. Annealing also decreases any heterogeneity in the composition of the nanoparticles. For example, on heating a KCl matrix of Pt:Fe::3:1 to 600 C, ordered Pt_3Ti nanoparticles grow to an average particle size of 5 nm from only 2 nm as prepared at room temperature (**Figures 2 through 6**). In a similar manner, we have prepared ordered intermetallic nano-particles of Pt_3Co , Pt_3Cr , $PtFe$, Pt_3Fe , $PtNi$, Pt_2Mo , $PtSn$, Pt_3Sn , Pt_3V . It is important to emphasize the key role that the KCl matrix plays in greatly slowing particle growth and in avoiding significant particle agglomeration.

The next step is to release the PtM_x product from the KCl matrix and to bind the nanoparticles to an appropriate support, say carbon black. We developed a simple route to do so. The support is first suspended in ethylene glycol (EG). When the NpKCl matrix is added, the EG dissolves the KCl (solubility: 1.5 g KCl/100 g EG). EG is also a weak surfactant that in concentrated form is sufficient to prevent particle agglomeration, but that can be removed from particles by heating under vacuum at 150 °C without leaving a residue. EG is labile at room temperature so that supports with binding sites that have stronger affinity than EG, such as carbon black, will preferentially bind the nanoparticles (**Figure 5**). If higher KCl solubility is needed, adding up to 15 mole % water, does not change the outcome of the transfer.

If time allows, some electrochemical observations will be presented and discussed.

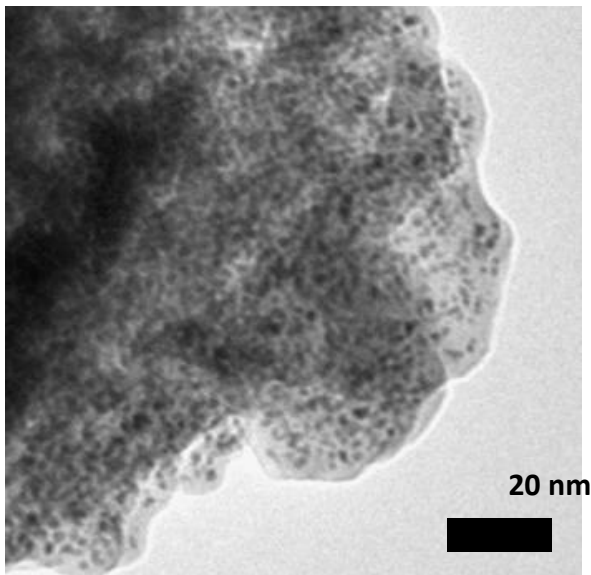


Figure 2. A TEM image of Pt₃Fe-15KCl synthesized at room temperature. 2 nm nanoparticles are isolated and dispersed on and/or in the KCl matrix (light colored).

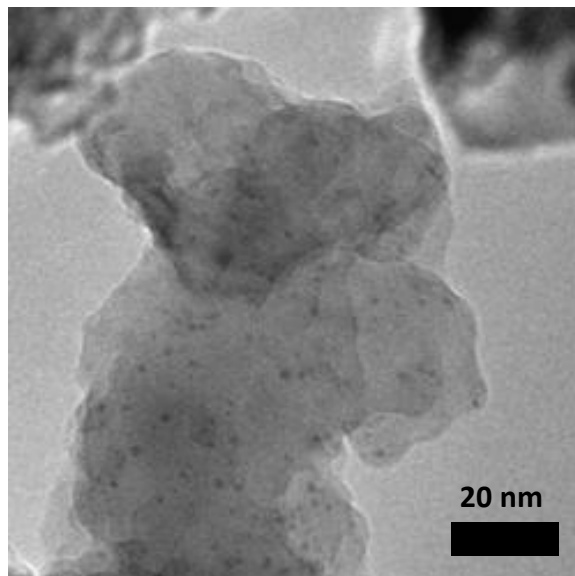


Figure 3. A TEM image of Pt₃Fe-160KCl synthesized at room temperature. The nanoparticles are highly dispersed in the KCl

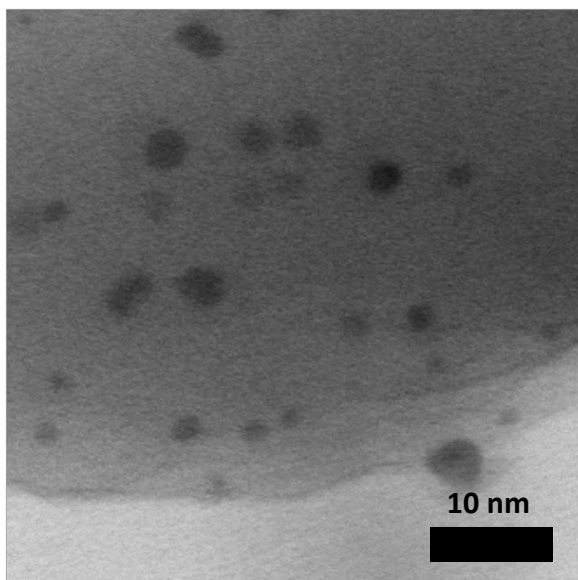


Figure 4. A TEM image of Pt₃Fe-160KCl annealed at 600 °C for 12 hours. The nanoparticles have grown to about 5 nm in size.

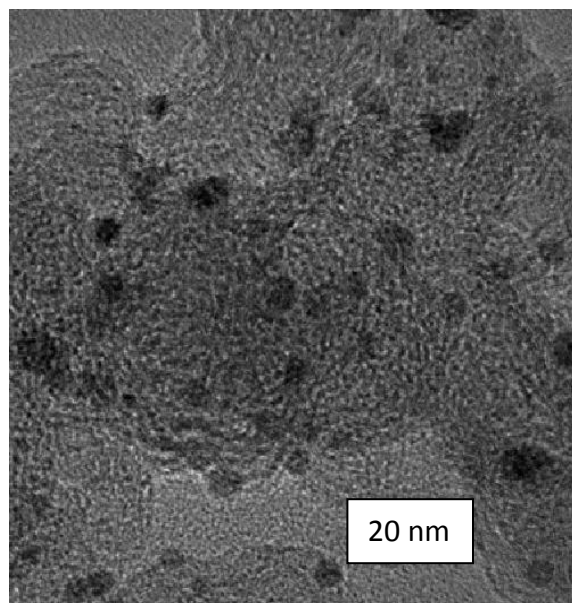


Figure 5. After thermal annealing a Pt₃Fe-80KCl composite at 600 °C for 12 hours, the Pt₃Fe was transferred to a Vulcan carbon support by sonicating a mixture of Pt₃Fe-80KCl and Vulcan in ethylene glycol and then washed in H₂O.

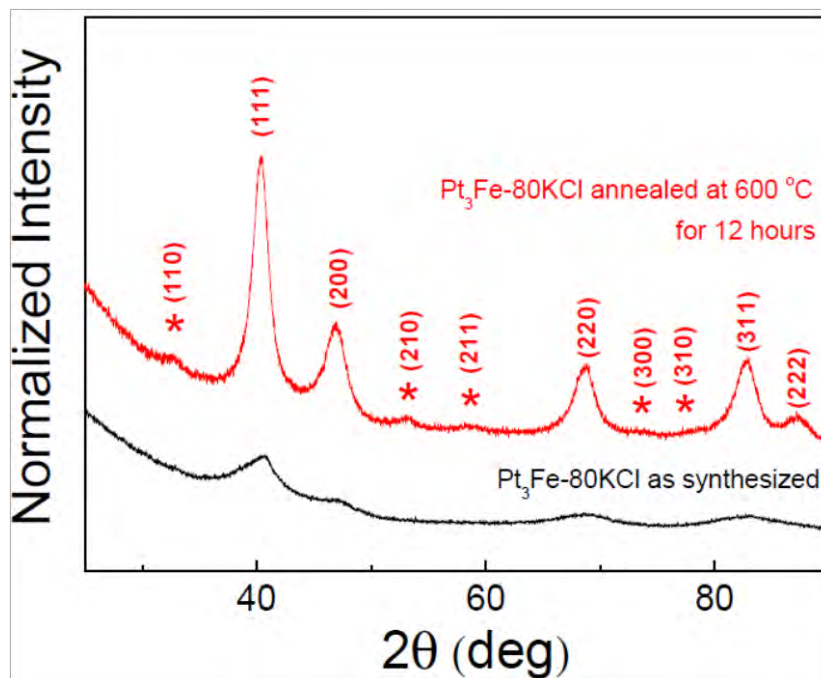


Figure 6. pXRD patterns of Pt₃Fe-80KCl nanoparticles before (black) and after (red) thermal annealing at 600 °C for 12 hours. In both cases, samples were washed with H₂O to remove KCl, so that diffraction comes from the particles only. The very broad peaks seen for the room temperature sample (black) are expected for 2 nm diameter nanoparticles. After annealing, the weak superlattice peaks expected for the ordered Cu₃Au structure type are indicated by an asterisk.

References

1. Bonnemann, H. and G. Khelashvili, *Efficient fuel cell catalysts emerging from organometallic chemistry*. Applied Organometallic Chemistry, 2010. **24**: p. 257–268.
2. Bonnemann, H., W. Brijoux, and T. Jousen, *The Preparation of Finely Divided Metal and Alloy Powders*. Angew. Chem. Int. Ed. Engl., 1990. **29**: p. 273-275.

Publications

1. "An in-situ STEM study of the growth mechanisms during annealing of Pt-Fe nanoparticles in a KCl matrix", Hao Chen, Yingchao Yu, Huolin L. Xin, Kathryn A. Newton, Héctor D. Abruña and Francis J. DiSalvo, ACS Nano (submitted)
2. "An unconventional strategy for synthesizing nanoparticles with desired size and structure", Hao Chen, Deli Wang, Kathryn A. Newton, Héctor Abruña and Francis J. DiSalvo, JACS (submitted)
3. "Facile Synthesis of PtNi Intermetallic Nanoparticles: Influence of Reducing Agent and Precursors on Electrocatalytic Activity", B.M. Leonard, Q. Zhou, D. Wu and F.J. DiSalvo, *Chem. Mater.* **23**, 1136-1146 (2011)
4. "Intermetallics as Novel Supports for Pt Monolayer O₂ Reduction Electrocatalysts: Potential for Significantly Improving Properties", T. Ghosh, M.B. Vukmirovic, F.J. DiSalvo and R.R. Adzic, *J. Am. Chem. Soc., Commun.* **132**, 906-907 (2010)

Rational Design and Nanoscale Integration of Multi-Heterostructures as Highly Efficient Photocatalysts

Xiangfeng Duan
Department of Chemistry and Biochemistry
University of California, Los Angeles,
Los Angeles, CA 90095

Nanoscale integration of dissimilar materials can enable exciting opportunities to precisely control and fine tune their electronic and optical properties, and create a new generation of integrated material systems with synergistic functions not possible in individual components. The objective of this project is to design and synthesize highly complex multi-hetero-nanostructures that integrate a nanoscale photovoltaic device with two distinct redox nanocatalysts. Photoexcitation of these heteronanostructures creates electron-hole pairs that are quickly separated and transported to the integrated nanocatalysts to drive thermodynamically uphill redox reactions. Systematic studies will be carried out to develop general strategies for the synthesis of such complex nanostructures, and to investigate their fundamental electronic, optical and photocatalytic properties. The rational design of nanoscale architectures and seamless integration of multiple functional components in a single nanostructure can enable efficient optical absorption, charge generation, separation, transportation and utilization for productive redox chemistry. It therefore has the potential to enable a new generation of highly effective photocatalysts for efficient harvest and conversion of solar energy into chemical fuel.

Title: Molecular Magnets Based on a Modular Approach: Investigation of Coupling, Anisotropy and Electronic Factors on Bistability

PI: Professor Kim R. Dunbar, Department of Chemistry, Texas A&M University, College Station, Texas

Until recently, research into the phenomenon of magnetic bistability in molecules, commonly referred to as Single Molecule Magnets (SMMs), has focused primarily on increasing the ground-state spin value (S) to raise the thermal barrier for spin reorientation, but success has been limited. The past few years, however, have witnessed a veritable explosion of exciting breakthroughs in the design of SMMs. One remarkable discovery is that mononuclear transition and lanthanide metal complexes with a small number of spins can also exhibit slow paramagnetic relaxation, compounds that are known as single ion single molecule magnets (SI-SMMs).¹⁻⁷ Another relatively unexplored avenue to increasing the blocking temperatures of polynuclear SMMs is to incorporate early 3d and 4d/5d transition metal ions that exhibit strong spin-orbit coupling into cyanide-bridged clusters, thereby introducing anisotropy into the M_1 -CN- M_2 metal-ligand bond through exchange interactions.⁸⁻¹⁰ In addition to anisotropic exchange, theory has predicted that certain combinations of metal ions in the M-CN-M' linkage should exhibit extremely strong coupling. The synthesis of new cyanide molecules guided by these premises and the assessment of their structural, electronic and magnetic properties constitute the foundation for our DOE funded research. Simply stated, the scope of our DOE funded project is to design, synthesize and fully characterize new molecular nanomagnets which differently than bulk magnetic materials. We are investigating such "quantum magnets" based on strongly anisotropic metal ions by preparing homologous families of compounds in order to gain insight into the complex interplay of metal ion, ligand, and supramolecular interactions and how they affect the properties of these materials. Our strategies are guided by theoretical predictions regarding the energies of magnetic interactions as well how the ligand field of the metal affects the zero field splitting parameter that leads to Ising (or easy axis) anisotropy.

Recent Progress

New magnets based on 4d and 5d transition metal ions

We recently isolated linear trimers based on $[M^{III}(CN)_6]^{3-}$ ($M = Fe, Ru$ and Os) and Mn^{III} ions that exhibit exchange-biased single-molecule magnetic (SMM) behavior due to extensive intermolecular interactions, the first such evidence for this phenomenon in cyanide based SMMs. This result provides us with an ideal platform to probe the effect of supramolecular interactions on the bistability of a small magnetic unit. We have also incorporated 4d and 5d cyanometallates (Os^{III} , Ru^{III} and Mo^{III}) into trigonal bipyramidal clusters of the type $([M(tmphen)_2]_3[M'(CN)_6]_2)$ resulting in the first ferromagnetic interaction observed between Mo^{III} and Co^{II}/Ni^{II} through cyanide and the cluster $[Fe(tmphen)_2]_3[Os(CN)_6]_2$ which undergoes a thermally-induced reversible intramolecular electron transfer - highlighted in *Nature Chemistry*. A very exciting recent finding is that a molecule with $Mo(III)$ and $V(II)$, namely $[V(tmphen)_2]_3[Mo(CN)_6]_2$, exhibits the strongest exchange coupling to date through a cyanide ligand estimated at -130 cm^{-1} .

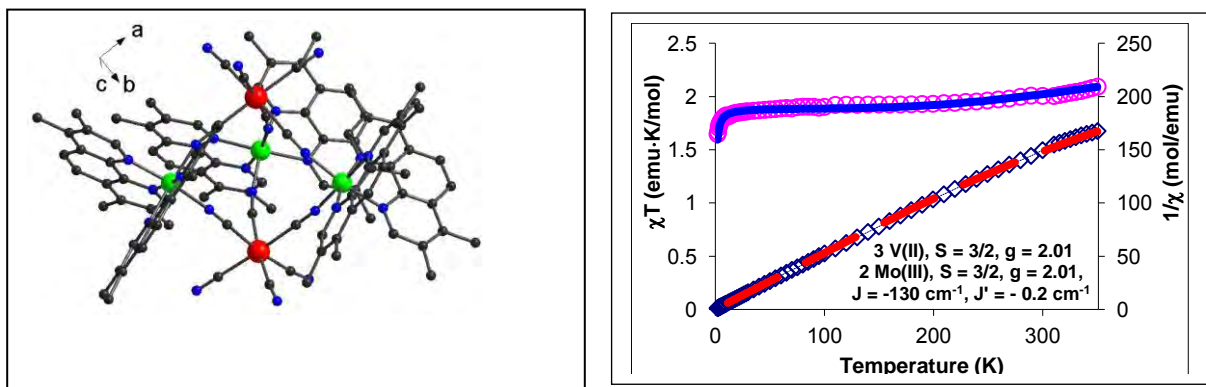


Figure 1. Depiction of the molecular structure of the new Mo_2V_3 TBP cluster (left) and the magnetic data (right).

Efforts by our group have also yielded new structures incorporating $[\text{Mo}(\text{CN})_7]^{4-}$, namely two new octahedral clusters ($[\text{M}(\text{tmphen})_2]_4[\text{Mo}(\text{CN})_7]_2(\text{solvent})$; $\text{M} = \text{Cr}^{\text{II}}, \text{Mn}^{\text{II}}$) with possible SMM behavior and an extraordinary dicosanuclear cluster that holds the record for the highest ground state spin value of any cyanide-bridged cluster known to date, a molecule featured on the cover of *Angewandte Chemie*. By far the most exciting result has come very recently in an unpublished result with the $[\text{Mo}(\text{CN})_7]^{4-}$ chemistry. The first trinuclear cluster based on the $[\text{Mo}(\text{CN})_7]^{4-}$ unit $[\text{Mn}(\text{L}_{\text{N5Me}})(\text{H}_2\text{O})]_2[\text{Mo}(\text{CN})_7] \cdot 6\text{H}_2\text{O}$ was synthesized and fully characterized. Antiferromagnetic coupling was found between the Mo^{III} and Mn^{II} in the compound. Detailed magnetic measurements reveal this compound to be a single-molecule magnet with a blocking temperature of 3.8 K (at 1 Hz) and a barrier of $\sim 44.1 \text{ cm}^{-1}$. These numbers set the record for a cyano-bridged SMM. Moreover, hysteresis loops with obvious steps corresponding to quantum tunneling were observed up to 2.4 K. This compound is a proof-of-concept case for a SMM composed of spin centers that engage in anisotropic magnetic coupling and its properties confirm a long-standing debate about whether this strategy would work. This result represents a major milestone in our work.

Future Plans

Future efforts are being directed at the expansion of the trigonal bipyramidal, tetranuclear and linear trinuclear families of molecules to include 4d/5d metal ions as well as early 3d metal ions such as

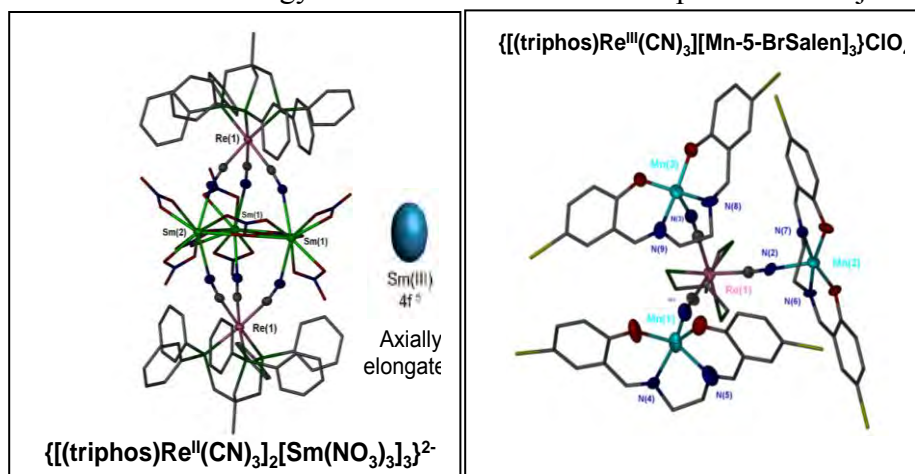


Figure 2. Two new $\text{Re}(\text{II})$ compounds as new anisotropic trigonal symmetry molecules being pursued in the next year.

Ti^{III} and V^{III}, efforts that are being guided by theoretical models of our collaborators Boris Tsukerblat from Israel and Sophia Klokishner from Moldova. Their work has led to the conclusion that trigonal symmetry is very important for engendering SMM behavior in a number of different polyhedral geometries. We have already made excellent progress with the incorporation of Re^{II} ions into new types of clusters as depicted in Figure 2.

References

1. Ishikawa, N.; Sugita, M.; Ishikawa, T.; Koshihara, S.; Kaizu, Y. *J. Am. Chem. Soc.* **2003**, *125*, 8694.
2. AlDamen, M. A.; Clemente-Juan, J. M.; Coronado, E.; Martí-Gastaldo, C.; Gaita-Ariño, A. *J. Am. Chem. Soc.* **2008**, *130*, 8874.
3. AlDamen, M. A.; Cardona-Serra, S.; Clemente-Juan, J. M.; Coronado, E.; Gaita-Ariño, A.; Martí-Gastaldo, C.; Luis, F.; Montero, O. *Inorg. Chem.* **2009**, *48*, 3467.
4. Rinehart, J. D.; Long, J. R. *J. Am. Chem. Soc.* **2009**, *131*, 12558.
5. Freedman, D. E.; Harman, W. H.; Harris, T. D.; Long, G. J.; Chang, C. J.; Long, J. R. *J. Am. Chem. Soc.* **2010**, *132*, 1224.
6. Cremades, E.; Ruiz, E. *Inorg. Chem.* **2011**, *50*, 4016–4020.
7. Lin, P.-H.; Smythe, N.C.; Gorelsky, S. I.; Maguire, S.; Henson, N. H.; Korobkov, I.; Scott, B. L.; Gordon, J. C.; Baker, R. Tom; Murugesu, M. *J. Am. Chem. Soc.* **2011**, *133*, 15806–15809.
8. Shatruk, M.; Avendaño, C.; Dunbar, K. R. *Prog. Inorg. Chem.*, **2009**, *56*, 155-334.
9. Pali, A.; Tsukerblat, B.; Klokishner, S.; Dunbar, K. R.; Clemente-Juan, J. M.; Coronado, E. *Chem. Sov. Rev.*, (invited critical review, featured on the cover), **2011**, *40*, 3130–3156.
10. Wang, X.-Y.; Avendano, C.; Dunbar, K. R. *Chem. Sov. Rev.* (invited critical review), **2011**, *40*, 3213-3238.

DOE Publications 2010-present

1. Cyanide Lability and Linkage Isomerism of Hexacyanochromate(III) Induced by the Co(II) ion. Carolina Avendano, Ferdi Karadas, Matthew Hilfiger, Michael Shatruk, and Kim R. Dunbar, *Inorg. Chem.*, **2010**, *49*, 583–594.
2. An Unprecedented Charge Transfer Coupled Spin Transition in a Cluster with Fe(II) and Os(III) Centers. Matthew G. Hilfiger, Meimei Chen, Tatiana V. Brinzari, Tanya M. Nocera, Doros T. Petasis, Janice L. Musfeldt, Catalina Achim, Kim R. Dunbar, *Angew. Chem. Int. Ed.*, **2010**, *49*, 1410-1413.
3. A Homologous Heterospin Series of Mononuclear Lanthanide/TCNQF₄ Organic Radical Complexes. Nazario Lopez, Hanhua Zhao, Andrey V. Prosvirin, Wolfgang Wernsdorfer and Kim R. Dunbar, *Dalton Trans.*, **2010**, *39*, 4341-4352.
4. Control of Charge-Transfer in a Series of Ru₂^{II,II}/TCNQ Two-Dimensional Networks by Tuning Electron-Affinity of TCNQ Units: A Route to Synergistic Magnetic/Conducting Materials. Hitoshi Miyasaka, Natsuko Motokawa, Satoshi Matsunaga, Masahiro Yamashita, Kuniyoshi Sugimoto, Tatsuya Mori,[‡] Naoki Toyota, and Kim R. Dunbar, *J. Am. Chem. Soc.*, **2010**, *132*, 1532-1544.
5. Use of a Rhenium Cyanide Nanomagnet as a Building Block for New Clusters and Extended Networks. Ferdi Karadas, Carolina Avendaño, Andrey V. Prosvirin, and Kim R. Dunbar, *Dalton Trans.*, **2010**, *39*, 4986-4977.

6. Cyanide-Bridged $\text{Co}^{\text{II}}_2\text{M}^{\text{II}}$ and $\text{Co}^{\text{II}}_2\text{M}^{\text{II}}_2$ Complexes Based on the $\text{Co}^{\text{II}}(\text{triphos})(\text{CN})_2$ Building-Block: Syntheses, Structures, Magnetic Properties and Density Functional Theoretical Studies. Ferdi Karadas, Michael Shatruk, Lisa M. Perez, and Kim R. Dunbar, *Chem. Eur. J.*, **2010**, *16*, 7164-7173.
7. Trigonal Bipyramidal Magnetic Molecules Based on $[\text{Mo}^{\text{III}}(\text{CN})_6]^{3-}$. Xin-Yi Wang, Matthew Hilfiger, Andrey Prosvirin, and Kim R. Dunbar, *Chem. Commun.*, **2010**, *46*, 4484-4486.
8. A Docosanuclear $\text{Mo}_8\text{Mn}_{14}$ Cluster Based on $[\text{Mo}(\text{CN})_7]^{4-}$. Xin-Yi Wang, Andrey V. Prosvirin, and Kim R. Dunbar, *Angew. Chem. Int. Ed.*, **2010**, *49*, 5081-5084 (Featured on the Cover).
9. Temperature and Light Induced Bistability in a $\text{Co}_3[\text{Os}(\text{CN})_6]_2$ Prussian Blue Analog. Carolina Avendano, Matthew G. Hilfiger, Andrey Prosvirin, Codi Sanders, Darryl Stepien, Kim R. Dunbar, *J. Am. Chem. Soc.*, **2010**, *132*, 13123-13125.
10. Structural Studies of the 1:1 Complex of o-3,4-Dimethyltetrathiafulvalene (o-Me₂TTF) and 1,2,4,5-tetracyanobenzene (TCNB). Eric Reinheimer, Hanhua Zhao, and Kim R. Dunbar. *J. Chem. Cryst.* **2010**, *40*, 514-519.
11. Light-Induced Charge Transfer and LIESST Effect in Pentanuclear Cyanide-Bridged Clusters. Kristen E. Funck, Andrey Prosvirin, Corine Mathonière, Rodolphe Clérac, Etienne Harté, Marguerite Kalisz, and Kim R. Dunbar, *Inorg. Chem.*, **2011**, *50*, 2782-2789.
12. Molecular Magnetic Materials Based on 4d and 5d Transition Metals. Xin-Yi Wang, Carolina Avendano and Kim R. Dunbar, *Chem. Sov. Rev.* **2011**, *40*, 3213-3238, (Invited Critical Review).
13. Beyond the spin model: Exchange coupling in molecular magnets with unquenched orbital angular momenta. Andrei Palii, Boris Tsukerblat, Sophia Klokishner, Kim R. Dunbar, Juan Modesto Clemente-Juan, Eugenio Coronado, *Chem. Sov. Rev.*, (Invited Critical Review), **2011**, *40*, 3130-3156.
14. Layered, Two-Dimensional Hydrogen Bonding Nets in the Structure of the 1:1 Encounter Complex TMTTF-TCNB: Combined Structural and Spectroscopic Study. Eric W. Reinheimer, Vibronic model for Cooperative Spin-Crossover, Hanhua Zhao and Kim R. Dunbar, *J. Chem. Crystallogr.*, **2011**, *41*, 936-943.
15. Vibronic model for Cooperative Spin-Crossover in Pentanuclear $\{[\text{M}^{\text{III}}(\text{CN})_6]_2-[\text{M}^{\text{II}}(\text{tmphen})_2]_3\}$ (M/M' = Co/Fe, Fe/Fe) Compounds. Sergei. Ostrovsky, Andrei Palii, Sophia Klokishner, Michael Shatruk, Kristen E. Funck, Kim R. Dunbar, Boris, Tsukerblat, *J. Phys. Chem. C.*, **2011**, *115*, 21666-21677.
16. Anion-Templated Self-Assembly of Highly Stable Fe(II) Pentagonal Metallacycles with Short Anion-□ Contacts. Ian D. Giles, Helen T. Chifotides, Michael Shatruk and Kim R. Dunbar, *Chem. Commun.*, **2011**, *47*, 12604-12606.
17. A Mn(III) Chain Derived from Mn_{12} -Acetate that Exhibits Both Glauber Dynamics and Antiferromagnetic Ordering Regimes. Andrey Prosvirin, Hanhua Zhao and Kim R. Dunbar, **2012**, *Jon Zubieta special issue of Inorg. Chim. Acta.*, **2012**, in press.
18. Spin-Crossover Materials: Properties and Applications in “*Charge Transfer-Induced Spin Transitions in Cyanometallate Materials*”, Chapter 6. “Malcolm Halcrow, Editor. Wiley-Blackwell. Kim R. Dunbar, Michael Shatruk, Catalina Achim, **2012**, in press. (Book Chapter)
19. An unprecedented double layered Fe_{36} phosphonate cage. Christine M. Beavers, Tina Tezgerevska, Andrey V. Prosvirin, John D. Cashion, Brendan F. Abrahams, Carmel Abrahams, Kim R. Dunbar, and Anne F. Richards, submitted to *Inorg. Chem.*, **2012**.

SISGR: Design and Synthesis of Chemically and Electronically Tunable Nanoporous Organic Polymers for Use in Hydrogen Storage Applications

Hani M. El-Kaderi,

Department of Chemistry, Virginia Commonwealth University, Richmond, Virginia 23284-2006, United States

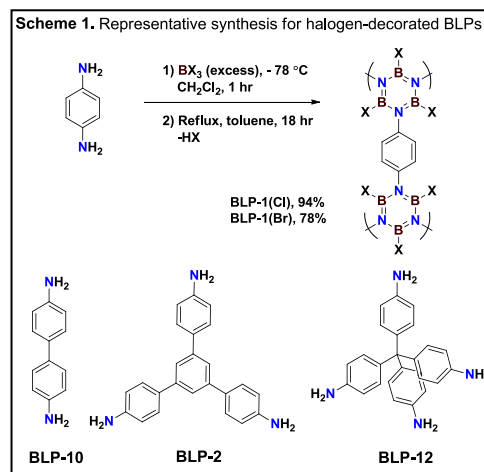
Program Scope

The objective of our research is to design and synthesize new classes of highly nanoporous organic polymers that are linked by strong covalent bonds and composed of chemically and electronically tunable building blocks for use in hydrogen storage and selective CO₂ capture. The new polymers, termed borazine-linked polymers (BLPs) and benzimidazole-linked polymers (BILPs), feature functionalized pore walls and exhibit significant hydrogen uptakes and one of the highest CO₂/N₂ and CO₂/CH₄ selectivities reported to date. In addition to their remarkable selectivity for CO₂, BILPs are thermally stable (~420 °C) and remain chemically intact under aqueous systems which reflects their potential use under practical conditions.

Recent Progress

This project is aimed at the synthesis and characterization of two new classes of porous organic polymers: borazine-linked polymers (BLPs) and benzimidazole-linked polymers (BILPs). In these polymers the resulting chemical connectivity between building units can potentially lead to structures analogous to those of COFs linked by B-O bonds.^{1,2} BLPs and BILPs feature functionalized pore walls and moderate surface areas. One significant motivation for pursuing isolated B₃N₃ rings in porous materials was the potential of the borazine rings to undergo hydrogenation by molecular dihydrogen in the presence of a catalyst. Thereby BLPs would store hydrogen by both chemical (B-H and N-H) and physical (physisorption within the pores) means.

Borazine-linked polymers (BLPs). We have described for the first time the incorporation of borazine units bearing three different B-substituents (H, Cl, Br) as building blocks for the construction of porous networks to assess the impact of pore decoration on hydrogen storage and selective gas binding. In halogen-decorated BLPs, treatment of arylamines with the corresponding boron trihalide followed by thermolysis in toluene under refluxing conditions produced the desired polymer (Scheme 1). We have extended this approach to prepare seven polymers in good yields using various amine building units. The chemical composition and structural aspects of these polymers were investigated by spectral (FT-IR, ¹¹B and ¹³C solid-state NMR, SEM) and analytical methods (elemental analysis) while porosity was examined by N₂ porosity measurements. Unlike COFs, all BLPs are amorphous which precluded their investigation by XRD techniques. From their porosity measurements, halogen-decorated BLPs exhibit moderate surface areas and relatively high gas uptakes in comparison to porous organic polymers (Table 1). The highest gas uptake was reported for BLP-12(Cl) which has the highest surface area and pore volume values; it stores 1.75 wt% of



hydrogen with an isosteric heat of adsorption of 7.08 kJ/mol which is somewhat higher than those reported for 2D and 3D COFs as a result of the narrower halogen decorated pores.

Table 1. Porous properties and H₂ uptakes of BLPs. SA_{Lang}: Calculated by the Langmuir method. P_{vol}: Calculated from nitrogen adsorption at P/P₀ = 0.9. PSD: Calculated using NLDFT.

Polymer	SA _{Lang} (m ² g ⁻¹)	P _{vol} (cm ³ g ⁻¹)	PSD (nm)	H ₂ , 77 K (wt%)	H ₂ Q _{st} (kJ mol ⁻¹)
BLP-1(Cl)	1828	0.746	1.33	1.00	7.06
BLP-1(Br)	730	0.303	1.27	0.68	7.14
BLP-2(Cl)	1699	0.649	1.27	1.30	7.19
BLP-2(Br)	1221	0.571	1.27	0.98	7.49
BLP-12(Cl)	2091	0.853	1.13	1.75	7.08
BLP-1(H)	1360	0.69	1.27	1.33; (3.97, 40 bar)	6.8
BLP-2(H)	1178	0.59	1.13	1.43; (2.48, 40 bar)	6.8
BLP-12(H)	2866	1.08	1.27	1.93; (4.25, 40 bar)	6.0

We have expanded the field of BLPs by the synthesis of halogen-free polymers following the same thermolysis approach described above to produce several borazine-rich polymers with very high surface areas. All BLPs were isolated as white powders in good yields and subjected to a battery of characterization methods: PXRD, SEM, TGA, FT-IR, and Ar porosity measurements. Halogen-free BLPs are thermally stable up to ~420 °C and were subjected to hydrogen storage experiments under low and high pressure conditions. Our studies indicate that halogen-free BLPs can store significant amounts of hydrogen under high pressure settings as in the case of BLP-12(H) which stores 4.25 wt% at 77 K and 40 bar.

Benzimidazole-Linked-Polymers (BILPs). In addition to our work on BLPs, we have developed a simple synthetic route for several organic polymers by using condensation reactions between a variety of aryl-o-diamine and aryl-aldehyde building units to form BILPs. BILPs have remarkable chemical and thermal stabilities and considerable H₂ uptakes as well as high CO₂ selectivity over N₂ and CH₄. The notably enhanced CO₂ capture and selectivity of BILPs compared to other purely organic or organic-inorganic hybrid materials such as MOFs, for example, were attributed to their subnano pore dimensions and imidazole-functionalized pore walls that facilitate selective CO₂ capture and storage. Similarly, these textural properties of BILPs resulted in high H₂ uptakes and binding affinities at low pressure and cryogenic conditions as shown in Figure 1 and summarized in Table 2.

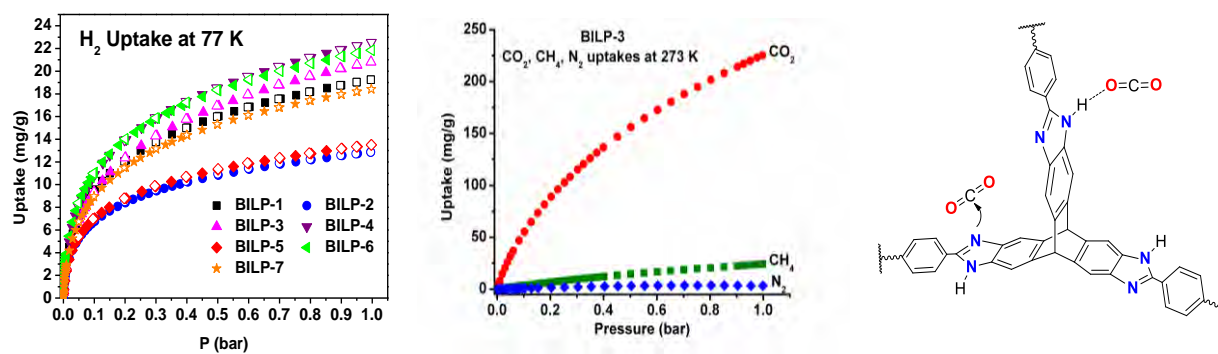


Figure 1. Hydrogen uptake isotherms, selective CO₂ uptake by BILP-3 and its functional unit showing potential CO₂ binding sites.

Table 2. Gas uptake and selectivity (CO₂/N₂ and CO₂/CH₄) for BILPs.

Polymer	SA _{BET} ^a	H ₂ /1 bar ^b			CO ₂ /1 bar ^b			CH ₄ /1 bar ^b			N ₂ /1 bar ^b		Selectivity ^c	
		77K	87K	Q _{st}	273 K	298 K	Q _{st}	273 K	298 K	Q _{st}	273 K	298 K	CO ₂ /N ₂	CO ₂ /CH ₄
BILP-1	1172	19	14	7.9	188	131	26.7	23	16	16.3	5.0	7.3	70 (36)	10 (7)
BILP-2	708	13	10	8.0	149	104	28.6	14	9	18.4	3.4	2.5	113 (71)	17 (12)
BILP-3	1306	21	15	8.0	225	145	28.6	24	17	16.6	3.3	2.4	59 (31)	8 (5)
BILP-4	1135	23	16	7.8	235	158	28.7	26	18	13.0	1.1	3.8	79 (32)	10 (7)
BILP-5	599	14	10	8.3	128	87	28.8	15	10	14.6	0.2	2.7	95 (36)	10 (6)
BILP-6	1261	22	16	8.2	211	121	28.4	27	19	13.2	6.8	6.7	63 (39)	8 (5)
BILP-7	1122	18	14	8.3	193	122	27.8	19	12	14.7	5.6	5.4	62 (34)	9 (7)

^aSurface area (m² g⁻¹) was calculated from Ar isotherm. ^bGas uptake in mg g⁻¹ and the isosteric enthalpies of adsorption (Q_{st}) in kJ mol⁻¹. ^cSelectivity (mol mol⁻¹) was calculated from initial slope calculations at 273 K and (298 K).

All BILPs exhibit excellent chemical stability that allow for their handling and purification under ambient conditions. They remain intact upon washing with a 2M aqueous solution of HCl or NaOH. BILPs also exhibit high thermal stability according to thermogravimetric analysis which showed decomposition only after ~420 °C. Porosity and gas storage measurements (Table 2) reveal that BILPs are some of the most attractive purely organic materials for gas storage applications. BILPs with high surface area in particular exhibit noteworthy hydrogen storage capabilities (1.9-2.3 wt % at 77 K and 1 bar). In addition, these polymers in general can store significant amounts of CO₂ (up to 5.3 mmol g⁻¹ at 273 K and 1 bar) with very high selectivities. The presence of amphoteric building units in the pore walls of BILPs can allow for post-synthesis modification with light metal ions (Li⁺, Na⁺, etc.) for enhanced hydrogen storage capacities which will be addressed in future work.

Future Plans

Our future research goals will focus on developing new synthetic methods to enhance the crystallinity and porosity of BLPs and BILPs to attain higher hydrogen storage capacities in these polymers especially under elevated pressure conditions. Additionally, pore surface modification by post-synthesis processes or by the use of pre-functionalized building blocks will also be explored to enhance H₂ isosteric heat of adsorption. Future studies will also address the potential of borazine-rich BLPs in chemical hydrogen storage. Chemical and physical tuning of the BILPs' pores will also be targeted to enhance their performance in selective CO₂ capture and sequestration.

References

1. El-Kaderi, H. M.; Hunt, J. R.; Mendoza-Cortés, J. L.; Côté, A. P.; Taylor, R. E.; O'Keeffe, M.; Yaghi, O. M. *Science* **2007**, *316*, 268-272.
2. Côté, A. P.; El-Kaderi, H. M.; Furukawa, H.; Hunt, J. R.; Yaghi, O. M. *J. Am. Chem. Soc.* **2007**, *129*, 12914-12915.

Publications

1. "Highly Selective CO₂/CH₄ Gas Uptake by a Halogen-Decorated Borazine-Linked Polymer," Reich, T. E., Behera, S.; Jackson, K. T.; Li, S.; Jena. P.; El-Kaderi, H. M., *J. Mater. Chem.* **2012**, (DOI:10.1039/C2JM31123B.).
2. "Synthesis and Characterization of Porous Benzimidazole-Linked Polymers and Their Performance in Small Gas Storage and Selective Uptake," Rabbani, M. G.; El-Kaderi, H. M. *Chem. Mater.* **2012**, *48*, 1411.
3. "High CO₂ uptake and selectivity by triptycene-derived benzimidazole-linked polymers," Rabbani, M. G.; Reich, T. E.; Jackson, K. T.; Kassab, R. M.; El-Kaderi, H. M. *Chem. Commun.* **2012**, *48*, 1411.
4. "Impact of tailored chemical and textural properties on the performance of nanoporous borazine-linked polymers in small gas uptake and selective binding," Reich, T. E.; El-Kaderi, H. M. *J. Nanopart. Re.* **2012** (submitted)
5. "Synthesis of highly porous borazine-linked polymers and their application to H₂, CO₂, and CH₄ storage," Jackson, K. T.; Rabbani, M. G.; Reich, T. E.; El-Kaderi, H. M. *Polym. Chem.* **2011**, *2*, 2775.
6. "Design, Synthesis, and Characterization of Halogen-Decorated Porous Borazine-Linked Polymers and their performance in hydrogen storage application," Reich, T. E., Jackson, K. T.; Li, S.; Jena. P.; El-Kaderi, H. M. *J. Mater. Chem.*, **2011**, *21*, 10629.
7. "Template-Free Synthesis of a Highly Porous Benzimidazole-Linked Polymer for CO₂ Capture and H₂ Storage," Rabbani, M. G.; El-Kaderi, H. M. *Chem. Mater.*, **2011**, *23*, 1650.
8. "Synthesis and Characterization of Highly Porous Borazine-Linked Polymers via Dehydrogenation/Dehydrocoupling of Borane-Amine Adducts and their Applications to Gas Storage," Jackson, K. T. Virginia Commonwealth University, Richmond, VA, December **2011**, Ph.D. thesis.
9. "Designed Synthesis and Characterization of Halogenated Borazine-Linked Polymers and their Application to Gas Storage," Reich, T. E. Virginia Commonwealth University, Richmond, VA, December **2011**. PhD. thesis.
10. "Highly Porous Benzimidazole-Linked Polymers for Use in Gas storage and Separation Applications," Rabbani, M. G.; El-Kaderi, H. M. Provisional Patent (Issued on Jan 14th, **2011** by Virginia Commonwealth University).

Pore Space Engineering and Functionalization in Porous Metal-Organic Framework Materials

Pingyun Feng, Department of Chemistry, University of California Riverside

Program Scope

The overall objective of this project is to develop synthetic strategies to synthesize porous materials with geometrical features and chemical functionalities useful for hydrogen storage applications. Specific aims of this project are:

- *Design and synthesize new metal-organic frameworks (MOF) using lightweight chemical elements to help improve gravimetric hydrogen storage capacity.*
- *Develop new synthetic strategies to generate novel active binding sites on metal ions and ligands to enhance solid-gas interactions for increased gas uptake near ambient conditions.*
- *Develop synthetic methods to create porous frameworks with novel architectural features such as partitioned pore space for the optimum size match with hydrogen molecule.*

Recent Progress

The project places a strong emphasis on the use of lightweight elements (Li in particular) as the structural building block. In addition to being the lightest metal, lithium possesses desirable binding affinity for H₂ if active binding sites can be created. Compared with other metal ions, lithium is unique in its synthetic and structural chemistry, because of its small ionic radius, low oxidation state, and high solvation enthalpy. Therefore, innovative synthetic methods need to be developed to realize lithium based porous materials. Other strategies being studied for enhancing H₂ storage capacity include a comparative study of the related lightweight Mg²⁺, the creation of high-density binding sites on ligands, and partition of pore-space for better size match with H₂.

A highly stable porous material constructed from lithium aryloxy clusters.

In order to further enhance the adsorption property, an emergent and promising strategy is to introduce lightweight elements into the framework, which may lead to an increase in the gravimetric uptake capacity. A new porous material based on Li₄O₄ cubane cluster has been realized. While Li₄(OPh)₄ type clusters linked by neutral ligands (e.g., 1,4-dioxane) are well-known in the literature, none is porous or stable. Our success was through the use of a very unique ditopic ligand 4-pyridinol. Because 4-pyridinol serves dual roles (i.e., cluster formation using -OH side and intercluster crosslinking using both -OH and pyridyl sides), this strategy eliminates the pore-blocking effect of the dangling -OPh ligand (found in literature examples), leading to the high stability and accessible porosity. The synthesized material exhibits a zeolite topology and possesses large channels (Fig. 1). Considering that it is based on low-valent lithium framework, this material has an unbelievably high thermal stability up to at least 500°C. Its BET and Langmuir surface areas reach 440.3m²/g and 632.5m²/g, respectively and its hydrogen

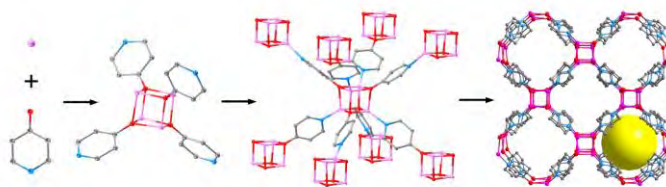


Figure 1. Illustration of the self-assembly process from molecular species Li⁺ and 4-pyridinol to Li₄O₄ cubane clusters, and finally to 3-D framework. (purple: Li; red: O; blue: N; grey: C)

storage capacity is 1.4 wt% H₂ at 77 K-1atm. While these numbers are modest compared to the best metal-organic framework materials (MOFs) based on some other metal ions, they are nevertheless the highest among lithium-based MOFs, demonstrating the significant potential of this system.¹

A porous magnesium-carboxylate framework with nanotubular channels

Because highly negative tetraanionic ligands can increase the metal-to-ligand ratio (for the simple reason of charge balance), it can increase the density of active metal sites and gas uptake capacity as shown by MOF-74 (one of the best materials for gas sorption applications).² In this work, we sought to mimic the tetraanionic ligand used in MOF-74 (Mg₂(dobdc), H₄dobdc = 2,5-dihydroxyterephthalic acid) by investigating the reaction of Mg²⁺ with a tetracarboxylate (biphenyl-3,3',5,5'-tetracarboxylic acid or H₄bptc) (Fig. 2) and were able to synthesize a new Mg-MOF (denoted CPF-1).

CPF-1 is built from 4₁-helical inorganic chains (space group: *I4*₁22), connected to each other with a tetracarboxylate to form 1D cylindrical nanotubular channels with tetragonal symmetry, in contrast with the 1D hexagonal channels in MOF-74 (Fig. 2). We were able to achieve a higher density of solvent sites on Mg²⁺ sites with each Mg²⁺ bonded to two solvent molecules. However, solvent sites on two adjacent Mg²⁺ sites are oriented toward each other, which leads to the bridging mode for the coordinated solvent molecules. This apparently complicates the sample activation due to the more difficult removal of bridging solvent molecules. The present data show that its storage capacity (1.3 wt% H₂ at 77 K-1atm, 84cm³/g of CO₂ at 273K-1atm) is lower than that of MOF-74-Mg. Still, our material is the second highest among all known Mg-MOFs,² demonstrating the potential of the synthesis strategy for further advancing the hydrogen uptake capacity.

Single-walled metal-organic channels with high density of open donor sites for gas uptake

In addition to uncoordinated metal sites, uncoordinated functional groups of organic ligands can play a key role in gas sorption. Thus, having available the largest possible number of exposed functional sites (on either metals or ligands) can contribute to enhanced gas sorption. Of particular interest are functional groups such as aromatic pyridyl-type N-donors found in metal azolate frameworks.

For the purpose of increasing the percentage of open donor sites, individual triazole or tetrazole ligands are less effective, because at least two N-donor sites will be used up for the framework connectivity, and the maximum percentage of open N-donor sites would be only 33% for a triazole and 50% for a tetrazole framework. Hence, we are especially interested in ligands

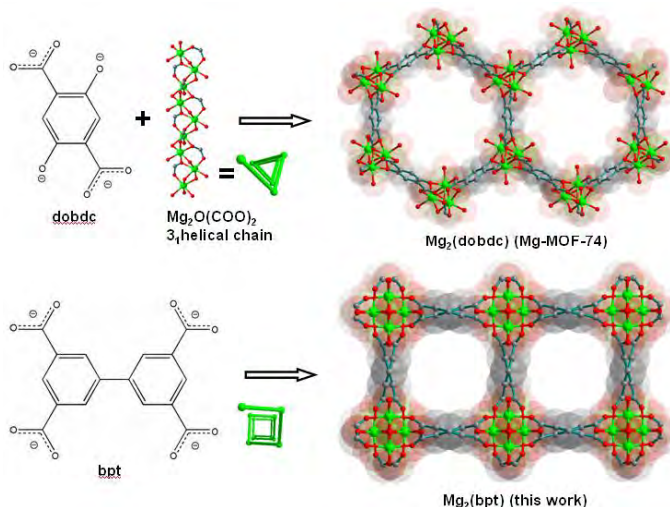


Figure 2. A comparison between two MOFs based on tetraanionic ligands. (top) Mg₂(dobdc) (Mg-MOF-74) and (bottom) CPF-1.

containing multiple triazole and tetrazole groups (e.g., polytriazole such as 1,3,5-tris(2*H*-tetrazol-5-yl)benzene or H₃BTT in short), and such a ligand can achieve a high connectivity even if they only use one N-donor site (per triazole or tetrazole group) for bonding with metals. The highest percentage of open donor sites would be 67% for a triazole and 75% for a tetrazole, assuming each ligand uses just one N-donor site for the framework formation. However, such a high percentage of open donor sites have not been achieved prior to this work.

Here, by using a urea derivative (1,3-dimethylpropyleneurea) as the co-solvent in *N,N*-dimethylacetamide (DMA), an interesting porous framework (denoted CPF-6) with 1D square single-atom-walled channel system has been prepared (Fig. 3). This material has a highly porous 3-D framework with a large percentage (67%) of N-donor sites unused for bonding with metals. This feature, coupled with the low-framework density resulting from single-walled channels, contributes to a high gas storage capacity (ca. 1.9wt% H₂ at 77K-1atm, 98cm³/g CO₂ at 273K-1atm).

Future Plans

To develop high-capacity hydrogen storage materials, we will need to further develop synthetic methods to synthesize porous materials that combine multiple features including lightweight building block, active binding sites, and high stability. A systematic study of solvent systems that can bind reversibly to metal ions such as Li⁺ without adversely affecting the crystallization process is important. Also important is to create a stable support framework system for Li⁺ with active binding sites, because monomeric lithium sites with open sites may not be sufficiently stable. The application of the pore partition strategy, particularly to the lightweight building units, would make it possible to integrate advanced architectural features with desirable chemical compositions and functionality.

References

1. Abrahams, B. F.; Grannas, M. J.; Hudson, T. A.; Robson, R. "A Simple Lithium(I) Salt with a Microporous Structure and Its Gas Sorption Properties." *Angew. Chem. Int. Ed.* **2010**, *49*, 1.
2. Caskey, S. R.; Wong-Foy, A. G.; Matzger, A. J. "Dramatic Tuning of Carbon Dioxide Uptake via Metal Substitution in a Coordination Polymer with Cylindrical Pores." *J. Am. Chem. Soc.* **2008**, *130*, 10870-10871

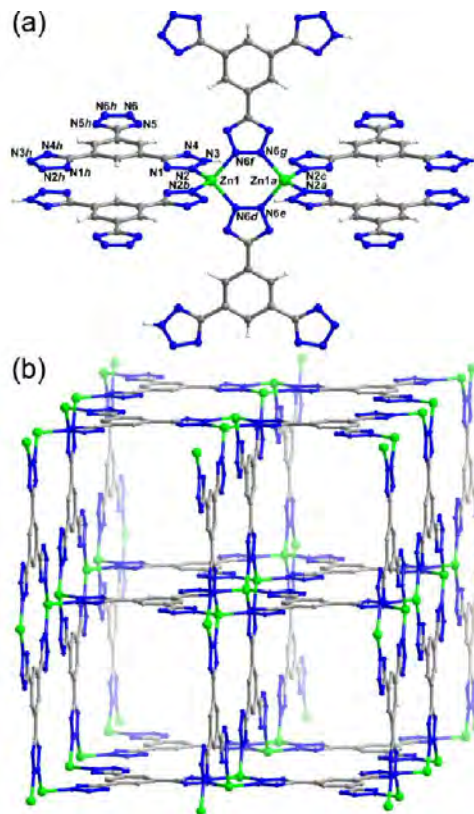


Figure 3. (a) View of the zinc dimer bridged by two tetrazolate groups (in bidentate fashion) and completed by four other tetrazolate groups (in unidentate fashion), (b) the 3-D extended network showing large channels.

Publications

- (1) Zhang, J.; Chen, S.; Nieto, R. A.; Wu, T.; Feng, P.; Bu, X. "A Tale of Three Carboxylates: Cooperative Asymmetric Crystallization of Three-Dimensional Microporous Framework from Achiral Precursors", *Angew. Chem. Int. Ed.* **2010**, *49*, 1267-1270.
- (2) Zheng, S.; Wu, T.; Zhang, J.; Chow, M.; Nieto, R., Feng, P.; Bu, X. "Porous Metal Carboxylate Boron Imidazolate Frameworks", *Angew. Chem. Int. Ed.* **2010**, *49*, 5362-5366.
- (3) Zheng, S.; Li, Y.; Wu, T.; Nieto, R., Feng, P.; Bu, X. "Porous Lithium Imidazolate Frameworks Constructed with Charge-Complementary Ligands", *Chem. Eur. J.* **2010**, *16*, 13035-13040.
- (4) Zhang, J.; Bu, J.; Chen, S.; Wu, T.; Zheng, S.; Chen, Y.; Nieto, R., Feng, P.; Bu, X. "Urothermal Synthesis of Crystalline Porous Materials", *Angew. Chem. Int. Ed.* **2010**, *49*, 8876.
- (5) Zheng, S.; Bu, J. T.; Li, Y.; Wu, T.; Zuo, F.; Feng, P.; Bu, X. "Pore Space Partition and Charge Separation in Cage-within-Cage Indium-Organic Frameworks with High CO₂ Uptake", *J. Am. Chem. Soc.* **2010**, *132*, 17062-17064.
- (6) Zheng, S.; Zuo, F.; Wu, T.; Irfanoglu, B.; Chou, C.; Nieto, R. A.; Feng, P.; Bu, X. "Cooperative Assembly of 3-Ring-Based Zeolite-Type Metal-Organic Frameworks and Johnson-Type Dodecahedra", *Angew. Chem. Int. Ed.* **2011**, *50*, 1849-1852.
- (7) Zhao, X.; Wu, T.; Zheng, S-T.; Wang, L.; Bu, X., Feng, P. "Zeolitic Porous Lithium Organic Framework Constructed from Cubane Clusters", *Chem. Commun.* **2011**, *47*, 5536-5538.
- (8) Zheng, S.; Wu, T.; Irfanoglu, B.; Zuo, F.; Feng, P.; Bu, X. "Multi-Component Self-Assembly of A Nested Co₂₄@Co₄₈ Metal Organic Polyhedral Framework", *Angew. Chem. Int. Ed.* **2011**, *50*, 8034-8037.
- (9) Zhao, X.; Wu, T.; Bu, X.; Feng, P. "A Mixed Ligand Route for Construction of Tetrahedrally Coordinated Porous Lithium Frameworks", *Dalton Trans.* **2011**, *40*, 8072-8074.
- (10) Zheng, S.; Bu, J. J.; Wu, T.; Chou, C.; Feng, P.; Bu, X. "Porous Indium-Organic Frameworks and Systematization of Structural Building Blocks", *Angew. Chem. Int. Ed.* **2011**, *50*, 8858-8862.
- (11) Jiang, G.; Wu, T.; Zheng, S-T; Zhao, X.; Lin, Q.; Bu, X.; Feng, P. "A nine-connected mixed-ligand nickel-organic framework and its gas sorption properties", *Crystal Growth & Design* **2011**, *11*, 3713-3716.
- (12) Lin, Q.; Wu, T.; Zheng, S.; Bu, X.; Feng, P. "A Chiral Tetragonal Magnesium-Carboxylate Framework with Nanotubular Channels", *Chem. Commun.* **2011**, *47*, 11852-11854.
- (13) Zhao, X.; Wu, T.; Bu, X.; Feng, P. Lithium Cubane Clusters as Tetrahedral, Square Planar, and Linear Nodes for Supramolecular Assemblies, *Dalton Trans.* **2012**, *41*, 3902-3905.
- (14) Lin, Q.; Wu, T.; Zheng, S-T; Bu, X.; Feng, P. "Single-Walled Polytetrazolate Metal-Organic Channels with High Density of Open Nitrogen-Donor Sites and Gas Uptake", *J. Am. Chem. Soc.* **2012**, *134*, 784-787.
- (15) Zheng, S.; Wu, T.; Zuo, F.; Chou, C-T; Feng, P.; Bu, X. "Mimicking Zeolite to Its Core: Porous Sodalite Cages as Hanger for Pendent Trimeric M₃(OH) Clusters (M = Mg, Mn, Co, Ni, Cd)", *J. Am. Chem. Soc.* **2012**, *134*, 1934-1937.
- (16) Zhai, Q.; Lin, Q.; Wu, T.; Zheng, S-T; Bu, X.; Feng, P. "Induction of Trimeric [Mg₃(OH)(COO)₆] in a Porous Framework by a Desymmetrized Tritopic Ligand", *Dalton Trans.* **2012**, *41*, 2866-2868.
- (17) Lin, Q.; Wu, T.; Bu, X.; Feng, P. A "Twelve-Connected Porous Framework Built from Rare Linear Cadmium Tricarboxylate Pentamers", *Dalton Trans.* **2012**, *41*, 3620-3622.
- (18) Zheng, S.; Wu, T.; Chou, C-T; Fuhr, A.; Feng, P.; Bu, X. Development of Composite Inorganic Building Blocks for Metal-Organic Frameworks, *J. Am. Chem. Soc.* **2012**, *134*, 4517.

Chemical Frustration: A Design Principle for the Discovery of New Complex Intermetallic and Alloy Phases

Daniel C. Fredrickson, Dept. of Chemistry, University of Wisconsin-Madison

Program Scope

The difficulty of guiding the crystal structures of intermetallics is a limiting factor in the development of new materials based on metals and alloys. Structural complexity in intermetallics is increasingly being traced to the coexistence of competing bonding or packing modes,¹ a conflict which may be termed *chemical frustration* by analogy with magnetic phenomena. The focus of this research program is the development of the theme of chemical frustration into a predictive theoretical model for the synthesis of new intermetallic phases. We are working toward this goal through the pursuit of the following three objectives.

Objective 1: Synthesis of new chemically frustrated intermetallics. In the first objective, we are testing the hypothesis of chemical frustration as a source of structural complexity through attempts to synthetically induce conflicts in intermetallic systems. Our strategy for doing this can be connected to the analogy to magnetic phenomena mentioned above (Figure 1; see also Pub. 3 in the publication list below). The classic example of magnetic frustration is the situation in which three unpaired electrons at the corners of a triangle attempt to couple antiferromagnetically: when any two of the electrons are paired, the third cannot take part in antiferromagnetic coupling without engaging in a ferromagnetic one as well.² A chemical analogy to this can be created by replacing the triangle of spins with the triangular form of a ternary phase diagram, where frustration can be envisioned as arising when the binary subsystems (as represented by the triangle edges) exhibit strong preferences for bonding modes which are incompatible with each other.

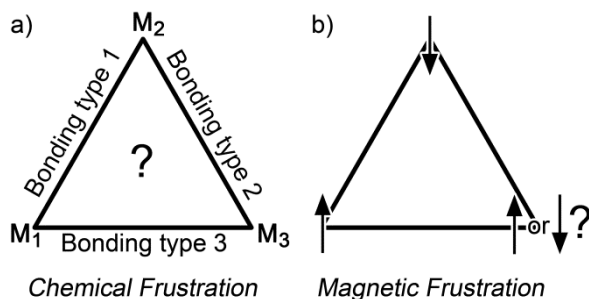


Figure 1. Schematic comparison of (a) chemical and (b) magnetic forms of frustration.

We are synthetically exploring three families of ternary systems in which this form of chemical frustration is expected to occur. In intermetallic carbides, the desire of carbon for octahedral coordination environments in carbides competes with the tetrahedral close packing (TCP) exhibited by many intermetallic phases. In the alkaline earth matrix systems, the tendency of alkaline earth elements to aggregate into small clusters of elemental phases is pitted against the TCP arrangements of transition metal-based compounds. Finally, in the ionic seed systems

we explore the transition between ionic lattices and TCP packing by beginning with binary systems with large electronegativity differences and introducing a third element of intermediate electronegativity that forms TCP structures with the other two elements.

Objective 2: Theoretical analysis of the impact of chemical frustration on electronic structure and phase stability. In parallel with the synthetic exploration of chemically frustrated systems, we are also developing theoretical and computational tools for analyzing this tension within crystal structures. A common outcome of incompatible bonding modes is the spatial segregation of bonding types into different domains. Analyzing this requires an approach which can draw clear connections between local structural features and the electronic structure. Such is afforded by the Method of Moments³ as applied to DFT-calibrated Hückel tightbinding calculations, which provides a direct link between the shape of a density of states curve and the topology of contacts within a crystal structure. In this project, we are adapting the Method of Moments to the problems of bonding description, and the detection of frustration within metals.

Objective 3: Development of guidelines for guiding crystal structures through chemical frustration. While our project begins with separate experimental and theoretical endeavors, our overall goal is to combine these two sides into theoretically-informed synthetic approaches to guiding the structures of intermetallic compounds.

Recent Progress

In the theoretical component of this project, we have developed the μ_3 -acidity analysis, which uses the Method of Moments to extend the fundamental molecular concept of Lewis acids and bases to metals, alloys, and intermetallics. Through calculations using this approach we have rationalized the stability of 23 intermetallic compounds formed between first-row transition metals as μ_3 -acid/base adducts, the stability ranges of the CsCl- and Laves phase types in these systems, and some of the structural features of Ti-Ni compounds (see Pubs. 4 and 5). We are currently preparing a manuscript describing how the effectiveness of μ_3 -acid/base interactions is influenced by the choice of crystal structure adopted, and how optimizing these interactions can lead to structural complexity.

Our experimental efforts have led to a number of new phases (see Pubs. 1, 3, and 6). Synthesis and structural analysis in the Gd-Fe-C intermetallic carbide system has led to the crystal structures of $\text{Gd}_{13}\text{Fe}_{10}\text{C}_{13}$ (Figure 2) and its oxygenated derivative. These compounds join a growing family of fascinating structures that emerge from Lanthanide-transition metal-carbon systems,⁴ but are unprecedented in their H-shaped C_2FeFeC_2 fragments. These

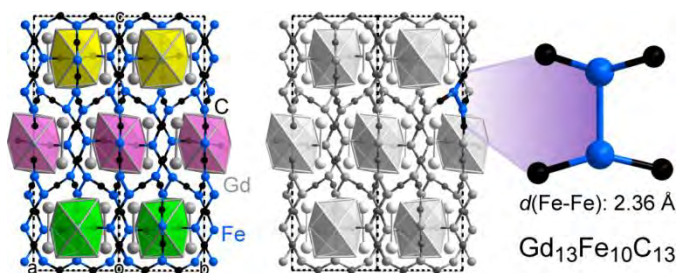


Figure 2. The crystal structure of $\text{Gd}_{13}\text{Fe}_{10}\text{C}_{13}$.

fragments exhibit short Fe-Fe contacts of 2.36 to 2.38 Å, the shortest yet observed (to our knowledge) for such bonds unsupported by classical ligands. A bonding analysis using DFT-calibrated Hückel calculations points to the presence of multiple bonding at these contacts.

Explorations of the alkaline earth matrix system Ca-Cu-Cd have also been particularly productive. We here have determined the structures of three new compounds: $\text{Ca}_5\text{Cu}_2\text{Cd}$, $\text{Ca}_2\text{Cu}_2\text{Cd}_9$, and a monoclinic quasicrystal approximant. The first two of these compounds adopt ternary variants of known binary types, which are nonetheless interesting because of two striking features. (1) Despite their ternary compositions, the local coordination environments approximate binary and elemental phases (Figure 3). In other words, at a very small length scale, the ternary phase exhibits phase segregation consistent with a form of chemical frustration. (2) No binary versions are present in the binary subsystems of Ca-Cu-Cd, i.e. their stability depends on the ternary composition. The stabilizing effect of the ternary compositions was traced through DFT-calibrated μ_2 -Hückel chemical pressure calculations to the expanded palette of atomic sizes moving from two to three elements. The third compound to emerge from the Ca-Cu-Cd system is a new variant of the Bergman phase structure type, in which the usual bcc packing of Bergman clusters is interrupted by disordered interfaces inserted between the (110) planes. Our investigations into the factors stabilizing this compound are on-going.

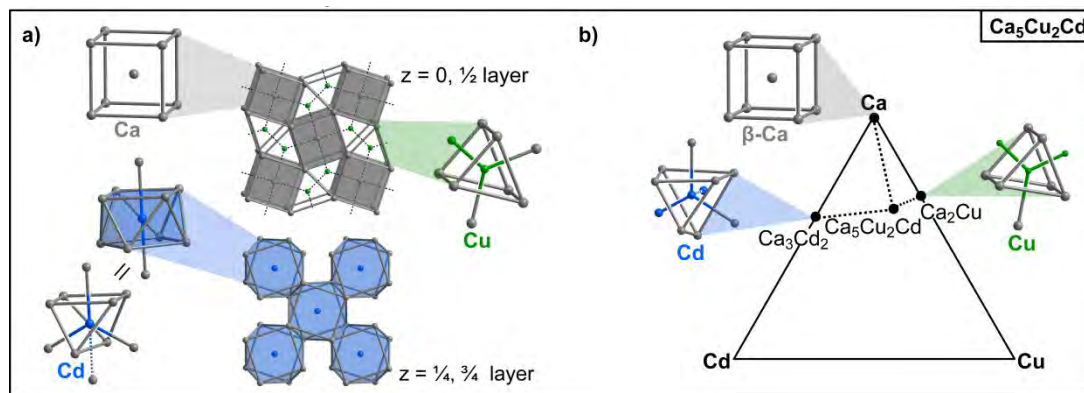


Figure 3. Comparison of local coordination environments in (a) $\text{Ca}_5\text{Cu}_2\text{Cd}$ with those in (b) simpler elemental and binary phases in the Ca-Cu-Cd system.

Future Plans

Our plan for the next year is to continue the separate pursuits of objectives 1 and 2 while seeking out avenues for their interaction (in anticipation of shifting our focus to objective 3 in the fourth year of this project). In terms of our synthetic work, we will be devising new ternary systems to explore based on the results of our initial synthetic survey. For the intermetallic carbides systems, we will perform investigations into other lanthanide-containing systems, with an emphasis being placed on finding new compounds with multiple bonding between transition metals (TMs) and charting the lanthanide rich corners and centers of the phase diagrams. Our first syntheses in the alkaline earth matrix systems revealed little tendency for interactions

between the TM element pairs tested, such as Cu/Zn and Cu/Cd. We will adjust for this by combining the alkaline earth metals with TM pairs with more distinct properties to increase the TM-TM' affinity, as in the Ca-Ir-Zn system. Synthetic investigations into the ionic seeds systems will also continue.

The focus of our theoretical efforts will be on expanding the generality of the μ_3 -acidity analysis, and its ability to inspire new synthetic experiments. This will include adapting it to systems beyond transition metal-based compounds to include phases with lanthanide, alkaline-earth and main group elements. Other areas of development will be the creation of a DFT-based version of the method, in collaboration with Prof. J.R. Schmidt at UW-Madison, and the use of this approach to analyze the spatial segregation of bonding modes in complex intermetallics. Finally, we will incorporate the concept of μ_3 -acid/base interactions into the design of a new set of chemically-frustrated ternary systems for future synthetic work.

References

1. (a) Conrad, M.; Harbrecht, B.; Weber, T.; Jung, D. Y.; Steurer, W. *Acta Crystallogr. B* **2009**, *65*, 308; (b) Fredrickson, D. C.; Lee, S.; Hoffmann, R. *Angew. Chem. Int. Ed.* **2007**, *46*, 1958; (c) Fredrickson, D. C.; Lidin, S.; Venturini, G.; Malaman, B.; Christensen, J. *J. Am. Chem. Soc.* **2008**, *130*, 8195; (d) Janssen, T.; Chapuis, G.; Boissieu, M. d. *Aperiodic crystals: from modulated phases to quasicrystals*; Oxford University Press: Oxford ; New York, 2007.
2. Greedan, J. E. *J. Mater. Chem.* **2001**, *11*, 37.
3. (a) Burdett, J. K.; Lee, S. *J. Am. Chem. Soc.* **1985**, *107*, 3050; (b) Lee, S. *Annu. Rev. Phys. Chem.* **1996**, *47*, 397.
4. (a) Dashjav, E.; Prots, Y.; Kreiner, G.; Schnelle, W.; Wagner, F. R.; Kniep, R. *J. Solid State Chem.* **2008**, *181*, 3121; (b) Davaasuren, B.; Borrmann, H.; Dashjav, E.; Kreiner, G.; Widom, M.; Schnelle, W.; Wagner, F. R.; Kniep, R. *Angew. Chem., Int. Ed.* **2010**, *49*, 5687; (c) Benbow, E. M.; Dalal, N. S.; Latturmer, S. E. *J. Am. Chem. Soc.* **2009**, *131*, 3349.

Publications

1. V. M. Berns; T. E. Stacey; M. Sapiro; D. C. Fredrickson. $Mg_{11}Cu_6Al_{12}$, a new link in the structural chemistry of $MgCu_2$ -type clusters. *Eur. J. Inorg. Chem.* **2011**, *26*, 3936-3949.
2. D. C. Fredrickson. Electronic packing frustration in complex intermetallic structures: The role of chemical pressure in Ca_2Ag_7 . *J. Am. Chem. Soc.* **2011**, *133*, 10070-10073.
3. N. H. Harris; A. B. Hadler; D. C. Fredrickson. In search of chemical frustration in the Ca-Cu-Cd System: Chemical pressure relief in the crystal structures of Ca_5Cu_2Cd and $Ca_2Cu_2Cd_9$. *Z. Anorg. Allg. Chem.* **2011**, *637*, 1961-1974.
4. T. E. Stacey; D. C. Fredrickson. The μ_3 model of acids and bases—Extending the Lewis Theory to Intermetallics. *Inorg. Chem.* **2012**, *51*, 4250-4264.
5. T. E. Stacey; D. C. Fredrickson. Perceiving Molecular Themes in the Structures and Bonding of Intermetallic Phases: The Role of Hückel Theory in an Ab Initio Era. *Dalton Trans.* **2012**, Advance Article. DOI: 10.1039/c2dt30298e
6. A. B. Hadler; D. C. Fredrickson. $Gd_{13}Fe_{10}C_{13}$: Indications of Fe-Fe Multiple Bonding Emerging from Chemical Frustration, submitted.

Cathode Catalysis in Hydrogen/Oxygen Fuel Cells: New Catalysts, Mechanism, and Characterization

PIs: Andrew A. Gewirth, Paul J.A. Kenis, Ralph G. Nuzzo, and Thomas B. Rauchfuss

Department of Chemistry, Department of Chemical and Biomolecular Engineering, and the Fredrick Seitz Materials Research Laboratory

University of Illinois at Urbana-Champaign, Urbana, IL 61801

Program Scope

In this project, we are engaged in a comprehensive plan of research directed at developing new catalysts and new understandings relevant to the operation of low temperature hydrogen-oxygen fuel cells. The focal point of this work is one centered on the Oxygen Reduction Reaction (ORR), the electrochemical process that most fundamentally limits the technological utility of these environmentally benign energy conversion devices. It is therefore to the single greatest challenge limiting wide-spread implementation of hydrogen-oxygen fuel cells -- providing robust low cost cathodes that efficiently reduce dioxygen to water – that we address the work described in this proposal.

Utilizing support from this project, we developed a new class of ORR catalyst, based on Cu dimers and multimers. These new materials exhibit ORR onsets at potentials higher than any other Cu-based material in neutral and basic environments and are inspired by the three-Cu active site in laccase which has the highest ORR onset potential of any material known. By directly coupling laccase to a Au electrode we showed that this three-Cu active site in laccase is especially competent for the ORR. We also used microfluidic methods to evaluate these catalysts in both the acidic and basic electrochemical environments. We have developed new XAS and microscopy based techniques with which to study the ORR, which provide insight into the ORR active site with unprecedented resolution. These techniques have helped us to develop insights into ORR reaction mechanisms on important electrocatalytic materials. In turn, these insights are providing directions to synthesize new ORR catalytic materials.

Recent Accomplishments

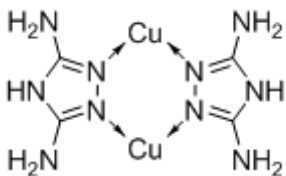


Figure 1: 3,5-diamino-1,2,4-triazole ligands bridging two copper centers. Typical Cu...Cu spacing is 3.5 Å. Counter-ions and ligated water are omitted.

New Catalysts for the Oxygen Reduction Reaction

An important accomplishment was the development of a new class of catalysts for the ORR.^{2 2} We found that direct precipitation of an insoluble copper triazole (Figure 1) coordination complex formed from 3,5 diamino 1,2,4 triazole (DAT) onto a carbon black support leads to the formation of an efficient catalyst for the 4 e⁻ reduction of O₂ to H₂O. The oxygen reduction activity is reported over a wide pH range from 1 to 13 and the onset of the oxygen reduction reaction occurs at potentials as high as 0.86 V_{RHE}. This potential is the highest ever reported for a Cu complex ORR catalyst. (Figure 2) Ex-situ magnetic susceptibility

measurements confirm the presence of multi-Cu sites, since the on- electrode sample exhibits room temperature antiferromagnetic coupling which can only be explained by the presence of Cu dimer sites. A secondary outcome attendant this work was to develop a new way to entrain molecular materials on carbon electrode surfaces. We discovered that a soluble ligand and soluble metal could be stabilized on an electrode if the complex they formed was insoluble. This precipitation method enables very smooth conformal coatings of molecular catalyst on the electrode.

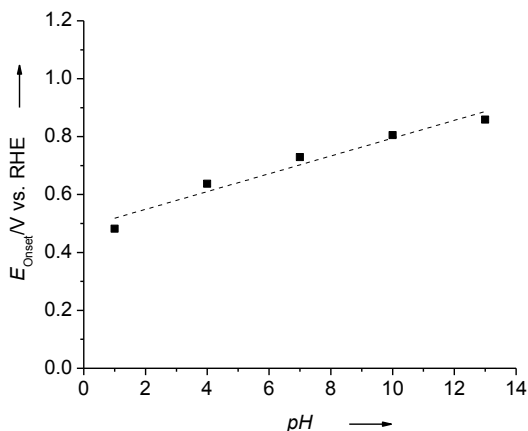


Figure 2 Potentials at which the onset of O_2 reduction occurs at electrodes modified with CuDAT in electrolytes of varying pH and a linear fit (31 ± 4 mV per pH unit slope and 0.49 ± 0.03 V y -intercept). Electrodes were rotated at 1600 rpm in 0.1 M HClO_4 ; 0.1 M NaClO_4 + 0.04 M Britton-Robinson Buffers (pH 4, 7, 10); or 0.1 N NaOH saturated with O_2 . Potential scanned at 5 mV/s. Onset potential chosen as the potential at which the current density reaches $-5 \mu\text{A cm}^{-2}$ which is ca. the most positive potential at which a non-zero current can be visually resolved on a full scale voltammogram.

high oxygen flux to the working electrode by utilizing a thin poly(dimethylsiloxane) (PDMS) window.⁴ This cell design enables in situ XAS investigations of the oxygen reduction reaction (ORR) at high operating current densities greater than 1 mA in an oxygen-purged environment. When the cell was used to study the ORR for a Pt on carbon electrocatalyst, the data revealed a progressive evolution of the electronic structure of the metal clusters that is both potential-dependent and strongly current-dependent. In particular, we showed that the white line intensity from the Pt L_3 edge was higher in the presence of O_2 than N_2 at all potentials. (Figure 3) This shows directly

that oxygen exposure induces charge transfer from

Cu-containing ORR catalysts are a focus of work since multicopper oxidases (exemplified by laccase) activate oxygen at a site containing 3 Cu atoms with ca. 3.5 Å spacings and exhibit remarkable ORR activity at potentials approaching 1.2 V RHE.³ A Cu-containing complex entrained on an electrode surface that exhibited this level of reactivity would be highly desirable.

There remain a number of outstanding issues related to the mechanism of the ORR on Pt and other surfaces. In particular, changes in the surface structure and bonding of Pt electrocatalyst particles during the ORR event is still unclear. We developed an in situ electrochemical X-ray absorption spectroscopy (XAS) cell that enables

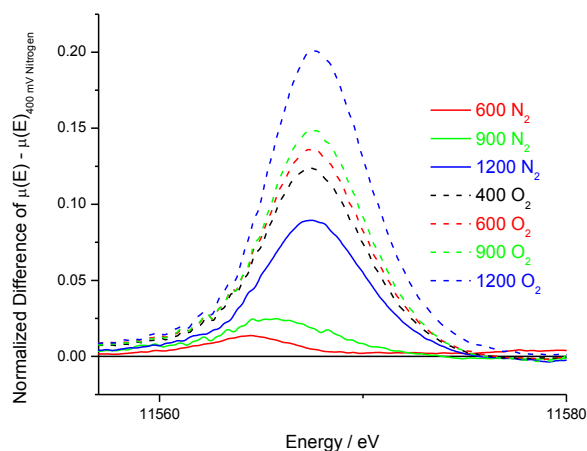


Figure 3. XANES difference ($\Delta\mu$) plots of the electrode at varied potentials under O_2 and N_2 , calculated by subtracting the XANES values at 400 mV under N_2 from each white line region.

that oxygen exposure induces charge transfer from

the Pt to the adsorbed O. Further, this charge transfer increases with decreasing potential. The trends establish a direct correlation to d-state occupancies that directly tracks the character of the Pt–O bonding present.

The focus on coordination of Cu with ligands containing N to form competent ORR catalysts possibly mimicking laccase has led to a reexamination of other such ligands. We recently examined the tris(2-pyridylmethyl)amine (TPA) ligand, recently used in a nonaqueous context for ORR,⁵ and showed that this ligand, complexed with Cu, yields the most positive potential onset for the ORR in aqueous acidic solution relative to any Cu-containing complex thus far examined.⁶ However, there is little understanding yet developed concerning the nature of the active site in this system.

We also demonstrated that non precious metal catalysts, such as those from Cu DAT, from Fe phthalocyanin, and from pyrolyzed Fe phthalocyanin materials all exhibit poisoning by small molecules added to the electrolyte. In the case of CuDAT, the small molecules included azide and fluoride, molecules identical to those that poison multicopper oxidase enzymes which also perform the ORR. In the case of the Fe-containing materials, we showed that both were poisoned by CN⁻, consistent with the presence of metal-centered ORR activity.⁷

The Cu DAT and related complexes are being developed as mimics for the four-Cu active site of laccase, which are highly active for the ORR. In laccase, only three of the Cu atoms form the site at which the ORR occurs, while the fourth Cu acts to transfer electrons from the site of oxidation on the other side of the protein where oxidation occurs.⁸ An important question relates to the rate determining step (rds) of the ORR in laccase. In order to address this issue, we recently developed a novel method of immobilizing laccase on a Au surface, using an anthracene thiol, backfilled with a short chain thiol to allow space for the laccase to adsorb with the correct orientation on the Au surface.⁹ The stabilized laccase enables direct electron transfer between the enzyme and the Au surface, and direct determination of the Tafel slope for the ORR process. The Tafel slope is found to be 140 mV/decade, which can only be consistent with the first electron transfer between the substrate and the electron transfer associated type 1 Cu center being the rate determining step. Consequently, this implies that the 3 Cu active site is in fact kinetically competent and that the ORR occurs quickly there.

Future Plans

In the future we specifically propose to undertake research that has three synergistic program elements. These are: (1) design and synthesis of new advanced solid-state and molecular cathode materials; (2) physico-spectroscopic characterization of the molecular mechanisms of catalysis and the atomistic structures that mediate it; and (3) develop test-bed platforms that facilitate critical performance measurements of catalytic materials, ones integrated at both the sub-cell component and full device levels.

References:

1. Piontek, K.; Antorini, M.; Choinowski, T., Crystal structure of a laccase from the fungus *Trametes versicolor* at 1.90-angstrom resolution containing a full complement of coppers. *Journal of Biological Chemistry* **2002**, 277 (40), 37663-37669.
2. Thorum, M. S.; Yadav, J.; Gewirth, A. A., Oxygen reduction activity of a copper complex of 3,5-diamino-1,2,4-triazole supported on carbon black. *Angew. Chem., Int. Ed.* **2009**, 48 (1), 165-167.

3. (a) Blanford, C. F.; Foster, C. E.; Heath, R. S.; Armstrong, F. A., Efficient electrocatalytic oxygen reduction by the 'blue' copper oxidase, laccase, directly attached to chemically modified carbons. *Faraday Discuss* **2008**, *140*, 319-335; (b) Mano, N.; Soukharev, V.; Heller, A., A laccase-wiring redox hydrogel for efficient catalysis of O₂ electroreduction. *J. Phys. Chem. B* **2006**, *110* (23), 11180-11187.
4. , N. a. S.; Frenkel, A.; Gewirth, A. A.; Nuzzo, R. G., In Situ Electrochemical X-ray Absorption Spectroscopy of Oxygen Reduction Electrocatalysis with High Oxygen Flux. *Journal of the American Chemical Society* **2012**, *134*, 197-200.
5. Fukuzumi, S.; Kotani, H.; Lucas, H. R.; Doi, K.; Suenobu, T.; Peterson, R. L.; Karlin, K. D., Mononuclear Copper Complex-Catalyzed Four-Electron Reduction of Oxygen. *Journal of the American Chemical Society* **2010**, *132* (20), 6874-+.
6. Thorseth, M.; Gewirth, A. A., in preparation. **2012**.
7. Thorum, M. S.; Hankett, J. M.; Gewirth, A. A., Poisoning the Oxygen Reduction Reaction on Carbon Supported Fe and Cu Electrocatalysts: Evidence for Metal-Centered Activity *Journal of Physical Chemistry Letters* **2011**, in press.
8. Solomon, E. I.; Sundaram, U. M.; Machonkin, T. E., Multicopper Oxidases and Oxygenases. *Chem. Rev* **1996**, *96* (7), 2563-2605.
9. Thorum, M. S.; Anderson, C. A.; Hatch, J. J.; Campbell, A. S.; Marshall, N. M.; Zimmerman, S. C.; Lu, Y.; Gewirth, A. A., Direct, Electrocatalytic Oxygen Reduction by Laccase on Anthracene-2-methanethiol-Modified Gold. *Journal of Physical Chemistry Letters* **2010**, *1* (15), 2251-2254.
10. Ouellette, W.; Yu, M. H.; O'Connor, C. J.; Hagrman, D.; Zubieta, J., Hydrothermal chemistry of the copper-triazolate system: A microporous metal-organic framework constructed from magnetic {Cu-3(mu₃-OH)(triazolate)₃}²⁺ building blocks, and related materials. *Angewandte Chemie-International Edition* **2006**, *45* (21), 3497-3500.

Selected Publications resulting from work supported

1. "I et g t f Pt Pt₃Co and Pt₃Co/Mo Cathodes for the ORR in a Microfluidic H₂/O₂ Fuel Cell" F B ett H D g J W D Ng L Be e A We w P J A Ke *Journal of The Electrochemical Society*, **2010**, *157* (6), B837-B845.
2. "Oxygen Reduction Activity of a Copper Complex with 3,5-Diamino-1,2,4-triazole Supported on Carbon Bl " Y d J Gew t A A *Angewandte Chemie* **2009** *48*, 165-7.
3. "I e t e d t f D xy ge f F e l Cell Appl t : t e l d C lle ge " Gew t A. A.; Thorum, M. S. *Inorganic Chemistry* **2010** *49*, 3357-66.
4. "D e t l e t t lytic Oxygen Reduction by Laccase on Anthracene-2-methanethiol Modified G ld" t t e w Cy A A de J e e y J H t A d e w C p b e l l N l Marshall, Steven C. Zimmerman, Yi Lu, and Andrew A. Gewirth *J. Phys. Chem. Lett.* **2010** *1* (15), 2251-2254.
5. "A Carbon-Supported Copper Complex of 3,5-Diamino-1,2,4-triazole as a Cathode Catalyst for Al l e F e l Cell Appl t " F.R. Brushett, M.S. Thorum, N.S. Lioutas, M.S. Naughton, C. Tornow, H.R.M. Jhong, A.A. Gewirth, P.J.A. Kenis, *J. Am. Chem. Soc.* **2010** *132*(35), 12185-12187.
6. "A Permeation-B e d f l d D e t F A d F e l Cell (DFAFC)" Mitrovski, S. M.; Gewirth, A. A.; Nuzzo, R. G. *Electrophoresis* **2011** *32*, 947-956..
7. "P g t e Oxyge e d t e t C r b o n Supported Fe and Cu Electrocatalysts: Evidence for Metal-Ce t e e d A t t y" H e t t J Gew t A A *J. Phys. Chem. Lett.* **2011**, 295-298.
8. "D xy ge d H y d g e P e x d e e d t w t H e y d e l" t t e w A e t Christopher S. Letko, Thomas B. Rauchfuss, Andrew A. Gewirth *Inorg Chem.*; **2011** *50*, 6158-6162.
9. , N. a. S.; Frenkel, A.; Gewirth, A. A.; Nuzzo, R. G., In Situ Electrochemical X-ray Absorption Spectroscopy of Oxygen Reduction Electrocatalysis with High Oxygen Flux. *J. Am. Chem. Soc.* **2012**, *134*, 197-200.

Low Temperature Synthesis of Carbide-Derived-Carbons from Binary and Ternary Carbides in the Si-Ti-C System

PI: Prof. Yury Gogotsi

Research team: Min Heon (PhD student), Dr. Volker Presser (Res. Asst. Prof.)

Department of Materials Science and Engineering, Drexel University, Philadelphia, PA 19104

1. Program Scope

The project investigates the synthesis of carbide-derived carbons (CDC) via low-temperature chlorination (*i.e.*, below 800°C). Low temperature metal extraction by chlorine yields an attractive route to achieve lower energy consumption during synthesis, but it is complicated by a relatively low conductivity of the resulting porous carbon, which may limit its application as electrodes in electrochemical double layer capacitors, so called supercapacitors. The influence of electronic conductivity of carbon on the electrochemical performance of supercapacitors is still poorly understood and the tunability in carbon structure and porosity makes carbide-derived carbons an attractive material for systematic and parametric studies.

The scope of the program is the investigation of TiC and SiC thin film transformation to carbon – for SiC-CDC in the temperature range between 500 and 800 °C and for TiC-CDC between 200 and 500 °C. Silicon carbide is known to be a challenging precursor material for CDC synthesis as its native oxide provides a diffusional barrier; thus higher temperatures were needed to achieve complete transformation to carbon.

Thin films were chosen because they serve as a good model system. The ability of thin-film supercapacitor electrodes to respond to charge and discharge at high rates (due to a shorter diffusional path compared to conventional electrodes) makes them attractive for high power supercapacitors. They can also be integrated with silicon chips. The benefits of thin films (< 1 μm) extend to fast reaction kinetics for the carbide-carbon transformation (compared to conventional carbide powder particles which are several μm in thickness). However, the build-up of internal tensile stress due to a nearly-conformal transformation of carbide to carbon and the different thermal expansion of the CDC film and the substrate poses complications.

2. Recent Progress

2.1 Patterned Thin Film approach

We chose magnetron sputtering for depositing carbide films. This work was done through collaboration with Rowan University¹ where we used reactive DC magnetron sputtering with a Si target and acetylene (C₂H₂) gas as a carbon source to obtain SiC films. TiC films were obtained by exchanging the Si with a Ti target. This method provided us with the possibility to produce carbide thin films with sub-micrometer thickness on a variety of substrates (thermally grown silica on silicon, glassy carbon, highly oriented pyrolytic graphite, and sapphire). We also used CVD SiC films in some experiments. After carbide deposition, the transition metal atoms (Ti) or metalloid atoms (Si) were extracted by etching in dry chlorine gas and pure carbon was produced per the following reaction:

$MC + 2 Cl_2 \rightarrow MCl_4 + C$ (M = Si, Ti).

Subsequently, the samples were annealed in hydrogen gas at the same temperature as that of chlorine treatment, to remove chlorine and tetrachlorides from the pores of carbon.

Magnetron sputtering provided sufficiently large sample areas, which were homogeneously coated with the carbide thin film ($>1 \text{ cm}^2$).

This way, subsequent patterning of the films made it possible to obtain interdigitated electrodes that, unlike what is commonly used in supercapacitors, which required no porous separator between the individual electrode fingers. Different methods were tested to manufacture patterned electrodes: ion milling with the focused ion beam gun of a dual beam electron microscope, laser machining, and reactive ion etching lithography. The concept behind this “top-down” patterning method is depicted in Fig. 1.

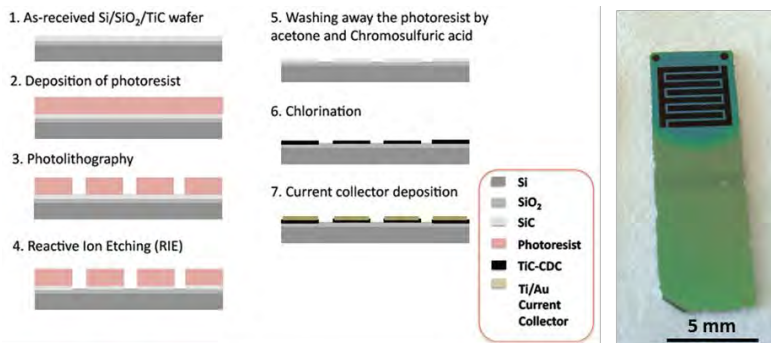


Fig. 1: Schematic representation of the patterned CDC thin film electrode manufacturing and a resulting device obtained from reactive ion etching lithography.

2.2 Structure of SiC-CDC Thin Films

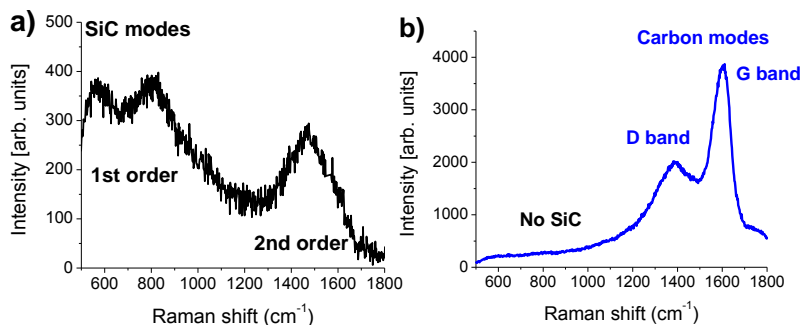


Fig. 2: Raman spectra of a 100 nm thick SiC on Si (a), and SiC-CDC on Si after chlorination (b); the film thickness remained constant.

SiC films were obtained by sputtering of SiC on Si substrates. Raman spectroscopy was used to confirm full carbide-to-carbon-transformation after chlorination. Typical Raman spectra of SiC and SiC-CDC thin films are shown in Fig. 2. Complete transformation of the carbide into carbon (SiC-CDC) was achieved

after chlorination in the temperature range from 500 to 800 °C. Chemical analysis showed that the only impurities after the synthesis are trace amounts of chlorine (probably present as $SiCl_4$) and some oxygen (from the exposure to the laboratory atmosphere after the synthesis) – both are comparable to the results for SiC-CDC obtained from SiC powders. Like the TiC-CDC thin films (next section) all SiC-CDC showed some cracking, which increased at higher synthesis temperatures.

2.3 Structure of TiC-CDC Thin Films

The Ti:C ratio of magnetron sputtered films was varied between 78:22 to 40:60 to create non-stoichiometric TiC-films and to explore the influence of film deposition parameters and carbon content in TiC on the final microstructure and film texture (Fig. 3). For this, the substrate was heated to 700 °C to produce textured TiC in the (111) orientation which created a pillar-like film

morphology of TiC-crystals perpendicular to the substrate, and the texture was maintained for TiC-CDC.

A systematic study of various substrate materials was conducted, using HOPG (highly ordered pyrolytic graphite), glassy carbon, and single crystal sapphire (Al_2O_3) and silica thermally grown on silicon. The goal was to understand the influence of the substrate on cracking, which increased in magnitude at higher synthesis temperatures. HOPG and glassy carbon represent conductive substrates for direct electrochemical characterization of the resulting samples without additional wiring. As shown in **Fig. 4**, carbon films were successfully produced on all substrates.

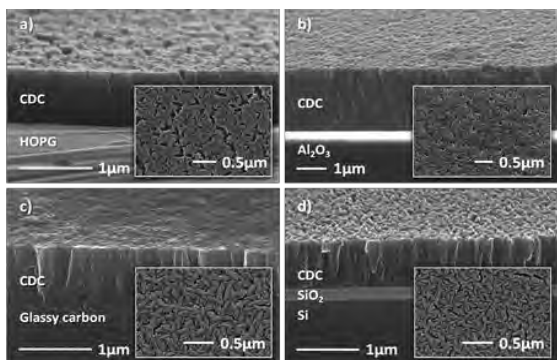


Fig. 4: Scanning electron micrographs of CDC films on highly ordered pyrolytic graphite (HOPG) produced at 500 °C (a), on Al_2O_3 produced at 400 °C (b), on glassy carbon produced at 300 °C (c), and oxidized Si wafer produced at 300 °C (d).

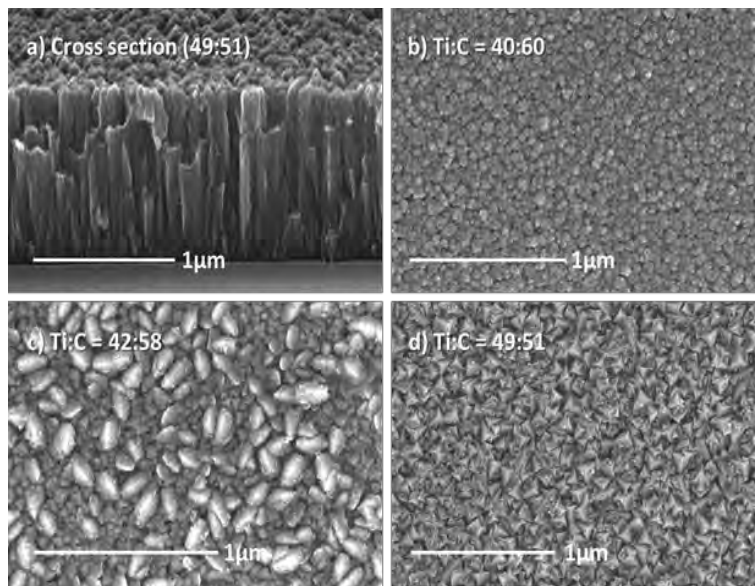


Fig. 3: Fracture surface (a) and surface morphology (b-d) of TiC films on sapphire substrates

The thickness of the initial carbide film and the synthesis temperature affect crack density and eventual delamination, as the removal of Ti atoms induces tensile stress in the film, which increases with the film thickness during synthesis. Uniform porous carbon films were synthesized for a thickness of up to 3 μm on Si wafers by chlorination below 400 °C. CDC films on HOPG showed pronounced crack formation after synthesis, which may be related to the weak adhesion of the initial carbide film to the carbon substrate and thermal expansion mismatch. Glassy carbon, sapphire and silicon showed good adhesion and minor crack formation.

2.4 Electrochemical Performance of TiC-CDC Thin Films

In addition to the proof-of-concept of the interdigitated electrode architecture, electro-chemical characterization was carried out on bulk film electrodes in a 2-electrode setup (with an oversized activated carbon counter electrode used as quasi-reference). CDC films were tested in 1.5 M tetraethylammonium tetrafluoroborate (TEA-BF_4) in acetonitrile (ACN), which is a common organic electrolyte. Cyclic voltammograms are shown in **Fig. 5** and they are characteristic for capacitive behavior typical for electric double layer capacitors. Carbon films produced at 400 °C showed the highest volumetric capacitance of $\sim 180 \text{ F/cm}^3$ at 20 mV/s scan

rate, which is about 3 times higher than conventional activated carbon electrodes with binders (about 50-60 F/cm³).

Future Plans

Our next steps are to complete the structural characterization of the TiC-CDC thin film by investigation the film porosity with small angle X-ray scattering (SAXS). From the SAXS pattern it is possible to calculate the pore size distribution by the maximum entropy

method (MEM) and to obtain the specific surface area. This is important in order to compare the TiC-CDC thin film porosity with conventional CDC synthesized under identical conditions; yet, conventional gas sorption is not applicable to CDC thin film because of the small amount of sample material. Electrochemical scanning probe microscopy (in collaboration with ORNL) will be used for in situ electrochemical characterization of the CDC films. Room temperature synthesis of CDC will be attempted using electrochemical methods and different carbide precursors. Furthermore, we plan to systematically continue the electrochemical investigation of interdigitated electrodes in organic electrolytes, rather than bulk film characterization; transitioning to gel electrolytes will be the logical next step to obtain a quasi-solid, binder- and separator-free supercapacitor.

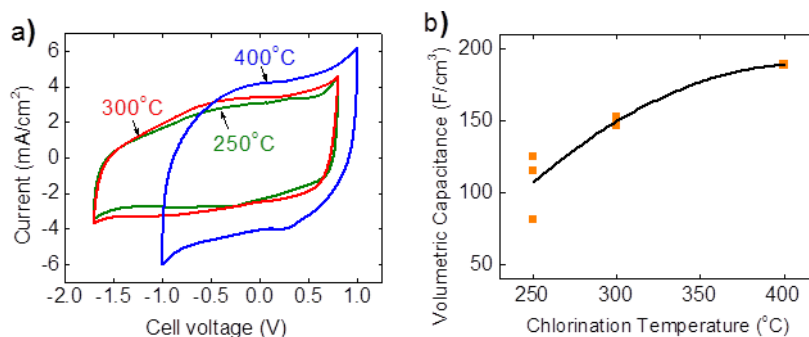


Fig. 5. Cyclic voltammograms of CDC films produced at 250, 300, and 400 °C (a) and volumetric capacitance vs. chlorination temperature (b).

Publications

1. C. R. Pérez, S.-H. Yeon, J. Ségalini, V. Presser, P.-L. Taberna, P. Simon, Y. Gogotsi, Structure and Electrochemical Performance of Carbide-Derived Carbon Nanopowders, *Advanced Functional Materials* (2012) in press
2. S. Osswald, J. Chmiola, Y. Gogotsi, Structural Evolution of Carbide-Derived Carbons upon Vacuum Annealing, *Carbon* (2012) in press
3. V. Presser, J. McDonough, S.-H. Yeon, Y. Gogotsi, Effect of Pore Size on Carbon Dioxide Sorption by Carbide Derived Carbon, *Energy & Environmental Science*, 4 (8), 3059 - 3066 (2011)
4. V. Presser, M. Heon and Y. Gogotsi, Carbide-Derived Carbons – From Porous Networks to Nanotubes and Graphene; *Advanced Functional Materials* 21, 810-833 (2011) [invited feature and cover article]
5. M. Heon, S. Lofland, J. Applegate, R. Nolte, E. Cortes, J. D. Hettinger, P.-L. Taberna, P. Simon, P. Huang, M. Brunet, and Y. Gogotsi, Continuous carbide-derived carbon films with high volumetric capacitance; *Energy and Environmental Science* 4, 135-138 (2011)

Materials and Interfacial Chemistry for Next Generation Electrical Energy Storage

J. B. Goodenough and A. Manthiram – The University of Texas at Austin, Austin, TX 78712

S. Dai, M. Paranthaman, C. A. Bridges, R. R. Unocic, X. Sun, D. Jiang, and G. M. Veith – Oak Ridge National Laboratory, Oak Ridge, TN 37831

Program Scope

Electrochemical energy storage systems are critically needed for transportation and for effectively using renewable energy sources. This project has two major emphases that enable the development of new materials for next-generation batteries. First, we aim to improve the understanding and control of the fundamental processes that occur at the interfaces of the anode and cathode. Second, we focus on improving Li^+ -ion diffusion in solid electrolytes with higher voltage limits. Specifically, these processes are examined with *ex-situ* and *in-situ* studies of Li^+ -ion transport across the electrode-electrolyte interfaces as well as in the electrodes and electrolytes. Example systems investigated are spinel-layered composite and olivine cathodes, alloy anodes, dual-electrolyte systems, and solid Li^+ -ion conductors. This work lays a foundation for transformative advances in batteries for vehicle and stationary storage applications.

Recent Progress

Spinel-layered composite cathodes: High voltage, high capacity spinel-layered composite cathode materials have been synthesized by controlling the Li/metal ratio in the precursor, with the formula $x\text{Li}[\text{Li}_{0.2}\text{Mn}_{0.6}\text{Ni}_{0.17}\text{Co}_{0.03}]\text{O}_2 \cdot (1-x)\text{LiMn}_{1.5}\text{Ni}_{0.425}\text{Co}_{0.075}\text{O}_4$ ($x = 0, 0.25, 0.5, 0.75, \text{ and } 1$). The 5 V spinel undergoes Jahn-Teller distortion on discharging down to 2 V, but maintains its capacity with good cyclability due to the small volume and c/a ratio changes. The sloping region originating from the layered phase gradually changes to a ~ 3 V plateau during 50 cycles, due to the evolution of a new cubic spinel-like phase. The presence of Mn^{4+} in the 3 V spinel-like phase suppresses Jahn-Teller distortion!

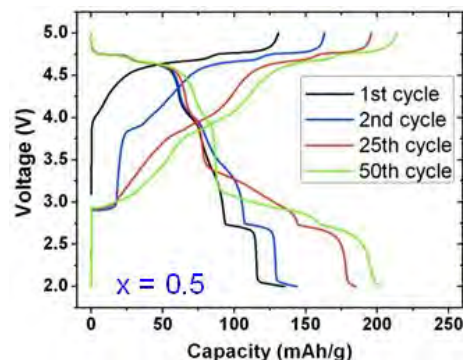


Figure 1: Charge-discharge curves of layered-spinel composites.

Doped olivine cathodes: Vanadium-doped LiFePO_4 cathodes have been obtained by a novel low-temperature microwave-assisted solvothermal (MW-ST) method (Table 1), employing a vanadyl (VO) precursor. Neutron diffraction and elemental analysis indicate the formation of cation-deficient $\text{LiFe}_{1-3x/2}\text{V}_x\text{PO}_4$. However, electrochemical measurements and FTIR suggest the

presence of a V=O bond similar to that in LiVOPO₄. Synthesis with less iron or more iron precursors than dictated by LiFe_{1-3x/2}V_xPO₄ leads to the formation of impurity phases.

Table 1: Elemental analysis results and Fe occupancy determined by neutron diffraction refinement

Sample	Fe/P	Li/P	V/P	Expected Fe Occupancy	Calculated Fe Occupancy
LiFe _{0.925} V _{0.05} PO ₄	0.92	0.99	0.051	0.925	0.923(5)
LiFe _{0.85} V _{0.10} PO ₄	0.82	0.99	0.99	0.85	0.860(5)
LiFe _{0.775} V _{0.15} PO ₄	0.79	0.97	0.97	0.775	0.808(6)

Nano-olivine cathodes: Flowering LiFePO₄ plates, LiMnPO₄ plates, and LiCoPO₄ rods have been realized. The [010] direction parallel to the platelets and the LiMPO₄/MPO₄ interface perpendicular to [010] degrades the rate capability of LiMnPO₄ compared to LiFePO₄. Also,

decoration of the surface of C-LiFePO₄ with N or S reduces the resistance of Li⁺ transfer across the electrolyte-electrode interfaces.

Nanocomposite alloy anodes: A Cu₂Sb-Al₂O₃-C nanocomposite anode exhibiting superior cycle life has been developed. The Al₂O₃/C matrix eliminates agglomeration and buffers the volume expansion, leading to > 500 cycles. The reaction mechanism appears to depend on crystallite size or carbon. Because the crystallites are 2 – 10 nm, XRD could not be used to determine the reaction mechanism. Future work with X-ray absorption spectroscopy could help in this regard.

Dual-electrolyte Li-air cells: A rechargeable dual-electrolyte Li-air cell with a phosphate buffer catholyte has been developed with the configuration Li | 1 M LiPF₆ in EC/DEC | LISICON | 0.1M H₃PO₄ + 1M LiH₂PO₄ | Pt air. It offers an energy density of 221 mAh/g × 3.5 V = 773 Wh/kg. The H₃PO₄ catholyte delivers high capacity while the LiH₂PO₄ provides good stability to the solid electrolyte by maintaining a moderate pH. Only mild degradation occurs upon cycling and the bulk and boundary resistances of the solid electrolyte (LTAP) membrane exhibit little change during the test, indicating that the phosphate buffer is a promising catholyte for high capacity dual-electrolyte Li-air cells. The relevant reaction that occurs is $\text{Li} + \text{H}_3\text{PO}_4 + 1/4 \text{O}_2 \leftrightarrow \text{LiH}_2\text{PO}_4 + 1/2 \text{H}_2\text{O}$.

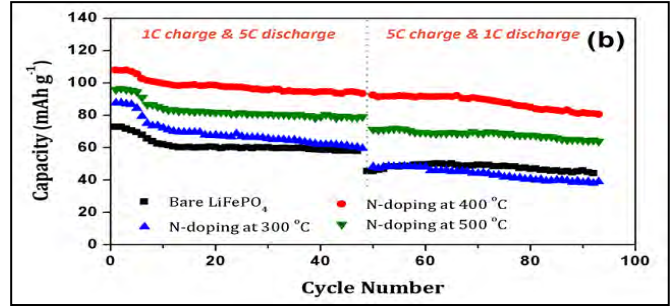


Figure 2: Cyclability of bare and N-doped LiFePO₄.

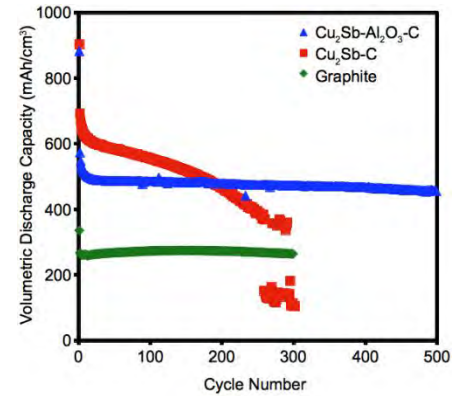


Figure 3: Cycling performance of Cu₂Sb-Al₂O₃-C anode material.

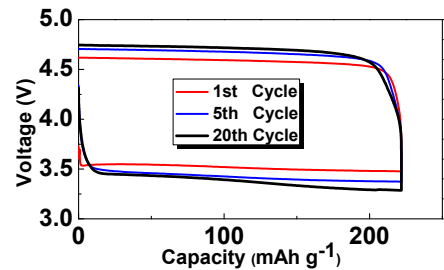


Figure 4: Charge-discharge curves of the cell with H₃PO₄ + LiH₂PO₄ electrolyte.

A second rechargeable dual-electrolyte Li-air cell has been developed with the configuration Li | 1 M LiPF₆ in EC/DEC | LISICON | 0.1M H₃PO₄+1M Li₂SO₄ | Pt + IrO₂ air. By utilizing all the three protons in H₃PO₄, an ultra-high energy density of 740 Ah/g×3.3 V = 2442 Wh/kg was achieved. IrO₂ was added as an oxygen evolution catalyst to lower the over-voltage during charge. The relevant reaction that occurs is $3\text{Li} + \text{H}_3\text{PO}_4 + 3/4 \text{O}_2 \leftrightarrow \text{Li}_3\text{PO}_4 + 3/2 \text{H}_2\text{O}$. The voltage profiles retain almost the same shape under different current densities, indicating the distinct cell chemistry of the cell. The concept allows a flow-through mode for grid-energy storage, offering a low-cost approach for large-scale storage.

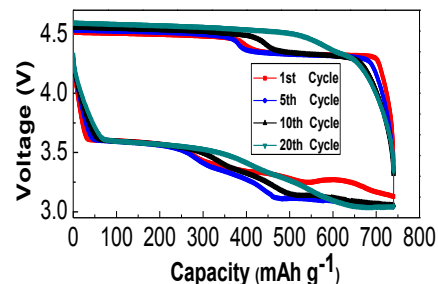


Figure 5: Charge-discharge curves of the cell with H₃PO₄+Li₂SO₄ electrolyte.

Solid Li⁺-ion electrolytes: A solid electrolyte separator has been developed for dual-electrolyte cells. A lithium anode can be used with this separator, which maximizes voltage while still blocking dendrites from Li anode. A Li anode need not rob Li irreversibly from the cathode on initial charge. This design can be used with air, flow-through liquid, or solid cathodes. The Li⁺-ion conductivity in garnet Li_{7-x}La₃Zr_{2-x}Ta_xO₁₂ has been optimized by tuning the lithium content. The maximum conductivity is achieved for x = 0.6, and neutron diffraction is on-going at ORNL to determine whether the maximum σ_{Li^+} is where short-range order sets in.

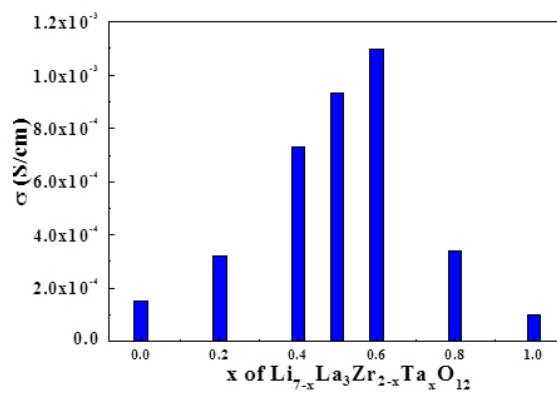


Figure 6: Dependence of Li⁺ content on Li⁺-ion conductivity in Li_{7-x}La₃Zr_{2-x}Ta_xO₁₂.

Future Plans

Our future work will continue to develop a basic science understanding of materials for advanced energy storage. Specifically, we will focus on the following:

- Study the effect of synthesis temperature on the structural and electrochemical characteristics of the layered-spinel composite system $x\text{Li}[\text{Li}_{0.2}\text{Mn}_{0.6}\text{Ni}_{0.2}]\text{O}_2 - (1-x)\text{Li}[\text{Mn}_{1.5}\text{Ni}_{0.5}]\text{O}_4$ ($0 \leq x \leq 1$)
- Analyze neutron and X-ray diffraction data with Rietveld and point distribution function refinements to better understand the structure of vanadium-doped LiFePO₄
- Study the interface between the Sb-based alloy and Al₂O₃ to understand the role Al₂O₃ plays in performance improvement, and thereby optimize the composition/microstructure
- Perform *in situ* X-ray absorption spectroscopy to understand the reaction mechanism of Cu₂Sb-Al₂O₃-C and the influence of particle size, carbon content, and synthesis conditions
- Develop composite polymer-garnet Li⁺-electrolyte membranes for mechanically and chemically robust separators of dual-electrolyte cells

Publications

1. H. Xie, Y. Li, J.B. Goodenough, "NASICON-type $\text{Li}_{1+2x}\text{Zr}_{2-y}\text{Ca}_x(\text{PO}_4)_3$ with high ionic conductivity at room temperature," *RSC Advances* **1**, 1728-1731 (2011).
2. Y. Li, C.-A. Wang, H. Xie, J. Cheng, J.B. Goodenough, "High lithium ion conduction in garnet-type $\text{Li}_6\text{La}_3\text{ZrTaO}_{12}$," *Electrochemistry Communications* **13**, 1289-1292 (2011).
3. H. Xie, J.A. Alonso, Y. Li, M.T. Fernandez-Diaz, J.B. Goodenough, "Lithium ordering of cubic $\text{Li}_7\text{La}_3\text{Zr}_2\text{O}_{12}$ with stuffed garnet structure," *Chemistry of Materials* **23**, 3587-3589 (2011).
4. S. Yoon and A. Manthiram, "Hollow Core-Shell Mesoporous TiO_2 Spheres for Lithium-Ion Storage," *Journal of Physical Chemistry C* **115**, 9410-9416 (2011).
5. D. Applestone, S. Yoon, and A. Manthiram, " $\text{Mo}_3\text{Sb}_7\text{-C}$ Composite Anodes for Lithium-Ion Batteries," *The Journal of Physical Chemistry* **115**, 18909-18915 (2011).
6. A. Gupta, R. Murugan, M.P. Paranthaman, Z. Bi, C.A. Bridges, M. Nakanishi, A.P. Sokolor, K.S. Han, E.W. Hagaman, H. Xie, C.B. Mullins, J.B. Goodenough, "Optimum Lithium-ion Conductivity in Cubic $\text{Li}_{7-x}\text{La}_3\text{Hf}_{2-x}\text{Ta}_x\text{O}_{12}$," *Journal of Power Sources* **209**, 184-188 (2012).
7. H. Xie, K.-S. Park, J.B. Goodenough, "Reversible lithium insertion in the garnet framework of $\text{Li}_3\text{Nd}_3\text{W}_2\text{O}_{12}$," *Electrochemistry Communications* **19**, 135-137 (2012).
8. Y. Lu, D. Zhang, L. Wang, M. Xu, J. Song, J.B. Goodenough, "Electrochemical Behavior of a Graphite Electrode Prepared by Anodic Electrophoretic Deposition," *Journal of Electrochemical Society* **159**, A321-A324 (2012).
9. H. Xie, Y. Li, J.B. Goodenough, "Low-temperature Synthesis of $\text{Li}_7\text{La}_3\text{Zr}_2\text{O}_{12}$ with Cubic Garnet-type Structure," *Materials Research Bulletin* **47**, 1229-1232 (2012).
10. L. Li, X. Zhao, and A. Manthiram, "A Dual-electrolyte Rechargeable Li-Air Battery with Phosphate Buffer Catholyte," *Electrochemistry Communications* **14**, 78-81 (2012).
11. D. Applestone, S. Yoon, and A. Manthiram, " $\text{Cu}_2\text{Sb-Al}_2\text{O}_3\text{-C}$ Nanocomposite Alloy Anodes with Exceptional Cycle Life for Lithium-Ion Batteries," *Journal of Materials Chemistry* **22**, 3242-3248 (2012).
12. E.-S. Lee, A. Huq, H.-Y. Chang, and A. Manthiram, "High-voltage, High-energy Layered-Spinel Composite Cathodes with Superior Cycle Life for Lithium-Ion Batteries," *Chemistry of Materials* **24**, 600-612 (2012).
13. S. Yoon, E. Lee, and A. Manthiram, "Microwave-solvothermal Synthesis of Various Polymorphs of Nanostructured TiO_2 in Different Alcohol Media and Their Lithium-Ion Storage Properties," *Inorganic Chemistry* **51**, 3505-3512 (2012).
14. D. Applestone and A. Manthiram, " $\text{Cu}_6\text{Sn}_5\text{-TiC-C}$ Nanocomposite Alloy Anodes with High Volumetric Capacity for Lithium Ion Batteries," *RSC Advances* DOI:10.1039/C2RA20325A.
15. D. Applestone and A. Manthiram, "Symmetric Cell Evaluation of the Effects of Electrolyte Additives on $\text{Cu}_2\text{Sb-Al}_2\text{O}_3\text{-C}$ Nanocomposite Anodes," *Journal of Power Sources* (submitted).
16. S. Wang, X. Zhao, T. Cochell, and A. Manthiram, "3D Porous Nitrogen-doped Carbon Nanotube/Graphite Felt as Advanced Electrode Materials for Vanadium Redox Flow Batteries," *Chemical Communications* (submitted).
17. D. W. Shin, C. A. Bridges, A. Huq, M. P. Paranthaman, and A. Manthiram, "Role of Cation Ordering and Surface-segregation in High-voltage Spinel $\text{LiMn}_{1.5}\text{Ni}_{0.5-x}\text{M}_x\text{O}_4$ (M = Cr, Fe, and Ga) Cathodes for Lithium-Ion Batteries," *Energy and Environmental Science* (submitted).

Dynamic Supracolloidal Assemblies

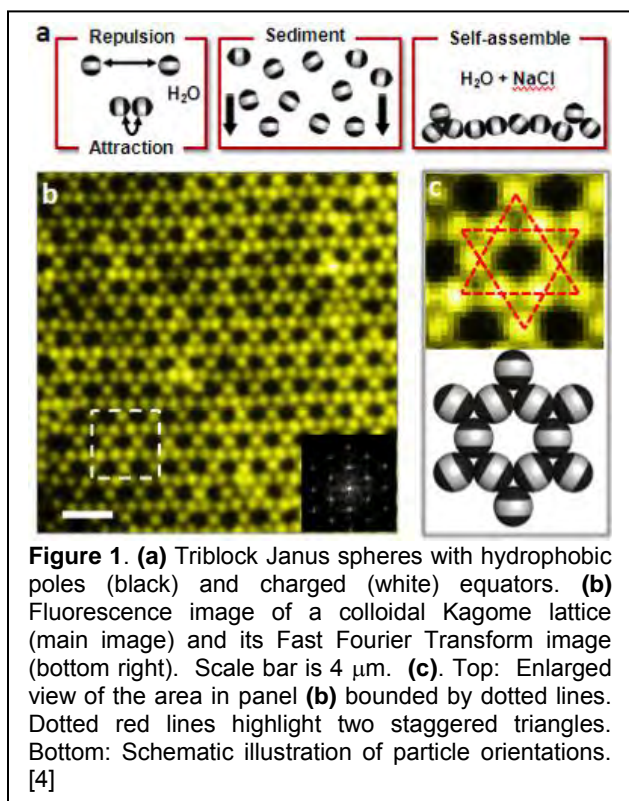
Steve Granick

Programming Function via Soft Materials, Research Core 1
Frederick Seitz Materials Research Laboratory
Materials Science and Engineering Department
University of Illinois at Urbana-Champaign

RESEARCH APPROACH. The overarching goal is to establish the fundamental knowledge required to transform diverse classes of information- and function-encoded building blocks into multiscale functional assemblies that guide photon-electron conversion processes for light capture and utilization. This core research area is devoted to dynamic supracolloidal assemblies - - created by controlling the equilibrium and nonequilibrium phase behavior, spatial organization, and connectivity of colloidal particles, clusters, and mixtures thereof through self, driven and chemically amplified assembly and disassembly pathways.

RECENT PROGRESS. To achieve equilibrium configurations, the tendency to become kinetically trapped in the form of glasses or gels must be overcome without mitigating the short-range interactions that drive the desired assembly pathway(s). Alternatively, to kinetically trap desirable nonequilibrium structures, an understanding of the origin and nature of dynamic barriers is required. Towards these objectives, we are synthesizing Janus spheres, dicolloids, and rods, investigating their dynamic assembly, and developing theoretical models to predict their behavior (*Granick, Lewis, Moore, Schweizer, Zukoski*).

(i) Janus and triblock spheres – Building on the group’s advances in synthesis and assembly [1], *Granick* has probed the kinetic pathways of self-assembly of Janus spheres with a hemispherical hydrophobic attraction and showed key differences from those characteristic of molecular amphiphiles. Visualization combined with theory and molecular dynamics simulation showed that small, kinetically favored isomers fuse, before they equilibrate, into fibrillar triple helices with at most six nearest neighbors per particle, as reported in *Science* [2]. The time scales of colloidal rearrangement combined with the directional interactions resulting from Janus geometry make this a prototypical system to elucidate, on a mechanistic level and with single-particle resolution, how chemical anisotropy and reaction kinetics coordinate to generate highly ordered structures. These ideas were extended to the creation of triblock Janus spheres [3,4],



micrometer-sized spheres are prepared with an electrostatic repulsion in the middle and hydrophobic attraction at their poles, and design principles were formulated to form intended superstructures from these information-encoded building blocks. We showed how these spheres can be induced to self-assemble into a complex predetermined colloidal crystal—in this case a colloidal kagome lattice (Figure 1), as reported in *Nature* [4]. This open network is of interest for several reasons. With respect to enhanced functionality, the resulting lattice structure possesses two families of pores, one that is hydrophobic on the rims of the pores and another that is hydrophilic. This strategy of ‘convergent’ self-assembly from easily fabricated colloidal building blocks encodes the target supracolloidal architecture, not in localized attractive spots, but instead in large redundantly attractive regions, and can be extended to form other supracolloidal networks.

(ii) Slow Dynamics and Viscoelasticity of Dicolloid Suspensions - To test novel predictions of *Schweizer* for the kinetic arrest and elasticity of homogeneous nonspherical particles, a family of charged homogeneous dicolloids with modest shape anisotropy have been designed and synthesized by emulsion polymerization (*Zukoski*) [5,6].

The shear elasticity is found to be tunable over a remarkably wide range by controlling colloid shape, interparticle forces, and volume fraction, consistent with theory. All shear moduli grow exponentially with volume fraction and a theoretically inspired universal master plot can be constructed for all particle shapes under repulsive interaction conditions (Figure 2), as reported in *Physical Review Letters* [5]. The underlying universal behavior is a consequence of the idea that the relevant fundamental stress is controlled by the single particle volume, and the relevant volume fraction is the distance from the emergence of transient solidity. The statistical dynamical theory has also now been fully generalized to treat the coupled translational and rotational dynamics of dicolloids that interact via short-range attractive forces (*Schweizer*). Calculations of the stress required to force flow (*Schweizer*) are consistent with the striking experimental discovery (*Zukoski*) that these dicolloids mechanically yield in two steps due to sequential unlocking of the orientational and translational dynamical constraints.

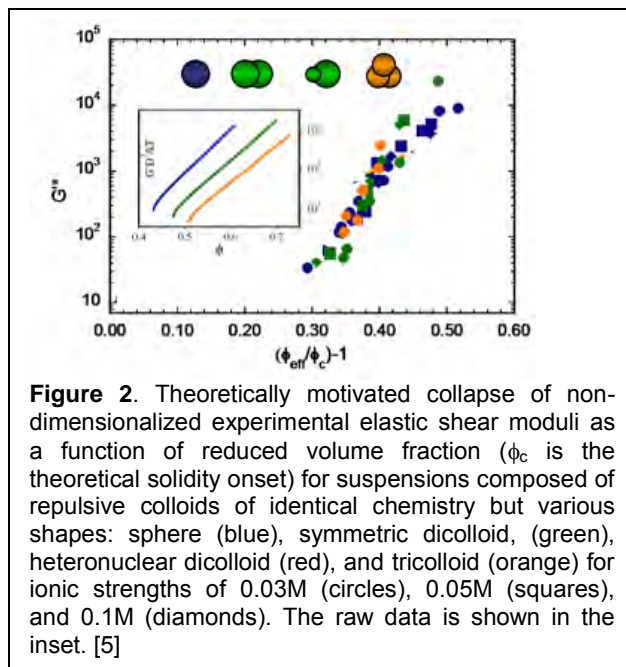


Figure 2. Theoretically motivated collapse of non-dimensionalized experimental elastic shear moduli as a function of reduced volume fraction (ϕ_c is the theoretical solidity onset) for suspensions composed of repulsive colloids of identical chemistry but various shapes: sphere (blue), symmetric dicolloid, (green), heteronuclear dicolloid (red), and tricolloid (orange) for ionic strengths of 0.03M (circles), 0.05M (squares), and 0.1M (diamonds). The raw data is shown in the inset. [5]

(iii) Janus Dicolloid Suspensions - To test novel predictions of *Schweizer* for the kinetic arrest and elasticity of nonspherical particles, a family of charged Janus dicolloids with modest shape anisotropy have been synthesized by emulsion polymerization (*Zukoski*) [7]. These particles are produced by swelling seeds with a second monomer that contains a secondary amine, which is protonated at low solution pH. The negative charges used to stabilize the seed particles are cross-linked to the seed side of the dicolloid while the nitrogen containing group distributes itself more uniformly over the dicolloid surface. At high pH, these particles carry a net negative

charge and show signs of very weak dipolar attractions produced from a negative lobe and a neutral lobe. At low pH, the particles have a substantial positive charge, suspensions again are well described as containing dicolloid particles experiencing uniform electrostatic repulsions. Near their isoelectric point, the particles form strings and clusters (Figure 1). We find evidence of head to tail clustering and suggest the multiple constraints seen in yielding are associated with “unraveling” these clusters - such that there is a first yield point associated with breaking antiparallel bonds but retaining head to tail bonds while a second yield point is associated with a stress of sufficient magnitude to break head to tail bonds. The problem raises rich problems of how to equilibrate colloidal structures, and these are under intensive experimental and theoretical investigation [8-18].

(iv) Homogeneous and Janus Colloidal Rods

- *Lewis* and *Granick* are probing the self- and electric field-driven assembly of homogeneous and Janus silica rods. Colloidal rods (Figure 2) with tunable aspect ratios have been synthesized to explore the effects of shape and chemical anisotropy on the formation of supracolloidal assemblies. Homogeneous silica rods either assemble into horizontal motifs with random orientation or align vertically with an applied electric field (*Lewis*) (Figure 3). Janus rods can be formed in either orientation simply coating these particles with a thin gold layer, following the approach reported previously for producing Janus and triblock spheres (*Granick*). Vertically coated rods, i.e., Janus matchsticks, align with their tips oriented along the direction of the applied electric field (Figure 3). Their observed directionality, which is intrinsic to the Janus matchstick geometry, leads to the formation of colloidal bilayers and unique multipod assembly driven by valency rules we have formulated to describe the end-tips [19].

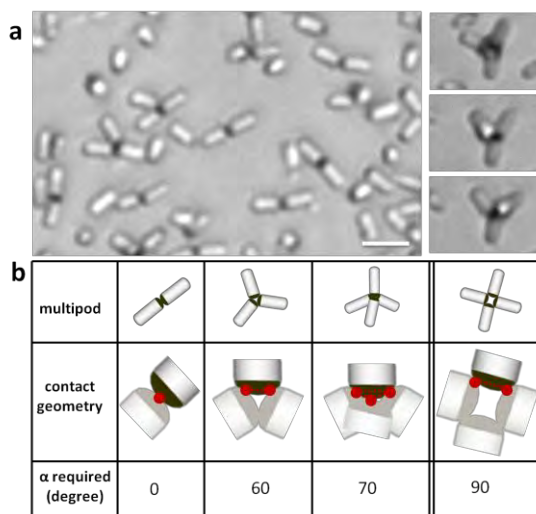


Figure 3. Self-assembly into multipods at 4.4 mM NaCl. (a) Optical images of bipods and tripods that coexist with tetrapods. The right panel shows a time-resolved series of optical images of a tetrahedral cluster as it rotates by Brownian motion. (b) A schematic table showing the valency selection rule: each multipod geometry requires a minimum patch angle α . For a patch angle of 90° , tetrahedral clusters are favored over those with a planar configuration [19].

FUTURE PLANS

These exciting developments will be pursued. For the coming year, the research team is focused on the dynamic self- and field-driven assembly of Janus dicolloids and rods encoded with chemical and topographical instruction sets. We plan to move further beyond self-assembly approaches and explore how mesoscale assembly can be driven by efficient feeding of energy into the system.

REFERENCES (CITED FROM PUBLICATIONS LISTED BELOW)

PUBLICATIONS - CORE AREA (1)

1. Jiang, S., Chen, Q., Tripathy, M., Luijten, E., **Schweizer, K. S.**, and **Granick, S.**, "Janus Particle Synthesis and Assembly", *Adv. Mat.*, **22**, 1060 (2010).
2. Q. Chen, J. Whitmer, S. Jiang, S.C. Bae, E. Luijten, and **S. Granick**, "Supracolloidal Reaction Kinetics of Janus Spheres", *Science*, **331**, 199 (2011).
3. Q. Chen, E. Diesel, J. Whitmer, S.C. Bae, E. Luijten, and **Steve Granick**, "Triblock Colloids for Directed Self-Assembly," *JACS*, **133**, 7725 (2011).
4. Q. Chen, S.C. Bae, and **S. Granick**, "Directed self-assembly of a colloidal kagome lattice", *Nature*, **469**, 381 (2011). Highlighted: *Nature Materials*, **10**, 171 (2011).
5. Kramb, R. C., Zhang, R., **Schweizer, K. S.**, and **Zukoski, C. F.**, "Glass Formation and Shear Elasticity in Dense Suspensions of Repulsive Particles", *Phys. Rev. Lett.*, **105:5**, 055702 (2010).
6. Larsen, R. J., Kim, J-W, **Zukoski, C. F.**, and Weitz, D., "Elasticity of Dilatent particle Suspensions Under Flow", *Phys Rev. E*, **81**, 011502 (2010).
7. Mock, E. B. and **C. F. Zukoski**, "Emulsion Polymerization Routes to Chemically Anisotropic Particles", *Langmuir*, **26:17**, 13747-13750 (2010).
8. Zhang, R. and **K. S. Schweizer**, "Dynamic Free Energies, Cage Escape Trajectories, and Glassy Relaxation in Dense Fluids of Uniaxial Hard Particles", *J.Chem. Phys.*, **133**, 104902 (2010).
9. R. Jadrlich and **K.S. Schweizer**, "Percolation, Phase Separation and Gelation in Fluids and Mixtures of Spheres and Rods", *J. Chemical Physics*, **135**, 234902 (2011).
10. R.C. Kramb and **C.F. Zukoski**, "Yielding in Dense Suspensions: Cage, bond and rotational confinement", *J. Phys: Condensed Matter*, **23**, 035102(13pp) (2011).
11. R.C. Kramb and **C.F. Zukoski**, "Nonlinear Rheology and Yielding in Dense Suspensions of Hard Anisotropic Colloids", *J. Rheol.*, **55:5**, 1069-1084(2011).
12. R.C. Kramb and **C.F. Zukoski**, "Exploration of the Volume Fraction Above Which Suspensions of Spherical And Weakly Anisotropic Colloid Particles Cannot Flow", *J. Rheol.*, **55:5**, 1085-1101 (2011).
13. R.C. Kramb, R. Zhang, **K.S. Schweizer**, and **C.F. Zukoski**, "Re-entrant Kinetic Arrest and Elasticity of Concentrated Suspensions of Spherical and Nonspherical Repulsive and Attractive Colloids", *J. Chemical Physics*, **134**, 014502 (2011).
14. R.J. Larsen and **C.F. Zukoski**, "Effect of particle Size on Glass transition", *Phys Rev E*, **83:5**, Article Number 051504 (2011).
15. R.J. Larsen and **C.F. Zukoski**, "Molecular Mixture as an Effective Single-Component System", *J Phys Chem B*, **115:14**, 3981-3991 (2011).
16. M. Tripathy and **K.S. Schweizer**, "Activated Dynamics in Dense Fluids of Attractive Nonspherical Particles. I. Kinetic Crossover, Dynamic Free Energies, and the Physical Nature of Glasses and Gels", *Physical Review E*, **83**, 041406 (2011).
17. M. Tripathy and **K.S. Schweizer**, "Activated Dynamics in Dense Fluids of Attractive Nonspherical Particles. II. Elasticity, Barriers, Relaxation, Fragility and Self-Diffusion", *Physical Review E*, **83**, 041407 (2011).
18. R. Zhang and **K.S. Schweizer**, "Kinetic Arrest, Dynamical Transitions and Activated Relaxation in Dense Fluids of Attractive Nonspherical Colloids", *Physical Review E-Rapid Communications*, **83**, 060502(R) (2011).
19. K. Chaudhary, Q. Chen, J. Juárez, **S. Granick**, **J. A. Lewis**, "Janus Colloidal Matchsticks," submitted.

Spectroscopic Studies of Materials for Electrochemical Energy Storage

Steven G. Greenbaum, Department of Physics & Astronomy, Hunter College of CUNY

Program Scope

This research program centers on spectroscopic investigations of materials germane to lithium metal and lithium ion batteries. The primary analytical tools used in this investigation are solid state nuclear magnetic resonance (NMR) and synchrotron x-ray absorption spectroscopy (XAS). The NMR measurements are conducted primarily at Hunter College and the XAS is done at Brookhaven's NSLS through an existing collaborative arrangement with NIST's beamline facilities there. The materials research is highly collaborative and leverages the efforts of long-time and more recent colleagues at universities and national labs. Some of these collaborators are listed in the sections below in the context of specific projects.

Single crystal olivines, LiMPO_4 , where $M = \text{Co, Fe, Mn, and Ni}$ are being investigated by ^7Li and ^{31}P NMR to extract the local magnetic environments about the Li and phosphate ions, knowledge of which will provide vital experimental input to colleagues engaged in first principle calculations related to ion transport properties. New methods of probing the composition of the Solid Electrolyte Interphase (SEI) are now under development and are being exploited in this project, including the use of ^{13}C isotopic enrichment of electrolyte solvents. This strategy is also being applied in studies of reversible conversion reaction between Li and metal fluorides. Ion transport is being investigated in polymer electrolytes of two basic kinds, membranes containing ionic liquids, and solvent-free PEO-based materials in which partial chain alignment is achieved by magnetic means. Novel electrolytes based on ionic liquids are also being investigated, in particular with regard to their charge and mass transport properties.

Finally, several related projects not conceived at the time the proposal was submitted in 2009 are underway, including investigations of ionic liquid-based electrolytes for sodium-air batteries, studies of SEI formation in the Si/Li system, and synchrotron XAS measurements in thin film CuS electrodes.

Recent Progress

The work summarized herein dates back to the beginning of this BES grant funding in the Fall of 2010. In collaboration with colleagues from CNRS/Orsay, Universite Jules Verne de Picardie, and North Carolina State University, our group was the first to demonstrate the feasibility of natural abundance ^{13}C NMR standard pulsed field gradient methods to measure diffusion in ionic liquids (ILs). Several ILs based on some well-known cations such as N-alkyl-N-methylpyrrolidinium (PY1R⁺) and newly synthesized fluorine and hydrogen-free anions such as 4,5-dicarbonitrile-1,2,3-triazole (DCTA⁻) were prepared by W. Henderson's group at NC State, as shown in Fig. 1.

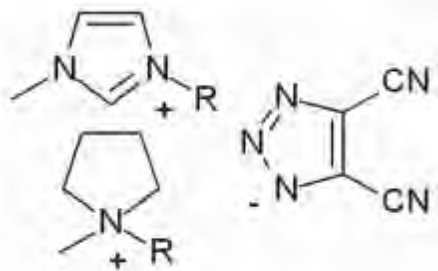


Figure 1. IL cation and anion structures studied in this work: 1-alkyl-3-methylimidazolium (IM10R⁺), N-alkyl-N-methylpyrrolidinium (PY1R⁺), and 4,5-dicyanotriazole-1,2,3-triazole (DCTA⁻), where R is an alkyl group (i.e. 2, ethyl; 3, propyl; 4, butyl).

The ¹³C direct detection (no cross polarization) spectrum of a representative IL, with spectral assignment is displayed in Fig. 2. The planar anion is believed to reduce cation-anion interactions and the absence of fluorine may be beneficial for safety reasons, but presents an NMR spectroscopic challenge.

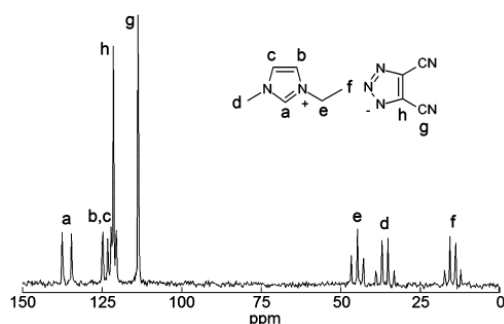


Figure 2. ¹³C NMR spectrum of IM₁₀₂ DCTA at 25°C.

By means of standard NMR pfg methods, but with about 8 hours of signal averaging per sample per temperature, we were able to measure the natural abundance ¹³C self-diffusion coefficients of the anions and cations. The values obtained for the cations were checked by the much more efficient proton NMR pfg and the good agreement obtained between ¹H and ¹³C values provide a strong measure of confidence for the anion values. [1]

We obtained single crystals of LiMPO₄ (M = Fe, Co, Ni, Mn) from colleagues at DoE Ames Lab and Iowa State University, which we then investigated by broad band NMR, including the use of a custom designed low field NMR apparatus necessitated by the very strong paramagnetic broadening and shifting characteristic of these compounds. [2] A ³¹P NMR rotation pattern about the [010] crystallographic axis of LiFePO₄ is shown in Fig. 3. The simulated spectra are in pretty good agreement with the experimental ones, with the major source of disagreement attributed to alignment error when moving the crystal from the x-ray diffractometer to the NMR spectrometer. Similar rotation patterns were obtained about the three orthogonal principal crystallographic axes in the Fe and Co analogues for both ³¹P and ⁷Li. Diagonalizing the NMR chemical shift tensor, one finds the principal axis system of the NMR nuclei and the direction cosines with respect to the crystallographic axes, depicted in Fig. 4 for ³¹P (not shown for ⁷Li). Interestingly, the Li tensor appears to be approximately diagonal in the crystallographic frame and the principal component of the nuclear electric quadrupole tensor (not shown) is along or nearly along [010], which coincidentally or not, is the direction of maximum Li ion mobility.

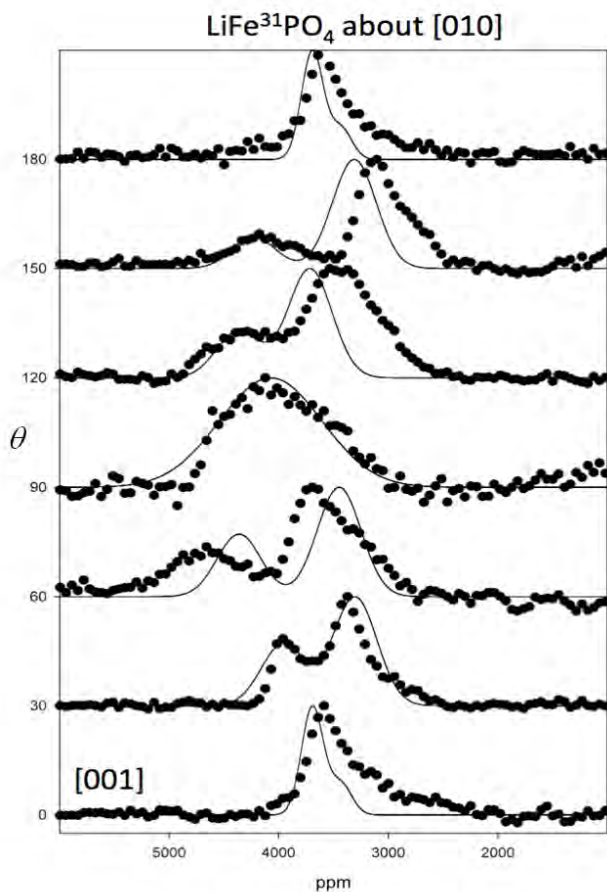


Figure 3. Representative ^{31}P resonances of a single crystal of LiFePO_4 rotated about $[010]$ as a function of rotation angle θ between $[001]$ and the magnetic field ($0^\circ \leq \theta \leq 180^\circ$). The solid line simulations were created using Gaussian functions

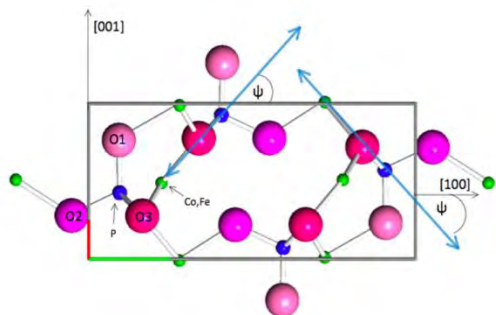


Figure 4. Phosphate sites in a 4-unit cell of the LiMPO_4 olivine lattice structure of space group $Pnma$. The view is along $[010]$ with phosphorus (blue), iron or cobalt (green), and oxygen (O1, O2, O3) atoms given. The fourth oxygen atom of the phosphate tetrahedron is structurally identical to O3 and directly behind O3 in this view. The largest paramagnetic principal axis is shown in the plane as the double arrow for the two phosphate sites, oriented at ψ relative to the $[100]$ direction. Note that the arrow closely follows the line defined by the P-O3-M arrangement.

Additional results, in collaboration with NASA/JPL, on characterization of SEI formation on lithium ion MCMB anodes using solid state ^7Li , ^{19}F , and ^{31}P NMR in cells containing various electrolyte additives and subjected to accelerated aging will be presented. [3]

Future Plans

The projects either currently underway or planned for the next 12 months are: (i) analysis of the Ni and Mn analogues of LiMPO_4 and discussion with theoreticians (e.g. Prof. Ceder, MIT) about using the magnetic data to augment the accuracy of calculations; (ii) using ^{13}C enriched carbonates to study SEI formation in BiF_3 conversion electrodes; (iii) investigating charge and mass transport in polymer/IL gel electrolytes; (iv) continued study of the effect of novel Li ion electrolytes on SEI formation; (v) beginning to investigate IL- Na salt mixtures for possible application in Na air batteries. (vi) synchrotron XAS study of CuS-based cathodes developed for 3D microbatteries. The last two projects are in collaboration with Tel Aviv University.

References

1. Publication #1 (below).
2. Publication #2 (below).
3. Publication #3 (below).

Publications (only published or accepted papers listed; grant started 9/2010)

“Diffusion Coefficients from ^{13}C PGSE-NMR Measurements— Fluorine-Free Ionic Liquids with DCTA^- and DCA^- Anions”, with Cristelle Portet, Sufia Khatun, Eric Fox, Patrick Judeinstein, Michel Armand, and Wesley Henderson, *Journal of Physical Chemistry Letters*, **3**, 441-444 (2012).

^7Li and ^{31}P Nuclear Magnetic Resonance Studies of Single Crystal LiMPO_4 ($M = \text{Co}, \text{Fe}$)”, with P. Sideris, R. Samuelli, P.E. Stallworth, and D. Vaknin, *Journal of the American Ceramic Society*, in press.

“Solid State Multinuclear Magnetic Resonance Investigation of Electrolyte Decomposition Products on Lithium Ion Electrodes”, with J.H.S.R. DeSilva, V. Udinwe, P.J. Sideris, M. C. Smart, F.C. Krause, C. Hwang, and K. A. Smith, *Electrochemical Society Transactions*, in press.

“Effect of Peptide Nanotube Filler on Structural and Ion-transport Properties of Solid Polymer Electrolytes”, with K. Goldstein, D. Golodnitsky, E. Peled, L. Adler-Abramovich, E. Gazit, and S. Khatun, *Solid State Ionics*, in press.

“Advanced Techniques to Elucidate Electrochemical Reactions in Lithium Ion Batteries”, with P.J. Sideris, *Encyclopedia of Sustainability Science and Technology*, Springer, in press.

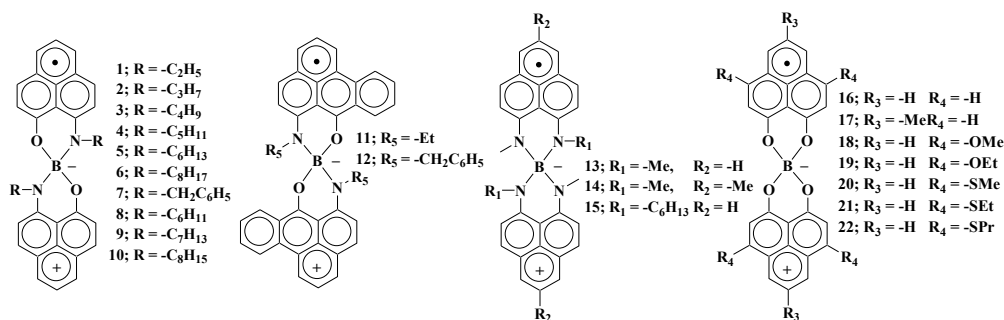
Solid State Electronic Structure and Properties of Neutral Carbon-Based Radicals

Robert C. Haddon, University of California, Riverside, CA, 92521

Program Scope

We have shown that neutral carbon-based radicals exhibit unusual conductivity, magnetic and optical properties, and our work is focused on the synthesis of suitably modified radicals in order to investigate the effect of electronic structure on the solid state properties of these compounds.

Scheme 1



Experimental work in our group has produced crystals of a new class of carbon-based radicals (**1** – **22**, Scheme 1), which has led to the discovery of a neutral organic solid with the highest conductivity yet reported. These compounds incorporate the phenalenyl (PLY) system as the molecular building block^[1] and they are spiro-conjugated at boron so that the spin density is delocalized over orthogonal π -systems in two dimensions.^[2] Crystals of **8** show the highest room-temperature conductivity ($\sigma_{RT} = 0.3$ S/cm), among the phenalenyl-based neutral radical conductors, a high-symmetry crystal structure and a metal-like temperature-independent Pauli paramagnetism.^[3]

Recent Progress

Benzannulated Phenalenyl Radical (12). We crystallized and characterized the first benzannulated phenalenyl (**12**) neutral radical conductor which shows unprecedented solid state properties: radical RVB (resonating valence bond) and σ -dimer CDW (σ -charge density wave) phases coexist over the whole temperature range (Figures 1 and 2).^[4] The structure is dominated by two sets of intermolecular interactions: (1) a π -chain structure with superimposed π -overlap of the benzannulated phenalenyls along [0 0 1], and (2) an inter-chain overlap involving a pair of carbon atoms (C4, C24) along [0 1 0]. The π -chain-type stacking motif is reminiscent of previously reported phenalenyl radicals and the room temperature structure (space group P2/c) together with the conductivity of $\sigma_{RT} = 0.03$ S/cm and the Pauli-like magnetic susceptibility are best described by the resonating valence bond (RVB) model. The inter-chain interaction is unstable with respect to the formation of a σ -charge density wave (σ -CDW) involving pairs of C4 carbon atoms between adjacent radicals (Figure 1) and this phase is characterized by the P2₁/c space group which involves a doubling of the unit cell along the [0 1 0] direction. The

RVB and CDW phases compete for structural occupancy throughout the whole temperature range (15 to 293 K) with the RVB phase predominating at 15 and 293 K and the σ -CDW phase achieving a maximum structural occupancy of about 60% at 150 K where it produces clearly discernible effects on the magnetism and conductivity (Figure 2).

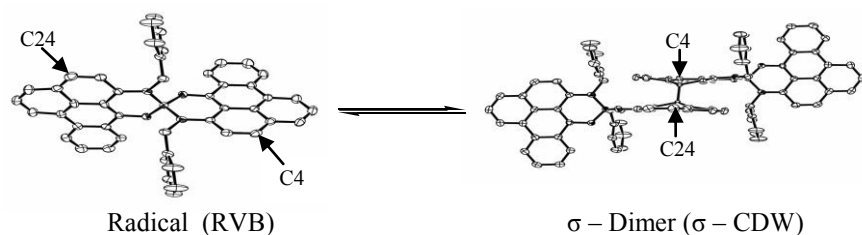


Figure 1. ORTEP drawing of radical **12** showing the carbon atoms with close interchain contacts (293 K), and the σ -dimer which forms by bonding of C4(C24) pairs of atoms (150 K).

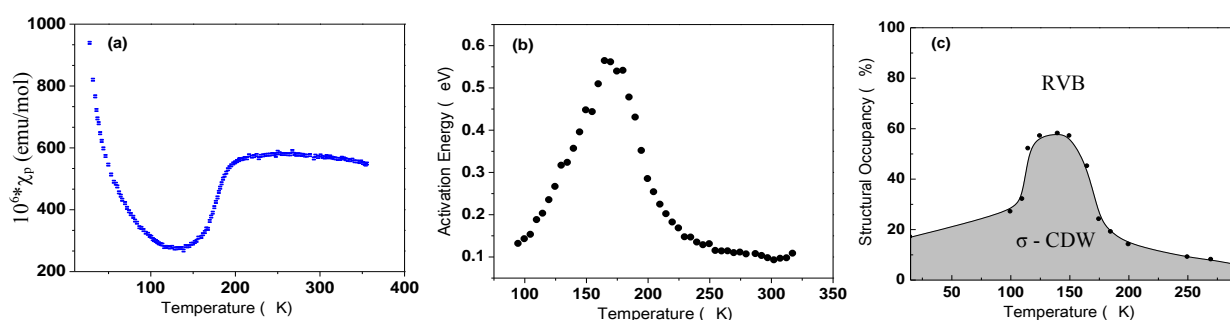


Figure 2. Variation of (a) magnetic susceptibility and (b) Activation energy of the conductivity of **12**. (c) Structural occupancy of RVB and σ -CDW phases.

Hysteretic Phase Transition in the Spiro-Biphenalenyl Radical (3). Previously we developed an experimentally based structural analysis to examine the degree of localization of the spin and charge in the phenalenyl-based neutral radical molecular conductors based on the relationship between bond order and bond length,^[5] and we used this method to investigate the solid state electronic structure and properties of the phenalenyl-based butyl-substituted neutral radical (**3**), which shows a hysteretic phase transition just above room temperature.^[6] We find two distinct electronic states in the hysteresis loop which accompanies the phase transition; by comparing the changes in the crystal structures of butyl radical and the related ethyl radical (**1**) at various temperatures, we showed that the change in the interplanar π - π distance within dimers is the most important structural parameter in determining the physical properties of the radicals. We suggest that the presence of a high temperature state inside the hysteresis loop during the cooling cycle is due to thermodynamic stability while the existence of the low temperature state during the heating cycle is due to the presence of a large energy barrier between the two states (estimated to be greater than 100 kJ/mol), as a result of the large amplitude motion of the phenalenyl rings and the associated lattice reorganization energy which is required at the phase transition (Figure 3).

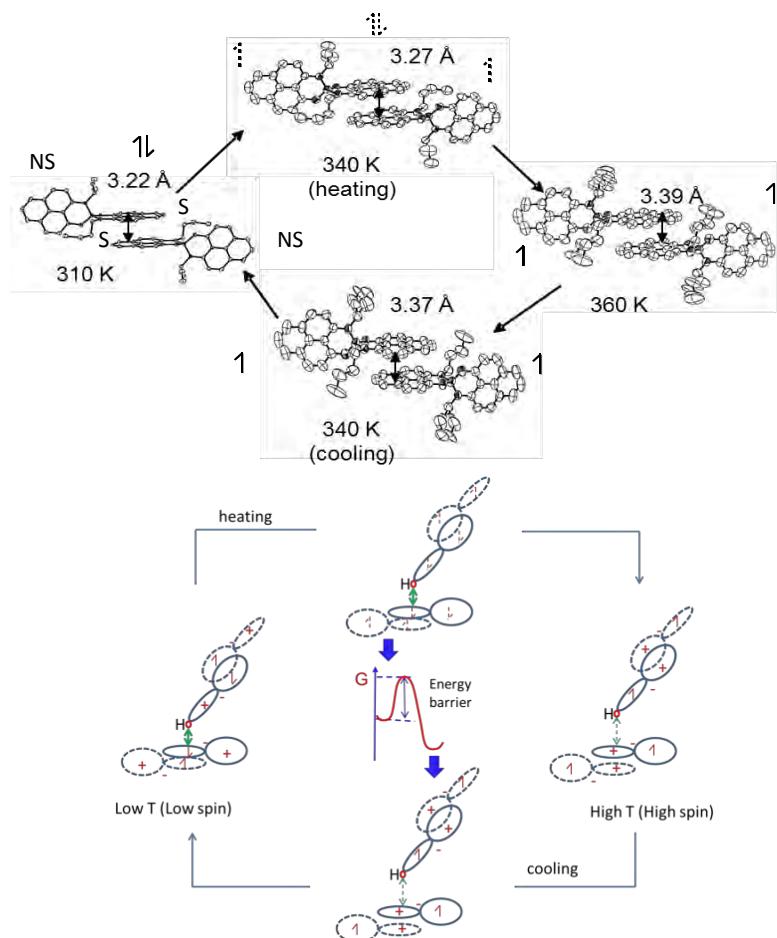


Figure 3. Top: ORTEP view of **3** at temperatures of 310 K, 340 K (heating and cooling), and 360 K showing superimposed PLY (S) and non-superimposed PLY (NS) within the dimer of **3** (radical **1** has similar π -dimers). The structures show the interplanar separations and the limiting spin and electron density distributions of the butyl radical (**3**) as a function of temperature; the center structures refer to the two branches of the hysteresis loop. Bottom: Schematic showing of the change of C-H \cdots π distance during the phase transition and the energy barrier that is responsible for the hysteresis in butyl radical (**3**).

Future Plans

We have recently developed a synthetic scheme which allows the introduction of alkylthio, disulfide and diselenide functionalities into the spiro-biphenalenyl boron neutral radical precursors, and we have crystallized the first sulfur containing radicals (**20** - **22**). The crystal structures of **21** and **22** show that the radicals exist as one dimensional (1-D) π -chains of superimposed phenalenyl units (Figure 4), and the molecular units pack more efficiently than the oxygen-substituted analogues (**18** and **19**).^[7-9] There are significant spin-spin interaction between the molecules along the π -chains and the room temperature electrical conductivities of both compounds are found to be $\sigma_{RT} = 1.5 \times 10^{-2}$ S/cm (Figure 4).

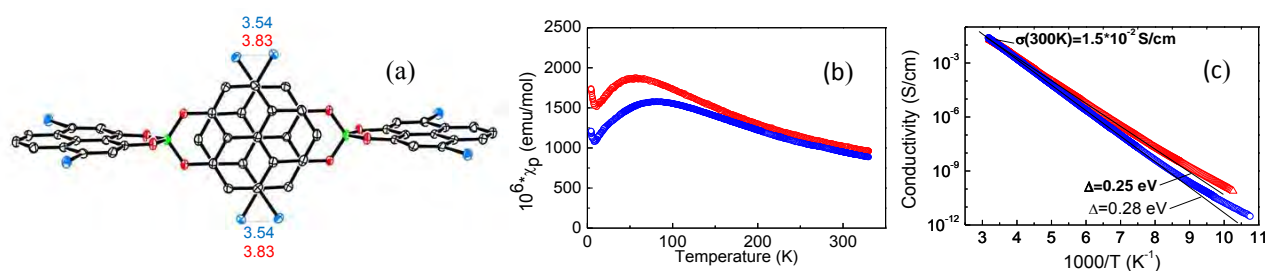


Figure 4. (a) Superimposed π -overlap, showing the close contact between the S-alkyl substituents. (b) Magnetic susceptibilities and (c) conductivities of **21** (blue) and **22** (red).

The introduction of sulfur and selenium into organic molecular conductors is well known to enhance the intermolecular interactions and electronic stabilization of various oxidation states

which results in improved solid state properties and thus we plan to explore additional sulfur and selenium derivatives. We also intend to increase the band-width of the spiro-biphenalenyl boron neutral radicals by pursuing the synthesis of additional benzo-derivatives (see **11** and **12**), and by application of pressure to some of the materials that exhibit particularly low conduction activation energies ($E_a < 0.1$ eV, **1**, **8**).^[3]

References

- [1] R. C. Haddon, *Nature* **1975**, *256*, 394.
- [2] R. C. Haddon, S. V. Chichester, J. H. Marshall, *Tetrahedron* **1986**, *42*, 6293.
- [3] S. K. Pal, M. E. Itkis, F. S. Tham, R. W. Reed, R. T. Oakley, R. C. Haddon, *Science* **2005**, *309*, 281.
- [4] P. Bag, M. E. Itkis, S. K. Pal, B. Donnadiou, F. S. Tham, H. Park, J. A. Schlueter, T. Siegrist, R. C. Haddon, *J. Am. Chem. Soc.* **2010**, *132*, 2684.
- [5] R. Haddon, A. Sarkar, S. K. Pal, X. Chi, M. E. Itkis, F. S. Tham, *J. Am. Chem. Soc.* **2008**, *130*, 13683
- [6] S. K. Pal, P. Bag, A. Sarkar, X. L. Chi, M. E. Itkis, F. S. Tham, B. Donnadiou, R. C. Haddon, *J. Am. Chem. Soc.* **2010**, *132*, 17258.
- [7] A. Sarkar, S. K. Pal, M. E. Itkis, P. Liao, F. S. Tham, B. Donnadiou, R. C. Haddon, *Chem. Mater.* **2009**, *21*, 2226.
- [8] A. Sarkar, M. E. Itkis, F. S. Tham, R. C. Haddon, *Chem. Eur. J.* **2011**, *17*, 11576.
- [9] A. Sarkar, F. S. Tham, R. C. Haddon, *J. Mater. Chem.* **2011**, *21*, 1574.

Publications

1. Bag, P.; Itkis, M. E.; Pal, S. K.; Donnadiou, B.; Tham, F. S.; Park, H.; Schlueter, J. A.; Siegrist, T.; Haddon, R. C., Resonating Valence Bond and σ -Charge Density Wave Phases in a Benzannulated Phenalenyl Radical. *J. Am. Chem. Soc.*, **2010**, *132*, 2684 - 2694.
2. Pal, S. K.; Bag, P.; Sarkar, A.; Chi, X.; Itkis, M. E.; Tham, F. S.; Donnadiou, B.; Haddon, R. C.; Hysteretic Spin and Charge Delocalization in a Phenalenyl-Based Molecular Conductor. *J. Am. Chem. Soc.*, **2010**, *132*, 17258 -17264.
3. Sarkar, A.; Itkis, M. E.; Tham, F. S.; Haddon, R. C., Synthesis, Structure, and Physical Properties of a Partial π -Stacked Phenalenyl-Based Neutral Radical Molecular Conductor. *Chem. Eur. J.*, **2011**, *17*, 11576 - 11584.
4. Kubo, T.; Katada, Y.; Shimizu, A.; Hirao, Y.; Sato, K.; Takui, T.; Uruichi, M.; Yakushi, K.; Haddon, R. C., Synthesis, Crystal Structure, and Physical Properties of Sterically Unprotected Hydrocarbon Radicals. *J. Am. Chem. Soc.*, **2011**, *133*, 14240 - 14243.
5. Sarkar, A.; Tham, F. S.; Haddon, R. C., Synthesis, Crystallization, Electrochemistry and Single Crystal X-ray Analysis of a Methoxy Substituted tris-Phenalenyl Based Neutral Radical. *J. Mater. Chem.*, **2011**, *21*, 1574 - 1581.
6. Sarkar, A.; Pal, S. K.; Itkis, M. E.; Tham, F. S.; Haddon, R. C., Sulfur and Selenium Substituted Spiro-Biphenalenyl-Boron Neutral Radicals. *J. Mater. Chem.*, **2012**, *22*, 8245 - 8256.

Controlling Magnetic and Ferroelectric Order Through Geometry-Synthesis, Ab Initio Theory, and Characterization of New Multi-Ferroic Fluoride Materials

Prof. P. Shiv Halasyamani, Department of Chemistry, University of Houston, 136 Fleming Building, Houston, TX 77204-5003

Prof. Craig Fennie, School of Applied and Engineering Physics, Cornell University, 224 Clark Hall, Ithaca, NY, 14853

Program Scope

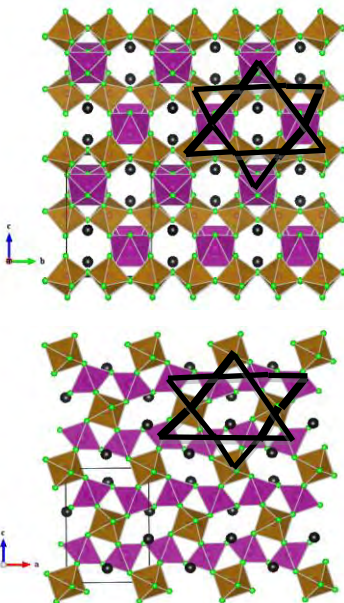
This research program involves the synthesis, crystal structure, characterization, and theory on new magnetically ordered mixed-metal fluoride materials. A major objective of the research is to develop the chemical and physical insight to rationally design new multi-functional multi-ferroic fluoride materials. These materials represent a promising class of EMO (electronic, magnetic, and/or optical) materials that respond in a technologically useful way to external stimuli, e.g., electric, magnetic, optical, and/or acoustic fields. Multi-ferroic materials are defined as possessing more than one ‘ferro’ property such as ferroelectricity, ferroelasticity, and ferro-, anti-ferro, or ferrimagnetism. As such, we will investigate new magnetically ordered geometric ferroelectric complex fluoride materials. Our approach involves a two-fold strategy: (i) bulk synthesis, crystal growth, and subsequent characterization (characterization will involve structural – powder and single crystal X-ray diffraction – and ‘non-structural’ – ferroelectric and magnetic susceptibility measurements) of new mixed-metal fluorides that are geometrically ferroelectric and exhibit magnetic ordering (Halasyamani), and (ii) first-principles theoretical studies of their structural, dielectric, and magnetic properties (Fennie). Ultimately, our goal is to develop new microscopic models that lead to the desired macroscopic properties in these magnetic-ferroelectric fluorides, as well as the routes to synthesize such materials. In combining such models with the basic tenets of crystal chemistry and symmetry principles, the development of a general set of design criteria is possible that, in the spirit of the 2007 DOE BESAC Grand Challenges report, will aid in the identification of new multi-ferroic fluorides with the desired properties built-in from the bottom-up, i.e., from a model to a real material. When combined with first-principles computational methods, these design criteria provide a powerful tool to survey the vast space of possible materials in order to select the most promising candidates that will exhibit geometric ferroelectricity and magnetic ordering.

Recent Progress

We recently developed a low temperature hydrothermal method for the synthesis of mixed-metal fluorides.¹ We demonstrated this method through the selective pure-phase synthesis

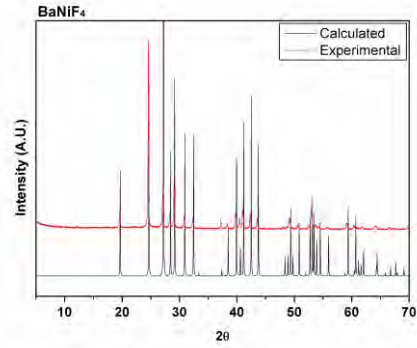
of the multi-ferroic BaMF₄ (M = Mg, Mn, Co, Ni, and Zn) family. The method consists of combining BaF₂, MF₂ (M = Mg, Mn, Co, Ni, or Zn), CF₃COOH, and H₂O in a small autoclave (23 ml). The autoclave is closed, heated to 230°C for 24h, and cooled slowly to room temperature. Pure and polycrystalline BaMF₄ is recovered in 70-80% yields, based on BaF₂ (see Figure).

Using this synthetic method, we synthesized a new charge-ordered magnetically frustrated mixed-metal fluoride with a pyrochlore-related structure.² The material, RbFe₂F₆ (RbFe²⁺Fe³⁺F₆) was synthesized through mild hydrothermal conditions. The materials exhibit a three-dimensional pyrochlore-related structure consisting of corner-shared Fe²⁺F₆ and Fe³⁺F₆ octahedra (see Figure). In addition, Kagome-type nets are observed in both the ac- and bc-planes.



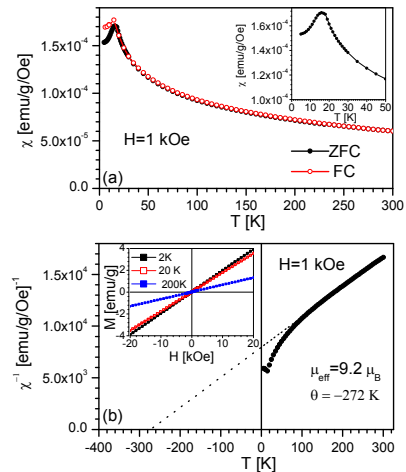
RbFe₂F₆ in the ac- and bc-planes – note the Kagome-nets (black lines) in both planes.

calculations using the Kugel-Khomskii model⁴ identified four most essential Fe-Fe exchange integrals (J₁-J₄) that define the underlying magnetic structure of the system (see Figure). All the exchange integrals are found to be antiferromagnetic in nature and their calculated magnitudes (see Table) show that the orthorhombic distortion of the crystal structure of the material lifts the magnetic frustration of the system partially, however not completely. The estimated Curie-Weiss temperature within mean field theory was -281 K, which is in good agreement with the experimental value.



Calculated (black) and experimental (red) powder X-ray diffraction data for BaNiF₄.

Magnetic data clearly reveal strong antiferromagnetic interactions (a Curie-Weiss temperature of -270K) but sufficient frustration to prevent ordering until 16K (see Figure). A frustration ratio, Θ/T_N , of 17 was determined. No structural phase transformation was detected from the variable-temperature neutron diffraction data. First-principles density functional theory (DFT) calculations confirmed the charge ordered insulating state of the material. The

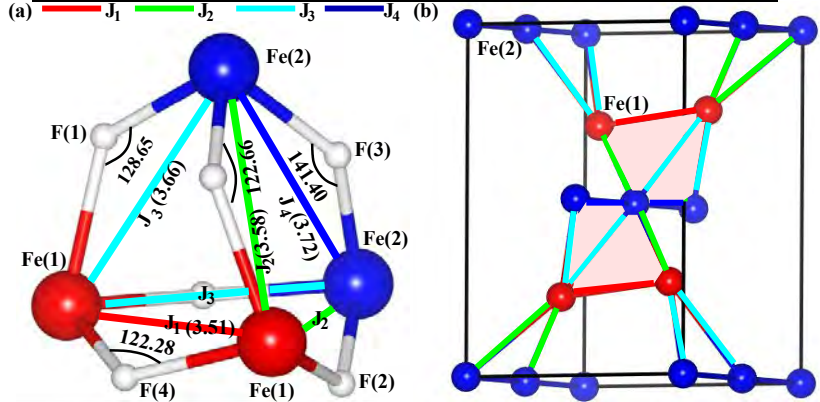


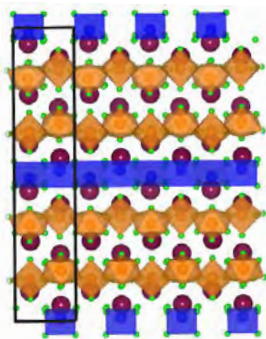
Temperature dependence of (top) the dc magnetic susceptibility measured at 1 kOe (after zero field and field cooling), and (bottom) the inverse magnetic susceptibility with a Curie-Weiss fit (dotted line).

J_1	-0.9
J_2	-0.7
J_3	-1.5
J_4	-1.7

The calculated magnetic exchange integrals (J) in meV are listed.

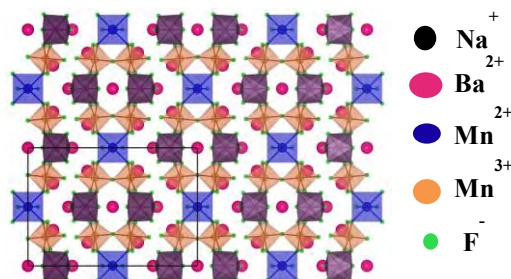
The Fe_4 tetrahedron unit (a) and the magnetic unit cell (b), that consists of a connected network of Fe_4 tetrahedra (pink shaded region).



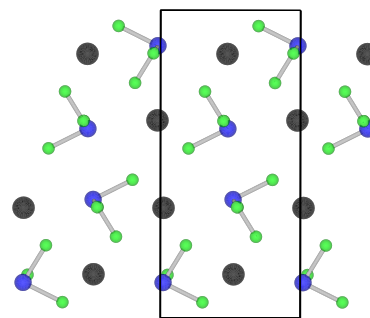


Using this synthetic technique, we have also synthesized $\text{Ba}_3\text{Mn}_3\text{F}_{14}$ and $\text{Ba}_7\text{NaMn}_7\text{F}_{34}$. The former exhibits a layered crystal structure (see Figure left), with Mn^{2+} and Mn^{3+} on distinct crystallographic sites. With $\text{Ba}_7\text{NaMn}_7\text{F}_{34}$, both Mn^{2+} and Mn^{3+} are observed, however crystallographic disorder occurs on one site (see Figure). With both materials, synthetic efforts are continuing toward phase-pure synthesis. Magnetic measurements and

theoretical calculations are also in progress.



We have also recently synthesized CsSnF_3 . This is a rare example of a Sn(II) fluoride material. The material was synthesized by a low temperature solvothermal route, and uses methanol as the solvent instead of water. The structure consists of discrete $(\text{SnF}_3)^-$ anions that are separated by Cs^+ cations (see Figure). Theoretical calculations exploring the structure and bonding of this compound, including a comparison to CsPbF_3 (which is known to form in a distorted perovskite) are currently underway.



Future Plans

In addition to the above:

1. We plan to expand our synthetic efforts. The following systems are planned for investigation:
 - a. Tetragonal tungsten bronze (TTB) fluorides: A polar TTB fluoride that is known is $\text{K}_3\text{Fe}_5\text{F}_{15}$ ³ that contains an ordered arrangement of both Fe^{2+} and Fe^{3+} cations. We plan to substitute the Fe^{2+} cations with other M^{2+} cations, e.g., Ni^{2+} , Cu^{2+} , and Zn^{2+} , and investigate their multi-functional behavior.
 - b. Materials related to the mineral Coulsellite ($\text{CaNa}_3\text{AlMg}_3\text{F}_{14}$): The Mg^{2+} cations form Kagome-type nets in the structure. We plan to replace the Mg^{2+} cation with transition metal cations with unpaired electrons, e.g., Mn^{2+} , Fe^{2+} , Co^{2+} , Ni^{2+} , and Cu^{2+} . In doing so, a magnetically frustrated material will be created.
2. Our theoretical effort will follow to main themes:

- a. Continue to explore the physics and chemistry of new compounds synthesized by our experimental colleagues
- b. Materials Genome initiative: In the spirit of the recently discussed Materials Genome initiative we will create databases of known fluoride compounds and apply an approach we are developing based on first-principles calculations and Bond-Valence approach to mine the data to help point the way to new multiferroic fluorides. Some specific systems include layered perovskites, for example, comparing the compounds that form in the polar ABO_4 (e.g., $BaMF_4$ compounds) and those that form in the non-polar, $TlAlO_4$ structure.

References

1. Kim, S. W., Chang, H. Y., Halasyamani, P. S., *J. Am. Chem. Soc.*, **2010**, *132*, 17684-17685.
2. Kim, S. W., Kim, S.-H., Halasyamani, P. S., Green, M. A., Bhatti, K. P., Leighton, C., Das, H., Fennie, C. J., *Chem. Sci.*, **2012**, *3*, 741-751.
3. Ravez, J., *J. Physique III*, **1997**, *7*, 1129-1144.
4. K. I. Kugel and D. I. Khomskii, *Sov. Phys. Usp.* *25*, 231 (1982).

Publications

“Selective Pure-Phase Synthesis of the Multiferroic $BaMF_4$ ($M = Mg, Mn, Co, Ni, \text{ and } Zn$) Family”, Sun Woo Kim, Hong Young Chang, and P. Shiv Halasyamani, *J. Am. Chem. Soc.*, **2010**, *132*, 17684-17685.

“ $RbFe^{2+}Fe^{3+}F_6$: Synthesis, structure, and characterization of a new charge-ordered magnetically frustrated pyrochlore-related mixed-metal fluoride”, Sun Woo Kim, Sang-Hwan Kim, P. Shiv Halasyamani, Mark A. Green, Kanwal Preet Bhatti, C. Leighton, Hena Das, and Craig J. Fennie, *Chem. Sci.*, **2012**, *3*, 741-751.

Crystallization-driven assembly of conjugated-polymer-based nanostructures

Ryan C. Hayward, Department of Polymer Science & Engineering, University of Massachusetts Amherst

Program Scope

The goal of this project is to harness solution-state crystallization of conjugated polymers to construct well-defined nanoscale building blocks that will facilitate fabrication of optoelectronic devices, especially photovoltaic cells, in scalable and cost-effective ways. We seek to ultimately control the organization, and therefore the electronic properties, of matter on length-scales spanning: (i) the molecular, to achieve highly crystalline semiconducting polymer-based materials capable of efficient charge transport, (ii) the nanoscale, to position electron donating and accepting materials with domain sizes comparable to exciton diffusion lengths (~ 10 nm) to facilitate charge separation, and (iii) the colloidal scale, such that well-defined crystalline nanoscale building blocks can be hierarchically organized into device layers with optimal structures.

Recent Progress

In collaboration with the Emrick group at UMass, we have recently developed an approach to self-assemble hybrid organic/inorganic donor/acceptor semiconducting nanowires through solution-state crystallization of conjugated polymers [1]. In short, we rely on the well-known assembly of poly(3-hexyl thiophene) (P3HT) into nanowire or fibril structures induced by a reduction in solvent quality. When this crystallization-driven assembly process is conducted in the presence of CdSe nanorods grafted with appropriate P3HT ligands, these ligand polymers can be incorporated into the growing polymer nanowire. We have shown that this process yields closely associated hybrid assemblies with nanorods flanking the edges of polymer fibrils. While effective, this method suffers from several key limitations, including the synthetic challenges to prepare P3HT-grafted CdSe nanorods, the slow kinetics of assembly (requiring nearly 1 week to reach completion, compared to < 1 day for pristine P3HT fibrils), and the relatively short lengths of hybrid structures (< 1 micrometer, compared to many μ meters for pristine fibrils). We hypothesize that the latter two effects are the result of steric frustration of the growing P3HT fiber by the presence of nanorods at the crystal face. When a nanorod first has a polymer ligand “captured” by the crystal, it will be largely immobilized in front of the crystal surface, where the remaining polymer ligands (~ 100 per nanorod) may partially shield the crystal face, thereby slowing the rate of addition of polymer chains.

Motivated by this hypothesis, we focused our recent efforts on an improved alternative route based on polymers end-functionalized with a group capable of serving as a ligand for CdSe nanoparticles, in particular a thiol or phosphonic acid [2]. This polymer is then induced to form crystalline nanowires by a reduction in solvent quality, where we anticipate that the chain ends will be largely excluded to the edges of the polymer fibril. In this case, the nanowire sides should be densely coated with ligand functionalities that can be used in a subsequent “ligand exchange”, whereby CdSe nanoparticles or nanorods coated with their native alkane ligands (trioctyl phosphine oxide, TOPO) adsorb onto the fibril. Notably, the synthetic steps required are simpler and more robust than those required to prepare nanoparticles with directly grafted P3HT ligands.

As shown in Figure 1, this two-step method is successful for generation of hybrid CdSe/P3HT assemblies. In addition to single fibrils flanked by nanoparticles, we generally observe a high incidence of larger structures consisting of multiple alternating “lanes” of polymer fibrils interspersed with nanoparticles. Such structures are consistent with the proposed mechanism of assembly, as a single nanowire flanked by adsorbed particles would present exposed CdSe-TOPO surfaces on its edges, thus rendering it strongly attractive towards adsorption of another P3HT fibril. Photoluminescence measurements indicate that fluorescence from the CdSe nanoparticles is almost completely quenched upon formation of hybrid assemblies, though whether this reflects energy transfer, charge transfer, or both remains to be determined.

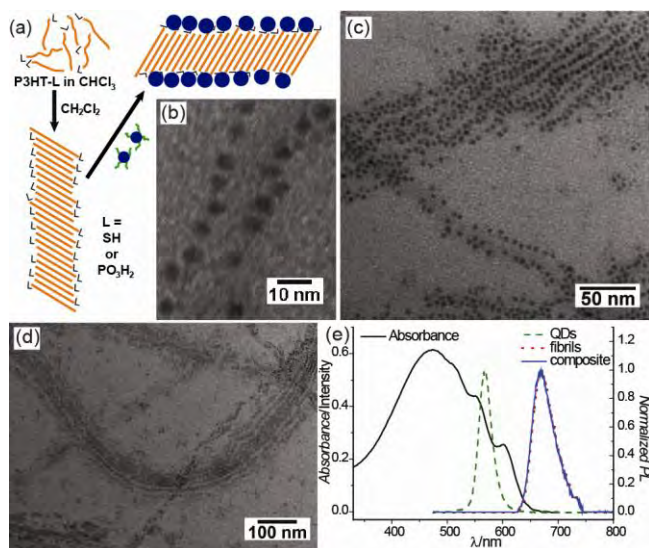


Figure 1. (a) Schematic illustration of hybrid nanowire assembly by nanoparticle adsorption to ligand-functionalized polymer nanowires. (b) – (d) TEM images showing individual fibers flanked by CdSe nanoparticles and larger scale “superhighway” bundles. (e) UV-vis absorbance of composites, and photoluminescence spectra.

Future Plans

Our ongoing work and plans for the near future are focused on three main areas: (i) improving our understanding and control of nucleation and growth kinetics in solution state crystallization of semiconducting polymers and small molecules, (ii) generalization of strategies to form hybrid donor/acceptor nanowires to other types of organic acceptors and different donor polymers, and (iii) characterization of the photophysical properties of the resulting hybrid

nanostructures through a combination of ensemble techniques (including transient absorption and fluorescence upconversion) and single-nanostructure characterization methods.

References

[1] F.A. Bokel, P.K. Sudeep, E. Pentzer, T. Emrick, R.C. Hayward, *Macromolecules*, **44**, 1768-1770 (2011).

[2] E.B. Pentzer, F.A. Bokel, R.C. Hayward, T. Emrick, *Advanced Materials*, **24**, 2254-2258 (2012).

Publications

E.B. Pentzer, F.A. Bokel, R.C. Hayward, T. Emrick “Nanocomposite "Superhighways" by Solution Assembly of Semiconductor Nanostructures with Ligand-Functionalized Conjugated Polymers”, *Advanced Materials*, **24**, 2254-2258 (2012).

i) Program Scope Our DOE program, entitled ‘Quantum Dot and Quantum Wire Solids’, has generally focused on two related topics. First, we are developing nanomaterials based platforms for various applications related to energy efficiency and energy conversion, with particular attention towards understanding the role the phonon physics plays in the performance metrics of finite sized systems. Second, we have been investigating, also in nanomaterials, the surface science of weakly bound adsorbates, and how those adsorbates influence physical properties at the nanoscale. These two areas are intimately connected in multiple ways. For example, many energy associated applications of nanomaterials, ranging from superconductors to thermoelectrics to photovoltaics, rely on precisely controlling charge carrier locations, mobilities, and concentrations. For high surface-to-volume nanomaterials, this requires one to pay strict attention to surface chemistries and other passivation techniques, and phenomena such as adsorbed water can strongly influence the ultimate performance metrics of a device. For my presentation, I will briefly provide examples of some of the nanomaterials/devices that we have built and tested, and say a few words regarding how surface chemistries and surface passivations influence the performance metrics. I will spend the bulk of my presentation discussing surface science at the nanoscale.

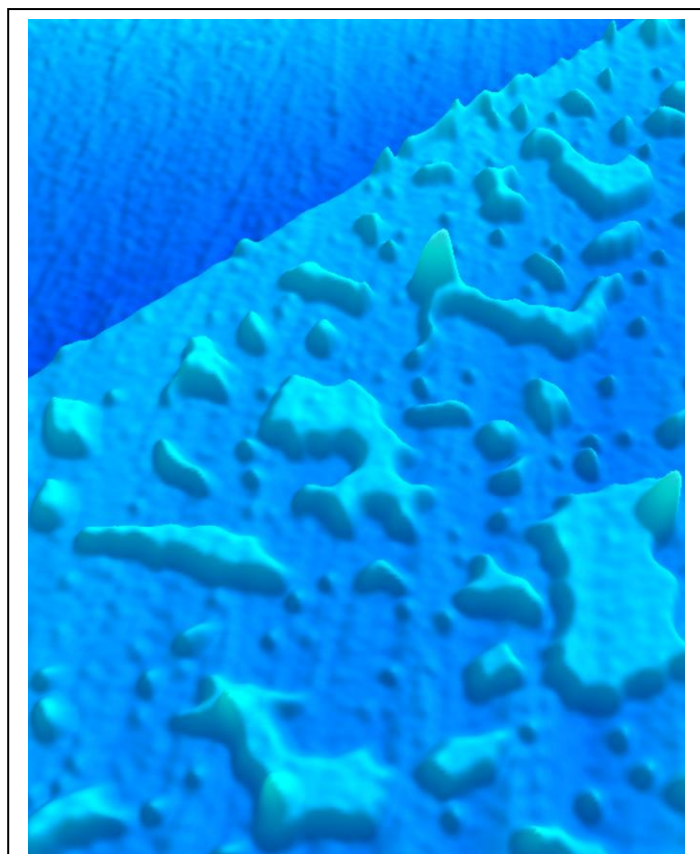
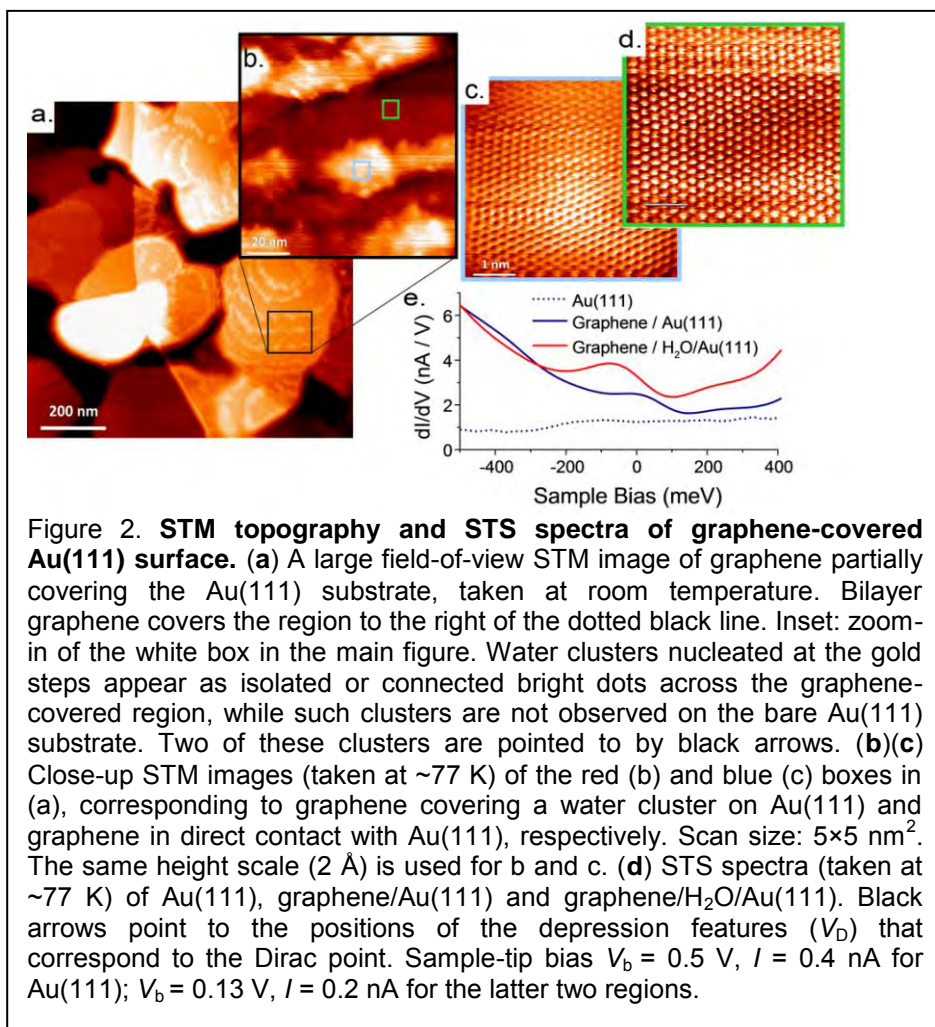


Figure 1. Graphene templating reveals the structures of 2-molecule thick ice crystals on mica, as measured under ambient conditions and 40% relative humidity. The flat region at top left is beyond the edge of the templating graphene sheet, and in that region, water can not be imaged using standard probe microscopy techniques. (from Xu, et al., *Science*, 2010)

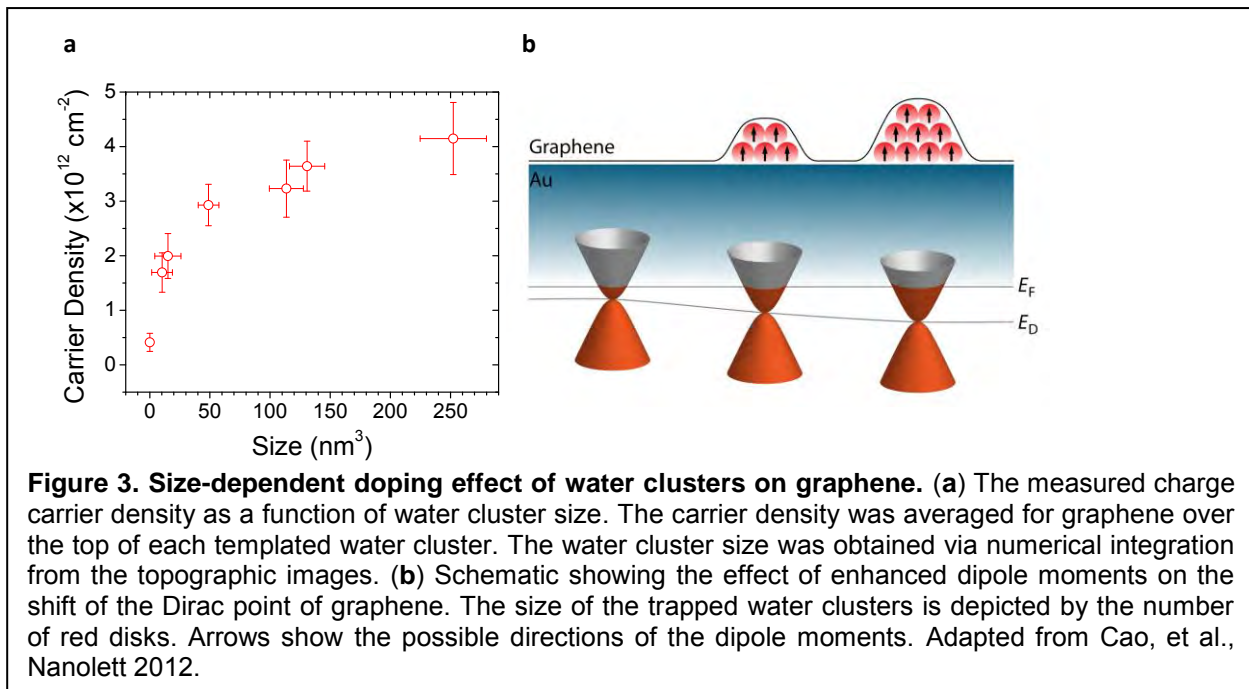
ii) Recent Progress Over the past two years we have discovered and developed the technique of graphene templating as an approach towards investigating the molecular structure of weakly bound surface adsorbate layers (Xu, et al., *Science*, 2010; Cao, et al., *JACS* 2011; Cao, et al., *Nanolett.* 2011), as well as an approach towards understanding how such adsorbates influence the electronic properties of nanomaterials (Cao, et al., *Nanolett.* 2012). The technique itself is simple in concept. Weakly adsorbed adlayers, especially under ambient conditions, have been historically very difficult to study, because their fragile nature. The method of graphene templating relies on the surface-conformal layer of single (or few-layer) graphene sheets. Depositing a graphene sheet onto a surface that has been exposed to, for example, water vapor at a known humidity, preserves and protects the adsorbed water layer, and allows the structure of that layer to be directly imaged. We used the technique to demonstrate that water adsorbed onto at least certain hydrophilic surfaces has an ice-like



state film growth mechanisms that are observed in semiconductor processing and, in fact, often used to grow quantum dots on surfaces. We also investigated water adsorption on a series of hydrophobic surface in an attempt to address a long-standing question regarding why hydrophobic surfaces can have as much adsorbed water as do hydrophilic surfaces. We investigated 3 hydrophobic surfaces: graphite, H/Si(111), and organically functionalized mica. The details of what adsorbed water structure varied significantly from surface to surface, but there were also striking similarities. We found that, on each surface, the water adsorbed as nanoscale droplets with very low contact angles, onto defects and step edges. We also found that, although the adsorbed water structures varied widely between hydrophilic and hydrophobic surfaces, the actual amount of adsorbed water was very similar. The observations on both hydrophilic and hydrophobic surfaces were wholly consistent with a significant amount of previous literature, but permitted a significantly higher resolution investigation of this surface chemistry (see Xu, et al., Science 2010; Cao, et al., JACS 2011; Cao, et al., Nanolett 2011 and references within). The net results highlighted that surface science at the nanoscale can be very, very different from that observed at the macroscopic level.

Very recently, we turned the approach around to interrogate how adsorbed water influences the electronic structure of graphene (Fig 2). For those experiments, we templated adsorbed water on Au(111) surfaces, and interrogated the system using scanning tunneling

structure, even under ambient condition (Figure 1). As relative humidity is increased, a single layer of ice, two water molecules thick, and of the same crystal structure as common ice, extends to cover the entire surface. At high relative humidities, a second layer forms, but, before it is complete, nanoscale water droplets are formed. Similar, but distinct, phenomena was observed for weakly adsorbed organic molecules (THF and hexane). The growth of these adlayers thus somewhat resembles the various heteroepitaxial solid-



microscopy. We attempted to resolve the following conundrum: it has been known for several years that water adsorbed onto graphene can alter its electrical properties. In seeming contradiction to (macroscopic) transport experiments,^{4,5} density functional theory calculations have shown that there were no doping effects for *single* water molecules on freestanding graphene.^{6,7} However, an electrostatic-field-mediated doping mechanism has been proposed basing on the enhanced dipole moments of water *clusters*.^{6,8} This model potentially closes the gap with experiment.. We were able to interrogate the influence of templated water clusters of varying sizes, and we found a strong size dependence, indicating that the smallest water clusters (<10 nm³) barely influenced the graphene electronic structure, while clusters larger than 50 nm³ exerted a strong influence (Fig 3).

iii) Future Plans We are beginning to investigate the influence of surface adsorbed water on surface frictional propertie, as well continuing to investigate the influence of adsorbates on the electronic structure of nanomaterials. We are also investigating precisely integrated quantum dot/nanowire systems for energy conversion applications. Early work on constructing such systems can be found in Guo, et al., 2012.

References

1. Martin, J.; Akerman, N.; et al., *A. Nat. Phys.* **2008**, *4*, 144.
2. Zhang, Y. B.; Brar, V. W.; Girit, C.; Zettl, A.; Crommie, M. F. *Nat. Phys.* **2009**, *5*, 722.
3. Deshpande, A.; Bao, W.; Zhao, Z.; Lau, C. N.; LeRoy, B. J. *Appl. Phys. Lett.* **2009**, *95*, 243502.
4. Novoselov, K. S.; Geim, A. K.; et al. *Science* **2004**, *306*, 666.
5. Schedin, F.; Geim, A. K.; Morozov, S. V. Et al., *Nat. Mater.* **2007**, *6*, 652
6. Wehling, T. O.; Katsnelson, M. I.; Lichtenstein, A. I. *Chem. Phys. Lett.* **2009**, *476*, 125.
7. Leenaerts, O.; Partoens, B.; Peeters, F. M. *Phys. Rev. B* **2008**, *77*, 125416.
8. Wehling, T. O.; Lichtenstein, A. I.; Katsnelson, M. I. *Appl. Phys. Lett.* **2008**, *93*, 202110.

Publications over Past Two Years Acknowledging DOE BES Support

1. Ke Xu, Peigen Cao, and James R. Heath, Achieving the theoretical depairing current limit in superconducting nanomesh films", *Nanolett.* **11**, 4206-4210 (2010).
2. Jen Kan Yu; Mitrovic, S; Tham D; Varghese J; Heath JR. "Thermal Conductivity Reduction in Phononic Nanomesh Films." *Nat Nanotech*, **5**, 718 (2010). doi:10.1038/nnano.2010.149 21 citations
3. Ke Xu, Peigen Cao, and James R. Heath. "Graphene Visualizes the First Water Adlayers on Mica at Ambient Conditions." *Science*, **329**, 1188 (2010) DOI: 10.1126/science.1192907 [link to article](#). [link to Science perspective](#)
4. Douglas Tham and James R. Heath. "Ultra-Dense sub-wavelength nanowire array photovoltaic as engineered optical thin films." *NanoLetters*, **10**(11), 4429-4434. DOI: 10.1021/nl102199b. [link](#)
5. Peigen Cao, Ke Xu, Joseph O. Varghese, and James R. Heath. "Atomic Force Microscopy Characterization of Room-Temperature Adlayers of Small Organic Molecules Through Graphene Templating." *J. Am. Chem. Soc.* (communication) **133**(8) 2334 (2011).
6. Ru Guo Huang, Douglas Tham, Dunwei Wang, and James R. Heath. Ring Oscillators from Enhancement-mode 10 nm Width Silicon Nanowire FETs. *Nano Research* **4**, 1005-1012 (2011). DOI 10.1007/s12274-011-0157-2. [link to article](#)
7. P. Cao, K Xu, J.O. Varghese, J. R. Heath. The microscopic structure of adsorbed water on hydrophobic surfaces under ambient conditions. *Nanolett.* **11**, 5581-5586 (2011). [link](#)
8. P. Cao, JO Varghese, K Xu, and J.R. Heath. Visualizing Local Doping Effects of Individual Water Clusters on Gold(111)-Supported Graphene. *NanoLett* **12**(3) 1469-1463 (2012) doi: 10.1021/nl2041673.
9. Huang RG and Heath JR Silicon Nanowire Charge-Trap Memory Incorporating Self-Assembled Iron Oxide Quantum Dots. Submitted 4/2012.

Charge Recombination, Transport Dynamics, and Interfacial Effects in Organic Solar Cells

Alan J. Heeger, Guillermo C. Bazan, Thuc-Quyen Nguyen, Fred Wudl

Departments of Chemistry, Materials and Physics, University of California, Santa Barbara, CA 93106

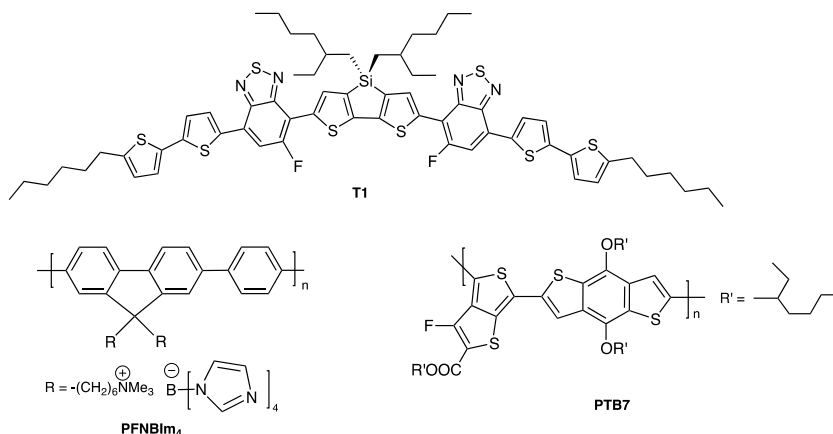
Program Scope

The objective of this project is to take advantage of new device strategies, function-specific materials, and interfacial phenomena to improve the performance (open circuit voltage, short circuit current, fill-factor and power conversion efficiency) of polymer-based photovoltaic devices fabricated by processing all layers from solution. Fundamental understanding of charge generation, transport, and recombination dynamics in thin film bulk heterojunction (BHJ) polymer:fullerene blends and in solar cells made from such BHJ blends will be studied using transient photoconductivity and impedance spectroscopy. Light intensity and temperature-dependent current-voltage measurements will reveal the charge recombination kinetics. Devices utilizing conjugated polyelectrolyte (CPE) and oligoelectrolyte interlayers to improve open-circuit voltage and fill factor will be explored with an emphasis on establishing a deeper understanding of the working mechanism. New CPEs and oligoelectrolytes will be synthesized and their functions as interlayers in BHJ solar cells will be investigated. Sensitive probes and experimental methods that enable detailed characterization of the interfaces, the local molecular organization and the charge generation at the nanoscale will provide details of the structure/property relationships across multiple length scales.

Recent Progress

1) Improve Bulk Heterojunction Solar Cell Performance Using a Conjugated Polyelectrolyte Interlayer and Solvent Treatment of the Active Layer

Among the performance-limiting factors of organic solar cells, the nature of the contact between the top electrode and the active layer has not been explored thoroughly. The characteristics of this contact influences all aspects of device performance, such as the fill factor (FF), short-circuit current (J_{SC}), and open-voltage (V_{OC}), and there is much to be done to understand at a fundamental level and improve this facet of device design. For conjugated polymer-based solar cells, different metal cathodes and the use of a thin interlayer between the cathode and the active layer such as LiF, ferroelectric random copolymers, conjugated polyelectrolyte (CPE), oligoelectrolyte, or metal oxide (ZnO and Cs_2CO_3) have been shown to improve the device performance.



We have recently

Scheme 1. Relevant molecular structures.

obtained universal improvements in solar cell performance through the use of a CPE material, PFN⁺BIm₄⁻, as a cathode interlayer for solution processed small molecule-based BHJ solar cells with a device structure: ITO/PEDOT:PSS/T1:PCBM/PFN⁺BIm₄⁻/Al. See Scheme 1 for description of molecular structures. It is worth noting that this work is the first demonstration of CPE enhancement of a high efficiency small molecule device. The addition of a PFN⁺BIm₄⁻ interlayer increased power conversion efficiency with a thermally evaporated Al cathode from 4.8% to 7.0%, a result of improved V_{OC} from 0.72 V to 0.81 V, J_{SC} from 11.3 mA/cm² to 12.2 mA/cm², and a large improved in the FF from 58.4% to 70.5% (Table 1).

Table 1. Device characteristics of control device (T1:PCBM/Al) and devices with solvent treatment (T1:PCBM/MeOH treatment/Al) and CPE interlayer (T1:PCBM/CPE/Al) and contact angle measurements of the films without the Al cathode.

Device	J _{SC} (mA/cm ²)	V _{OC} (V)	FF (%)	PCE (%)	Contact Angle
T1:PCBM/Al	11.3	0.72	58.4	4.8	168°
T1:PCBM/MeOH treatment/Al	12.0	0.80	66.1	6.4	170°
T1:PCBM/CPE/Al	12.2	0.81	70.5	7.0	97°

Contact angle and XPS measurements confirm the presence of the CPE interlayer atop of the BHJ active layer. For samples spin-coated with CPE solution, we observed an average contact angle of 97° (hydrophilic surface), while those without CPE interlayer had an average contact angle of 168° (hydrophobic surface). To our surprise, we also observe a noticeable increase in device performance for solvent treatment of the active layer (i.e., by simply spin-coating methanol without CPE atop the active layer). While the solvent control yields modest improvements in FF and J_{SC}, a nearly equal improvement in V_{OC} is observed. The result is suggestive of a multi-faceted effect involving both solvent modification of the BHJ properties and the nature of the organic/cathode interface.

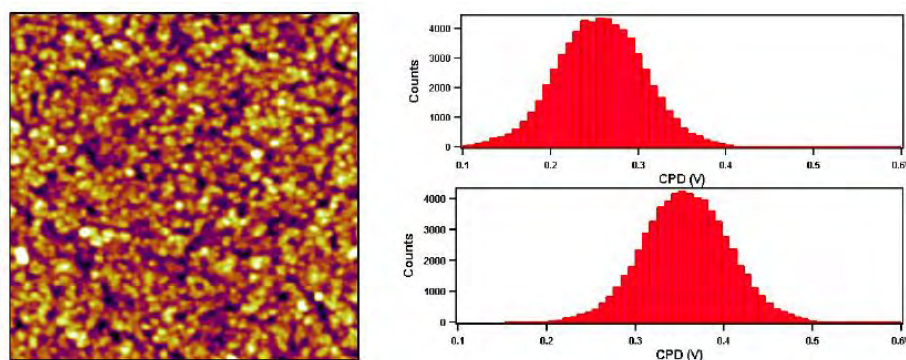


Figure 1. A 5µm x 5µm tapping mode image of the methanol-treated surface, with contact potential difference histograms as measured by SKPM of control (top right) and methanol-treated (bottom right) devices.

Solvent treatment also leads to improvement of polymer-based BHJ solar cell performance. We observe that a significant increase in fill factor, along with improvements in J_{SC} and V_{OC}, can be obtained with solvent treatment, with the best devices reaching a PCE of 8.0%.

This result shows that, for the low bandgap polymer (PTB7):PCBM system, interactions between solvent and active layer may be just as critical as contributions from a thin CPE interlayer. We have performed photo-conducting AFM (pc-AFM) and scanning Kelvin probe microscopy (SKPM) on active layer surfaces for control and solvent treated PTB7:PCBM solar cells in the area between evaporated Al cathodes. Methanol treated devices exhibit no distinct changes in topography after treatment. However, the photocurrent collected at 0 V is almost double for the methanol treated device. SKPM surface potential histograms (Figure 1) show a 100 meV shift in contact potential difference for the methanol treated device. Our preliminary results indicate that the solvent treatment of the active layer lead to higher photocurrent and surface potential than that of the control device.

In another approach to enhance the PCE of BHJs by interfacial control, we designed fullerene assembly directing molecules. An example is shown in Figure 2 in the form of a diheptyl ether **2**.

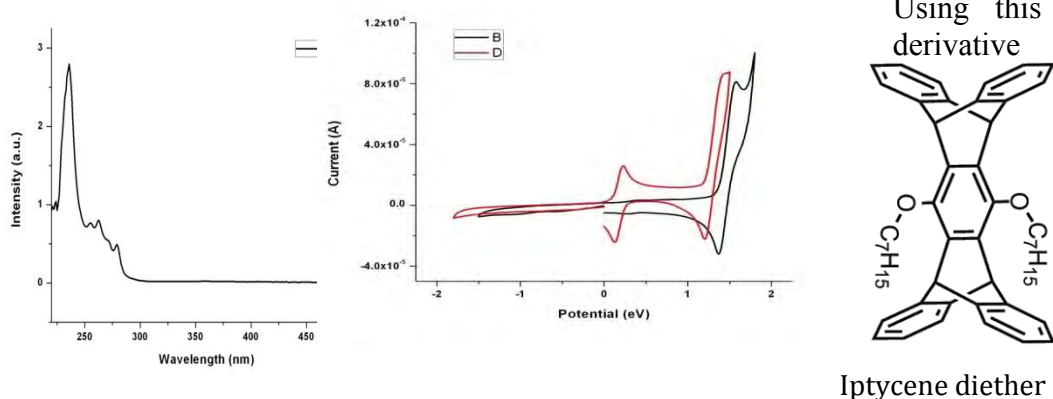


Figure 2 UV-vis spectrum, cyclic voltammetry and electronic levels of

2

additive in 16% relative to PCBM (Figure 4), produces an enhancement of ca 20% in PCE of a P3HT PCBM photovoltaic device.

2) A Solution Processed MoO_x Anode Interlayer for Use within Organic Photovoltaic Devices

The MoO_x layer gives excellent results as shown recently with the new small molecule donors where 7% efficiency was demonstrated.

3) Manifestation of carrier relaxation through the manifold of localized states in PCDTBT:PC₇₀BM bulk heterojunction material: The role of PC₈₄BM traps on the carrier transport

We present a critical discussion of the various physical processes occurring in organic bulk heterojunction (BHJ) solar cells based on recent experimental results. The investigations span from photoexcitation to charge separation, recombination, and sweep-out to the electrodes. Exciton formation, relaxation, and decay in PCDTBT and P3HT are investigated by femtosecond-resolved fluorescence up-conversion spectroscopy

Future Plans

Ongoing work will attempt to isolate and better understand the mechanisms of the CPE interlayers and solvent treatment that lead to the improved device performance. Pc-AFM and SKPM will be employed to map put change in surface topography, photocurrent networks, and surface potential as a function of solvent treatment and CPE interlayer thickness. Furthermore,

there is the possibility that the methanol treatment leads to changes in the “buried” electrode, namely PEDOT/ITO. The extent to which this interface is modified will be explored by taking advantage of metal oxide contacts, which are anticipated to be less sensitive to methanol.

Publications

In press

“Post Deposition Treatment of an Arylated-Carbazole Conjugated Polymer for Solar Cell Fabrication,” Xiaofeng Liu, Wen Wen, and Guillermo C. Bazan, Submitted to *Adv. Mater*

The Electronic Structure of Conjugated Polymer PCDTBT and of Its Donor-Acceptor Repeat Unit: A Combined Experimental and Computational Study; Natalie Banerji, Eric Gagnon, Pierre-Yves Morgantini, Sebastian Valouch, Ali Reza Mohebbi, Jung-Hwa Seo, Mario Leclerc, and Alan J. Heeger
Journal of Physical Chemistry, Accepted and in Press

Efficiency Increase Flexible Bulk Heterojunction Solar Cells with a Nano-Patterned Indium Zinc Oxide Anode Dong Hwan Wang, Jason Seifert, Dae-Geun Choi, Jong Hyeok Park, and Alan J. Heeger. This work has been submitted to *Advanced Energy Materials* for publication.

Ribbons, Vesicles and Baskets: Supramolecular Assembly of a Coil-Plate-Coil Emeraldicene Derivative, Mingfeng Wang, Ali Reza Mohebbi, Yanming Sun, Fred Wudl, *Angew. Chem Int Ed.* **2012**, in press

Short Circuit Current Improvement of P3HT PCBM Solar Cells Ali Reza Mohebbi, Fred Wudl, ,Manuscript in preparation **2012**.

Published

A Solution Processed MoO_x Anode Interlayer for Use within Organic Photovoltaic Devices; Jacek Jasieniak, Jason Seifert, Jang Jo, Tom Mates and Alan J. Heeger
Article first published in *Advanced Functional Materials* online: 4 APR 2012 DOI: 10.1002/adfm.201102622 The printed version will appear shortly.

Manifestation of carrier relaxation through the manifold of localized states in PCDTBT:PC₇₀BM bulk heterojunction material: The role of PC₈₄BM traps on the carrier transport; Wei Lin Leong, Gerardo Hernandez-Sosa, Sarah R. Cowan, Daniel Moses*, and Alan J. Heeger; *Advanced Materials*, vol. 24, p.2273 (2012)

Progress Report: Charge Formation, Recombination and Sweep-out Dynamics in Organic Solar Cells; Sarah R. Cowan, Natalie Banerji, Wei Lin Leong, and Alan J. Heeger

This work was published as a Feature Article in Advanced Functional Materials (2012)

DOI: 10.1002/adfm.201101632

Optical Spectroscopy and Scanning Tunneling Microscopy Studies of Molecular Adsorbates and Anisotropic Ultrathin Films

PI: John C. Hemminger, Department of Chemistry, University of California, Irvine

Program Scope

The emphasis of our research is to develop sufficient fundamental understanding to allow the controlled preparation of nano-structured samples that display novel optical properties and chemical reactivity. The research places an emphasis on the impact of ordering phenomena on the molecular and mesoscopic scale on surface properties of materials. In this research we combine the use of optical probes (Polarization and angle dependent laser reflectivity and Laser Raman Scattering, and laser induced desorption coupled with Fourier transform mass spectrometry (LD-FTMS)) with modern surface imaging experiments (electron microscopy, and variable temperature ultra high vacuum scanning tunneling microscopy (STM)). These experiments are combined with conventional methods of UHV surface science (High Resolution Electron Energy Loss Vibrational Spectroscopy (HREELS), Auger electron spectroscopy (AES), x-ray photoelectron spectroscopy (XPS) and thermal desorption spectroscopy (TDS)). The conventional surface probes provide well-tested methods for the preparation and characterization of substrates. The optical probes used in our experiments provide methods for the characterization of the structure dependent optical properties of novel molecular and nanometer scale surface structures as well as molecular identification and quantification of adsorbates in monolayers and ultrathin films. The emphasis of our research will be on the generation of novel nanometer scale morphologies and the resultant optical and chemical reactivity properties. These experiments will involve more complex molecular adsorbates, which we are well equipped to study using techniques such as LD-FTMS.

We will use a combination of STM and SEM to study the growth of mesoscopically ordered nanometer sized metal structures on well-defined substrates such as highly ordered pyrolytic graphite (HOPG). We will continue to develop methods (e.g. photochemical deposition) to decorate nanometer scale metal oxide structures with transition metal nanoparticles.

The fundamental understanding generated by this research will lead to the ability to better control in advance the growth of mesoscopically ordered nanometer scale structures that exhibit predictable physical and chemical properties.

Recent Progress

During the last year progress has been made in three areas of our research program: (1) Using methods we have previously developed to synthesize stable metal (e.g., Al, Ti, Fe, Ni) oxide nanoparticles on HOPG we have now developed photoelectrochemical methods to deposit metal nanoparticles selectively onto the metal oxide nanoparticles. (2) We have upgraded our UHV high resolution electron energy loss spectrometer (HREELS) to allow rapid introduction of externally prepared samples (e.g., nanoparticles on nanoparticle samples of (1)). This has allowed us to initiate vibrational spectroscopy studies of molecular adsorbates and reactions on Pt nanoclusters deposited on nanoparticle TiO_2 , and (3) We have obtained high resolution STM images of these films and are moving ahead with STM imaging and reaction experiments of Pt nanostructures on the Al_2O_3 nanoparticles supported on HOPG.

Previous work in our laboratory funded by this grant has led to the development of methods to produce ordered arrays of relatively monodispersed nanoparticles of metals (e.g., Au, Ag, Pt) on highly oriented pyrolytic graphite (HOPG) substrates. Simple atomic vapor deposition of the metal onto the HOPG substrate while the HOPG substrate is held at sufficiently high temperature to allow surface atom diffusion results in decoration of steps on the HOPG and subsequent nucleation and growth of metal nanoparticles along the HOPG steps. We have reported on this synthetic work in previous annual progress reports and in literature publications.^{1,2} Additionally, we have reported previously on the novel polarization dependent optical properties of the ordered arrays. The HOPG substrate temperature that is required to obtain selective nucleation of the nanoparticles at the HOPG steps is different for each metal—varying with the strength of metal—graphite interaction. The size and number density of the nanoparticles can be adjusted to some extent by varying the parameters of the vapor deposition (HOPG substrate temperature, atom flux to the surface, total metal deposition). During the past year we have extended this work to easily oxidized metals (e.g., Ti, Al, Fe). In these experiments the metal is deposited in high vacuum onto the HOPG with the substrate at high temperature. As with the less easily oxidized metals, nucleation and growth occurs at the HOPG steps resulting in nanoparticles at the steps. Exposure of the easily oxidized metal nanoparticle to either oxygen or air results in complete oxidation of the metal nanoparticle. For example, TiO₂ nanoparticles are easily generated in this manner. Figure 1 shows an SEM image of TiO₂ nanoparticles on HOPG that were generated in this manner.

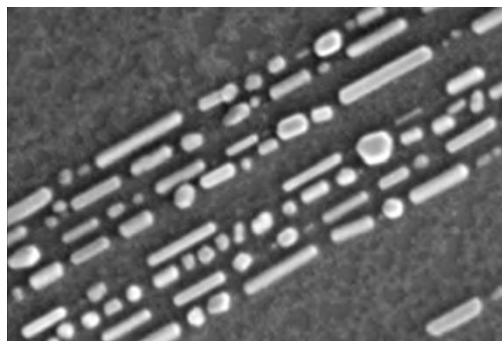


Figure 1. SEM image of TiO₂ nanoparticles that were generated by vapor deposition of Ti on the HOPG while the substrate was held at 550 C, followed by room temperature exposure of the sample to oxygen. The nanoparticles are 10-15 nm wide and occur as either rods or faceted particles.

We have also been able to obtain TEM images of individual particles from samples such as that shown in Figure 1. The TEM images exhibit diffraction with fringe spacings consistent with the rutile structure of TiO₂. In addition XPS spectra show Ti peaks with binding energy consistent with fully oxidized Ti.

Photodeposition of metals onto the TiO₂ nanoparticles:

We have successfully used photodeposition methods to selectively deposit metals onto the TiO₂ nanoparticles for samples such as the one shown in Figure 1. In this approach, the sample is placed in an aqueous solution of the metal salt of interest in an electrochemical cell. The sample is then irradiated with UV radiation with photon energy in excess of the TiO₂ bandgap. Bandgap radiation generates electron-hole pairs in the TiO₂ that result in reduction of the metal ions from solution at the surface of the TiO₂ nanoparticle. Since the metal deposition is driven by bandgap

excitation of the TiO_2 the deposition only occurs on the TiO_2 nanoparticle with no deposition on the HOPG substrate.

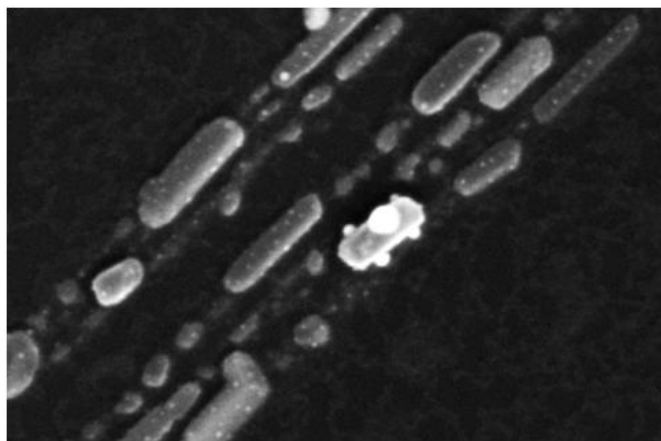


Figure 2. SEM image showing TiO_2 nanoparticles that have been decorated with Ag nanoparticles using the photochemical deposition method described in the text. The TiO_2 particles are $\sim 10\text{nm}$ wide. The small Ag nanoparticles are 1—2nm diameter.

Figure 2 shows an SEM image of an HOPG sample with Ag nanoparticles decorating TiO_2 nanoparticles. The Ag was deposited onto the TiO_2 nanoparticles using photodeposition from a AgNO_3 solution and TiO_2 bandgap radiation. The amount of Ag metal deposition can be followed via the photocurrent in the electrochemical photodeposition cell. Background experiments show that Ag deposition does not occur when the sample is exposed to the solution in the dark. Similar experiments have been carried out to photodeposit 1-2 nanometer diameter Au nanoparticles onto TiO_2 nanoparticles using an HAuCl_4 solution as the source of Au ions.

The recent results just described now provide well characterized TiO_2 nanoparticle substrates for transition metal nanoparticle catalysts. This will allow us to study the impact of the substrate nanoparticle size and morphology on the transition metal catalyst activity.

Future Plans

The planned activities for the next year will follow on from the recent developments of the program.

1. We will continue to refine the synthesis of transition metal oxide nanoparticles decorated with transition metal nanoparticles, including expanding to Fe_2O_3 nanoparticles. In addition, we will begin catalytic reactivity studies of the TiO_2 nanoparticles on HOPG that are decorated with Au or Pt nanoparticles.
2. We plan to utilize the UHV HREELS instrument, now fitted with a fast entry chamber to study a variety of new samples prepared by the ex-situ synthesis methods we have developed. Our plans include vibrational spectroscopy studies of adsorbates on the TiO_2 nanoparticles decorated with Pt nanoparticles (such as those shown in Figure 2 of this abstract).

References cited in the report

1. Polarization-Dependent Surface Enhanced Raman Scattering from Silver 1-D Nanoparticle Arrays, Wei Luo, Wytze van der Weer, Ping Chu, D. L. Mills, Reginald M. Penner, and John C. Hemminger, *Journal of Physical Chemistry C*, 112(31), 11609-11613 (2008) DOI: 10.1021/jp803455s.

2. Physical vapor deposition of one-dimensional nanoparticle arrays on graphite: Seeding the Electrodeposition of gold nanowires, C. E. Cross, J. C. Hemminger, and R. M. Penner, *Langmuir*, **23** (20), 10372 -10379, (2007)

Publications Based on BES Supported Research (2010—present)

1. Smaller is Faster and More Sensitive: The Effect of Wire Size on the Detection of Hydrogen by Single Palladium Nanowires. Yang, F., Kung, S.-C., Cheng, M., Hemminger, J. C., Penner, R. M. (2010). *ACS Nano*, *4*(9), 5233-5244.

2. Single-Molecule Imaging of Platinum Ligand Exchange Reaction Reveals Reactivity Distribution. Esfandiari, N. M., Wang, Y., Bass, J. Y., Cornell, T. P., Otte, D. A. L., Cheng, M. H., Hemminger, J. C., McIntire, T. M., Mandelshtam, V. A., Blum, S. A. (2010). *JACS*. (Publication Date (Web): August 23, 2010 (Communication) DOI: 10.1021/ja105517d).

3. Single-Molecule Imaging of Platinum Ligand Exchange Reaction Reveals Reactivity Distribution. N. Melody Esfandiari, Yong Wang, Jonathan Y. Bass, Trevor P. Cornell, Douglas A. L. Otte, Ming H. Cheng, John C. Hemminger, Theresa M. McIntire, Vladimir A. Mandelshtam and Suzanne Blum, *JACS Communications*, *132*, 15167-15169, (2010). DOI: 10.1021/ja105517d

4. High-Throughput Measurement of the Seebeck Coefficient and the Electrical Conductivity of Lithographically Patterned Polycrystalline PbTe Nanowires. Yongan Yang, David K. Taggart, Ming H. Cheng, John C. Hemminger, and Reginald Penner *Physical Chemistry Letters*, *1*, 3004-3011,(2010). DOI: 10.102/jz1011128d

5. Photodeposition of Ag or Pt onto TiO₂ Nanoparticles Decorated on Step Edges of HOPG. James Taing, Ming H. Cheng, and John C. Hemminger *ACS Nano*, *5*(8), 6325-6333 (2011). DOI:10.1021/nn201396v

6. Mesoporous Manganese Oxide Nanowires for High-Capacity, High Rate, Hybrid Electrical Energy Storage. Wenbo Yan, Talin Ayvazian, Jungyun Kim, Yu Liu, Keith C. Donovan, Wendong Xing, Yongan Yang, John C. Hemminger, and Reginald Penner *ACS Nano*, *5*(10), 8275-8287 (2011). DOI: 10.1021/nn2029583

7. Tunable Photoconduction Sensitivity and Bandwidth for Lithographically Patterned Nanocrystalline Cadmium Selenide Nanowires. Sheng-Chin Kung, Wendong Xing, Wytze E. van der Veer, Fan Yang, Keith C. Donovan, Ming Cheng, John C. Hemminger, and Reginald M. Penner *ACS Nano*, *5*(9), 7627-7639, (2011). DOI: 10.1021/nn202728f

Title

SISGR: Linking Ion Solvation and Lithium Battery Electrolyte Properties

PI

Wesley Henderson

Department of Chemical & Biomolecular Engineering, North Carolina State University

Program Scope

The research objective of this proposal is to provide a detailed analysis of how solvent and anion structure govern the solvation state of Li^+ cations in solvent-LiX mixtures and how this, in turn, dictates the electrolyte physicochemical and electrochemical properties which govern (in part) battery performance. Lithium battery electrolytes remain a poorly understood and hardly studied topic relative to the research devoted to battery electrodes. This is due to the fact that it is the electrodes which determine the energy (capacity) of the battery. The electrolyte, however, plays a crucial role in the power, low and/or high temperature performance, lifetime, safety, cost, etc. In particular, the state-of-the-art electrolyte composition consisting of LiPF_6 with ethylene carbonate (EC) and a linear carbonate such as ethyl methyl carbonate (EMC) has undergone only minor changes over the past 20 years. This electrolyte is poorly optimized for use with new electrode materials for advanced Li-ion batteries with high-voltage cathodes, Li-air, Li-S and other critical battery chemistries. The development of a "looking glass" into the molecular interactions (i.e., solution structure) in bulk electrolytes through a synergistic experimental approach involving three research thrusts complements work by other researchers to optimize multi-solvent electrolytes and efforts to understand and control the electrode-electrolyte interface, thereby enabling the rational design of electrolytes for a wide variety of battery chemistries and applications (low/high temperature, high power, etc.) (electrolytes-on-demand). These three research thrusts include:

- (1) conduction of an in-depth analysis of the thermal phase behavior of diverse solvent-LiX mixtures,
- (2) exploration of the ionic association/solvate formation behavior of select LiX salts with a wide variety of solvents, and
- (3) linking structure to properties—determination of electrolyte physicochemical and electrochemical properties for comparison with the ionic association and phase behavior.

Thrust I involves the creation of a library of binary solvent-LiX phase diagrams. These are highly informative when combined with the ionic association information provided by Thrust II. Solvate crystal structures are determined to provide insight into the manner of Li^+ ...solvent and Li^+ ...anion coordination and to serve as model compounds for the Raman spectroscopic analysis used in Thrust II to determine the degree of ionic association.

Thrust II will develop a Li^+ Solvation Scale for Solvents by directly examining Li^+ ...anion interactions in a wide variety of solvents to determine which types of solvates exist in solution—solvent-separated ion pairs (SSIPs), contact ion pairs (CIPs) and aggregates (AGGs) in which the anions remain uncoordinated (to a Li^+ cation) or are coordinated to one or more cations.

Thrust III involves the determination of a variety of solvent-LiX electrolyte properties over a broad temperature and concentration range including conductivity, ion/solvent diffusion coefficients, viscosity, density, etc. This detailed data, in combination with the information from Thrusts I and II, will result in a comprehensive understanding of the electrolyte/battery

composition-property-performance relationships which will be essential in utilizing this fundamental information for improved electrolyte selection (formulation) for new battery chemistries. Information has been shared throughout the project with collaborators who are utilizing the data to aid in understanding variations in diffusion coefficients (for the ions and solvent) and to optimize molecular simulations which will provide further insight unobtainable directly from experimental data. This work will clearly delineate which solvent and anion structural features are critical for determining electrolyte bulk properties and how these properties are interrelated.

Recent Progress

Phase diagrams have been prepared for numerous nitrile, carbonate and ester solvents with a range of lithium salts (Fig. 1). Examples of phase diagrams for acetonitrile (AN) mixtures are shown in Fig. 2. A comparison of the phase behavior (which phase forms first from dilute solution, the melting point (T_m) of this solvate phase, etc.) for a single solvent with different salts or different solvents with a single salt is very informative with regard to the ionic association tendency (of the different anions) and solvation interactions. Structures of the crystalline solvate phases (i.e., $(AN)_6:LiPF_6$, $(AN)_5:LiPF_6$, $(AN)_2:LiBF_4$, $(AN)_1:LiBF_4$ and $(AN)_1:LiTFSI$) have been determined where possible. Raman spectroscopy has then been used to determine the average solvation number of a given solvent (vs. concentration and temperature) mixed with the different salts. Raman

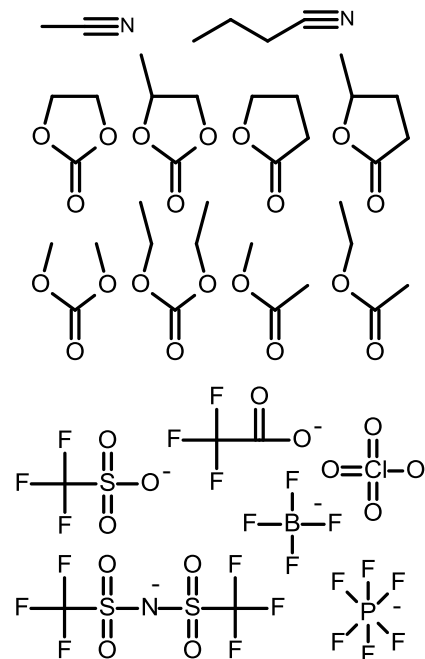


Fig. 1. Structure of the solvents and anions studied.

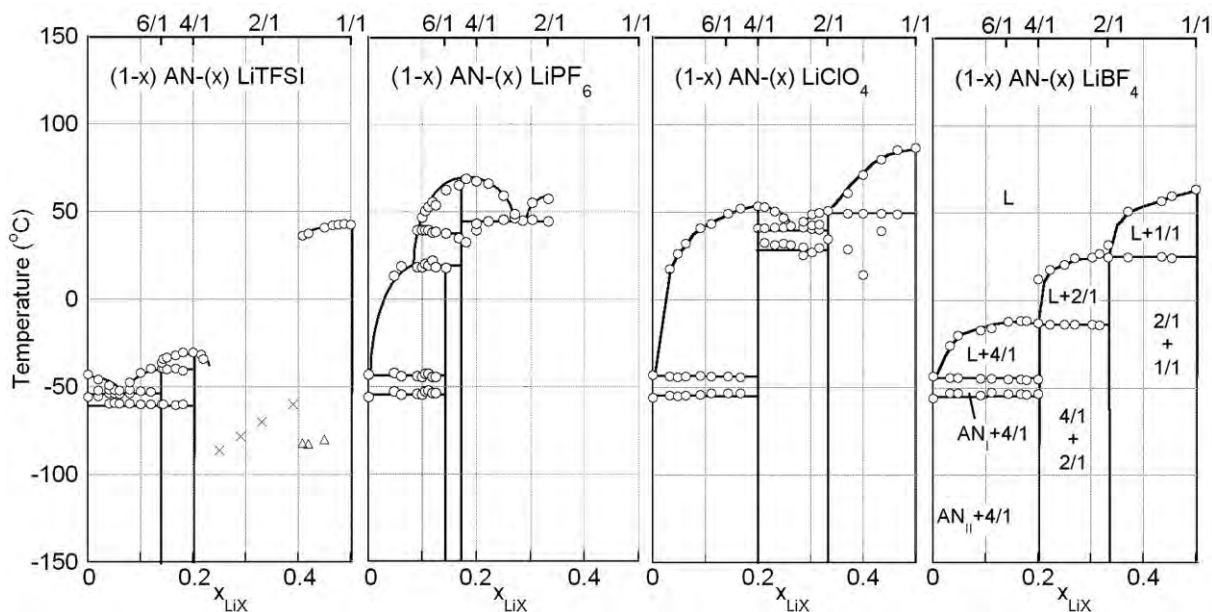


Fig. 2. Phase diagrams for $(AN)_n$ -LiX mixtures with LiTFSI, $LiPF_6$, $LiClO_4$ and $LiBF_4$. The bottom axis shows the salt mole fraction (x), while the top axis shows the AN/Li mole ratio. The solid and liquid (L) phases are indicated for the $LiBF_4$ phase diagram. The \times symbols indicates a T_g for fully amorphous samples, whereas the triangles are the T_g for a partially crystalline sample.

spectroscopy is also used to examine the distribution of different solvate species (i.e., manner of anion coordination - Fig. 3) in both the solid state (crystalline) and liquid phases. To aid in this, a diverse range of solvate crystal structures have been determined for different salts and then these solids are characterized to correlate the Raman band variation (of structures with known anion...Li⁺ coordination) with temperature (Fig. 4). Such spectroscopic analysis tools (for liquid electrolytes) are being created for the different salts (i.e., LiTFSI, LiPF₆, LiClO₄ and LiBF₄) which will be used for the Li⁺ Solvation Scale (this is necessary to properly deconvolute the spectra for this work). Once the solution structure of the solvent-salt electrolytes has been rigorously analyzed experimentally (with phase diagrams and spectroscopy), the information is provided to a collaborator to validate quantum chemical (QC) calculations and molecular dynamics (MD) simulations to add further insight into the solvation/ionic association interactions. The transport properties (i.e., conductivity, molar conductivity - Fig. 5, viscosity, etc.) are then explored in detail and correlated with the solution structure information to explain the mechanisms/origin of the measured properties and how this is linked to solvation/ionic association.

Future Plans

Future plans include the completion of the work which has been initiated, especially with regarding to the analysis of the acyclic carbonates and esters with several lithium salts, the characterization of additional model salts (i.e., LiNO₃, LiCF₃SO₃) to further improve the understanding of solvation/ionic association and the development of the Li⁺ Solvation Scale (for which the necessary Raman spectroscopic analysis background work has nearly been completed). Additional future work would include the characterization of other solvents (i.e., glymes, dinitriles, sulfones, fluorinated solvents) and the expansion of the work already completed including the use of additional characterization methods (diffusion coefficients, pseudo-transference number measurements, FTIR spectroscopic analysis of solvation/ionic association).

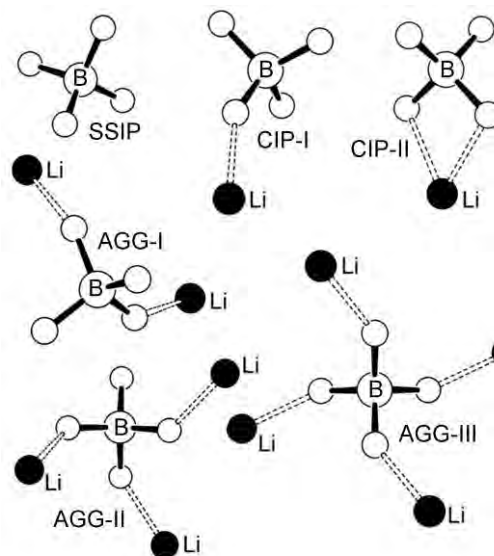


Fig. 3. Forms of BF₄⁻...Li⁺ cation coordination found in crystalline solvates (the AGG-III structure is for pure LiBF₄).

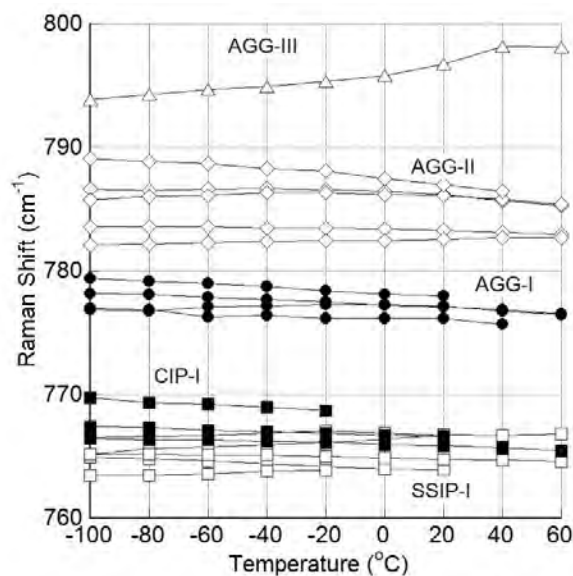


Fig. 4. Raman BF₄⁻ anion band variation vs. temperature from the characterization of crystalline solvates with known structures.

References

None

Publications

- Seo DM, Borodin O, Han S-D, Ly Q, Boyle PD, Henderson WA. *J. Electrochem. Soc.* 2012, In-Press. Electrolyte Solvation and Ionic Association (II): Acetonitrile-Lithium Salt Mixtures—Highly Dissociated Salts
- Seo DM, Borodin O, Han SD, Ly Q, Boyle PD, Henderson WA. *J. Electrochem. Soc.* 2012, 159, A553. Electrolyte Solvation and Ionic Association (I): Acetonitrile-Lithium Salt Mixtures - Intermediate and Highly Associated Salts
- Seo DM, Boyle PD, Henderson WA. *Acta Crystallogr.* 2011, E67, m547. Poly[[[(acetonitrile)-lithium(I)]- μ 3-tetrafluoridoborato]
- Seo DM, Boyle PD, Henderson WA. *Acta Crystallogr.* 2011, E67, m534. Poly[bis(acetonitrile- κ N)bis[μ 3-bis(trifluoromethanesulfonyl)imido- κ 4O,O':O":O"]dilithium]
- Seo DM, Boyle PD, Borodin O, Henderson WA. *Phys. Chem. Chem. Phys.* (2012) Under Review. Li^+ Cation Coordination by Acetonitrile—Insights from Crystallography
- Seo DM, Afroz T, Han SD, Allen JL, Boyle PD, Henderson WA. In-Preparation. Solvation and Ionic Coordination Interactions in Lithium Solvates
- Seo DM, Borodin O, O'Connell M, Ly Q, Boyle PD, Henderson WA. In-Preparation. Electrolyte Solvation and Ionic Association (III): Acetonitrile-Lithium Salt Mixtures—Transport Properties
- Seo DM, Johansson P, Allen JL, Boyle PD, Henderson WA. In-Preparation. Solvate Structures and Spectroscopic Characterization of Lithium tetrafluoroborate (LiBF_4)
- Seo DM, Borodin O, O'Connell M, Ly Q, Boyle PD, Henderson WA. In-Preparation. Electrolyte Solvation and Ionic Association (VII): Cyclic Carbonates and Esters with LiClO_4
- Seo DM, Borodin O, Han SD, Gardner L, Boyle PD, Henderson WA. In-Preparation. Electrolyte Solvation and Ionic Association (VIII): Cyclic Carbonates and Esters with LiTFSI
- Seo DM, Borodin O, Boyle PD, Henderson WA. In-Preparation. Electrolyte Solvation and Ionic Association (IX): Cyclic Carbonates and Esters with LiPF_6

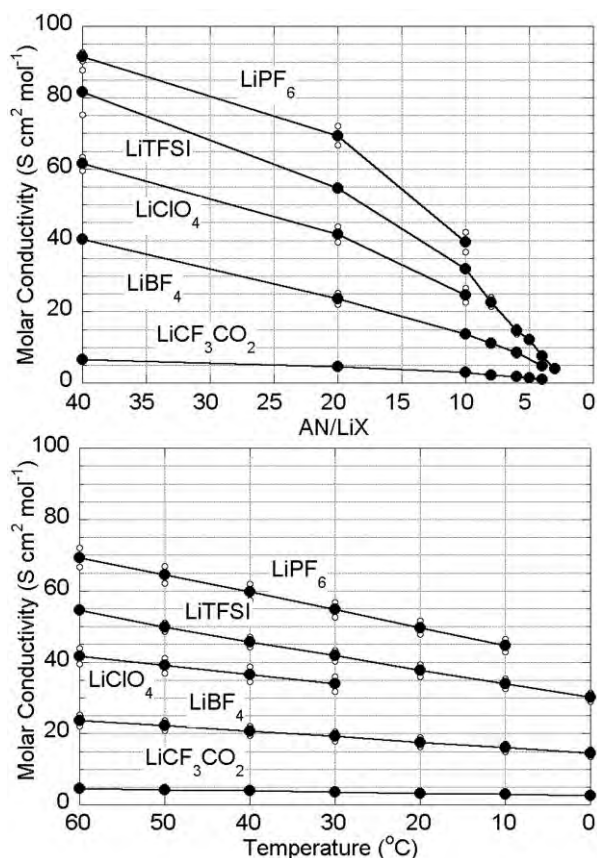


Fig. 5. Molar conductivity of (top) $(\text{AN})_n\text{-LiX}$ mixtures (60°C) for varying AN/LiX (n) concentrations and (bottom) $(\text{AN})_n\text{-LiX}$ mixtures ($n = 20$ - filled circles are average values, individual measurements shown as small open circles) with varying temperature.

Actinide Transition-Metal Chalcogenides and Pnictides

James A. Ibers, Department of Chemistry, Northwestern University, Evanston, IL;
Collaborating Investigator: Lynda Soderholm, Argonne National Laboratory, Argonne, IL

Program Scope

The scope is, the synthesis and characterization of new transition-metal chalcogenides and pnictides of Th, U, and Np, to characterize them structurally, to determine selected physical properties, and to develop theoretical insights into these properties.

Recent Progress

The synthesis and characterization of a number of new U chalcogenides and an old Np binary selenide are currently in progress. Some examples are:

a) $Ba_9Ag_{10}U_4S_{24}$. Single crystals of $Ba_9Ag_{10}U_4S_{24}$ (Fig. 1) were synthesized from a stoichiometric reaction among BaS, Ag_2S , U and S at 1273 K. The formal oxidation state could be explained by Ba^{2+} , $Ag_{10}^{(1+)}$, $U_4^{(5+)}$ and $S_{24}^{(2-)}$, with no S-S bonds.

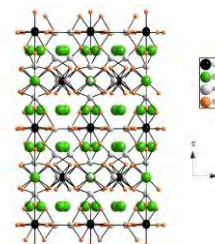


Figure 1. The structure of $Ba_9Ag_{10}U_4S_{24}$

b) $Rh_2U_6S_{15}$ and $Cs_2M_2U_6Se_{15}$ ($M = Ti, Cr$). Single crystals of these compounds were synthesized by reaction of the elements in a CsCl flux. The first compound contains M^{3+} whereas the latter compounds contain M^{2+} . A temperature sweep at 5T of $Cs_2Cr_2U_6Se_{15}$ exhibits simple ferromagnetic behavior. The known analogues $Rh_2U_6Se_{15.5}$ and $Ir_2U_6Se_{15.5}$ exhibit antiferromagnetic behavior.

c) $Cs_2U_3Se_7$. Single crystals of this material were synthesized by the reaction among Cs, Se, and As in a Cs_2S_3 flux at 1273 K. The structure is shown in Fig. 2. Extensive magnetic measurements have been performed as well as specific heat measurements. These may be summarized as follows: The first magnetic transition at $T_N = 90$ K indicates antiferromagnetic

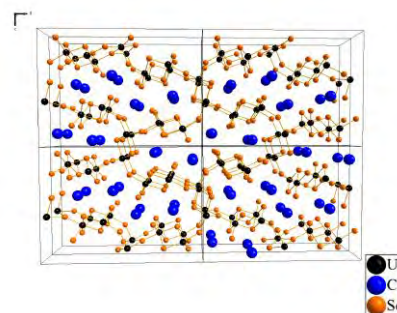


Figure 2. The structure of $Cs_2U_3Se_7$.

ordering. There are at least two observed transitions in the ZFC 50 Oe measurement. The second transition at $T = 50$ K could be explained by canted antiferromagnetic ordering. The effective magnetic moment calculated from Curie-Weiss Law is $3.41 \mu_B$, which is close to the theoretical value of $3.58 \mu_B$ for the free-ion value for U^{4+} . A plot of the magnetization between -5 and 5 T at 5 K is nonlinear. This behavior

is indicative of noncollinear antiferromagnetic behavior. At 5 T the magnetic moment for each uranium atom in $\text{Cs}_2\text{U}_3\text{Se}_7$ is $0.33 \mu_B$. Cycling the magnetization between 5 and -5 T shows the presence of hysteresis between 0.02 and -0.02 T. Missing is an ac magnetic measurement. This will be performed by Bob Cava at Princeton.

d) NpSe_3 . This is an old compound that was studied by X-ray powder diffraction methods as well as magnetic measurements and ^{237}Np Mössbauer spectroscopy in the 1970's and 1980's. These measurements did not resolve the question of the oxidation state of Np in NpSe_3 . Because the structure is a key to understanding interactions and electron distributions within An_xQ_y systems (An = actinide, Q = S, Se, Te), it is important to examine such binary systems. Neptunium triselenide, NpSe_3 , was synthesized by the stoichiometric reaction of the elements in an Sb_2Se_3 flux at 1223 K. Its structure has been determined by single-crystal X-ray diffraction methods (Fig. 3). Np-Se interatomic distances range from 2.859(2) to 2.927(3) Å; the Se-Se bond length is 2.340(3) Å, typical of a single bond. The compound may thus be charge-balanced and formulated as $\text{Np}^{4+}\text{Se}_2(\text{Se}_2^{2-})$.

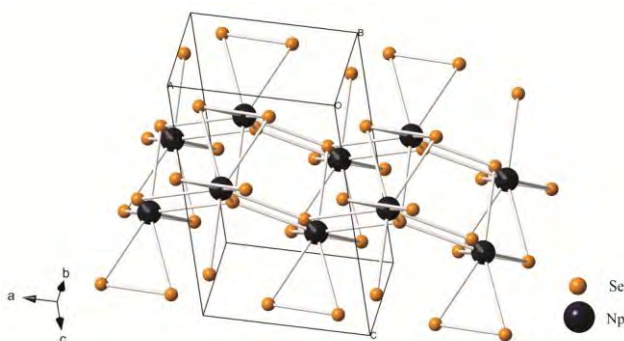


Figure 3. The structure of NpSe_3 .

Future Plans

- 1) Northwestern: Complete the current projects, including those detailed above.
- 2) Argonne/Notre Dame: Our efforts at ANL have been dormant for many months owing to various issues both within and without The Actinide Facility. Our attempts to move Np metal out of ANL and to Albrecht-Schmitt's facility at Notre Dame are buried at ANL under unbelievable piles of red tape and are not progressing. In the interim, attempts are being made at Notre Dame to synthesize Np metal from NpO_2 , a nontrivial task.

Publications (last two years)

Wells, D. M.; Chan, G. H.; Ellis, D. E.; Ibers, J. A. *J. Solid State Chem.* **2010**, *183*, 285-290. $\text{UTa}_2\text{O}(\text{S}_2)_3\text{Cl}_6$: A ribbon structure containing a heterobimetallic $5d-5fM_3$ cluster.

Wells, D. M.; Ibers, J. A. *Z.Anorg. Allg. Chem.* **2010**, *636*, 440-442. The $[\text{U}_2\text{I}_{10}]^{2-}$ Anion: Synthesis and Structure of $[\text{Ta}_7(\text{Se}_2)_{14}][\text{U}_2\text{I}_{10}]_2$.

Jin, G.B.; Raw, A. D.; Skanthakumar, S.; Haire, R. G.; Soderholm, L.; Ibers, J.A. *J. Solid State Chem.* **2010**, *183*, 547-550. Single-crystal structures of uranium and neptunium oxychalcogenides $AnOQ$ ($An = \text{U}, \text{Np}$; $Q = \text{S}, \text{Se}$).

Bugaris, D. E.; Copping, R.; Tyliszczak, T.; Shuh, D. K.; Ibers, J. A. *Inorg. Chem.* **2010**, *49*, 2568-2575. $\text{La}_2\text{U}_2\text{Se}_9$: An Ordered Lanthanide/Actinide Chalcogenide with a Novel Structure Type.

Bugaris, D. E.; Ibers, J. A. *Dalton Trans.* **2010**, *39*, 5949-5964. Syntheses and characterization of some solid-state actinide (Th, U, Np) compounds.

Bugaris, D.E.; Wells, D.M.; Yao, J.; Skanthakumar, S.; Haire, R.G.; Soderholm, L.; Ibers, J.A. *Inorg. Chem.* **2010**, *49*, 8381-8388. Dichalcogenide Bonding in Seven Alkali-Metal Actinide Chalcogenides of the KTh_2Se_6 Structure Type.

Ibers, J. A. *Nature Chem.* **2010**, *21*, 996. Neglected neptunium.

Jin, G. B.; Ringe, E.; Long, G. J.; Grandjean, F.; Sougrati, M.T.; Choi, E.S.; Wells, D.M.; Balasubramanian, M.; Ibers, J. A. *Inorg. Chem.* **2010**, *49*, 10455-10467. Structural, Electronic, and Magnetic Properties of UFeS_3 and UFeSe_3 .

Manos, E.; Kanatzidis, M. G.; Ibers, J. A. Actinide Chalcogenide Compounds, in "The Chemistry of the Actinides and Transactinide Elements", Morss, L. R.; Edelstein, N. M.; Fuger, F., Eds. Springer, Dordrecht, 2010. Vol. 6, pp. 4005-4077.

Wells, D. M., Ringe, E.; Kaczorowski, D.; Gnida, D.; André, G.; Haire, R. G.; Ellis, D. E.; Ibers, J. A. *Inorg. Chem.* **2011**, *50*, 576-580. Structure, Properties, and Theoretical Electronic Structure of UCuOP and NpCuOP .

Oh, G. N.; Ibers, J. A. *Acta Crystallogr.* **2011**, *E67*, i9. $\text{Cs}_2\text{UPd}_3\text{Se}_6$.

Koscielski, L. A.; Ibers, J. A. *Acta Crystallogr.* **2011**, *E67*, i16. Tetrayttrium(III) trisulfide disilicate.

Jin, G. B.; Skanthakumar, S.; Haire, R.G.; Soderholm, L.; Ibers, J.A. *Inorg. Chem.* **2011**, *50*, 1084-1088.

Syntheses, Structures, and Magnetic Properties of Np_3S_5 and Np_3Se_5 .

Bugaris, D.E.; Choi, E.S.; Copping, R.; Glans, P.-A. Minasian, S.G.; Tyliczszak, T.; Kozimor, S.A.; Shuh, D. K.; Ibers, J. A. *Inorg. Chem.* **2011**, *50*, 6656-6666. Pentavalent and Tetravalent Uranium Selenides, $Tl_3Cu_4USe_6$ and $Tl_2Ag_2USe_4$: Syntheses, Characterization, and Structural Comparison to Other Layered Actinide Chalcogenide Compounds.

Oh, G.N.; Ibers, J. A. *Acta Crystallogr.* **2011**, *E67*, i9. $Cs_2UPd_3Se_6$.

Oh, G.N.; Ibers, J. A. *Acta Crystallogr.* **2011**, *E67*, i46. Manganese(II) octauranium(IV) heptadecasulfide.

Jin, G. B.; Skanthakumar, S.; Haire, R.G.; Soderholm, L.; Ibers, J. A. *Inorg. Chem.* **2011**, *50*, 9688-9695. Neptunium Thiophosphate Chemistry: Intermediate Behavior between Uranium and Plutonium.

Raw, A.D.; Ibers, J.A. *Acta Crystallogr.* **2011**, *E67*, i70. Zirconium(IV) dilanthanum(III) pentasulfide.

Andrews, L.; Wang, X.; Liang, B.; Ruipérez, F.; Infante, I.; Raw, A.D.; Ibers, J.A. *Eur. J. Inorg. Chem.* **2011**, 4457-4463. Matrix Infrared Spectroscopy and a Theoretical Investigation of SUO and US_2 .

Oh, G. N.; Ibers, J. A. *Acta Crystallogr.* **2011**, *E67*, i75. The β -polymorph of uranium phosphide selenide.

Oh, G. N.; Ringe, E.; Van Duyne, R. P.; Ibers, J. A. *J. Solid State Chem.* **2012**, *185*, 124-129. Synthesis, structure, and optical properties of $CsU_2(PO_4)_3$.

Bugaris, D. E.; Ibers, J. A. *Inorg. Chem.* **2012**, *51*, 661-666. $Ba_8Hg_3U_3S_{18}$: A Complex Uranium(4+)/Uranium(5+) Sulfide.

Raw, A. D.; Ibers, J. A. *J. Solid State Chem.* **2012**, *186*, 177-181. Syntheses and crystal structures of the quaternary uranium lanthanide oxyselenides $UYb_2O_2Se_3$ and $U_2Ln_2O_4Se_3$ ($Ln = Pr, Sm, Gd$).

Relationships Between the Adhesion, Friction and Nano/Micro-Structure of Materials, Surfaces and Films (DOE Award number: DE-FG02-87ER 45331)

Jacob Israelachvili, Dept Chemical Engineering, Materials Department, and Materials Research Laboratory, University of California (UCSB), Santa Barbara, CA 93106.

Program Scope

The aims are to apply recently developed experimental techniques [2], and develop new ones, to make simultaneous static and dynamic measurements of the adhesion, friction, structure, and wear of both model (smooth) and especially “engineering” surfaces and materials ... conducted under a wide range of conditions of both fundamental and practical interest (Fig. 1), including high speeds. The project involves modifications and new attachments to the Surface Forces Apparatus (SFA) allowing for *simultaneous* measurements of interaction forces and other physical properties, such as electric field effects, and additional imaging techniques, of the surfaces and thin films. There are close collaborations with top theoreticians/modelers worldwide.

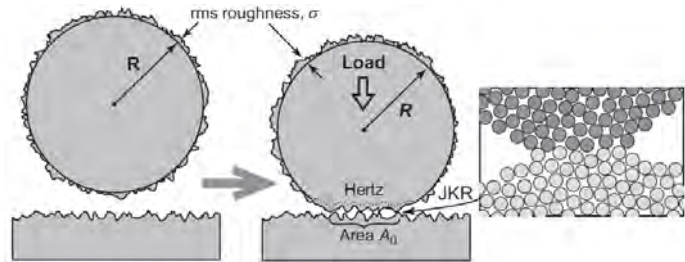


Fig. 1. The adhesion and friction forces between "real" (rough or patterned surfaces as opposed to "ideal" molecularly smooth surfaces) are being measured at all length scales (from the nano to the macro) and time scales.

Recent Progress (includes work done during the 4 months unfunded period)

Material failure (crack initiation and propagation): We completed a comprehensive study of how polymeric materials make the transition from brittle to ductile failure [1], i.e., how solid-like cracks can make a *continuous* transition to liquid-like “snapping”. The results (not shown here) how a fascinating, and non-intuitive transition from simple cracking to liquid bridge snapping via a very complex transition regime involving Saffman-Taylor fingering and cavitation instabilities.

Tribology: In 2011 we developed and started to use the new experimental force-measuring and imaging techniques (Ref. 2 and Fig. 2) to measure tribological mechanisms under “extreme conditions” of pressure and speed

(up to 20 m/s) [5, 6], and identified a new type of stick-slip at sliding speeds above a few cm/s that gives rise to oscillatory, rather than sharp, stick-slip spikes. This is commonly referred to as “shudder” in cars or “chatter” in machinery. Our experiments show that this common phenomenon is not due to traditional/conventional stick-slip friction, but is more related to mechanical "resonance coupling" between the moving parts and

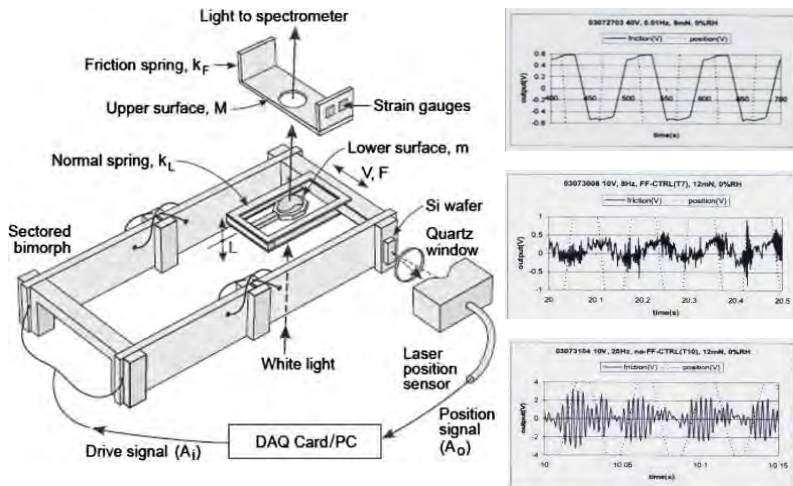


Fig. 2. Left: High speed friction SFA setup using fast-feedback piezo-electric feedback (or a rotating disk -- not shown) [5]. Right: Progressive increase in the back-and-forth sliding speed changes the friction from smooth to oscillatory, that depends on the inertia of the system [5, 6].

surfaces in the system. Other findings in the related area of the tribology and thin film rheology of nanoparticle systems are described in refs [3, 7, 8, 10].

Electrochemical forces between and "wear" of surfaces: We have used a new electrochemical attachment to the SFA (Fig. 3) to measure the electric double-layer and other forces in electrolyte solutions between various asymmetric (differently chemically functionalized) surfaces, including

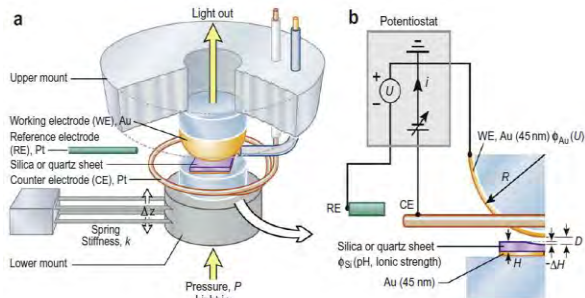


Fig. 3. The EC-SFA showing the electrochemical attachment to the SFA for both measuring natural and applying electric fields and potentials [4, 9].

different roughness and natural or applied electrochemical potentials [Fig. 4 and refs 4, 9]. These studies are providing new fundamental insights on interaction forces, particularly on the practically important phenomena of electrochemical dissolution, corrosion and damage, where we have found and quantified how chemical dissolution of a surface is very significantly enhanced when it is brought into close proximity with another surface that has a different (more negative or more positive) electrochemical potential difference.

Future Plans

Adhesion and friction of randomly rough and anisotropically patterned or lubricated surfaces: We are currently investigating the adhesion and (anisotropic or "3D") adhesion and friction of

randomly rough, anisotropically patterned and nanoparticle-coated surfaces Fig. 5) and of molecular anisotropy of the (lubricant) liquids. Our aim to obtain *quantitative* adhesion and friction laws or models for these systems that can describe their adhesion (Fig. 6) and friction in terms of simple equations, analogous to the Hertz and JKR models for smooth surfaces, or the Stribeck Curve friction law, with "effective" parameters (e.g., for the material stiffness and surface/interfacial energies) that take into account the surface topographies.

5) and of molecular anisotropy of the (lubricant) liquids. Our aim to obtain *quantitative* adhesion and friction laws or models for these systems that can describe their adhesion (Fig. 6) and friction in terms of simple equations, analogous to the Hertz and JKR models for smooth surfaces, or the Stribeck Curve friction law, with "effective" parameters (e.g., for the material stiffness and surface/interfacial energies) that take into account the surface topographies.

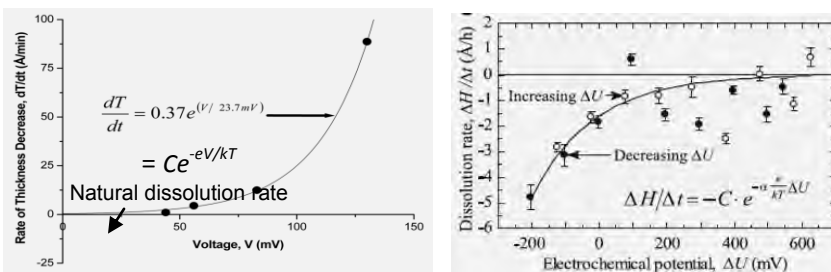
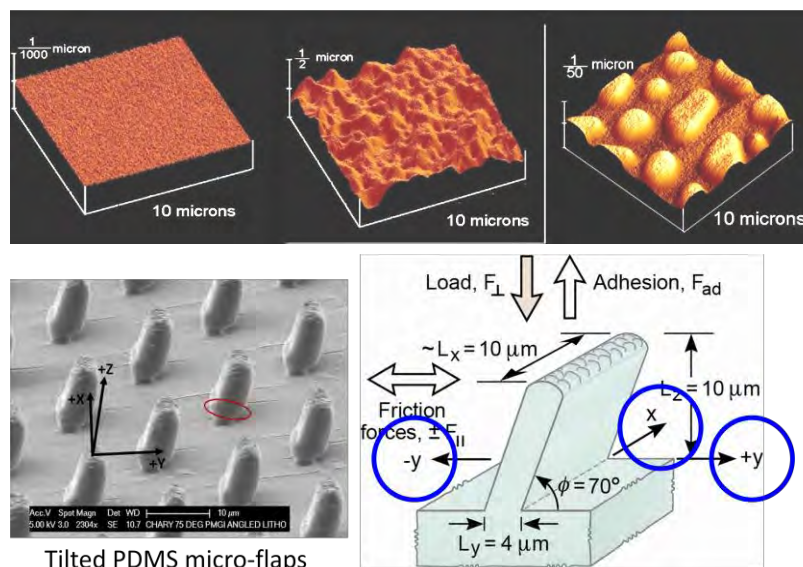


Fig. 4. Left: *Natural* dissolution rates of silica when pressed by mica surfaces in electrolyte solutions vs the measured potential difference V between the two surfaces. Right: Rates vs externally *applied* potential, ΔU .

Fig. 5. Some examples of the types of surfaces being made to study the effects of random and ordered surface structures, including crystal lattices for smooth surfaces, both dry and lubricated, polymeric and ceramic. Angled flaps (bottom right) provide an example of an anisotropic surface structure. (See Figs 6 and 7 a for some preliminary adhesion and friction results on these structures).



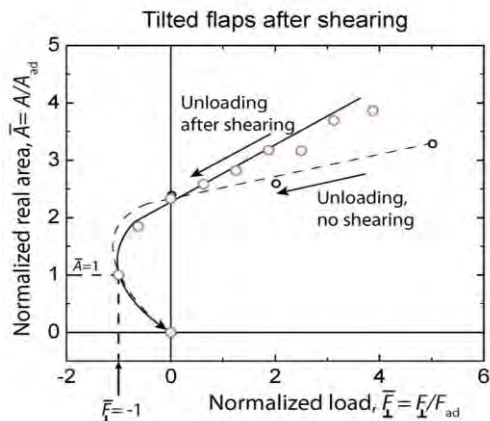


Fig. 6. Unloading path taken between two rough surfaces before and after shearing, showing "JKR-like" behavior, but with an effective stiffness and surface (adhesion) energy much reduced from the values of the bulk materials and smooth surfaces.

separated by nanometer thin layer of hexadecane. We are finding that the magnitude and "off-axis" directions of the friction forces depend on many factors, including the "twist angle" between the two surface lattices, the sliding direction, the anisotropic molecular structure of the lubricating fluid between the two surfaces, and the immediate previous history of the sliding motion. "Off-axis" friction cause very complex relative motions of surfaces. Most importantly, we are finding that during reciprocated (back-and-forth) sliding the surfaces never stop moving during the cyclic motion (Fig. 7), which avoids the damage-inducing "stiction spikes" that occurs with isotropic surfaces or lubricants when they come transiently to rest. These effects can be displayed on "friction maps" or "limit cycles" (Fig. 7).

Nanoparticle assemblies: Closely related to the above are our ongoing studies of the 3D organization and stability of various surfactant-coated nanoparticle assemblies and thin films [7,8,10], including a detailed investigation of the effects of water (humidity) on the adhesion, interfacial energies and contact angle hysteresis of physisorbed vs chemisorbed monolayers on nanoparticle surfaces.

The AFM-SFA and measuring forces in 3D: Also closely related to the above, we are developing the AFM attachment that will allow for simultaneous SFA and AFM-type measurements to be made in the same experiments. A prototype has been successfully tested in the SFA (Fig. 9) and is currently in use; the fabrication of a micro-scale version is currently in progress.

Fig. 8. The cross-spring flexure design for mounting an AFM tip suitable for measuring tip-surface interactions in 3D (xyz sensitivity) using piezo strain gauges.

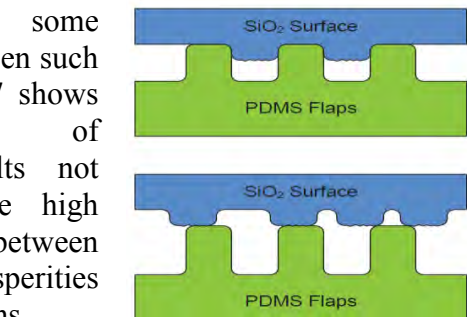


Fig. 7. Schematic illustration of why adhesion and friction are higher for surfaces with matching topographies.

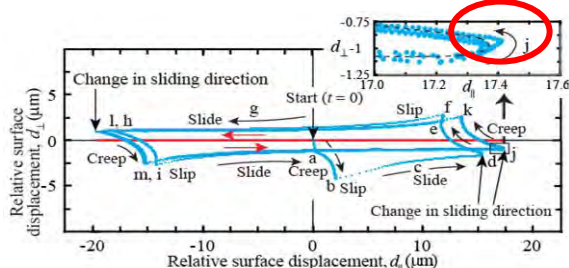
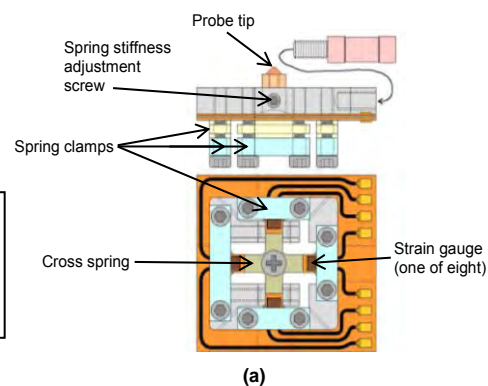


Fig. 7. The off-axis 2D displacement responses of a surface during the application of a back-and-forth shearing force in 1D (red line). The anisotropic hexadecane molecules align at an angle to the shearing force during the cyclic motion (blue path), causing the surfaces to move off-axis. On reversing, as the molecules rotate, the moving surface make a circular turning motion (red oval) rather than stopping momentarily before reversing.



(a)

Other studies in progress: We are continuing with our studies of electric field effects [3, 4, 9] on colloidal, adhesion and friction forces, molecular structure in thin films (e.g., of liquid crystals or anisotropic nano-particles), and later plan to study magnetic field effects.

Collaborations: We are currently collaborating with the following world-class theoreticians/modelers: Bob MacMeeking, Matt Begley, Bo Person, Mark Robbins, Jay Fineberg, Erun Bouchbinder, and (maybe) Uzi Landman.

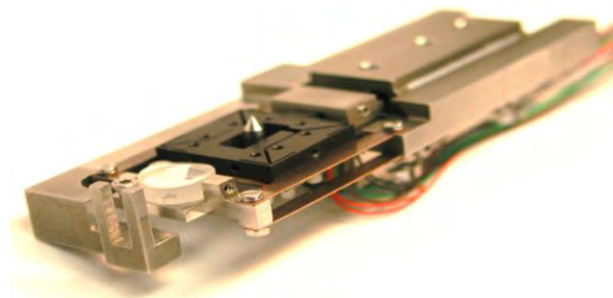


Fig. 9. AFM-SFA attachment that contains both a macroscopic (mica or silica) surface (front) and a microscopic 3D sensing AFM tip (behind the disk) that can be used simultaneously in SFA experiments.

References / Publications (2 years: 2010-2011)

1. **Liquid- to Solid-Like Failure Mechanisms of Thin Polymer Films at the Micro- and Nanoscales.** Hongbo Zeng, Boxin Zhao, Jacob N. Israelachvili, and Matthew Tirrell. *Macromolecules* **43** (2010) 538-542.
2. **Recent advances in the surface forces apparatus (SFA) technique.** J Israelachvili, Y Min, M Akbulut, A Alig, G Carver, W Greene, K Kristiansen, E Meyer, N Pesika, K Rosenberg and H Zeng. *Reports on Progress in Physics* **73** (2010) 1-16.
3. **Reversible shear thickening at low shear rates of electrorheological fluids under electric fields.** Yu Tian, Minliang Zhang, Jile Jiang, Noshir Pesika, Hongbo Zeng, Jacob Israelachvili, Yonggang Meng, Shizhu Wen. *Physical Review E*(2011) **83**, 011401.
4. **Effect of surface roughness and electrostatic surface potentials on forces between dissimilar surfaces in aqueous solution.** Markus Valtiner, Kai Kristiansen, George W. Greene, and Jacob N. Israelachvili. *Adv. Matls.* (2011) **23**, 2294–2299.
5. **High-Speed Friction Measurements Using a Modified Surface Forces Apparatus.** D. D. Lowrey, K. Tasaka, J. H. Kindt X. Banquy, N. Belman, Y. Min, N. S. Pesika, G. Mordukhovich, J. N. Israelachvili. *Tribol Lett* (2011) 42, 117–127.
6. **Measurement and characterization of ‘resonance friction’ at high sliding speeds in a model automotive wet clutch.** Xavier Banquy, Daniel D. Lowrey, Nataly Belman, Younjin Min, Gregory Mordukhovich, Jacob N. Israelachvili. *Tribology Letters* (2011) **43**, 185-195.
7. **Surface-Induced Patterns from Evaporating Droplets of Aqueous Carbon Nanotube Dispersions.** Hongbo Zeng, Kai Kristiansen, Peng Wang, Joakim Bergli, and Jacob Israelachvili. *Langmuir* (2011) **27** (11) 7163–7167.
8. **Imaging the microscopic structure of shear thinning and thickening colloidal suspensions.** Xiang Cheng, Jonathan H. McCoy, Jacob N. Israelachvili and Itai Cohen. *Science* (2011) **333** (6047) 1276-1279.
9. **Pressure solution – the importance of the electrochemical surface potentials.** Kai Kristiansen, Markus Valtiner, George W. Greene, James R. Boles, and Jacob N. Israelachvili. *Geochimica et Geophysica Acta* **75** (2011) 6882–6892.
10. **Microtribology of Aqueous Carbon Nanotube Dispersions,** Kai Kristiansen, Hongbo Zeng, Peng Wang, Jacob N. Israelachvili. *Adv. Functional Materials* 21 (2011) 4555-4564.

Enhanced Mixed Electronic-Ionic Conductors through Cation Ordering

Allan J. Jacobson, University of Houston, Dane Morgan, University of Wisconsin, Clare Grey, Stony Brook University (Cambridge University)

Program Scope

The performance of many energy conversion and storage devices depend on the properties of mixed ionic-electronic conducting (miec) materials. Mixed or ambipolar conductors simultaneously transport ions and electrons and provide the critical interface between chemical and electrical energy in devices such as fuel cells, ion transport membranes, and batteries. Enhancements in storage capacity, reversibility, power density and device lifetime all require new materials and a better understanding of the fundamentals of ambipolar conductivity and surface reactivity.

The high temperature properties of the ordered perovskites $AA'B_2O_{5+x}$, where A = rare earth ion, Y and A' = Ba, Sr are being studied. The work is motivated by the high oxygen transport and surface exchange rates observed for members of this class of mixed ionic and electronic conductors. The objectives of the work are to:

1. Understand how the cation and associated anion order lead to exceptional ionic and electronic transport properties and surface reactivity in $AA'B_2O_{5+x}$ perovskites;
2. Use this understanding to develop optimized A-site cation ordered perovskites for use in electrochemical devices;
3. Understand the effects of nanostructure and strain on structure and properties;
4. Develop fundamental understanding of defect chemistry, oxygen diffusion and surface exchange in $AA'B_2O_{5+x}$ perovskites and related defect mixed-metal oxides.

A combined experimental and computational approach, including structural, electrochemical, and transport characterization and modeling is used. The approach attacks the problem simultaneously at global (e.g., neutron diffraction and impedance spectroscopy), local (e.g., pair distribution function, nuclear magnetic resonance) and molecular (ab initio thermokinetic modeling) length scales.

Recent Progress

Experiments: The oxygen non-stoichiometries of $PrBaCo_2O_{5+x}$ and $NdBaCo_2O_{5+x}$ have been measured by Coulometric titration using a cell built by stacking two alumina tubes, where one has one end closed and the other has both sides open, and Pyrex glass rings. [1] The top of the cell was covered with an YSZ disk, which served as both an oxygen sensor and an oxygen pump. The oxygen non-stoichiometry change $\Delta\delta$ was recorded as a function of pO_2 at $10^{-6} \leq pO_2 \leq 0.21$ atm and at 750, 800, 850, 900, and 950 °C. An example is shown in Fig. 1 at 750 °C. Measurements were made on pumping oxygen out of the cell and then back in. The data are characterized by a large hysteresis effect indicative of a first order phase transformation. In the intermediate regions the kinetics are extremely slow (days) and it was necessary to program the system so that the same criterion for the attainment of equilibrium was used everywhere. The pO_2 values defining the hysteresis effect change with temperature but always occur at a stoichiometry corresponding to $PrBaCo_2O_{5.25}$. The most likely explanation for this behavior is the presence of a two phase region between $PrBaCo_2O_{5+x}$ and a new ordered structure

PrBaCo₂O_{5.25}. We have reported similar behavior in the perovskite to Brownmillerite transformation in SrCo_{0.8}Fe_{0.2}O_{3-x}. [2] Measurements on NdBaCo₂O_{5+x} reveal the same behavior.

The oxygen non-stoichiometry in PrBaCo₂O_{5+x} and NdBaCo₂O_{5+x} was also measured as a function of temperature and oxygen partial pressure by neutron diffraction. (in collaboration with Steven McIntosh (Lehigh), Rosemary Cox-Galhotra (Virginia Tech) Jason Hodges and Ashfia Huq (ORNL))

Neutron diffraction patterns were collected for PrBaCo₂O_{5+x} and NdBaCo₂O_{5+x} at SNS in flowing 0.01 %, 0.1% 1% and 100% O₂ at temperatures of 550, 650, 750 and 825 °C. The data were processed by the Rietveld method using the GSAS program. Various structure models have been tested and used to determine the variations of the atom positions, the oxygen non stoichiometry and the lattice parameters. In the data shown below all atoms were refined with anisotropic thermal parameters. The behavior of the oxygen non stoichiometry shows several interesting trends (Fig. 2). At high pO₂, the behavior is as expected, namely the vacancy concentration increases with increasing temperature. At 1% O₂ and 500 °C, the deviation from the nearly linear behavior at higher temperature indicates that the system has not completely re-equilibrated from the previous condition (10% O₂ and 825 °C). At lower pO₂ (0.1 % and 0.01 %) the non-stoichiometry is nearly constant with temperature suggesting that the system has hit the phase boundary shown by the coulometric data on the non-stoichiometry.

Modeling: We have validated the our ab initio approaches on the defect chemistry of LaMnO_{3-δ} to demonstrate that the many approximations needed to treat the perovskites give reliable guidance for defect chemistry. Figure 3 shows the stoichiometry from experiments and a defect model derived from our ab initio energies. [3] The good agreement validates the accuracy of the ab initio approaches.

This work also demonstrated that the defects in LaMnO_{3-δ}

(and presumably (La,Sr)MnO_{3-δ}) have significant interactions that play a key role in the defect energetics. This result is critical for guiding accurate modeling of defect chemistry in many perovskite systems.

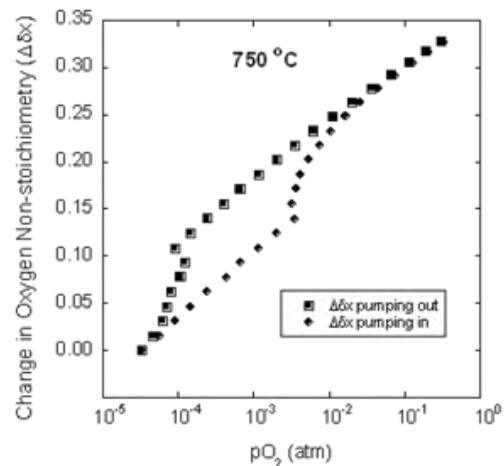


Figure 1: Relative stoichiometry data for PrBaCo₂O_{5+δx} at 750 °C.

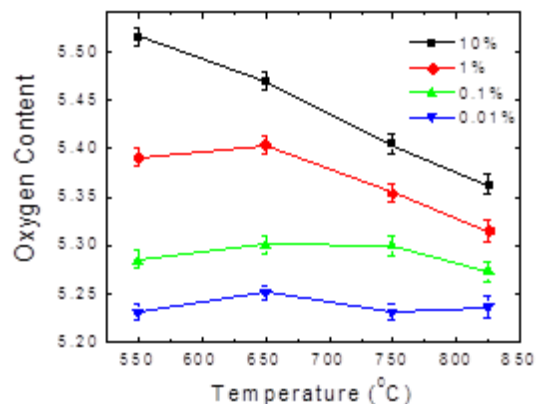


Figure 2: Oxygen non-stoichiometry of PrBaCo₂O_{5+x} as a function of T and pO₂.

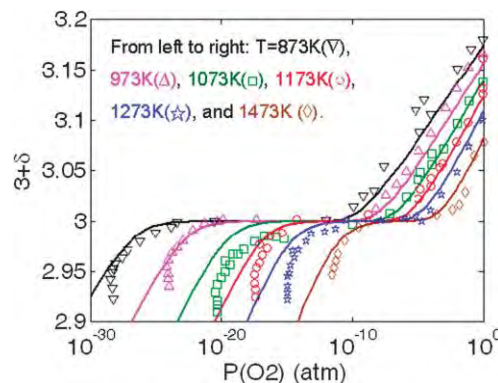


Figure 3: LaMnO_{3+d} composition as a function of pO₂ from experiment and ab initio based model (from ref. [3]).

Present work is focused on two directions. First, we are exploring the energetics of A-site cation ordering, particularly for La-Sr given their wide use and observed ordering in our recent work. [4] Our results show only a very weak ordering tendency in (La,Sr)MnO₃ and (La,Sr)CoO₃, suggesting that the ordering seen in Ref. [4] requires a strong coupling to oxygen vacancies. We have also begun studying the migration energy for O diffusion in ABaCo₂O_{5.5} (A= La, Pr, Sm, Gd, Y) to understand the role of A-site dopant on the oxygen kinetics. Initial results suggest that size effects can explain many of the trends we are seeing.

Future Plans

A detailed model to analyze the oxygen non-stoichiometry data for PrBaCo₂O_{5+x} and NdBaCo₂O_{5+x} will be developed. We will determine the nature of the ordered phase at the composition PrBaCo₂O_{5.25}. We will extend the measurements of both thermodynamic and kinetic properties to include the Sm, Eu, and Gd analogs and to investigate the effects of Fe substitution for Co in PrBaCo_{2-x}Fe_xO_{5.5} with x =0.5, 1, 1.5, and 2.0.

We will continue ab initio based thermodynamic and kinetic studies on (ABa)Co₂O_{5+x} systems to parallel the experimental efforts. The goal of this work is to understand the dominant oxygen ordering and assist in the development of the oxygen non-stoichiometry model and well as determine which cations yield the best kinetics and why.

References

- 1 Yoo, J.; Jacobson, A. J., *Proceedings Electrochemical Society* **2003**, 2002-26(Solid-State Ionic Devices III), 354-363.
- 2 Liu, L. M.; Lee, T. H.; Qiu, L.; Yang, Y. L.; Jacobson, A. J., *Materials Research Bulletin* **1996**, 31(1), 29-35.
- 3 Lee, Y. L.; Morgan, D., *Physical Chemistry Chemical Physics* **2012**, 14(1), 290-302.
- 4 Donner, W.; Chen, C.L.; Jacobson, A. J.; Lee, Y.-L.; Gadre, M.; Morgan, D., *Chemistry of Materials*, **2011**, 23(4), 984-988.

Publications

1. Materials for Solid Oxide Fuel Cells, A. J. Jacobson, Chem. Mater. **2010**, 22(3) 660-674.
2. Electrically driven oxygen separation through gadolinia-doped ceria using PrBaCo₂O_{5+x} and NdBaCo₂O_{5+x} electrodes, M. Yadav, W. Gong and A. J. Jacobson. J Solid State Electrochem. **2011**, 15(2), 293-301, DOI 10.1007/s10008-010-1082-0.
3. Oxygen Non-Stoichiometry in Nano-crystalline La_{0.5}Sr_{0.5}CoO_{3-x} Thin Films, S. Wang, S. Cho, H. Wang, and A. J. Jacobson, ECS Transactions, **2011**, 35(1), 1891-1897.
4. Epitaxial Strain-Induced Chemical Ordering in La_{0.5}Sr_{0.5}CoO₃ Films on SrTiO₃, W. Donner, C.L. Chen, A.J. Jacobson, Y.-L. Lee, M. Gadre, D. Morgan, Chemistry of Materials, **2011**, 23(4), 984-988.
5. Strain Effects on Defect Chemistry in Epitaxial Perovskite Thin Films for Solid Oxide Fuel Cells, M. Gadre, Y.-Lin Lee, N. Swaminathan, D. Morgan, ECS Transactions, **2011**, 35(1), 2113-2118.

6. Prediction of solid oxide fuel cell cathode activity with first-principles descriptors, Y.-L. Lee, J. Kleis, J. Rossmeisl, Y. Shao-Horn, D. Morgan, *Energy & Environmental Science*, **2011**, 4(10), 3966.
7. Cation Interdiffusion Model for Enhanced Oxygen Kinetics at Oxide Heterostructure Interfaces, M. Gadre, Y.-L. Lee, D. Morgan, *Phys. Chem. Chem. Phys.*, 14 (8), 2606 – 2616 (**2012**).
8. Ab initio and empirical defect modeling of $\text{LaMnO}_{3-\delta}$ for solid oxide fuel cell cathodes, Y. L. Lee, D. Morgan, *Physical Chemistry Chemical Physics* **2012**, 14 (1), 290-302.
9. Surface Strontium Enrichment on Highly Active Perovskites for Oxygen Electrocatalysis in Solid Oxide Fuel Cells, E. Crumlin, E. Mutoro, Z. Liu, M. E. Grass, M. Biegalski, Y.-L. Lee, D. Morgan, H. Christen, H. Bluhm, Y. Shao-Horn, *Energy & Environmental Science* 5 (3), p. 6081-6088 (**2012**).
10. Thin-Film Solid Oxide Fuel Cell Materials, A. J. Jacobson in “Functional Materials for Energy Applications” in press **2012**.
11. Cation Interdiffusion Model for Enhanced Oxygen Kinetics at Oxide Heterostructure Interfaces, M. J. Gadre, Y.-L. Lee, D. Morgan, to be published in *Physical Chemistry Chemical Physics* **2012**.
12. $\text{NdBaCo}_2\text{O}_{5+\delta}$ structural parameters determined by *in-situ* neutron diffraction, R. A. Cox-Galhotra, A. Huq, J. P. Hodges, J.-H. Kim, C. Yu, X. Wang, A. J. Jacobson, S. McIntosh to be submitted to *Chemistry of Materials* **2012**.
13. The Oxygen Non-stoichiometries of $\text{PrBaCo}_2\text{O}_{5+x}$ and $\text{NdBaCo}_2\text{O}_{5+x}$ Determined by Coulometric Titration W. Gong, D. Rupasov, C. Yu, and A. J. Jacobson, to be submitted to *J. Electrochem. Soc.* **2012**.
14. Effect of Interlayer Thickness on the Electrochemical Properties of Bi-layer Cathodes for Solid Oxide Fuel Cells, Q. Su, D. Yoon, Y. N. Kim, W. Gong, A. Chen, S. Cho, A. Manthiram, A. J. Jacobson, H. Wang to be submitted to *J. Power Sources*.

Molecular and Nanoscale Engineering of High Efficiency Excitonic Solar Cells

Samson A. Jenekhe, Guozhong Cao and David S. Ginger
University of Washington, Departments of Chemical Engineering, Chemistry, and
Materials Science and Engineering, Seattle, WA 98195

Program Scope

By coupling tailored materials design of both organic and inorganic materials closely with device measurements and optical spectroscopy we propose to use new materials to harvest more of the solar spectrum while generating larger cell voltages by uncovering the fundamental factors such as energy level offsets, relative dielectric constants, interfacial chemistry, and morphology that control relative branching ratios between geminate recombination and free carrier generation at a range of model donor/acceptor interfaces. These studies will identify the design rules and fundamental performance limits for new organic and hybrid organic/inorganic photovoltaic materials. We thus propose to: (1) develop new p-type polymers with tailored energy level offsets and different morphologies (e.g. nanowires) to systematically explore the effects of energetics and morphology on recombination loss in polymer/fullerene systems; (2) explore new n-type polymers with a range of energy levels, optical bandgaps and carrier mobilities to enable investigation of effects of energetics and morphology on device performance and recombination loss in polymer/polymer bulk heterojunction (BHJ) solar cells for comparison with fullerene acceptors; (3) design and study new hybrid inorganic quantum dot/polymer combinations for extending the response of solution-processable solar cell materials into the near and mid-IR, while exploring the role of acceptor dielectric constant and surface chemistry; (4) manipulate the surface chemistry and facets of ZnO nanostructures towards studies of effects of dielectric constant and morphology on charge injection rate and surface recombination rate in organic/inorganic hybrid systems; and (5) use test beds of experimental tools to probe and quantify the performance limits and loss mechanisms in BHJ solar cells based on various model donor/acceptor pairs produced in this project.

Recent Progress

Photoinduced Charge Transfer and Polaron Dynamics in Polymer and Hybrid Photovoltaics: Organic versus Inorganic Acceptors. We used photoinduced absorption (PIA) spectroscopy to study charge generation and recombination in a series of bulk heterojunction blends relevant to organic photovoltaics (OPVs) and hybrid solar cells. We drew on the full synthetic breadth of our team to compare both organic and inorganic electron acceptors, including the fullerene, phenyl-C₆₁-butyric acid methyl ester (PCBM), oxides such as ZnO, and

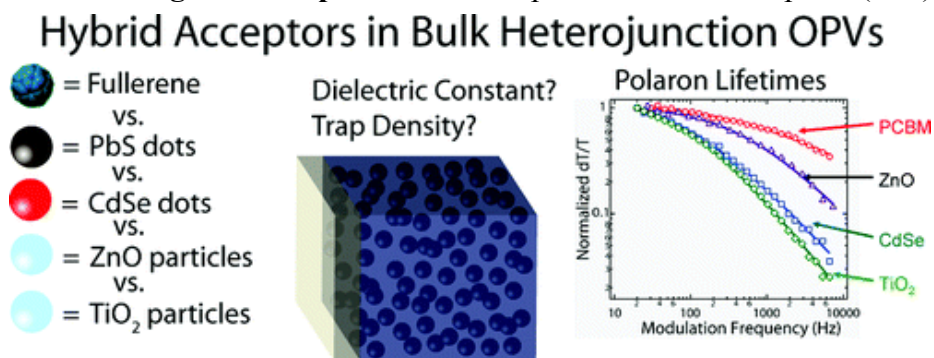


Fig. 1. Illustration of BHJ polymer OPVs exploring various organic and inorganic electron acceptors and corresponding PIA spectra for polymer/acceptor (PCBM, ZnO, CdSe, or TiO₂). The pump modulation dependence of the PIA signal for some of the polymer (donor)/acceptor blend films investigated.

the fullerene, phenyl-C₆₁-butyric acid methyl ester (PCBM), oxides such as ZnO and TiO₂, and

colloidal quantum dots, including CdSe and PbS nanocrystals. We used a variety of donor host polymers, including poly(3-hexylthiophene) (P3HT), poly[2-methoxy-5-(3',7'-dimethyloctyloxy)-*p*-phenylenevinylene] (MDMO-PPV), and poly(2,3-bis(2-hexyldecyl)quinoxaline-5,8-diyl-*alt*-*N*-(2-hexyldecyl)-dithieno[3,2-*b*:2',3'-*d*]pyrrole) (PDTPQx-HD). In every case, we observed longer average carrier lifetimes in blends with inorganic acceptors as compared to blends with PCBM. The PIA data also indicated that the internal electric fields are attenuated in the inorganic blends, consistent with increased screening between the photogenerated carriers due to the higher dielectric constants of the inorganic nanoparticles. Using ligand exchange experiments, we further demonstrated that surface electron trapping on the inorganic colloids contributes to at least part of the increased lifetime in the PDTPQx-HD/PbS blends and that ligand exchange to remove traps can be used to improve the performance of these polymer/low-band-gap quantum dot hybrid photovoltaics (*J. Phys. Chem. C* **2011**, *115*, 24403).

Effects of Polymer Side Chains on Charge Photogeneration and Efficiency of BHJ Solar Cells. Our previous work suggested that for the same conjugated polymer backbone the *type* (alkyl, alkoxy, aryl), *size*, *topology* (linear, branched) and *distribution* (uniform, alternating, random) of side chains can have a large impact on the morphology (crystallinity, π -stacking orientations), charge transport and photovoltaic properties of the materials and thus should also

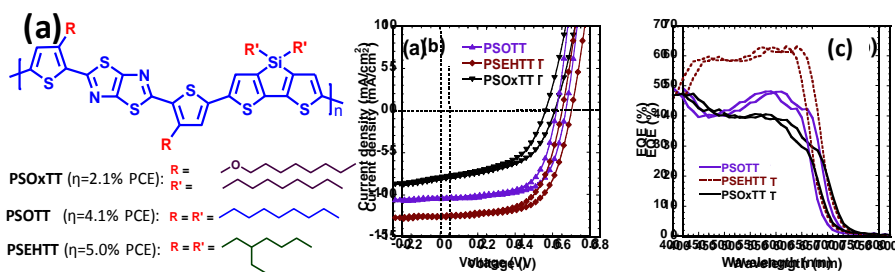


Fig. 2. (a) Molecular structures of copolymers, PSO_xTT, PSOTT, and PSEHTT. (b) The current density – voltage characteristics of PSOTT:PC₇₁BM (1:2), PSEHTT:PC₇₁BM (1:2), and PSO_xTT:PC₇₁BM (1:2) solar cells. (c) EQE spectra of the solar cells, measured on devices with an active area of 9 mm².

be fully considered in the design of new polymers for solar cells. To further investigate the effects of side chains on charge photogeneration and efficiency of BHJ solar cells, we have synthesized a series of new thiazolothiazole-dithienosilole based donor-acceptor copolymers with different side chains (Fig. 2a). Changing side chains on the polymer from linear octyloxy to octyl, and linear octyl to branched ethylhexyl, the average power conversion efficiency was improved from 2.1% in PSO_xTT to 4.1% in PSOTT to 5.0% in PSEHTT, respectively. The PSEHTT:PC₇₁BM device showed the highest photoconversion efficiency with a monochromatic EQE around 60% over the 450–650 wavelength range. Transient optical absorption studies indicate that these differences in photovoltaic device performance correlate with differences in geminate recombination losses. These results provide new insights toward the design of optimum polymers for high performance excitonic solar cells (*Adv. Energy Mater.* **2011**, *1*, 854).

TiO₂ Nanocrystallite Aggregates for Dye-sensitized Solar Cells (DSCs) - Prepared Using an Electrospray Method. Nanocrystallite aggregates have been demonstrated to be an effective method to significantly enhance the power efficiency in ZnO DSCs, increasing the efficiency from 2.4 to 5.2% PCE. The enhancement is due to the generation of light scattering, which may extend the traveling distance of incident light within the photoelectrode film and

thereby increase the optical absorption of the photoelectrode. However, ZnO is not stable in the ruthenium dye solution, preventing the formation of fully covered self-assembled monolayer of dyes, and thus limits further improvement in the efficiency of this system.

Chemically stable TiO_2 nanocrystallite aggregates would take the advantage of light scattering while achieving a full coverage of dye molecules. We have applied an electro spray method to fabricate TiO_2 nanocrystallite aggregates from commercially available TiO_2 nanoparticles (Fig. 3). The advantage of this method is that the most favorable facets of the TiO_2 nanoparticles are retained so as to achieve the most ideal dye adsorption. The other merit of this method is that the size

and porosity of the aggregates can be readily tuned by adjusting the solid content and additives in the colloidal dispersion and the voltage applied for the electro spray. DSCs with TiO_2 nanocrystallite aggregates have an efficiency of 5.9% PCE. Many groups around the world have been following our idea of using nanocrystallite aggregates to advance fundamental understanding and efficiency of DSCs.

Future Plans

In the next year we plan to emphasize experiments enabled by the team's complementary expertise to study new (p- and n-type) donor and acceptor materials from Jenekhe as hosts for PbS quantum dots from Ginger that operate in both "normal" and "inverted" structures with high-surface area metal oxide electrodes from Cao. Jenekhe will chemically tailor the thiazolothiazole-based polymer family (side chains, molecular weight), Ginger the PbS quantum dot sizes and surfaces, and Cao the ZnO/TiO_x particle sizes, shapes and surfaces to maximize hybrid device performance in solid state bulk heterojunction, depleted heterojunction, and hybrid (bulk+depleted) heterojunction configurations. At the same time we will use optical spectroscopy to screen these evolving materials combinations for suitable use with non-toxic p-type Cu_2S and FeS_2 nanoparticles, while continuing to probe the basic processes controlling performance in the testbed PbS-based devices. Examples of specific experiments include studies of hole transfer from the PbS dots to the organics as a function of driving force (by synthetic control of dot size and polymer host redox potentials), and studies to correlate local device efficiency with scanning probe data and SEM images of the metal oxide electrodes to understand the specific correlations between local nanotexturing of the oxide and overall photocurrent collection. We also plan to test the hypothesis that sometimes the quantum dot domains are behaving as local Schottky diode cells after ligand exchange—operating in parallel with the hybrid BHJ rather than in direct electronic contact with it.

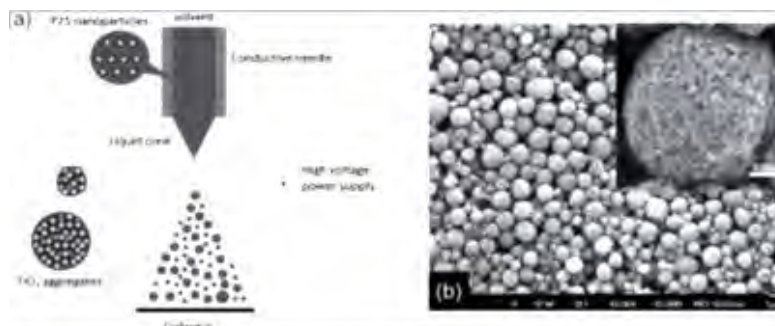


Fig. 3. Electro spray method for the fabrication of TiO_2 nanocrystallite aggregates. (a) Schematic diagram showing set-up for electro spray fabrication of TiO_2 nanocrystallite aggregates, and (b) SEM images of TiO_2 nanocrystallite aggregates produced with the electro spray method.

Publications (Selected from 35 total journal papers in the last 2 years)

1. Xin, H.; Guo, X.; Ren, G.; Watson, M. D.; Jenekhe, S. A. "Efficient Phthalimide Copolymer-Based Bulk Heterojunction Solar Cells: How the Processing Additive Influences Nanoscale Morphology and Photovoltaic Properties". *Adv. Energy Mater.* **2012**, *2*, 575-582.
2. Zhang, Q. F.; Yodyingyong, S.; Xi, J. T.; Myers, D.; and Cao, G. Z. "Oxide nanowires for solar cell applications". *Nanoscale* **2012**, *4*, 1436-1445.
3. Noone, K. M.; Subramaniyan, S.; Zhang, Q. F.; Cao, G. Z.; Jenekhe, S. A.; Ginger, D. S. "Photoinduced Charge Transfer and Polaron Dynamics in Polymer and Hybrid Photovoltaic Thin Films: Organic vs Inorganic Acceptors". *J. Phys. Chem. C* **2011**, *115*, 24403-24410.
4. Ren, G. Q.; Ahmed, E.; Jenekhe, S. A. "Non-Fullerene Acceptor-Based Bulk Heterojunction Polymer Solar Cells: Engineering the Nanomorphology via Processing Additives". *Adv. Energy Mater.* **2011**, *1*, 946-953.
5. Subramaniyan, S.; Xin, H.; Kim, F. S.; Jenekhe, S. A. "New Thiazolothiazole Copolymer Semiconductors for Highly Efficient Solar Cells". *Macromolecules* **2011**, *44*, 6245-6248.
6. Subramaniyan, S.; Xin, H.; Kim, F. S.; Shoaee, S.; Durrant, J. R.; Jenekhe, S. A. "Effects of Side Chains on Thiazolothiazole-Based Copolymer Semiconductors for High Performance Solar Cells". *Adv. Energy Mater.* **2011**, *1*, 854-860.
7. Zhang, Q. F.; Park, K.; Xi, J. T.; Myers, D.; Cao, G. Z. "Recent Progress in Dye-Sensitized Solar Cells Using Nanocrystallite Aggregates". *Adv. Energy Mater.* **2011**, *1*, 988-1001.
8. Ahmed, E.; Ren, G. Q.; Kim, F. S.; Hollenbeck, E. C.; Jenekhe, S. A. "Design of New Electron Acceptor Materials for Organic Photovoltaics: Synthesis, Electron Transport, Photophysics, and Photovoltaic Properties of Oligothiophene-Functionalized Naphthalene Diimides". *Chem. Mater.* **2011**, *23*, 4563-4577.
9. Kim, F. S.; Ren, G.; Jenekhe, S. A. "One-Dimensional Nanostructures of π -Conjugated Molecular Systems: Assembly, Properties, and Applications from Photovoltaics, Sensors, and Nanophotonics to Nanoelectronics," *Chem. Mater.* **2011**, *23*, 682-732.
10. Ren, G.; Wu, P.-T.; Jenekhe, S. A. "Solar Cells Based on Block Copolymer Semiconductor Nanowires: Effects of Nanowire Aspect Ratio," *ACS Nano* **2011**, *5*, 376-384.
11. Q.F. Zhang and G.Z. Cao, "Nanostructured Photoelectrodes for Dye-sensitized Solar Cells," *Nano Today* **2011**, *6*, 91-109.
12. Reid, O. G.; Xin, H.; Jenekhe, S. A.; Ginger, D. S. "Nanostructure determines the intensity-dependence of open-circuit voltage," *J. Appl. Phys.* **2010**, *108*, 084320.
13. Xin, H.; Reid, O. G.; Ren, G.; Kim, F. S.; Ginger, D. S.; Jenekhe, S. A. "Polymer Nanowire/Fullerene Bulk Heterojunction Solar Cells: How Nanostructure Determines Photovoltaic Properties," *ACS Nano* **2010**, *4*, 1861-1872.
14. Noone, K. M.; Strein, E.; Anderson, N. C.; Wu, P.-T.; Jenekhe, S. A.; Ginger, D. S. "Broadband Absorbing Bulk Heterojunction Photovoltaics Using Low-Bandgap Solution-Processed Quantum Dots," *Nano Lett.* **2010**, *10*, 2635-2639.
15. Yodyingyong, S.; Zhou, X.Y.; Zhang, Q. F.; Triampo, D.; Limketkai, B.; Cao, G. Z. "Enhanced photovoltaic performance of nanostructured hybrid solar cell using highly oriented TiO₂ nanorods," *J. Phys. Chem. C* **2010**, *114*, 21851-21855.

SISGR: Fundamental Studies of Charge Transfer in Quantum Confined Nanostructure Heterojunctions and Applications to Solar Energy Conversion

Song Jin, John C. Wright, and Robert J. Hamers

Department of Chemistry, University of Wisconsin-Madison, Madison, WI 53706

(jin@chem.wisc.edu, wright@chem.wisc.edu, rjhamers@wisc.edu)

Program Scope

We create new nanostructures and their heterojunctions with well-defined surface chemistry and develop new laser spectroscopies that probe charge transport at the quantum mechanical level. They provide the fundamental understanding required to enable transformative coherent solar energy nanotechnologies.

Recent Progress

An ideal large-scale solar technology should utilize inexpensive and sustainable earth-abundant materials and possess the ultrafast coherent charge transfer dynamics that characterizes the most efficient solar conversion. However, earth-abundant materials pose substantial challenges that must be solved. Nanotechnology offers new approaches for meeting these challenges. The complexity of earth abundant materials hinders our ability to exploit them without more sophisticated characterization methods. We seek new paradigms for making and characterizing efficient nanoscale earth-abundant heterostructures. Our research incorporates typical characterization methods including surface photovoltage (SPV) and ultrafast pump-probe and transient absorption but it also incorporates the recently developed multiresonant coherent multidimensional spectroscopy (CMDS) methods that can spectrally resolve individual excitonic and multiexcitonic quantum states, resolve their coherent and incoherent dynamics, narrow inhomogeneous line profiles, resolve surface states, define the correlations between states, and measure the Coulombic coupling and relative transition moments of biexcitonic states.

We have developed nanomaterials of several earth-abundant semiconductors and their nanoscale heterostructures. Single-crystal iron pyrite (FeS_2) nanowires (NWs) have been synthesized via thermal sulfidation. We have developed an improved method to synthesize hematite ($\alpha\text{-Fe}_2\text{O}_3$) NWs via thermal oxidation that reduces reaction time while improving NW density and uniformity. These hematite NWs can be doped with Si to significantly improve their conductivity. We have also developed a facile method for converting $\alpha\text{-FeF}_3\cdot 3\text{H}_2\text{O}$ NWs to porous semiconducting $\alpha\text{-Fe}_2\text{O}_3$ NWs of high aspect-ratio on FTO substrates via a simple thermal treatment in air. Photoelectrochemical (PEC) investigations of these nanostructured photoelectrodes showed promising photocurrent and photovoltage without intentional doping. Preliminary Ti-doping treatments improved the photocurrent. Further improvement and better understanding using time-resolved surface photovoltage (TR-SPV) and other spectroscopic techniques are needed and are on-going. We also have investigated organic ligands to stabilize

CdSe and other chalcogenide nanocrystals against corrosion and to improve stability of CdSe-based solar devices by using ligands that will remove the resulting holes from the nanocrystals.

We have developed a new method to synthesize epitaxial heterostructures of quantum dots (QDs) on NWs by integrating the colloidal QD synthesis with the NWs prepared via vapor phase or other synthesis, as shown in the example of PbSe QDs with α -Fe₂O₃ NWs (Fig. 1).

The key to our success is a vacuum surface treatment that we have developed to remove the surface absorbed water that is often present on the surface of oxides, and this ensures the integration of the two nanostructures. The results are epitaxial QD-decorated NW structures with the size of QDs tunable by controlling the temperature of the colloidal synthesis. The heteroepitaxy between PbSe and Fe₂O₃ (Fig. 1F&G) that has not been previously observed illustrates that fortuitous heteroepitaxy can occur readily in nanoscale heterostructures. This discovery creates a general approach for preparing heteroepitaxial nanostructures. These nanostructures will be the model systems for the multidimensional spectroscopy investigation.

Our recent progress extended earlier picosecond experiments that demonstrated feasibility to femtosecond time scales that provide the full capabilities of multiresonant CMDS. Fig. 2 shows examples of this system's capabilities. It can scan any combination of excitation frequencies, output frequencies, and excitation pulse time delays. Fig. 2a shows the 2D frequency spectrum of PbSe QDs with excitation pulse time delays where the first pulse creates a 1S exciton and the next two pulses creates output coherences that probe either the 1S biexciton or exciton. It also shows that the 1S exciton is coupled to a continuum of higher energy states. The coherent and incoherent dynamics can be probed at any set of frequencies within the 2D spectrum.

Fig. 2b shows the relaxation dynamics at one point in the 2D spectrum. Note that it also shows a weak beating that is characteristic of coherence transfer

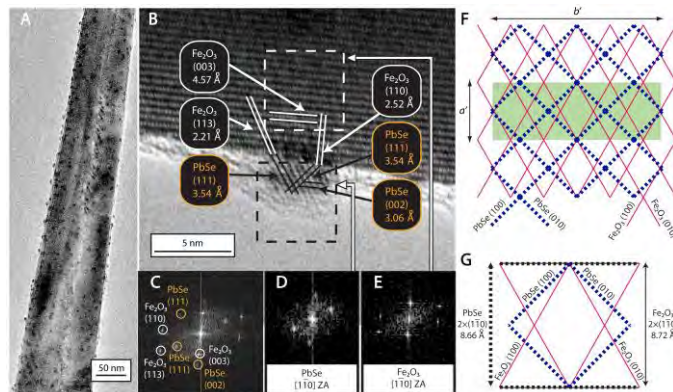


Fig. 1. TEM analysis of the epitaxial PbSe QD-Fe₂O₃ NW heterostructures and the illustration of the crystallographic relationship at the interface.

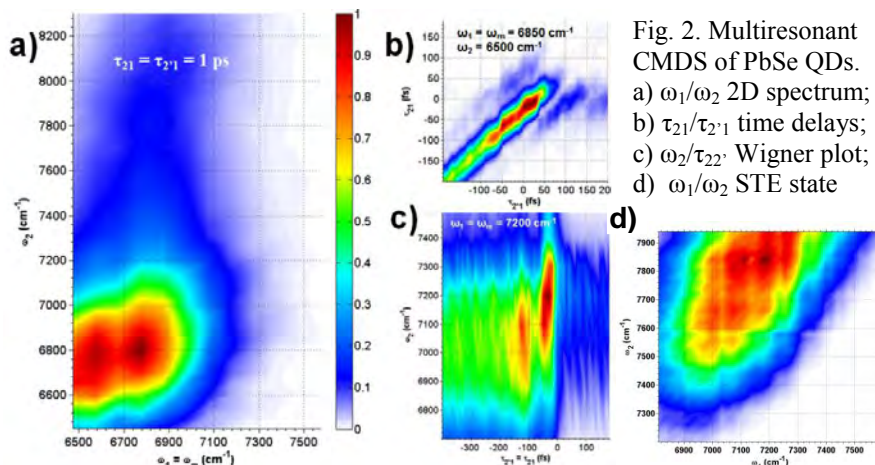


Fig. 2. Multiresonant CMDS of PbSe QDs. a) ω_1/ω_2 2D spectrum; b) τ_{21}/τ_{21} time delays; c) ω_2/τ_{22} Wigner plot; d) ω_1/ω_2 STE state

between states. Fig. 2c shows another example where an excitation frequency and a time delay are scanned so the relative dynamics of different states is displayed. Fig. 2d shows the 2D spectrum of a surface trapped exciton (STE), which appears as a cross-peak between the 1S exciton and the STE states. Note that the diagonal character results from the CMDS line-narrowing capabilities and the slope reflects the relative effects of size heterogeneity on the 1S and STE states.

Fig. 3 shows our recent development of femtosecond surface photovoltage (SPV). It directly measures charge separation. SPV is an inherently nonlinear process where the interaction region mixes two modulated optical beams to create new output signals at the sum and difference frequencies. Fig. 3 shows preliminary experiments that demonstrate the detection of an ultra-fast SPV signal with time response on the <100 fs time scale.

Future Plans

The strength of our research program is its integration of our team's breadth, depth, and experience for synthesizing, modifying, characterizing, and understanding complex nanostructures. Our method for synthesizing epitaxial heterojunctions is the foundation for our goal of creating efficient solar materials with abundant semiconductors. We are further developing this methodology to create epitaxial heterostructures between various nanomaterials we have already made, and we will explore doping and surface modifications to optimize charge transfer efficiency, eliminate surface states, and enhance stability.

We will use the multiresonant CMDS methods to observe the changes in the individual quantum states in earth abundant nanostructures over the entire time scale from charge creation to charge recombination. This capability will be implemented using pump-CMDS probe methods where an initial excitation creates excitons or multiexcitons and a time delayed set of CMDS pulses provides multidimensional spectra of the quantum states' evolution. We will take advantage of our capability for resolving not only individual quantum states of a nanostructure but also its surface states. Multiresonant CMDS experiments will first explore the states and dynamics of the individual nanomaterials and later explore the changes that result from creating heterostructures. We will be particularly interested in understanding the changes during charge transfer across epitaxial heterojunctions and the involvement of surface and interface states. The experiments will include observing the quantum state changes upon doping, surface passivation, and biasing within an operational PEC. We will correlate the behavior of the quantum states and their dynamics observed in the CMDS experiments with PEC properties of the nanostructures prepared under different synthetic procedures in order to guide optimization of the charge transfer and solar efficiency. We will develop interface selective even-order wave mixing (EOWM) spectroscopy to specifically isolate the dynamics of quantum states at the electrode-solvent interface of a working PEC cell.

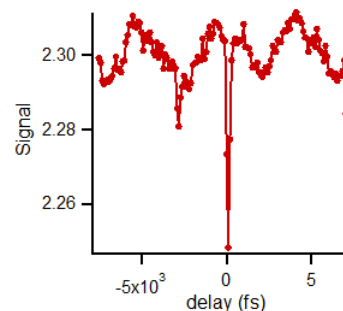


Fig. 3. Preliminary femtosecond-surface photovoltage measurements showing resolution of <100 fs.

Furthermore, the femtosecond SPV method we have developed will be combined with atomic force microscopy (AFM) and the CMDS system to probe the charge separation dynamics in individual nanostructures and the quantum state resolved dynamics simultaneously. While CMDS can provide direct femtosecond dynamics they are limited in their spatial resolution. SPV measurements can probe the dynamics of photoexcited charge carriers on nanometer length scales using a nanoscale electrical probe located from an AFM or STM near a sample. We will develop and apply the TR-SPV spectroscopy for characterizing nanoscale heterostructures at the space-time limit. We will combine femtosecond optical excitation with a conductive AFM tip to have a nano-scale electrical probe of the charge separation. Information will be encoded in the time- and/or phase-modulation of the incident beams at audio frequencies; demodulation of the signal picked up by the electrical probe will reveal the nonlinear character of the response.

We will use our unique femtosecond CMDS system and SPV-AFM to investigate the quantum states in the epitaxial heterostructures, particularly the coupling between donor and acceptor states and the coherent and incoherent dynamics resulting from the epitaxial interface. This research will lead to a fundamental understanding of charge transfer in nanoscale heterostructures and it will provide an in-depth characterization that informs and guides the synthetic efforts to build efficient heterostructures and develop new nanomaterials.

References (see the next section)

Publications

- Block, S. B.; Yurs, L. A.; Pakoulev, A. V.; Selinsky, R. S.; Jin, S.; Wright, J. C.; “Multiresonant Multidimensional Spectroscopy of Surface-Trapped Excitons in PbSe Quantum Dots” *submitted*.
- Selinsky, R. S.; Shin, S.; Lukowski, M. A.; R. J.; Jin, S.; “Epitaxial Heterostructures of Lead Selenide Quantum Dots on Hematite Nanowires” *in revision*.
- Caban-Acevedo, M.; Faber, M. S.; Tan, Y.; Hamers, R. J.; Jin, S.; “Synthesis and Properties of Semiconducting Iron Pyrite (FeS₂) Nanowires” *Nano Lett.* **2012**, *12*, 1977-1982.
- Yurs, L. A.; Block, S. B.; Pakoulev, A. V.; Selinsky, R. S.; Jin, S.; Wright, J. C.; “Spectral Isolation and Measurement of Surface-Trapped State Multidimensional Nonlinear Susceptibility in Colloidal Quantum Dots” *J. Phys. Chem. C* **2012**, *116*, 5546-5553.
- Li, L.; Yu, Y.; Meng, F.; Tan, Y.; Hamers, R. J.; Jin, S.; “Facile Solution Synthesis of α -FeF₃·3H₂O Nanowires and Their Conversion to α -Fe₂O₃ Nanowires for Photoelectrochemical Application” *Nano Lett.* **2012**, *12*, 724-731.
- Yurs, L. A.; Block, S. B.; Pakoulev, A. V.; Selinsky, R. S.; Jin, S.; Wright, J. C.; “Multiresonant Coherent Multidimensional Electronic Spectroscopy of Colloidal PbSe Quantum Dots” *J. Phys. Chem. C* **2011**, *146*, 22833–22844. (Featured on the cover).
- Lukowski, M. A.; Jin, S.; “Improved Synthesis and Electrical Properties of Si-Doped α -Fe₂O₃ Nanowires” *J. Phys. Chem. C* **2011**, *115*, 12388-12395.
- Song Jin, Matthew J. Bierman, Stephen A. Morin, “A New Twist on Nanowire Formation: Screw Dislocation-Driven Growth of Nanowires and Nanotubes” *J. Phys. Chem. Lett.* **2010**, *1*, 1472-1480.

SISGR: BI-CONTINUOUS MULTI-COMPONENT NANOCRYSTAL SUPERLATTICES FOR SOLAR ENERGY CONVERSION

Cherie R. Kagan, Christopher B. Murray, James M. Kikkawa, Nader Engheta, University of Pennsylvania, Philadelphia, PA 19104

Program Scope

Our program explores three-dimensional multi-component nanocrystal (NC) superlattices, wherein combinations of NCs self-assemble into well-defined, crystalline architectures [Fig. 1].^{1,2} We focus on crystal structures having bi-continuous, NC-sub-lattices and identify n and p-type semiconductor NC building blocks that form Type-II energy offsets to drive charge separation onto electron and hole transporting sub-lattices and provide wide coverage of the solar spectrum. We aim to discover the design rules and optimize the architectures of bi-continuous, multi-component NC superlattices to efficiently convert solar radiation into electricity. Our interdisciplinary team combines NC synthesis, assembly, and structural characterization with optical spectroscopy, electrical measurements, and modeling of nanoscale materials and the physical phenomena that govern the flow of energy and the transfer and transport of charge important in converting solar energy into electricity.

Recent Progress

Wet-chemical synthetic routes have been developed to prepare a wide-range of semiconductor,³ metal,^{D3} and metal-oxide^{D1} NC samples tunable in size from ~2-20 nm in diameter and monodisperse to $\leq 5\%$, providing many different building blocks for the self-assembly of single and multi-component NC superlattices. NCs display new mesoscopic phenomena found in neither bulk nor molecular system that depend on

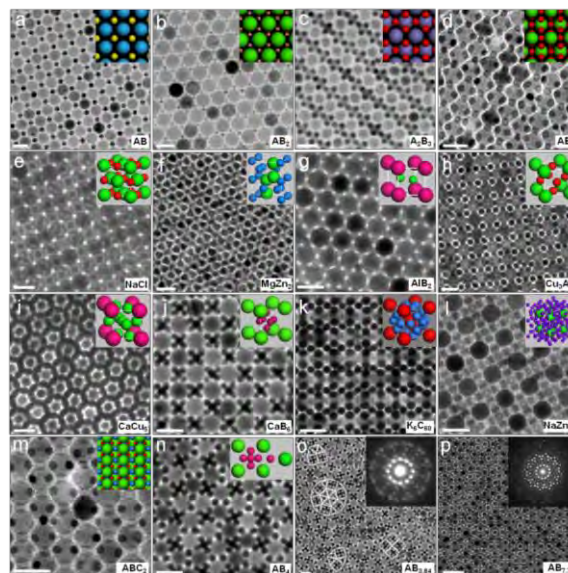


Fig. 1 TEM images of multi-component NC superlattice structures having the structural analogs of binary phases: (a) AB, (b) AB₂, (c) A₂B₃, (d) AB₃, (e) NaCl, (f) MgZn₂, (g) AlB₂, (h) Cu₃Au, (i) CaCu₅, (j) CaB₆, (k) K₆C₆₀, (l) NaZn₁₃, tertiary structures: (m) ABC₂, and quasi-crystalline motifs: (n) AB₄, (o) AB_{3.84}, and (p) AB_{7.7}. Scale bar = 20 nm

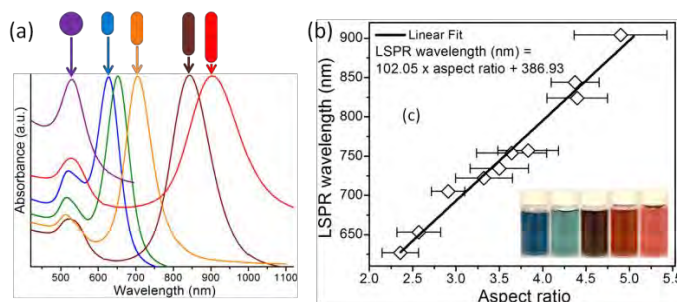


Fig. 2 Au nanorod (NR) (a) absorption and (b) calculated wavelength of the longitudinal surface plasmon resonance (LSPR) as a function of NR aspect ratio. Inset: Au NRs with increasing NR aspect ratio (from left to right) in solution.

crystallite size and shape. We recently developed an improved synthesis of Au nanorods and corroborating simulations,^{D13} which allows the longitudinal surface plasmon resonance to be tuned from 627 nm to now 1246 nm [Fig. 2].

We developed methods,³ which have now been broadly applied, to organize NC superlattices from the wide-range of synthetically achieved NC chemistries. We recently developed processes to assemble NC superlattices over large areas [Fig. 3], to form uniform layers of controlled thickness (from monolayer to many multilayers), or superlattices structured periodically on the micron scale in NC thickness.^{D4} This is realized by assembling the NC superlattices at the liquid-air interface, which allows the superlattices to be subsequently transferred to arbitrary surfaces and integrated into measurement and device architectures.

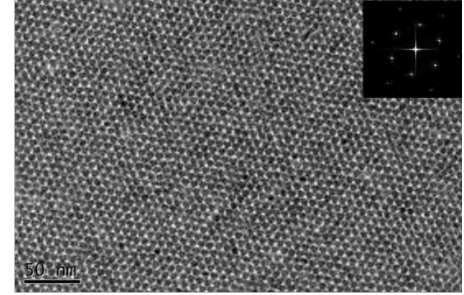


Fig. 2 Superlattice of 7 nm PbTe NCs assembled at the liquid-air interface

Collective physical phenomena between neighboring NCs in close-packed arrays give rise to novel and fascinating electronic, optical, and optoelectronic properties.³ We recently extended our studies of electronic energy transfer to mixed CdSe-CdTe NC arrays. In competition with energy transfer, carrier tunneling between neighboring NCs allows for charge transport and observations of photo- and dark- conductivity. In early reports, conductivities were very small as the long, insulating aliphatic ligands used in the synthesis and assembly of the NCs gave rise to highly resistive materials requiring low-level current measurements. Recently, through the introduction of a new, compact thiocyanate ligand, we demonstrated dramatically enhanced photoconductivity and gain, the highest reported in the literature.^{D11} We realized high performance, balanced electron and hole mobilities in PbS nanocube FETs which we exploited to demonstrate the first non-sintered quantum dot based circuits.^{D12}

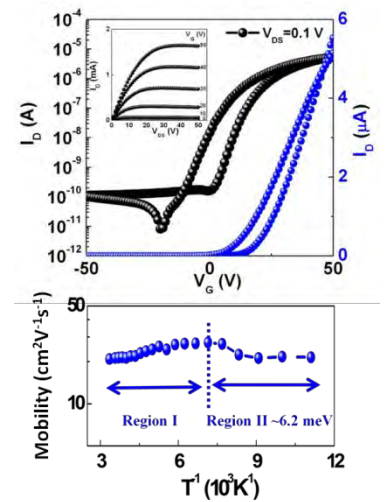


Fig. 4 Transfer and (inset) output characteristics of high mobility CdSe NC thin film transistor. Temperature dependent mobility showing increasing mobility with decreasing temperature (region I).

The thiocyanate ligand chemistry is non-corrosive, which allowed us to integrate these NC FETs and circuits on flexible plastics. While most studies of photoconductivity and charge transport have been pursued on small bandgap Pb-chalcogenides, we demonstrated dramatic performance enhancement in wider band gap CdSe NC thin films: by combining strong-coupling (through the use of the thiocyanate ligand) and by doping (through a process of thermal diffusion not previously used in NC thin films), we realized band transport and carrier mobilities as high as 27 cm²/Vs [Error! Reference source not found.].^{D14}

We have synthesized multifunctional NC superlattices, focusing on the binary crystallization of colloidal NCs using combinations of semiconducting and metallic NC building blocks. We have

identified more than thirty different binary nanocrystal superlattice (BNSL) structures, of which more than half of these colloidal crystalline structures were reported for the first time.^{D6} Examples of these BNSL structures, those that are bi-continuous and therefore a focus of the research program, are shown in **Fig. 1(c, f, i, k, l)**. Electrostatically adjusting the NCs to be charge neutral favors the formation of bi-continuous structures as it eliminates the repulsive interactions that exist between like charged NCs. We have demonstrated that static electrical charges on sterically stabilized NCs influence BNSL stoichiometry and, with additional contributions from entropic, van der Waals, steric, and dipolar forces, stabilize a rich variety of additional crystal structures. In addition to BNSLs, we have also recently demonstrated ternary nanocrystal superlattices (TNSLs) comprised of three distinct NC components.^{D8}

Future Plans

Our team will develop the synthesis of NC building blocks that are earth abundant and of controlled size and shape as constituents in the assembly of multi-component NC superlattices. We will develop common platforms to correlate structure, optical and electrical measurements to investigate the same region of multi-component NC superlattices. Using compact ligand chemistries, we will probe and optimize charge transfer and transport processes in the crystalline architectures of type-II BNSLs. We will explore the origin of traps that limit the mobility-lifetime product in NC solids and use chemical methods to passivate these. We will integrate plasmonic building blocks in the design of TNSLs and use plasmonic enhancement to increase energy harvesting.

References

- ¹ Redl, F. X.; Cho, K.-S.; Murray, C. B.; O'Brien, S. Three-dimensional binary superlattices of magnetic nanocrystals and semiconductor quantum dots. *Nature* **2003**, *423*, 968-971.
- ² Shevchenko, E. V.; Talapin, D. V.; Kotov, N. A.; O'Brien, S.; Murray, C. B. Structural diversity in binary nanoparticle superlattices. *Nature* **439**, 55-59 (2006).
- ³ Murray, C. B.; Kagan, C. R.; Bawendi, M. G. Synthesis and Characterization of Monodisperse Nanocrystals and Close-Packed Nanocrystal Assemblies. *Ann. Rev. Mater. Sci.* **30**, 545-610 (2000).

Publications (additionally referenced in abstract above)

- ^{D1} "Morphologically controlled synthesis of colloidal upconversion nanophosphors and their shape-directed self-assembly," X. C. Ye, J. E. Collins, Y. J. Kang, J. Chen, D. T. N. Chen, A. G. Yodh, and C. B. Murray, *Proc. Nat. Acad. Sci.* **107**, 22430-22435 (2010).
- ^{D2} "Collective Dipolar Interactions in Self-Assembled Magnetic Binary Nanocrystal Superlattice Membranes" J. Chen, A. G. Dong, J. Cai, X. C. Ye, Y. J. Kang, J. K. Kikkawa, C. B. Murray, *Nano Lett.* **10**, 5103-5108 (2010).

- ^{D3} “Size- and Shape-Selective Synthesis of Metal Nanocrystals and Nanowires Using CO as a Reducing Agent” Y. J. Kang, X. C. Ye, C. M. Murray, *Angew. Chem.-Int. Ed.* **49**, 6156-6159 (2010).
- ^{D4} “Multiscale Periodic Assembly of Striped Nanocrystal Superlattice Films on a Liquid Surface,” A. Dong, J. Chen, S. J. Oh, W.-K. Koh, F. Xiu, X. Ye, D.-K. Ko, K. L. Wang, C. R. Kagan, C. B. Murray, *Nano Lett.* **11**, 841-846 (2011).
- ^{D5} "Carrier Distribution and Dynamics of Nanocrystal Solids Doped with Artificial Atoms Context Sensitive Links" D.-K. Ko, J. J. Urban, C. B. Murray, *Nano Lett.* **10**, 1842-1847 (2010).
- ^{D6} “Polymorphism in Self-Assembled AB(6) Binary Nanocrystal Superlattices” X. Ye, Chen, J. Chen, C. B. Murray, *J. Am. Chem. Soc.* **133**, 2613-2620 (2011).
- ^{D7} “A Generalized Ligand-Exchange Strategy Enabling Sequential Surface Functionalization of Colloidal Nanocrystals” A. G. Dong, X. C. Ye, J. Chen, Y. J. Kang, T. G. Gordon, J. M. Kikkawa, Y. C. Ye, and C. B. Murray, *J. Am. Chem. Soc.* **133**, 998-1006 (2011).
- ^{D8} “Two-Dimensional Binary and Ternary Nanocrystal Superlattices: The Case of Monolayers and Bilayers” A. Dong, X.C. Chen, J. Chen, and C. B. Murray, *Nano Lett.* **11**, 1804-1809 (2011).
- ^{D9} "Tailoring hot-excitonic emission in semiconducting nanowires via whispering gallery nanocavity plasmons" Chang-Hee Cho, Carlos O. Aspetti, Michael E. Turk, James M. Kikkawa, Sung-Wook Nam, and Ritesh Agarwal, *Nat. Mater.* **10**, 669-675 (2011).
- ^{D10} “Near-Infrared Absorption of Monodisperse Silver Telluride (Ag₂Te) Nanocrystals and Photoconductive Response of Their Self-Assembled Superlattices,” Y.-W. Liu, D.-K. Ko, S. J. Oh, T. R. Gordon, V. Doan-Nguyen, T. Paik, Y. Kang, X. Ye, L. Jin, C. R. Kagan, and C. B. Murray, *Chem. Mater.* **23**, 4657-4659, (2011).
- ^{D11} “Thiocyanate Capped Nanocrystal Colloids: A Vibrational Reporter of Surface Chemistry and a Solution-based Route to Enhanced Coupling in Nanocrystal Solids,” A. T. Fafarman, W.-K. Koh, B. T. Diroll, D. K. Kim, D.-K. Ko, S. J. Oh, X. Ye, V. Doan-Nguyen, M. R. Crump, D. C. Reifsnnyder, C. B. Murray, and C. R. Kagan, *J. Am. Chem. Soc.* **133**, 15753–15761, (2011).
- ^{D12} “Thiocyanate-capped PbS nanocubes: ambipolar transport enables quantum dot-based circuits on a flexible substrate,” W.-K. Koh, S. R. Saudari, A. T. Fafarman, C. R. Kagan, and C. B. Murray, *Nano Lett.* **11**, 4764–4767 (2011).
- ^{D13} “Programmable Synthesis of Monodisperse Gold Nanorods through Engineering of Rod-like Micelles,” X. X. Ye, L. Jin, H. Caglayan, J. Chen, G. Xing, C. Zheng, V. Doan-Nguyen, Y. Kang, N. Engheta, C. R. Kagan, C. B. Murray, *ACS Nano*, **6**, 2804-2817 (2012).
- ^{D14} “Band-like transport in strongly-coupled and doped quantum dot solids: A route to high-performance thin-film electronics,” J.-H. Choi, A.T. Fafarman, S. J. Oh, D.-K. Ko, D. K. Kim, B. T. Diroll, S. Muramoto, J. G. Gillen, C. B. Murray, C. R. Kagan, *Nano Lett.*, **12**, 2631-2638 (2012).
- ^{D15} “Remote Doping and Schottky Barrier Formation in Strongly Quantum Confined Single PbSe Nanowire Field-Effect Transistors,” S. J. Oh, D. K. Kim, C. R. Kagan, *ACS Nano*, *ASAP* (2012).

Chemistry and Properties of Complex Intermetallics from Metallic Fluxes

(Grant DE-FG02-07ER46356)

Mercouri G Kanatzidis, Department of Chemistry, Northwestern University, Evanston, IL 60208

Program Scope

This project investigates the reaction chemistry and synthesis of novel intermetallic compounds with complex compositions and structures using metallic fluxes as solvents. The metallic fluxes offer several key advantages in facilitating the formation and crystal growth of new materials and they are liquid aluminum, gallium and indium. We focus on the ability of these fluxes to produce phases which are difficult to predict a-priori and are likely to feature novel characteristics. Specifically, we seek to: (a) to discover mainly Si (or Ge)-based compounds with new structures, bonding and exotic physicochemical properties; the aim is to discover exciting new materials displaying unusual bonding and enhanced cooperative phenomena, such as magnetic ordering, phase transitions, spin and charge density waves, as well as other properties such as oxidation resistance. (b) to learn more about the reaction chemistry that is responsible for stabilizing such materials and to study their structural interrelationships to ultimately be able to predict their existence. (c) to identify and characterize the complex phases present in many advanced Al-matrix alloys. Such phases play a key role in determining (either beneficially or detrimentally) the mechanical properties of Al-matrix alloys. This project enhances our basic knowledge of the solid state chemistry and physics of intermetallics, produce new materials with unusual or enhanced bulk properties and ultimately help improve our understanding of component/matrix interactions that could lead to better Al-matrix alloys. This work is performed predominantly with two graduate students.

Recent Progress

Indium flux chemistry: Our work with In flux has led to some interesting quaternary phases so far, such as the $RE_4Ni_2InGe_4$ ($RE = Dy, Ho, Er, Tm$) and $RE_7Co_4InGe_{12}$ ($RE = Dy, Ho, Yb$). We have uncovered a rich chemistry revealed by the thorough examination of the ternary $RE/Au/In$ system and so we decided to incorporate also a tetrelide such as Ge in order to search for more complex structures and compositions and to compare with the analogous $RE/T/Al/Si$ or Ge and $RE/T/Ga/Ge$ or Si systems investigated previously.¹⁻¹³ Among the rare earth compounds, the Yb-based intermetallics which are considered as the hole counterparts to the isostructural cerium compounds (i.e. f^{13} vs. f^1 systems), have received considerable attention for the past few years. This interest originates from their ability to exhibit various peculiar properties such as intermediate-valence, heavy fermion or Kondo behavior and unusual magnetism. These properties are generally believed to arise from the strong hybridization (interaction) between the localized $4f$ electrons and the delocalized s , p , d conduction electrons.

$Yb_3AuGe_2In_3$, is particularly interesting and was grown from In flux. It crystallizes as an ordered variant of the $YbAuIn$ structure. We studied the magnetic properties, X-ray Absorption Near Edge Spectroscopy (XANES), electrical resistivity, thermoelectric power and heat capacity measurements are reported. These studies suggest

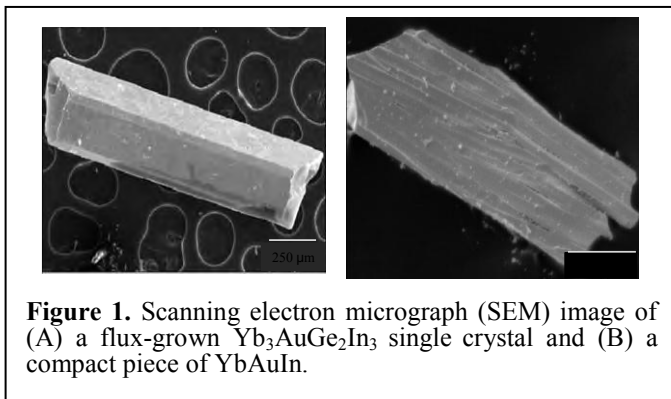


Figure 1. Scanning electron micrograph (SEM) image of (A) a flux-grown $Yb_3AuGe_2In_3$ single crystal and (B) a compact piece of $YbAuIn$.

that $\text{Yb}_3\text{AuGe}_2\text{In}_3$ is an intermediate or heterogeneous mixed-valence system. Similar studies are also reported for the parent isostructural YbAuIn in an attempt to investigate the similarities and/or differences between the two compounds. Crystals of $\text{Yb}_3\text{AuGe}_2\text{In}_3$ grow in indium flux generally as metallic silver rods and in a smaller portion as thinner needles. Figure 1 shows SEM images of a typical rod type $\text{Yb}_3\text{AuGe}_2\text{In}_3$ and YbAuIn crystals. When other rare earth metals such as Ce, Sm, Eu, Dy and Pr were employed under the same reaction conditions we did not observe analogs of $\text{Yb}_3\text{AuGe}_2\text{In}_3$. In contrast, the REAuIn family of compounds forms with most of the RE atoms including Yb.

Crystal Structure. $\text{Yb}_3\text{AuGe}_2\text{In}_3$ crystallizes as an ordered variant of the YbAuIn structure. YbAuIn contains two crystallographically independent gold sites in trigonal prismatic coordination. The overall structure of the compound is illustrated in Figure 2. The Au atoms have trigonal prisms formed by the In atoms and those of Ge are built up from ytterbium atoms. Both types of trigonal prisms are capped on the rectangular faces: $[\text{AuIn}_6]$ by three ytterbium atoms and $[\text{GeYb}_6]$ by three indium atoms, leading to coordination number nine for gold and germanium sites. The three-dimensional arrangement that the rare earth atoms adopt in this structure type leads to three exceptional features: i) The RE ions within the same layer form triangles so when it comes to antiferromagnetic coupling between nearest neighbors, this topology can cause frustration of the magnetic interactions. ii) The fact that the magnetic RE atoms are stacked in $[\text{Yb}_3\text{Au}]$ layers that alternate with the non-magnetic $[\text{GeIn}_3]$ layers, can give rise to indirect exchange interactions. iii) The crystalline electric field surrounding the lanthanide ions frequently induces strong anisotropy, which leads either to Ising or XY spin behavior. Examples of compounds adopting this arrangement are the families of REAuIn and RENiAl .

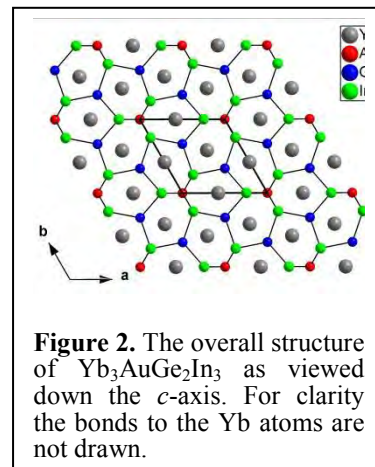


Figure 2. The overall structure of $\text{Yb}_3\text{AuGe}_2\text{In}_3$ as viewed down the c -axis. For clarity the bonds to the Yb atoms are not drawn.

Magnetism. Figure 3(A) shows the molar magnetic susceptibility (χ_m) of a ground sample of $\text{Yb}_3\text{AuGe}_2\text{In}_3$ measured with applied field of 500 G. The magnetic susceptibility data follow a modified Curie-Weiss (CW) law that includes a temperature independent component according to the equation $\chi(T) = \chi_0 + C / (T - \theta_p)$. χ_0 includes the sum of the temperature-independent contributions, e.g. van Vleck paramagnetism and Pauli paramagnetism (due to conduction electrons). The effective magnetic moment μ_{eff} was deduced from the Curie constant C , ($C = \mu_{\text{eff}}^2 / 8$). A nonlinear least-squares fit to this equation resulted in $\chi_0 = 3.2 \times 10^{-3}$ emu/mol of Yb atom, Curie - Weiss constant of $\theta_p = -1.5$ K indicating antiferromagnetic interactions and an effective moment of $0.52 \mu_B / \text{Yb}$ atom. The inset in Figure 4(A) shows the plot of $1/(\chi - \chi_0)$ versus temperature. The estimated effective moment of $0.52 \mu_B$, is only $\sim 11.5\%$ of the value expected for the free-ion Yb^{3+} , $4.54 \mu_B$. This indicates that the compound contains both Yb^{2+} and Yb^{3+} species. In order to confirm the presence of Yb^{3+} species in the title compound we performed XANES studies.

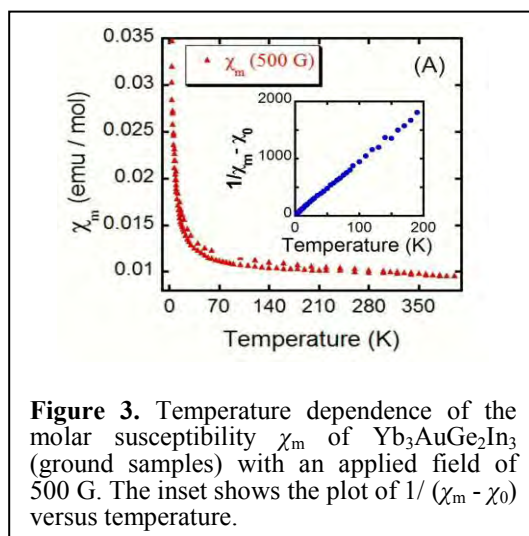


Figure 3. Temperature dependence of the molar susceptibility χ_m of $\text{Yb}_3\text{AuGe}_2\text{In}_3$ (ground samples) with an applied field of 500 G. The inset shows the plot of $1/(\chi_m - \chi_0)$ versus temperature.

XANES. To further probe the Yb valence state in $\text{Yb}_3\text{AuGe}_2\text{In}_3$ and YbAuIn , we performed X-ray absorption measurements at the Yb L_{III} -edge (Advanced Photon Source ANL). The near-edge spectra for both compounds obtained at temperatures of ~ 15 - 18 K and 300 K and at ambient pressure showed no significant difference between the two temperatures,

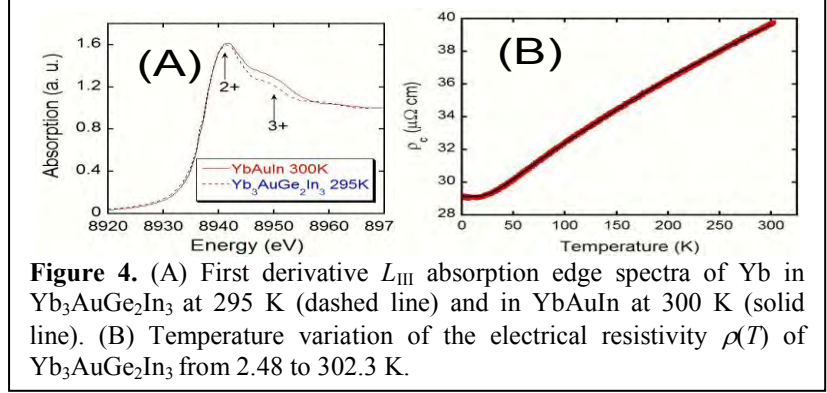


Figure 4. (A) First derivative L_{III} absorption edge spectra of Yb in $\text{Yb}_3\text{AuGe}_2\text{In}_3$ at 295 K (dashed line) and in YbAuIn at 300 K (solid line). (B) Temperature variation of the electrical resistivity $\rho(T)$ of $\text{Yb}_3\text{AuGe}_2\text{In}_3$ from 2.48 to 302.3 K.

suggesting that the Yb valence remained stable in the measured temperature range. The spectra at 295 and 300 K (room temperature) for $\text{Yb}_3\text{AuGe}_2\text{In}_3$ and YbAuIn , respectively, are given in Figure 4(A). The main absorption peak (white line resonance) of the spectrum for both spectra is centered at ~ 8941.5 eV, which is attributed to divalent Yb atoms. The spectra also reveal the presence of a weaker feature (shoulder) at ~ 8949.5 eV, indicating that some trivalent Yb is also present. The relative amounts of the two electronic configurations were determined by decomposing the normalized Yb XANES into a pair of arc-tangents and Lorentzians functions (representing the white line resonance). Fitting of the data with the above technique for $\text{Yb}_3\text{AuGe}_2\text{In}_3$, resulted in $\sim 85.2\%$ of Yb^{2+} and $\sim 14.8\%$ of Yb^{3+} which leads to an average Yb valence of ~ 2.15 . For YbAuIn , similar analysis led to an average Yb valence of ~ 2.22 . In the case of YbAuIn however, while majority of the Yb is present in the intermediate state, a careful inspection and analysis of the EXAFS indicates that the sample might also contain ~ 3 - 5% of a trivalent oxide impurity component. Taking into account the possible presence of an oxide component we determine the intrinsic valence of Yb in YbAuIn to be ~ 2.17 .

Resistivity. The $\text{Yb}_3\text{AuGe}_2\text{In}_3$ compound is clearly metallic. The temperature variation of the electrical resistivity $\rho(T)$ of $\text{Yb}_3\text{AuGe}_2\text{In}_3$ between 2.48 and 302.3 K is presented in Figure 4(B). The resistivity data measured on single crystals along the c -axis and at zero applied field reveal metallic conductivity with a room temperature resistivity value $\rho(300\text{K})$ of $39.6 \mu\Omega \text{ cm}$. When a magnetic field of 6 Tesla was applied the compound showed no magnetoresistance.

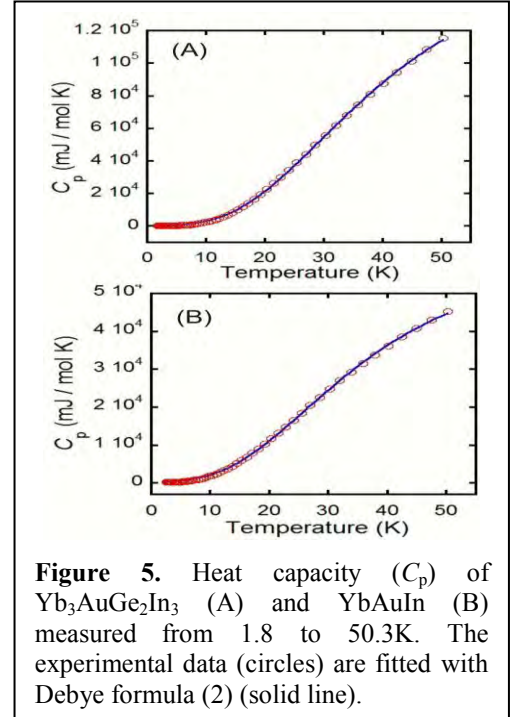


Figure 5. Heat capacity (C_p) of $\text{Yb}_3\text{AuGe}_2\text{In}_3$ (A) and YbAuIn (B) measured from 1.8 to 50.3K. The experimental data (circles) are fitted with Debye formula (2) (solid line).

Heat Capacity . The temperature dependent specific heat from 1.8 to 50 K for $\text{Yb}_3\text{AuGe}_2\text{In}_3$ is shown in Figure 5(A). The data can be described well by a Debye function (2) where the first and second term correspond to the electronic and the phonon contribution, respectively. N is the number of the atoms in the formula unit and $x = \hbar\omega/k_B T$.

$$C_p(T) = \gamma T + 9NR \left(\frac{T}{\Theta_D} \right)^3 \int_0^{\Theta_D/T} \frac{x^4 dx}{(e^x - 1)^2} - KT^3 \quad (2)$$

A fit to the experimental points resulted in a Debye temperature Θ_D of about 178 K, and an electronic specific heat coefficient $\gamma \approx 31 \text{ mJ} / \text{mol K}^2$, which was determined from $\gamma (= C_p / T)_{T \rightarrow 0}$ at low

temperatures. The observed Θ_D value is slightly higher than the value obtained from the resistivity measurements (166 K). Therefore the compound does not appear to be a heavy-fermion material according to the arbitrary classification of these compounds into “light”, “moderate” and classical heavy-fermions with γ values lying in the range of ~ 50 -60, 100-400 and > 400 mJ / mol K² respectively.

The temperature dependent specific heat data measured at a temperature range of 1.8 to 50 K for YbAuIn are shown in Figure 5(B). The data can also be described well by the Debye function (2). A least-square fit to the experimental points resulted in a Debye temperature Θ_D of about 156 K, and an electronic specific heat coefficient $\gamma \approx 84$ mJ/mol K², which was determined from $\gamma (= C_p/T)_{T \rightarrow 0}$ at low temperatures. According to the arbitrary classification of the heavy-fermion compounds mentioned above, YbAuIn could be classified as a “light” heavy-fermion compound.

Future Plans: This program is in its last year. There are no future plans. A renewal proposal will not be submitted.

References

- (1) Hundley, M. F.; Sarrao, J. L.; Thompson, J. D.; Movshovich, R.; Jaime, M.; Petrovic, C.; Fisk, a. Z. *Phys. Rev. B* **2001**, *65*, 024401.
- (2) Macaluso, R. T.; Sarrao, J. L.; Moreno, N. O.; Pagliuso, P. G.; Thompson, J. D.; Fronczek, F. R.; Hundley, M. F.; Malinowski, A.; Chan, J. Y. *Chem. Mater.* **2003**, *15*, 1394.
- (3) Chen, X. Z.; Larson, P.; Sportouch, S.; Brazis, P.; Mahanti, S. D.; Kannewurf, C. R.; Kanatzidis, M. G. *Chem. Mater.* **1999**, *11*, 75.
- (4) Chen, X. Z.; Small, P.; Sportouch, S.; Zhuravleva, M.; Brazis, P.; Kannewurf, C. R.; Kanatzidis, M. G. *Chem. Mater.* **2000**, *12*, 2520.
- (5) Chen, X. Z.; Sportouch, S.; Sieve, B.; Brazis, P.; Kannewurf, C. R.; Cowen, J. A.; Patschke, R.; Kanatzidis, M. G. *Chem. Mater.* **1998**, *10*, 3202.
- (6) Zhuravleva, M. A.; Evain, M.; Petricek, V.; Kanatzidis, M. G. *J. Am. Chem. Soc* **2007**, *129*, 3082.
- (7) Zhuravleva, M. A.; Kanatzidis, M. G. *Z. Naturforsch B : Sec. B* **2003**, *58*, 649.
- (8) Zhuravleva, M. A.; Pcioneck, R. J.; Wang, X. P.; Schultz, A. J.; Kanatzidis, M. G. *Inorg. Chem.* **2003**, *42*, 6412.
- (9) Lattner, S. E.; Bilc, D.; Mahanti, S. D.; Kanatzidis, M. G. *Chem. Mater.* **2002**, *14*, 1695.
- (10) Lattner, S. E.; Bilc, D.; Mahanti, S. D.; Kanatzidis, M. G. *Inorg. Chem.* **2003**, *42*, 7959.
- (11) Lattner, S. E.; Kanatzidis, M. G. *Inorg. Chem.* **2008**, *47*, 2089.
- (12) Wu, X. U.; Lattner, S. E.; Kanatzidis, M. G. *Inorg. Chem.* **2006**, *45*, 5358.
- (13) Sieve, B.; Chen, X. Z.; Henning, R.; Brazis, P.; Kannewurf, C. R.; Cowen, J. A.; Schultz, A. J.; Kanatzidis, M. G. *J Am Chem Soc* **2001**, *123*, 7040.

Publications in 2010-2012 period

1. Peter, S. C.; Kanatzidis, M. G. *Zeitschrift Fur Anorganische Und Allgemeine Chemie* **2012**, *638*, 287.
2. Peter, S. C.; Malliakas, C. D.; Nakotte, H.; Kothapilli, K.; Rayaprol, S.; Schultz, A. J.; Kanatzidis, M. G. *Journal of Solid State Chemistry* **2012**, *187*, 200.
3. Chondroudi, M.; Peter, S. C.; Malliakas, C. D.; Balasubramanian, M.; Li, Q. A.; Kanatzidis, M. G. *Inorganic Chemistry* **2011**, *50*, 1184.
4. Peter, S. C.; Chondroudi, M.; Malliakas, C. D.; Balasubramanian, M.; Kanatzidis, M. G. *Journal of the American Chemical Society* **2011**, *133*, 13840.
5. Peter, S. C.; Rayaprol, S.; Francisco, M. C.; Kanatzidis, M. G. *European Journal of Inorganic Chemistry* **2011**, 3963.
6. Sebastian, C. P.; Kanatzidis, M. G. *Journal of Solid State Chemistry* **2010**, *183*, 2077.
7. Sebastian, C. P.; Kanatzidis, M. G. *Journal of Solid State Chemistry* **2010**, *183*, 878.
8. Sebastian, C. P.; Malliakas, C. D.; Chondroudi, M.; Schellenberg, I.; Rayaprol, S.; Hoffmann, 9. R. D.; Pottgen, R.; Kanatzidis, M. G. *Inorganic Chemistry* **2010**, *49*, 9574.
10. Sebastian, C. P.; Salvador, J.; Martin, J. B.; Kanatzidis, M. G. *Inorganic Chemistry* **2010**, *49*, 10468.

Rational Synthesis of Superconductors

(FWP 70053)

Mercouri G. Kanatzidis, Materials Science Division, Argonne National Laboratory

Program Scope

This project is a material synthesis program using a multi-faceted approach that combines the rational design of novel materials with structural and electronic characterization probes. One strategy adopted is the conception of homology to investigate pnictide and intermetallic systems and narrow gap semiconductors. We focus on materials with a high degree of structural and compositional freedom and chemical/electronic complexity with which to investigate: (a) density-wave instabilities (spin and charge), and their suppression through chemical doping in order to generate superconductivity that may emerge from phase competition, and (b) how narrow energy band gaps and facile doping properties could lead to a superconducting state. The project focuses on relationships between structure, composition, electronic structure and physical properties. In the long term, we expect to understand phase competition and clarify the influence of various building blocks on the physical properties and enhance our ability to further design members exhibiting superconductivity.

Recent Progress

Synthesis of high quality superconductors: The overwhelming body of work with ternary iron arsenide today is focused on substitution doping of transition metals (e.g. Co, Ni, etc) into the Fe sites because it is easier to grow relatively homogeneous large crystals. K substitution on the Ba site however is very challenging because of the extreme volatility of the alkali metal which produces grossly inhomogeneous crystals unsuitable for many studies. We have refined the synthesis procedures and successfully generated high quality samples, both polycrystalline and single crystal, of $\text{Ba}_{1-x}\text{K}_x\text{Fe}_2\text{As}_2$ and $\text{Ba}_{1-x}\text{Na}_x\text{Fe}_2\text{As}_2$ across the entire phase diagram, with sharp superconducting transitions as low as 4K, showing that the compositional fluctuations have been reduced from previous studies.

Our compositionally precise samples allowed revising the previous phase diagrams reported, Figure 1. The tetragonal-orthorhombic and antiferromagnetic transitions are suppressed with K-doping in $\text{Ba}_{1-x}\text{K}_x\text{Fe}_2\text{As}_2$, falling to zero at $x \leq 0.3$. The magnetic and structural phase transitions are coincident and first-order over the entire phase diagram, with a strong biquadratic coupling of the magnetic structure to the nuclear lattice. The onset of superconductivity is at $x = 0.135$ with all three phases coexisting until $x \geq 0.24$. As already observed in $\text{Ba}(\text{Fe}_{1-x}\text{Co}_x)_2\text{As}_2$, but in contrast to earlier reports of phase separation, there is evidence of a coupling of the magnetic and superconducting order parameters close to the onset of superconductivity.

Synthesis of novel pnictide compounds: The new compound CaFe_4As_3 displaying low-temperature Fermi-liquid behavior, with enhanced electron-electron correlations was discovered in our laboratory. Antiferromagnetic ordering was observed below T_N of 96 K, possibly via a SDW. The SDW comprises of spins from three Fe^{2+} and one Fe^+ atoms. Anisotropic charge transport studies show a drop in

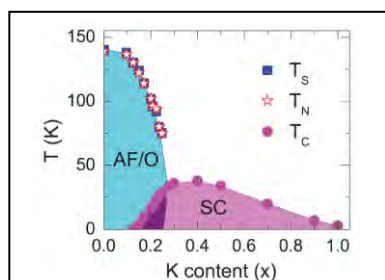


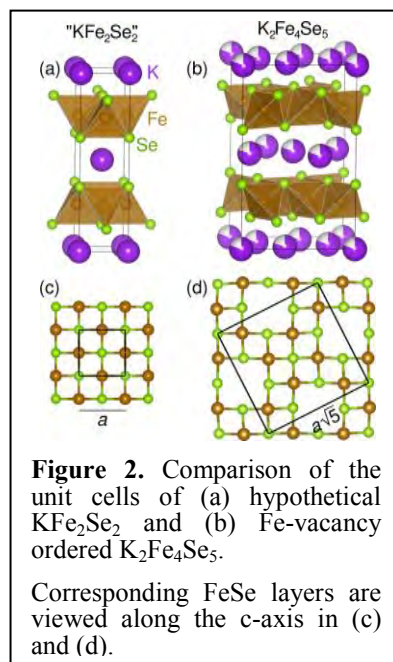
Figure 1. Phase diagram of $\text{Ba}_{1-x}\text{K}_x\text{Fe}_2\text{As}_2$ with the superconducting critical temperatures T_c (circles), the Néel temperatures T_N (stars), and the structural transition temperatures T_s

resistivity at 26 K, correlated with a similarly abrupt increase in the magnetic susceptibility. The magnetic structure of the SDW was shown to be incommensurate with respect to the $[\text{Fe}_4\text{As}_3]^{2-}$ lattice. Below 85 K, an incommensurate longitudinal SDW with magnetic moments directed along the b -axis was observed. Below 25 K, there is a first-order phase transition (ferromagnetism).

Detailed investigation of superconductivity and phase identification in the alkali iron selenide ($A_x\text{Fe}_{2-y}\text{Se}_2$; $A = \text{K}, \text{Cs}$) system: The recent discovery of superconductivity in a ThCr_2Si_2 -type chalcogenide of $A_x\text{Fe}_{2-y}\text{Se}_2$ has challenged many theories about high- T_C Fe-based superconductors. The reported T_C near 31 K is higher than any other chalcogenide, including its parent FeSe, where miniscule changes in Fe stoichiometry can tune T_C and cause it disappear altogether. The mechanisms of this behavior as well as the structure of the superconducting phase are still hotly debated.

For $\text{K}_x\text{Fe}_{2-y}\text{Se}_2$ (Figure 2), we optimized the synthetic procedure and mapped the phase equilibria in order to investigate the interplay between stoichiometry, crystal structure, and superconductivity. A multi-step, moderate-temperature synthesis route was developed to single phase $\text{K}_x\text{Fe}_{2-y}\text{Se}_2$ powders with variation of x , by which we found that the tendency for Fe^{2+} is so strong that bulk KFe_2Se_2 with mixed oxidation states $\text{Fe}^{2+}/\text{Fe}^+$ cannot be formed at high temperatures and the Fe-vacancy ordered compound $\text{K}_2\text{Fe}_4\text{Se}_5$ where 1/5 Fe sites are vacant and valence is stable at Fe^{2+} . SQUID magnetometry measurements showed that the samples with stoichiometry in the vicinity of $\text{K}_2\text{Fe}_4\text{Se}_5$ are antiferromagnetic insulators and not dopable to produce superconductivity. We also developed a synthetic route to superconducting samples by adapting published methods and growing single crystals of $\text{K}_x\text{Fe}_{2-y}\text{Se}_2$ using an excess of K and Fe contained in a sealed Nb tube.

Structural differences between superconducting and non-superconducting samples are very subtle, and high-resolution structural characterization proved crucial to probe structure-property relations with an eye toward a structural trigger of T_C . By performing high-resolution synchrotron Rietveld refinements on our full collection of samples we determined the stoichiometry and fully defined the unit cells. No variation of T_C versus Se-Fe-Se bond angles was seen, contrary to what is seen in iron pnictides. Instead we discovered a narrow range of c -axis lengths where superconductivity is present for melt-processed crystals. We found that there is no direct correlation between superconductivity and Fe valence, nor the degree of Fe-vacancy ordering as proposed in the literature. Furthermore, the fact that T_C is invariant for all samples (either 30 K or not present) implies that K content and Fe valence cannot dope the superconducting fraction. Our specific heat measurements of superconducting samples showed no enthalpy release at T_C . This precludes bulk superconductivity, and when combined with the invariant T_C , points to the fact that superconductivity most likely arises from an interfacial effect that is itself far from $\text{K}_2\text{Fe}_4\text{Se}_5$ stoichiometry.



Narrow Gap Semiconducting Materials for Candidates of Superconductor: On the opposite side of the property spectrum are semiconductors which do not exhibit spin density wave states and historically have not been a source of superconductor materials. Recent results, however, are helping to change this view and promise to open up vast new phase space for investigations. Metal chalcogenide semiconductors can also be doped to superconductivity upon conventional chemical doping. For example, TiSe_2 , Bi_2Se_3 and Bi_2Te_3 which possess energy gaps of 0.05 eV, 0.3 eV, and 0.15 eV respectively can be doped with transition metals such as Fe, Cr, Cu and Pd to become superconductors. In the same context, we discovered that the narrow band gap semiconductor CsBi_4Te_6 (Figure 3) can be doped to become a superconductors and will explore further inside narrow semiconducting chalcogenide systems.

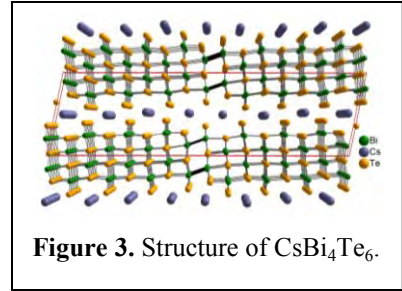


Figure 3. Structure of CsBi_4Te_6 .

CsBi_4Te_6 are doped to both p- and n-type conductors and its superconducting transition around 4 K was identified by measurements of resistivity and field dependence and angular dependence magnetic susceptibility. The point contact spectra confirmed the presence of superconducting gap. In Figure 4, as seen in the magnetic field evolution of the spectra the zero-bias peak does not completely disappear at a field of 1 Tesla and quantitative analysis on the superconducting gap is currently under way.

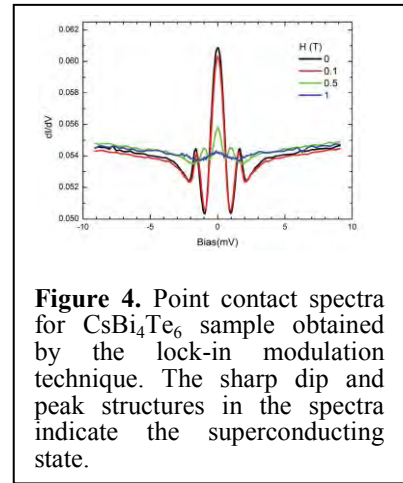


Figure 4. Point contact spectra for CsBi_4Te_6 sample obtained by the lock-in modulation technique. The sharp dip and peak structures in the spectra indicate the superconducting state.

Future Plans

The two primary goals of this FWP work are 1) design and synthesis of new compounds exhibiting electronic instabilities or materials with narrow band gaps as superconducting candidates by applying the concept of phase homologies and 2) study the complexity in the electronic materials to understand and control their electronic properties. In this program we use phase homologies to predict and synthesize new materials in a rational manner (as opposed to a less predictive exploratory approach) and thus the target compounds have defined structural building blocks with controllable dimensions as one of the tunable parameters.

The science-driver underpinning this project is the study and understanding of new and exotic superconductors in the class of complex pnictides (i.e. phosphides, arsenides, antimonides) that feature spin density wave states, intermetallic alloys, and narrow gap semiconductors and we will investigate the following systems.

1. $(\text{REO})_n(\text{A})_m(\text{FePn})_{n+m}$ and $(\text{REO})_n(\text{AE})_{m/2}(\text{FePn})_{n+m}$ (A = alkali metal e.g. Na, K, Rb; AE = alkaline earth element, e.g. Ca, Sr, Ba; Pn = P, As): These can be considered as intergrowth structures between the parent $(\text{REO})(\text{FePn})$ and AFePn fragments. In this series the PbO-type FePn slab stays intact.
2. $(\text{AE})\text{Fe}_{2+m}\text{As}_2\text{X}_m$ (X = group 13, 14, 15 element, e.g. Ga, Si, P, etc.) with thicker iron pnictide slabs with systematically varying m . The first member is $(\text{AE})\text{Fe}_2\text{As}_2$ ($m = 0$). The second, third members etc have thicker arsenide slabs stabilized with an element X

from group 14 or 15 (i.e. Si, Ge). The corresponding phosphide analogs $\text{BaFe}_{2+m}\text{P}_2\text{X}_m$ are also possible.

3. $(\text{Pb}_{1-m}\text{M}_m\text{S})_n(\text{FeAs})$ where $(\text{Pb}_{1-m}\text{M}_m\text{S})_n$ (where M = divalent atom e.g. Sn, Pb, Ca, Sr, Ba): New sulfide/arsenide families with alternating rock salt type layer with the iron pnictide slabs.
4. LaMn_2X_2 , CaMn_2X_2 , REFe_2X_2 and CaCo_2X_2 ($X = \text{Si, Ge}$): Antiferromagnetic ordering in layered phases appears to be common and raises the broad question of the relationship of magnetic interactions with quantum criticality, and the competition of electronic localization with itinerancy. In this respect, we will investigate the corresponding silicide and germanide families of iron and manganese starting from the base members.
5. $\text{K}_x\text{Fe}_{2-y}\text{Se}_2$ and $\text{Cs}_x\text{Fe}_{2-y}\text{Se}_2$: While $\text{K}_x\text{Fe}_{2-y}\text{Se}_2$ has a distinct superconducting transition at 30 K, $\text{Cs}_x\text{Fe}_{2-y}\text{Se}_2$ has a wider superconducting window in a 10 - 30 K range. We will investigate doping dependence of superconductivity and identify the nature of superconductivity and superconducting phase of $\text{A}_x\text{Fe}_{2-y}\text{Se}_2$.

Publications in 2010-2012 period

1. S. Avci, O. Chmaissem, E. A. Goremychkin, S. Rosenkranz, J. P. Castellan, D. Y. Chung, I. S. Todorov, J. A. Schlueter, H. Claus, M. Kanatzidis, A. Daoud-Aladine, D. Khalyavin, and R. Osborn *Phys. Rev. B* **2012**, *85*, 18457. (DOI: 10.1103/PhysRevB.85.184507)
2. Chung, Duck Young; Uher, Ctirad; Kanatzidis, Mercuri G. **2012** *Chem. Mater.* in print. (DOI: 10.1021/cm300490v)
3. Arham, H. Z.; Hunt, C. R.; Park, W. K.; Gillett, J.; Das, S. D.; Sebastian, S. E.; Xu, Z. J.; Wen, J. S.; Lin, Z. W.; Li, Q.; et al *Phys. Rev. Lett.* **2012**, submitted; arXiv 1201.2479v.
4. R. J.-P. Castellan, S. Rosenkranz, E. A. Goremychkin, D. Y. Chung, I. Todorov, M. G. Kanatzidis, I. Eremin, J. Knolle, A. V. Chubukov, S. Maiti, M. Norman, F. Webery, H. Claus, T. Guidi, R. I. Bewley, and R. Osborn *Phys. Rev. Lett.* **2011**, *107*, 177003-1-4. (DOI:10.1103/PhysRevLett.107.177003)
5. S. Avci, O. Chmaissem, E. A. Goremychkin, S. Rosenkranz, J.-P. Castellan, D. Y. Chung, I. S. Todorov, M. G. Kanatzidis, A. Daoud-Aladine, D. Khalyavin, and R. Osborn *Phys. Rev. B* **2011**, *83*, 172503. (DOI:10.1103/PhysRevB.83.172503)
6. Todorov, Iliya; Chung, Duck Young; Claus, Helmut; Gray, Kenneth; Li, Quing'an; Schlueter, John; Bakas, Thomas; Douvalis, Alexios; Gutmann, Matthias; Kanatzidis, Mercuri *Chem. Mater.* **2010**, *22*, 4996-5002.
7. Todorov, Iliya; Chung, Duck Young; Claus, Helmut; Malliakas, Christos; Douvalis, Alexios P.; Bakas, Thomas; He, Jiaqing; Dravid, Vinayak P.; Kanatzidis, Mercuri G. *Chem. Mater.* **2010**, *22*, 3916-3925.
8. P. Manuel, L. C. Chapon, I. S. Todorov, D. Y. Chung, J.-P. Castellan, S. Rosenkranz, R. Osborn, P. Toledano, and M. G. Kanatzidis *Phys. Rev. B* **2010**, *81*, 184402.

Charging and Polarization of Organic Semiconductors in Energy-efficient Circuits and Energy Capture Modules: Synthesis, Electronics, and Spectroscopy

Howard E. Katz, PI, and Andreas G. Andreou, co-PI, Departments of Materials Science and Engineering and Electrical and Computer Engineering, Johns Hopkins University; William L. Wilson, Materials Research Laboratory, University of Illinois

Program Scope

We are engaged in a comprehensive study of interfacial static charging and polarization at organic semiconductor-dielectric and semiconductor-semiconductor interfaces. The objective is to understand and control these effects to develop energy-saving organic semiconductor circuits and organic-based energy capture systems. The activities include materials synthesis, interfacial physical characterization, and circuit implementation. Scanning probe microscopy of statically charged interfaces correlated to device current-voltage relationships are a major focus. Variable-threshold-voltage transistors are fabricated that employ static voltages “prestored” in or near the dielectric for tuning and adaptation. Such transistors have been incorporated into logic circuits; such circuits save energy, as devices can be biased at optimum operating points to have higher gain and reduce power per unit operating current. In addition to optimizing the characteristics of individual transistors, non-volatile storage allows for the integration of programmable switches in energy capture modules such as polymer solar cells that will allow maximum power harvesting and graceful degradation of organic photovoltaic arrays.

A second polarized interface that we are exploring is the one formed by adjacent p and n semiconductors. We will elaborate on a result from the current program in which we showed for the first time that organic pn junctions display a gate-tunable built-in potential that is consistent with models originally derived for inorganic pn junctions. We are exploring material combinations that are used in bulk heterojunction solar cells and bilayer photodiodes. P-N interfacial polarization can affect voltages in complementary circuits containing adjacent films of p and n organic semiconductors. Tuning of p-n polarizations will facilitate photoinduced charge separation in organic and polymer solar cells. As a further extension, the controlled blending and doping of the copolymer semiconductors with densities of states defined for maximum thermoelectric power factors will also be investigated.

For both types of interfaces, we are designing and synthesizing materials, and performing morphological and spectroscopic analysis, scanning probe potential mapping, and device analysis to uncover charge distributions responsible for the activity of the materials in the various applications. We are also building circuits from the devices. The impact will be to lower the energy footprint of emerging, alternative electronic components and to increase the efficiency of solar cells and thermoelectrics based on organic semiconductors.

Recent Progress

By using corona charging on atactic polystyrene dielectric before semiconductors and contacts were patterned, we have adjusted the threshold voltage in both p-type (pentacene) and n-type (an NTCDI derivative) organic transistors with no loss in stored charge owing to annealing of substrates. Simultaneous tuning of the threshold voltage on both n- and p-type transistors enabled us to achieve the optimum operating switching point and gain in the inverters

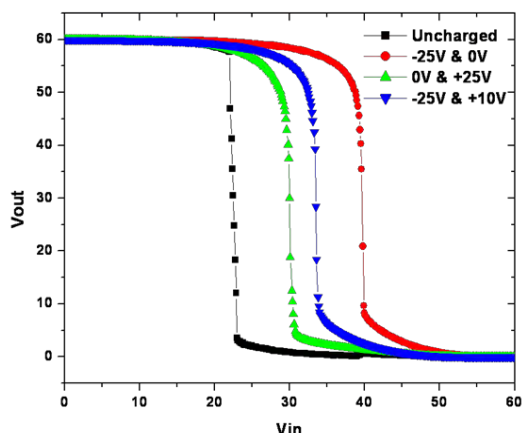


Figure 1. Charged inverter input-output characteristics. Charging refers to surface charge on dielectrics before semiconductor deposition.

from 74 on control samples to a maximum of 105 on threshold voltage tuned samples. The inverter gains as a result of fine-tuning both n- and p-type threshold voltages are the highest ever attained in organic semiconductor inverters.¹ Input-output characteristics are shown in Figure 1.

V_t shifts can include a contribution from the polarization at the gate dielectric-OSC interface, and from static charge in the dielectric.² This polarization is difficult to measure in conventional vertical architectures. Therefore, we investigate the charge trapping at a lateral gate dielectric-OSC interface using Kelvin probe microscopy (KPM).³ In this geometry, the gate dielectric/OSC interface is exposed, facilitating the imaging of the charge storage. Furthermore, we quantify the injected and releasable static charge using thermally stimulated discharge current (TSDC). The interface chosen is analogous to the pentacene-polystyrene used for the inverters.

To see the effect of charge storage in the dielectric, the samples were examined in ambient conditions before and after charging. Before the samples were charged, the electrode on the PS was grounded while the electrode on the pentacene was varied between -10V and +9V (“small voltages”). The bias was started at 0V, stepped down to -10V, stepped up to +9V and brought back to zero, revealing the hysteresis. KPM line scans were performed on the samples as the

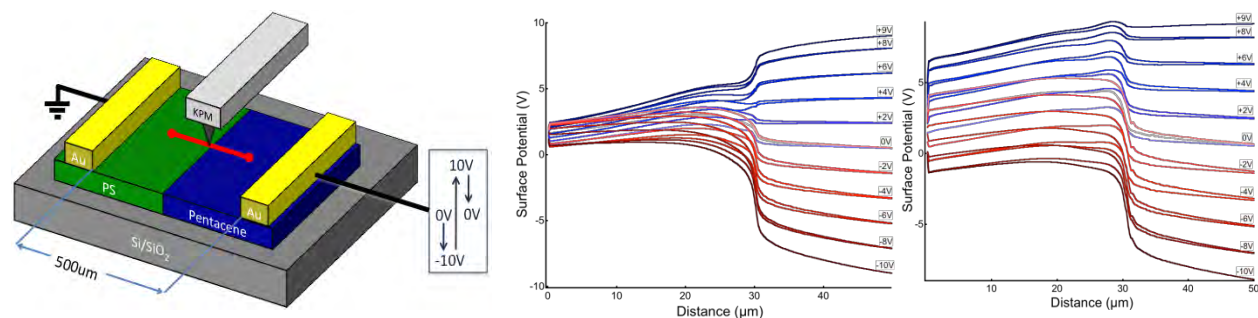


Figure 2. (A) Schematic of the heterojunction, with the KPM scan in red. (B) Uncharged sample surface potential at various applied biases. The sample was initially scanned in the negative direction to -10V then the bias was stepped up to +9V and finally back to 0V. (C) The sample was removed from the KPM and charged at +200V for 10 minutes, then returned to the KPM and rescanned.

bias applied to the pentacene was varied, showing the potential drop across the pentacene, PS and interface. The sample was then charged by applying a *much higher voltage* ($\pm 200V$) to the pentacene for approximately 10 minutes. The charged sample was then rescanned as the potential between the electrodes was varied again in a small voltage range. Figure 2 shows the device layout and SKPM scans across the interface as various voltages are applied, before and after charging the interface. The voltage drops at the junction are clearly observed, and vary with the voltage applied during scanning. More significantly, the interfacial voltage is actually reversed by static charging prior to the scans! This is an indication of the capability of that

interface to store static charge with sufficient stability to survive further device operation. Indeed, in followup work now being prepared for publication, *we showed for the first time that this stored charge directly shifts V_t of transistors made in the same lateral geometry*, with pairs of electrodes acting as source and drain on the pentacene side.

We have made circuits using materials from the above experiments on flexible silicon substrates. Figure 3 shows one such circuit. The circuits incorporate the capability for static charge tuning,

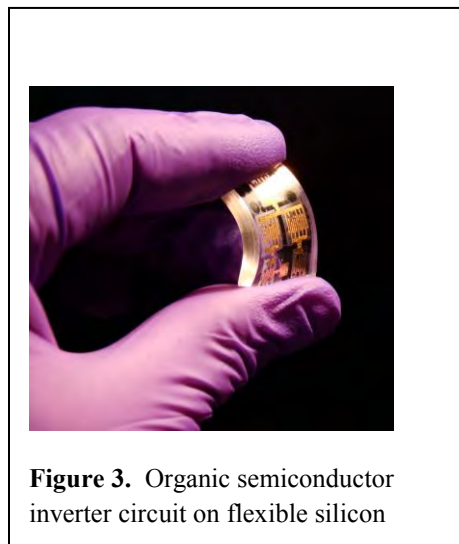


Figure 3. Organic semiconductor inverter circuit on flexible silicon

as shown above. The process is compatible with technology used to make polymer solar cells, and the circuits can be used in a variety of monitoring and controlling functions to enhance the performance and reliability of energy-capture modules.

Future Plans

We will utilize different material combinations in our scanning probe study of organic electronic interfaces, and begin nonlinear spectroscopic analysis of the charged materials to identify charged chemical functional groups. We will integrate and tune circuits such as in Figure 3 to operate alongside solar cells. We will extend our junction studies to include relevance to thermoelectrics as well.

References

- 1 Dhar, B. M., Ozgun, R., Jung, B. J., Katz, H. E. & Andreou, A. G. Optimum bias of CMOS organic field effect transistor inverter through threshold adjustment of both p- and n-type devices. *Electronics Letters* 46, 1335-1336, doi:10.1049/el.2010.1603 (2010).
- 2 Dhar, B. M., Ozgun, R., Dawidczyk, T., Andreou, A. & Katz, H. E. Threshold voltage shifting for memory and tuning in printed transistor circuits. *Materials Science & Engineering R-Reports* 72, 49-80, doi:10.1016/j.mser.2010.11.001 (2011).
- 3 Dawidczyk, T. *et al.* Kelvin Probe Microscopic Visualization of Charge Storage at Polystyrene Interfaces with Pentacene and Gold. *Applied Physics Letters* 100, 073305 (2012).

Publications

Lecover, R.; Williams, N.; Marcovic, N.; Reich, D.H. Naiman, D.Q.; Katz, H.E. "Next-Generation Polymer Solar Cell Materials: Designed Control of Interfacial Variables" ACS Nano DOI: 10.1021/nm301140w 2012

Dawidczyk, T.; Johns, G.L.; Ozgun, R.; Alley, O.; Andreou, A.G.; Markovic, N.; Katz, H.E. "Kelvin Probe Microscopic Visualization of Charge Storage at Polystyrene Interfaces with Pentacene and Gold" Applied Physics Letters, 100, 073305 (2012)

Kola, S.; Sinha, J.; Katz, H.E. "Organic Transistors in the New Decade: Toward N-Channel, Printed, and Stabilized Devices" J. Pol. Sci., Pol. Phys. DOI: 10.1002/polb.23054 (2012)

Wall, B.D.; Diegelmann, S. R.; Zhang, S.; Dawidczyk, T.J.; Wilson, W.L.; Katz, H.E.; Mao, H.Q.; Tovar, J.D. Aligned Macroscopic Domains of Optoelectronic Nanostructures Prepared via Shear-Flow Assembly of Peptide Hydrogels (cover article) *Adv. Mater.* 23 5009-5014 (2011)

Dhar, B.M.; Ozgun, R.; Dawidczyk, T.; Andreou, A.; Katz, H.E. "Threshold Voltage Shifting for Memory and Tuning in Printed Transistor Circuits" (invited) *MSE Reports*, doi:10.1016/j.mser.2010.11.001 (2011)

Ozgun R.; Jung, B.J.; Dhar, B.M.; Katz, H.E.; Andreou, A.G. "Silicon-on-insulator (SOI) Integration for Organic Field-effect Transistor (OFET) Circuits" *ICSAS/IEEE* 2253-2256 (2011)

Dhar, B.M.; Ozgun, R.; Jung, B.J.; Lee, K.; Katz, H.E.; Andreou, A.G. "Optimum Bias of CMOS Organic Field Effect Transistor Inverter through Threshold Adjustment of both p and n Devices" *Electronics Letters*, 46, 1335-1336 (featured article) (2010)

Jung, B.J.; Lee, K.; Sun, J.; Andreou, A.G.; Katz, H.E. "Air-operable, High-mobility Organic Transistors with Unsubstituted Naphthalenetetracarboxylic Diimide Cores: Environmental and Bias Stress Stability" *Adv. Funct. Mater.*, 20, 2930-2944 (2010)

Katz, H.E.; Searson, P.; Poehler, T.O. "Polymer Batteries and Charge Storage Devices" *J. Mater. Res.* 25, 1561-1574 (2010)

Sun, J.; Yeh, M.; Jun, B.J.; Zhang, B.; Feser, J.; Majumdar, A.; Katz, H.E. "Simultaneous Increase in Seebeck Coefficient and Conductivity in a Doped polyalkylthiophene Blend with Defined Density of States" *Macromolecules*, 43, 2897-2903 (2010)

Dhar, B.M.; Kini, G.; Xia, G.; Jung, B.J.; Markovic, N.; Katz, H.E. "Field-effect Tuned Lateral Organic Diodes" *Proc. Nat. Acad. Sci.*, 107, 3972-3976 (2010).

Zheng, Q.; Jung, B.J.; Sun, J.; Katz, H.E. "Ladder-Type Oligo-*p*-Phenylene-Containing Copolymers with High Open-Circuit Voltages and Ambient Photovoltaic Activity" (cover article) *J. Am. Chem. Soc.* 132, 5394-5404 (2010)

Reuter, K.; Kempa, H.; Huebler, A.; Deshmukh, K.; Katz, H.E. "Full-Swing Mass-Printed Organic Inverters Using a Charged Perfluorinated Electret" *Organic Electronics*, 11, 95-99 (2010)

Biaxiality in Thermotropic Bent-Core and Tetrapodic Nematic Liquid Crystals

Principal Investigator: Satyendra Kumar, Kent State University, Kent, Ohio
Co-Principal Investigators: Quan Li and Sam Sprunt, Kent State University, Kent, OH
Alejandro Rey, McGill University, Montreal, Canada
Mohan Srinivasarao, Georgia Inst. of Technology, Atlanta, GA

Program Scope

The scope of the project is to acquire a sound understanding of the phenomena of biaxiality in liquid crystals (LC) in specifically designed and synthesized bent-core mesogens having 5- and 6- aromatic rings with different apex angle, different linkage and terminal groups, and a chiral center, and in siloxane tetrapodic compounds. In addition to understanding molecular origins of the physical and electro-optical properties of these unique materials, theoretical models and their predictions are being tested through investigations of the topology of phase diagrams, critical behavior at the transitions between the isotropic and uniaxial and biaxial nematic (N) phases, viscoelasticity, and statics and dynamics of topological defects in 3D near $s = 1/2$ and $s = 1$ disclinations. The results of such fundamental studies should enable the design of molecules with desired phase behavior and properties leading to new science and disruptive technologies.

Recent Progress

A. Synthesis of Molecules with Unique Mesomorphism

1. Achiral Bent-Core Mesogens: A series of achiral mesogens with general structure **1** (Fig. 1) were synthesized [7] to understand the role of the nature and position of substitutions (X, X', X'', Y, Z, Z', and Z'') on central rigid core, linkage unit (L) and terminal chains (R and R') on the formation and stability of the N phase. The results reveal that:

(a). The molecules that are non-symmetric at the central core, rigid arms, and terminal chains exhibited a stable N phase over a wide temperature range.

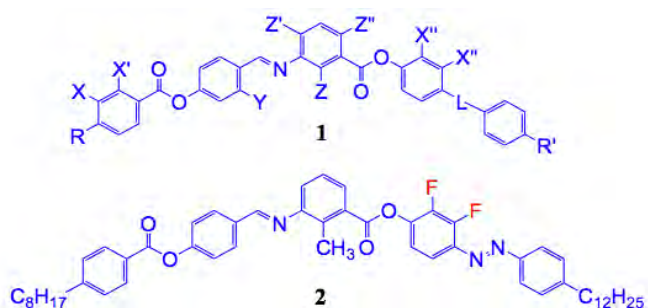


Fig. 2 General structure **1**, and a synthesized achiral fluorinated bent-core compound **2** with only the N phase.

(b). The chemical nature of linking group, lateral substitutions on the rigid arms and the terminal chain lengths were secondary in governing the nematic temperature range. Azo linkages favored a wider N range than the esters and imines.

(c). Lateral fluoro substitutions (compound **2**) enhanced the N phase stability and suppressed the smectic phases. When **F** substitution is close to the

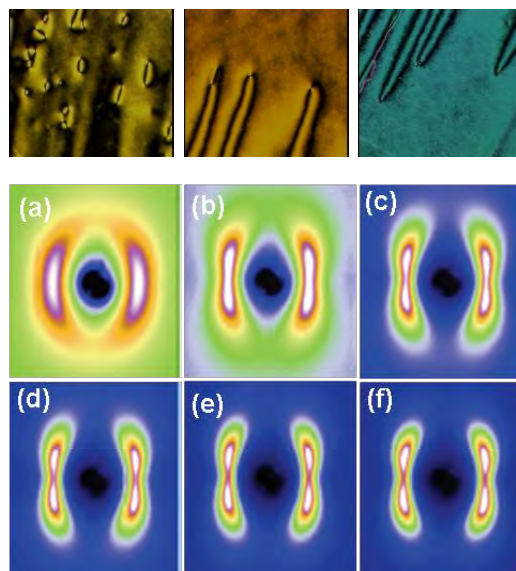


Fig. 1. Optical micrograph (top panel) of mesogen **2** under homeotropic condition in the N phase at (L to R) 157°C, 150°C; and 145°C. Small angle x-ray diffraction in the N phase (a) 153.8°C, (b) 125.6°C, (c) 101.9°C, (d) 92.5°C, (e) 84.0°C, and (f) 74.2°C.

central core, only the N phase was stabilized. Textural studies and synchrotron x-ray measurements indicate the possibility of the biaxial nematic order (Fig. 2).

2. Chiral Bent-Core Mesogens: Two mesogens, combining the unique structure of bent-core molecules with chiroptic properties, were synthesized [8, 9]. *These exhibited the first bent-core chiral N phase.* The smectic phase was completely suppressed due to the intermolecular steric interactions and the unsymmetrical molecular shape. Due to intrinsic biaxiality of the bent-core, *these materials provide a unique opportunity to explore the hitherto unknown biaxial chiral N phase.*

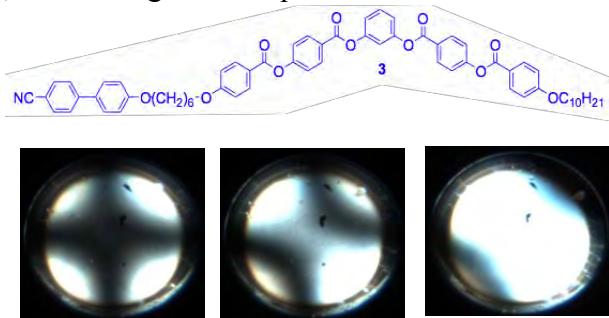


Fig. 3: Conoscopic images of compound **3** at 108°C in 5 μm thick homeotropic cell at an angle of 90, 80 and 70° between polarizer and analyzer axes.

3. Hybrid Calamitic and Bent-Core Mesogens: A number of hybrid dimeric mesogens using calamitic and bent-core structural units were synthesized [20]. Mesogen **3** (Fig. 3) exhibited the N and the biaxial smectic-A (SmA) phase, representing *an important and alternate route towards achieving the biaxial N phase without the customary underlying SmC phase, i.e., without the presence of cybotactic groups.*

B. Structure and Biaxial Nematic Order

A number of experimental techniques were employed to investigate the uniaxial and biaxial N phases of compound **A131** which has the same structure as mesogen **2** except that the two **F** atoms are replaced by two **H** atoms. The nematic order, its evolution with temperature, and the degree of phase biaxiality in bent-core mesogen were studied by polarized micro-Raman scattering. The values of both uniaxial, P_{200} and P_{400} , and biaxial order parameters P_{220} , P_{420} , and P_{440} were determined [2, 3]. Temperature dependence of P_{200} and P_{400} and a theoretical fit to P_{200} for the uniaxial N phase are shown in Fig. 4. It is very clear that P_{200} and P_{400} deviate from uniaxial behavior upon crossing over to the biaxial N phase.

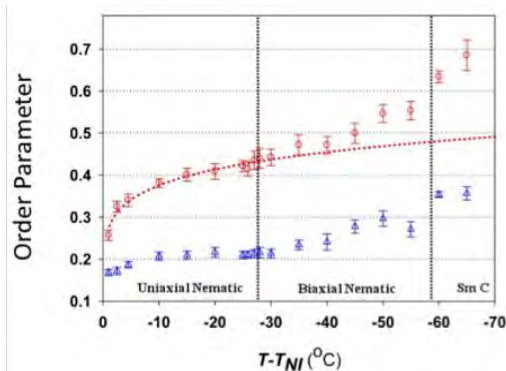


Fig. 4: Temperature dependence of P_{200} : (\circ) and P_{400} : (Δ).

From the measured values of order parameters, we constructed [4] the most probable orientation distribution function and calculate a number of parameters related to the nematic flow behavior of these materials. We are now attempting to perform experiments to understand the response to imposed shear flow. Measurements of the orientational elastic constants and associated viscosities [11] in the N phase of ClPbis10BB reveal qualitative differences between the bent-core and the conventional nematics, possibly due to the presence of nanoscale molecular clusters (*cybotactic groups*).

The presence of cybotactic groups has often been used to explain anomalous results with little common understanding of the term. In order to understand this phenomenon, we

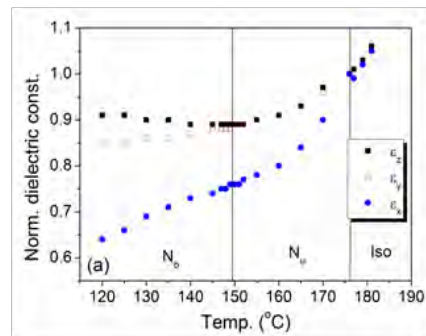


Fig. 5. Thermal evolution of three dielectric constants of **A131** in the isotropic and uniaxial and biaxial N phases measured using 10 kHz at field strength of 0.1 V/ μm .

conducted a comprehensive study [19] of positional order correlations (i.e., size of cybotactic groups) in a large number of calamitic, bent-core, and lyotropic materials. *A clear picture has now emerged*; the nematic phases fall into one of the three categories: **(i)** with short range smectic positional correlations ($\sim 1-2$ molecules) and weak temperature dependence, **(ii)** Arrhenius-type thermal dependence of correlations that extend from 3-10 molecules, and **(iii)** power-law divergence of the correlation length as the transition to a lower phase is approached. One can further argue, on the basis of published data, that every fluid, with the possible exception of superfluid *He*, has cybotactic groups. This work appeared as a book chapter [19].

C. Defect Mechanics Theory for Complex Mesophases

The conformation adopted by disclination lines in nematic LCs reflects the background elasticity of the mesophase and offers a new route for mechanical characterization. The widely used Landau-de Gennes model is used to understand the energetics of planar disclinations containing both bending and tension and to establish the specific relation between them and the Frank moduli. We have extended this model to non-planar disclination lines with torsion. Given that the disclination elasticity is proportional to the Frank elasticity, temperature is an efficient variable to soften the lines. Another novel approach is to explore the preferential adsorption of solutes and nanoparticles on defect cores, which will provide additional core energy under bending. We developed a new multiple order parameter phase field model [16, 17] for mesophases, solvents and nanoparticles, that is able to describe temperature-composition phase diagrams, textures, and defect cores.

This research extends the attributes of disclination line defects from simple tension to tension/bending/twisting moduli and from a simple low orientational order filament system to a binary mixture with couplings between bending and positional order.

D. Structure of the Biaxial de Vries Smectic-C Phases

Since their discovery in 1979 by de Vries, the microscopic structure and molecular order in the uniaxial smectic-A (SmA) and the biaxial smectic-C (SmC) phases have remained elusive and the de Vries' elegant diffuse cone model untested. Interest in these materials has recently grown as they offer a pathway to the superior ferroelectric SmC phase based technology.

Our x-ray study of the materials provided [13, 14] by Lemieux (Queen's University) has, for the first time, *directly* accessed the director tilt (Fig. 7, top), orientational order parameters of both the hydrocarbon (HC) and siloxane (SiO) parts of the molecule, and smectic layer spacing. The large angle x-ray peaks arising from lateral separation between the HC and SiO segments show that they tilt by different angle and possess different degree of orientational order. This led us to understand submolecular organization in these phases, (Fig. 5, bottom). The SmC order parameter critical exponent β is 0.26 ± 0.01 for one of the compounds, in excellent agreement with theoretically predicted tricritical and 2D Ising behavior.

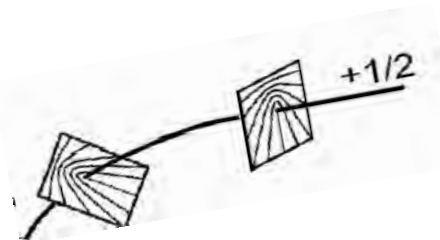


Fig. 6. Curvature of disclination lines reveals quantitative information on the Frank elasticity of the mesophase.

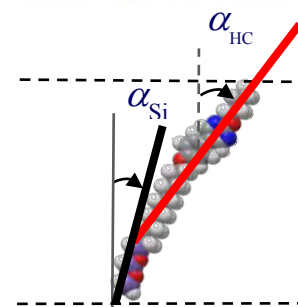
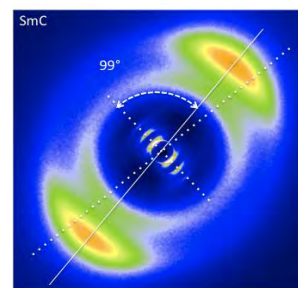


Fig. 7. (Top) Diffraction pattern in the SmC phase showing molecular tilt, (bottom) molecular organization in smectic layer with Si and HC parts tilted differently.

Future Plans

- Raman study of differential depolarization ratio in the biaxial N phase of the bent-core and lyotropic systems will continue to facilitate a comparison. The effect of large non-linear susceptibility on Raman measurements will be assessed and theoretical framework developed.
- Structure, order, and electrooptical properties of the N, biaxial SmA, chiral N phases of the molecules discussed in §A1-A3 above and their homologs will be investigated to lead to the design and synthesis of mesogens with desired phases, properties, and temperature range.
- Investigate new De Vries materials and their mixtures with conventional smectics to understand the precise nature of phases and what makes them different.
- Continue multiscale modeling needed for the biaxial phases of bent-core and de Vries systems

Publications (listed by the year of publication):

1. H.-G. Yoon, et al., *Nematic biaxiality in a bent-core material*, Phys. Rev. E **81**, 051706 (2010).
2. M.S. Park, B.-J. Yoon, J. O. Park, V. Prasad, S. Kumar and M. Srinivasarao, *Raman scattering study of phase biaxiality in a thermotropic bent-core nematic liquid crystal*, Phys. Rev. Lett. **105**, 027801 (2010).
3. M. S. Park, B.-J. Yoon, J. O. Park, S. Kumar, M. Srinivasarao, *Reply to Comment on “Raman scattering study of phase biaxiality in a thermotropic bent-core nematic liquid crystal”*, Phys. Rev. Lett. **107**, 109802 (2011).
4. M. S. Park, et al., *A simple method for obtaining the information of orientation distribution using polarized Raman spectroscopy: Orientation study of structural units in poly(lactic acid)*, Macromols., **44**, 2120 (2011).
5. M. S. Park, A. Aiyar, J. O. Park, E. Reichmanis, and M. Srinivasarao, *Solvent evaporation induced liquid crystalline phase in poly(3-hexyl thiophene)*, J. Am. Chem. Soc., **133**, 7244 (2011) (communications).
6. B. Park, A. Aiyar, M. S. Park, M. Srinivasarao and E. Reichmanis, *Conducting channel formation in poly(3-hexylthiophene) field effect transistors: bulk to interface*, J. Phys. Chem. C. **115**, 11719 (2011).
7. M. Mathews, S. Kang, S. Kumar and Q. Li, *Designing bent-core nematogens towards biaxial nematic liquid crystals*, Liq. Cryst. **38**, 31 (2011).
8. K. Rameshbabu, A. Urbas and Q. Li, *Synthesis and characterization of thermally irreversible photochromic cholesteric liquid crystals*, J. Phys. Chem. B **115**, 3409 (2011).
9. M. Mathews, R. Zola, D. Yang and Q. Li, *Thermally, Photochemically and electrically switchable reflection colors from self-organized chiral bent-core liquid crystals*, J. Mat. Chem. **21**, 15673 (2011).
10. Y. Li, A. Urbas and Q. Li, *Synthesis and characterization of light-driven dithienylcyclopentene switches with axial chirality*, J. Org. Chem. **76**, 7148 (2011).
11. M. Majumdar, P. Salamon, A. Jakli, J. T. Gleeson, and S. Sprunt, *Elastic constants and orientational viscosities of a bent-core nematic liquid crystal*, Phys. Rev. E **83**, 031701 (2011).
12. J. Seltmann, A. Marini, B. Mennucci, S. Dey, S. Kumar, M. Lehmann, *Nonsymmetric bent-core liquid crystals based on a 1,3,4-thiadiazole core unit and their nematic mesomorphism*, Chem. Mater. **23**, 2630 (2011).
13. H.-G. Yoon, D.M. Agra-Kooijman, K. Ayub, R.P. Lemieux, S. Kumar, *Direct observation of diffuse cone behavior in de Vries smectic-A and -C phases of organosiloxane mesogens*, Phys. Rev. Lett. **106**, 087801 (2011).
14. H.-G. Yoon, D.M. Agra-Kooijman, K. Ayub, R. P. Lemieux, and S. Kumar, *Diffuse cone behavior and microscopic structure of the de Vries smectic-A and Sm-C phases*, Proceedings SPIE **8114**, 811400 (2011).
15. A. D. Rey, M. Golmohammadi and E. E. Herrera Valencia, *A Model for mesophase wetting thresholds of sheets, fibers and fiber bundles*, Soft Matter, **7**, 5002 (2011).
16. E. R. Soulé, A. D. Rey, *Hedgehog defects in mixtures of a nematic liquid crystal and a non-nematogenic component*, Soft Matter **8**, 1395 (2012), [DOI: 10.1039/C1SM06741A].
17. E. Soulé, J. Milette, L. Reven, A. D. Rey, *Phase equilibrium and structure formation in gold nanoparticles - nematic liquid crystals composites: Experiments and Theory*, Soft Matter, **8** (10), 2860 (2012).
18. Y. Wang and Q. Li, *Light-driven chiral molecular switches or motors in LCs*, Adv. Mat. **24**, 1926 (2012).
19. B.R. Acharya and S. Kumar, *X-ray Diffraction from nematic phase of bent-core mesogens and cybotactic groups*, Book Chapter in “Liquid Crystals Beyond Displays”, Editor Q. Li, John Wiley & Sons (2012).
20. Y. Wang, H.-G. Yoon, H. K. Bisoyi, S. Kumar, and Q. Li, *Hybrid and bent-core mesogens and their biaxial smectic-A and nematic phases*, Submitted (2012).

Deterministic Assembly of Fluid and Solid Inks

Jennifer A. Lewis (PI, Core 2 Lead)

Frederick Seitz Materials Research Laboratory
Materials Science and Engineering Department
University of Illinois at Urbana-Champaign

PROGRAM SCOPE

The overarching goal of our DOE materials research cluster is to establish the fundamental knowledge required to transform diverse classes of information- and function-encoded building blocks into multiscale functional assemblies that guide photon-electron conversion processes for light capture and utilization.

Our approach to *Programming Function via Soft Materials* integrates three core research areas:

(1) Dynamic supracolloidal assemblies – created by controlling the equilibrium and nonequilibrium phase behavior, spatial organization, and connectivity of colloidal particles, clusters, and mixtures thereof through self, driven and chemically amplified assembly and disassembly pathways.

(2) Deterministic assembly of fluid and solid inks – to precisely pattern micro/nanostructured materials in the form of conductive pathways via omnidirectional printing and as solid “inks” composed of III-V heterojunctions via transfer printing.

(3) Functional architectures for light capture and utilization – in flexible “skin-like” motifs. Light collection and light emitting systems based on large microcell arrays represent new technologies that are uniquely enabled by our scalable approaches and fundamental understanding of function-encoded building block synthesis and assembly.

This abstract focuses solely on Deterministic Assembly of Fluid and Solid Inks.

RECENT PROGRESS

The creation of unusual devices composed of flexible/stretchable circuits that are heterogeneously integrated in large-area, conformal layouts has been pioneered by our cluster team through a combination of fluid and solid ink assembly methods (Lewis, Nuzzo, Rogers, and Schweizer).

(i) Structure and Assembly of Fluid Inks – Lewis and Schweizer are designing silver microwire-microparticle inks for direct-write assembly of conductive microelectrodes for flexible photovoltaics (Rogers, Nuzzo) [1-2]. Schweizer has developed the first unified theory of percolation, phase separation, physical bond formation and kinetic arrest to establish criteria for the formation of

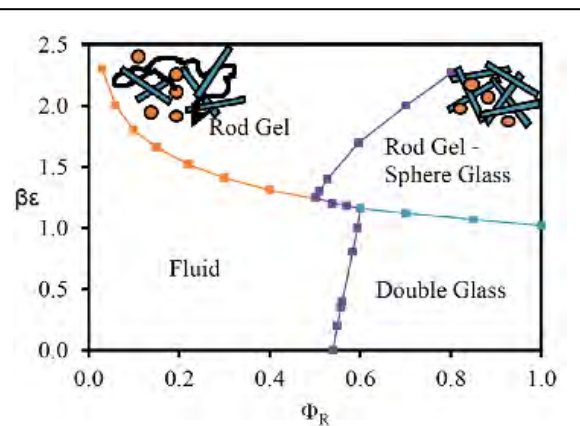


Figure 1. Predicted nonequilibrium phase diagram for a dense mixture of repulsive sphere colloids and attractive rods ($L/D=5$) for mixtures of varying attraction strength and rod volume fraction.

homogeneous phase physical gels and the role of phase separation in creating heterogeneous gels (Figure 1).[2] The strong effect of nanoparticle aspect ratio was demonstrated, with isotropic rod gels of controlled elastic properties predicted to be quite easy to realize in practice. Extension to conductive sphere-rod mixtures reveals remarkable dynamic complexity that depends on rod aspect ratio and interparticle attractions. A theory for how to control both the linear shear modulus and yield stress was created, thereby providing design tool for tailoring mechanical and nonlinear flow properties. A theory for electrical hopping conductivity in amorphous metallic rod-sphere gel inks has also been formulated, and preliminary calculations suggest significant improvements over the silver particle inks employed in solar microcell applications can be achieved by appropriate blending with conductive microwires.

(ii) Conductive Ink Printing for Flexible Concentrator Photovoltaics – *Lewis* has demonstrated the conformal printing of concentrated silver inks with tailored viscoelastic behavior to form interconnects between sparsely populated InP microcell arrays on glass and polyimide substrates (Figure 2). These devices are being developed for concentrator PV applications. Both silver interconnects (~ 50 microns wide) and busbars (~ 1 mm wide) are patterned over large areas (4"x4" wafers) via direct-write assembly. The silver inks are conductive as patterned, and approach bulk-like conductivity upon annealing at 175°C in air (not shown). These and related inks have also been used in other applications [3-9], including pen-on-paper flexible electronics [3], conformal printing of electrically small antennas [4], and ultrafine scale printing of silver microgrids (5 microns wide) for transparent conductive displays [5]. Recently, *Lewis* has developed a new reactive silver ink that exhibits nearly bulk conductivity upon annealing at 90°C for 15 min [10]. This ink opens new avenues for printed electronics and optoelectronic devices on low-cost plastics.

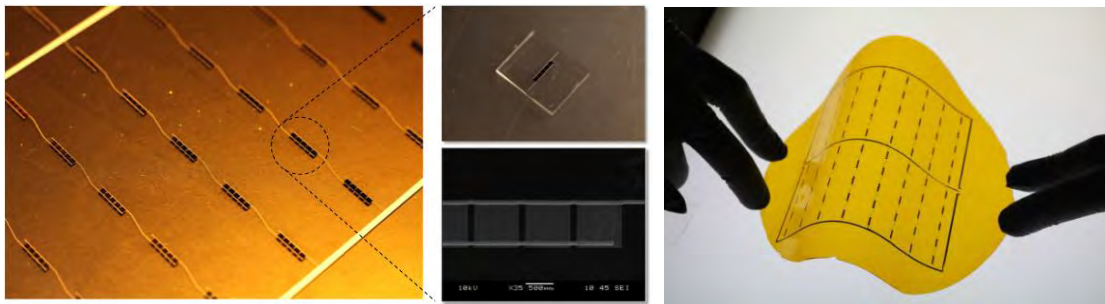


Figure 2. Optical and SEM images of printed silver interconnects and busbars on a fully populated glass substrate (left), test coupons (middle), and polyimide substrate (right).

(ii) Transfer Printing of Solid Inks - Reversible control of adhesion is an important requirement for stamps designed for deterministic assembly by transfer printing. In past work, we exploited viscoelastic effects in the materials used for these stamps, to achieve control through modulation of the peeling rates. Although useful for many applications, the difference between ‘on’ and ‘off’ states in adhesion that can be accomplished in this manner is limited. *Rogers* recently developed new approaches, supported by detailed experimental and theoretical studies, for pressure-modulated adhesion between flat objects and elastomeric surfaces that have sharp features of surface relief in optimized geometries.[11] Specifically, we showed that the strength of non-specific adhesion can be switched by more than three orders of magnitude, in a reversible fashion. Implementing these concepts in advanced stamps enables versatile modes for deterministic assembly of solid materials in micro/nanostructured forms. As an example, we printed two and three-dimensional collections of silicon platelets and membranes to illustrate

some capabilities. To show utility in device fabrication, we built an unusual type of transistor that incorporates a printed gate electrode, an air gap dielectric and an aligned array of single walled carbon nanotubes. Figure 3 shows printed structures in these contexts.

Rogers, Li, Moore and Nuzzo have recently developed solid inks with higher levels of functionality than previously reported, while retaining forms favorable for deterministic assembly by transfer printing. [12-19] The schemes require only interconnect metallization to be performed on the final device substrate, thereby minimizing the need for any specialized processing technology. The result has important consequences in large-area electronics for display systems, flexible/stretchable electronics, or other non-wafer-based devices (carried out in Core 3).

FUTURE PLANS

Our interdisciplinary research team is now focused on expanding the palette of fluid and solid inks for heterogeneously integration of functional skin-like architectures for light harvesting and utilization. In the coming year, we plan to move beyond photovoltaic and solid-state lighting applications and explore how our unique mesoscale assembly efforts can be harnessed to create new planar and 3D architectures for energy harvesting [19] and storage.

REFERENCES (CITED FROM PUBLICATIONS LISTED BELOW)

PUBLICATIONS - CORE AREA (2)

1. R. Jadrich and K.S. Schweizer, "Percolation, Phase Separation and Gelation in Fluids and Mixtures of Spheres and Rods", *J. Chemical Physics*, 135, 234902 (2011).
2. (Invited Review) J.C. Conrad, S.R. Ferreira, J. Yoshikawa, R.F. Shepherd, B.Y. Ahn, and J.A. Lewis, "Designing Colloidal Suspensions for Directed Materials Assembly", *Current Opinions in Colloid and Interface Science*, 16, 71-79 (2011).
3. A. Russo, B.Y. Ahn, J.J. Adams, E.B. Duoss, J.T. Bernhard, and J.A. Lewis, "Pen-on-Paper Flexible Electronics", *Adv. Mater.*, 23, 3426-3430 (2011).
4. (Cover Article) J.J. Adams, E.B. Duoss, T.F. Malkowski, M.J. Motala, B.Y. Ahn, R.G. Nuzzo, J.T. Bernard, and J.A. Lewis, "Conformal Printing of Electrically Small Antennas on Three-Dimensional Surfaces", *Advanced Materials*, 23:11, 1335-1340 (2011).
5. (Invited) B.Y. Ahn, D.J. Lorang, and J.A. Lewis, "Transparent conductive grids via direct writing of silver nanoparticle inks", *Nanoscale*, 3:7, 2700-2 (2011). [DOI:10.1039/c1nr10048c]
6. B.Y. Ahn, S.B. Walker, S.C. Slimmer, A. Russo, A. Gupta, E. Duoss, T.F. Malkowski, and J.A. Lewis, "Planar and Three-Dimensional Printing of Conductive Inks", *JoVE* (online).

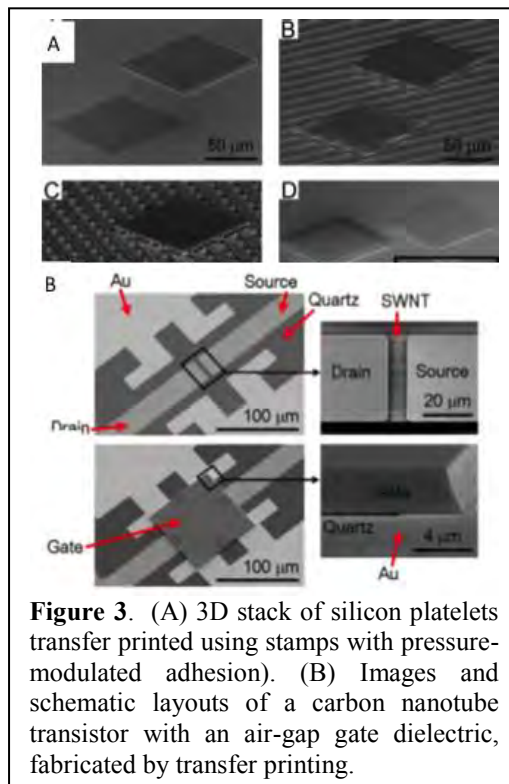


Figure 3. (A) 3D stack of silicon platelets transfer printed using stamps with pressure-modulated adhesion. (B) Images and schematic layouts of a carbon nanotube transistor with an air-gap gate dielectric, fabricated by transfer printing.

7. (Cover Article) Ahn, B. Y., Hansen, C. J., Shoji, D., Hong, E., Dunand, D., and Lewis, J. A., "Printed Origami", *Adv. Mat.*, 22, 2251-54 (2010).
8. E. Hong, B.Y. Ahn, S. Shoji, J.A. Lewis, and D.C. Dunand, "Microstructure and Mechanical Properties of Reticulated Titanium Scrolls", *Advanced Engineering Materials*, 13:12, 1122-1127 (2011).
9. Ahn, B. Y., Lorang, D. J., Duoss, E. B., and Lewis, J. A., "Direct-Write Assembly of Microperiodic Planar and Spanning ITO Microelectrodes", *Chemical Communications*, 46:38, 7118-20 (2010).
10. S.B. Walker and J.A. Lewis, "Reactive Silver Inks for Patterning High-Conductivity Features at Mild Temperatures", *Journal of the American Chemical Society*, (2012).
11. Kim, S., Wu, J., Carlson, A., Jin, S. H., Kovalsky, A., Glass, P., Liu, Z., Ahmed, N., Elgan, S. L., Chen, W., Ferreira, P. M., Sitti, M., Huang, Y., and **Rogers, J. A.**, "Microstructured Elastomeric Surfaces with Reversible Adhesion and Examples of Their Use in Deterministic Assembly by Transfer Printing", *Proc. Nat. Acad. Sci. USA*, **107**(40), 17095–17100 (2010).
12. (Invited review) Rogers, J. A., Someya, T., and Huang, Y., "Materials and Mechanics for Stretchable Electronics", *Science*, 327, 1603 (2010).
13. Unarunotai, S., Koepke, J. C., Tsai, C.-L., Du, F., Chialvo, C. E., Murata, Y., Haasch, R., Petrov, I., Mason, N., Shim, M., Lyding, J., and Rogers, J. A., "Layer-by-Layer Transfer of Multiple, Large Area Sheets of Graphene Grown in Multilayer Stacks on a Single SiC Wafer", *ACS Nano*, 4:10, 5591–5598 (2010).
14. Unarunotai, S., Murata, Y., Chialvov, C., Mason, N., Petrov, I., Nuzzo, R., Moore, J., and Rogers, J., "Conjugated Carbon Monolayer Membranes: Methods for Synthesis and Integration", *Adv. Mat.*, 22, 1072–1077 (2010).
15. Yoon, J., Jo, S., Chun, I. S., Jung, I., Kim, H.-S., Meitl, M., Menard, E., Li, X., Coleman, J. J., Paik, U., and Rogers, J. A., "GaAs Photovoltaics and Optoelectronics Using Releasable Multilayer Epitaxial Assemblies", *Nature* 465, 329-333 (2010).
16. M.T. DeJarld, J.C. Shin, W. Chern, D. Chanda, K. Balasundaram, J.A. Rogers, and X. Li, "Formation of High Aspect Ratio GaAs Nanostructures with Metal Assisted Chemical Etching", *Nano Lett.*, 11, 5259-5263 (2011).
17. J.A. Rogers, M.G. Lagally, and R.G. Nuzzo, "Synthesis, Assembly and Applications of Semiconductor Nanomembranes", *Nature*, 477, 45-53 (2011).
18. Park, S.-I., Le, A.-P., Wu, J., Huang, Y., Li, X. and Rogers, J. A., "Light Emission Characteristics and Mechanics of Foldable Inorganic Light-Emitting Diodes", *Adv. Mat.*, 22:28, 2062 (2010).
19. X. Feng, B.D. Yang, Y. Liu, Y. Wang, C. Dagdeviren, Z. Liu, A. Carlson, J. Li, Y. Huang and J.A. Rogers, "Stretchable Ferroelectric Nanoribbons with Wavy Configurations on Elastomeric Substrates", *ACS Nano*. 5:4, 3326-3332 (2011).

Functional architectures for light capture and utilization

Xiuling Li

Programming Function via Soft Materials, Research Core III

Frederick Seitz Materials Research Laboratory

Department of Electrical and Computer Engineering

University of Illinois at Urbana-Champaign

RESEARCH SCOPE. The overarching goal is to establish the fundamental knowledge required to transform diverse classes of information- and function-encoded building blocks into multiscale functional assemblies that guide photon-electron conversion processes for light capture and utilization. This core research area is devoted to Functional architectures for light capture and utilization -- in flexible “skin-like” motifs. Light collection and light emitting systems based on large microcell arrays represent new technologies that are uniquely enabled by our scalable approaches and fundamental understanding of function-encoded building block synthesis and assembly.

RECENT PROGRESS. Harnessing our unique deterministic assembly capabilities, we have created flexible, highly transparent solar cell arrays, flexible inorganic LED arrays, and flexible PZT arrays in unusual layouts (Rogers, Li, Nuzzo, Johnson).

(i) Flexible, concentrator solar cell arrays – Our prior work on synthesis of functional micro/nanoscale materials focused primarily on monocrystalline silicon, for applications in electronics and photovoltaics. However, compound semiconductors, like gallium arsenide, provide advantages over silicon for many applications, due to their direct bandgaps and high electron mobilities. Examples range from efficient photovoltaic devices to radio frequency electronics and most forms of optoelectronics. Growing large, high quality wafers of these materials, and intimately integrating them on silicon or amorphous substrates such as glass or plastic is expensive, thereby restricting their use. During the last couple of years, **Rogers and Li** developed concepts that address many of these challenges through the use of functional films formed in thick, multilayer epitaxial assemblies created in a single deposition sequence on a growth wafer, and then distributed over large areas on foreign substrates by printing, in a step and repeat mode. In a paper published in *Nature* (2010), we reported specialized designs that enable release and separation of the individual active layers to yield large quantities of high quality material for subsequent device integration by transfer printing in large area formats on diverse

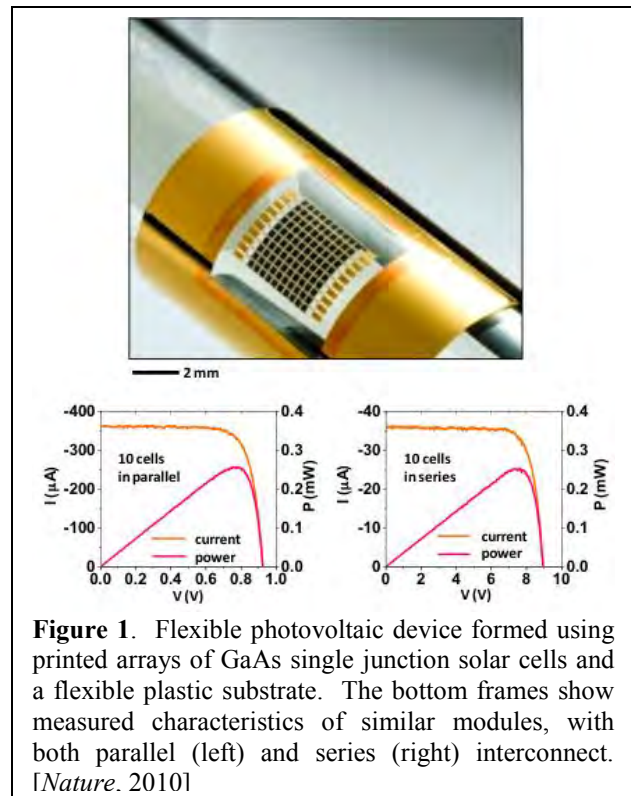
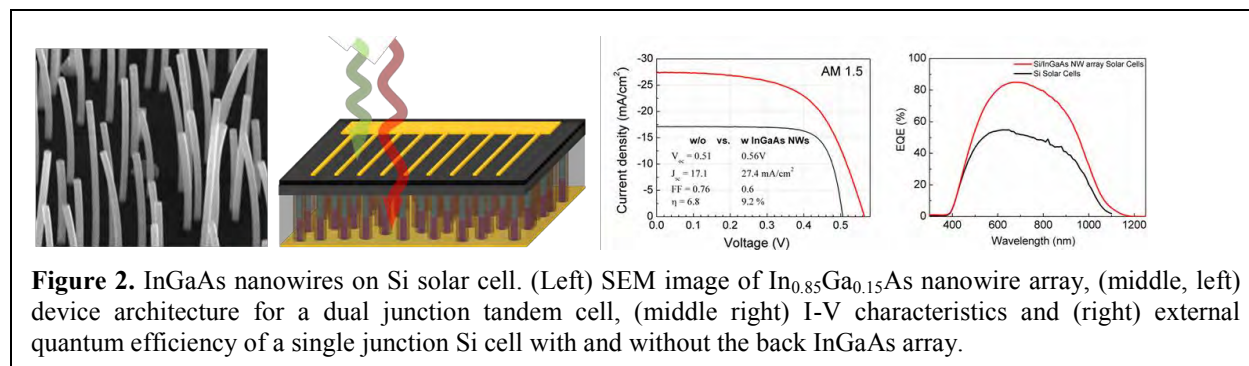


Figure 1. Flexible photovoltaic device formed using printed arrays of GaAs single junction solar cells and a flexible plastic substrate. The bottom frames show measured characteristics of similar modules, with both parallel (left) and series (right) interconnect. [*Nature*, 2010]

classes of substrates, in a manner that also allows the wafer to be re-used for additional growths. Demonstrations in high-speed electronics, near infrared imagers and efficient photovoltaic modules were also reported. Figure 1 provides an image of a representative PV module formed using these ideas.

Rogers, Nuzzo, and Johnson have demonstrated advances in flexible, concentrator PV arrays composed of monocrystalline silicon microcells coupled with luminescent waveguides. Specifically, they designed, assembled and theoretically optimized a type of composite luminescent concentrator PV system that embeds large scale, interconnected arrays of microscale silicon solar cells in thin matrix layers doped with luminophores. Photons that strike cells directly generate power in the usual manner, while those incident on the matrix launch wavelength-downconverted photons that reflect and waveguide into the sides and bottom surfaces of the cells to increase their power output by more than 300%. Unlike conventional luminescent photovoltaics, this design can be implemented in ultrathin, mechanically bendable layouts. Experimental and computational modeling efforts have been carried out to provide quantitative descriptions of the underlying materials science and optics.

Li and Rogers are also developing a method for heterogeneous integration of III-V nanowires with Si substrates for tandem solar cells (Figure 2). The nanowire geometry provides the added benefit of enhancing solar cell performance through greater light absorption and carrier collection efficiency. The nanowire approach also uses less material than thin films. We have demonstrated the growth of dislocation free nanowires in the nearly the entire composition range of $\text{In}_x\text{Ga}_{1-x}\text{As}$ ($x = 0.1 - 1.0$), the p-n junction formation, tunnel junction formation at the III-V/Si interface, and preliminary solar cell results.



(ii) Flexible LED arrays - Properties that can now be achieved with advanced, blue InGaN light emitting diodes (LEDs) lead to their potential as replacements for existing infrastructure in general illumination, with enormous positive implications on power efficiency. Further advances in this technology will benefit from re-examination of the modes for incorporating this materials technology into lighting modules that manage light conversion, extraction and distribution, in ways that most critically minimize adverse thermal effects associated with operation, with packages that fully exploit the unique aspects of these light sources. Over the last year, Rogers and Nuzzo developed ideas in anisotropic etching, microscale device assembly/integration, and module configuration that address these challenges in unconventional ways. We built various device demonstrators to provide examples of the capabilities, including thin, flexible lighting ‘tapes’ based on patterned phosphors and large collections of small, light emitters on plastic substrates. Quantitative modeling and experimental evaluation of heat flow in such structures illustrates one particular, important aspect of their operation: small, distributed

LEDs can be passively cooled simply by direct thermal transport through thin film metallization used for electrical interconnect, providing an enhanced and scalable means to integrate these devices in modules for white light generation.

(iii) Flexible PZT arrays – Rogers recently expanded into systems that can harvest mechanical energy, in conceptually similar ‘skin-like’ formats. As an example, we developed materials, assembly and mechanics approaches that allow brittle ferroelectric ceramics, such as lead zirconate titanate (PZT), to be exploited in flexible and stretchable formats. In particular, we adapted ideas previously developed in PFvSM research, to create ‘wavy’ geometries in nanoribbons of PZT, on soft, elastomeric supports. The result is a hard/soft material construct that offers linear elastic responses to large strain deformations (i.e. stretchable properties), without any loss in ferroelectric or piezoelectric properties. Theoretical and computational analysis of the mechanics accounts for these characteristics and also shows that the amplitudes of the waves can be continuously tuned with an applied electric field, to achieve a vertical (normal) displacement range that is near one thousand times larger than is possible in conventional planar layouts. The results suggest new design and application possibilities in piezoelectric devices, both for harvesting and actuation. Figure 3 shows an optical image of a ‘wavy’ PZT nanoribbon, and a three-dimensional finite element model that captures the underlying physics.

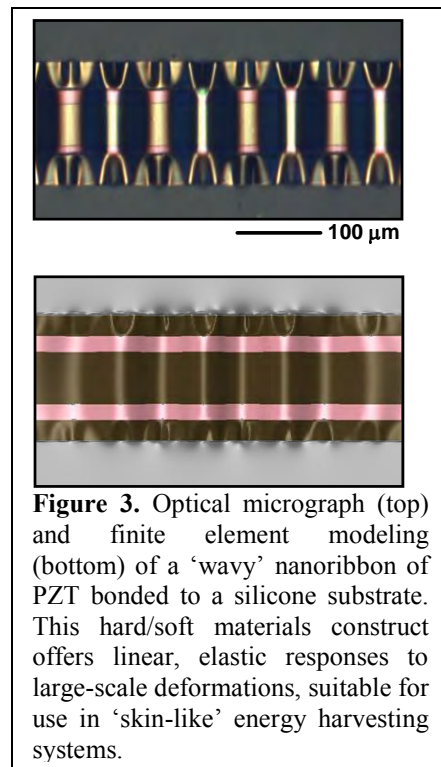


Figure 3. Optical micrograph (top) and finite element modeling (bottom) of a ‘wavy’ nanoribbon of PZT bonded to a silicone substrate. This hard/soft materials construct offers linear, elastic responses to large-scale deformations, suitable for use in ‘skin-like’ energy harvesting systems.

FUTURE PLANS

Building upon the above successes, we plan to further develop and exploit deterministic strategies for the design, assembly, and integration of multiscale functional objects in “skin-like” architectures for efficient light capture and utilization.

REFERENCES (CITED FROM PUBLICATIONS LISTED BELOW)

PUBLICATIONS - CORE AREA (3)

1. **(Inside Cover Feature Article)** Arpin, K. A., Mihi, A., **Johnson, H. T.**, Baca, A. J., **Rogers, J. A.**, **Lewis, J. A.**, and Braun, P. V., “Multidimensional Architectures for Functional Optical Devices”, *Adv. Mat.*, **22:10**, 1084-1101 (2010).
2. **(Cover Article)** Baca, A. J., Yu, K. J., Xiao, J., Wang, S., Yoon, J., Ryu, J. H., Stevenson, D., **Nuzzo, R. G.**, Rockett, A. A., Huang, Y., and **Rogers, J. A.**, “Compact Monocrystalline Silicon Solar Modules With High Voltage Outputs and Mechanically Flexible Designs”, *Energy and Environmental Science*, **3**, 208–211 (2010).
3. Kim, R.-H., Kim, D.-H., Xiao, J., Kim, B. H., Park, S.-I., Panilaitis, B., Ghaffari, R., Yao, J., Li, M., Liu, Z., Malyarchuk, V., Kim, D. G., Le, A.-P., **Nuzzo, R. G.**, Kaplan, D. L., Omenetto, F. G., Huang, Y., Kang, Z., and **Rogers, J. A.**, “Waterproof AllInGaP Optoelectronics on Stretchable Substrates with Applications in Biomedicine and Robotics”, *Nature Materials* **9:11**, 929-937 (2010).

4. Lambeth, R. H., Park, J., Liao, H., Shir, D. J., Jeon, S., **Rogers, J. A.** and **Moore, J. S.**, “Proximity Field Nanopatterning of Azopolymer Thin Films”, *Nanotechnology*, **21**, 165301 (2010).
5. Park, S.-I., Le, A.-P., Wu, J., Huang, Y., **Li, X.** and **Rogers, J. A.**, “Light Emission Characteristics and Mechanics of Foldable Inorganic Light-Emitting Diodes”, *Adv. Mat.*, **22:28**, 2062 (2010).
6. Sanchez, S. I.; Small, M. W., Sivaramkrishnan, S., **Wen, J.-G.**, **Zuo, J.-M.**, and **Nuzzo, R.G.**, “Visualizing Materials Chemistry at Atomic Resolution”, *Analyt. Chem.*, **82**, 2599-2607 (April 1, 2010).
7. Unarunotai, S., Murata, Y., Chialvov, C., **Mason, N.**, **Petrov, I.**, **Nuzzo, R.**, **Moore, J.**, and **Rogers, J.**, “Conjugated Carbon Monolayer Membranes: Methods for Synthesis and Integration”, *Adv. Mat.*, **22**, 1072–1077 (2010).
8. **(Inside Cover Feature Article)** Yao, J., Le, A., **Gray, S.**, **Moore, J.**, **Rogers, J.**, and **Nuzzo, R.**, “Functional Nanostructured Plasmonic Materials”, *Adv. Mat.*, **22:10**, 1102-1110 (2010).
9. Yoon, J., Jo, S., Chun, I. S., Jung, I., Kim, H.-S., Meitl, M., Menard, E., **Li, X.**, Coleman, J. J., Paik, U., and **Rogers, J. A.**, “GaAs Photovoltaics and Optoelectronics Using Releasable Multilayer Epitaxial Assemblies”, *Nature* **465**, 329-333 (2010).
10. **(Cover Article)** J.J. Adams, E.B. Duoss, T.F. Malkowski, M.J. Motala, B.Y. Ahn, **R.G. Nuzzo**, J.T. Bernard, and **J.A. Lewis**, “Conformal Printing of Electrically Small Antennas on Three-Dimensional Surfaces”, *Advanced Materials*, **23:11**, 1335-1340 (2011).
11. A.M. Bowen, J.A. Ritchey, **J.S. Moore**, and **R.G. Nuzzo**, “Programmable Chemical Gradient Patterns by Soft Grayscale Lithography”, *Small*, **7:23**, 3360-3362, (2011).
12. M.T. DeJarld, J.C. Shin, W. Chern, D. Chanda, K. Balasundaram, **J.A. Rogers**, and **X. Li**, “Formation of High Aspect Ratio GaAs Nanostructures with Metal Assisted Chemical Etching”, *Nano Lett.*, **11**, 5259-5263 (2011).
13. H. Kim, E. Brueckner, J. Song, Y. Li, S. Kim, C. Lu, J. Sulking, K. Choquette, Y. Huang, **R.G. Nuzzo**, and **J.A. Rogers**, "Unusual Strategies for Using Indium Gallium Nitride Grown on Silicon (111) for Solid-State Lighting", *Proceedings of the National Academy of Sciences USA*, **108:25**, 10072-10077 (2011).
14. **J.A. Rogers**, M.G. Lagally, and **R.G. Nuzzo**, "Synthesis, Assembly and Applications of Semiconductor Nanomembranes", *Nature*, **477**, 45-53 (2011).
15. A.V. Semichaevsky, **H.T. Johnson**, J. Yoon, **R. Nuzzo**, L. Li and **J.A. Rogers**, "Theory of optimal design of waveguiding light concentrators in photovoltaic microcell arrays", *Applied Optics*, **50**, 2799-2808 (2011).
16. J.C. Shin, K.H. Kim, K.J. Yu, H. Hu, L. Yin, C.-Z. Ning, **J.A. Rogers**, J.-M. Zuo, and **X. Li**, "InxGal-xAs Nanowires on Silicon: One-Dimensional Heterogeneous Epitaxy, Bandgap Engineering, and Photovoltaics", *Nano Letters*, **11**, 4831-4838 (2011).
17. J. Yao, A.-P. Le, M.V. Schulmerich, J. Maria, T.-W. Lee, S.K. Gray, R. Bhargava, **J.A. Rogers** and **R.G. Nuzzo**, "Soft Embossing of Nanoscale Optical and Plasmonic Structures in Glass", *ACS Nano*, **5:7**, 5763-5774 (2011).
18. J. Yoon, L. Li, A.V. Semichaevsky, J.H. Ryu, **H.T. Johnson**, **R.G. Nuzzo** and **J.A. Rogers**, "Flexible Concentrator Photovoltaics Based on Microscale Silicon Solar Cells Embedded In Luminescent Waveguides", *Nature Communications*, **2:343**, DOI: 10.1038/ncomms1318 (2011).
19. H. Zhang, A.J. DeConinck, S.C. Slimmer, P.S. Doyle, **J.A. Lewis**, and **R.G. Nuzzo**, “Genotyping by Alkaline Dehybridization Using Graphically Encoded Particles“, *Chemistry—A European Journal*, **17**, 2867-2873 (2011).
20. J.C. Shin, D. Chanda, W. Chern, K.J. Yu, **J.A. Rogers**, and **X. Li**, “Experimental Study of Design Parameters in Periodic Silicon Micropillar Array Solar Cells Produced by Soft Lithography and Metal Assisted Chemical Etching”, *IEEE J. Photovoltaics*, **2**, 129 – 133 (2012).

Project Title: Materials Science of Electrodes and Interfaces for High-Performance Organic Photovoltaics

PI: Tobin J. Marks, Co-PIs: R.P.H. Chang, A. J. Freeman, T.O. Mason, K.R. Poeppelmeier, Northwestern University, Evanston, IL 60208

Program Scope. This program pursues an integrated basic research effort by an experienced, highly collaborative interdisciplinary team with expertise in solid-state chemistry, interfacial materials, quantum theory, solar cell fabrication and characterization, and low temperature processing. The team addresses, in unconventional ways, critical electrode-interfacial issues underlying organic photovoltaic (OPV) performance--controlling band offsets between transparent electrodes and organics, addressing current loss/leakage at interfaces, and investigating cost-effective low temperature, large-area cell fabrication. Current research foci are: 1. Design (based on theory) and synthesis of advanced 2-D and 3-D TCO electrode layers with high conductivity and transparency, while minimizing the use of indium. 2. Developing theory-based understanding of the ideal interfacial layers between oxide electrodes and OPV active materials. 3. Exploring and developing new processing techniques and cell architectures for next-generation large-area flexible OPVs. The goal is to develop for the photovoltaic community the fundamental scientific understanding needed to design, fabricate, prototype, and ultimately implement high-efficiency solar cells incorporating these new concepts.

Recent Progress

Thin Film TCO Growth (Chang, Mason, Marks). Studies of TCO electrical and optical properties have aimed at understanding the transition between the amorphous and crystalline states, and how this affects the electrical and optical properties. Thus, Zn-In-Sn-O (ZITO) films were grown by pulsed-laser deposition, and three different material compositions were investigated: ZITO-30, ZITO-50 and ZITO-70 in which 30%, 50%, and 70%, respectively, of the indium in the In_2O_3 structure is replaced by substitution with Zn and Sn in equal molar proportions (co-substitution): $\text{In}_{2-2x}\text{Zn}_x\text{Sn}_x\text{O}_3$, where $x = 0.3, 0.5, 0.7$. All ZITO films grown at 25°C are amorphous. The first evidence of crystallinity is observed at higher growth temperatures as the degree of co-substitution is increased. A decrease in mobility and conductivity is also observed as the degree of co-substitution is increased. The highest mobility for ZITO-30 and ZITO-50 is observed at growth temperatures just prior to crystallization. The effect of deposition temperature on carrier concentration is surprisingly minor compared to the effect of O_2 partial pressure during growth.

Bulk GITO Phase Space (Poeppelmeier, Mason, Freeman). The co-substitution scheme that led to the synthesis of ZITO has also been applied to the Ga_2O_3 - In_2O_3 - SnO_2 (GITO) phase space, producing the tetragonal phase $\text{Ga}_{3-x}\text{In}_{5+x}\text{Sn}_2\text{O}_{16}$ (T-phase),¹ where $0.3 < x < 1.6$, and a Ga, Sn co-substituted In_2O_3 (bixbyite), as shown in **Fig. 1**. The electrical conductivity of bulk T-phase specimens, measured by 4-point probe, is found to range from 500 to 1500 S/cm with increasing In : Ga ratio at room temperature. All compositions (x-values) are found to be optically transparent, with a common band gap of ~ 3.1 eV by diffuse reflectance spectroscopy. Of even greater interest, the bixbyite solid solution, when lightly doped with Sn, is found to have a *very high* bulk conductivity in excess of 4000 S/cm. The high conductivity and transparency of these bulk GITO phases are of interest for OPV applications and we anticipate still higher values for crystalline thin films. Furthermore, the T-phase is found to exhibit a significant temperature dependence of conductivity. As the synthesis temperature increased from 1250°C to 1350°C (followed by

quenching), the electrical conductivity increases five-fold. Ongoing work focuses on the origin of this dramatic increase in carrier content and/or mobility. Our prior work showed a direct correspondence between optimized conductivity and the so-called “octahedral site density” of cations. Current work is aimed at testing this relationship in the T-phase, which exhibits a wide range of coordination environments, as depicted in **Fig. 2**. So far, this investigation has identified the T-phase as one member of a large class of compounds related to the scheelite structure. Structurally analogous compounds with various cation oxidation states, such as +2

and +5 in the case of $\text{Mn}_3\text{Ta}_2\text{O}_8$ and +1, +3, and +6 in the case of $\text{Na}_5\text{Lu}(\text{WO}_4)_4$, have been identified in this class in the literature. Some semi-conducting compounds, such as $\text{Zn}_3\text{Ta}_2\text{O}_8$ and $\text{Zn}_3\text{Nb}_2\text{O}_8$ have already been synthesized in an attempt to follow this trend, but they form significantly different crystal structures.

Interfacial Layers (IFLs) (Chang, Marks). The remarkable functionality of NiO interfacial layers in enhancing bulk heterojunction (BHJ) OPV performance is being investigated by integrated characterization of the electrical, micro-structural, electronic structural, and optical properties of thin NiO films grown on glass/ITO electrodes. These layers are found to be advantageous in BHJ OPV applications due to favorable energy band levels, interface passivation, p-type character, crystallinity, smooth surfaces, and optical transparency. The NiO overlayers are fabricated via pulsed-laser deposition and are found to have a work function of ~ 5.3 eV. They are investigated by both topographic and conductive AFM and shown to passivate interfacial charge traps. The films have an average optical transparency of $>80\%$ in the visible range, crucial for efficient OPV function, and have a near-stoichiometric NiO surface composition. By grazing-incidence X-ray diffraction, the NiO thin films are shown to grow preferentially in the (111) direction and to have the fcc NaCl crystal structure. Diodes of p-n structure and first-principles electronic structure calculations indicate that the NiO interlayer is preferentially conductive to holes, with a lower hole charge carrier effective mass versus that of electrons. Implications of these attributes in advancing efficiencies for state-of-the-art OPV systems-in particular, improving the open circuit voltage have been demonstrated.

In regard to organic IFLs, the design, synthesis, characterization and device implementation of a novel IFL for insertion between the ITO anode and active layer of poly(3-hexylthiophene) : [6,6]-phenyl-C₆₁-butyric acid methyl ester (PCBM) bulk-heterojunction OPVs was completed. The precursor, 5,5'-bis[(*p*-trichlorosilylpropylphenyl)phenylamino]-2,2'-bithiophene (PABTSi₂), covalently anchors to the ITO surface via the $-\text{SiCl}_3$ groups and incorporates a bithiophene unit to align the HOMO energy with that of P3HT (5.0 eV). The synthesis and subsequent electrochemical analysis of anchored PABTSi₂ indicates a HOMO energy of 4.9 eV, while the

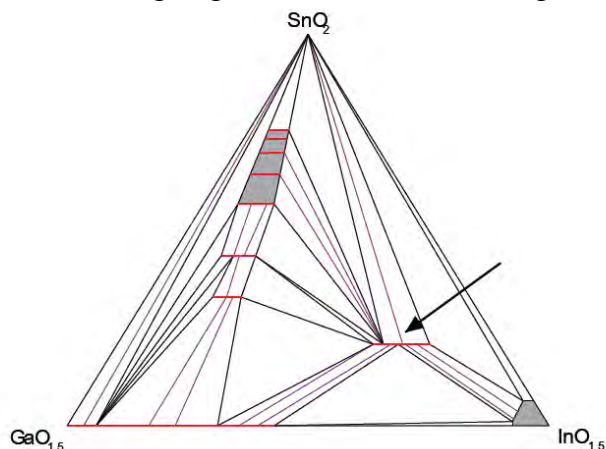


Fig. 1. Previously reported Ga_2O_3 - In_2O_3 - SnO_2 phase diagram. Phases of interest: the “T-phase” (arrow) and bixbyite (the shaded area at the bottom-right corner).

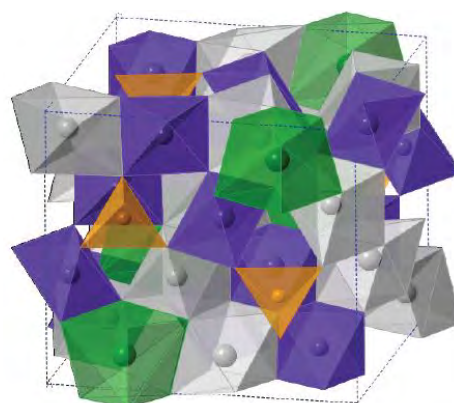


Fig. 2. T-phase crystal structure model: 4-fold (orange), 6-fold (purple), 7-fold (gray), and 8-fold (green) coordination polyhedra.

LUMO level remains sufficiently high, at 2.2 eV, to effectively block electron leakage to the OPV ITO anode. For the P3HT:PCBM OPV fabrication, PABTSi₂ is used as a spin-coated and crosslinked (via -SiCl₃ hydrolysis and condensation) as a 1:2 blend with poly[9,9-dioctylfluorene-co-N-[4-(3-methylpropyl)]-diphenylamine] (TFB). Such devices exhibit an average power conversion efficiency of 3.34%, a fill factor of 62.7%, an open-circuit voltage of 0.54 V, and a short-circuit current of 9.31 mA/cm², parameters rivaling those of optimized PEDOT:PSS-based devices, but with far greater thermal durability.

3-D ITO Nanorod Electrodes (Chang, Marks, Poepelmeier). Recently we demonstrated the ability to grow both random and patterned ITO nanorods using VLS techniques in combination with high resolution e-beam lithography at ANL. The goal of this work is to demonstrate that 3-D nanorod electrodes can afford high OPV efficiencies. The unique design of these electrodes is based on reducing cell recombination losses while at the same time retaining good light absorption. Estimates from preliminary results using this new architecture design for DSSCs show that cell efficiency can be increased by as much as 30%!

Future Plans

Thin Film TCOs (Chang, Mason, Marks). Work in the coming period will focus on understanding the transport, microstructural, and device electrode properties of amorphous TCO films such as ZITO, especially as a function of growth process—vapor phase or solution. The attraction of amorphous phases such as ZITO is the great mechanical flexibility, lack of grain boundaries, smoothness, and low In content. All of these are attractive for the cost-effective fabrication of efficient, flexible OPVs by roll-to-roll processes. The work on 3-D nanorod electrodes will also continue. It is our goal that by a combination of the use of unique materials and electrode architectures, efficiencies for both OPV and DSSC can be increased by as much as 50% during the next two years.

Bulk GITO Phase Space (Poepelmeier, Freeman, Mason). To better understand the T-phase compound electrical properties, band structure calculations will be conducted in collaboration with the Freeman group. The full-potential linearized augmented plane wave (FLAPW) calculations will provide theoretical analyses of conduction and valence band minima, as well as the correct band gap, calculated with the XLDA method, and the optical properties. Work function calculations will also be performed. For transport analysis, our calculations, combined with the experimental evidence, will provide a theoretical explanation on the significant temperature dependence of the T-phase conductivity. Of interest is which cations/coordinations dominate the density of states at the conduction band minimum. Work function measurements will also be conducted on all T-phase and bixbyite compositions by Kelvin Probe to assess the viability of these compounds as OPV electrodes. With its substantially larger band gap, Ga₂O₃ is of interest for the potential to modify surface electrical properties, especially the GITO work function. Additionally, phase diagram studies will clarify the nature of the In₂O₃ corner of the GITO phase diagram, which is not fully understood. Furthermore, the temperature dependence of the T-phase electrical conductivity will be further studied.

Novel phases outside the GITO phase space are also of interest. The scheelite structure contains cation environments that bear a striking resemblance to the In and Ga sites in the T-phase, but the cations occupying these sites have different oxidation states. Thus the geometry of these compounds suggests that n-type co-substitution of GITO with more economical cations is feasible. Possible dopants to accomplish this include +2 cations that have good TC properties; of particular interest is Mg. This design is intended to lead to advanced 2-D TCO layers with high conductivity and transparency while minimizing or excluding In. Additionally, the relationship between the

dopant cation size and its correlation with conductivity will be tracked to predict alternative dopants for this process.

Interfacial Layers (Marks, Chang, Freeman). In the coming grant period, efforts will focus in three areas. First, theoretical studies will analyze how the TCO band structure interacts with the covalently tethered IFL molecules as an effective construct for hole transport and electron blocking. Second, IFL molecule design will focus on modulation of the above band-orbital overlap and how this interaction can be tuned by IFL molecule electronic structure and dipole moment. Third, IFL design will turn to some of the unique interfacial scientific challenges offered by inverted OPVs where metal oxides are used as transport and blocking layers.

Publications Acknowledging this Grant

1. Buchholz, D.B.; Proffitt, D.E.; Wissler, M.D.; Mason, T.O.; Chang, R.P.H. Electrical and band-gap properties of amorphous zinc-indium-tin oxide thin films. *Prog. Nat. Sci.-Mater. Int.* **2012**, *22*, 1-6.
2. Lee, B.; Buchholz, D.B.; Guo, P.; Hwang, D.K.; Chang, R.P.H. Optimizing the Performance of a Plastic Dye-Sensitized Solar Cell. *J. Phys. Chem. C.* **2011**, *155*, 9787-9796.
3. Irwin, M.D.; Servaites, J.D.; Buchholz, D.B.; Leever, B.J.; Liu, J.; Emery, J.D.; Zhang, M.; Song, J.H.; Durstock, M.F.; Freeman, A.J.; Bedzyk, M.J.; Hersam, M.C.; Chang, R.P.H.; Ratner, M.A.; Marks, T.J. Structural and Electrical Functionality of NiO Interfacial Films in Bulk Heterojunction Organic Solar Cells. *Chem. Mater.* **2011**, *23*, 2218-2226.
4. Lee, B.; Hwang, D.K.; Guo, P.; Ho, S.T.; Buchholz, D.B.; Wang, C.Y.; Chang, R.P.H. Materials, Interfaces, and Photon Confinement in Dye-Sensitized Solar Cells, *J. Phys. Chem. B* **2010**, *114*, 14582-14591.
5. Hains, A.W.; Ramanan, C.; Irwin, M.D.; Liu, J.; Wasielewski, M.R.; Marks, T.J. Designed Bithiophene-Based Interfacial Layer for High-Efficiency Bulk-Heterojunction Organic Photovoltaic Cells. Importance of Interfacial Energy Level Matching. *ACS Appl. Mater. Interfaces* **2010**, *2*, 175-185.
6. Proffitt, D.E.; Buchholz, D.B.; Chang, R.P.H.; Bedzyk, M.J.; Mason, T.O.; Ma, Q. X-Ray Absorption Spectroscopy Study of the Local Structures of Crystalline Zn-In-Sn Oxide Thin Films. *J. Appl. Phys.* **2009**, *11*, 113524.
7. Hopper, E.M.; Zhu, Q.; Song, J.H.; Peng, H.; Freeman, A.J.; Mason, T.O. Electronic and thermoelectric analysis of phases in the $\text{In}_2\text{O}_3(\text{ZnO})_k$ system. *J. Appl. Phys.* **2011**, *109*, 13713.
8. Hains, A.W.; Liu, J.; Martinson, A.B.F.; Irwin, M.D.; Marks, T.J. Anode Interfacial Tuning via Electron-Blocking/Hole-Transport Layers and Indium Tin Oxide Surface Treatment in Bulk-Heterojunction Organic Photovoltaic Cells. *Adv. Funct. Mater.* **2010**, *20*, 595-606.
9. Hopper, E.M.; Sauvage, F.; Chandiran, A.K.; Grätzel, M.; Poepfelmeier, K.R.; Mason, T.O. Electrical properties of Nb-, Ga-, and Y-substituted nanocrystalline anatase TiO_2 prepared by hydrothermal synthesis. *J. Am. Ceram. Soc.*, in press.
10. Hopper, E.M.; Zhu, Q.; Gassmann, J.; Klein, A.; Mason, T.O. Surface electronic properties of polycrystalline bulk and thin film $\text{In}_2\text{O}_3(\text{ZnO})_k$ compounds. *Appl. Surf. Sci.*, submitted.

Symmetry Breaking for the Synthesis of Nanostructured Porous Materials

Principal Investigator: Adam J. Matzger

Co-Investigator: Antek G. Wong-Foy

Department of Chemistry and the Macromolecular Science and Engineering Program

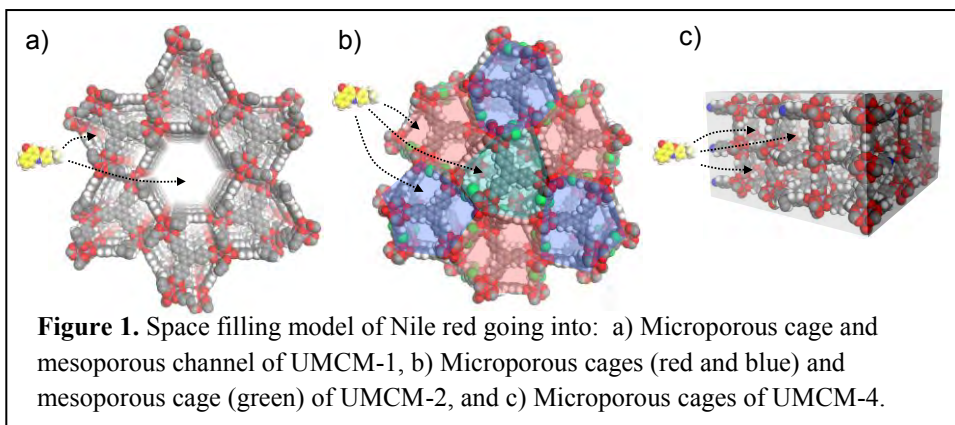
University of Michigan, Ann Arbor, MI 48109-1055

Program Scope

The overarching theme of the program is to develop, understand, and deploy new methods for sorbent synthesis. The development of new high performance sorbents is critical for a variety of established (separations, purification) and emerging (hydrogen storage, carbon capture) technologies. Coordination polymers offer tremendous promise for such applications and complement greatly established materials such as zeolites and carbons. The specific goals of the project can be broadly defined as those involving reduced symmetry linker design for producing coordination polymers and coordination polymers involving mixed linkers (coordination copolymers).

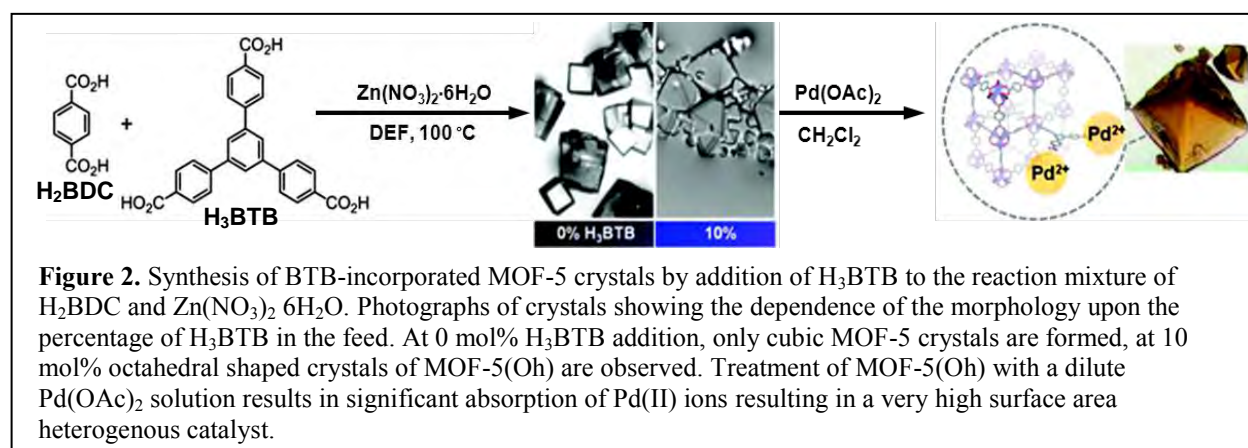
Recent Progress

The considerable potential of mixing linkers with different topologies and identical coordinating functionality was first demonstrated with the production of UMCM-1 (UMCM = University of Michigan crystalline material).¹ Derived from the commercially available linkers, terephthalic acid (H₂BDC) and benzene tribenzoic acid (H₃BTB), this material possesses large mesoporous channels flanked by microporous cages. Soon after, UMCM-2 followed² with a record setting BET surface area of 5200 m²/g and its analogs such as MOF-210.³ More recently other combinations of carboxylate linkers have led to UMCM-3 and UMCM-4, the latter with an unusual combination of terephthalate linkers (BDC) acting both as pillars and as organizing elements within 2D sheets containing BTB.⁴ Although the pore dimensionality of these frameworks differed significantly in terms of having pores aligned in radically different fashions, the potential to exploit these topological novelties in facilitating



anisotropic guest transport was uncertain due to the limited ability of single crystal X-ray diffraction to yield information on defects in materials. By applying single molecule methods, in collaboration with the Biteen group at the University of Michigan, we were able to directly observe the diffusion of individual Nile red guest molecules inside three different UMCMs in real time using single-molecule fluorescence microscopy (Figure 1).⁵ Trajectory analysis revealed that most molecules observed in UMCM-2 crystals are immobilized by this material with a torturous three dimension network of interconnected pores. By contrast most molecules in UMCM-1, with a mesoporous channel structure, move according to a 1D random walk. In the pillared sheet-like material UMCM-4, 2D random walking is operative. In all cases guest motion is not homogeneous in the crystals, and several subpopulations of molecules, each with its own mobility range, were identified in each crystal. In addition, due to structural heterogeneities, molecules that are reversibly trapped or adsorbed at a single site switch between different modes of motion along the way, depending on the physical and chemical properties of the local environments in which they reside and the features with which they interact. These studies serve to inform separations occurring with coordination polymers in the large molecule regime. This is a growing and important area of application where significant gains in energy efficient separations might be realized.⁶

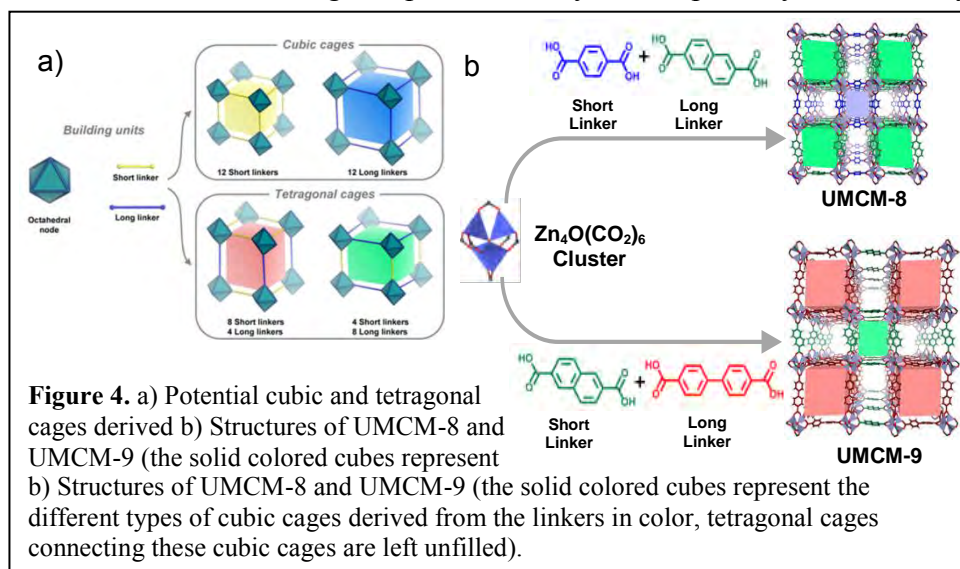
In the course of our studies with mixed linkers we have observed that there are threshold concentrations of ligands required for efficient production of new phases. For example, UMCM-1 does not form as an initial phase during solvothermal synthesis until the BDC concentration exceeds about 10 mol%. Initially we had assumed, based primarily on gas sorption and PXRD analysis, that the cubic phase produced below this concentration was MOF-5 [$\text{Zn}_4\text{O}(\text{BDC})_3$]_n. However, further scrutiny by NMR spectroscopy of the decomposed material indicated the presence of BTB within the material clearly displaying the gross structure of MOF-5. Based on the change in morphology from a cubes to octahedra during addition of increasing concentration of BTB we term this material MOF-5(O_h) (Figure 2, middle). Through a mechanism that we ascribe to the presence of uncoordinated carboxylate groups, defective MOF-5(O_h) produced with 10 mol% BTB in the feed adsorbs a considerable amount of palladium ions from a dilute Pd(OAc)₂ solution (Figure 2, right). This affords a very high surface area heterogeneous catalyst



(~2500 m²/g BET surface area) that is effective for the nondirected C–H activation and functionalization of, for example, naphthalene. This approach opens the potential for similarly functionalizing other coordination polymers to greatly simplify the process of introducing catalytically active metals in a uniformly dispersed fashion. Such materials are of particular interest to test models for enhanced adsorption of hydrogen in MOFs through the proposed spillover mechanism.⁷

One of the keys to success of the mixed linker strategy is that by incorporating more than only type of linker around a highly symmetrical metal cluster, the symmetry of the cluster is broken. This translates into the symmetry breaking at the network nodes and forces more complex topologies than those based, for example, on simple Archimedean solids. The end result of this is that framework interpenetration is suppressed. In spite of exceptional porosity, UMCM-1,-2,-3, and -4 show no propensity towards interpenetration. Each of these materials is built with a combination of a dicarboxylate and a tricarboxylate. In principle the network node desymmetrization need not be so drastic; however, until recently this hypothesis has not been tested. We will discuss the product constructed with BDC and NDC (NDC = naphthalene-2,6-dicarboxylate) linkers which is denoted as UMCM-8.⁸ The BET surface area of UMCM-8 is 4030 m²/g, which matches well with the theoretical surface area (4005 m²/g). The structure arises from a combination of cubic and tetragonal cages thus thwarting interpenetration. In addition the structure of UMCM-9, with a surface area approaching 5000 m²/g will be highlighted. Hand in hand with this effort we have been reassessing the procedures by which porosity is ultimately

realized in a coordination polymer. Grouped under the general heading of “activation” this is a critical step towards making viable sorbents and the potential of flow supercritical CO₂ activation will be discussed.



Future Plans

We are particularly focused on the further development of the mixed linker strategy exploiting linear linkers that are commercially available at a reasonable price and therefore have the potential make high performance sorbents capable of exceeding the properties of zeolites and carbons such that the overall economics of deployment makes sense.

In the area of mixed linker and reduced symmetry linkers we are poised to test some of the hypotheses about constructing greatly expanded analogs using the principles of isorecticular chemistry in the context of relatively low symmetry networks.

References

1. Koh, K.; Wong-Foy, A. G.; Matzger, A. J. A Crystalline Mesoporous Coordination Copolymer with High Microporosity. *Angew. Chem.-Int. Edit.* **2008**, *47*, 677680.
2. Koh, K.; Wong-Foy, A. G.; Matzger, A. J. A Porous Coordination Copolymer with over 5000 m²/g BET Surface Area. *J. Am. Chem. Soc.* **2009**, *131*, 4184-4185.
3. Furukawa, H.; Ko, N.; Go, Y. B.; Aratani, N.; Choi, S. B.; Choi, E.; Yazaydin, A. O.; Snurr, R. Q.; O'Keeffe, M.; Kim, J.; Yaghi, O. M. Ultrahigh Porosity in Metal-Organic Frameworks. *Science* **2010**, *329*, 424-428.
4. Koh, K.; Wong-Foy, A. G.; Matzger, A. J. Coordination Copolymerization Mediated by Zn₄O(CO₂R)₆ Metal Clusters: a Balancing Act between Statistics and Geometry. *J. Am. Chem. Soc.* **2010**, *132*, 15005-15010.
5. Liao, Y.; Yang, S. K.; Koh, K.; Matzger, A. J.; Biteen, J. S. Heterogeneous Single-Molecule Diffusion in One-, Two-, and Three-Dimensional Microporous Coordination Polymers: Directional, Trapped, and Immobile Guests. *Nano Lett.* **2012**, ASAP.
6. Cychosz, K. A.; Ahmad, R.; Matzger, A. J. Liquid Phase Separations by Crystalline Microporous Coordination Polymers. *Chem. Sci.* **2010**, *1*, 293-302.
7. Park, T.-H.; Hickman, A. J.; Koh, K.; Martin, S.; Wong-Foy, A. G.; Sanford, M. S.; Matzger, A. J. Highly Dispersed Palladium(II) in a Defective Metal-Organic Framework: Application to C-H Activation and Functionalization. *J. Am. Chem. Soc.* **2011**, *133*, 20138-20141.
8. Koh, K.; Van Oosterhout, J. D.; Roy, S.; Wong-Foy, A. G.; Matzger, A. J. Exceptional Surface Area from Coordination Copolymers Derived from Two Linear Linkers of Differing Lengths. *Chem. Sci.* **2012**, in press.

Publications

Park, T.-H.; Hickman, A. J.; Koh, K.; Martin, S.; Wong-Foy, A. G.; Sanford, M. S.; Matzger, A. J., "Highly Dispersed Palladium(II) in a Defective Metal-Organic Framework: Application to C-H Activation and Functionalization" *J. Am. Chem. Soc.*, **2011**, *133*, 20138-20141.

Liao, Y.; Yang, S. Y.; Koh, K.; Matzger, A. J.; Biteen, J. S., "Heterogeneous Single-Molecule Diffusion in One-, Two-, and Three-Dimensional Microporous Coordination Polymers: Directional, Trapped, and Immobile Guests" *Nano Lett.*, **2012**, ASAP.

Koh, K.; Van Oosterhout, J. D.; Roy, S.; Wong-Foy, A. G.; Matzger, A. J., "Exceptional surface area from coordination copolymers derived from two linear linkers of differing lengths" *Chem. Sci.*, **2012**, in press.

SYNTHESIS OF MOLECULE/POLYMER-BASED MAGNETIC MATERIALS

Joel S. Miller, Department of Chemistry, University of Utah, Salt Lake City, UT 84112

Program Scope

The design/synthesis/characterization/exploitation of organic-based magnetic materials, and those combining magnetism with other technologically important properties (*e.g.*, electrical, optical, and mechanical). These materials are important for future electronic/photonics devices, especially due to the need for rare earth-free materials, reduced energy consumption and environmentally friendlier processing and disposal.

Recent Progress

The magnetic behavior of $M^{II}(\text{TCNE})[\text{C}_4(\text{CN})_8]_{1/2}$ ($M = \text{Mn}, \text{Fe}$) was reinvestigated, and are antiferromagnets, not ferrimagnets,⁴ with 67 and 84 K T_c s, respectively.⁴ A spin-flop transition occurs at 19.5 kOe at 5 K for **Mn**, while **Fe** is a Class 1 metamagnet with a tricritical temperature of 62 K. **Fe** also exhibits a constricted hysteretic behavior with a 5 K critical field of 12,600 Oe, and coercive field and remanent magnetization of 4,800 Oe and 1,850 emuOe/mol, respectively.

Mn has a reversible P-induced transition from an antiferromagnet to a high magnetization ferrimagnet above 0.5 kbar (Fig. 1), and in the ferrimagnetic state T_c increases with P and is ~97 K at 12.6 kbar (Fig. 2), the magnetization increases a thousand fold (Fig. 3), and the material becomes a hard magnet with a significant remnant magnetization. The phase diagram is shown in Fig. 2. This piezomagnetic transition suggest applications in transducers, sensors, and actuators.⁵

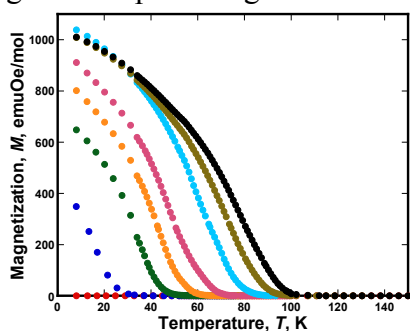


Fig 1. Remanent magnet for **Mn** Ambient pressure (●), 0.95 (●), 3.88 (●), 4.95 (●), 6.37 (●), 8.86 (●), 10.8 (●), 12.6 kbar (●).⁵

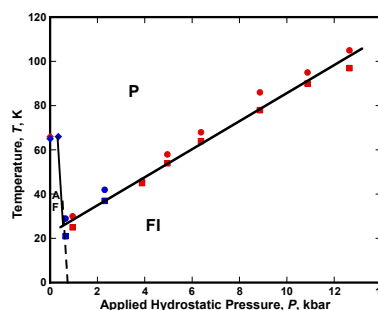


Fig 2. Phase diagram for **Mn**: AF= antiferromagnetic; P = paramagnetic; FI = ferrimagnetic⁵

The reaction of Mn^{II} and ACN ($A = \text{Na}, \text{K}, \text{Rb}, \text{Cs}$)^{6,7} forms 3-D Prussian blue analogues (PBA), $\text{A}_2\text{Mn}[\text{Mn}(\text{CN})_6]$. While $A = \text{Cs}$ leads to a typical PBA ($T_c = 21$ K), $A = \text{K}, \text{Rb}$ as well as hydrated-Na are structurally different with monoclinic, not cubic unit cells, with nonlinear MnCNMn linkages.³ Dehydration of the sodium-hydrated materials forms $\text{Na}_2\text{Mn}[\text{Mn}(\text{CN})_6]$, which has an unexpected hexagonal unit cell.⁶ This is at variance with the previous report that $\text{K}_2\text{Mn}[\text{Mn}(\text{CN})_6]$ possesses a cubic unit cell. This is attributed to the ionic nature of high spin Mn^{II} accommodating a reduced $\text{M-CN-M}'$ angle and minimizing void space. $\text{K}_2\text{Mn}^{II}[\text{Mn}^{II}(\text{CN})_6]$ and $\text{Rb}_2\text{Mn}^{II}[\text{Mn}^{II}(\text{CN})_6]$ are a ferrimagnets below 41 and 35 K.⁷ Most interestingly is the increase in T_c as the $\angle\text{Mn-N-C}$ decreases from linearity (Fig. 3).⁶ Hence, the bent cyanide

bridges play a crucial role in the superexchange mechanism by increasing the coupling via shorter Mn-Mn distances, and perhaps enhanced overlap.

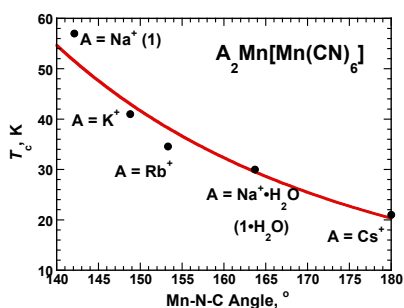


Fig. 3. Correlation of increasing T_c with nonlinearity of the $\angle\text{MnNC}$ for $A_2\text{Mn}[\text{Mn}(\text{CN})_6]$.⁷

The magnetic structure of ferrimagnetic $\text{K}_2\text{Mn}[\text{Mn}(\text{CN})_6]$ was determined at 4 K.^{8,9} The high spin, $S = 5/2$ N-bonded Mn^{II} ion has a moment of $4.4 \mu_B$ while the low spin, $S = 1/2$ C-bonded Mn^{II} ion has a moment of $-1.0 \mu_B$; hence, $\text{K}_2\text{Mn}[\text{Mn}(\text{CN})_6]$ has a non-compensated, collinear, antiparallel magnetic moments oriented along the b axis (Fig. 4). The T_c is 40.6 ± 0.3 K, and the critical exponent $\beta = 0.38$ (Fig. 5).

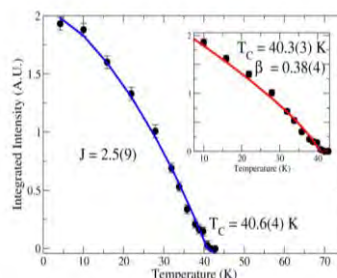
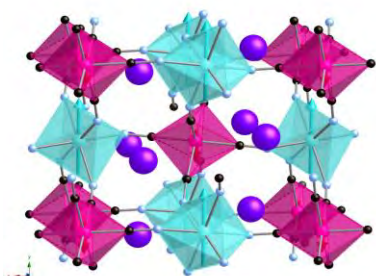


Fig. 4. Experimental magnetic structure for $\text{K}_2\text{Mn}^{\text{II}}[\text{Mn}^{\text{II}}\text{CN}_6]$ with the magnetic moments (\uparrow) along b , not a bond.^{8,9} Fig. 5. Total integrated intensity for several Bragg peaks near T_c is a fit to a critical order parameter ($-$).^{8,9}

The reaction of $[\text{NEt}_4]\text{CN}$ and Mn^{II} forms both $[\text{NEt}_4]_2[\text{Mn}_3(\text{CN})_8]$ ¹⁰ and $[\text{NEt}_4][\text{Mn}_3(\text{CN})_7]$,^{10,11} and neither exhibit a fcc structure typical of Prussian blue structured materials.³ $[\text{NEt}_4][\text{Mn}_3(\text{CN})_7]$ differs from $[\text{NEt}_4]_2[\text{Mn}_3(\text{CN})_8]$ as the terminal cyanides that point above and below the layers are orientationally disordered and provides bridging for a 3-D structure.

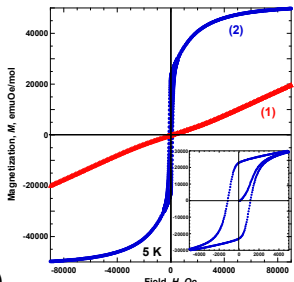
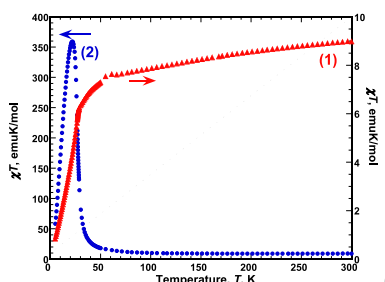
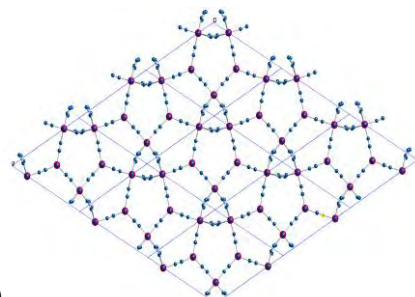


Fig. 10. $\chi T(T)$ (a) and 5-K $M(H)$ (b) for $[\text{NEt}_4]\text{Mn}_3(\text{CN})_7$ (1) (σ) & $[\text{NEt}_4]_2\text{Mn}_3(\text{CN})_8$ (2) (\bullet) in a 1 kOe applied field. Inset: 5-K coercivity.



Both exhibit direct antiferromagnetic coupling between each low spin $S = 1/2$ octahedral Mn^{II} and the two high spin $S = 5/2$ tetrahedral Mn^{II} sites within a layer, and exhibit different magnetic behaviors (Fig. 10). Layered $[\text{NEt}_4]_2[\text{Mn}_3(\text{CN})_8]$ orders as a ferrimagnet at 27 K, with a coercive field and remanant magnetization of 1140 Oe and 22,800 emuOe/mol, respectively. In contrast, the direct bonding via bridging cyanides between ferrimagnetic layers leads to antiferromagnetic coupling between the layers, and 3-D structured $[\text{NEt}_4]\text{Mn}_3(\text{CN})_7$ has different magnetic behavior (Fig. 10), and is the first antiferromagnetic Prussian blue analog ($T_c = 27$ K) having neither a coercive field, nor a response in the imaginary ac susceptibility, $\chi''(T)$.

Thermolysis of either $[\text{NEt}_4]_2[\text{Mn}_3(\text{CN})_8]$ or $[\text{NEt}_4][\text{Mn}_3(\text{CN})_7]$ form antiferromagnetic $\text{Mn}(\text{CN})_2$ ($T_c = 73$ K) that possesses consisting of two independent, interpenetrating diamondoid

networks.¹² The reaction of Mn^{II} and [NMe₄]CN forms [NMe₄]₂Mn^{II}₅(CN)₁₃ that has a highly disordered structural motif with square pyramidal, trigonal bipyramidal, and octahedral Mn^{II} sites with a single layer motif of three pentagonal and one triangular fused rings similar to β-U₃O₈ (Fig. 11).¹³ The layers are bridged in a complex manner. [NMe₄]₂Mn^{II}₅(CN)₁₃ has one low-spin octahedral and 4 pentacoordinate high-spin Mn^{II} sites, and order as antiferromagnet at 11 K.

Future Plans

Our multidisciplinary research builds on these and other accomplishments and targets the several projects to understand the structure-function relationship to ultimately enable the preparation of stable, technologically useful, high-*T_c* organic-based magnets. This will include the synthesis of new materials as well as their magnetic characterization, including pressure dependent studies.

References

- ¹ S. H. Lapidus, A. C. McConnell, P. W. Stephens, J. S. Miller, *Chem. Comm.* 47, 7602 (2011).
- ² K. H. Stone, P. W. Stephens, A. C. McConnell, E. Shurdha, K. I. Pokhodnya, J. S. Miller, *Adv. Mater.* 22, 2514 (2010).
- ³ The structure was refined by Peter W. Stephens from the Rietveld refinement of synchrotron powder diffraction data collected at the NSLS at BNL.
- ⁴ A. C. McConnell, E. Shurdha, J. D. Bell, J. S. Miller, submitted.
- ⁵ A. C. McConnell, J. S. Miller, in preparation.
- ⁶ C. M. Kareis, S. H. Lapidus, J.-H. Her, P. W. Stephens, J. S. Miller, *J. Am. Chem. Soc.* 134, 2246 (2012).
- ⁷ J.-H. Her, P. W. Stephens, C. M. Kareis, J. G. Moore, K. S. Min, J.-W. Park, G. Bali, B. S. Kennon, J. S. Miller, *Inorg. Chem.* 49, 1524 (2010).
- ⁸ J.-H. Her, C. M. Brown, W. W. Shum, P. W. Stephens, C. M. Kareis, J. S. Miller, in prep.
- ⁹ The structure was refined by Craig M. Brown; NIST Center for Neutron Research.
- ¹⁰ J.-H. Her, P. W. Stephens, C. M. Kareis, J. G. Moore, J. S. Miller, *Angew. Chem. internat. Ed.* 49, 7773 (2010)
- ¹¹ C. M. Kareis J.-H. Her, P. W. Stephens, J. G. Moore, J. S. Miller, *Chem. Eur. J.* 18, X (2012).
- ¹² C. M. Kareis S. H. Lapidus, P. W. Stephens, J. S. Miller, *Inorg. Chem.* 51, 3046 (2012).
- ¹³ S. H. Lapidus, P. W. Stephens, C. M. Kareis J. S. Miller, in preparation.

Publications

1. Structures and Magnetostructural Correlation of Ferrimagnetic *meso*-Tetraphenylporphinatomanganese(III) dimethyl-*N,N'*-dicyanoquinonediiminide, [MnTPP]⁺[Me₂DCNQI]⁻, J. L. Arthur, S. H. Lapidus, P. W. Stephens, J. S. Miller, *Science China Chem.* 55, 0000-0000 (2012).
2. Organic-based Magnets: The Importance of Structural Determinations from the Rietveld Refinement of Powder X-ray Data, J. S. Miller, P. W. Stephens, *Trans. Am. Cryst. Assoc.*
3. Structure and Magnetostructural Correlation of Two Desolvated Polymorphs of Ferrimagnetic *meso*-Tetrakis(4-chlorophenyl)porphinatomanganese(III) Tetracyanoethenide, [MnTCIPP]⁺[TCNE]⁻, J.-H. Her, P. W. Stephens, J. D. Bagnato, J. S. Miller, *J. Phys. Chem. C* 114, 20614-20620 (2010).
4. Magnetically Ordered Molecule-based Materials, J. S. Miller, *Chem. Soc. Rev.* 40, 3266-3296 (2011).

5. Mn(TCNE)_{1.5}(I₃)_{0.5} (TCNE = Tetracyanoethylene) - a 3-D Networked Structured High Temperature Organic-based Magnet), K. H. Stone, P. W. Stephens, A. C. McConnell, E. Shurdha, K. I. Pokhodnya, J. S. Miller, *Adv. Mater.* **22**, 2514-2519 (2010).
6. Solid-State NMR Spectra and Long, Intradimer Bonding in the π -[TTF]₂²⁺ (TTF = Tetrathiafulvalene) Dication, M. D. Halling, J. D. Bell, R. J. Pugmire, D. M. Grant, J. S. Miller, *J. Phys. Chem. A* **114**, 6622-6629 (2010).
7. Anomalous Non-Prussian Blue Structure and Magnetic Ordering of K₂Mn^{II}[Mn^{II}(CN)₆] and Rb₂Mn^{II}[Mn^{II}(CN)₆], J.-H. Her, P. W. Stephens, C. M. Kareis, J. G. Moore, K. S. Min, J.-W. Park, G. Bali, B. S. Kennon, J. S. Miller, *Inorg. Chem.* **49**, 1524-1534 (2010).
8. Anomalous Stoichiometry, Layered Structure, and Magnetic Ordering of the Prussian Blue Analog [NEt₄]₂Mn^{II}₃(CN)₈, J.-H. Her, P. W. Stephens, C. M. Kareis, J. G. Moore, J. S. Miller, *Angew. Chem. internat. Ed.* **49**, 7773-7775 (2010).
9. Optical control of magnetization in a room-temperature magnet: V-Cr Prussian blue analog, K. D. Bozdog, J.-W. Yoo, N. P. Raju, A. C. McConnell, J. S. Miller, A. J. Epstein, *Phys. Rev. B* **094449-1/5** (2010).
10. High field linear magnetoresistance in fully spin-polarized high-temperature organic-based ferrimagnetic semiconductor V(TCNE)_x films, x ~ 2, N. P. Raju, V. N. Prigodina, K. I. Pokhodnya, J. S. Miller, A.J. Epstein, *Synth Met.* **160**, 307-310 (2010).
11. Molecule-based Magnets, J. S. Miller, D. Gatteschi, *Chem. Soc. Rev.* **40**, 3065-6 (2011).
12. Stabilization of Magnetic Ordering Observed for the Bridging NCN Group, J. L. Arthur, C. E. Moore, A. L. Rheingold, J. S. Miller, *Inorg. Chem.* **50**, 2735-2737 (2011).
13. Structure and Magnetic Ordering of a 2-D Mn(TCNE)I(OH₂) (TCNE = tetracyanoethylene) Organic-Based Magnet (*T_c* = 171 K), S. H. Lapidus, A. C. McConnell, P. W. Stephens, J. S. Miller, *Chem. Comm.* **47**, 7602-7604 (2011) + Cover
14. Unusual Long, Multicenter Cation···Anion Bonding Observed for Several Polymorphs of [TTF][TCNE], M. Capdevila-Cortada, J. J. Novoa, J. D. Bell, C. E. Moore, A. L. Rheingold, J. S. Miller, *Chem. Eur. J.* **17**, 9326-9341 (2011).
15. Dinuclear Co^{II}(NCMe)₅Co^{II}(NCS)₄ Possessing Octahedral and Tetrahedral Co^{II} Sites, E. Shurdha, C. E. Moore, A. L. Rheingold, J. S. Miller, *Inorg. Chem.* **50**, 10546-8 (2011).
16. *N,N*-7-Tricyanoquinomethanimine (TCQMI) as a cyano acceptor in the synthesis of new molecule-based magnetic systems, J. L. Arthur, C. E. Moore, A. L. Rheingold, S. H. Lapidus, P. W. Stephens, J. S. Miller, *Adv. Functional Mater.* **22**, 0000-0000 (2012).
17. Zero-dimensional Organic-based Magnets Possessing Decamethylmetallocene, J. S. Miller, *J. Mater. Chem.* **20**, 1846-1857 (2010) + Front Cover
18. Thin Film Co[TCNE]₂ and V_yCo_{1-y}[TCNE]₂ Magnetic Materials, P. K. Erickson, J. S. Miller, *J. Mag. Magnet. Mater.* **324**, 2218-2223 (2012).
19. Structure and Magnetic Ordering of the Anomalous Layered (2-D) Ferrimagnetic [NEt₄]₂Mn^{II}₃(CN)₈ and 3-D Antiferromagnetic Bridged-Layered [NEt₄]₂Mn^{II}₃(CN)₇ Prussian Blue Analogs, C. M. Kareis J.-H. Her, P. W. Stephens, J. G. Moore, J. S. Miller, *Chem. Eur. J.* **18**, 0000-0000 (2012).
20. Interpenetrating Three-Dimensional Diamondoid Lattices and Antiferromagnetic Ordering (*T_c* = 73 K) of Mn(CN)₂, C. M. Kareis S. H. Lapidus, P. W. Stephens, J. S. Miller, *Inorg. Chem.* **51**, 3046-3050 (2012).
21. Non-Prussian Blue Structures and Magnetic Ordering of Na₂Mn^{II}[Mn^{II}(CN)₆] and Na₂Mn^{II}[Mn^{II}(CN)₆]•2H₂O, C. M. Kareis, S. H. Lapidus, J.-H. Her, P. W. Stephens, J. S. Miller, *J. Am. Chem. Soc.* **134**, 2246-2254 (2012).

Mechanistic Studies of Charge Injection from Metallic Electrodes into Organic Semiconductors Mediated by Ionic Functionalities (DE-SC0002368)

**Thuc-Quyen Nguyen, Guillermo C. Bazan, and Alexander Mikhailovsky,
Department of Chemistry and Biochemistry, University of California Santa Barbara, Santa Barbara, CA 93106**

Project Scope

Organic semiconducting materials composed of π -delocalized organic frameworks and ionic functionalities *aka* conjugated polyelectrolytes (CPEs) have been recently shown to provide potential solutions to some of the key bottleneck problems associated with organic optoelectronic devices. Specifically, inserting a thin layer of these materials between an organic semiconductor and a cathode in organic light emitting diodes substantially improves electron injection from high work function metals.¹ In photovoltaic devices, introduction of a CPE layer below the cathode has shown a significant increase of the device parameters, such as open circuit voltage and fill factor.² While successful from an engineering perspective, the demonstration of enhanced performance by introduction of ionic organic semiconductors within specific device configurations highlights the need for a more complete understanding of their intrinsic electronic properties and for establishing reliable structure/function relationships. Indeed, more than one mechanism for the reduction of charge injection barriers can be considered^{3,4} and there is healthy debate on how ionic organic semiconductors interface with metallic electrodes and with the more conventional uncharged organic semiconductors. This project coordinates a comprehensive program comprising molecular design, organic synthesis capabilities, an array of structural and electronic characterization techniques across multiple scales, and device fabrication and evaluation.

Synthetic effort is focused on the design and fabrication of CPEs and oligoelectrolytes with specific backbones, functional groups, and ionic moieties according to the requirements dictated by the device structure and function. Besides synthesized materials, naturally occurring non-conjugated charged molecules, such as DNA and heparin have been utilized in the project.

A significant portion of the project is dedicated to the fabrication and characterization of electronic devices, such as organic light emitting diodes (OLEDs) and organic field effect transistors (OFETs) using charge bearing materials in order to determine their chemical and electronic properties and to elucidate the mechanisms of the performance enhancement in such devices. A variety of characterization techniques have been employed for characterization of CPE layers and their interfaces with adjacent metal and organic materials in devices. Various scanning probe techniques, such as atomic force microscopy (AFM), conductive AFM (C-AFM), electrostatic force microscopy (EFM), scanning Kelvin probe microscopy (SKPM), along with XPS, UPS, and NEXAFS are employed to study the morphology of the CPE layer surface and interfaces. Additionally, charge transport properties in CPEs are of particular interest. The characterization data are correlated with the CPE chemical structure, device performance and fabrication conditions.

The ultimate goal of the project is to determine the fundamental mechanisms in CPEs responsible for the enhancement of charge carrier injection from metals with substantial work function mismatch and increased performance of organic OLEDs and OFETs. It is anticipated

that this knowledge will enable us to intelligently design and synthesize CPEs optimized for specific organic electronics applications.

Recent Progress

Introduction of CPE interlayer between the organic layer and high work function cathode has been reported to reduce the barriers for the injection of electrons resulting in the drop of the polymer LED (PLED)'s operational bias voltage and increased power efficacy.¹ However, synthesis and purification of CPEs often require significant efforts and rely on technologies harmful for the environment. From this point of view, it may be interesting to study the function of naturally occurring charge bearing molecules which can be extracted from renewable natural resources. In this presentation, we report on the use of deoxyribonucleic acid (DNA) extracted from fishing industry byproducts as an interlayer for improvement of charge injection and transport in PLEDs and OFETs.

Two mechanisms have been proposed for the improved electron injection. The first is

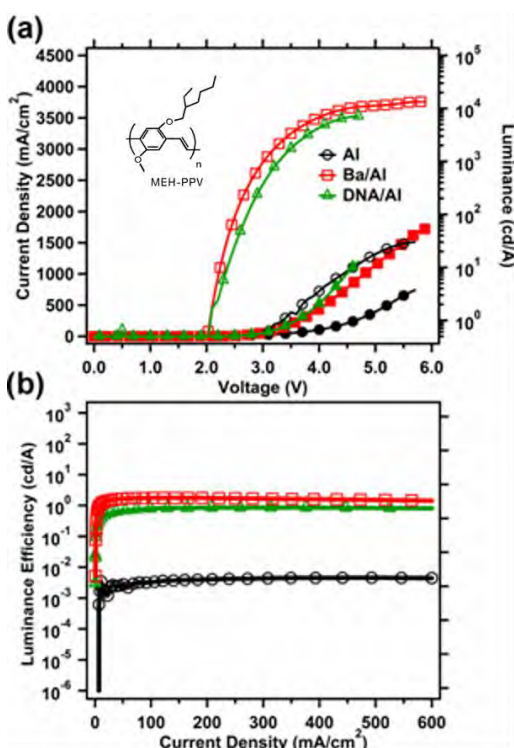


Figure 1. (a) J-V curves and (b) L-V for OLEDs with different cathode structure

usually observed with thicker CPE layers and involves an initial ion migration upon application of an external bias, which leads to redistribution of the electric field within the device and formation of a steep electrical field gradient close to the electrode aiding electron injection into the LUMO of the underlying polymer.³ The second approach involves the presence of an aligned dipole layer that modifies the effective work function of the cathode. These conditions lead to faster device turn on times and direct electron injection into the electroluminescent layer.⁴ The latter mechanism can be implemented in thin layers of non-conjugated materials, such as DNA. We studied the effects of salmon DNA extracted from the fish processing byproducts on the performance of model PLEDs with the structure ITO/PEDOT:PSS/MEH-PPV/DNA/Al. Control devices were fabricated with the structure ITO/PEDOT:PSS/MEH-PPV/Ba/Al and ITO/PEDOT:PSS/MEH-PPV/Al. The work function of Al has a significant mismatch with LUMO energy level in MEH-PPV and devices without DNA interlayer demonstrated significantly

increased turn-on bias voltage and reduced efficiency with respect to devices with Ba/Al cathode which have nearly ohmic contact with MEH-PPV (See Figure 1). However, introduction of DNA layer between MEH-PPV and Al cathode brings PLEDs performance to the level observed in devices with alkali electrode that was manifested in reduction of the operational bias voltage accompanied by the increased light output. The nearly-instant onset of the electroluminescence enabled us to conclude that redistribution of ions is not responsible for the phenomena observed and most likely the DNA interlayer affects the charge injection process via formation of interfacial

dipole layer which effectively reduces the work function of the cathode material. Deposition of DNA layer on top of the polymer demonstrated to be very sensitive to the solvent and casting conditions. The wetting of the polymer surface by DNA solution was poor and good quality films were obtained only if water-methanol mixtures were used for the casting of devices. C-AFM studies revealed that the hole current is suppressed by DNA and the hole-blocking properties of the DNA could contribute to the increase of PLED performance

The idea of using DNA as a charge injection enhancer was extended to OFETs. These devices can also benefit from the improvement of charge injection due to reduction of the contact resistance and turn-on voltage and increase of the on/off ratio. Also, in FETs designed for the

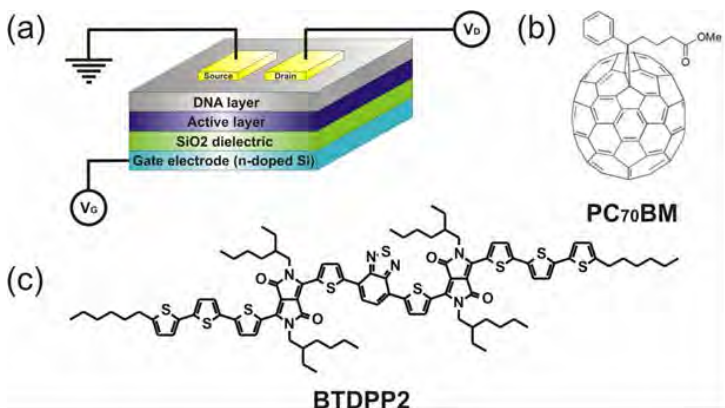


Figure 2. (a) Structure of an OFET with DNA layer (Au was used for source and drain electrodes). Channel materials for (b) n-type and (c) ambipolar devices.

ambipolar charge transport, significant potential barriers are inevitable at either source and drain electrodes or at both of them. From this point of view, it might be interesting to investigate whether introduction of electrode interlayers fabricated from charge-bearing materials can facilitate the ambipolar operation of an OFET. We have fabricated OFETs with the structure shown in Figure 2. Initially, n-type only OFETs were fabricated using PC₇₀BM (Figure 2(b)) in the active layer. The device characterization

data indicate clearly at least 15-fold reduction of the contact resistance along with decrease of the threshold and turn-voltages in devices with DNA layer. Increase of the field effect mobility was

observed relative to the control devices as well. The observations strongly suggest that the enhancement of OFET parameters stems from the improvement of the electron injection. Similarly to OLEDs, devices with DNA layers demonstrate nearly instant response to the applied voltage that can be interpreted that ion motion is not responsible for the phenomena observed but this is the interfacial dipole layer formed by DNA that alters the device operation.

Ambipolar OFET operation was investigated using BTDDPP2 small molecule (Figure 2 (c)) as a material for the OFET channel. Both control devices and OFETs with DNA layer exhibited ambipolar operation (Figure 3). Nevertheless, addition of the charge injection interlayer has a significant effect on the field effect mobilities for both electron and holes and

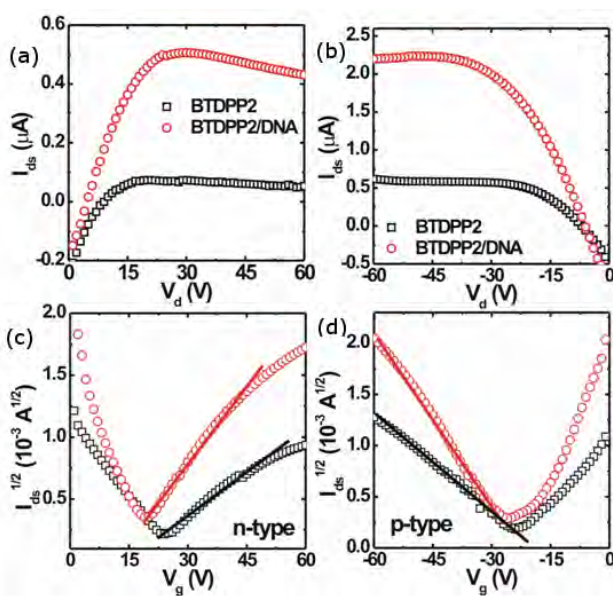


Figure 3. Output and transfer characteristics for (a,c) p- and (b,d) n-type modes in ambipolar OFETs.

can be seen clearly in both transfer and output characteristic of the devices. Enhancement of the charge injection for both electrons and holes is explained by the ability of DNA to repolarize and change the direction of the interfacial dipole under the influence of the gate field.

Future Plans

In the coming year we plan to continue work with naturally occurring charged molecules for enhancement of the charge injection in organic devices. At the same time, we will continue to study the fundamental mechanisms responsible for the phenomena observed using synthetic CPE materials which allow for more precise control of the polymer layer parameters, such as film morphology, amount of charge, ionic and electronic mobilities. Mechanisms responsible for the interface formation between the polymer, CPE, and the metal are of the great interest for us as well.

References

1. Huang, F. *et al.*; *JACS* **126**, p. 9845-9853 (2004).
2. Seo, J.H. *et al.*; *JACS* **133**, p. 8416-8419 (2011).
3. Hoven, C. V.; Peet, J.; Mikhailovsky, A.; Nguyen, T.-Q. *J. Appl. Phys.* **94**, 033301 (2009).
4. Seo, J. H.; Yang, R.-Q.; Brzezinski, J. Z.; Walker, B.; Bazan, G. C.; Nguyen T.-Q. *Adv. Mater.* **21**, 1006 (2008)

Publications

1. Lin, C.Y.; Garcia, A.; Zalar, P.; Brzezinski, J.Z.; Nguyen, T.-Q.; "Effect of Thermal Annealing on Polymer Light-Emitting Diodes Utilizing Cationic Conjugated Polyelectrolytes as Electron Injection Layers", *J. Phys. Chem. C* **114**, p. 14786-15790 (2010).
2. Ortony, J.H.; Chatterjee, T.; Garner, L.E.; Chworos, A.; Mikhailovsky, A.; Kramer, E.J.; Bazan, G.C.; "Self-Assembly of an Optically Active Conjugated Oligoelectrolyte", *JACS* **133**, p. 8380-8387 (2011).
3. Seo, J.H.; Namdas, E.B.; Gutacker, A.; Heeger, A.J.; Bazan, G.C.; "Solution-Processed Organic Light-Emitting Transistors Incorporating Conjugated Polyelectrolytes", *Adv. Funct. Mat.* **21**, p.3667-3672 (2011).
4. Zalar, P.; Kamkar, D.; Naik, R.; Ouchen, F.; Grote, J.G.; Bazan, G.C.; Nguyen, T.-Q.; "DNA Electron Injection Interlayers for Polymer Light-Emitting Diodes", *JACS* **133**, p. 11010-11013 (2011).
5. Yan, H.P.; Wang, C.; Garcia, A.; Swaraj, S.; Gu, Z.R.; McNeill, C.R.; Schuettfort, T.; Sohn, K.E.; Kramer, E.J.; Bazan, G.C.; Nguyen, T.-Q.; Ade, H.; "Interfaces in organic devices studied with resonant soft x-ray reflectivity", *J. of Appl.Phys.* **110**, art 102220 (2011).
6. Zalar, P; Henson, Z.B.; Welch, G.C.; Bazan, G.C.; Nguyen, T.-Q.; " Color Tuning in Polymer Light-Emitting Diodes with Lewis Acids", Accepted for publication in *Angewandte Chemie* (2012).

RAFT Polymerization of Emulsified Microemulsions

Jennifer O'Donnell, Department of Chemical and Biological Engineering, Iowa State University, Ames, IA 50011

Program Scope

The current work seeks to develop a fundamental understanding of the reversible addition-fragmentation chain transfer (RAFT) polymerization mechanism^{1,2} in confined nanostructures. Initial work has focused on RAFT polymerizations in emulsified inverse microemulsions, which consist of monomer drops on the order of 100 nm in diameter containing surfactant-stabilized water drops on the order of 5 nm in diameter. Glatter et al. have shown that microemulsions within emulsified drops are in thermodynamic equilibrium.^{3,4} Thus, monomer diffusion between initiated and uninitiated drops is expected to be hindered, and the rate of monomer conversion and polymer molecular weight are expected to differ from traditional RAFT emulsion polymerizations. Several polymerizations have been performed with RAFT chain transfer agent (CTA) concentrations ranging from 0.002 to 0.100 moles of CTA per mole of monomer, which is lauryl acrylate. The rate of monomer conversion has been monitored by reaction calorimetry, polymer molecular weight has been measured by gel permeation chromatography, and particle size has been determined by dynamic light scattering.

Recent Progress

RAFT emulsified microemulsion polymerizations of lauryl acrylate reached 70 % monomer conversion at all CTA/LA ratios investigated (**Figure 1**), as expected if monomer diffusion between uninitiated and initiated drops is in fact hindered by the thermodynamic stability of the microemulsion within the drops. As the CTA/LA ratio increases, the time necessary for the polymerization to reach 70 % monomer conversion also increases, and correspondingly, the maximum rate of polymerization decreases (**Figure 1**). This decrease in polymerization rate is commonly observed in RAFT polymerizations due to the stability of the intermediate macroRAFT radical, which effectively decreases the concentration of propagating polymer radicals. In addition to the decrease in the maximum polymerization rate with increasing CTA/LA ratio, the location of the rate maximum shifts to a greater percent monomer conversion until the CTA/LA ratio reaches 0.043 mol CTA/mol LA (**Figure 1**). At greater CTA/LA ratios, the location of the rate maximum remains fixed. A shift in the location of the rate maximum to a greater monomer conversion indicates that either the concentration of monomer at the locus of polymerization remains high or the concentration of propagating radicals continues to increase. The concentration of propagating radicals is in fact expected to continually increase due to thermal decomposition of the initiator. However, further

experiments, such as in situ small angle neutron scattering, are necessary before the cause of the shift in the location of the rate maximum can be conclusively identified.

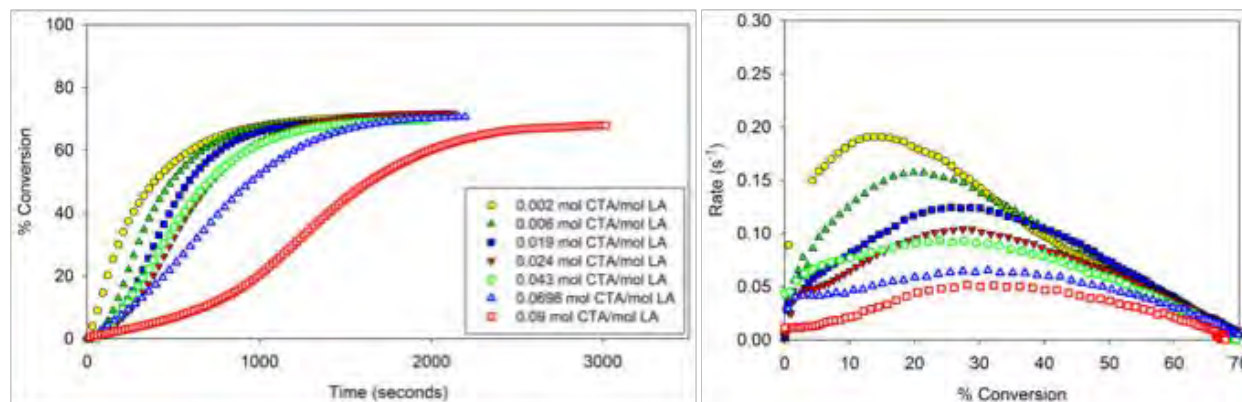


Figure 1. Percent monomer conversion as a function of time (left) and rate of monomer conversion as a function of percent monomer conversion (right). The legend applies to both figures.

Number average molecular weight (M_N) of the final polymer product has been determined by gel permeation chromatography, and compared to predicted values based on the

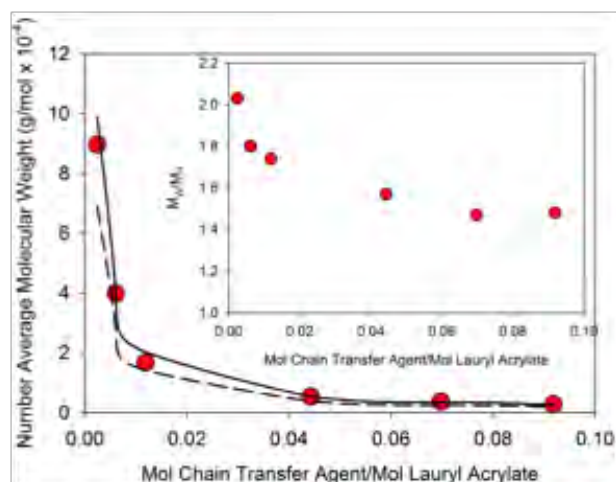


Figure 2. Number average molecular weight (M_N) and polydispersity (M_w/M_N , inset) of the final polymer product as a function of CTA/LA ratio. Solid line is prediction for 100% monomer conversion, and dotted line is prediction for 70% monomer conversion.

ratio of monomer to chain transfer agent (**Figure 2**). At CTA/LA ratios less than 0.043, the final M_N is greater than predicted, which indicates that all of the CTA was not activated during the polymerization. However, at CTA/LA ratios greater than 0.043, the final M_N does agree with predicted values. These results indicate very slow diffusion of the CTA from uninitiated to initiated drops during the polymerization, so that long polymerization times are required for activation of all of the CTA. The polydispersity of the final polymer product also decreases as the CTA/LA ratio increases (**Figure 2, inset**), which is consistent with greater CTA activation and improved control of the polymerization.

The diameter of the final polymer product was measured by dynamic light scattering (**Figure 3**). All of the polymerizations produced polymer particles with a diameter significantly greater than the particle diameter produced by uncontrolled emulsified microemulsion polymerization (50 nm). At CTA/LA ratios less than 0.043, the final polymer particle diameter ranges from 150-200 nm, while at CTA/LA ratios greater than 0.070 the final polymer particle diameter ranges from 400-500 nm. The increase in particle diameters at low CTA/LA ratios relative to uncontrolled emulsified microemulsion polymerizations indicates that the slower

polymerization times facilitate some diffusion of monomer from uninitiated to initiated drops. The large particle diameters produced at high CTA/LA ratios indicate that drop coalescence also occurs during long polymerizations, when the polymerizing particles are swollen with monomer for an extended time. The coalescence of polymerizing drops and monomer drops is also consistent with the molecular weight data, which indicates greater activation of the CTA because CTA activation is now no longer solely dependent upon the rate of diffusion between uninitiated and initiated drops. Transmission electron microscopy shows that small 5 nm clusters of the Na^+ associated with the surfactant used to stabilize the original microemulsion exist within the polymer particles, which is consistent with retention of the original microemulsion structure.

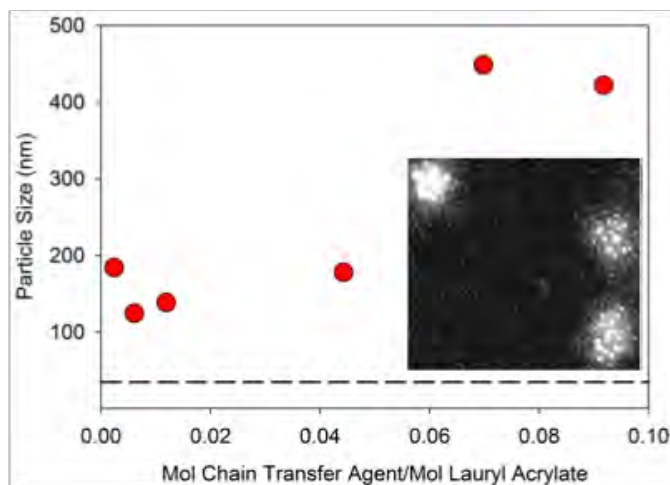


Figure 3. Final polymer particle diameter as a function of CTA/LA ratio, and a TEM micrograph showing clusters of Na^+ from the surfactant used to stabilize the microemulsion.

Transmission electron microscopy shows that small 5 nm clusters of the Na^+ associated with the surfactant used to stabilize the original microemulsion exist within the polymer particles, which is consistent with retention of the original microemulsion structure.

Future Plans

Future work will study the effect of CTA location on the RAFT polymerization mechanism. High molecular weight and low molecular weight amphiphilic diblock copolymers of poly(2-hydroxyethyl acrylate)-b-poly(lauryl acrylate) will be synthesized by RAFT solution polymerization, and used to replace the traditional surfactants Pluronic F127 and dioctyl sodium sulfosuccinate (AOT), respectively. These high molecular weight amphiphilic diblock copolymers will fix the location of the CTA to the corona of the emulsified microemulsion drop, and the low molecular weight amphiphilic copolymers will fix the location of the CTA to the interface between the small microemulsion drops and the monomer. The RAFT CTA end group will be removed from a fraction of the synthesized amphiphilic block copolymers using previously developed methods, so that the concentration of CTA in the emulsified microemulsion polymerizations can be varied. Reaction calorimetry, gel permeation chromatography, and dynamic light scattering will be used to determine the rate of monomer conversion, the polymer molecular weight, and the final particle size, as in previous investigations.

References

1. J. Chiefari, Y. K. Chong, F. Ercole, J. Krstina, J. Jeffery, T. P. T. Le, R. T. A. Mayadunne, G. F. Meijs, C. L. Moad, G. Moad, E. Rizzardo and S. H. Thang, *Macromolecules*, 1998, 31, 5559-5562.

2. G. Moad, E. Rizzardo and S. H. Thang, *Australian Journal of Chemistry*, 2009, 62, 1402-1472.
3. L. de Campo, A. Yaghmur, L. Sagalowicz, M. E. Leser, H. Watzke and O. Glatter, *Langmuir*, 2004, 20, 5254-5261.
4. A. Yaghmur, L. de Campo, L. Sagalowicz, M. E. Leser and O. Glatter, *Langmuir*, 2005, 21, 569-577.

Publications

No current publications have resulted from this work.

“Measuring the importance of valence to the chemistry of nanocrystal surfaces”

Jonathan S Owen, Department of Chemistry, Columbia University

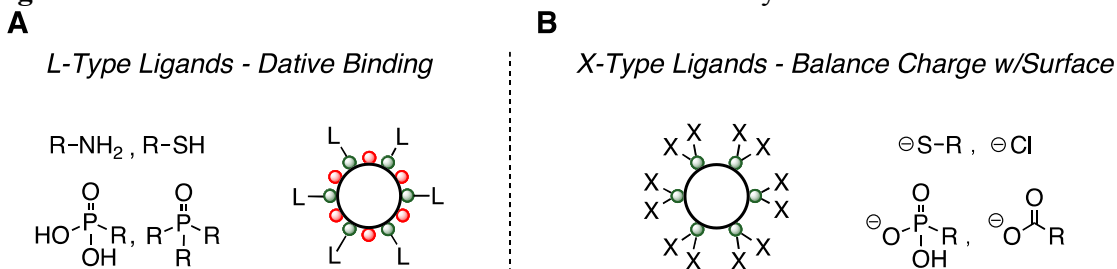
Program Scope

The goal of this project is to understand and control the interplay between nanocrystal stoichiometry, surface ligand binding and exchange, and the optoelectronic properties of semiconductor nanocrystals in solution and in thin solid films. We are pursuing three research directions with this goal in mind: 1) We seek to characterize nanocrystal nonstoichiometry and its influence on the number of L-type and X-type binding sites, the thermodynamics of ligand binding, and the kinetics and mechanisms of ligand exchange. 2) Using this information we aim to develop a quantitative understanding of the relationship between surface ligand passivation and photoluminescence quantum yield. 3) We aim to develop methods to replace the organic ligands on the nanocrystal with halide ligands and controllably deposit these nanocrystals into thin films. Electrical measurements on these films will make it possible to evaluate the effect of the nonstoichiometric ligand layer on surface passivation and internanocrystal electronic coupling.

Recent Progress

Introduction. In nanometer scale crystals the interaction of charges with surface atoms dominates electronic properties like photoluminescence quantum yield, fluorescence blinking, vibrational cooling of excited carriers, and charge trapping. These features result from mid-band gap electronic states derived from surface atoms. As a result, a detailed understanding of nanocrystal surface structure and ligand exchange chemistry is central to utility of nanocrystals in next generation optoelectronic devices. Despite the importance of nanocrystals to this technological goal, the valence of atoms on nanocrystal surfaces is an essentially unexplored avenue of their chemistry. This project aims to distinguish between dative ligands that are adsorbed to nanocrystal surfaces (Figure 1A) and ligands that balance charge with a nonstoichiometric nanocrystal lattice (Figure 1B). Studies of nanocrystal stoichiometry and ligand exchange reactivity indicate that ligands, which balance charge with nonstoichiometric nanocrystals, are an important ligation motif.¹ These findings contrast strongly with the prevailing description of nanocrystal surface structure, particularly of CdSe quantum dots, where the dative ligand-binding model is widely accepted. We are building upon this distinction to obtain predictive control over electronic states within the nanocrystals band gap and to design surface modification strategies for thin-film fabrication.

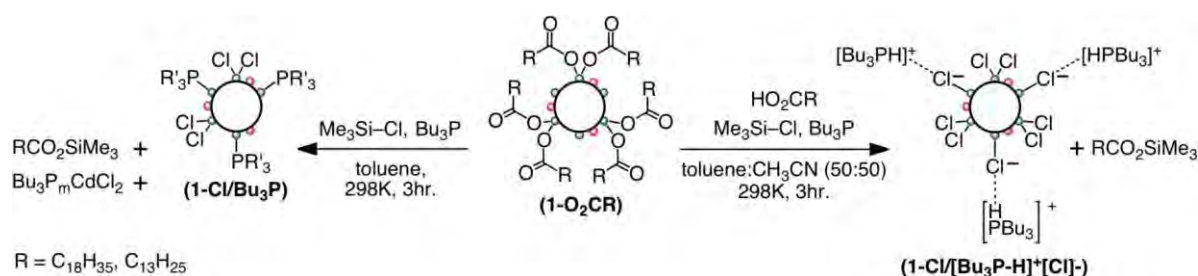
Figure 1. Idealized stoichiometric and Cd-rich CdSe nanocrystal surfaces.^a



^a Red = surface Se, green = surface Cd, white = a stoichiometric CdSe crystal.

Phosphine and amine complexes of halide terminated nanocrystals. The distinction presented above allows one to more accurately analyze the exchange of surfactant ligands bound to nanocrystal surfaces. Removing organic ligands from the nanocrystal surface is an important step toward transforming these soluble materials into thin-films that efficiently transport charge. We have developed a technique to exchange nanocrystal surface ligands for a surface monolayer of metal-halide (Figure 2). Our initial efforts have produced CdCl₂ terminated CdSe nanocrystals that are soluble in organic solution because of their trialkylphosphine supporting ligands. ³¹P NMR spectroscopy, UV-Visible absorption spectroscopy and Rutherford backscattering spectrometry support the structural assignment shown in Figure 2, where 20-40 phosphine ligands bind each 700-1000 atom nanocrystal.

Figure 2. Chloride exchange and complexation by tri-*n*-butylphosphine or tri-*n*-butylphosphonium chloride.^a

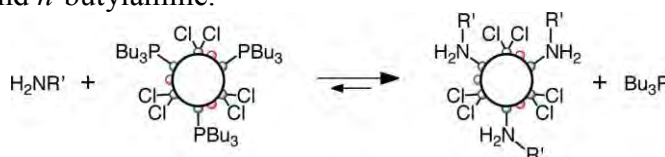


^a Red = surface Se, green = surface Cd, white = a stoichiometric CdSe crystal.

***In situ* monitoring of ligand exchange.**

Trialkylphosphine bound nanocrystals make it possible to monitor ligand binding with ³¹P NMR spectroscopy. Traditionally ligand adsorption has been studied with fluorescence spectroscopy leading to conflicting results. Using NMR we have measured relative ligand binding affinities *in situ*. Competitive ligand binding experiments led to the following order of relative binding affinity: H₂NR >> PBu₃ > O=PR₃ > NR₃ clearly demonstrating that sterics are a dominant factor controlling surface binding affinity (Figure 3).

Figure 3. Competitive binding of tri-*n*-butylphosphine and *n*-butylamine.^a

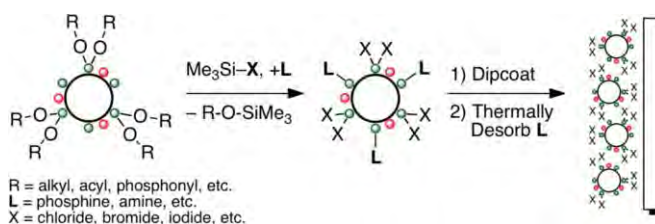


^a Red = surface Se, green = surface Cd, white = a stoichiometric CdSe crystal.

Thin solid films of halide terminated nanocrystals.

Nanocrystal thin films composed of the halide-terminated nanocrystals described above can be deposited from solution followed by desorption of the organic ligand shell *en vacuo* (Figure 4). Ready access to gram quantities of the nanocrystals described above has allowed us to reproducibly deposit crack free films with

Figure 4. Spin coating thin films of halide-terminated nanocrystals.^a



^a Red = surface Se, green = surface Cd, white = a stoichiometric CdSe crystal.

a spin coater. Thermal desorption of the organic ligand shell provides ready access to films with decreased internanocrystal separation and enhanced electronic coupling. This coupling is clearly visible from the red shift in the film absorption spectrum upon thermal annealing *en vacuo*. Grazing incidence x-ray diffraction measurements as well as TEM and SEM analysis support the ligand desorption process shown in Figure 4. Aluminum top-contacted field effect transistor devices made from vacuume annealed films show N-type conduction and charge mobilities of $\sim 1 \text{ cm}^2 \text{ V}^{-1} \text{ s}^{-1}$.

Future Plans

In the near term, we plan to study Langmuir binding and exchange rates using NMR spectroscopy. This will allow us to directly investigate the relationship between surface coverage and photoluminescence. Both metal-ion adsorption and dative ligand binding will be investigated for this purpose. We also aim to tune nanocrystal stoichiometry prior to thin-film deposition and evaluate the effect of excess metal-halide layers on sintering and charge mobility in thin films.

Publications

“Tri-*n*-alkylphosphine Complexes of Chloride-Terminated Cadmium Selenide Nanocrystals”, Anderson, N. C.; Owen, J. S.; *Full article Submitted to J. Am. Chem. Soc.*

References

¹ “Reaction Chemistry and Ligand Exchange at Cadmium Selenide Nanocrystal Surfaces”, Owen, J. S.; Park, J.; Trudeau, P.-E.; Alivisatos, A. P.; *J. Am. Chem. Soc.* **2008**, *130*, 12279-12281.

Project title: Basic surface chemistry and physics of carbon-based electronic materials modified by silane molecular layers.

PI: Prof. Vitaly Podzorov, Physics Department, Rutgers University, Piscataway, NJ 08854

Program Scope.

The scope of this project is to investigate fundamental aspects of self-assembled monolayers (SAMs) grown at the surface of organic semiconductors and other electronic materials, recently discovered in our group (Fig. 1) [1]. Understanding the growth mechanism and structure of these SAMs, as well as investigating the effect of SAM-induced high surface conductivity, are the main thrusts of the project.

Molecular self assembly is an exciting research area of modern materials science, playing an important role in a variety of emerging applications, such as organic and molecular electronics, bioengineering, sensors and actuators. The current effort in this field has been focused on two experimental platforms: SAMs on metals (e.g., Au) and SAMs on inorganic oxides (e.g., SiO₂). We have recently discovered the third platform, molecular self-assembly at the surface of carbon-based electronic materials (organic semiconductors, graphene and CNTs), which opens new opportunities for fundamental research and applications (Fig. 1) [1, 2, 3]. One of the most intriguing aspects of the new discovery is that formation of an FTS self-assembled monolayer on these materials induces a high-density mobile charges, with n up to 10^{14} cm⁻², resulting in a large surface conductivity, $\sigma \approx 10^{-5}$ S-square⁻¹ [1]. The effect is due to an interfacial electron transfer from the semiconductor to the SAM, resulting in a 0.54 V potential drop across the 1.3 nm-thick SAM, as recently revealed by Kelvin probe microscopy in rubrene [4]. This project focuses on understanding fundamental properties of the surfaces functionalized with SAMs:

- ***Understanding the growth mechanism and structure of SAMs on organic surfaces;***
- ***Studies of electronic transport effects induced by the SAMs in these materials.***

The latter topic is especially important, as it is related to the basic research on fundamental transport properties of organic semiconductors (band-like vs. hopping transport models, polaronic effects) [5] and graphene (surface doping and shift of Dirac point) [3]. This novel system allows us to access the transport regime of a 2D polaronic conductor at ultra-high charge carrier densities induced by the SAM.

One of our immediate goals was to experimentally determine the mobility (μ), density (n) and effective mass (m^*) of the charge carriers induced by the SAM in organic crystals. Our DOE-supported work on this has recently resulted in the development of a novel effective method for electrostatic gating of fragile and sensitive semiconductors, including fragile organic crystals and SAM-coated

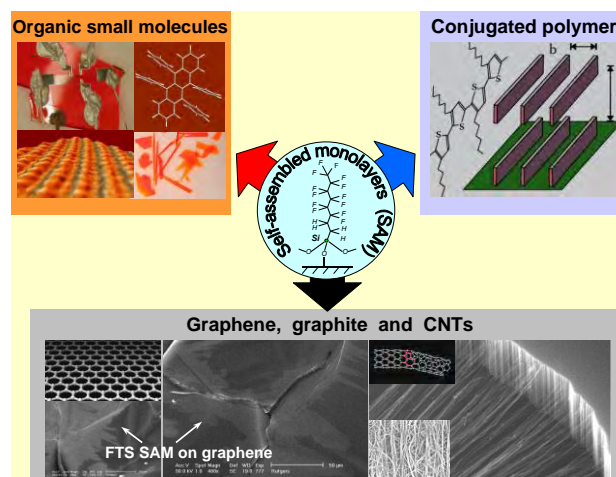


Fig. 1. Three classes of carbon-based electronic materials that can be functionalized with silane self-assembled monolayers (SAM). Large modulations of electrical conductivity are observed when an FTS SAM is grown on these surfaces.

surfaces (*Adv. Mater.* 2011) [6]. This progress is described in the following section.

Recent progress.

One of the central issues in organic and molecular electronics is extreme sensitivity of these materials to the standard semiconductor fabrication processing, including exposure to plasmas, elevated temperatures in a variety of deposition methods, reactive gases in CVD and ALD and exposure to solvents during wet processing. These kinds of processes can be frequently detrimental to functional organic interfaces, including accumulation channels in transistors and donor-acceptor junctions in solar cells. For instance, one of the important illustration of this problem relates to a deposition of dielectric layer on organic material for OFETs: conventional techniques, such as sputtering, CVD or ALD, turn out to be largely incompatible with the delicate surfaces of molecular films or crystals because of a high-density surface defects they generate (one notoriously famous example is the sputtering of Al_2O_3 on molecular crystals by *rf* sputtering). For this reason, several alternative methods of OFET fabrication have been developed over the recent few years, such as parylene conformal dielectric coatings in OFETs, PDMS stamp OFETs, and lamination of organic crystal on Si/SiO₂ wafers (see, e.g., [5]). However, all these methods are rather complex - they require the use of optical or e-beam lithography, high-vacuum processing, metallization, usage of high-quality Si wafers or PDMS technology. These methods are also costly and time consuming.

In this phase of the project, we have developed a new remarkably simple, versatile and inexpensive method of OFET fabrication. We borrowed the idea from vacuum food packing technology (FoodSaver[®]), where a piece of food can be tightly encapsulated in a plastic film by pumping the air out of a plastic pocket. This forces the plastic film to collapse to the surface of the object creating a tight insulating layer. In our devices, we suspend a thin membrane made out of commercially available insulating polymer films (a few μm -thick Mylar[®], Saran[®] or Glad[®] wraps) above the surface of an organic crystal with pre-fabricated contacts, and then force the membrane to collapse onto the surface of the crystal by pulling a vacuum from under the membrane. After the interface is formed, a gate electrode is painted on top, completing the fabrication of a single-crystal OFET that usually takes not more than ~ 10 min (Fig. 2) (for a video visit [7]).

This method, enabling an efficient express analysis of various organic and inorganic semiconductors, results in remarkably high-quality FETs, because: (a) the process is performed at room temperature, without using plasmas or other harsh environments, and (b) there is no surface chemistry required for formation of the insulating layer (contrary to ALD) – the process is purely mechanical. Therefore, it is applicable to various “capricious” systems, such as gentle surfaces of molecular crystals or molecular monolayers. We found that our method results in excellent OFET performance (Fig. 3).

Figure 3 shows an example of a rubrene

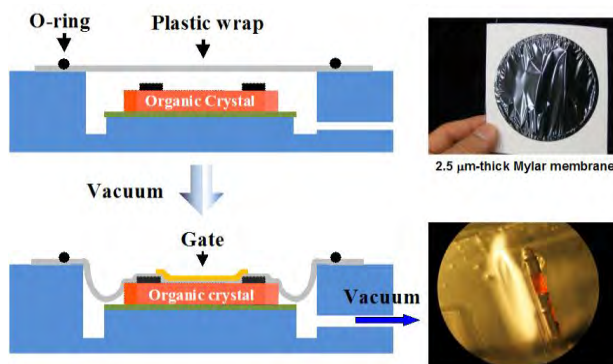


Fig. 2. Vacuum lamination of insulating plastic membranes (for instance, 2.5 μm -thick Mylar or Glad food wrap) to create defect-free semiconductor-insulator interface in high-performance OFETs. The photograph in the lower right corner is a rubrene single crystal device with graphite contacts and a Mylar membrane vacuum-laminated at its surface.

single-crystal OFET created using this method. The device exhibits a behavior of a classic textbook FET: (a) perfectly linear device characteristics in the linear and saturation regimes are observed, as expected from a correctly working OFET, (b) mobility is independent of the carrier density (or V_G), (c) negligible contact resistance, (d) nearly zero-threshold operation, (e) negligible hysteresis (V_G is swept back and forth in Fig. 3). *We believe, this method may become a wide-spread tool in semiconductor research due to its simplicity, low-cost and un-perturbing nature of the interfaces formed.*

Now that we have developed a novel, very gentle method for gating delicate semiconducting systems, we can apply it to the SAM-organic samples in order to decouple the SAM-induced carrier density, n , and mobility, μ . Simple conductivity measurements do not allow to do so, because $\sigma = en\mu$, and hence an extra “knob” of control is required to disentangle n and μ . The charge carrier density and mobility at the FTS-rubrene interface could be reliably measured, if a robust FET structure can be deposited on top of the FTS-coated crystal. Although such attempts have been made in our original work,^[1] parylene insulator does not grow well on alkylated surfaces. For this reason, reliable electrical measurements of n and μ for this system have been unavailable.

Here, we have applied our new method to FTS SAM coated rubrene crystals in order to reliably measure n and μ at the SAM-rubrene interface. First, we measured the FET characteristics of a pristine rubrene crystal (the dashed lines in the upper panel of Fig. 4). The mobility was $\mu \sim 3 \text{ cm}^2\text{V}^{-1}\text{s}^{-1}$, and the carrier density at $V_G = -40 \text{ V}$ was $n = 7.5 \times 10^9 \text{ cm}^{-2}$. Next, we detached the Mylar film, coated the crystal with FTS SAM and measured FET-like transfer characteristics again (solid lines in the upper panel of Fig. 4). SAM-induced carrier density n_0 has been approximately found by extrapolating the linear fits to these curves to zero current, as shown in the lower panel of Fig. 4. This yielded a large positive depletion gate voltage, $V_0 \approx 2 \text{ kV}$, and the corresponding $n_0 \approx 1.4 \cdot 10^{13} \text{ cm}^{-2}$, which is more than three orders of magnitude higher than the typical carrier density in pristine OFETs. The slope, dI_{SD}/dV_G , in these devices gives the hole mobility in the SAM-induced accumulation layer, $\mu \sim 0.4 \text{ cm}^2\text{V}^{-1}\text{s}^{-1}$. This value is ~ 6 times smaller than μ in pristine rubrene with Mylar dielectric, which might be an indication of a significant hole-hole interaction in the high carrier density regime, or it can be due to an increased carrier scattering by the charged FTS monolayer.

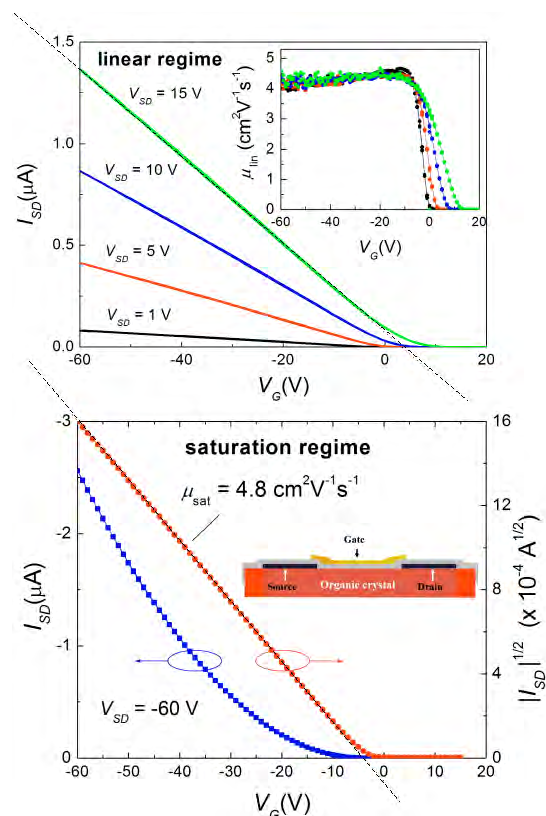


Fig. 3. Excellent transistor characteristics of a rubrene single-crystal OFET created using the vacuum lamination method developed in this project. Measurements performed in a linear (upper panel) and a saturation (lower panel) regimes are shown. V_G is swept back and forth in these measurements.

In summary, we have introduced a novel efficient method of high-performance OFET fabrication, which is non-destructive, reversible and non-perturbing, so that delicate systems, such as e.g. *molecular monolayers*, can be probed. By using this method, we were able to measure carrier density and mobility in FTS-induced accumulation layer in rubrene. *We emphasize that the described method is an attractive approach providing unique opportunities for the fundamental studies of charge transport in organic and inorganic FETs.*

Future plans.

Our future plans include: (a) application of this method of FET fabrication to inorganic semiconductors, including single-crystal and thin-films of ZnO, SrTiO and layered dichalcogenides (WSe₂, ZrS₂); (b) investigation of *T*-dependent magneto-transport of highly conducting 2D accumulation layer in FTS SAM-rubrene system; and (b) using free-standing polymer membranes (e.g., ultra-thin Mylar) coated by alkylated SAMs as a platform for developing flexible organic electronic devices.

References.

- ¹ M. F. Calhoun, J. Sanchez, D. Olaya, M. E. Gershenson, V. Podzorov, *Nat. Mater.* **7**, 84 (2008).
- ² C.-Y. Kao, *et al.*, *Adv. Funct. Mater.* **19**, 1906 (2009).
- ³ B. Lee, *et al.*, *Nano Lett.* **10**, 2427 (2010).
- ⁴ D. J. Ellison, B. Lee, V. Podzorov and C. D. Frisbie, *Adv. Mater.* **23**, 502 (2011).
- ⁵ R. W. I. de Boer, M. E. Gershenson, A. F. Morpurgo, V. Podzorov, *Phys. Status Solidi A* **201**, 1302 (2004).
- ⁶ H. T. Yi, Y. Chen, K. Czelen and V. Podzorov, *Adv. Mater.* **23**, 5807 (2011).
- ⁷ <http://www.youtube.com/watch?v=ET0cudXYfVQ>

Publications (solely supported by this DOE BES award).

1. H. T. Yi, Y. Chen, K. Czelen, V. Podzorov “Vacuum lamination approach to fabrication of high-performance single-crystal OFETs” *Adv. Mater.* **23**, 5807 (2011).
2. <http://www.youtube.com/watch?v=ET0cudXYfVQ>
3. C. Blesch “Eureka! Kitchen Gadget Inspires Scientist to Make More Effective Plastic Electronics”, *Rutgers Media Relations* (2012)
<http://news.rutgers.edu/medrel/research/rh-2012/eureka-kitchen-gadge-20120126>

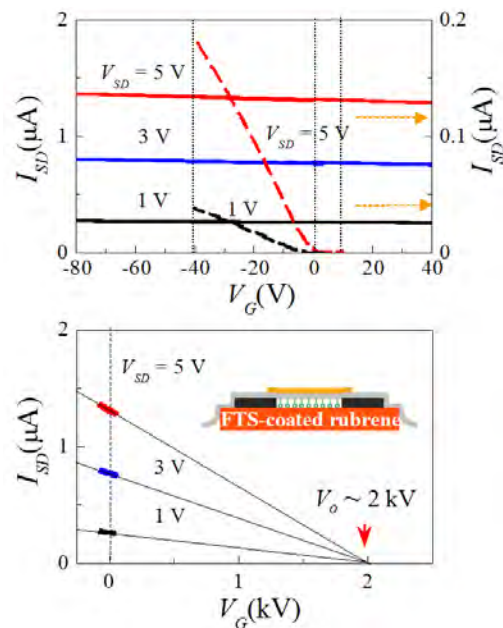


Fig. 4. *Upper panel:* Transfer characteristics of a pristine rubrene OFET (dashed lines), and the same crystal after it was coated with FTS SAM (solid lines). Vacuum-laminated Mylar was employed as a gate insulator. *Lower panel:* The same transfer curves of the gated FTS-rubrene sample re-plotted in a wider V_G range. The red arrow indicates the extrapolated depletion point, V_0 . This measurement shows that $n_0 \approx 1.4 \times 10^{13}\text{ cm}^{-2}$ and $\mu \sim 0.4\text{ cm}^2\text{ V}^{-1}\text{ s}^{-1}$

1. Activation of Hydrogen under Ambient Conditions and Unusual Element Hydride Reactivity by Main Group Molecules

2. Philip P. Power, Department of Chemistry, University of California at Davis, One Shields Avenue, Davis, California 95616

3(i). Program Scope

The primary goals of the research, as originally proposed in 2007, were to investigate the reactions under mild conditions (25°C, 1 atmosphere) of hydrogen and related molecules with a range of heavier (principal quantum number $n \geq 3$) main group species having strained geometry (i.e. bent or pyramidalized, in comparison to their congeneric derivatives of principal quantum number 2 which have linear or planar structures), diradical character, or open-shell configurations, (Figure 1) and to determine the mechanisms of these reactions. In many cases, the strained geometries observed resemble and represent molecular models for the geometries of atoms at the exposed surfaces of solid state materials (e.g. the elements Si and Ge) which exhibit high reactivity.¹ The ultimate objectives of this research are the achievement of reversibility in the absorption and release of small molecules, and to develop simple catalytic processes based on derivatives of abundant main group elements, such as aluminum or silicon. The reactive heavier main group species are characterized by frontier HOMOs and LUMOs that are not widely separated in energy (<4 eV) and are frequently of suitable symmetry to interact synergistically in a push-pull fashion. Initial work supported by the DOE focused primarily on reactions with hydrogen and ammonia.²⁻⁴ The more recent work over the past two years, which will be the main theme of this presentation, mainly concerns the reactions of the main group complexes with olefins and other unsaturated molecules leading to isomerization, C-H activation, insertion reactions, and with transition metal multiple bonded species to afford metathesis of the heavier element alkyne analogues.

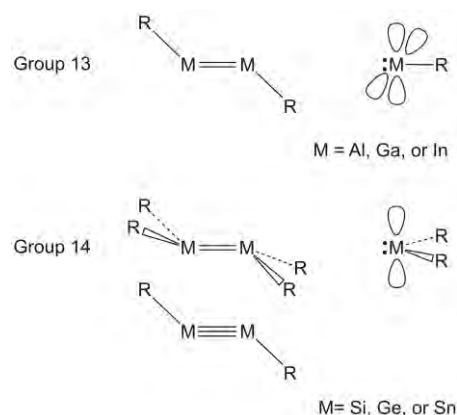


Figure 1: Schematic drawings of strained geometry and open shell heavier group 13 and 14 element compounds.

3(ii). Recent Progress

The first investigations of the reactions of the main group complexes with cyclic olefins, as illustrated by the reaction of a distannylyne ArSnSnAr ($\text{Ar} = \text{C}_6\text{H}_3\text{-2,6}(\text{C}_6\text{H}_3\text{-2,6-Pr}^i_2)_2$) with cyclooctatetraene (COT), (Figure 2) resulted in unprecedented complete homolysis of the metal-metal multiple bond to give an inverted sandwich product featuring an almost planar delocalized aromatic $\text{C}_8\text{H}_8^{2-}$ ring and uniformly short

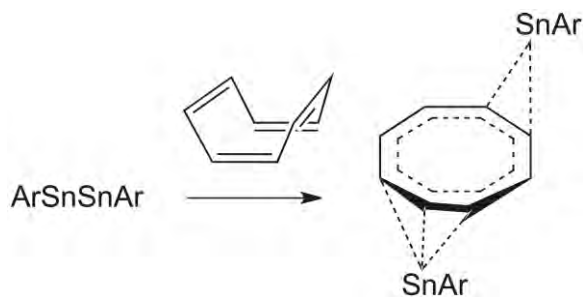


Figure 2: Tin-Tin triple bond cleavage by cyclooctatetraene (COT) ($\text{Ar} = \text{C}_6\text{H}_3\text{-2,6}(\text{C}_6\text{H}_3\text{-2,6-Pr}^i_2)_2$).

C-C bonds.⁴ The reaction with the corresponding digermine gave the analogous inverted sandwich product initially, but this isomerized reversibly at room temperature to give a tetracyclic diene-digermene in which a single bonded Ge-Ge moiety had inserted into a C=C bond (Figure 3).⁵ The significance of the isomerization in Figure 3 lies in the fact that it involves the cleavage of an unstrained C=C bond in COT that appears to occur by oxidative addition across a multiple Ge-Ge bond.

Investigations of the reaction mechanism show that the reaction most likely proceeds intramolecularly by initial

interaction of the digermine with one of the C=C double bonds of COT to give a

structure in which the incorporated ArGeGeAr unit can dissociate its formal Ge-Ge double bond, and subsequently rearrange to the inverted sandwich structure. The rearrangement pathway to the tetracyclic structure is unclear, but DFT calculations indicate that it probably involves the complexed $\text{GeAr}^{\text{Pr}^4}$ moieties participating in both C=C cleavage and Ge-Ge σ -bond formation in a concerted manner. The tin derivative does not undergo the isomerization shown in Figure 3 because the non-bonded pairs of the tin atoms in the inverted sandwich structure lie at much lower energies than those in germanium, so that the tetracyclic cage structure becomes inaccessible.

Reaction of the digermine

ArGeGeAr with cyclopentene, cyclopentadiene, and 1,4-cyclohexadiene afforded very different reaction sequences. For example, treatment of ArGeGeAr with cyclopentene resulted in double C-H bond activation of the olefinic moiety in the reaction described by Figure 4.⁶ We have shown that this reaction proceeds by initial C-H bond cleavage involving double dehydrogenation of a cyclopentene to form a hydridodigermene Ar(H)GeGe(H)Ar and cyclopentadiene. A second molecule of cyclopentene then reacts with Ar(H)GeGe(H)Ar to give the cyclopentene derivative Ar(H)GeGeAr(*c*-C₅H₉), which is also the first example of an unsymmetric digermene. The cyclopentadiene then reacts with ArGeGeAr to give the dihydridogermene Ar(H)GeGe(H)Ar and ArGe(η^5 -C₅H₅). The intermediacy of the dihydridogermene was demonstrated by performing addition reactions with olefins, which insert into the Ge-H bonds to form the corresponding alkyl digermene derivatives. The net result of these three reactions is the stoichiometry given in Figure 4. A possible radical mechanism for this reaction was excluded by use of radical clocks such as 1,6-heptadiene. The latter yielded a simple addition of the two double bonds to the digermine, rather than the cyclization expected for a radical pathway.

A different type of C-H activation together with C-C bond cleavage

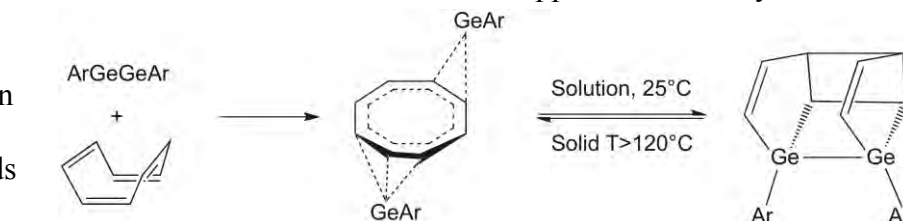


Figure 3: Germanium-Germanium triple bond cleavage with COT and isomerization of the inverted sandwich structure to a tetracyclic with C-C bond cleavage and Ge-Ge Bond formation.

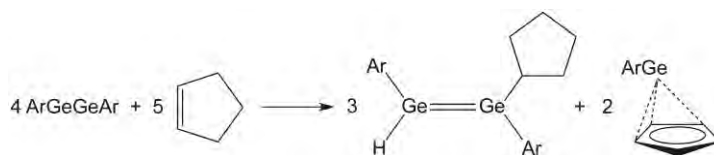


Figure 4: Overall stoichiometry of the C-H bond activation of cyclopentene by ArGeGeAr.

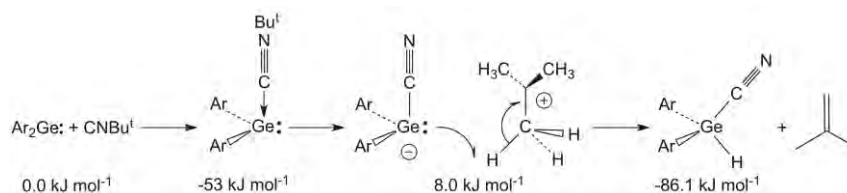


Figure 5: Mechanism of C-H activation in the interaction of CNBu^t with ArGeGeAr.

was demonstrated by the reaction of a germylene with an isocyanide (Figure 5). Thus, Ar_2Ge reacts with CNBu^t to form the adduct $\text{Ar}_2\text{GeCNBu}^t$ at room temperature, but this species spontaneously rearranges to eliminate 2-butene with formation of $\text{Ar}_2\text{Ge}(\text{H})\text{CN}$. The mechanism of this reaction, which was investigated by computational methods, involves intramolecular C-H activation of one of the Bu^t methyl groups with simultaneous C-N bond cleavage to eliminate the 2-butene. A radical mechanism was excluded by the use of a radical clock.⁷

The dimetallynes ArMMAr ($\text{M} = \text{Ge}$ or Sn) have also been shown to undergo metathesis reactions involving their M-M multiple bonds with other single and multiple bonded complexes, as illustrated in Figure 6. In contrast to the reactions of most transition metal multiple bonded compounds with alkynes, these reactions occur readily at 25°C. Other reactions of the dimetallynes that will be discussed are their reactions with various oxidizing reagents⁸

to give diradicaloid species, $\text{ArMMAr} + (\eta^5\text{-C}_5\text{H}_5)(\text{CO})_2\text{Mo}\equiv\text{Mo}(\text{CO})_2(\eta^5\text{-C}_5\text{H}_5) \rightarrow 2 \text{ArM}\equiv\text{Mo}(\eta^5\text{-C}_5\text{H}_5)(\text{CO})_2$

and their ability to reduce hydrocarbons in a similar manner to the alkali metals.⁷

Figure 6: Metathesis reaction of the heavier alkyne ArMMAr ($\text{M} = \text{Ge}$ or Sn) with a transition metal multiple bonded species.

Initial investigations of the reactions of open shell group 13 metal derivatives with olefins have also demonstrated a high reactivity toward olefins. Thus, the gallium compound ArGaGaAr was shown to react readily with ethylene, propene, or styrene to form products with six-membered Ga_2C_6 ring structures.⁹ In a study analogous to that performed with the group 14 species, ArGaGaAr was found to react with several cyclic olefins including norbornadiene and COT.¹⁰ DFT calculations showed that the barrier to the addition of one or two double bonds to ArGaGaAr was very low — below 5 kcal mol^{-1} in most cases.

3(iii). Future Plans

The reactivity studies supported by DOE have shown that the strained geometry, open-shell main group molecules display a reactivity pattern which resembles that seen at the surfaces of the crystalline main group elements. Their reactivity is, in fact, more characteristic of transition metal complexes with open valence shells than of normal main group molecules. The reactions that have been established for hydrogen, olefin, and alkyne addition, C-H, C-C, and C-N bond activation, insertion and metathesis reactions are all of key importance because they represent the individual steps in various homogenous catalytic cycles known for transition metal complexes whose reactivity is related to those of the germanium and gallium molecules described above. The primary objectives of our future work in the area will be to expand the range of these reactions to a wider selection of open shell main group molecules involving more than one reactive site. In particular, we plan to focus on derivatives of two of the most abundant main group elements, aluminum and silicon. Our goal is to combine what has been discovered with current funding into catalytic cycles for hydrogenation, C-H activation, or olefin or alkyl metathesis using these inexpensive elements.

3(iv). References

1. Buriak, J. M. *Chem. Rev.* **2002**, *102*, 1271-1308.
2. Peng, Y.; Brynda, M.; Ellis, B. D.; Fettingner, J. C.; Rivard, E.; Power, P. P. *Chemical Communications*. **2008**, 6042-6044.
3. Zhu, Z.; Wang, X.; Peng, Y.; Lei, H.; Fettingner, J. C.; Rivard, E.; Power, P. P. *Angewandte Chemie International Edition*. **2009**, *48*, 2031-2033.
4. Peng, Y.; Ellis, B. D.; Wang, X.; Power, P. P. *Journal of the American Chemical Society*. **2008**, *130*, 12268-12269.
5. Summerscales, O. T.; Jimenez-Halla, J. O.; Merino, G.; Power, P. P. *Journal of the American Chemical Society*. **2011**, *133*, 180-182.
6. Summerscales, O. T.; Fettingner, J. C.; Power, P. P. *Journal of the American Chemical Society*. **2011**, *133*, 11960-11963.
7. Summerscales, O. T.; Caputo, C. A.; Knapp, C. E.; Fettingner, J. C.; Power, P. P. Unpublished results, **2012**.
8. Summerscales, O. T.; Olmstead, M. M.; Power, P. P. *Organometallics*. **2011**, *30*, 3468-3471.
9. Caputo, C. A.; Zhu, Z.; Fettingner, J. C.; Power, P. P. *Chemical Communications*. **2011**, *47*, 7506-7508.
10. Caputo, C. A.; Guo, J-D.; Nagase, S.; Fettingner, J. C.; Power, P. P. *Journal of the American Chemical Society*. **2012**, *134*, 7155-7164.

3(v). Publications Acknowledging DOE Support Since Mid-2010

1. Summerscales, O. T.; Wang, X.; Power, P. P. *Angew. Chem. Int. Ed.* **2010**, *49*, 4788-4790.
2. Summerscales, O. T.; Jimenez-Halla, J. O.; Merino, G.; Power, P. P. *Journal of the American Chemical Society*. **2011**, *133*, 180-182.
3. Caputo, C. A.; Zhu, Z.; Fettingner, J. C.; Power, P. P. *Chemical Communications*. **2011**, *47*, 7506-7508.
4. Summerscales, O. T.; Olmstead, M. M.; Power, P. P. *Organometallics*. **2011**, *30*, 3468-3471.
5. Summerscales, O. T.; Fettingner, J. C.; Power, P. P. *Journal of the American Chemical Society*. **2011**, *133*, 11960-11963.
6. Power, P. P. *Accounts of Chemical Research*. **2011**, *44*, 627-637.
7. Brown, Z. D.; Vasco, P.; Fettingner, J. C.; Tuononen, H. M.; Power, P. P. *Journal of the American Chemical Society*. **2012**, *134*, 4045-4048.
8. Caputo, C. A.; Guo, J-D.; Nagase, S.; Fettingner, J. C.; Power, P. P. *Journal of the American Chemical Society*. **2012**, *134*, 7155-7164.
9. Brown, Z. D.; Guo, J-D.; Nagase, S.; Power, P. P. *Organometallics*. **2012**. In-press as soon as publishable. DOI: 10.1021/om300271c.

MOLECULAR PROCESSES UNDERLYING THE STRUCTURE AND ASSEMBLY OF THIN FILMS AND NANOPARTICLES AT COMPLEX INTERFACES

Geraldine L. Richmond
Department of Chemistry
1253 University of Oregon
Eugene, Oregon 97403-1253
richmond@uoregon.edu

Program Scope and Motivation

In our nation and around the globe there is an increased recognition of the serious challenges that we face both today and in the future to develop sustainable and environmentally benign energy resources. Such challenges include developing more efficient ways to recover and use our existing fossil fuels, minimizing or sequestering excess green house gases resulting from their usage, increasing the efficiency of current alternative energy sources and developing of new ones. Materials chemistry has a leading role to play in these areas as well as in addressing many other important societal issues that rely on advanced technologies. Over the past decade we have witnessed many exciting advances in the laboratory towards the development of new materials, in the area of molecular architecture and nanoscience, as well as in the development of new bio-inspired materials that seek to emulate materials that have evolved in nature. Many of these new materials are being made in more complex and reactive environments than in the past. The assembly of thin films at liquid/solid and liquid/liquid interfaces fall into this category as well the multitude of unique nanostructured materials that assemble in solvents and at surfaces. This increased complexity of the materials growth environment is usually accompanied by less predictability, often because of our limited knowledge of the fundamental molecular interactions that lead to the assembly and stability of molecules at these interfaces.

The focus of the science in this project is to obtain a molecular level picture of adsorption and assembly at complex “soft” interfaces. The studies include (1) adsorption to the surface of hydrophobic self-monolayer surfaces in aqueous solutions of ions and acids and (2) nanoparticle and macromolecular assembly at aqueous/hydrophobic liquid surfaces. The fundamental studies being pursued have direct relevance to many important areas of interest to the Department of Energy including carbon sequestration, biomolecular assembly, oil recovery, environmental remediation, surface wetting, flotation, nanoparticle structure, and monolayer film assembly. We employ a variety of experimental techniques including surface vibrational sum frequency spectroscopy (VSFS), Raman spectroscopy, infrared reflection adsorption spectroscopy (IRRAS), atomic force microscopy (AFM), contact angle, surface tension and zeta potential measurements. The closely coupled computer simulation capabilities that we have developed over the past decade also provide important complementary insights into our understanding of these molecular processes occurring at these wet interfaces.

Recent Progress on Project:

(1) SAMs Under Water: The Impact of Ions at Soft Hydrophobic Surfaces

The focus of this study has been on exploring the behavior of aqueous solutions of salts and acids in contact with hydrocarbon and fluorocarbon SAMs using vibrational sum-frequency spectroscopy. The studies take a systematic approach to understanding how each component of the SAM/water interface contributes to the overall observed behavior of ions and water in the

boundary region. Spectroscopic comparison of hydrocarbon- and fluorocarbon-terminated SAMs exploits the sensitivity of VSFS to differences in the molecular interactions of water with these two chemical functionalities at the interface. We are able to distinguish between water at the terminus of these two monolayer systems from that of H₂O in other regions of the interface, such as those closer to the substrate or deeper into the bulk liquid. Contributions from the substrate are determined by examining and comparing the VSFS response from SiO₂ in contact with various ion and acid solutions. Further insights into the influence of the substrate and monolayers on interfacial water and electrolytes are obtained from studies of aqueous solutions of acids, bases and ions in contact with a hydrophobic organic liquids where a substrate is not a factor.

Some striking similarities can be found between the water/monolayer interface and the water/hydrophobic liquid interface. The interface between water and the hydrophobic terminus of the monolayers is relatively sharp, as is found to be general behavior for water adjacent to nonpolar liquids. The degree of interaction is dependent on the molecular form of the hydrophobic phase, with a progressively stronger interaction as one moves from fluorocarbon monolayers, to hydrocarbon monolayers and alkanes, to more polarizable liquids like CCl₄. This weak interaction is identical in strength for water bonded to the hydrocarbon SAMs and various alkanes examined. The presence of ions and acids has no significant impact on this weak interaction between water and the free-OH mode in all cases. The behavior of more highly coordinated water a bit deeper into the water displays very different behavior at the SAM interfaces relative to the CCl₄/water interface. We attribute this to the influence of electrostatic fields at the SiO₂/monolayer interface that is present due to water molecules and ions permeating the monolayers. The presence of OH⁻ ions increases water bonding and orientation at the monolayer containing interfaces examined, but had the opposite effect on the CCl₄/H₂O interface. At the liquid/liquid interface, OH⁻ serves to disrupt the hydrogen-bonding network. For the monolayer surfaces, OH⁻ deprotonates substrate silanols, which creates an electrostatic field to orient water molecules. Salt screening experiments remove this electrostatic component and reveal those water molecules whose interactions are governed by their direct interactions with their nonaqueous neighbors.

(2) Solute Adsorption at Fluorocarbon and Hydrocarbon SAMs Under Water

Understanding molecular scale interactions of adsorbates with fluorocarbon and hydrocarbon surfaces is of great importance for biological and industrial applications seeking to leverage the unique properties of fluorocarbons relative to their hydrocarbon counterparts. In any of these systems, the coatings of interest are exposed to an array of chemical agents of varying functionality. Two of particular note are molecules with hydroxy and/or amine functionalities. Alcohols and similar small organic molecules are known to cause degradation of lubricant films in microelectromechanical applications. Amines and amine chlorides are present in biological molecules and are commonly used in applications where cationic surfactants are required. In this study, we have employed VSFS to examine the adsorption of methanol and amines in aqueous solution to hydrocarbon (HC) and fluorocarbon (FC) SAMs surfaces grown on SiO₂.

These studies show that methanol adsorbs to the fluorinated FDS interface at very low concentration due to the strong hydrophobicity of the monolayer. As CH₃OH adsorbs, it does so with a constant molecular orientation, displacing interfacial water molecules. This displacement alters the hydrogen bonding network of interfacial water molecules and thus the coordination of the methanol OH group. On the hydrocarbon ODS interface, we see nearly identical behavior. However, due to the favorable interactions between the hydrocarbon SAM and MeOH, methanol perturbs the monolayer structure slightly. For both FC and HC interfaces, BuNH₃⁺ begins to populate the interface and displace water, at relatively low bulk concentrations behaving like a

soluble salt. However, at high concentrations the amine adsorbs to the monolayer surface and gives the interfacial region a net positive charge, like a surfactant. At pH 2, this results in electrostatically induced water coordination before there is any ordered adsorption at the interface. Similarly, for both FC and HC SAMs at pH 5.7, BuNH₃Cl first acts mostly as an ion and screens the interfacial charge before reversing it at high concentrations. In the high concentration regime, key differences in the behavior of BuNH₃Cl at FC and HC interfaces become apparent. On the hydrocarbon surface, BuNH₃Cl adopts a relatively horizontal orientation which maximizes its interactions with the ODS chains. At the fluorinated interface, the terminal methyl group of BuNH₃Cl is oriented towards the fluorocarbon layer, which minimizes the interactions between the adsorbate and the lipophobic monolayer. These observed differences in adsorbate molecular orientation at fluorocarbon and hydrocarbon surfaces shows that lipophobic interactions between fluorocarbon and hydrocarbons can affect adsorption processes. These results help explain differences in biomolecule adsorption at fluorocarbon and hydrocarbon surfaces and may lead to different lubricant designs for fluorinated and hydrogenated surfaces.

(3) Molecular Insights in Nanoparticle Assembly at Liquid/Liquid Interfaces

The ability for nanoparticles to self-assemble at the oil/water interface makes them very attractive for applications such as emulsion stabilization, soil and water remediation and biomedical engineering. Particle interfacial behavior at the oil/water interface differs significantly from surfactant self-assembly, where surfactants have distinct hydrophilic and hydrophobic moieties. The surface organization of particles is strongly influenced by particle size, surface charge and particle-particle interaction. Spherical silica (SiO₂) nanoparticles are ideal model system for studying the organization of particles at the oil/water interface due to their non-toxicity, ease of surface grafting and availability. In these studies we have been able to measure spectroscopically for the first time the self-assembly of carboxylate - modified silica nanoparticles at the oil/water interface. We have employed VSFS coupled with surface tension measurements to make these measurements. The studies show that the carboxylic acid and hydrocarbons on the nanoparticles show a high degree of orientation when they assemble at the interface and that this ordering increases with time even though no further adsorption is measured. We have also found that altering the particle surface charge via pH increases the adsorption and orientation of SiO₂ bound moieties at the oil/water interface. The studies demonstrate the unique capabilities for examining nanoparticle assembly at oil surfaces and the interesting structuring that they display when upon adsorption.

(4) Polyelectrolyte Assembly at Liquid/Liquid Interfaces

Building on the nanoparticles studies described in (3) we are interested in how polyelectrolyte-modified nanoparticles behave at liquid/liquid interfaces. Such nanoparticles are good candidates for emulsion stabilizers due to the tunability of both the polyelectrolyte and particle. As a build-up to these studies we have been examining the adsorption of polyacrylic acid (PAA) at the oil/water interface so that we can distinguish the free polymers from those that are bound to the nanoparticle. From these surface spectroscopic and thermodynamics studies we report the unique molecular characteristics that PAA exhibits when they adsorb at a fluid interface between water and simple insoluble organic oil. PAA is found to adsorb to the interface from aqueous solution in a multi-stepped process with a very thin initial layer of oriented polymer followed by multiple layers of randomly oriented polymer. The adsorption/desorption

process is highly pH dependent and distinctly different than what might be expected from bulk aqueous phase behavior.

Ongoing and Near-Future Plans

Because of the exciting results that we are obtaining regarding nanoparticle and macromolecular assembly at liquid surfaces in these DOE sponsored studies, much of our ongoing and near-future plans will be focusing in this area. For the macromolecular studies we will be examining the mechanism of co-adsorption of surfactants and macromolecular polyelectrolytes at the oil-water interface. This is a very important area of research for which there is little molecular level information. Interfacial tension, zeta potential and VSF experiments will be conducted. The experimental results will be complemented with MD simulations.

Our second area of focus will be on polyelectrolyte-modified nanoparticles. These types of nanoparticles are good candidates for emulsion stabilizers due to the tunability of both the polyelectrolyte and particle. For instance, the adsorption of the polyelectrolyte (PE) to the particle surface and also the net charge on the particles are determined by factors such as PE concentration and solution pH. Polyelectrolytes can thus tune the hydrophobicity of charged particles and enhance their adsorption at the oil-water interface. Many previous studies of polyelectrolyte binding to nanoparticles as well as emulsions stabilized using these colloidal particles have focused on measured macroscopic quantities such as solution conductivity, viscosity, and zeta potential. Not much is thus understood about the molecular behavior of these colloidal particles at the liquid/liquid interface and how tuning particle hydrophobicity affects this behavior. Our VSFS and interfacial tension studies will provide molecular level information pertaining to the adsorption of anionic PEs onto cationic particles as well as the interfacial behavior of these hydrophobically functionalized nanoparticles at the oil-water interface by using PMA/Al₂O₃ particle solutions as a model system. Specific experiments will include varying the concentration of PMA in solution to see how the amount of polyelectrolyte adsorbed to the particle affects interfacial adsorption, pH studies to see how changing the charge and bulk structure of PMA affects its adsorption to Al₂O₃ particles and their subsequent interfacial activity, and salt studies to see the effects of charge screening.

Publications

- “Molecular Insights into the Self-Assembly of Nanoparticles at the Water/Oil Interface”, H. Staleva, J. Hensel and G.L. Richmond, in preparation.
- “The Water/Hydrophobic Interface: Neutral and Charged Solute Adsorption at Fluorocarbon and Hydrocarbon SAMs”, A. J. Hopkins, and G.L. Richmond, submitted.
- “Ordered Polyelectrolyte Assembly at the Oil-Water Interface”, D.K. Beaman, E. J. Robertson and G.L. Richmond, *PNAS*, 109 (3226-3231) 2012.
- “SAMS Under Water: The Impact of Ions on the Behavior of Water at Soft Hydrophobic Surfaces”, A.J. Hopkins, C. McFearin and G.L. Richmond, *J. Phys. Chem. C*, 115 (11192-11203) 2011.
- “The Unique Assembly of Macromolecules at Water/Hydrophobic Liquid Interfaces”, D. K. Beaman, E. J. Robertson and G.L. Richmond, *Langmuir*, 27 (2104-2106) 2011.
- “Specific Ion Effects of Salt Solutions at the CaF₂/water Interface” A.J. Hopkins, S. Schroedle and G.L. Richmond, *Langmuir* 26 (10784–10790) 2010.

Nanoscale Manipulation and Imaging of Liquid Crystals

Charles Rosenblatt

Department of Physics, Case Western Reserve University, Cleveland, Ohio 44106

rosenblatt@case.edu

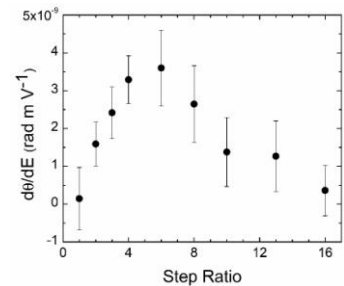
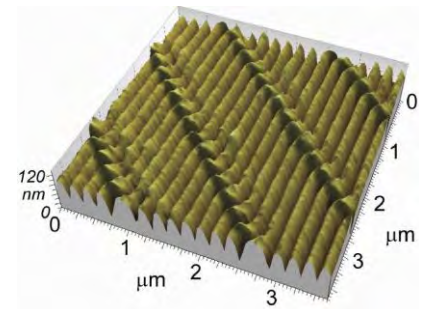
Program Scope

Scanning probe microscopy and a variety of lithographic techniques have spurred a revolution in nanoscopic control and optical imaging of materials. Studies in liquid crystals and other soft materials have benefited greatly from these tools [1-5], as manipulation and imaging can be achieved down to the nanometer scale. The program has two broad and interconnected goals: 1) investigation of nanoscopic and macroscopic liquid crystal phenomena — including symmetry properties — arising from nanoscopically-controlled surface modification, and 2) studies of nanocolloids in liquid crystals, with emphasis on the nature of the nanocolloid surface. As might be expected, the specific emphasis has evolved over the course of the project, and now focuses most strongly on nanotubes in liquid crystals, the creation of 2D chiral surface patterns at the nanoscale and their transmission of chirality into the adjacent achiral liquid crystal, and the effects of controlled surface topography and its relationship with chiral symmetry breaking.

Recent Progress

1. *Spatially controllable surface chirality at the nanoscale*

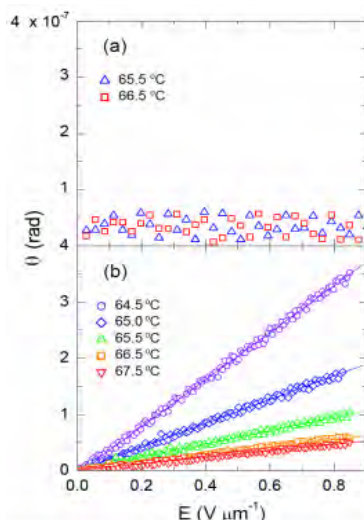
[6] Two-dimensional chirality is the inability to superpose an object onto its mirror image by rotation and translation within a plane. Because of the absence of translational symmetry normal to a substrate, 2D chiral patterns on a substrate actually are 3D chiral — but with the chirality localized near the surface. This is referred to as “surface chirality”. We have demonstrated a mechanical approach for precisely manipulating surface chirality at nanoscopic length scales. We use an AFM to scribe a chiral step pattern into a polyimide alignment layer, and can obtain exquisite control of the chiral strength by varying the steps’ length-to-width ratio R . To examine the strength of the chirality, we coat the scribed surface with a nematic liquid crystal and apply an electric field normal to the surface. Owing to the surface’s chiral environment, we observe an electroclinic effect localized to the surface, and the liquid crystal in the cell’s interior elastically follows the surface rotation. We find that the chiral strength $d\theta/dE$, is nonmonotonic in R . The maximum chiral strength occurs when the “chiral cores”, *i.e.*, the jogs in the pattern, are separated by a distance comparable to twice the nematic extrapolation length L , where L is the twist elastic constant divided by the azimuthal



anchoring strength coefficient. This behavior suggests that the chiral cores interact up to a distance $2L$, beyond which the spatially-averaged chiral strength decreases to zero, as the density of chiral cores $\propto 1/R$. Our results demonstrate that chiral handedness and strength can be controlled precisely on nanoscopic length scales and can be varied spatially over the surface.

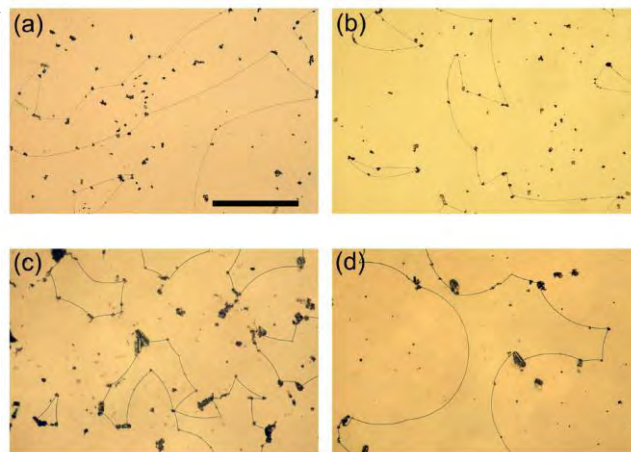
2. Carbon nanotube-induced chirality in an achiral liquid crystal [7] A small quantity of

carbon nanotubes dispersed in an achiral liquid crystal matrix transmits chirality a short distance into the LC, and the LC+CNT mixture was found to exhibit a bulk-like electroclinic effect [8] in the nematic phase. The magnitude of the effect increases rapidly on cooling, showing significant pretransitional behavior on approaching the nematic – smectic-*A* transition temperature (T_{NA}) from above. The variation of the electroclinic coefficient is negligible over the frequency range 100 Hz – 100 kHz in the in the nematic phase well above T_{NA} and in the smectic-*A* phase, whereas the



Electroclinic effect in the nematic phase: (a) tilt angle θ vs. E ($f = 1$ kHz) for bulk $\overline{8S5}$ at two different values of T ; (b) tilt angle θ vs. E ($f = 1$ kHz) for $\overline{8S5}$ +MWCNTs at five different values of T listed in the legend.

electroclinic coefficient falls off significantly with increasing frequency just above T_{NA} . Additionally, we showed that the LC+CNT mixture exhibits a macroscopic mechanical twist [9]. We determined the nanotube-induced chiral pitch length P as a function of the average nanotube concentration by measuring the radii of curvature of reverse twist disclination lines in 90° nematic twist cells. The results suggest that the nanotubes' spatial concentration can vary significantly across the cell, and that at high average concentration the nanotubes undergo aggregation, resulting in an apparent saturation of P^{-1} at high concentrations. We also have been able to determine the macroscopic helical twisting power of the nanotubes.



Micrographs of a 90° twist cell showing bowed disclinations of 5CB+MWCNT samples for four different average CNT concentrations C_w : (a) 0.0001, (b) 0.008, (c) 0.002, and (d) 0.003 weight fraction. The bar in (a) represents $250 \mu\text{m}$

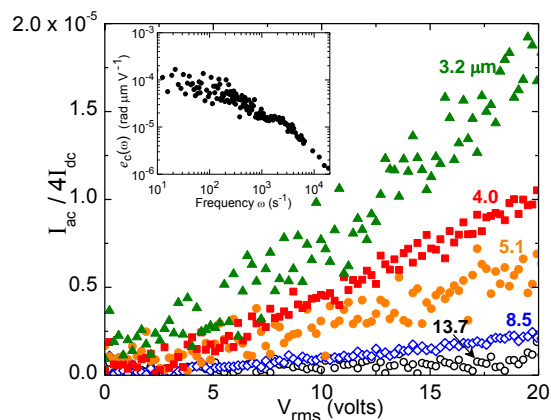
3.

Since antiquity chiral phenomena have been “bottom – up”, where the chiral constituents, such as molecules, give rise to chiral-specific macroscopic behavior. Examples include the macroscopic twist distortion associated with cholesteric liquid crystals, circular dichroism, and optical rotatory power. Here we approach chirality from the opposite direction: A macroscopic torsional strain is used to induce conformational deracemization of the configurationally achiral molecules. To accomplish this, we impose a macroscopic helical twist on an achiral nematic

liquid crystal by rotating the azimuthal easy axis of one substrate with respect to the other. On application of an electric field the director rotates in the substrate plane. This electroclinic effect [10], which requires the presence of chirality, is strongest at the two substrates, increases with decreasing pitch, and depends strongly on the liquid crystal – surface interaction. We developed a simple model involving a trade-off among bulk elastic energy, surface anchoring energy, and entropy associated with molecular deracemization that suggests the imposed director twist induces a deracemization of chiral conformations of the molecules —effectively “top-down” chiral induction — quantitatively consistent with experiment.

Future Plans

- We intend to investigate the orientation profile of the liquid crystal around the chiral-inducing carbon nanotubes by means of optical nanotomography [11], a technique that we have developed and exploited using funds from a previous DoE grant. This technique is based on using the tapered optical fiber of a near field scanning optical microscope to measure the optical phase retardation of polarized light from the optical fiber aperture to the surface as a function of height above the surface. The resulting signal can be deconvoluted to provide optical imaging with resolution of 100 x 100 nm in the xy-plane and 1 to 2 nm in the z-direction.
- With Prof. Maurizio Nobili of University of Montpellier (France), we have begun to use our technique of optical nanotomography to examine the angular distribution of the local liquid crystal “easy axes” written to a polymer substrate by UV illumination. Ordinarily the azimuthal easy axis is a delta function around some angle φ_0 . Using optical microscopy Nobili noticed that there is a small *angular distribution* around φ_0 , which we will examine with area resolution about 25 times better than possible with diffraction limited optics. Our goal is to quantify this effect, and then determine its cause(s).
- With chemist colleague Prof. Robert Lemieux (Queen’s University, Kingston, Ontario) we are examining chiral periodic mesoporous organosilicas (PMO), which are prepared by the surfactant-templated condensation of bridged organosilsesquioxane monomers, e.g., $(\text{EtO})_3\text{Si-R-Si}(\text{OEt})_3$. By controlling the nature of the organic segment R, the type of surfactant and the condensation conditions, one can control the physical and chemical properties of the resulting PMO and produce highly ordered porous structures with a periodicity on the nanometer scale. The idea is that achiral liquid crystals fill the nanometer-sized pores, and the chirality of the PMO is transmitted into the liquid crystal, which we probe by optical means. By varying the pore size, we can estimate the range of chiral transmission into the achiral liquid crystal.



The intensity ratio $I_{ac}/4I_{dc}$ corresponds to the director’s electroclinic rotation, vs. applied voltage for five different cell widths d . Here the imposed helical pitch $\propto d^{-1}$. Inset: Electroclinic coefficient $e_c(\omega)$ versus frequency at fixed voltage of 8 V_{rms} and $d = 3.2$ mm.

References

1. M. Rüetschi, P. Grütter, J. Fünfschilling, and H.-J. Güntherodt, *Science*, 265, 512 (1994)
2. A.J. Pidduck, S.D. Haslam, G.P. Bryan-Brown, R. Bannister, I.D. Kitely, *Appl. Phys. Lett.* 71, 2907 (1997)
3. Bing Wen, M.P. Mahajan, and C. Rosenblatt, *Appl. Phys. Lett.* 76, 1240 (2000)
4. M. Zhu, G. Carbone, and C. Rosenblatt, *Appl. Phys. Lett.* 88, 253502 (2006).
5. J.H. Kim, M. Yoney, and H. Yokoyama, *Nature* 420, 159 (2002)
6. J. Pendery, S. Ferjani, C. Rosenblatt, and R.G. Petschek, *Europhys. Lett.* 96, 26001 (2011)
7. Rajratan Basu, Rolfe G. Petschek, and Charles Rosenblatt, *Phys Rev. E* 83, 041707 (2011)
8. S. Garoff and R. B. Meyer, *Phys. Rev. Lett.* 38, 848 (1977)
9. R. Basu, C.-L. Chen, and C. Rosenblatt, **J. Appl. Phys.** 109, 083518 (2011)
10. R. Basu, J. Pendery, R.G. Petschek, R.P. Lemieux, and C. Rosenblatt, *Phys. Rev. Lett.* 107, 237804 (2011)
11. A. De Luca, V. Barna, T. Atherton, G. Carbone, M. Sousa, and C. Rosenblatt, *Nature Phys.* 4, 869 (2008).

Publications (2010 – 2012)

- “Mechanically generated surface chirality at the nanoscale,” S. Ferjani, Y. Choi, J. Pendery, R.G. Petschek, and C. Rosenblatt, **Phys. Rev. Lett.** 104, 257801 (2010)
- “Direct visualization and measurement of the extrapolation length on cooling toward the nematic — smectic-A phase transition temperature,” Y. Choi and C. Rosenblatt, **Phys. Rev. E** 81, 051708 (2010)
- “Mechanically generated surface chirality: Control of chiral strength,” S. Ferjani, J. Pendery, and C. Rosenblatt, **Appl. Phys. Lett.** 97, 121905 (2010)
- “Carbon nanotube-induced chirality in an achiral liquid crystal,” Rajratan Basu, Krysta A. Boccuzzi, Sameh Ferjani, and Charles Rosenblatt, **Appl. Phys. Lett.** 97, 121908 (2010)
- “Spatially controllable surface chirality at the nanoscale,” J. Pendery, S. Ferjani, C. Rosenblatt, and R.G. Petschek, **Europhys. Lett.** 96, 26001 (2011)
- “Chiral nanotube-induced macroscopic helical twist in an achiral nematic liquid crystal,” R. Basu, C.-L. Chen, and C. Rosenblatt, **J. Appl. Phys.** 109, 083518 (2011)
- “Macroscopic torsional strain and induced molecular conformational chirality,” [*i.e.*, Top-Down Chiral Induction] R. Basu, J. Pendery, R.G. Petschek, R.P. Lemieux, and C. Rosenblatt, **Phys. Rev. Lett.** 107, 237804 (2011)
- “Nematic electroclinic effect in a carbon nanotube-doped achiral liquid crystal,” Rajratan Basu, Rolfe G. Petschek, and Charles Rosenblatt, **Phys Rev. E** 83, 041707 (2011)
- “Chiral induction in thioester and oxoester liquid crystals by dispersed carbon nanotubes,” R. Basu, C. Rosenblatt, and R. P. Lemieux, **Liq. Cryst.** 39, 199 (2012)
- “Surface induced orientational order and role of isotropic-nematic interface fluctuations in the appearance of an induced nematic phase,” E.S. Pikina and C. Rosenblatt, **Eur. Phys. J. E** (submitted)

SISGR: Improved electrical energy storage with electrochemical double layer capacitance based on novel carbon electrodes, new electrolytes, and thorough development of a strong science base

Rod Ruoff (Email: r.ruoff@mail.utexas.edu; Phone: 512 471 4691)

Cockrell Family Regents Chair

Dept of Mechanical Engineering and the Materials Science and Engineering Program, Cockrell School of Engineering, The University of Texas at Austin, 1 University Station, C2200, Austin, TX 78712-0292

Program Scope

Electrical energy storage (EES) is critical to the ongoing development of alternative energy systems currently required for long term national security. Indeed, "revolutionary breakthroughs in EES are perhaps the most crucial need for this nation's secure energy future", and are essential for the development of electrical vehicles and charging stations, hybrid electrical devices, fuel cells, home energy management systems, and the transition of our nation to a smart grid. Despite substantial research on the two primary methods of EES - batteries and electrochemical double-layer capacitors (also referred to as 'ultracapacitors'), EES technologies fall significantly short of the requirements needed for widespread implementation. EES devices with substantially higher energy and power densities and fast recharge times are necessary if all-electric/plug-in-hybrid vehicles are to be deployed broadly as replacements for gasoline-powered vehicles. Though EES devices have been the subject of a great deal of investigation over many decades, fundamental research is critically needed to further improve their performance and meet current needs.

The Ruoff group has pioneered the development of new carbon materials that have been termed "chemically modified graphenes" (CMGs) and have demonstrated their utility in electrochemical double layer capacitance (EDLC) systems. CMGs are one-atom thick sheets of carbon, with tailored functionalities. The surface area of a single graphene sheet is 2630 m²/g, much higher than most of the currently available activated carbons. Materials with surface areas of this magnitude, or even greater, have recently been prepared in our laboratories and show remarkable electronic properties, rendering them applicable in EES devices. As an extension of this work, we envision the design and synthesis of other high surface area carbon materials (such as well-defined graphene nanoribbons, porous graphene, and other activated porous carbons) that possess useful electronic and electrochemical properties. To fully optimize the devices, we will also develop a detailed scientific understanding of the double layer capacitance between ions in the electrolyte and the charged carbon surfaces. These efforts will result in scientifically directed choices of the electrolyte and the CMG type and configuration, and ultimately, optimal design of the overall ultracapacitor cells with significantly enhanced values of specific capacitance and stored energy.

With practical improvements of the carbon materials comprising the electrode, the broad use of EES devices, such as ultracapacitors, will be enabled. The highest commercially available ultracapacitor energy densities are in the range of about 4-7 Wh/kg (based on the weight of a fully packaged symmetric ultracapacitor cell) and are based upon activated carbons with specific capacitances of 80-85 F/g and organic electrolytes (that operate up to 2.7 V). Current performance of activated carbons in the laboratory is in the range of 120 to 180 F/g with organic electrolytes or ionic liquid electrolytes. Further improvements in the carbon electrode material including in conjunction with use with ionic liquid electrolytes are envisioned to enhance performance and secure the primary objectives defined above.

Recent Progress

Our team is now studying the interplay between graphene-based and graphene-derived carbons as the electrode materials in EDLC systems on the one hand, and electrolytes including novel electrolytes such as newly synthesized ionic liquids (ILs), on the other.

1) *A new porous carbon by activation of microwave-exfoliated graphite oxide*

We have made important advances including a paper published in *Science* in 2011¹ (team led by Ruoff) that describes a new type of carbon with atom-thick walls and a distribution of mesopores and micropores with BET specific surface area as high as 3100 m²/g that favors high gravimetric capacitance as well as high electrical energy storage on a gravimetric basis, with both organic or IL electrolytes. This carbon is made by ‘KOH-activation’ of microwave-expanded graphite oxide (MEGO) at 800 °C under flowing argon gas and is thus referred to as ‘activated MEGO’ or ‘aMEGO’. More recently the Ruoff team has shown that aMEGO performs very well as the cathode in a hybrid battery-electrocapacitor system² and that by compressing it, exceptionally high capacitance can also be achieved on a volumetric basis (manuscript in preparation).

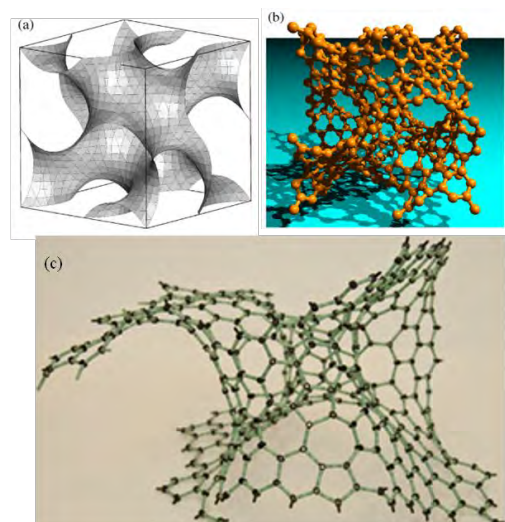


Figure 1. (a) The “G (gyroid) TPMS”. (b) One cubic cell of the G TPMS decorated with trivalently bonded C atoms using hexagonal and octagonal rings of carbon (384 atoms per cubic cell). (c) A home-built model showing 5, 6, 7, and 8 sided polygons in the atomic structure yielding an open and highly curved pore structure.

2) *Solid-state NMR to study novel carbons and ionic liquids*

The Ishii group used solid state NMR (SSNMR) for the study of the chemistry and molecular-level structural changes in the production of CMGs by chemical reduction of ¹³C-labeled graphene oxide with ¹⁵N-labeled hydrazine by high-resolution ¹³C and ¹⁵N SSNMR in collaboration with the Ruoff group.³ This allowed identification of ¹⁵N species having a ¹⁵N

chemical shift of 190 ppm, which was incorporated from ^{15}N -labeled hydrazine to the edge of the graphene sheet. These experiments and ^{13}C - ^{15}N REDOR experiments suggest that hydrazine treatment of GO causes insertion of an aromatic N_2 moiety in a five-membered ring at the platelet edges and also restores sp^2 networks on the basal planes (published in *Nat. Comm.*).³ The results present a novel avenue to dope aromatic N species into graphene platelet, which is likely to enhance the conductivity of the CMG based on density function calculations.³ Using *ab initio* calculations of ^{15}N and ^{13}C SSNMR chemical shifts, we tested the feasibility of these proposed edge structures in GO and RGO (Ishii et al. in preparation). The results are consistent with the model. Preliminary SSNMR analysis of MEGO and aMEGO, including their interactions with solvent, is also ongoing.

3) *Characterization of IL Electrolyte Dynamics and Transport Properties*

In collaboration with the Alam group at Sandia National Labs we have also utilized pulse field gradient (PFG) diffusion NMR and solution ^{14}N NMR to help measure the chemical and physical transport for a series of novel ILs. (Alam et al. , 2011) This data provides important basic information about the role of different cation/anion pair formation, and the impact this has on the performance of the ILs. Ultimately our goal is to use these results to map and understand the interactions that are occurring between the IL electrolytes and the electrode materials within the capacitors.

4) *Microstructure and Capacitance of IL Electrolytes*

Some examples of a wide range of efforts underway include investigating the effect of interactions of azolium azolates (Rogers) type ionic liquids (ILs), namely [BMIM][4,5-dicyanoimidazolate] and [BMIM][2-methyl-5-nitroimidazolate], with graphene and graphite for potential use in advanced battery and ultracapacitor applications. To gain a fundamental understanding of the ILs' physical and chemical interactions with graphite oxide (GO), the ILs are intercalated between the GO layers in liquid media and the system studied as a function of annealing temperature that produces expanded thermally reduced graphene (TRG). The anion and cation moieties of the ILs in GO-IL intercalated compounds investigated were found to influence the decomposition temperature and the degree of thermal stabilization of the TRG-IL intercalation compounds.⁴ In an effort to further optimize ILs as electrolytes for use in ultracapacitors, we are currently exploring the relationship between the ILs' physicochemical and colloidal properties and their ultracapacitor performance. The experimental findings suggest that GO-IL composites are good model systems to understand oxygen interactions with various electrolyte systems and ultimately good candidates to achieve high surface area materials (carbon-electrolyte interactions).

Future Plans

Our further efforts will focus on the research topics of

- 1) Studies of the activation of microwave-exfoliated graphite oxide

- 2) Structural characterization of aMEGO and MEGO by Solid-state NMR
- 3) Porous carbon thin films
- 4) Quantum capacitance and density of states of graphene, doped graphene, and multilayer graphene
- 5) Bottom up Synthesis of new types of Porous Carbon Materials
- 6) *In-situ* characterizations: IR, Raman spectroscopy, , Low energy ion scattering
- 7) Characterization of IL Electrolyte Transport Properties at the Carbon Interface
- 8) Microstructure and Capacitance of IL Electrolytes

References

- (1) Zhu, Y.; Murali, S.; Stoller, M. D.; Ganesh, K. J.; Cai, W.; Ferreira, P. J.; Pirkle, A.; Wallace, R. M.; Cychosz, K. A.; Thommes, M.; Su, D.; Stach, E. A.; Ruoff, R. S. *Science* 2011, 332, 1537-1541.
- (2) Stoller, M. D.; Murali, S.; Quarles, N.; Zhu, Y.; Potts, J. R.; Zhu, X.; Ha, H.-W.; Ruoff, R. S. *Phys. Chem. Chem. Phys.* 2012, 14, 3388-3391.
- (3) Park, S.; Hu, Y.; Hwang, J. O.; Lee, E.; Casabianca, L. B.; Cai, W.; Potts, J. R.; Ha, H.; Chen, S.; Kim, S. O.; Kim, Y. H.; Ishii, Y.; Ruoff, R. S. *Nature Commun.* 2012, 3, 638.
- (4) Acik, M.; Dreyer, D. R.; Bielawski, C. W.; Chabal, Y. *J. Phys. Chem. C* 2012, *accepted*.

Publications

- (1) Zhu, Y.; Murali, S and Ruoff, R. S. *et. al. Science* **2011**, 332, 1537.
- (2) Zhu, Y.; Stoller, M. D. and Ruoff, R. S. *et. al. ACS Nano* **2010**, 4, 1227.
- (3) Zhu, Y.; Murali, S. and Ruoff, R. S. *et. al. Adv. Mater.* **2010**, 22, 3906.
- (4) Zhu, X.; Zhu, Y. and Ruoff, R. S. *et. al. ACS Nano* **2011**, 5, 3333.
- (5) Zhu, X.; Zhu, Y. and Ruoff, R. S. *et. al. J. Power Sources* **2011**, 196, 6473.
- (6) Stoller, M. D.; Murali, S. and Ruoff, R. S. *et. al. Phys. Chem. Chem. Phys.* **2012**, 14, 3388.
- (7) Stoller, M.; Mangnuson, C. W. and Ruoff, R. S. *et. al. Energy Environ. Sci.* **2011**, 4, 4685.
- (8) Kim, T. Y.; Lee, H. W. and Suh, K. S. *et. al. ACS Nano* **2011**, 5, 436.
- (9) Potts, J. R.; Lee, S. H. and Ruoff, R. S. *et. al. Carbon* **2011**, 49, 2615.
- (10) Alam, T. M.; Dreyer, D. R. and Ruoff, R. S. *et. al. J. Phys. Chem. A* **2011**, 115, 4307.
- (11) Acik, M.; Dreyer, D. R.; Bielawski, C. W.; Chabal, Y. *J. Phys. Chem. C* **2012**, *in revision*.
- (12) Acik, M.; Chabal, Y. *J. Japan. J. Appl. Phys.* **2011**, 50.
- (13) Acik, M.; Lee, G. and Chabal, Y. *et. al. J. Phys. Chem. C* **2011**, 115, 19761.
- (14) Acik, M.; Chabal, Y. *J. Appl. Surf. Sci.* **2012**, *under review*.
- (15) Gong, C.; Acik, M. and Cho, K. *et. al. J. Phys. Chem. C.* **2012**, *under review*.
- (16) Kim, S.; Zhou, S. and Riedo, E. *et. al. Nat. Mater* **2012**, *under review*.
- (17) Park, S.; Hu, Y. Ishii, Y. and Ruoff, R. S. *et. al. Nature Commun.* **2012**, 3, 638.
- (18) Lee, S.; Hwang, G. S. *J. Appl. Phys.* **2011**, 110, 093524.
- (19) Paek, E.; Pak, A.; Hwang, G. S. *to be submitted* **2012**.
- (20) Pak, A.; Paek, E.; Hwang, G. S. *to be submitted* **2012**.
- (21) Paek, E.; Pak, A.; Hwang, G. S. *to be submitted* **2012**.
- (22) Zhang, L. L.; Zhao, X. and Ruoff, R. S. *et. al. Nano Lett.* **2012**, *published online*.
- (23) Ji, H. X.; Zhang, L. L. and R.; Ruoff, R. S. *et. al. Nano Lett.* **2012**, *published online*.

Interfacial Behavior of Polymers: Using Interfaces to Manipulate Polymers

T.P.Russell, University of Massachusetts, Amherst, MA 01003

Program (DE-FG02-96ER45612)

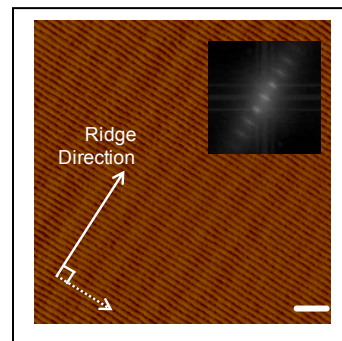
Scope: The interactions of polymers, block copolymers and nanoparticles at interfaces control their assemblies in thin films. Manipulating these interactions or overcoming these interactions opens pathways to generate functional materials. Solvent annealing processes, where interfacial interactions are mediated, represent one route to achieve this control and to impart mobility to polymeric materials. The mechanism by which the directed self-assembly of the copolymer microdomains order into highly ordered and oriented arrays of microdomains with long-range lateral order is ill-understood and being investigated. Initial results indicated that the entropy of the block copolymer chains, in addition to specific interactions, play a crucial role. To this end, the topology of the polymer chain is being investigated where the behavior of linear, bottle-brush and catenane chains is being investigated on planar and topographically patterned surfaces. Subsequently, methods will be developed to remove the minor component, so as to generate templates and scaffolds for the fabrication of nanoscopic elements for potential device applications.

Directly related to these goals is the influence of confinement on the morphology of block copolymers. When the natural period of the block copolymer is not commensurate with the dimensions of the confining geometry, whether this is in a thin film or a cylindrical geometry, the copolymer must respond by altering its fundamental morphology. Transitions, as for example cylinders to helices, are being quantitatively investigated to develop guidelines by which specific morphologies can be generated in a routine manner. X-ray and neutron scattering and electron microscopy are being used to investigate the morphological transitions. In addition, as the dimension of the confining volume become comparable to the dimension of the polymer chain, the dynamics of the polymer, including the entanglement density and chain mobility, can be perturbed. Using neutron scattering to determine the chain dimensions of the confined polymer, along with the rheological characteristics, like viscosity, will be used to understand the influence of confinement on chain dynamics.

Block copolymer microdomain morphologies with characteristic lengths scales in the tens of nanometer size scale can be obtained with simple linear diblock copolymer. To push the size of the microdomains to the single nanometer or to the hundreds of nanometer length scales require alternate routes. Ion complexation of the minor component, using low molecular weight salts, linear polymers or functional nanoparticles, is being used to drive the copolymer into the strong segregation limit where nanometer-sized domains can be achieved and where defect energies become costly. The enhanced lateral ordering of the diblock copolymer over macroscopic distances is being studied by grazing incidence x-ray scattering, transmission x-ray and neutron scattering, transmission electron microscopy and scanning force microscopy. The influence of the additive interfacial interactions presents and alternate handle on manipulating to ordering of the polymers in thin films. The additive can also alter the dielectric constant of the minor component enabling the use of electric fields to control the orientation and ordering of the copolymer microdomains in thin films. To attain morphologies with characteristic length scales hundreds of nanometers in size, bottle brush copolymers are being used wherein the crowding of the chain at the microdomain interfaces results in a stretching of the backbone chain and a marked increase in the domain size. Controlling the orientation and lateral ordering of these bulky copolymers poses a significant challenge.

Recent Progress: Unidirectionally Aligned Line Patterns Driven by Entropic Effects on Faceted Surfaces: A simple, versatile approach to the directed self-assembly of block

copolymers into a macroscopic array of unidirectionally aligned cylindrical microdomains on reconstructed faceted single crystal surfaces or on flexible, inexpensive polymeric replicas was discovered. High fidelity transfer of the line pattern generated from the microdomains to a master mold is also shown. A single-grained line patterns over arbitrarily large surface areas without the use of top-down techniques is demonstrated, which has an order parameter typically in excess of 0.97 and a slope error of 1.1 deg. This degree of perfection, produced in a short time period, yet to be achieved by any other methods. The exceptional alignment arises from entropic penalties of chain packing in the facets coupled with the bending modulus of the cylindrical microdomains. This is shown, theoretically, to be the lowest energy state. The atomic crystalline ordering of the substrate is transferred, over multiple length scales, to the block copolymer microdomains, opening avenues to large-scale roll-to-roll-type and nanoimprint processing of perfectly patterned surfaces and as templates and scaffolds for magnetic storage media, polarizing devices, and nanowire arrays.



Future Plans: The mechanism underpinning the ordering and orientation of the block copolymer microdomains using solvent annealing will be investigated using real-time GISAXS and neutron scattering. In particular, efforts will be made to unravel the independent roles of enthalpy and entropy in the ordering wherein solvent mediates interfacial interactions, markedly enhances the chain dynamics, and introduces a strong, highly directional field normal to the film surface. Entropic factors will be investigated by altering the chain topology from linear to bottle-brush to catenane, while maintaining an invariance of the chemical composition of the copolymer. Size scales of the block copolymer microdomains will be driven to the single nanometer size-scale, increasing the areal density of elements to the tens of teradots of elements per square inch regime, orders of magnitude over that which can be currently achieved and, in parallel, route will be probed by which the etching contrast can be enhanced as the film thickness invariably becomes thinner.

Publications (2010, 2011)

1. S. Park, S. C. Moon, D. Chen, R. J. Farris and TPR, "Preparation of 1-inch Gold Nanowires from PS-b-P4VP Block Copolymers," *Journal of Materials Chemistry* **20**(6), 1198-1202 (2010).
2. H. Cho, H. Park, TPR and S. Park, "Precise Placements of Metal Nanoparticles from Reversible Block Copolymer Nanostructures," *Jour of Mat Chem* **20** (24), 5047-5051, (2010).
3. Serghei, D. Chen, D. H. Lee and TPR, "Segmental dynamics of polymers during capillary flow into nanopores," *Soft Matter* **6** (6), 1111-1113, (2010).
4. G. V. Kolmakov, R. Revanur, R. Tangirala, T. Emrick, TPR, A. J. Crosby and A. C. Balazs, "Using Nanoparticle-filled Microcapsules for Site-specific Healing of Damaged Substrates: Creating a 'Repair-and-Go' System," *ACS Nano* **4**(2), 1115-1123 (2010).
5. H. D. Koh, S. Park and TPR, "Fabrication of Pt/Au Concentric Spheres from Triblock Copolymer," *ACS NANO* **4**(2), 1124-1130 (2010).
6. S. Park and TPR, "Nanoscale Patterning in Block Copolymer Thin Films," *Nano* **5**(1), 1-11, (2010).
7. S. Park, D. Lee and TPR, "Self-Assembly of Block Copolymers on Flexible Substrates," *Advanced Materials* **22** (16), 1882-1884, (2010).
8. J. L. Lutkenhaus, K. McEnnis, A. Serghei and T. P. Russell, "Confinement Effects on Crystallization and Curie Transitions of Poly(vinylidene fluoride-co-trifluoroethylene)," *Macromolecules* **43**(8), 3844-3850 (2010).

9. J. Xu, S. Park, S. Wang, TPR, B. Ocko and A. Checco, "Directed Self-Assembly of Block Copolymers on Two-Dimensional Chemical Patterns Fabricated by Electro-Oxidation Nanolithography," *Advanced Materials* **22** (20), 2268-2272, (2010).
10. X. Hu, D. Chen, S. Park, T. Emrick and TPR, "Guided Assemblies of Ferritin Nanocages: Highly Ordered Arrays of Monodisperse Nanoscopic Elements," *Advanced Materials* **22**(23), (2010).
11. J. Huang, B. Davidovitch, C. Santangelo, TPR and N. Menon, "Smooth Cascade of Wrinkles at the Edge of a Floating Elastic Film," *Physical Review Letters* **105** (3), 038302/1-038302/4, (2010).
12. X. Wei, W. Chen, X. Chen and TPR, "Disorder-to-Order Transition of Diblock Copolymers Induced by Alkyne/Azide Click Chemistry," *Macromolecules* **43** (14), 6234-6236, (2010).
13. K. Sun, J. Y. Lee, B. Y. Li, W. Liu, C. Q. Miao, Y. H. Xie, X. Y. Wei and TPR, "Fabrication and Field Emission Study of Atomically Sharp High-density Tungsten Nanotip," *Journal of Applied Physics* **108**, 036102, (2010).
14. H. Park, TPR and S. Park, "Spatial Control of Dewetting: Highly Ordered Teflon Nanospheres," *J Colloid Interface Sci.* **348**(2), 416-423, (2010).
15. Serghei, J. Lutkenhaus, D. Miranda, K. McEnnis, F. Kremer, TPR, "Density Fluctuations and Phase Transitions of Ferroelectric Polymer Nanowires," *Small* **6** (16), 1822, (2010).
16. L. Li, K. Matsunaga, J. Zhu, T. Higuchi, H. Yabu, M. Shimomura, H. Jinnai, R. Hayward and TPR, "Solvent-driven Evolution of Block Copolymer Morphology Under 3D Confinement," *Macromolecules* **43** (18), 7807-7812, (2010).
17. J. Tang, H. Wang, D. Lee, M. Fardy, Z. Huo, TPR and P. Yang, "Holey Silicon as an Efficient Thermoelectric Material," *Nano Letters* **10**(10), 4279-4283, (2010).
18. A. Serghei, W. Zhao, X. Wei, D. Chen and TPR, "Nanofluidics with Phase Separated Block-Copolymers: Glassy Dynamics During Capillary Flow," *Eur. Phys. J. Special Topics* **189**(1), 95-101, (2010).
19. M. Bihari, TPR and D. A. Hoagland, "Dissolution and Dissolved State of Cytochrome c in a Neat, Hydrophilic Ionic Liquid," *Biomacromolecules* **11**(11), 2944-2948, (2010).
20. H. Y. Lu, D. H. Lee and TPR, "Temperature Tunable Micellization of Polystyrene-block-poly(2-vinylpyridine) at Si-Ionic Liquid Interface," *Langmuir* **26**(22), 17126, (2010).
21. Z. Niu, J. He, TPR, and Q. Wang, "Synthesis of Nano/Microstructures at Fluid Interfaces," *Angewandte Chemie* **49**(52), 10052-10066 (2010).
22. D. F. Miranda, TPR and J. J. Watkins, "Ordering in Mixtures of a Triblock Copolymer with a Room Temperature Ionic Liquid," *Macromolecules* **43**(24), 10528-10535, (2010).
23. K. Sun, J. Y. Lee, B. Li, W. Liu, C. Miao, Y. Xie, X. Wei and TPR, "Fabrication and Field Emission Study of Atomically Sharp High-density Tungsten Nanotip Arrays," *Journal of Applied Physics* **108** (3), 4089-4094 (2010).
24. S. Park, S. Moon, D. Chen, R. Farris and TPR, "Preparation of 1 inch Gold Nanowires from PS-*b*-P4VP Block Copolymers," *Journal of Materials Chemistry* **20** (6), 1198-1202, (2010).
25. E. Kim, S. Choi, R. Guo, D. Y. Ryu, C. J. Hawker and TPR, "Transition Behavior of PS-*b*-PMMA Films on the Balanced Interfacial Interactions," *Polymer* **51**, 6313, (2010).
26. J. Xu, TPR, B. M. Ocko and A. Checco, "Block Copolymer Self-Assembly in Chemically Patterned Squares," *Soft Matter* **7**(8), 3915-3919, (2011).
27. B. Kim, S. W. Hong, S. Park, J. Xu, S. K. Hong and TPR, "Phase Transition Behavior in Thin Films of Block Copolymers by Use of Immiscible Solvent Vapors," *Soft Matter* **7**(2), 443-447, (2011).
28. W. Chen, J. Y. Wang, X. Y. Wei, J. Xu, A. Balazs, K. Matyjaszewski and TPR, "UV-Enhanced Ordering in Azobenzene-Containing Polystyrene-block-Poly(*n*-Butyl Methacrylate) Copolymer Blends," *Macromolecules* **44**(2), 278-285, (2011).

29. D. H. Lee, S. Park, W. Y. Gu and TPR, "Highly Ordered Nanoporous Template from Triblock Copolymer," *ACS Nano* **5**(2), 1207-1214, (2011).
30. W. Chen, X. Y. Wei, A. C. Balazs, K. Matyjaszewski and TPR, "Phase Behavior and Photoresponse of Azobenzene-Containing Polystyrene-block-poly(n-butyl methacrylate) Block Copolymers," *Macromolecules* **44**(5), 1125-1131, (2011).
31. W. Zhao, D. A. Chen, Y. X. Hu, G. M. Grason and TPR, "ABC Triblock Copolymer Vesicles with Mesh-Like Morphology," *ACS Nano* **5**(1), 486-492, (2011).
32. S. W. Hong, X. D. Gu, J. Huh, S. Xiao and TPR, "Circular Nanopatterns Over Large Areas from the Self-Assembly of Block Copolymers Guided by Shallow Trenches," *ACS Nano*, **5**(4), 2855-2860 (2011).
33. L. Li, C. Miesch, P.K. Sudeep, A.C. Balazs, T. Emrick, TPR and R.C. Hayward, "Kinetically Trapped Co-continuous Polymer Morphologies through IntrapHase Gelation of Nanoparticles," *Nano Letters* **11**(5), 1997-2003, (2011).
34. X. Wei, L. Li, J.P. Kalish, W. Chen and TPR, "A Study on the Kinetics of a Disorder-to-Order Transition Induced by Alkyne/Azide Click Reaction," *Macromolecules*, **44**(11), 4269-4275, (2011).
35. S. Xiao, XM Yang, K.Y. Lee, ver der Veerdonk RJ, Kuo D. and TPR, "Aligned Nanowires and Nanodots by Directed Block Copolymer Assembly," *Nanotechnology*, **22**(30), 305302, (2011).
36. H. Lu, B. Akgun and TPR, "Morphological Characterization of a Low-Bandgap Crystalline Polymer: PCBM Bulk Heterojunction Solar Cells," *Advanced Energy Materials*, **1**(5), 870-878, (2011).
37. T C. Wang, D.H. Lee, A. Hexemer, M.I. Kim, W. Zhao, H. Hasegawa, H. Ade and TPR, "Defining the Nanostructured Morphology of Triblock Copolymers Using Resonant Soft X-ray Scattering," *Nano Letters*, **11**(9), 3906-3911, (2011).
38. D. Chen, W. Zhao, D. Wei and TPR, "Dewetting on Curved Interfaces: A Simple Route to Polymer Nanostructures," *Macromolecules*, **44**(20), 8020-8027, (2011).
39. H. Lu, B. Akgun, X. Wei, L. Li, S. Satija and TPR, "Temperature-Triggered Micellization of Block Copolymers on an Ionic Liquid Surface," *Langmuir*, **27**(20), 12443-12450, (2011).
40. Z.M. Al-Badril, R.R. Maddikeril, Y. Zha, H.D. Thaker, P. Dobriyal, R. Shunmugam, TPR and G.N. Tew, "Room Temperature Magnetic Materials from Nanostructured Diblock Copolymers," *Nature Communications* **2**, 486,
41. W. Chen, J.-Y. Wang, W. Zhao, L. Li, X. Wei, A. C. Balazs, K. Matyjaszewski, and TPR, "Photocontrol over the Disorder-to-Order Transition in Thin Films of Polystyrene-block-poly(methyl methacrylate) Block Copolymers Containing Photodimerizable Anthracene Functionality," *Journal of the Am. Chem. Soc.*, **133**(43), 17217 (2011).
42. J. Xu, S.W. Hong, W. Gu, K.Y. Lee, D.S. Kuo, S. Xiao, and TPR, "Fabrication of Silicon Oxide Nanodots with an Areal Density Beyond 1 Teradot/Inch²," *Adv. Mat.*, **23**(48), 5755, (2011)
43. T. Irita, D. Chen, X. Li, J. Wang and TPR, "Thin Films of Semifluorinated Block Copolymers Prepared by ATRP," *Macromol. Chem. Phys.*, **212**, DOI: 10.1002/macp.201100321 (2011).

Patents (2010, 2011)

1. Russell, T.P., Park, S, Xu, T. and Lee D.H., "Self-assembly of block copolymers on topographically patterned polymeric substrates," USA, UMA 0028US, Provisional Application filed 2009.
2. Russell, T.P., Park, S., Wang, J.-Y., Kim, B. "Method of Producing Nanopatterned Articles and Articles Produced Thereby," Application #12566705. Filed 9/25/2009, Published 4/8/2010.

Dielectric Ceramics in Nanosheet Form

Tina T. Salguero, Assistant Professor
Department of Chemistry
University of Georgia
Athens, GA 30602

Program Scope

Nanosheets are characterized as being from one to several monolayers thick and up to tens of micrometers in lateral dimensions. The nanosheet morphology has several unique features that put it at the frontier of materials development, foremost the fact that nanosheets can combine remarkable, quantum effect-derived properties with large surface areas and the advantages of solution-based manipulation methods.

To date, well-defined nanosheets have been derived from lamellar materials via exfoliation processes; examples include selected perovskites, various transition metal oxides and chalcogenides, hexagonal boron nitride, and graphene. We are interested in materials for energy applications that go beyond these examples, specifically oxide ceramics including metal titanates and ruthenates. The important initial challenge is that there is no bulk precursor that can simply be exfoliated to provide nanosheets of these materials. However, when this preparative hurdle is surmounted, the scientific rewards will be substantial. At a fundamental level, these nanosheets will provide an opportunity to better understand the properties of complex oxide ceramics at a size regime down to one monolayer, as well as allow us to study the roles of surface functionalization and interface interactions.

Our approach in this new area of two-dimensional ceramic nanomaterials encompasses synthesis, characterization, and deposition methods. Specifically we propose:

(1) To develop innovative methodologies for preparing dielectric ceramics in nanosheet form. The first step is to prepare dielectric ceramics as nanosheets, a non-natural form of these materials. This synthetic challenge will require novel strategies and techniques encompassing solid-state inorganic chemistry as well as solution-based modification and processing. Our innovation is to apply topotactic chemical transformations to pre-existing nanosheet starting materials, which will enable us to prepare metal titanates $MTiO_3$ and ruthenates $MRuO_3$ in nanosheet form. We further plan to develop ways to scale-up the preparation of exceptional nanosheet materials as they are identified.

(2) To characterize the fundamental properties of dielectric ceramic nanosheets. Our innovation is to use the unique combination of morphology and surface functionalization of monolayer-thick ceramic nanosheets to tune their dielectric properties, and we fully expect to identify nanosheets with remarkable permittivity properties.

(3) To process dielectric ceramic nanosheets via solution-based techniques. We propose two ways to assemble and deposit nanosheet materials. The first is inkjet printing of nanosheet inks; because nanosheets typically exhibit liquid crystal properties, the solid components will be well-ordered when the ink dries, which leads to high-quality (near crystalline) materials. The second way is to use dielectric ceramic nanosheets in the assembly of layered, hybrid, and composite macroscale materials. The concept of nanosheet building blocks is based on bottom-up assembly strategies that will allow us to create novel materials with dielectric ceramic nanosheet components. Such well-ordered materials can contain tailored interfaces between

dissimilar materials, controlled layer thicknesses, gradients, varied nanosheet dimensionality (flat vs. crumpled), and so on. In addition, solution-based approaches will enable the preparation of macroscale samples on large and/or flexible substrates at ambient conditions.

Recent Progress

In preliminary studies, we have found reaction conditions that allow us to transform TiO_2 nanosheets into SrTiO_3 and BaTiO_3 nanosheets. Representative scanning electron microscopy (SEM) and transmission electron microscopy (TEM) images are shown in Figure 1 for SrTiO_3 and Figure 2 for BaTiO_3 . Both the SrTiO_3 and BaTiO_3 nanosheets exhibit a crumpled morphology. The SrTiO_3 nanosheets display poor crystallinity due to imperfect nanosheet re-stacking. In contrast, the BaTiO_3 nanosheets are well ordered, and preliminary diffraction as well as Raman spectroscopy results indicate that the crystallographic structure is tetragonal in nature. This is surprising in light of the “Curie point depression” effect often seen for BaTiO_3 nanoparticles. Atomic force microscopy (AFM) measurements provide a BaTiO_3 nanosheet thickness of 1.7 nm (Figure 3).

Future Plans

In the upcoming year of work, we plan to study the properties of SrTiO_3 and BaTiO_3 nanosheets and extend the synthetic methodology to other MXO_3 materials, particularly PbTiO_3 and SrRuO_3 .

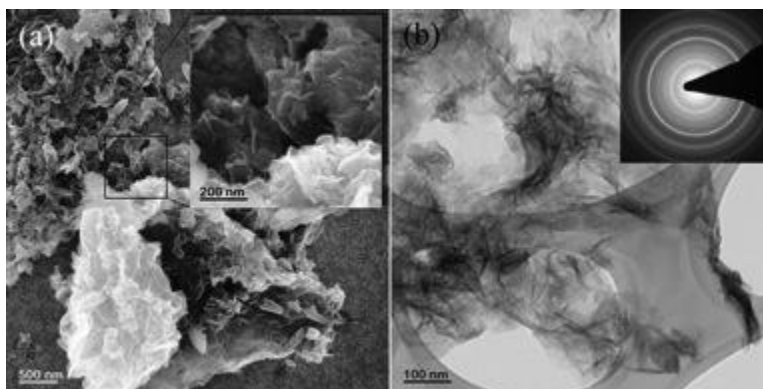


Figure 1. SEM (a) and TEM (b) images of SrTiO_3 nanosheets.

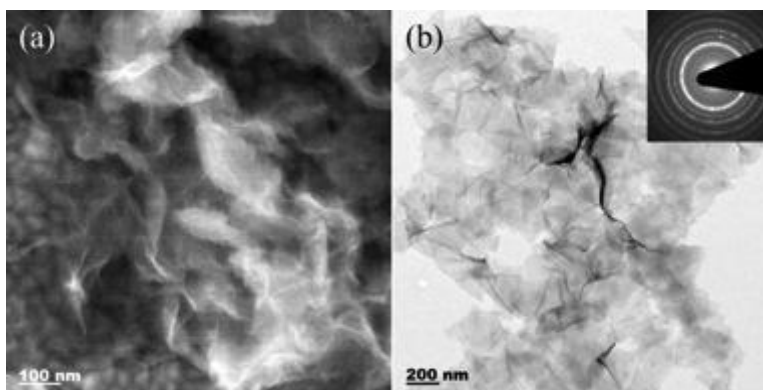


Figure 2. SEM (a) and TEM (b) images of BaTiO_3 nanosheets.

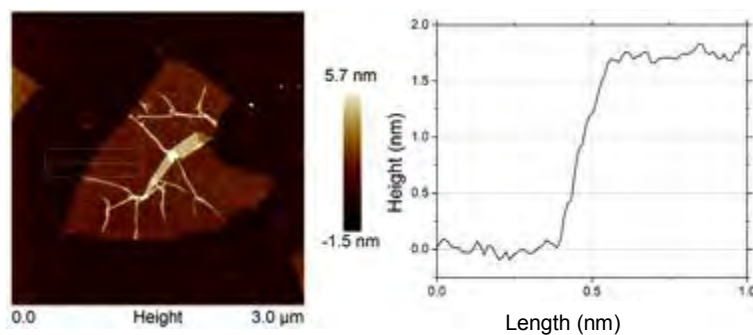


Figure 3. AFM image and height profile of a BaTiO_3 nanosheet.

Luminescence in Conjugated Molecular Materials under Sub-bandgap Excitation

Franky So
Department of Materials Science and Engineering
University of Florida

Program Scope

To achieve electroluminescence (EL) in an organic light-emitting diode (OLED), electrons and holes have to be injected into the emissive layer to form excitons or bound electron-hole pairs. The voltage applied across the OLED should be equal to the difference of the electron and hole quasi-Fermi levels of the semiconductor divided by the electron charge. Light emission is not normally observed until the applied voltage reaches the bandgap voltage of the semiconductor, which is defined as the bandgap energy, or for organic materials the lowest unoccupied molecular orbital (LUMO) and the highest occupied molecular orbital (HOMO) bandgap energy divided by e . However, we have previously demonstrated that a light emitting diode can be turned on at a voltage below its bandgap voltage when ZnO nanoparticles (NPs) are used as the electron transport layer. This sub-bandgap turn-on voltage is attributed to an Auger-assisted energy up-conversion process at the polymer/ZnO NP hetero-interface, i.e., the energy released from the non-radiative recombination of a hole in the polymer HOMO and an electron in the ZnO NP conduction band is transferred to an Auger electron in ZnO so that it has sufficiently high energy to inject into the LUMO level of the polymer. The efficiency of the energy up-conversion process depends strongly the nature of ZnO NPs. For example, the lowest turn-on voltage was observed in devices employing 2~3 nm size ZnO NPs. However, using sol-gel ZnO, sub-bandgap luminescence was not observed. The objective of this present work is to understand the electronic structure of these ZnO nanostructures and how they affect the carrier dynamics. Here, we studied the properties of both colloidal ZnO NPs and sol-gel ZnO nano-clusters, and determined how surface treatment affects their electronic properties and the resulting devices.

Recent Progress

Figure 1 show the transmission electron micrographs of the colloidal ZnO NPs used in this work. In order to study the properties of ZnO NPs, we used polymer solar cells as a testing vehicle. It is known that up to 30% of the atomic bonds in ZnO NPs are dangling bonds¹ and these defects give rise to a high density of recombination centers resulting in low power conversion efficiencies in these cells.

In order to passivate these colloidal ZnO NPs films, they are exposed to UV light at 254 nm after first annealing at 80 °C. The passivation effect on ZnO NP films by this UV ozone (UVO)

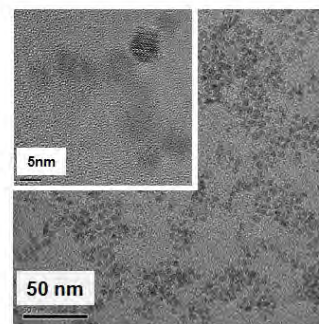


Figure. 1. TEM image of ZnO NPs

treatment was investigated by photoluminescence measurements. As shown in Figure 2a, in addition to the band-to-band emission of the ZnO NPs film at 372 nm, a strong broad emission band with a maximum at 519 nm was also observed for the untreated films and this emission band is known as an evidence of the presence of defect states in ZnO. It should be noticed that the defect emission band was not observed in the sol-gel ZnO films, indicating that the defect states are not present in the ZnO sol-gel films² as shown in Figure 2b. Upon UVO treatment, however, this broadband defect emission is effectively quenched, indicating a significant reduction of defects states. As a result, due to the reduction of the defect states emission, the band-to-band emission peaked at 372 nm peak increases in intensity. It should be also noted that the UVO treatment does not only treat the ZnO films surface, it also passivates the defects in the bulk due to the porosity of the ZnO NPs films, as the PL signal is coming from both bulk rather than just the surface. The passivation mechanism here is believed to be correlated with the reduction of oxygen vacancies by the penetration of oxygen in the NPs films.

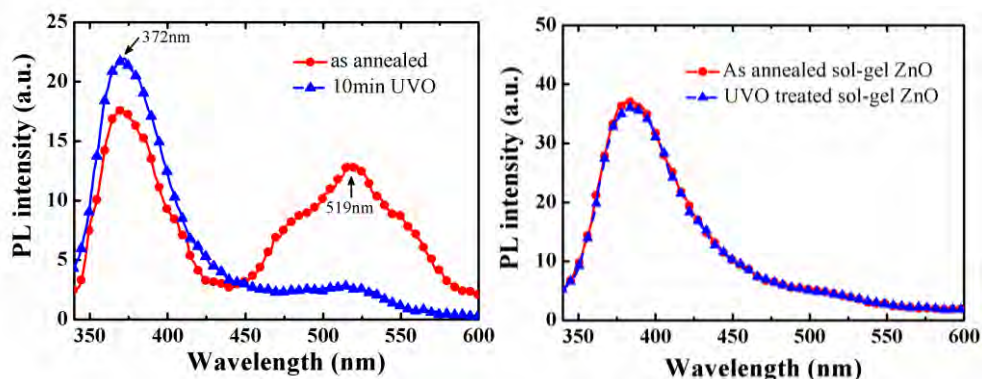


Figure 2. Photoluminescence spectra of colloidal film (a) and sol-gel film (b) before and after UVO treatment.

To study the effect of passivation on carrier lifetime, transient photo-current (TPC) measurements were carried out to study the photo-carrier decay dynamics of a bulk heterojunction polymer solar cell under an extraction field. During the measurements, the active layer of the device was photo-excited by a pulsed laser with an emission power attenuated to $\sim 10^2$ nJ pulse⁻¹ cm⁻², making sure the perturbation photocurrent < 0.1 mA/cm², while the sample was also under a constant illumination from a solar simulator. Since the pulse laser source, which emits at 527 nm, does not excite the ZnO NPs, photo-generated carriers due to the laser pulse only come from the polymer:fullerene blend. The photocurrent transient was measured by probing the voltage signals across a 30 Ω resistor connected in series with the solar cell, simulating the short circuit condition. The single exponential decay of the transient photocurrents perturbation for the inverted cells with treated and untreated ZnO NPs films, as shown in Figure 3a, is due to photo-generated carriers recombining either in the bulk or at the ZnO/photo-active layer interface. Determined from the photocurrent perturbation decay curves, the effective photo-carrier lifetimes are 130 ns and 210 ns for the untreated and UVO treated devices respectively. Since these devices have the same hole extraction contact and photo-active layer with identical transport properties, the difference in carrier lifetime must be attributed to

the difference in carrier recombination rate at the ZnO/photo-active layer interface. Moreover, at short circuit condition, bulk recombination is unlikely to be the dominant loss mechanism and usually shows a lifetime longer than 10 μ s since carriers are fairly depleted and extracted to the electrodes under an internal field $\sim 10^5$ V/cm. However, due to the presence of defects in the ZnO NPs, the photo-carriers excited by the laser pulse still recombine at a much faster rate via these mid-gap states at the ZnO/polymer interface. It should be mentioned that such a change of photocurrent transient was not observed in the devices made by the sol-gel ZnO in which defects emission was not observed. From the results of our transient photocurrent measurements, we conclude that defects in the ZnO colloidal NPs films are passivated by the UVO treatment which results in an increase in carrier lifetime.

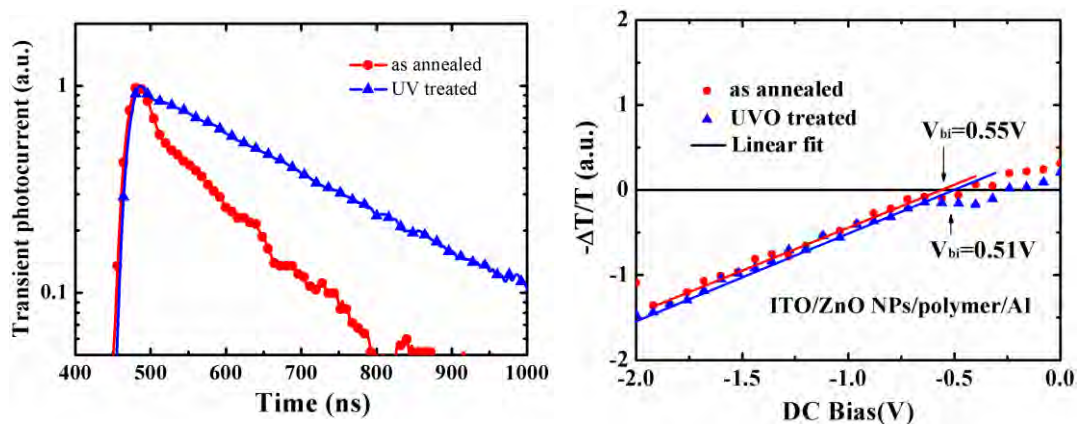


Figure 3. (a) Transient photo-current decay for the devices with as annealed and UV treated ZnO NP films. (b) DC bias dependence of electroabsorption signal of the two devices. The arrows mark the built-in potentials of the ZnO NPs/polymer/Al structure.

To understand how the UVO treatment affects the interface energetics, electroabsorption (EA) was done on samples with and without treatment. Figure 3b shows that the first harmonic EA signals vary linearly with the applied voltage bias until the internal field reaches zero. The flat band condition is reached when the DC bias compensates the built-in potential (V_{bi}) which is determined by the work function difference between the ZnO NPs layer and the top electrode. With UVO treatment on the ZnO NPs, as shown in Figure 3b, the built-in potential of the ZnO NPs/ polymer/ Al device only changes from 0.55 eV to 0.51 eV, indicating the change in interface energetics is small due to the UVO treatment on ZnO NPs.

To see the effect of UVO treatment on the final device performance, inverted polymer solar cells were fabricated based on poly-dithieno[3,2-b:2',3'-d]germole thieno[3,4-c]pyrrole-4,6-dione (PDTG-TPD)³. The device structure and the structure of PDTG-TPD are shown in Figure 4a and 4b, respectively. The external quantum efficiency (EQE) spectra for these cells are illustrated in Figure 4c. As shown by the EQE spectra, a maximum value of 72% at 675 nm is observed for the UVO treated PDTG-TPD cell while the maximum EQE for the untreated cell is 60%. This enhancement in EQE does confirm the passivation of ZnO NPs leading to reduction in carrier recombination in the resulting device.

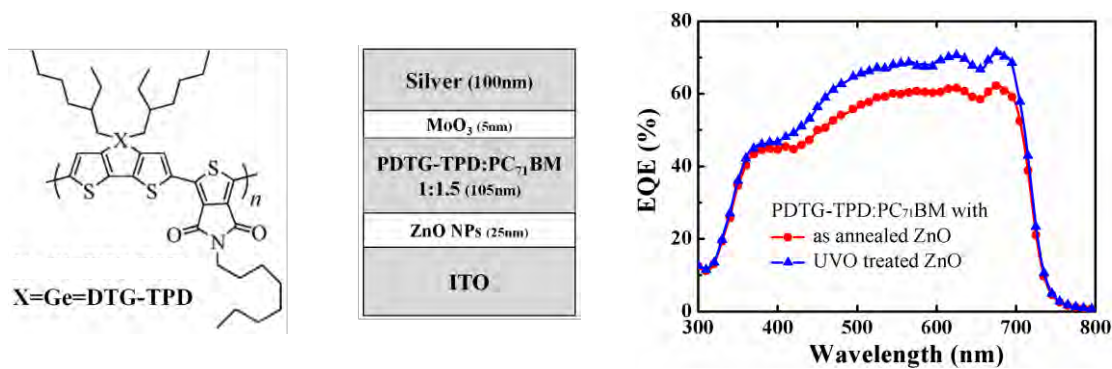


Figure 4. (a) Chemical structure of PDTG-TPD. (b) Inverted solar cell device structure. (c) External quantum efficiencies of as anneal and UVO treated cells.

Future Plans

We will focus on how passivation of ZnO defects affects the sub-bandgap luminescence. In addition to UVO treatment, sub-bandgap luminescence using fullerene and fullerene passivated ZnO will be studied.

References

1. V. A. Fonoberov, K. A. Alim, A. A. Balandin, F. X. Xiu, J. L. Liu, *Physical Review B* **2006**, *73*, 165317.
2. C. E. Small, S. Chen, J. Subbiah, C. M. Amb, S. W. Tsang, T. H. Lai, J. R. Reynolds, F. So, *Nature Photonics* **2012**, *6*, 115.
3. C. M. Amb, S. Chen, K. R. Graham, J. Subbiah, C. E. Small, F. So, J. R. Reynolds, *Journal of the American Chemical Society* **2011**, *133*, 10062.

Publications

1. S. Chen, K. Roy Choudhury, J. Subbiah, C.A. Amb, J.R. Reynolds and F. So, "Photo-Carrier Recombination in Polymer Solar Cells Based on P3HT and Silole-Based Polymer, *Adv. Energy Mater.* *1*, 963-969 (2011).
2. C.E. Small, S. Chen, J. Subbiah, C.M. Amb, T.H. Lai, S.W. Tsang, J.R. Reynolds, F. So, "High Efficiency Inverted Dithienogermole-Thienopyrrolodione Based Polymer Solar Cells", *Nature Photonics* *6*, 115-120(2012).
3. C.E. Small, S.W. Tsang, J. Kido, S.K. So, and F. So, "Study of charge injection in inverted organic unipolar devices using n-type hole injection layers", *Adv. Funct. Mater.* DOI: 10.1002/adfm.201200185 (2012)
4. S. Chen, C.E. Small, C.A. Amb, J. Subbiah, T.-H. Lai, S.W. Tsang, J. Manders, J.R. Reynolds, and F. So, "High efficiency inverted polymer solar cells with reduced interface recombination", *Adv. Energy Mater.* Accepted for publication.
5. S. Chen, S.W. Tsang, C.E. Small, J.R. Reynolds, F. So, "Inverted polymer solar cells", Invited paper, accepted for publication in *IEEE Photonics Journal* (2012).
6. S. Chen, J. Manders, S.W. Tsang, C.E. Small, J.R. Reynolds and F. So, "Metal oxides for organic solar cells", Invited review paper, *J. Mater. Chem.* (2012).

“Nanoscale Materials and Architectures for Energy Conversion”

Principal Investigator: Mahendra K. Sunkara, University of Louisville, Louisville, KY 40292, mahendra@louisville.edu; Madhu Menon (co-PI), University of Kentucky, Lexington, KY 40508.

PROGRAM SCOPE: This project specifically addresses the development and use of nanowire based structures toward creating new semiconductors and understanding fundamental processes occurring during the conversion of light and thermal energy to electronic and stored chemical energy. In this project, we proposed to create tailored one-dimensional semiconductor nanostructures and new semiconductor materials guided by computational predictions. Fundamental material properties such as photogeneration of electron/hole pairs, electron and hole transport, electron/hole recombination and thermionic emission are being investigated. Nanowire array platforms offer several advantages in terms of improving the transport of photogenerated carriers and also in creating single crystal layers of new materials. First principles computations are employed to understand electronic properties for discovery of new alloys based on III-nitrides. The experimental effort is guided by computational results toward creating new materials,

especially for solar fuels where no material has been yet discovered that meets all the essential criteria. Figure 1 illustrates the interesting properties of semiconducting nanowires such as: (a) fast surface charge transport characteristics for photogenerated carriers and low recombination in solar cells [1, 2]; (b) smaller diffusion length scales for reacting species toward doping/phase transformation [3]; and (c) short diffusion length scales for minority carriers for photoelectrochemical applications [4, 5]. In addition, the nanowires are being utilized as semi-rigid and strain relaxing substrates for producing thick crystalline layers necessary for photoelectrochemical applications.

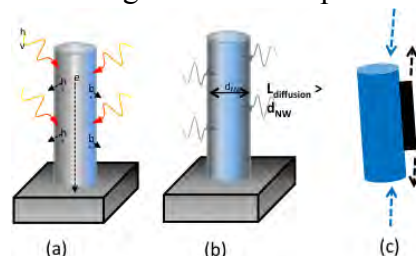


Figure 1. Nanowire architectures for energy conversion and synthesis of new materials: (a) smaller diffusional length scales for minority carriers; (b) smaller length scales for reaction with gas phase species; and (c) nanowires as substrates for growing crystalline layers of various materials.

RECENT PROGRESS:

1. Phase Transformations in Nanowires – Kirkendall effect to single crystal transformation: Nanowires potentially offer the advantage of tuning the material composition because the nanowire diameters are on the same order of reactant diffusion lengths. Prior phase transformation studies from our group showed the importance of nanowire diameter for phase transformation of tungsten oxide to tungsten nitride [3]. Recently, we studied the role of reactant species on phase transformation in nanowires such as sulfurization using hydrogen sulfide. Using MoO₃ nanowire arrays, we were able to produce core-shell structure of MoO₃-MoS₂ NWs that were shown to be excellent electrocatalysts for hydrogen evolution reaction [6]. Most importantly, the sulfurization of hematite nanowires resulted in single crystal – single crystal transformations when the nanowires were less than 20 nm in diameter. The sulfurization of thicker nanowires exhibit clear phenomena of Kirkendall effect in which iron from core diffused out and reacted with sulfur on the shell to produce pyrite type FeS_x crystals (Figure 3). The overall result is that the cores become completely hollow with walls composed of highly oriented FeS_x. The observation of Kirkendall effect under sulfurization is first of its kind and

opens up a set of interesting possibilities, i.e., to produce hollow nanotubes of various materials systems. For example, we can re-oxidize the resulting tubular structures to produce hollow, hematite one-dimensional structures while doping them using appropriate gas phase precursors.

3. III-Nitride Ternary Alloys: Epitaxial growth on planar substrates has been pursued for creating single crystal layers of materials. Such hetero-epitaxy onto planar substrates leads to phase segregation and misfit dislocations due to lattice mismatch-induced stresses and strain. Here, we showed that using hetero-epitaxy on nanowire substrates, one can grow thick layers without phase segregation. Specifically, using hetero-epitaxy, we were able to obtain single crystalline layers of $\text{In}_x\text{Ga}_{1-x}\text{N}$ alloys with composition over the entire range for indium from 0 to 100%.

The results suggest that the hetero-epitaxial growth on sub-30 nm sized nanowires is effective toward obtaining thick layers of InGaN alloys with control on composition over entire range. The as-grown, thick single crystalline $\text{In}_x\text{Ga}_{1-x}\text{N}$ layers have been shown to be photoactive with onset potentials consistent with the indium content ($x > 0.4$).

Photovoltage measurements on GaN nanowires and InGaN on GaN nanowires made on sapphire substrates have been measured. The OCP for GaN is -0.14V and for InGaN/GaN is 0.29 V (both w.r.t. SHE), indicating the difference in the conduction band edges. This is further confirmed in the photocurrent measurements shown in figure 4c and 4d where GaN NWs show a photocurrent onset at 0.1 V wrt Ag/AgCl while InGaN/GaN an onset potential of 0.4 V wrt. Ag/AgCl. As shown in the band lineup schematic in figure 4e, GaN has a conduction band edge about 0.4 – 0.6 V wrt SHE while a 60:40 InGaN alloy has the conduction band edge about - 0.3- - 0.5 V wrt SHE (a gap of ~ 0.5 V). This trend is consistent with results obtained on the GaN NWs and InGaN/GaN electrodes indicated in figure 4e with dark circles. The amount of photocurrent is limited due to non-conductivity of underlying substrate and the limited conduction from contact area. We are currently investigating the use of metallic substrates such as steel and thin

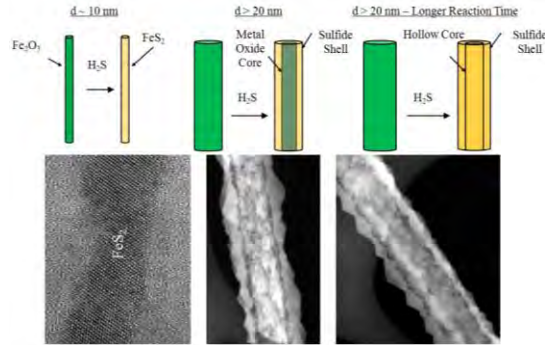


Figure 3. Sulfurization reaction with oxide nanowires illustrating kirkendall effect to produce hollow, one-dimensional structures.

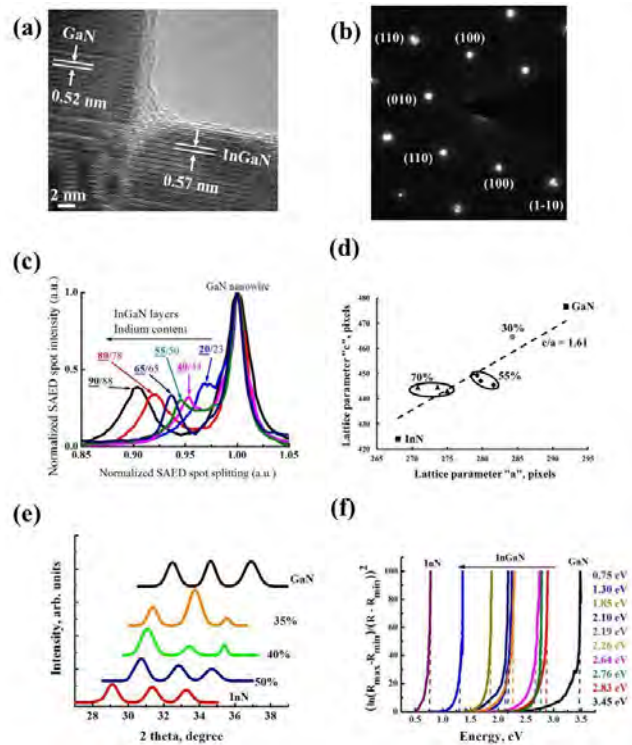


Figure 4. a) HRTEM image of the InGaN growth on GaN nanowires. b) SAED image of the InGaN growth on GaN nanowires showing the observed peak splitting. c) Compilation of the intensity profiles from SAED spot patterns of InGaN alloys showing the range of compositions synthesized. d) Compilation of the measured alloy compositions from lattice spacing measured from the CBED images. e) XRD patterns from InN, GaN and the range of InGaN compositions synthesized f) Band gap of the various InGaN compositions synthesized measured via diffuse reflectance.

GaN layers as protective coatings to improve the photoactivity. Theoretical computational studies predicted that dilute alloys of GaN with Sb (1-2 at%) can have the right band gap and band edge energetics for solar fuels. We made significant progress using metal organic chemical vapor deposition with synthesis of such alloys on planar substrates and are currently being investigated for the presence of antimony at low concentrations.

4. Tin Oxide Nanowire Based Hybrid Structures for Dye Sensitized Solar Cells – Alternate Redox Couples:

The commonly used iodide/tri-iodide redox electrolyte cannot be used for practical applications due its corrosive nature, toxicity, competition between tri-iodide and the dye for light absorption, high vapor pressure of iodine, association of tri-iodide with dye result in recombination losses. Alternate redox couples that can overcome these limitations are of significant interest for replacing the conventional iodide based electrolytes. However, several of these redox electrolytes cannot be used in nanoparticle (NP) based DSCs due to fast recombination kinetics of the electrons in nanoparticles with the oxidized species in electrolyte. Previously, our group showed that tin oxide nanowires exhibit, faster electron transport rates and lower electron recombination rates when compared to titania nanoparticles for DSCs using iodide/tri-iodide as redox electrolyte. [1,2]

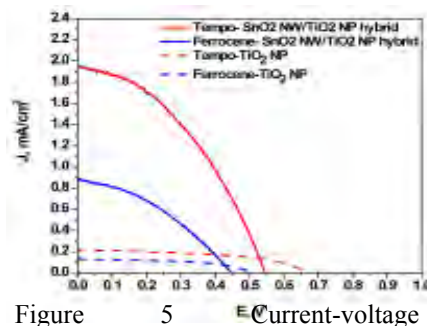


Figure 5 Current-voltage characteristics of SnO₂ NW / TiO₂ NP hybrid architectures and TiO₂ NP for tempo and ferrocene redox couples (1 Sun).

Recently, we investigated the use of tin oxide nanowires (NW) and their hybrid architectures to achieve significant improvement in the photovoltaic performance beyond that of nanoparticle based DSCs, when these alternate redox electrolytes are used. Attempts to lower the interfacial recombination rate have used passivating layers of Al₂O₃ or poly(methyl siloxane) on the nanoparticle surfaces, creating an overpotential for the recombination reaction to occur. [7, 8] Slow electron transport in nanoparticle networks results in low electron collection and hence the limits high photocurrent from being achieved. Significant enhancement in photocurrents can be achieved using hybrid architectures of SnO₂ NW coated with titania NP as shown in Figure 5.

4. FUTURE PLANS

On-going efforts include the following. (i) Investigate kirkendall effect during reactions involving sulfur, oxygen and other species with various kinds of nanowires; (ii) Synthesize dilute GaN alloys (specifically GaSbN) and InGaN alloys on both planar and nanowire substrates with proper back contact; and understand their electrical, optical and photoelectrochemical behavior; (iii) Understand fundamental charge transport and recombination kinetics with tin oxide nanowire based heterostructures when using redox couples other than iodide couple.

References

1. S. Gubbala, et al., Band-edge engineered hybrid structures for dye-sensitized solar cells based on SnO₂ nanowires. *Adv. Funct. Mater.*, 2008. **18**(16): p. 2411-2418.
2. S. Gubbala, et al., Surface properties of SnO₂ nanowires for enhanced performance with dye-sensitized solar cells. *Energy & Environ. Sci.*, 2009. **2**(12): p. 1302-1309.
3. J. Thangala, et al., Phase Transformation Studies of Metal Oxide Nanowires. *Crystal Growth & Design*, 2009. **9**(7): p. 3177-3182.

4. M.K. Sunkara, et al., Inorganic nanowires: a perspective about their role in energy conversion and storage applications. *J. Phys.*, 2011(Special Issue).
5. B. Chernomordik, et al., Photoelectrochemical activity of α -Fe₂O₃ nanowire array electrodes. 2010.
6. Z. Chen, et al., Core-shell MoO₃-MoS₂ Nanowires for Hydrogen Evolution: A Functional Design for Electrocatalytic Materials. *Nano Lett.*, 2011. DOI: 10.1021/nl2020476.
7. T.W. Hamann, O.K. Farha, and J.T. Hupp, Outer-Sphere Redox Couples as Shuttles in Dye-Sensitized Solar Cells. Performance Enhancement Based on Photoelectrode Modification via Atomic Layer Deposition. *J. of Phys. Chem. C*, 2008. 112(49): p. 19756-19764.
8. S.M. Feldt, et al., Characterization of Surface Passivation by Poly(methylsiloxane) for Dye-Sensitized Solar Cells Employing the Ferrocene Redox Couple. *Journal of Physical Chemistry C*, 2010. 114(23): p. 10551-10558.

5. SELECTED PUBLICATIONS RESULTING FROM DOE SUPPORT

1. C. Pendyala, J. H. Kim, J. B. Jasinski and M. K. Sunkara, "Nanowires as semi-rigid substrates for growth of thick, In_xGa_{1-x}N (x>0.4) epi-layers without phase segregation for photoelectrochemical water splitting", Submitted (2012).
2. B. Chernomordik, H. B. Russell, U. Cvelbar, J. B. Jasinski, V. Kumar, T. Deutsch, and M. K. Sunkara, "Photoelectrochemical activity of as-synthesized, α -Fe₂O₃ nanowire array electrodes for water splitting", *Nanotechnology* 23, 194009 (2012).
3. Z. Chen, D. Cummins, E.L. Clark, B. Reinecke, M.K. Sunkara, and T.F. Jaramillo, "Core-shell MoO₃-MoS₂ Nanowires for Hydrogen Evolution: A Functional Design for Electrocatalytic Materials", *Nano Letters*, 11 (10), pp 4168-4175 (2011).
4. L. Brockway, C. Pendyala, M.K. Sunkara, and S. Vaddiraju, " A post-synthesis decomposition strategy for Group III nitride quantum wires", *Crystal Growth and Design*, 11 (10), 4559-4564 (2011).
5. V. Kumar, J-H. Kim, J.B. Jasinski, E.L. Clark, and M.K. Sunkara, (2011) "Alkali assisted, atmospheric plasma production titania nanowire powders and arrays", *Crystal Growth and Design*, 11 (7), 2913 (2011).
6. M K Sunkara, C Pendyala, D Cummins, P Meduri, J. Jasinski, V Kumar, H B Russell, E L Clark, and J H Kim, "Inorganic nanowires: a perspective about their role in energy conversion and storage applications", *J. Phys. D: Appl. Phys.*, 44 (17), 174032 (2011).
7. J.B. Jasinski, S. Dumpala, G.U. Sumanasekera, M.K. Sunkara, and P.J. Ouseph, "Transmission Electron Microscopy Study of Moire Patterns of Few Layer Graphene", *Appl. Phys. Lett.*, 99, 073104 (2011).
8. S. Dumpala, J.B. Jasinski, G.U. Sumanasekera and M.K. Sunkara, "Synthesis of Conical Carbon Nanotube Arrays: Mechanistic Aspects and Growth on Foil Substrates", *Carbon*, 49(8), 2725-2734 (2011).
9. R.M. Sheetz, E. Richter, A.N. Andriotis, C. Pendyala, M.K. Sunkara and M. Menon, "Visible light absorption and large band gap bowing in dilute alloys of gallium nitride with antimony", *Phys. Rev. Lett.*, 84, 075304 (2011).
10. K. Ostrikov, I. Levchenko, U. Cvelbar, M.K. Sunkara and M. Mozetic, "From nucleation to nanowires: a single step process", *Nanoscale*, 2, 2012 (2010).
11. C. Pendyala, S. Vaddiraju, J-H. Kim, J. Jasinski, Z.Q. Chen and M.K. Sunkara, "Self nucleation and growth of Group III-antimonide nanowires", *Semicond. Sci. and Technol.*, 25, 024014 (2010).
12. Z. Chen, T. F. Jaramillo, T. G. Deutsch, A. Kleiman-Shwarsstein, A. J. Forman, N. Gaillard, R. Garland, K. Takanabe, C. Heske, M. Sunkara, E. W. McFarland, K. Domen, E. L. Miller, J. A. Turner, H. N. Dinh, "Accelerating materials development for photoelectrochemical (PEC) hydrogen production: Standards for methods, definitions, and reporting protocols", *J. Mater. Res.*, 25, No. 1, 3-16 (2010).

Bimetallic electrochemical displacement materials yielding high energy, high power, and improved reversibility

SUNY Distinguished Professor Esther S. Takeuchi, SUNY Distinguished Teaching Professor Kenneth J. Takeuchi, Research Assistant Professor Amy C. Marschilok

Program Scope

Bimetallic oxides ($M_xM'_yO_z$) and phosphorous oxides ($M_wM'_xP_yO_z$) are materials worthy of investigation as cathodes for secondary lithium batteries. Through appropriate material design, one metal (M^+) will be electrochemically reduced to form conductive metallic nanoparticles, while the second metal (M'^{n+}) will provide a framework that will enable reversible electron transfer.

Through targeted design, preparation, and electrochemical study of novel bimetallic electrochemical displacement materials, this project will contribute to the knowledge base that is needed to address the practical demands of energy storage systems. This project will fundamentally advance the three key performance metrics for energy storage: energy density, power delivery, and reversibility.

Recent Progress

Recent progress associated with the preparation, characterization, electrochemical evaluation of three materials will be described herein.

$Ag_2VO_2PO_4$

Nanocrystalline materials are desirable for electrochemical energy storage applications, as the high surface area enables fast ion diffusion and rapid electron transfer. However, structural and coordination environment characterization using conventional methods can be challenging, making it difficult to monitor structural changes upon lithiation of nanocrystalline materials. X-ray absorption spectroscopy methods such as x-ray absorption fine structure (XAFS), x-ray absorption near edge structure (XANES), and extended x-ray absorption fine structure (EXAFS) measurements can be powerful tools for mechanistic interrogation.

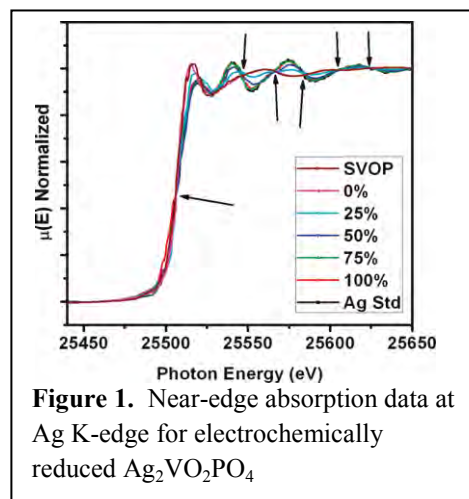


Figure 1. Near-edge absorption data at Ag K-edge for electrochemically reduced $Ag_2VO_2PO_4$

Using a combination of V K-, V L-, Ag K-, and O K-edge x-ray absorption fine structure (XAFS) spectroscopy, with XANES and EXAFS measurements, we determined the local vanadium and silver oxidation states, local coordination geometry, and stoichiometry for $\text{Ag}_2\text{VO}_2\text{PO}_4$ samples with varying extents of lithiation.

A comparison of the peak positions of discharged $\text{Ag}_2\text{VO}_2\text{PO}_4$ samples with the undischarged material and a silver metal standard, was undertaken (Figure 1). The data show five discrete isosbestic points suggesting the transformation of Ag^+ ions in $\text{Ag}_2\text{VO}_2\text{PO}_4$ to metallic $\text{Ag}^0_{(s)}$ without stabilization of any detectable intermediate Ag-containing phases. By comparing the peak positions of discharged $\text{Ag}_2\text{VO}_2\text{PO}_4$ samples with known binary vanadium oxide standards, a vanadium oxidation state of 4.64 ± 0.18 was deduced for the sample at 25% depth of discharge (Figure 2). During the initial two discharge steps, the contributions from Ag^0 were determined to be $31 \pm 6\%$ at 25% DOD and $59 \pm 5\%$ at 50% DOD. These results were significant as they confirmed that while reduction of Ag^+ was the predominant initial process upon discharge of $\text{Ag}_2\text{VO}_2\text{PO}_4$, some reduction of V^{5+} and V^{4+} was also occurring in parallel.

$\text{Ag}_{0.48}\text{VOPO}_4$

The electrochemistry of $\text{Ag}_{0.48}\text{VOPO}_4 \cdot 1.9\text{H}_2\text{O}$ was examined by reduction of the material versus lithium metal in an experimental cell. The discharge curve showed two voltage plateaus, the first at 3.7 V and second at 3.2 V.

The first higher voltage plateau is consistent with reduction by ~ 0.3 electron equivalents per formula unit, while the second plateau is consistent with ~ 0.6 electron equivalents. Thus, the overall reduction of $\text{Ag}_{0.48}\text{VOPO}_4 \cdot 1.9\text{H}_2\text{O}$ takes place by the addition of ~ 0.9 electron

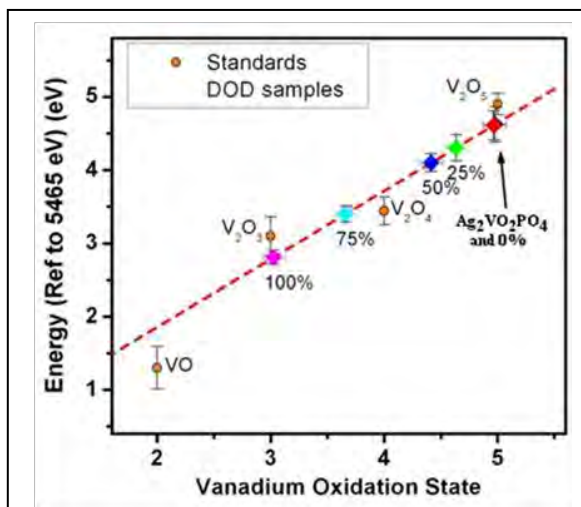


Figure 2. XAFS determination of the formal vanadium oxidation states of $\text{Ag}_2\text{VO}_2\text{PO}_4$ with varying extents of electrochemical lithiation

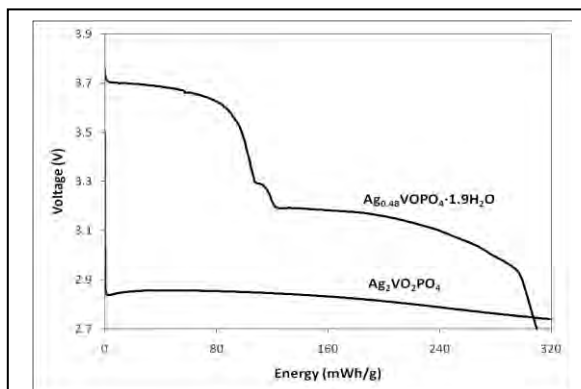


Figure 3. Discharge of Li / $\text{Ag}_2\text{VO}_2\text{PO}_4$ and Li / $\text{Ag}_{0.48}\text{VOPO}_4$ electrochemical cells

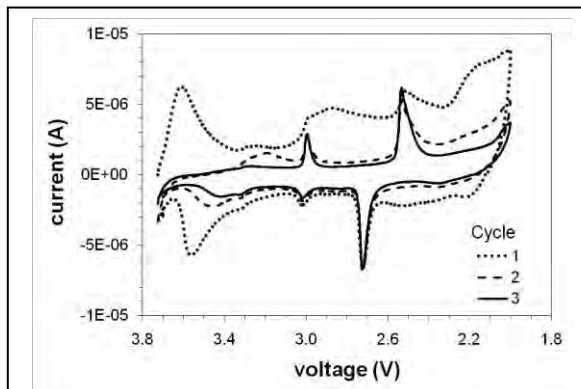


Figure 4. Cyclic voltammetry of $\text{Ag}_{0.48}\text{VOPO}_4$

equivalents in the two plateaus and a total of 1.26 electrons above 2.0 V. The voltage profile and specific energy of lithium cells containing $\text{Ag}_{0.48}\text{VOPO}_4 \cdot 1.9\text{H}_2\text{O}$ was compared with that of cells containing $\text{Ag}_2\text{VO}_2\text{PO}_4$ (Figure 3). Operating voltages of the $\text{Ag}_{0.48}\text{VOPO}_4 \cdot 1.9\text{H}_2\text{O}$ material were significantly higher, with $> 300 \text{ mWh g}^{-1}$ delivered above 2.9 V. Notably, the $\text{Ag}_{0.48}\text{VOPO}_4$ material displayed initial voltages even higher those of $\text{Ag}_2\text{V}_4\text{O}_{11}$.

Electrochemical reversibility was investigated by slow scan voltammetry using a three electrode configuration with lithium reference and auxiliary electrodes (Figure 4). The first reductive scan is complex with a series of cathodic peaks that appear at 3.6, 3.5, 2.9, 2.5, and 2.2 V. The reverse scan revealed a series of anodic peaks at voltages of 2.2, 2.7, 3.0, 3.3, and 3.5 V. While the broad peaks indicate some level of quasi-reversibility in the first scan, scan 2 and subsequent scans appear very different as two narrow major peaks appear at 3.0 V and 2.5 V on the cathodic scan and 2.7 V and 3.0 V on the anodic scan. These peaks remain consistent with further cycling, indicating that the $\text{Ag}_{0.48}\text{VOPO}_4$ material does display moderate rechargeability.

Future Plans

Future plans include synthesis, characterization and investigation of the electrochemistry of new $\text{M}_x\text{M}'_y\text{O}_z$ and $\text{M}_w\text{M}'_x\text{P}_y\text{O}_z$ materials, and including further probing of the discharge mechanisms of bimetallic materials.

References

1. Takeuchi, Esther S.; Marschilok, Amy C.; Tanzil, K.; Kozarsky, Eric S.; Zhu, Shali; Takeuchi, Kenneth J. *Chemistry of Materials*. **2009**, *21*, 4934-4939.
2. Patridge, Christopher J.; Jaye, Chernob; Abteu, Tesfaye A.; Ravel, Bruce; Fischer, Daniel A.; Marschilok, Amy C.; Zhang, Peihong; Takeuchi, Kenneth J.; Takeuchi, Esther S.; Banerjee, Sarbajit. *Journal of Physical Chemistry C*. **2011**, *115*, 14437-14447.
3. Kim, Young Jin; Lee, Chia-Ying; Marschilok, Amy C.; Takeuchi, Kenneth J.; Takeuchi, Esther S. *Journal of Power Sources*. **2011**, *196*, 3325-3330.
4. Zhu, Shali; Marschilok, Amy C.; Lee, Chia-Ying; Takeuchi, Esther S.; Takeuchi, Kenneth J. *Electrochemical and Solid State Letters*. **2010**, *13*(8), A98-A100.
5. Marschilok, Amy C.; Yau, Shali Z.; Menard, Melissa C.; Takeuchi, Esther S.; Takeuchi, Kenneth J. *submitted*.
6. Marschilok, Amy C.; Kim, Young Jin; Takeuchi, Kenneth J.; Takeuchi, Esther S. *submitted*.

Publications

1. Zhu, Shali; Marschilok, Amy C.; Lee, Chia-Ying; Takeuchi, Esther S.; Takeuchi, Kenneth J. *Electrochemical and Solid State Letters*. **2010**, *13*(8), A98-A100.
2. Zhu, Shali; Marschilok, Amy C.; Takeuchi, Esther S.; Yee, Gordon T.; Wang, Guangbin; Takeuchi, Kenneth J. *Journal of the Electrochemical Society*. **2010**, *157*(11), A1158-A1163.
3. Patridge, Christopher J.; Jaye, Cherno; Abtey, Tesfaye A.; Ravel, Bruce; Fischer, Daniel A.; Marschilok, Amy C.; Zhang, Peihong; Takeuchi, Kenneth J.; Takeuchi, Esther S.; Banerjee, Sarbajit. *Journal of Physical Chemistry C*. **2011**, *115*, 14437-14447.
4. Lee, Chia-Ying; Marschilok, Amy C.; Subramanian, Aditya; Takeuchi, Kenneth J.; Takeuchi, Esther S. *Physical Chemistry Chemical Physics*. **2011**, *13*, 18047-18054.
5. Marschilok, Amy C.; Lee, Chia-Ying; Subramanian, Aditya; Takeuchi, Kenneth J.; Takeuchi, Esther S. *Energy and Environmental Science*. **2011**, *4*, 2943-2951.
6. Farley, Katie E.; Marschilok, Amy C.; Takeuchi, Esther S.; Takeuchi, Kenneth J. *Electrochemical and Solid State Letters*. **2012**, *15*(2), A23-A27.
7. Yau, Shali Z.; Farley, Katie E.; Marschilok, Amy C.; Takeuchi, Esther S.; Takeuchi, Kenneth J. *Electrochemical Society Transactions*. **in press**.
8. Marschilok, Amy C.; Kim, Young Jin; Takeuchi, Kenneth J.; Takeuchi, Esther S. *Electrochemical Society Transactions*. **in press**.
9. Marschilok, Amy C.; Schaffer, Corey P.; Takeuchi, Kenneth J.; Takeuchi, Esther S. *Journal of Composite Materials*. **in press**.
10. Marschilok, Amy C.; Yau, Shali Z.; Menard, Melissa C.; Takeuchi, Esther S.; Takeuchi, Kenneth J. **submitted**.
11. Marschilok, Amy C.; Kim, Young Jin; Takeuchi, Kenneth J.; Takeuchi, Esther S. **submitted**.

Solvation and Phase Behavior of Lithium Trifluoromethanesulfonate in Ethylene Carbonate, γ -Butyrolactone, or Propylene Carbonate.

Paul C. Trulove (PI), Christopher J. Worosz, Kurt Sweely, Matthew P. Foley
Department of Chemistry, U. S. Naval Academy, Annapolis, MD 21402, USA

Wesley A. Henderson, Paul D. Boyle, Daniel M. Seo
North Carolina State University, Raleigh, NC 27695, USA

Program Scope

The solvation and phase behavior of the model battery electrolyte salt lithium trifluoromethanesulfonate (LiCF_3SO_3) in commonly used organic solvents; ethylene carbonate (EC), γ -butyrolactone (GBL), and propylene carbonate (PC) are explored. Data from differential scanning calorimetry (DSC), Raman spectroscopy, and X-ray diffraction are correlated to provide insight into the solvation states present within a sample mixture. Data from DSC analyses allow the construction of phase diagrams. Raman spectroscopy, as demonstrated by the work by Frech and coworkers¹, enable the determination of specific solvation states present within a solvent–salt mixture. Finally, X-ray diffraction data will provide exact information concerning the structure of a solvate.

Recent Progress

Our earlier work on this grant focused on LiCF_3SO_3 mixtures with either EC or GBL.^{2,3} Figure 1 contains phase diagrams derived from DSC analyses of the various solvent–salt mixtures investigated in this study; EC– LiCF_3SO_3 (A), GBL– LiCF_3SO_3 (B), and PC– LiCF_3SO_3 (C). The phase diagram of the EC– LiCF_3SO_3 indicated there were melting events at all molar ratios measured. The phase diagram of GBL– LiCF_3SO_3 , Figure 1 B, reveals three distinct regions. In the first region ($X_{\text{Li}} < 0.16$) a single melting transition is detected. The second region of intermediate molar ratios of GBL– LiCF_3SO_3 ($0.16 < X_{\text{Li}} < 3.1$), however, does not display any large endothermic melting events and thus falls into a crystallinity gap. The third region of the highest molar ratios ($X_{\text{Li}} > 3.1$) a series of melting events are detected across a wide range of temperatures.

Most recently, the study was extended to another common organic solvent found in battery electrolytes; propylene carbonate (PC). The phase diagram derived from DSC analyses of mixtures of PC– LiCF_3SO_3 is presented in Figure 1 C. With the exception of pure PC, the only detected transitions in any DSC analysis performed were glass transitions (T_g). The T_g appears to have a linear relationship with mole fraction of Li-ion.

PC is a mixture of solvents since it is a chiral molecule having 2 structural isomers. It only demonstrates a T_g when salt is present. The lack of large endothermic events in the DSC analyses could be a result of the mixed solvent system; R-(+)-PC and S-(-)-PC. Polarimetric

measurements of the PC solvent used in the study demonstrated it to be a racemic mixture with equal amounts of both isomers resulting in no detectable net optical rotation. Later studies used enantiomerically pure PC for comparison.

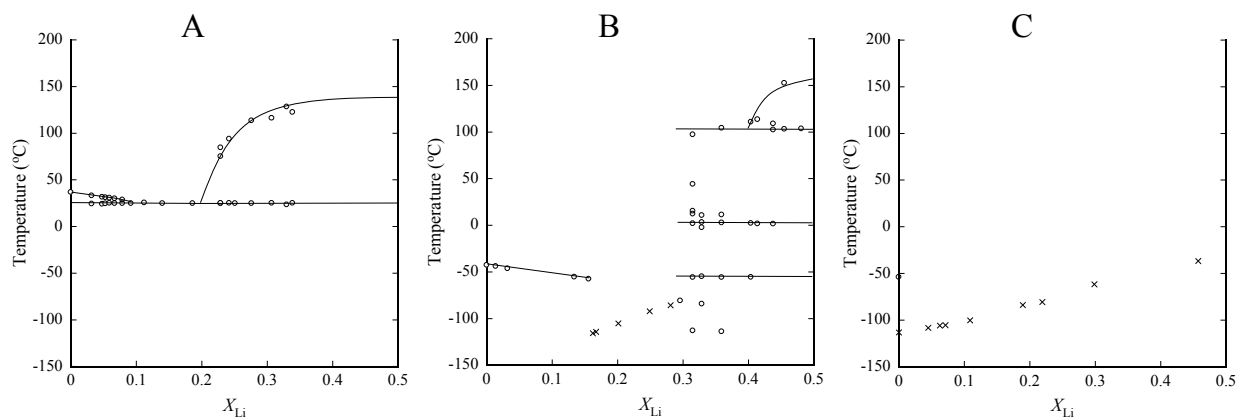


Figure 1. Phase diagrams of; EC–LiCF₃SO₃ (A), GBL–LiCF₃SO₃ (B), and PC–LiCF₃SO₃ (C) mixtures. Mole fraction of the Li-salt is plotted along X-axis. The open circles represent melting transitions and X's denote the temperatures at which glass transitions occur.

A structural comparison of the solvents employed explains the observed phase behavior. EC, the most symmetric of the solvents used, readily forms ordered solvate structures which leads to detection of first order phase transitions at all molar ratios. GBL lacks one of the mirror planes present in EC. This increased disorder within GBL–LiCF₃SO₃ mixtures leads to different phase behavior; a crystallinity gap and multiple melting events at higher mole fractions of salt. Finally, PC is chiral and has the lowest symmetry of the three solvents. This further increases disorder within mixtures of PC–LiCF₃SO₃ results in only glass transitions as possibilities.

Raman spectroscopy is employed to gain insight into the solvation states present within a sample mixture. Three general categories of solvation are employed; solvent-separated ion pair (SSIP), contact ion pair (CIP), and aggregates (AGG). Frech and coworkers studied LiCF₃SO₃ in various solvents and were able to determine wavenumber regions which can be associated with specific solvation categories. Generally, as the association between ions weakens, e.g. interposition of solvent molecules within ion pairs, the energy of the Raman scattered photons decrease and are detected at smaller wavenumbers (SSIP < CIP < AGG).¹

Mixtures of PC–LiCF₃SO₃ covering a wide range of molar ratios were prepared and analyzed with the aid of Raman spectroscopy. Figure 2 is a stack plot of a series of spectra collected at 25 °C for different molar ratios of PC–LiCF₃SO₃. The concentration of LiCF₃SO₃ decreases going from the bottom spectrum to the top. One can see that as the amount of LiCF₃SO₃ in a mixture decreases, the signal for the $\delta(\text{CF}_3)$ deformation shifts to smaller wavenumbers. This decrease in energy of the scattered photon results from change in population

of solvation states present within a sample mixture. It is interesting that in the most dilute samples measured, the dominant species is CIP.

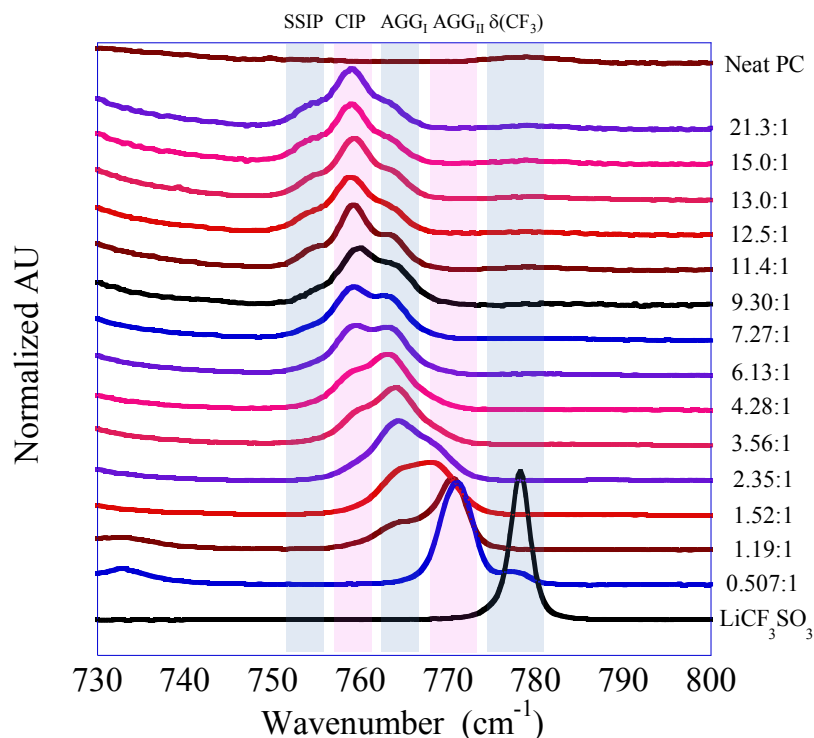


Figure 2. Stack plot of Raman spectra collected at 25 °C. Along the right y-axis are labels corresponding to the molar ratio of each sample. Highlighted regions indicate where specific solvation state dependent $\delta(\text{CF}_3)$ deformations occur.

Since PC is chiral, it becomes necessary to study the solvation and phase behavior of enantiomerically pure PC. Initial investigations into mixtures prepared using R-(+)-PC–LiCF₃SO₃ reveal some consequences associated with chirality. Significantly, there is an endothermic melting event occurring at approximately 150 °C for mixtures approaching a 1:1 molar ratio. We attribute the high-melting solvate to the lower entropy of the R-(+)-PC system. Additionally, as shown in Figure 3, kinetics play a greater role in the phase transition process and more complicated behaviors are detected. The large signal in the AGG_{II} region of the spectrum for 1.74:1 molar ratio mixture is greatly diminished in both more and less concentrated mixtures. Sample history and kinetics influence phase behavior resulting in the chance formation of more AGG_{II}.

Future Plans

DSC and Raman spectroscopic analyses of mixtures of LiCF₃SO₃ prepared with enantiomerically restricted R-(+)-PC reveal the presence of an apparent 1:1 solvate. Crystals of this aggregated species will be analyzed by X-ray diffraction in order to determine its structure.

In addition, the study will be extended to the other enantiomer, S-(-)-PC. Mixtures of LiCF_3SO_3 prepared using all three versions of PC will enable better understanding of the role played by solvent disorder within a solvate system. If the existence a 1:1 solvate is indicated by DSC analyses, crystals of that solvate will be prepared and interrogated by X-ray diffraction. Comparing crystal structure will improve basic knowledge of these model battery electrolytes. Additionally, if funding allows, we will apply understanding of solvate structure to measured conductivities.

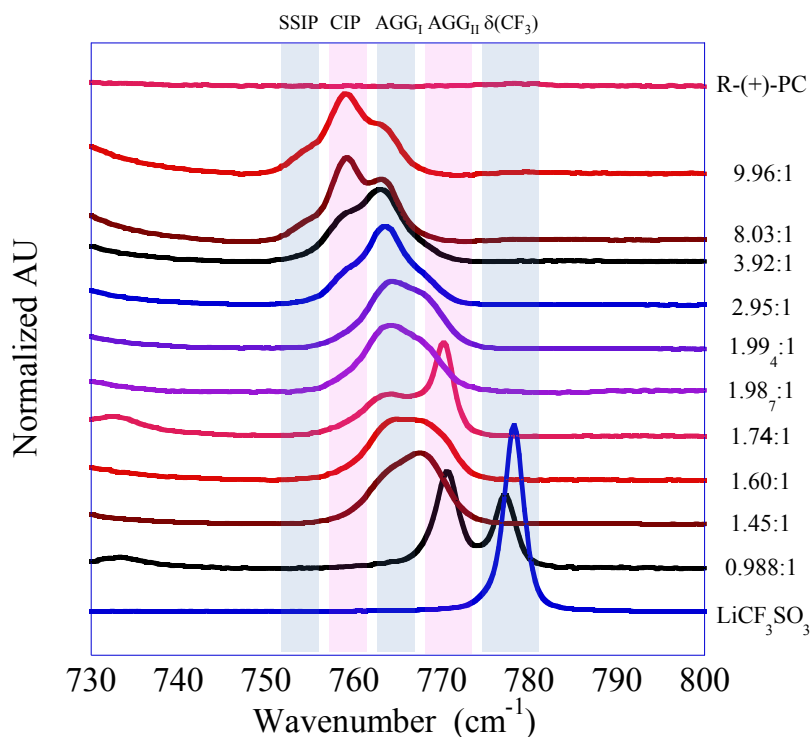


Figure 3. Raman spectra of R-(+)-PC- LiCF_3SO_3 mixtures collected at 25 °C. Along the right y-axis are labels corresponding to the molar ratio of each sample. Highlighted regions indicate where specific solvation state dependent $\delta(\text{CF}_3)$ deformations occur.

References

1. W. Huang, R. Frech, and R. A. Wheeler, *J. Phys. Chem.*, 98, p. 100 (1994).
2. M. P. Foley, D. M. Seo, P. D. Boyle, W. A. Henderson, H. C. De Long and P. C. Trulove, *ECS Trans.*, 35(29), 3 (2011).
3. M. P. Foley, D. M. Seo, P. D. Boyle, W. A. Henderson, H. C. De Long and P. C. Trulove, *ECS Trans.*, 41(25) 109 (2012).

Publications

1. M. P. Foley, D. M. Seo, P. D. Boyle, W. A. Henderson, H. C. De Long and P. C. Trulove, *ECS Trans.*, 35(29), 3 (2011).
2. M. P. Foley, D. M. Seo, P. D. Boyle, W. A. Henderson, H. C. De Long and P. C. Trulove, *ECS Trans.*, 41(25) 109 (2012).

Guided assembly of anisotropic micro- and nano-structures into mesoscale hierarchies of new properties

Vladimir Tsukruk and Mostafa El-Sayed

**School of Materials Science and Engineering and School of Chemistry & Biochemistry,
Georgia Institute of Technology, Atlanta, Georgia 30332, USA**

Program Scope

In this study, we focus on the synthesis and fabrication of inorganic, polymeric, and hybrid anisotropically-shaped microcrystals, microcapsules, plasmonic nanocrystals, and understanding their assembling behavior. This goal is motivated by the fact that despite the wide range of inorganic nano- and microstructures that have been studied, the guided formation of *organized macroscopic and mesoscale materials* from anisotropic building blocks has been rarely demonstrated. The near-field enhancement, optical coupling, and energy transport properties of assembled nanostructures highly dependent on the arrangement of the metal nanoparticles and on the matrix dielectrics are studied by using optical spectroscopy and ultrafast laser dynamics assisted by simulations of the metal nanostructures.

The anisotropically shaped, micro- and nanocontainers with nanoscale shells and functionalized microparticles were fabricated by layer-by-layer (LbL) assembly. The original spherical, cubic and tetrahedral micro- and nanoparticles from different inorganic materials were modified by wrapping them with polymeric shells. These sacrificial cores were removed to produce hollow microcontainers with ultrathin shells and well-defined sharp edges and robust shape. The mechanical stability of the flexible spherical, cubic and tetrahedral microcontainers has been evaluated under osmotic pressure and with computer simulation that mimic practical situations. The peculiar elastic properties and high permeability of microcontainers at different pH conditions have been revealed. The Langmuir-Blodgett (LB), LbL, and template-assisted methods are utilized to assemble the anisotropic micro- and nanoparticles in larger mesoscale structures.

The plasmonic-active nanoparticles were assembled into 2D structures having different interparticle distance and thus different plasmonic field distribution. Conjugated polymers of different dimensions were deposited on anisotropic plasmonic nanostructures such as gold and silver nanocubes. Such a coupling with the conjugated polymer shells resulted in highly variable optical properties which have been studied as a function of their separation and the conjugation length of the polymer. The observations are discussed in terms of changes in the rates of energy transfer and/or exciton-exciton annihilation processes.

Recent Progress

Fabrication and characterization of anisotropic micro- and nano- polymeric microcontainers.

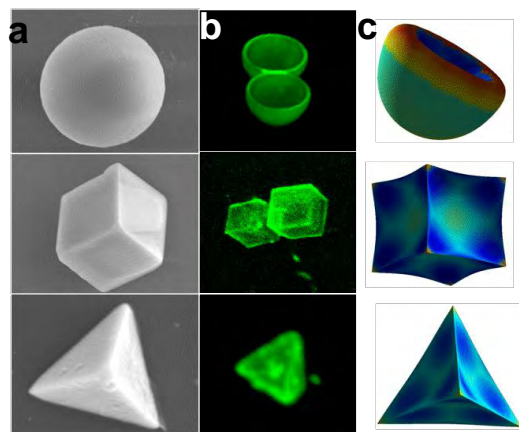


Figure 1. SEM images of the initial templates (a); confocal microscopy image of hollow microcontainers (b); and simulations of different shapes under osmotic pressure (c).

We exploited inorganic cubic (CdCO_3) and tetrahedral (SnS) nanocrystals as sacrificial cores for the preparation of anisotropic hollow capsules by hydrogen-bonded LbL assembly of tannic acid (TA) and poly(*N*-vinylpyrrolidone) (PVPON) which provided high compliance combined with chemical stability (Figure 1). We demonstrated that anisotropic, robust, and hollow microcapsules with cubic and tetrahedral shapes are stable at physiological pH and capable of retaining their anisotropic shape under different pHs. Tetrahedral shapes in comparison with cubic shapes present a new challenge in the preparation of shaped microcapsules due to additional stresses at the edges and corners. Finally, based on experimental results and corresponding computer modeling we suggested that introducing sharp edges

and vertices acting as a reinforcing frame can potentially prevent random buckling and collapse thus enhancing microcapsule stability under osmotic pressure variation (Figure 1).

The morphology, mechanical properties, and permeability of hydrogen-bonded LbL shells assembled on cubic cores have been studied in comparison with the traditional spherical shell assembled on spherical cores (Figure 2). We demonstrated that the morphology of LbL shells is dramatically affected by the nature of the core and the core-release process. The characteristic release processes of the sacrificial cubic core results in highly porous and highly softened LbL shells due to the CO_2 gas formation during reaction (Figure 2). The increasing porosity results in dramatic increase in permeability and softening of cubic shells with the elastic modulus dropping by almost an order of magnitude in comparison with spherical shells of the same composition. These dramatic changes in shell morphology, permeability, and stiffness discovered in this study, all are important for directed assembly and coupling of spherical microcapsules and anisotropic micro-containers.

Anisotropic cubic microcapsules based on water-soluble sodium chloride cubic cores were synthesized by LbL assembly of the hydrogen-bonded polymers from the anhydrous alcohol solutions. The cubic microcontainers that were observed mainly formed

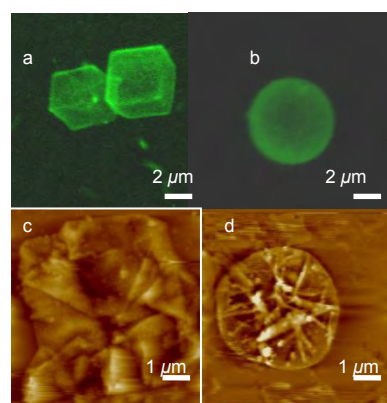


Figure 2. Confocal images of the cubic (a) and spherical (b) microcapsules and AFM images of dried cubic (c) and spherical (d) microcapsules.

the highly compacted 3D cubic arrays due to the face to face interactions and steric confinements in sharp contrast to the dense bcc assembly of the spherical capsules. The assembled spherical microcapsules create a large number of openings with extensive surface areas while the cubic microcapsules build close, compact aggregates. The global porosity of the cubic microcapsules assembly is mainly caused by the nanoporous shells which can be tuned by solvent composition.

Synthesis, assembling and studying the optical properties of the plasmonic metallic nanoparticles-conjugated polymer hybrid materials.

We studied the change in the optical properties of the poly(p-phenylene ethynylene) (PPE), conjugated polymers of different chain length 15 and 36 double bonds under the perturbation of assembled plasmonic silver nanocubes in monolayer with different inter-particle separation. The LB technique was used to assemble each of the PPE polymers onto a monolayer of gold or silver plasmonic nanoparticles of different interparticle separations. The localized surface plasmon resonance (LSPR) overlaps with the absorption of the PPE15 polymer but with the fluorescence of the PPE36 polymer. Decreasing the inter-particle distance increases the plasmonic field which enhances the excitation level in PPE15. This first increases the fluorescence intensity but then rapidly decreases it due the exciton-exciton annihilation processes. The change in the optical properties of the PPE36 polymer with an observed blue-shift with decreasing the interparticle separation suggests the reduction in the length of the conjugation due to possible twisting of the conjugated chain. When gold nanocages (AuNCs) are used whose LSPR peak overlaps with the emission of PPE polymer the polymer shell fluorescence intensity is quenched due to the energy transfer between the excited state of the polymer and the AuNCs, as well as due to the inter-chain energy transfer.

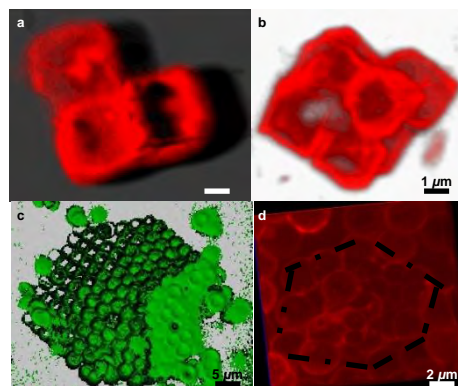


Figure 3. Assembly of the cubic microcapsules in buffer pH=3.5 (a, b) in contrast to the spherical capsules as evaluated by the confocal microscopy.

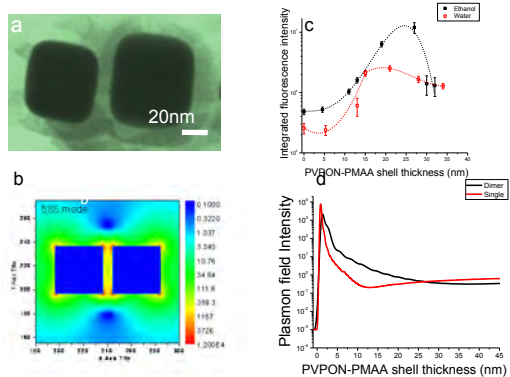


Figure 4. TEM of the PPE-LbL-AgNCs (a) with the electromagnetic field distribution (b). The fluorescent intensity of core-shell nanocubes (c). The plasmon field intensity versus the distance from the surface for individual AgNC and dimers (d).

The fluorescence behavior of the PPE on the core-shell AgNCs was evaluated as a function of the number of layers in LbL shells as well as the surrounding solvent at an excitation wavelength of 450 nm (which is close to the surface plasmon peak (SPR) of the bare 46 nm Ag nanocubes synthesized in this study). Figure 4 shows the observed change

The fluorescence behavior of the PPE on the core-shell AgNCs was evaluated as a function of the number of layers in LbL shells as well as the surrounding solvent at an excitation wavelength of 450 nm (which is close to the surface plasmon peak (SPR) of the bare 46 nm Ag nanocubes synthesized in this study). Figure 4 shows the observed change

in the fluorescence intensity of the PPE with increasing its separation from the plasmonic surface of AgNC is proposed to result from the interplay between a short-range fluorescent quenching and a relatively longer range plasmonic fluorescence enhancement mechanism for nanocube dimers. Discrete dipole approximation (DDA) calculation was carried-out to understand the fluorescence enhancement after the AgNCs surface is separated enough from the PPE polymer so that the plasmonic enhancement of the fluorescence is only operative (Figure 4).

Future Plans

We will focus on evaluation of the role of different inter-particulate forces (electrostatic, hydrogen, magnetic, capillary, and van der Waals) in mesoscale assembly of anisotropic colloidal structures from metal, polymer, and hybrid materials on functionalized surfaces and templates in conjunction with the investigation of their photophysical properties. Further research are planned with a strong focus on energy transport mechanisms between non-traditional anisotropic hybrid nanostructures and how these mechanisms are affected and can be tuned by plasmonic electrical fields inside and outside of the nanostructures, in proximity of different facets, and in a gap between nanostructures.

Related project publications (2010-2012)

- O.Shchepelina, V. Kozlovskaya, S. Singamaneni, E. Kharlampieva, V. V. Tsukruk, Synthetic Replicas of Anisotropic Particulate and Complex Continuous Templates. *J. Mater. Chem.* **2010**, *20*, 6587.
- M. A. Mahmoud, Proposed Molecular Mechanism for the Colloidal Nanocatalysis of the Hexacyanoferrate III-Thiosulfate Electron Transfer Reaction: On the Involvement of a Prussian Blue Analogue Complex Intermediate, *J. Catal.*, **2010**, *274*, 215.
- O.Shchepelina, V. Kozlovskaya, E. Kharlampieva, W. B. Mao, A. Alexeev and V. V. Tsukruk, Anisotropic Micro- and Nano-Capsules, *Macromol. Rapid Comm.* **2010**, *31*, 2041 (Cover Story).
- M. A. Mahmoud, M. A. El-Sayed, Plasmonic Field coupling effect on the energy transfer between Poly(paraphenyleneethynylene) Fluorescent Polymer and Au Nanocages, *J. Phys. Chem. C*, **2011**, *115*, 12726.
- O. Shchepelina, M. Lisunova, I. Drachuk, V. V. Tsukruk, Morphology and properties of cubic and spherical microcapsules with different core release. *Chem. Mater.*, **2012**, *24*, 1245.
- O. Shchepelina, I. Drachuk, M. K. Gupta, J. Lin, V. V. Tsukruk, Silk-on-Silk Layer-by-Layer Microcapsules. *Adv. Mater.* **2011**, *40*, 4655.
- M. Lisunova, M. Mahmoud, N. Holland, Z. Combs, M.A. El-Sayed, V.V. Tsukruk, The Unusual Fluorescence Intensity Enhancement of Poly(p-phenyleneethynylene) Polymer Separated from the Plasmonic Silver Nanocube Surface by H-bonded LbL Shells. *J. Mater. Chem.* **2012**, (Cover Story), Accepted.
- M. A. Mahmoud, A. Poncheri, M. A. El-Sayed, Dependence of the Photophysical Properties of Poly(paraphenyleneethynylene) polymer on Chains Length and Assembling into Langmuir-Blodgett Monolayer: Pure Polymer Versus Hybrid with Silver Nanocube Monolayer. *J. Phys. Chem. C* **2012**, submitted.



Optical and magnetic probes of charge dynamics in organic donor-acceptor bulk heterojunction for photovoltaic applications

Z. Valy Vardeny*

Physics & Astronomy Department, University of Utah, Salt Lake City, Utah 84112

Program Scope

The process of charge photogeneration in organic photovoltaic cells is still a matter of debate. In contrast to the labyrinth photosynthesis process that has evolved in nature [1], the charge photogeneration process in organic photovoltaic cells utilizes one type of heterojunction between two organic semiconductors [2]. The two organic semiconductors, dubbed donor (D-) and acceptor (A-) are cast from solution mixtures to form thin films having nanosize domains of relatively pristine materials and large D-A interface area. This type of architecture, dubbed 'bulk heterojunction' (BHJ) usually allows for light absorption in the bulk donor domains that generate excitons, followed by exciton dissociation at the D-A interfaces. However the processes by which the excitons reach the D-A interfaces and dissociate to generate separate charge polarons in the D-A nano-domains; or, alternatively recombine for a loss, are only now being the focus of attention [3]. *In our work we use a variety of optical and magnetic probes to investigate the charge dynamics in several organic D-A BHJ type films and devices.* Our arsenal includes both cw and ultrafast spectroscopies, as well as magneto-transport measurements [4].

Recent Progress

In our recent work we used the pump/probe transient photomodulation spectroscopy in an unprecedented broad spectral range (0.15-2.7 eV) to elucidate the early stages of the charge photogeneration process in the prototype D-A blend, namely the donor polymer regio-regular (RR-) (3 hexyl thiophene) [P3HT] and the fullerene acceptor molecule [6,6]-phenyl-C₆₁-butyric acid methyl ester [PCBM]. This blend shows separated donor and acceptor domains, and consequently has high solar power conversion efficiency, $\eta \sim 4\%$ [5]. We found compelling evidence that after the photoexcited excitons in the polymer domains reach the D-A interfaces, the charge generation process proceeds via the formation of charge transfer (CT) excitons at the interfaces (see Fig. 1). In RR-P3HT/PCBM with (1.2:1) weight ratio having maximum nano-domain separation the photogenerated excitons in the polymer domain reach the D-A interfaces forming CT excitons within ~ 10 ps. In contrast, in regio-random (RRa)-P3HT/PCBM blend where the D and A domain sizes are much smaller, the CT excitons at the D-A interfaces are generated within ~ 200 fs. In spite of this the subsequent exciton dissociation process in this blend is hampered by the large CT binding energy, which explains the small η -value ($< 0.1\%$) of

solar cells based on this blend. Our findings support a ‘two-step’ process for the charge photogeneration in organic D-A blends [3], and emphasize the important role of the CT exciton binding energy in generating free charges in organic solar cells [6].

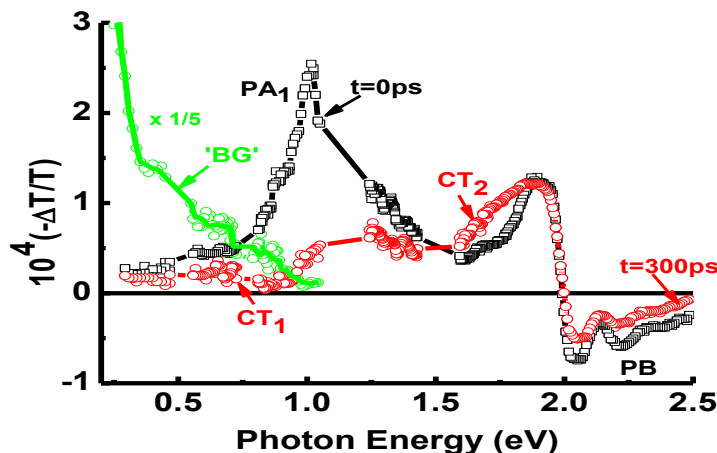


Figure 1: The ps transient photomodulation, $\Delta T(t)/T$ spectrum of RR-P3HT/PCBM blend film at $t=0$ and $t=300$ ps, respectively, measured at ambient. The exciton band PA_1 , and CT exciton bands CT_1 and CT_2 are indicated. The exciton PA_1 band decays, but polaron PA are not formed on their account; instead a two CT bands are generated. The green circles and line represent the background (BG) PA spectrum measured at $t = -5$ ps showing free polaron photogeneration at much later time, which is uncorrelated with the decay of the excitons (PA_1) in the polymer domains [taken from ref. 7].

Future plans

Having understood the importance of the D-A CT exciton role in the charge photogeneration process, the question is how we can improve the charge photogeneration efficiency in organic photovoltaic (OPV) cells. We realize that the competing mechanism to the charge photogeneration process is the geminate recombination (GR) process of the CT state. Since the CT exciton is generated in the singlet spin configuration, the possibility exists to enhance the intercrossing process from CT singlet to CT triplet, and thus reduce the GR loss.

Based on this conclusion we recently discovered a novel method to suppress CT recombination at the D-A domain interfaces and thus improve the OPV solar cell efficiency, by doping the device active layer with spin $\frac{1}{2}$ radicals such as Galvinoxyl [8]. At an optimal doping level of 3 wt%, the efficiency of a standard P3HT/PCBM solar cell improves by 15%. However in solar cells based on acceptor-rich blends the efficiency is enhanced by $\sim 340\%$. We propose a spin-flip mechanism to explain our results that should work only via *resonant exchange interaction* between the spin $\frac{1}{2}$ radicals and charged acceptors, which converts the CT spin state from spin singlet to triplet. We plan to thoroughly explore this proposed mechanism, and find additional spin $\frac{1}{2}$ radicals that may improve the OPV efficiency even more. In addition to OPV

related measurements we will also use transient spectroscopy and magneto-photocurrent to elucidate the generation and recombination processes in the spin-doped active blend. The spin $\frac{1}{2}$ radical doping may augment existing methods to yield higher OPV efficiencies, and may also be used to enhance the electroluminescence efficiency in organic light emitting devices.

* Supported by the DOE grant DE-FG02-04ER46109

References

1. M.R. Wasielewski, Chemical Reviews **92**, 435 (1992).
2. G. Li, R. Zhu and Y. Yang, Nature Photon. **6**, 153 (2012).
3. A. A. Bakulin, A. Rao, V. G. Pavelyev, P. H. M. van Loosdrecht, M. S. Pshenichnikov, D. Niedzialek, J. Cornil, D. Beljonne, and R. H. Friend, Science **335**, 1340 (2012).
4. T. Drori, C. X. Sheng, A. Ndobe, S. Singh, J. Holt, and Z. V. Vardeny, Phys. Rev. Lett. **101**, 037401 (2008).
5. T. Drori, J. Holt and Z. V. Vardeny, Phys. Rev. B **82**, 075207 (2010).
6. M. Hallerman, S. Haneder and E. Da Como, Appl. Phys. Lett. **93**, 053307 (2008).
7. S. Singh, B. Pandit, T. Basel, Z. V. Vardeny, S. Li and D. Laird, Phys. Rev. B (in the press).
8. S. Singh, Y. Zhang, and Z. V. Vardeny, *Jour of Synthetic Metals* **160**, 311 (2010).

Publications that resulted from DOE grant # DE-FG02-04ER46109

- (1) "Spin Dependent Reactions of Polaron Pairs in Organic Diodes", F. Wang, C. Yang, E. Ehrenfreund and Z. V. Vardeny, *Jour of Synthetic Metals* **160**, 297 (2010).
- (2) "Recent Advances in Organic Spin-Valves Devices", Z. V. Vardeny, F. Wang, and T. D. Nguyen, *Jour of Synthetic Metals* **160**, 210 (2010).
- (3) "Effect of Spin $\frac{1}{2}$ Radicals on the Ultrafast Photoexcitation Dynamics in RR-P3HT/PCBM Blends for Photovoltaic Applications", S. Singh, Y. Zhang, and Z. V. Vardeny, *Jour of Synthetic Metals* **160**, 311 (2010).
- (4) "Magneto-Optical Studies of [6,6]- phenyl-C₆₁-butyric acid methyl ester (PCBM)", G. Hukic-Markosian and Z. V. Vardeny, *Jour of Synthetic Metals* **160**, 614 (2010).
- (5) "Enhanced Performance of Polymer/Fullerene Bulk Heterojunction Photovoltaic Devices with $\frac{1}{2}$ spin Radical Doping", Ye Zhang, Golda Hukic-Markosian, Debra Mascaro, and Zeev Vally Vardeny, *Jour of Synthetic Metals* **160**, 262 (2010).
- (6) "Isotope effect in organic magneto-transport; the role of hyperfine interaction". T. D. Nguyen, Golda Hukic-Markosian, Fujian Wang, Leonard Wojcik, Xiao-Guang Li, Eitan Ehrenfreund, Z. V. Vardeny, *Nature Materials* **9**, 345 (2010).
- (7) "Threshold Excitation Studies of Random Lasers in π -Conjugated Polymers", A. Tulek, R. C. Polson, and Z. V. Vardeny, *Nature Physics* **6**, 303 (2010).

- (8) “Magnetic Field Effects in Pi-Conjugated Systems”, E. Ehrenfreund and Z. V. Vardeny, chapter four in “Organic Spintronics”, edited by Z.V. Vardeny CRC, Taylor & Francis, pp. 217-256 (2010).
- (9) “Optical Studies of the Charge Transfer Complex in Polythiophene/Fullerene Blends for Organic Photovoltaic Applications”, T. Drori, J. Holt and Z. V. Vardeny, *Phys. Rev. B* **82**, 075207 (2010).
- (10) “Nonlinear Optical Spectroscopy of Excited States in Di-substituted Polyacetylene”, C. -X. Sheng, M. Tong, and Z. V. Vardeny, *Phys. Rev. B* **81**, 205103 (2010).
- (11) “Magnetoconductance Response in Organic Diodes at Ultra-small Fields”, T. D. Nguyen, B. R. Gautam, E. Ehrenfreund, Z. V. Vardeny, *Phys. Rev. Lett.* **105**, 166804 (2010).
- (12) “Spatially mapping random laser cavities“, R. C. Polson and Z. V. Vardeny, *Optics Letters* **35**, 2801 (2010).
- (13) “Evidence for Excimer Excitations in Ordered π -Conjugated Polymer Films”, K. Aryanpour C. -X. Sheng, E. Olejnik, B. Pandit, D. Psiachos, S. Mazumdar and Z. V. Vardeny, *Phys. Rev. B* **83**, 155124 (2011).
- (14) “The Hyperfine Interaction Role in the Spin Response of π -Conjugated Polymer Films and Spin Valve Devices”, Tho D. Nguyen, Golda Hukic-Markosian, Fujian Wang, L. Wojcik, Xiao-Guang Li, Eitan Ehrenfreund, Z. V. Vardeny, *Synth. Metals* **161**, 598-602 (2011).
- (15) “Magneto-conductance of Unipolar and Bipolar Organic Diodes”, T. D. Nguyen, B. R. Gautam, E. Ehrenfreund, and Z. V. Vardeny, *Synth. Metals* **161**, 604-608 (2011).
- (16) “Magnetic Field Effects in Polymer Light-emitting Electrochemical Cells”, G. Li, T. D. Nguyen, and Z. V. Vardeny, *Appl. Phys. Lett.* **98**, 263302 (2011).
- (17) “The effects of Charge Injection in Single Wall Carbon Nanotubes Studied by Charge-Induced absorption Spectroscopy”, J. Kennedy and Z. V. Vardeny, *Appl. Phys. Lett.* **98**, 263110 (2011).
- (18) “Ultrafast optical studies of ordered poly(3-thienylene-vinylene) films. E. Olejnik, B. Pandit, T. Basel, E. Lafalce, C.-X Sheng, C. Zhang, X. Jiang, and Z. V. Vardeny, *Phys. Rev. B* (in the press).
- (19) “Two-step Charge Photogeneration Process in Polymer/Fullerene Blends for Organic Photovoltaic Applications”, S. Singh, B. Pandit, and Z. V. Vardeny, *Phys. Rev. B*. (in the press).
- (20) “Photoexcitation Dynamics in Polythiophene/fullerene Blends for Photovoltaic Applications”, C. -X. Sheng, B. Pandit, T. P. Basel, and Z. V. Vardeny, *Organic Electronics* **13**, 1031 (2012).
- (21) “Study of Photoexcitations in Poly(3-hexylthiophene) for Photovoltaic Applications”, G. Hukic, T. Basel. S. Singh, and Z. V. Vardeny, *Appl. Phys. Lett.* (in the press).

Extracting hot carriers from photo-excited semiconductor nanocrystals

Xiaoyang Zhu, Department of Chemistry & Biochemistry, University of Texas at Austin

Program Scope

In conventional solar cells, absorption of photons with energies above the semiconductor bandgap generates “hot” charge carriers that quickly “cool” to the band edges before they can be utilized to do work; this sets the solar cell efficiency at a limit of ~31%.¹ If instead, all of the energy of the hot carriers could be captured, solar-to-electric power conversion efficiencies could be increased, theoretically, to as high as 66%. A potential route to capture this energy is to utilize nanomaterials where quantization may slow down hot electron cooling. This may facilitate the transfer of hot electron/holes or allow the conversion of excess carrier energy to multiple electron/hole pairs. The latter process is carrier multiplication or multi-exciton generation (MEG) and may increase solar-to-electric power conversion efficiency to 44%.³ These scenarios are illustrated in Fig. 1. The current research program is aimed at quantitatively probing hot electron relaxation dynamics in QDs and establishing principles for charge extraction from photoexcited QDs.

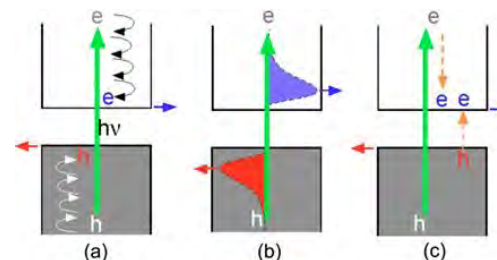


Fig. 1. Schematic illustration of (a) a conventional solar cell, (b) a hot-carrier solar cell, and (c) a multiexciton based solar cell.

Following initial demonstration of hot electron transfer from photoexcited PbSe QDs to TiO₂,⁴ we have focused on how hot electrons relax and how surface capping molecules and thin films affect QD electronic structure. During the past year, we succeeded in using femtosecond time-resolved two-photon photoemission (TR-2PPE) spectroscopy to carry out a complete mapping in time- and energy-domains of hot electron relaxation and MEG dynamics in PbSe quantum dots. We also discovered a new mechanism in electronic trap state formation on QD surfaces due a phase transition in capping molecules. In addition, we have carried out preliminary experiments on carbon nanomaterials, particularly synthetic graphene QDs, where the much slowed hot electron cooling dynamics (~10-100 ps time scale) has enabled us to unambiguously demonstrate the efficient injection of hot electrons into a TiO₂ electron acceptor.

Recent Progress

Direct mapping of hot electron relaxation & MEG dynamics in PbSe quantum dots

Here, we use femtosecond TR-2PPE spectroscopy⁵ to carry out a complete mapping of hot electron relaxation dynamics in QDs. A schematic representation of TR-2PPE is shown in Fig. 2. A pump laser pulse ($h\nu_1$) creates a hot electron-hole pair; after a controlled time-delay, a probe laser pulse ($h\nu_2$) ejects the excited electron, which is detected by an electron energy analyzer. The TR-2PPE spectrum represents the energy and population of hot electrons at each

pump-probe delay (t_d), thus providing a complete mapping in time and energy domains of electron relaxation dynamics.

The right panel in Fig. 2 shows a TR-2PPE spectrum for a PbSe QD thin film with 1,2-ethanedithiol (EDT) capping molecules and an optical gap of $E_g = 0.70$ eV. The spectrum shows hot electron population as they relax in energy with pump-probe delay time (t_d). The electron kinetic energy decreases monotonically to the bottom of the conduction band ($1S_e$) with increasing t_d . We find a linear scaling law for the hot electron relaxation rate (Γ) with its energy above the conduction band minimum: $\Gamma \propto (E_e - E_{CBM})$. The TR-2PPE spectrum in Fig. 2 for $h\nu_1 = 2.2$ eV ($> 3E_g$) and those at lower excitation photon energies ($h\nu_1 = 1.40$ or 1.80 eV) show no evidence for MEG where, the excess energy in a hot electron (hole) should decrease by a quantized amount ($\sim E_g$) to create a new electron-hole pair at the band edges. Primarily, there is an absence of population near the CBM on the short time scale (< 1 ps). The electron population in the conduction band can be entirely accounted for by a cascading energy relaxation process attributed to phonon scattering likely mediated by an e-h Auger process.

When the photon energy is increased to $h\nu_1 = 2.85$ eV ($> 4E_g$), we find direct evidence of MEG. The spectrum in Fig. 3a shows rich features at both positive and negative time-delays that can be assigned to the presence of optical resonance due to optical excitation to the second conduction band in PbSe. We remove the constant background (C) in 2PPE spectra due to two-photon photoemission from the pump laser pulse and the result is shown in Fig. 3b, which clearly reveals the short-lived resonant features of A and B on two sides of $t_d = 0$. For $t_d > 0$, the hot electron from the resonant state first decays with an ultrafast lifetime of ~ 100 fs in nearly a quantum step to give spectral feature D at ~ 0.9 eV below peak A. The ultrafast decay in electron energy also leads to a 10% increase in

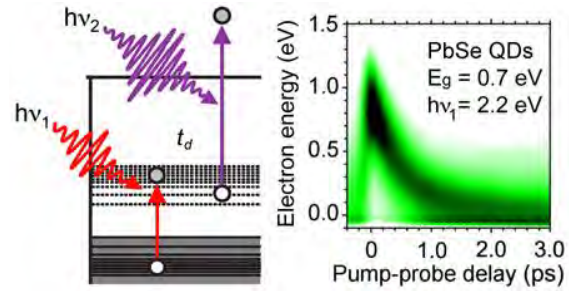


Fig. 2. Probing hot electron dynamics in QDs by TR-2PPE. The right shows pseudo-color representation of TR-2PPE spectra with $h\nu_1 = 2.20$ eV & $h\nu_2 = 4.28$ eV. The bandgap of the PbSe QDs is 0.70 eV.

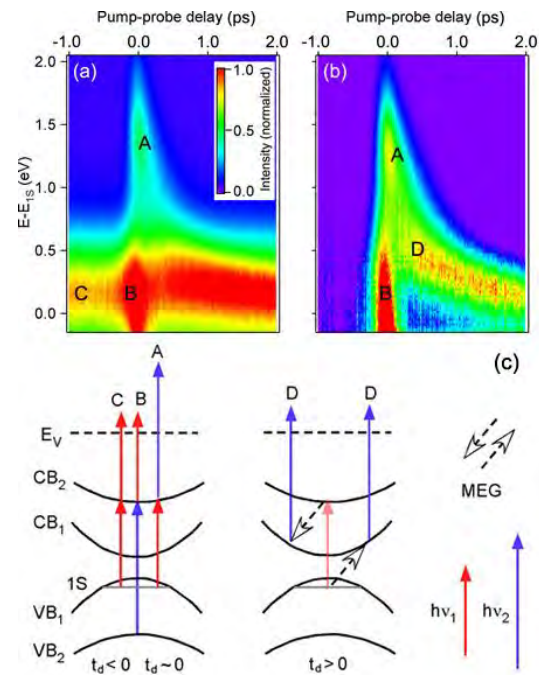


Fig. 3. (a) Pseudo-color representation of TR-2PPE spectra for PbSe QD films at an excitation photon energy of $h\nu_1 = 2.85$ eV and a probe photon energy of $h\nu_2 = 4.28$ eV; (b) The same data as in (a) with the spectral feature at negative time delays subtracted. (c) Schematic illustration of the TR-2PPE process at different pump-probe delays.

photoemission intensity. We take the quantized loss of hot electron energy and the corresponding increase in electron population as direct evidences for MEG. The observed MEG process is summarized in Fig. 3c ($t_d > 0$). Absorption of $h\nu_1 = 2.85$ eV excites a hot electron to the second conduction band. This is followed by *inter-band* transition to the lower conduction band and the concurrent excitation of a second electron pair, i.e, MEG. Compared to intra-band mechanism, the inter-band MEG process permits easier matching of energy and momentum simultaneously.

Hot electron injection from graphene QDs to TiO₂

There are a number of limitations with inorganic QDs for the harvesting of hot electrons or hot electron energy. These include i) the ultrashort hot electron lifetime; ii) heterogeneity of electronic structure and dynamics because of sensitivity to surface states; iii) limited absorption cross section requiring high solar concentration to reach the condition necessary for hot carrier solar cells. As an alternative, we are exploring carbon nanomaterials for hot carrier or multicarrier harvesting, particularly graphene or carbon nanotubes. For example, the rate of electron-electron scattering in

graphene is known to be much faster than that of electron-phonon scattering, leading to easy equilibration of hot electrons characterized by a transient electronic temperature higher than that of the phonon bath. We have explored the use of molecular analogs, usually called graphene QDs,⁶ adsorbed on the TiO₂ surface via -COOH anchors (Figs. 4 a & b). We use time resolved second harmonic generation (TR-SHG)⁴ to follow the transient interfacial electric field resulting from photo-induced electron transfer to TiO₂. Figs. 4 c & d show TR-SHG profiles for graphene QDs pumped at two different photon energies (c) or at the same photon energy, but different sample temperatures (d). While in all cases electron injection from photo-excited graphene QDs to TiO₂ occurs on ultrafast time scales (≤ 50 fs), the charge recombination dynamics are distinctly different. As shown in Fig. 4c, for graphene QDs excited at a higher photon energy, hot electrons are injected deeper into TiO₂ and the resulting polarons take longer time to come back to the surface for recombination. This mechanism is confirmed in Fig 4d for measurement at

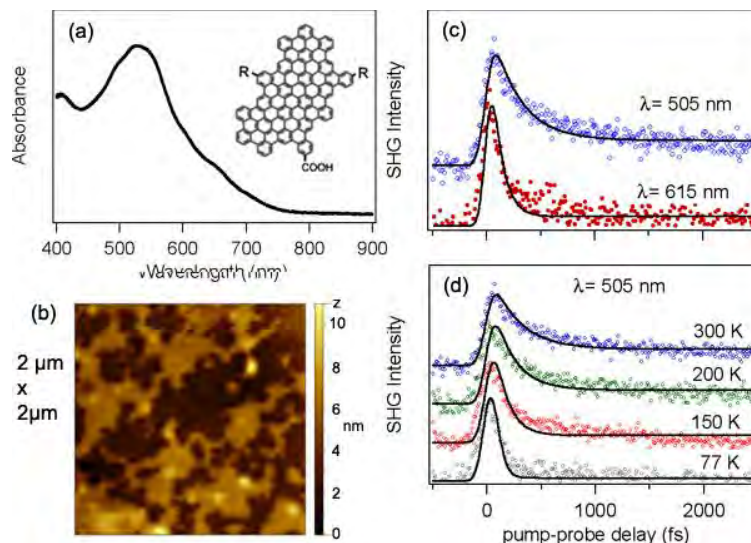


Fig. 4. (a) Absorption spectrum of the graphene QD; (b) AFM image of a submonolayer of graphene QD adsorbed on TiO₂(110); (c) TR-SHG spectra showing pump-induced rise and decay in transient electric field due to photo-induced electron transfer from graphene QD to TiO₂ at two wavelengths; (d) TR-SHG spectra at a fixed pump wavelength (505 nm) but different sample temperatures.

different sample temperatures. With increasing sample temperature, the mobility of polarons decreases due to enhanced scattering with phonons. As a result, charge recombination takes longer time at higher temperatures.

Future Plans

We will continue to focus on controlling QD surfaces and interfaces to the TiO₂ electron acceptor using core-shell structures and surface atomic passivation. We will continue to explore carbon nanomaterials, including carbon nanotubes and graphene QDs or nano-ribbons, for hot electron extraction of MEG. We will focus on probing hot carrier cooling and transfer dynamics by TR-2PPE and TR-SHG. The ultimate goal of this research program is to establish photophysical mechanisms and chemical control of interfaces for the harvesting of hot or multiple carriers from photoexcited nanomaterials.

References

(1) Shockley, W.; Queisser, H. J. *J. Appl. Phys.* **1961**, 32, 510; (2) Ross, R. T.; Nozik, A. J. *J. Appl. Phys.* **1982**, 53, 3813; (3) Hanna, M. C.; Nozik, A. J. *J. Appl. Phys.* **2006**, 100, 074510; (4) Tisdale, W. A.; Williams, K. J.; Timp, B. A.; Norris, D. J.; Aydil, E. S.; Zhu, X.-Y. *Science* **2010**, 328, 1543; (5) Chan, W.-L.; Ligges, M.; Jailaubekov, A.; Kaake, L.; Miaja-Avila, L.; Zhu, X.-Y. *Science* **2011**, 334, 1541; (6) Yan, X. Cui, B. Li, L-S., *Nano Lett.*, **2010**, 10, 1869.

Publications (DE-FG02-09ER46673)

- W. A. Tisdale, K. J. Williams, B. A. Timp, D. J. Norris, E. S. Aydil, X.-Y. Zhu, "Hot electron transfer from semiconductor nanocrystals," *Science* 328 (2010) 1543-1547.
- B. A. Timp, X.-Y. Zhu, "Electronic energy alignments at PbSe quantum dots / ZnO(1010) interfaces," *Surf. Sci.* 604 (2010) 1335-1341.
- W. A. Tisdale, X.-Y. Zhu, "Artificial atoms on semiconductor surfaces," *PNAS* 108 (2011) 965–970.
- A. Wolcott, V. Doyeux, C. A. Nelson, R. Gearba, K. W. Lei, K. G. Yager, A. D. Dolocan, K. Williams, D. Nguyen, X.-Y. Zhu, "Anomalously Large Polarization Effect Responsible for Excitonic Redshifts in PbSe Quantum Dot Solids," *J. Phys. Chem. Lett.* 2 (2011) 795–800.
- L. Miaja-Avila, J. Tritsch, A. Wolcott, W.-L. Chan, C. A. Nelson, X.-Y. Zhu, "Direct mapping of hot electron relaxation and multiexciton generation dynamics in PbSe quantum dots," *Nano Lett.* 12 (2012) 1588-1591.
- C. A. Nelson, X.-Y. Zhu, "Reversible electronic traps in PbS quantum dot solids induced by an order-disorder phase transition in capping molecules," *J. Am. Chem. Soc.* 134 (2012) dx.doi.org/10.1021/ja3004649.

Spectroscopy of Charge Carriers and Traps in Field-Doped Single Crystal Organic Semiconductors

Xiaoyang Zhu, Dept. of Chemistry & Biochemistry, University of Texas at Austin

C. Daniel Frisbie, Dept. of Chemical Engineering & Materials Sci., University of Minnesota

Program Scope

This research program aims to achieve quantitative, molecular level understanding of charge carriers and traps in field-doped crystalline organic semiconductors via in situ linear and nonlinear optical spectroscopy, in conjunction with transport measurements and molecular/crystal engineering. Organic semiconductors are emerging as viable materials for low-cost electronics and optoelectronics, such as organic photovoltaics (OPV), organic field effect transistors (OFETs), and organic light emitting diodes (OLEDs). Despite extensive studies spanning many decades, a clear understanding of the nature of charge carriers in organic semiconductors is still lacking. It is generally appreciated that polaron formation and charge carrier trapping are two hallmarks associated with electrical transport in organic semiconductors; the former results from the low dielectric constants and weak intermolecular electronic overlap while the latter can be attributed to the prevalence of structural disorder. These properties have led to the common observation of low charge carrier mobilities, e.g., in the range of 10^{-5} - 10^{-3} cm^2/Vs , particularly at low carrier concentrations. However, there is also growing evidence that charge carrier mobility approaching those of inorganic semiconductors and metals can exist in some crystalline organic semiconductors, such as pentacene, tetracene and rubrene. A particularly striking example is single crystal rubrene (Figure 1), in which hole mobilities well above $10 \text{ cm}^2/\text{Vs}$ have been

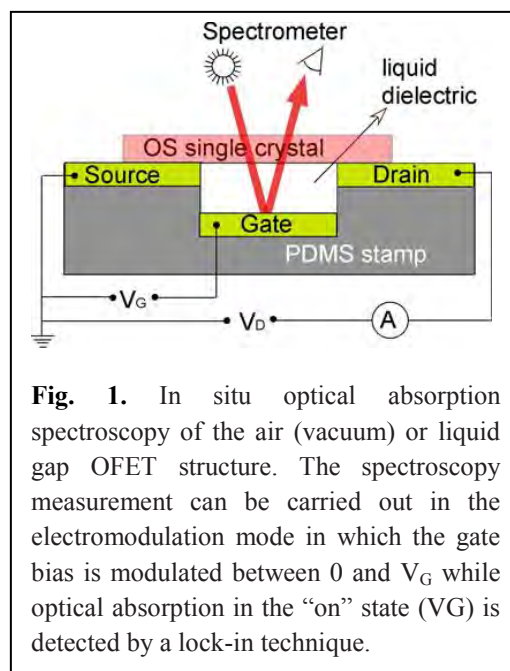


Fig. 1. In situ optical absorption spectroscopy of the air (vacuum) or liquid gap OFET structure. The spectroscopy measurement can be carried out in the electromodulation mode in which the gate bias is modulated between 0 and V_G while optical absorption in the “on” state (V_G) is detected by a lock-in technique.

observed in OFETs operating at room temperature. Temperature dependent transport and spectroscopic measurements both revealed evidence of free carriers in rubrene. Outstanding questions are: *what are the structural features and physical properties that make rubrene so unique? How do we establish fundamental design principles for the development of other organic semiconductors of high mobility?* These questions are critically important but not comprehensive, as the nature of charge carriers is known to evolve as the carrier concentration increases, due to the presence of intrinsic disorder in organic semiconductors. Thus, a complementary question is: *how does the nature of charge transport change as a function of carrier concentration?*

To answer these questions, the PIs are extending their successful collaboration that combines transport measurements with in situ spectroscopy; the new focus will be single crystal organic semiconductor field effect devices. The OFET structure provides control of surface charge concentration and the determination of carrier transport characteristics (e.g. mobility), while optical spectroscopy provides physical insight into the nature of charge carriers, as polarons and free carriers possess distinct optical signatures and also provide direct measurements of the energetics of charge carriers with respect to HOMO & LUMO bands.

Recent Progress

Recent research achievements are in two areas. The first is the development of absorption spectroscopy as a probe of charge carriers in gate-doped OFETs. We have focused on a model polymeric semiconductor, poly (3-hexylthiophene), and high capacitance dielectric materials (polymer electrolyte or ionic liquid) to probe gate-doping mechanisms. We have established fundamental limits and transitions in electrostatic and electrochemical doping regimes using polymer mixing theories. The second achievement is on the development of displacement current measurement (DCM) in studying the transient behavior of charge carriers and traps. We used the model system of polycrystalline pentacene thin film in a long-channel capacitor (LCC) geometry. The DCM techniques allowed us to determine not only charge carrier mobility, but more importantly, the nature of charge carrier traps at the pentacene-dielectric interface.

A. Electrostatic vs. Electrochemical Doping from In Situ Spectroscopy

We applied absorption spectroscopy to understand the molecular mechanism of gate-doping in OFETs with liquid dielectrics (ionic liquids & polymer electrolytes). A major advantage of these dielectric materials was the exceptionally high capacitance ($\geq 1 \mu\text{F}/\text{cm}^2$) which allowed one to achieve charge carrier density as high as $10^{14}/\text{cm}^2$ at gate voltages as low as 1 V. The low voltage operation was particularly important to the practical application of OFETs and the high doping level allowed one to explore interesting new carrier physics in organic semiconductors. The presence of mobile ions in these dielectric materials raised the critical question of whether the gate-doping mechanism was purely electrostatic or electrochemical (mixing). Using in situ absorption spectroscopy for a $\text{LiClO}_4/\text{PEO}$ polymer electrolyte gated device, we quantitatively measured the concentration of carriers in the organic semiconductor, in this case poly-3-hexyl-thiophene (P3HT). By monitoring the time-dependent

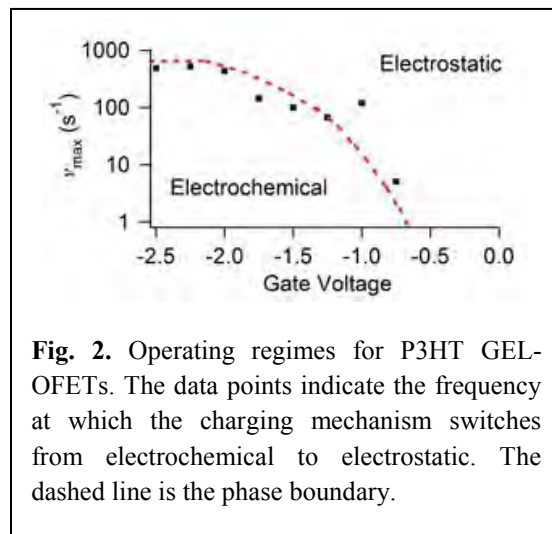


Fig. 2. Operating regimes for P3HT GEL-OFETs. The data points indicate the frequency at which the charging mechanism switches from electrochemical to electrostatic. The dashed line is the phase boundary.

buildup of charged species, we could determine the diffusion constants of carriers injected from a source electrode and that of mobile ions from the dielectric into the organic semiconductor (electrochemical doping) as a function of gate voltage. This allowed us to estimate the time scales (τ_m) for mixing for the first organic semiconductor molecular layer in contact with the dielectric and to construct a “phase” diagram for two doping mechanisms, as illustrated for an ion-gel gated P3HT OFET, Fig. 2. Here, we compared the maximum OFET switching speed (τ_{\max}) with $1/\tau_m$. When $\tau_{\max} > 1/\tau_m$, we were in the electrostatic region. When $\tau_{\max} < 1/\tau_m$, we had electrochemical doping.

Displacement Current Measurements.

In the area of transport, a principal direction has been to employ gate displacement current measurements on OFETs to understand transient charging and discharging dynamics in organic semiconductors, trapped charge concentrations, and total gate-induced charge. In standard transistor measurements, the DC current running through the conducting channel from source to drain electrode is measured either as a function of gate voltage or as a function of drain voltage. These traditional measurements give important device parameters, such as field-effect mobility, ON/OFF ratio, and threshold voltage. However, *transient* processes – including the injection of charge carriers from metal contacts into the OSC layer, the redistribution of carriers in the OSC layer to form the conducting channel, and the extraction of carriers from the OSC layer during the channel annihilation - are not explored in typical OFET measurements. Study of transient processes through displacement current measurements (DCM) provides additional information on carrier injection/extraction dynamics and trapping/detrapping properties. A typical device geometry we employed is shown in Fig. 3. This setup has allowed us to quantify charge carrier traps, trapping & de-trapping kinetics, and the roles of contact resistance.

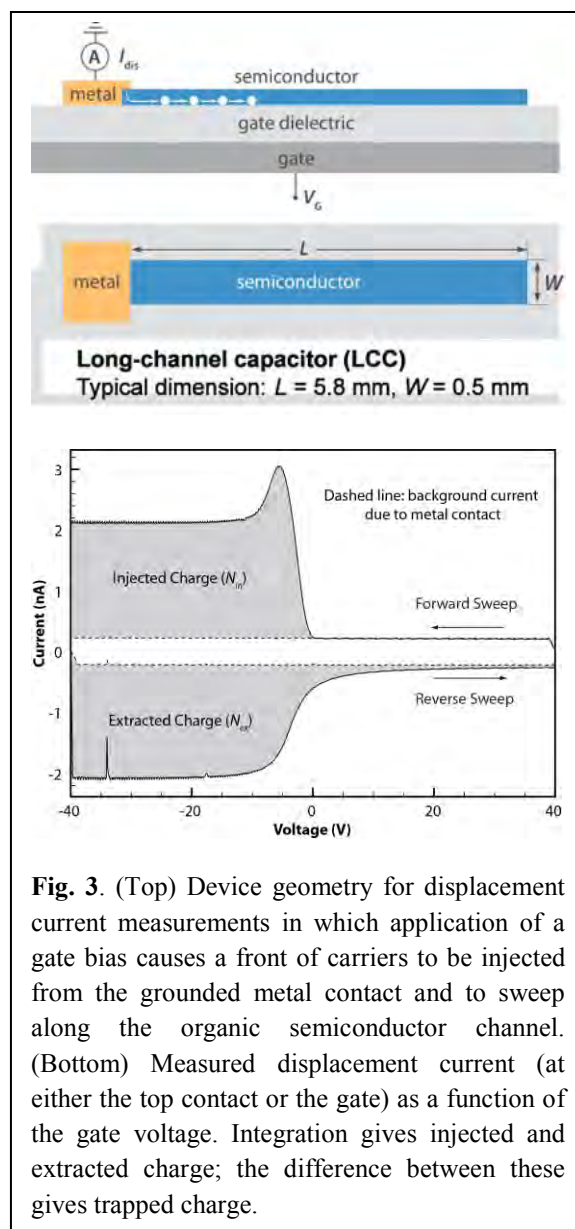


Fig. 3. (Top) Device geometry for displacement current measurements in which application of a gate bias causes a front of carriers to be injected from the grounded metal contact and to sweep along the organic semiconductor channel. (Bottom) Measured displacement current (at either the top contact or the gate) as a function of the gate voltage. Integration gives injected and extracted charge; the difference between these gives trapped charge.

Future Plans

We will use OFETs testbeds for exploring the physics of transport in single crystal organic semiconductors. This geometry provides exquisite control over the carrier concentration at the gate dielectric/crystal interface. This in turn allows the transport properties to be carefully examined as a function of charge concentration. The tunability of transport in these testbeds by means of the gate electrode makes single crystal OFETs ideal for the combined transport and spectroscopy studies we are carrying out here. We will use single crystal rubrene and pentacene OFETs as model systems and establish the physical nature of charge carriers by obtaining their spectroscopic signatures in a broad carrier density range and a broad temperature range. A particular focus will be on establishing the energetics of interfacial polarons resulting from the polarization of dielectric material by charge carriers at an organic semiconductor interface. An extreme example of this type of interfacial polaron is the direct pairing of a hole carrier with an anion across the semiconductor/dielectric interface when ionic liquid is used as a dielectric material. To explore the idea of polarization anisotropy as the cause for the exceptionally high room-temperature mobility in rubrene. While both rubrene and pentacene (or tetracene) possess layered structures and have similar electronic band widths, the one-order of magnitude higher mobility in rubrene may be attributed to its unique anisotropic polarizability, with the highly polarizable direction in the plane of the conducting layer, in contrast to the orthogonal situation in pentacene or tetracene. We propose to explore this mechanism by controlling interlayer spacing (and thus inter-layer electronic polarization) using rubrene and tetracene derivatives. We will establish the energetics from spectroscopy and mobility from transport measurements.

References

Publications (DE-FG02-10ER46675)

“Examination of Au, Cu, and Al contacts in organic field-effect transistors via displacement current measurements.” Liang, Y.; Chang, H.-C.; Ruden, P.P.; Frisbie, C.D. *J. Appl. Phys.*, **2011**, *110*, 064514. DOI: 10.1063/1.3638706.

“Quantify interfacial electric fields and local crystallinity in polymer/fullerene bulk heterojunction solar cells,” Gearba, I. R.; Morris, J.; Mills, T.; Black, D.; Pindak, R.; Zhu, X.-Y. *Adv. Funct. Mater.* **2011**, *21*, 2666-2673.

“Charge carrier extraction dynamics for organic field effect transistor structures.” Chang, H.-C.; Ruden, P.P.; Liang, Y.; Frisbie, C.D. *Appl. Phys. Lett.*, **2011**, *99*, 073306. DOI: 10.1063/1.3625945.

“Ultralow contact resistance in electrolyte-gated organic thin film transistors.” Braga, D.; Ha, M.J.; Xie W.; Frisbie, C.D. *Appl. Phys. Lett.*, **2010**, *97*, 193311. DOI: 10.1063/1.3518075

“Transient effects controlling the charge carrier population of organic field effect transistor channels.” Chang, H.C.; Ruden, P.P.; Liang, Y.; Frisbie, C.D. *J. Appl. Phys.*, **2010**, *107*, 104502. DOI: 10.1063/1.3368662.

“Mixing at the Charged Interface of a Polymer Semiconductor and a Polyelectrolyte Dielectric.” Kaake, L. G.; Paulsen, B. D.; Frisbie, C. D.; Zhu, X.-Y. *J. Phys. Chem. Lett.*, **2010**, *5*, 862-867. DOI: 10.1021/jz900471g.

“Intrinsic charge trapping in organic and polymeric semiconductors: a physical chemistry perspective,” L. Kaake, P. F. Barbara, X.-Y. Zhu, *J. Phys. Chem. Lett.* **2010**, *1*, 628–635.

INVITED TALKS

Ultrafast X-ray Laser Studies of Electronic Excited State Dynamics in Model Photocatalytic Coordination Complexes

Kelly J. Gaffney

PULSE Institute, SLAC National Accelerator Laboratory, Stanford University, Stanford, CA
94305 USA

Abstract

First light at the LCLS x-ray free electron laser at the SLAC National Accelerator Laboratory marked the beginning of hard x-ray laser science. With pulse energies in excess of a millijoule and pulse durations as short as 5 femtoseconds in duration, the LCLS provides a novel and potentially transformative approach for investigating chemical dynamics in complex systems.

The catalytic properties of coordination compounds derive from the ability of transition metal centers to bind substrates and shuttle electrons to and from the substrate. Numerous transition metal complexes also strongly absorb visible radiation making them targets for the development of photocatalysts. The electron and hole in the excited state can catalyze chemical reactions, but only for the duration of the electronic excited state. The charge distribution of the electron and hole, as well as the presence of low energy ligand field excited states greatly influence the lifetime of optically generated charge transfer excited states, but the detailed mechanism for the excited state quenching remains unclear in coordination chemistry.

Acquiring a mechanistic understanding of excited state relaxation in coordination chemistry requires a detailed understanding the coupled evolution of electrons and nuclei in electronic excited states. Ultrafast optical electronic spectroscopy can monitor both the nuclear and the electronic evolution that occurs during a chemical reaction, but this joint sensitivity often impedes the robust interpretation of experimental measurement. The LCLS provides the opportunity to simultaneously measure electronic dynamics with x-ray fluorescence and nuclear dynamics with elastic x-ray scattering, providing a robust means for disentangling the coupled motions of electrons and nuclei in electronic excited states.

Quantum to the Continuum: Opportunities for Mesoscale Science

John C. Hemminger

Chair, Basic Energy Sciences Advisory Committee

Department of Chemistry, University of California, Irvine, CA 92697

William Brinkman, Director of the DOE Office of Science, has asked the Basic Energy Sciences Advisory Committee (BESAC) to carry out a study of the opportunities for the Office of Basic Energy Sciences in the area of mesoscale science. An excerpt from Dr. Brinkman's request to the committee follows.

In referring to recent BESAC reports and to the series of BES Basic Research Needs Reports he stated:

"A central theme of these reports is the importance of atomic and molecular scale understanding of how nature works and how this relates to advancing the frontiers of science and innovation. I would now like BESAC to extend this work by addressing the research agenda for mesoscale science, the regime where classical, microscale science and nanoscale science meet. I see two parts to this new study:

- 1. Identify mesoscale science directions that are most promising for advancing the Department's energy mission.*
- 2. Identify how current and future BES facilities can impact mesoscale science.*

This study could prompt a national discussion of mesoscale science at the level heard during the initial formulation of the National Nanotechnology Initiative a decade ago."

In this presentation I will describe the process that BESAC has utilized to stimulate a discussion in the BES science community on the opportunities that exist in mesoscale science and describe the present state of the BESAC activities on this topic.

Mesoscale science embraces a wide variety of phenomena emerging at length scales larger than atomic and nano but smaller than macro. Mesoscale phenomena are often intermediate between quantum and classical, between isolated and interacting, and between simple and complex. They typically involve the interaction of many degrees of freedom, including mechanical, electrodynamic, electronic, ionic and chemical. Biology is an inspiring example of meso phenomena, often exhibiting striking functionality such as temperature regulation, muscle contraction and self-healing of tissue.

Examples of mesoscale materials and chemistry will be given, to stimulate audience input on the nature of mesoscale science and promising research directions. This input will be used in the coming Basic Energy Sciences Advisory Committee (BESAC) report on Opportunities for Mesoscale Science.

Please visit www.meso2012.com for more information or to contribute suggestions on promising research directions.

The DOE SunShot Initiative: Science and Technology to enable Solar Electricity at Grid Parity

R. Ramesh, Director, SunShot Initiative, US DOE

The SunShot Initiative's mission is to develop solar energy technologies through a collaborative national push to make solar Photovoltaic (PV) and Concentrated Solar Power (CSP) energy technologies cost-competitive with fossil fuel based energy by reducing the cost of solar energy systems by ~ 75 percent before 2020. Reducing the total installed cost for utility-scale solar electricity to roughly 6 cents per kilowatt hour (1\$/Watt) without subsidies will result in rapid, large-scale adoption of solar electricity across the United States and the world. Achieving this goal will require significant reductions and technological innovations in all PV system components, namely modules, power electronics, and balance of systems (BOS), which includes all other components and costs required for a fully installed system including permitting and inspection costs. This investment will re-establish American technological and market leadership, improve the nation's energy security, strengthen U.S. economic competitiveness and catalyze domestic economic growth in the global clean energy race. SunShot is a cooperative program across DOE, involving the Office of Science, the Office of Energy Efficiency and Renewable Energy and ARPA-E.

Title: Conjugated Polymer Semiconductors: Insights into Ordering at the Nano- Through Macro-scales

Elsa Reichmanis

School of Chemical and Biomolecular Engineering

Georgia Institute of Technology

Atlanta, GA 30332

ereichmanis@chbe.gatech.edu

Raman spectroscopy has elucidated the evolution of P3HT microstructure during solvent evaporation. Analysis of spectral changes of the characteristic C=C stretching peak in P3HT as a function of solvent (1,2,4-trichlorobenzene (TCB)) evaporation time, demonstrated that the π - conjugated polymer undergoes a series of phase transitions ranging from isotropic to liquid crystalline to finally, polycrystalline solid. In addition, *in-situ* measurements of the drain current as a function TCB evaporation reveal variations in the current that correspond well with the time-lines for the phase transition. Similar experiments performed with chloroform as a solvent show that the four contact mobility increases up to a peak value of $0.17 \text{ cm}^2/\text{Vs}$ after which it continuously decreased. These insights have further been extended to aid in the design of alternative semiconducting polymers having enhanced performance. A donor-acceptor semiconducting system that exhibits some of the characteristics expected of a liquid crystalline material has been synthesized and investigated. The results of these studies may open a new paradigm for effecting a long-range ordered structure having fewer defects in a simple, controllable, and cost-effective manner, which in turn could hold the key for the fabrication of devices with optimum performance.

Poster Sessions

Materials Chemistry Principal Investigators' Meeting

Poster Session 1

Monday, July 16, 7:00–10:00 pm

Session 1a. Electronic and Magnetic Materials

1. Solid State Electronic Structure and Properties of Neutral Carbon-Based Radicals
Robert C. Haddon, University of California, Riverside.....178
2. Controlling Magnetic and Ferroelectric Order through Geometry-Synthesis, Ab Initio Theory, and Characterization of New Multi-ferroic Fluoride Materials
P. Shiv Halasyamani, University of Houston, and Craig Fennie, Cornell University182
3. Spectroscopy of Charge Carriers and Traps in Field-Doped Single Crystal Organic Semiconductors
Xiaoyang Zhu, University of Texas, Austin331
4. Electronic and Ionic Conductors from Ordered Microporous Materials
Mircea Dincă, Massachusetts Institute of Technology134
5. Synthesis of Molecule/Polymer-Based Magnetic Materials
Joel Miller, University of Utah262
6. Diamondoid Science and Applications
Nick Melosh, SIMES, SLAC44
7. Basic Surface Chemistry and Physics of Carbon-Based Electronic Materials Modified by Silane Molecular Layers
Vitaly Podzorov, Rutgers University.....277
8. Polymer-Based Multicomponent Materials: Research on Multiblock Copolymer Systems
Alexei Sokolov, Oak Ridge National Laboratory.....85

Session 1b. Solar Energy Conversion Materials

9. Nanoscale Materials and Architectures for Energy Conversion <i>Mahendra Sunkara, University of Louisville</i>	307
10. Charge Recombination, Transport Dynamics, and Interfacial Effects in Organic Solar Cells <i>Alan Heeger, University of California, Santa Barbara</i>	194
11. Luminescence in Conjugated Molecular Materials under Sub-bandgap Excitation <i>Franky So, University of Florida</i>	303
12. Crystallization-Driven Assembly of Conjugated-Polymer-Based Nanostructures <i>Ryan Hayward, University of Massachusetts, Amherst</i>	187
13. Molecular and Nanoscale Engineering of High Efficiency Excitonic Solar Cells <i>Samson Jenekhe, University of Washington</i>	218
14. Optical and Magnetic Probes of Charge Dynamics in Organic Donor-Acceptor Bulk Heterojunction for Photovoltaic Applications <i>Z. Valy Vardeny, University of Utah</i>	323
15. Functional Architectures for Light Capture and Utilization <i>Xiuling Li, University of Illinois, Urbana-Champaign</i>	250
16. Dynamic Supracolloidal Assemblies <i>Steve Granick, University of Illinois, Urbana-Champaign</i>	170
17. Mechanistic Studies of Charge Injection from Metallic Electrodes into Organic Semiconductors Mediated by Ionic Functionalities <i>Alexander Mikhailovsky, University of California, Santa Barbara</i>	266

Session 1c. Tools and Techniques for Materials Characterization

18. Solid-State NMR of Complex Materials <i>Klaus Schmidt-Rohr, AMES Laboratory</i>	77
19. ¹²⁵ Te NMR and Transport Properties of Complex Thermoelectric Tellurides <i>Evgenii Levin, AMES Laboratory</i>	32

20. Optical Spectroscopy and Scanning Tunneling Microscopy Studies of Molecular Adsorbates and Anisotropic Ultrathin Films
John Hemminger, University of California, Irvine198
21. Physical Chemistry of Inorganic Nanostructures: Microscopy Investigations of Nanostructured Materials
Stephen Leone, Lawrence Berkeley National Laboratory11

Session 1d. Materials Relevant to Fuel Cells

22. Pore Space Engineering and Functionalization in Porous Metal-Organic Framework Materials
Pingyun Feng, University of California, Riverside.....150
23. Design and Synthesis of Chemically and Electronically Tunable Nanoporous Organic Polymers for Use in Hydrogen Storage Applications
Hani El-Kaderi, Virginia Commonwealth University.....146
24. Synthesis, Characterization and Properties of Nanoparticles of Intermetallic Compounds
Frank DiSalvo, Cornell University137
25. Tuning Sorption Properties of Metal-Organic Frameworks via Postsynthetic Covalent Modification
Seth Cohen, University of California, San Diego130
26. Activation of Hydrogen under Ambient Conditions and Unusual Element Hydride Reactivity by Main Group Molecules
Philip Power, University of California, Davis.....281

Materials Chemistry Principal Investigators' Meeting

Poster Session 2

Tuesday, July 17, 7:00–10:00 pm

Session 2a. Nanostructured Materials

1. Polymer-Based Multicomponent Materials: Polymer Nanocomposites
Alexei Sokolov, Oak Ridge National Laboratory81
2. RAFT Polymerization of Emulsified Microemulsions
Jennifer O'Donnell, Iowa State University270
3. Transport and Doping in Nanocrystal Solids with Electronically Active Organic Ligands
Paul Alivisatos, Lawrence Berkeley National Laboratory93
4. Directed Hierarchical Assemblies of Nanocomposites
Ting Xu, University of California, Berkeley97
5. Self-Assembly of Organic/Inorganic Nanocomposites: Characterization
Miguel Salmeron, Lawrence Berkeley National Laboratory101
6. Guided Assembly of Anisotropic Micro- and Nano-structures into Mesoscale Hierarchies of New Properties
Vladimir Tsukruk and Mostafa El-Sayed, Georgia Institute of Technology319
7. Chemical and Mechanical Properties of Surfaces, Interfaces, and Nanostructures:
Subtask #3: Synthesis and Assembly of Metal and Oxide Nanoparticles
Peidong Yang, Lawrence Berkeley National Laboratory69
8. Fundamentals of Semiconductor Nanowires
Peidong Yang, Lawrence Berkeley National Laboratory7
9. Physical Chemistry of Semiconductor Nanocrystals
Paul Alivisatos, Lawrence Berkeley National Laboratory3
10. Model Photocatalytic Nanostructures
Paul Alivisatos, Lawrence Berkeley National Laboratory15

11. Rational Design and Nanoscale Integration of Multi-heterostructures as Highly Efficient Photocatalysts <i>Xiangfeng Duan, University of California, Los Angeles</i>	141
12. Nanostructured Carbon Materials <i>Larry Curtiss, Argonne National Laboratory</i>	19

Session 2b. Inorganic Materials

13. Chemistry and Properties of Complex Intermetallics from Metallic Fluxes <i>Mercouri Kanatzidis, Northwestern University</i>	230
14. Dielectric Ceramics in Nanosheet Form <i>Tina Salguero, University of Georgia</i>	301
15. Low Temperature Synthesis of Carbide-Derived–Carbons from Binary and Ternary Carbides in the Si-Ti-C System <i>Yury Gogotsi, Drexel University</i>	162
16. Actinide Transition-Metal Chalcogenides and Pnictides <i>Jim Ibers, Northwestern University</i>	206
17. The Synthesis, Structures and Chemical Properties of Macrocyclic Ligands Covalently Bonded into Layered Arrays <i>Abraham Clearfield, Texas A&M University</i>	127
18. Synthesis and Structural Characterization of Novel Intermetallic Clathrates—Prospective Materials for Thermoelectric Applications <i>Svilen Bobev, University of Delaware</i>	115

Session 2c. Materials Behavior at Surfaces and Interfaces

19. Measuring the Importance of Valence to the Chemistry of Nanocrystal Surfaces <i>Jonathan Owen, Columbia University</i>	274
20. Interfacial Behavior of Polymers: Using Interfaces to Manipulate Polymers <i>Thomas Russell, University of Massachusetts, Amherst</i>	297
21. Biaxiality in Thermotropic Bent-Core and Tetrapodic Nematic Liquid Crystals <i>Satyendra Kumar, Kent State University</i>	242

22. Energy and Fuels from Multi-functional Electrochemical Interfaces: Electrocatalysis at Mesoscale <i>Vojislav Stamenkovic, Argonne National Laboratory</i>	40
23. Surface Science at the Nanoscale <i>James Heath, California Institute of Technology</i>	190
24. Chemical and Mechanical Properties of Surfaces, Interfaces and Nanostructures: Subtask #2: Surface Chemical Properties <i>Gabor Somorjai, Lawrence Berkeley National Laboratory</i>	65

Session 2d. Energy Storage Materials

25. Mitigating Breakdown in High Energy Density Perovskite Polymer Nanocomposite Capacitors <i>Richard Brutchey, University of Southern California</i>	119
26. Materials and Interfacial Chemistry for Next Generation Electrical Energy Storage <i>Sheng Dai, Oak Ridge National Laboratory</i>	24
27. Spectroscopic Studies of Materials for Electrochemical Energy Storage <i>Steve Greenbaum, Hunter College of the City University of New York</i>	174
28. Improved Electrical Energy Storage with Electrochemical Double Layer Capacitance Based on Novel Carbon Electrodes, New Electrolytes, and thorough Development of a Strong Science Base <i>Rod Ruoff, University of Texas, Austin</i>	293
29. Solvation and Phase Behavior of Lithium Trifluoromethanesulfonate in Ethylene Carbonate, γ -Butyrolactone, or Propylene Carbonate <i>Paul Trulove, US Naval Academy</i>	315
30. The Influence of Electrolyte Structure and Electrode Morphology on the Performance of Ionic-Liquid Based Supercapacitors: A Combined Experimental and Simulation Study <i>Dmitry Bedrov, University of Utah</i>	111

*Author Index
and
List of Participants*

Ade, H.	107	Granick, Steve	170
Alivisatos, A. Paul .. 3, 7, 11, 15, 89, 93, 97, 101		Greenbaum, Steven G.....	174
Andreou, Andreas G.....	238	Grey, Clare	214
Bates, F.....	81, 85	Haddon, Robert C.....	178
Bazan, Guillermo C.....	194, 266	Halasyamani, P. Shiv.....	182
Bedrov, Dmitry.....	111	Hamers, Robert J.....	222
Bobev, Svilen	115	Hayward, Ryan C.....	187
Boncella, Jim.....	57	Heath, James R.....	190
Borodin, Oleg.....	111	Heeger, Alan J.....	194
Boyle, Paul D.....	315	Hemminger, John C.....	198, 338
Bridges, C. A.....	24, 166	Henderson, Wesley A.....	111, 202, 315
Brutchey, Richard L.....	119	Heon, Min.....	162
Burns, Jonathan D.....	127	Hollingsworth, Jennifer A.....	28
Candanoza, Eliazar.....	127	Hong, M.....	77
Cao, Guozhong.....	218	Htoon, Han	28
Cava, R. J.....	123	Ibers, James A.....	206
Chang, R. P. H.....	254	Israelachvili, Jacob	210
Clearfield, Abraham	127	Jacobson, Allan J.....	214
Cohen, Seth M.....	130	Jenekhe, Samson A.....	218
Corbett, John D.....	49	Jiang, D.-E.....	24, 166
Cuk, Tanja	89, 93, 97, 101	Jin, Song	222
Curtiss, L. A.....	19	Kagan, Cherie R.....	226
Dadmun, M. D.....	81, 85	Kanatzidis, Mercouri G.....	230, 234
Dai, S.....	24, 166	Katz, Howard E.....	238
Devereaux, Thomas.....	44	Kenis, Paul J. A.....	158
Dincă, Mircea	134	Kikkawa, James M.....	226
DiSalvo, Frank.....	137	Kumar, Satyendra.....	242
Duan, Xiangfeng	141	Leone, Stephen R.....	3, 7, 11, 15
Dunbar, Kim R.....	142	Levin, E. M.....	32, 77
Edson, Joe.....	57	Lewis, Jennifer A.....	246
El-Kaderi, Hani M.....	146	Li, Quan.....	242
El-Sayed, Mostafa	319	Li, Xiuling	250
Enggheta, Nader	226	Lin, Qisheng.....	49
Engtrakul, Chai.....	57	Liu, Yi	89, 93, 97, 101
Feng, Pingyun.....	150	Long, Hai.....	57
Fennie, Craig	182	Macomber, Clay	57
Foley, Matthew P.....	315	Manoharan, Hari.....	44
Fréchet, Jean.....	89, 93, 97, 101	Manthiram, A.....	24, 166
Fredrickson, Daniel C.....	154	Markovic, Nenad M.....	19, 36, 40
Freeman, A. J.....	254	Marks, Tobin J.....	254
Frisbie, C. Daniel.....	331	Marschilok, Amy C.....	311
Gaffney, Kelly J.....	337	Mason, T. O.....	254
Gewirth, Andrew A.....	158	Matzger, Adam J.....	258
Ginger, David S.....	218	Mays, J. W.....	81, 85
Gogotsi, Yury	111, 162	Melosh, Nick	44
Goodenough, J. B.....	24, 166	Menon, Madhu	307

Mikhailovsky, Alexander	266	Takeuchi, Esther S.....	311
Miller, Gordon J.	49	Takeuchi, Kenneth J.....	311
Miller, Joel S.	262	Thimmaiah, Srinivasa.....	49
Morgan, Dane.....	214	Trulove, Paul C.....	315
Murray, Christopher B.	226	Tsukruk, Vladimir	319
Nguyen, Thuc-Quyen	194, 266	Unocic, R. R.....	24, 166
Nuzzo, Ralph G.....	158	Urban, V. S.....	81, 85
O'Donnell, Jennifer.....	270	Vajda, S.	19
Owen, Jonathan S.....	274	Vardeny, Z. Valy.....	323
Paranthaman, M. P.	24, 166	Veith, G. M.....	24, 166
Pellin, M. J.....	19	Veryovkin, Igor	73
Pines, Alexander.....	53	Wang, Lin-Wang.....	89, 93, 97, 101
Pivovar, Bryan.....	57	Wilson, William L.....	238
Podzorov, Vitaly.....	277	Wong-Foy, Antek G.....	258
Poeppelmeier, K. R.	254	Worosz, Christopher J.	315
Power, Philip P.....	281	Wright, John C.	222
Presser, Volker	162	Wudl, Fred.....	194
Ramesh, R.	339	Xu, Ting.....	89, 93, 97, 101
Rauchfuss, Thomas B.....	158	Yang, Peidong	3, 7, 11, 15, 61, 69
Reed, Donald T.....	127	Zapol, P.	19
Reichmanis, Elsa	340	Zhu, Xiaoyang.....	327, 331
Rey, Alejandro.....	242		
Richmond, Geraldine L.	285		
Rosenblatt, Charles.....	289		
Ruoff, Rod.....	293		
Russell, T. P.....	297		
Salguero, Tina T.....	301		
Salmeron, Miquel	61, 69, 89, 93, 97, 101		
Savina, Michael.....	73		
Scheiner, Peter.....	44		
Schmidt-Rohr, K.	32, 77		
Schweizer, K.	81, 85		
Seo, Daniel M.....	315		
Shen, Z. X.....	44		
So, Franky	303		
Soderholm, Lynda	206		
Sokolov, A. P.....	81, 85		
Somorjai, Gabor	61, 65, 69		
Springer, Sean	127		
Sprunt, Sam	242		
Srinivasarao, Mohan.....	242		
Stamenkovic, Vojislav R.....	36, 40		
Sumpter, B. G.....	81, 85		
Sun, X. G.....	24, 166		
Sunkara, Mahendra K.....	307		
Sweely, Kurt.....	315		

Participant List

Last Name	First Name	Organization	E-mail
Ade	Harald	North Carolina State University	harald_ade@ncsu.edu
Alivisatos	Paul	Lawrence Berkeley National Laboratory	APAAlivisatos@lbl.gov
Bajaj	Vikram	University of California, Berkeley	vikbajaj@berkeley.edu
Bedrov	Dmitry	University of Utah	d.bedrov@utah.edu
Bobev	Svilen	University of Delaware	bobev@udel.edu
Bridges	Craig	Oak Ridge National Laboratory	bridgesca@ornl.gov
Brutchey	Richard	University of Southern California	brutchey@usc.edu
Burns	Jonathan	Texas A&M University	jburns@chem.tamu.edu
Cao	Guozhong	University of Washington	gzcao@u.washington.edu
Cava	Robert	Princeton University	rcava@princeton.edu
Chang	R.P.H.	Northwestern University	r-chang@northwestern.edu
Christen	Hans	Oak Ridge National Laboratory	christenhm@ornl.gov
Clearfield	Abraham	Texas A&M University	clearfield@chem.tamu.edu
Cohen	Seth	University of California, San Diego	scohen@ucsd.edu
Corbett	John D.	Ames Laboratory	jcorbett@iastate.edu
Curtiss	Larry	Argonne National Laboratory	curtiss@anl.gov
Dadmun	Mark	Oak Ridge National Laboratory	Dad@utk.edu
Dai	Sheng	Oak Ridge National Laboratory	dais@ornl.gov
Devereaux	Tom	SLAC National Accelerator Laboratory	tpd@stanford.edu
Dinca	Mircea	Massachusetts Institute of Technology	mdinca@mit.edu
DiSalvo	Francis	Cornell University	fjd3@cornell.edu
Duan	Xiangfeng	University of California, Los Angeles	xduan@chem.ucla.edu
Dunbar	Kim	Texas A&M University	dunbar@chem.tamu.edu
El-Kaderi	Hani	Virginia Commonwealth University	helkaderi@vcu.edu
El-Sayed	Mostafa	Georgia Institute of Technology	melsayed@gatech.edu
Feng	Pingyun	University of California at Riverside	pingyun.feng@ucr.edu
Fennie	Craig	Cornell University	fennie@cornell.edu
Fitzsimmons	Tim	U.S. Department of Energy	Tim.Fitzsimmons@science.doe.gov
Fredrickson	Daniel	University of Wisconsin-Madison	danny@chem.wisc.edu
Gaffney	Kelly	SLAC National Accelerator Laboratory and Stanford University	kgaffney@slac.stanford.edu
Gennett	Tom	National Renewable Energy Laboratory	Thomas.Gennett@nrel.gov
Gersten	Bonnie	U.S. Department of Energy	Bonnie.Gersten@science.doe.gov
Gogotsi	Yury	Drexel University	yg36@drexel.edu
Granick	Steve	University of Illinois	sgranick@illinois.edu
Greenbaum	Steve	Hunter College of CUNY	steve.greenbaum@hunter.cuny.edu
Gross	Mihal	U.S. Department of Energy	Mihal.Gross@science.doe.gov
Haddon	Robert	University of California at Riverside	haddon@ucr.edu
Halasyamani	Shiv	University of Houston	psh@uh.edu
Hamers	Robert	University of Wisconsin-Madison	rjhamers@wisc.edu
Hayward	Ryan	University of Massachusetts, Amherst	rhayward@mail.pse.umass.edu
Heath	Jim	California Institute of Technology	heath@caltech.edu
Heeger	Alan	University of California, Santa Barbara	ajhe@physics.ucsb.edu
Hemming	John	University of California, Irvine	jchemmin@uci.edu

Henderson	Wesley	North Carolina State University	whender@ncsu.edu
Henderson	Craig	U.S. Department of Energy	Craig.Henderson@science.doe.gov
Hollingsworth	Jennifer	Los Alamos National Laboratory	jenn@lanl.gov
Horton	Linda	U.S. Department of Energy	linda.horton@science.doe.gov
Htoon	Han	Los Alamos National Laboratory	htoon@lanl.gov
Ibers	James	Northwestern University	ibers@chem.northwestern.edu
Ishii	Yoshitaka	University of Illinois at Chicago	yishii@uic.edu
Israelachvili	Jacob	University of California	jacob@engineering.ucsb.edu
Jacobson	Allan	University of Houston	ajjacob@uh.edu
Jenekhe	Samson	University of Washington	jenekhe@u.washington.edu
Jiang	De-en	Oak Ridge National Laboratory	jiangd@ornl.gov
Jin	Song	University of Wisconsin-Madison	jin@chem.wisc.edu
Kagan	Cherie	University of Pennsylvania	kagan@seas.upenn.edu
Kanatidis	Mercouri	Northwestern University	m-kanatidis@northwestern.edu
Katz	Howard	Johns Hopkins University	hekatz@jhu.edu
Kelley	Richard	U.S. Department of Energy	Richard.kelley60@gmail.com
Kini	Aravinda	U.S. Department of Energy	a.kini@science.doe.gov
Kumar	Satyendra	Kent State University	skumar@kent.edu
Kung	Harriet	U.S. Department of Energy	harriet.kung@science.doe.gov
Leone	Stephen	Lawrence Berkeley National Laboratory	srl@berkeley.edu
Levin	Evgenii	Ames Laboratory and Iowa State University	levin@iastate.edu
Lewis	Jennifer	University of Illinois	jalewis@illinois.edu
Li	Quan	Kent State University	qli1@kent.edu
Li	Xiuling	University of Illinois	xiuling@illinois.edu
Lin	Qisheng	Ames Laboratory	QSLIN@AMESLAB.GOV
Lograsso	Thomas	Ames Laboratory	lograsso@ameslab.gov
Manthiram	Arumugam	University of Texas at Austin	rmanth@mail.utexas.edu
Markovic	Nenad	Argonne National Laboratory	nmmarkovic@anl.gov
Markowitz	Michael	U.S. Department of Energy	mike.markowitz@science.doe.gov
Marks	Tobin	Northwestern University	t-marks@northwestern.edu
Marschilok	Amy	Stony Brook University	acm@buffalo.edu
Matzger	Adam	University of Michigan	matzger@umich.edu
Mays	Jimmy	University of Tennessee	jimmymays@utk.edu
Melcer	Natalia	U.S. Department of Energy	natalia.melcer@science.doe.gov
Melosh	Nick	Stanford University	nmelosh@stanford.edu
Mikhailovsky	Alexander	University of California, Santa Barbara	mikhailovsky@chem.ucsb.edu
Miller	Joel	University of Utah	jsmiller@chem.utah.edu
Morgan	Dane	University of Wisconsin-Madison	ddmorgan@wisc.edu
Nuzzo	Ralph	University of Illinois	r-nuzzo@illinois.edu
O'Donnell	Jennifer	Iowa State University	jodonnll@iastate.edu
Owen	Jonathan	Columbia University	jso2115@columbia.edu
Paranthaman	Mariappan	Oak Ridge National Laboratory	paranthamanm@ornl.gov
Pattison	Morgan	Solid State Lighting Services, Inc.	morgan@sslsinc.com
Pellin	Michael	Argonne National Laboratory	pellin@anl.gov
Pines	Alexander	Lawrence Berkeley National Laboratory	A_Pines@lbl.gov
Pivovar	Bryan	National Renewable Energy Laboratory	bryan.pivovar@nrel.gov

Podzorov	Vitaly	Rutgers University	podzorov@physics.rutgers.edu
Power	Philip	University of California, Davis	pppower@ucdavis.edu
Mohammad	Rabbani	Virginia Commonwealth University	mrabbani@vcu.edu
Rabuffetti	Federico	University of Southern California	federico.rabuffetti@usc.edu
Ramesh	Ramamoorthy	U.S. Department of Energy	ramamoorthy.ramesh@ee.doe.gov
Rankin	Stephen	University of Kentucky	srankin@engr.uky.edu
Reichmanis	Elsa	Georgia Institute of Technology	ereichmanis@chbe.gatech.edu
Rey	Alejandro	McGill University	alejandro.rey@mcgill.ca
Richmond	Geraldine	University of Oregon	richmond@uoregon.edu
Rosenblatt	Charles	Case Western Reserve University	rosenblatt@case.edu
Ruoff	Rodney	University of Texas at Austin	r.ruoff@mail.utexas.edu
Russell	Thomas	University of Massachusetts	russell@mail.pse.umass.edu
Salguero	Tina	University of Georgia	salguero@uga.edu
Salmeron	Miquel	Lawrence Berkeley National Laboratory	mbsalmeron@lbl.gov
Sasaki	Darryl	Sandia National Laboratories	dysasak@sandia.gov
Savina	Michael	Argonne National Laboratory	msavina@anl.gov
Schmidt-Rohr	Klaus	Ames Laboratory	srohr@iastate.edu
Sennett	Michael	U.S. Department of Energy	michael.sennett@science.doe.gov
So	Franky	University of Florida	fso@mse.ufl.edu
Sokolov	Alexei	Oak Ridge National Laboratory	sokolov@utk.edu
Somorjai	Gabor	University of California, Berkeley and Lawrence Berkeley National Laboratory	somorjai@berkeley.edu
Srinivasarao	Mohan	Georgia Institute of Technology	mohan@mse.gatech.edu
Stamenkovic	Vojislav	Argonne National Laboratory	vrstamenkovic@anl.gov
Sumpter	Bobby	Oak Ridge National Laboratory	sumpterb@ornl.gov
Sun	Xiao-Guang	Oak Ridge National Laboratory	sunx@ornl.gov
Sunkara	Mahendra	University of Louisville	mahendra@louisville.edu
Takeuchi	Esther	Stony Brook University	Esther.Takeuchi@stonybrook.edu
Thimmaiah	Srinivasa	Ames Laboratory	srini@ameslab.gov
Thiyagarjan	Thiyaga	U.S. Department of Energy	P.Thiyagarajan@science.doe.gov
Trulove	Paul	U.S. Naval Academy	trulove@usna.edu
Tsukruk	Vlaidmir	Georgia Institute of Technology	vlaidmir@mse.gatech.edu
Tumas	Bill	National Renewable Energy Laboratory	bill.tumas@nrel.gov
Unocic	Raymond	Oak Ridge National Laboratory	unocicrr@ornl.gov
Vajda	Stefan	Argonne National Laboratory	vajda@anl.gov
Vardeny	Z. Valy	University of Utah	val@physics.utah.edu
Veith	Gabriel	Oak Ridge National Laboratory	veithgm@ornl.gov
Veryovkin	Igor	Argonne National Laboratory	verigo@anl.gov
Wang	Lin-Wang	Lawrence Berkely National Laboratory	LWWang@lbl.gov
Wong-Foy	Antek	University of Michigan	atkwong@umich.edu
Wudl	Fred	University of California	wudl@chem.ucsb.edu
Xu	Ting	University of California, Berkeley	tingxu@berkeley.edu
Yang	Peidong	Lawrence Berkeley National Laboratory	p_yang@berkeley.edu
Zapol	Peter	Argonne National Laboratory	zapol@anl.gov
Zhu	Jane	U.S. Department of Energy	Jane.Zhu@science.doe.gov
Zhu	Xiaoyang	University of Texas at Austin	zhu@cm.utexas.edu